NASA Conference Publication 2382

The 1984 Goddard Space Flight Center Battery Workshop

Proceedings of a workshop held at
NASA Goddard Space Flight Center
Greenbelt, Maryland
November 13-15, 1984

NASA

NASA Conference Publication 2382

The 1984 Goddard Space Flight Center Battery Workshop

G. Morrow, *Editor*
Goddard Space Flight Center
Greenbelt, Maryland

Proceedings of a workshop held at
NASA Goddard Space Flight Center
Greenbelt, Maryland
November 13–15, 1984

NASA
National Aeronautics
and Space Administration

Scientific and Technical
Information Branch

1985

PREFACE

This document contains the proceedings of the 17th Annual Workshop held at Goddard Space Flight Center, Greenbelt, Maryland on November 13-15, 1984. The Workshop attendees included manufacturers, users, and government representatives interested in the latest results in battery technology as they relate to high reliability operations and aerospace use. The subjects covered included Multikilowatt Power System Strategies, Lithium Cell Technology and Safety, Nickel-Cadmium Technology, Nickel-Cadmium Testing and Flight Experience, and Nickel-Hydrogen Technology.

INTRODUCTION

George W. Morrow
Goddard Space Flight Center

This year the format of the Workshop has remained as it was in the past with the exception that each presenter was required to furnish a camera ready copy of the paper to be presented. This change took place for reasons of economy, not for the purpose of formalizing the conference. We have encouraged questions and comments from the audience and will continue to do so although the discussion periods following each presentation will no longer be included in these proceedings.

The first session, Multikilowatt Power System Strategies, deals with a topic new to the Workshop. It was included in the agenda to give the battery community insight into the Energy Storage Technology schemes being considered for future applications.

The second session, Lithium Cell Technology and Safety, filled out the first day. The sessions of the second day addressed Nickel-Cadmium Technology and Testing and Flight Experience. Nickel-Hydrogen Technology was the topic of the third and last day.

We hope that the 1984 Battery Workshop was as informative and enlightening as those in the past.

PREVIOUS BATTERY WORKSHOP PROCEEDINGS PUBLICATIONS

For your information, we have included a list of the acquisition numbers for all Battery Workshop proceedings since 1970. Copies of previous publications are available upon request. The document numbers and the addresses are as follows:

Year	Contents	Accession Number
1983	Workshop	N84-33668
1982	Workshop	N83-35230
1981	Workshop	N82-20402
1980	Workshop	N81-21493
1979	Workshop	N80-20820
1978	Workshop	N79-28669
1977	Workshop	N79-21565
1976	Workshop	N77-21550
1975	Workshop	N76-24704
1974	Workshop	N75-16976
1973	Workshop (1st day)	N75-15152
	Workshop (2nd day)	N75-17808
1972	Workshop (1st day)	N73-21956
	Workshop (2nd day)	N73-21957
1971	Workshop (Volume 1)	N72-27061
	Workshop (Volume 2)	N72-27062
1970	Workshop (1st day)	N71-28659
	Workshop (2nd day)	N71-28672

NASA may contact:

NASA Scientific and Technical Information Facility (STIF)
P.O. Box 8757
BWI Airport
Baltimore, MD., 21240
(301) 859-5300

All other interested parties contact:

National Technical Information Services (NTIS)
U.S. Department of Commerce
Springfield, VA, 22161
(703) 487-4600

CONTENTS
1984 GSFC Battery Workshop

Co-Chairmen: George W. Morrow
C. Michael Tasevoli
Goddard Space Flight Center

SESSION IV

TOPIC: NICKEL-CADMIUM TESTING AND FLIGHT EXPERIENCE

SESSION V

TOPIC: NICKEL-HYDROGEN TECHNOLOGY

SESSION I

MULTIKILOWATT POWER SYSTEM STRATEGIES

Chairman: F. E. Ford
Goddard Space Flight Center

GODDARD'S ROLE IN THE SPACE STATION PROJECT

Jerry Burdett
Goddard Space Flight Center

What I want to share with you is Goddard's enthusiasm and our pleasure of being a part of Space Station. I started working with the Task Force down at Headquarters in trying to sell this, and we had a big year in January when the President decided to go with the Space Station, and Goddard had an even bigger year in May when we found out what our work package was, and I'll try and share that with you. I think this one here tells you why Space Shuttle has been in development over 10 years, it's going operational as we can see now, we have about one launch per month coming up in the following year. And so what's next? . . . what's next is the Space Station. This is what our present configuration looks like and you have to realize that this configuration is really just what we at NASA have come up with. We will have contractors that will support us in this, we'll have two contractors per center (there's four centers involved) and their proposals are due in on Friday, so we are going to be very busy for the next two months. We hope to be under contract in April next year. This is a view of what we call the power tower. I figured you might be interested in power. It's a gravity gradient pointing down with the solar arrays articulated to track the sun. . . We have this end where we can attach payloads, we have this end with an attached payload looking at the earth, we have laboratories and living quarters, and we have heat rejection panels. This over here by itself is one of the platforms as a co-orbiting platform and there's a polar platform using the technology derived from these subsystems. This view will give you an idea of the size. Here we have a person free-flying and this is an articulated arm. These little circles are docking places for maintenance and repair and this is an enlarged antenna showing assembly in space.

The way we arrived at this configuration, and I won't go into a lot of detail on this, is that we did an iterative process. We took the base requirements from the NASA Centers, iterated these against other requirements, and came up with the unmanned platform on the right, and what our growth potential is on the left. And we really want to be able to have this to be technology transparent. So one of the key things we'd like to be able to do in the area of power for example, is as power technology changes and advances, we'd like to be able to change the power capability and technology in this facility. We're trying to come up with a proper mix of man and machine on Space Station. That's one of the challenges that we see for NASA, in that we're trying to blend the man culture, and what we call the unmanned or the free-flyer culture. We've been doing what we call free-flying spacecraft with robotics where they automatically control the power, and we're in the process on Space Station of unifying NASA in this approach. I found that working with the Task Force and working with the other centers is really a culture exchange and not a culture shock.

One of the functions of the Space Station is to provide an on-orbit laboratory. We'll have two laboratories involved, one for science and application technology (that is life sciences, plants, animals). Goddard has a responsibility for outfitting that Laboratory. The technology laboratory is the area of manufacturing zero G activities, crustal growth, etc., and Marshall has responsibility in their work package for outfitting that laboratory. We will have permanent observatories that are in orbit that we want to maintain; it's going to be a transportation node. The interesting thing in the logistics is to have a single point in space for the shuttle to go every flight. You can send it up with a constant payload. We plan to have a logistics module like a containerized shipping. You

load it, take it up, drop off a full one, bring back the empty with the refuse in it. The Space Station will be service and repair facility for free-flyers and platforms Goddard is involved with and has a responisiblity for servicing. We have the responsibility for servicing all of the users on Space Station in addition to the free-flyers.

The manufacturing facility I mentioned previously is for commercial users. It is the driver for the size of the power system. They're talking about kilowatts of power, 70 kilowatts to be exact; now whether that's what actually falls out in our design has to be determined. But the power that we're talking about is being driven by the manufacturing facility. The assembly facility, again this is Goddard pushing in the area of trying to be able to design and assemble on-orbit things that we cannot presently do on-orbit. In other words, things that are larger than the Shuttle bay itself. If you look at that power tower, that's 500 feet long, and that means you cannot get that whole thing into a single bay; it's going to take about seven shuttle loads to get that up, which means we're going to have to learn how to assemble in space. We're going to have to be able to do servicing in space, we're going to have to learn to assemble large arrays. This view shows an antenna, we have the idea that you might also want to be able to polish glass, you might want to be able to do optical alignments, recurving, cleaning of telescopes, etc. So this is the kind of activity we're talking about. As a goal we're trying to assure our leadership in the free world in space. We want to stimulate advanced technology. Internationally, we are talking about having a full laboratory, that will be an integral part of this Space Station.

Commercialization was one of the key topics in the President's announcement. We want to encourage commercialization. But in order to do that, most of you know that we have to provide the right environment. It's very important for us to provide a policy for what it's going to cost him to get on board (what we're going to charge for power for example); NASA has established an office at Headquarters under Ike Gillum for commercialization. Our commercial policy that we're worried about is a financial risk, institutional risk, and what technology we're going to work at or is going to be done there. We're trying to develop some seed money to encourage this. We expect these customers to be domestic and international, and international is one of the areas that we're really keenly interested in. We have a program under advanced development that came out of the planning for Space Station. For example: electrical power and thermal management are technology areas that have high potential of being able to grow with the Space Station. What we're trying to do is provide a scheme for focus technology, which is technology that is focused directly to the Space Station, prototyping, test beds of power, and thermal. We have a test bed for data systems, and in-flight experiments on shuttle which will verify whether it works or not.

The management of Space Station starts out with Level A being NASA Headquarters, they do policy and overall program direction. Level B, Johnson Space Center has been announced as the program management for technical control.

Something that we're excited about, and we're hoping to be able to provide in the future, is being responsible for this maintenance of free-flyers, we're going to want a bay of some kind so that we can bring free-flyers in for servicing and maintenance. Here is an indication of a guy pulling off a module to put here, that module is stored in this area. Ultimately, what we would like to see is the capability of having a service department or service station inside .

This is about all I wanted to share with you, Goddard's role. We are very excited about it, we're participating in the concept design, we're anxious to get started, and we're off and rolling.

POWER MANAGEMENT AND DISTRIBUTION

Floyd Ford
Goddard Space Flight Center

The first paper this morning was to be presented by Bob Robinson of JSC, and his topic was going to be on Power Management and Distribution Workshop that was held at Johnson back in April of 1984. Unfortunately, Mr. Robinson could not make it. The technical outcome of that workshop is so keyed to our deliberation and discussion that we have here this morning on large power systems, that I'm going to present a quick overview of the outcome of that workshop. Most of you probably have seen the proceedings on it, there is set of proceedings that was published. If you don't have a copy, you can contact Bob Robinson.

The workshop was two-and-a-half days long with the second half of the third day devoted to a panel-type discussion. The objective of that panel was to try to identify key technology issues related to a large multikilowatt power system. In this case, it was specifically geared towards the space station. As results of the deliberations of those people that took part, there were seven items that were identified out of that workshop. These items were documented in the proceedings of the workshop. The seven top issues were presented to the Johnson Management people and also to those people that were at the Johnson Space Center at that time, working on what became known as the skunk-works committee. I'd like to go briefly into the rationale. The first overall conclusion was that there were no major technology obstacles identified that would prevent us from doing the space station. And what you saw in that power tower is basically a solar array and some type of battery system that says 'yes' it can be done with existing technology. But in order to make it a more viable vehicle it said that quite a bit of advanced development is required, and there were four areas identified under the item one. In the first one no major technology issues were identified, but advanced development is required. The rationale that goes with item one is listed in this viewgraph, and basically says that solid-state devices and other electronic component technology for power conversion and switching exists for systems. Transmission line technology exists, and the automation and management technology exists, but it also recognized that for advanced development items, it would take three or four years for certain components to reach acceptable maturity. So, the baseline (and it's important to keep this perspective) is that we can do a large multiple-kilowatt power system with existing technology.

The second item which says conventional 28-volt bus power should not be considered for the main distribution. And the rationale for that was (some of it is very obvious) at 28 volts the magnitude of the current would be prohibitive, and for most of you that are working on a large system in the range of two to five kilowatts you very quickly realize how big a harness gets and how much loss you take through I^2R, losses, which also says that the transmission line and the distribution weight would be prohibitive. So basically the ground rule is don't do another 28-volt system for high power. Let's go to a higher voltage, which leads us to item three which said the voltage level should be as high as practical, consistent with local environment. And, the local environment being not well defined at this point, but the objective of that is you want to get the current levels to a manageable value, and that existing system components are compatible with the voltage levels. And, I might point out that at this workshop there were quite a few representatives from the aircraft industries, and it was one of my first exposures to that side of the technology house in terms of what

they had done with large high power buses for aircraft. And it's interesting that quite a bit of that technology will be applicable to large kilowatt systems in space.

Item C just says that the 200-volt range (there's nothing magic about 200 volts, I don't think the exact voltage has been determined and won't be determined until all the work from the Phase B effort is in) seems a viable compromise to all the problems on the environmental interaction that have been comtemplated and discussed. Item four, which deals with the question of AC versus DC, what the group said is that they could not see any real discriminating cost factors in making a selection between AC and DC high voltage distribution. And, for the reasons given here, is that the cost drivers are really not in the selection but in the component development and the engineering required to achieve the high power level. Power conditioning component technology requirement is the same for both systems and the selection for the AC and DC high voltage for primary distribution has to be evaluated and studied, so if not all conclusive. What it all says is that 'yes' high voltage is the way to go, but we're not sure what the exact voltage range should be and there's a lot of effort that has to be focused on this during the study phase.

Item five, which says an AC sine wave at a standardized TBD frequency, and voltage shoud be provided at the user (meaning the payload). And, these were the two underlying rationales supporting that, mainly that supplying every user with a condition-regulated power would not be cost-effective. In terms of the space station environment of large platforms, where the ground rules are changing on us is the fact that we don't know who all the users are going to be at this time. At the top of that power tower that Jerry showed earlier, is going to be an attachment for a lot of payloads. Some of those payloads have not been defined at this point, and when you envision a mission that is defined to last for 10 to 20 years, we have to back up and say 'we've got to maintain maximum flexibility in order to be able to accommodate the payloads that we don't know what they're going to be.' And it was felt that an AC sine wave at the interface is the most cost-effective, and could be done basically with available technology. It was interesting that there was a lot of discussion on the frequency (400 cycle, 2 kiloHertz, 100 kiloHertz)no one seemed to want to bite that bullet and say 'well this would be the best.' Everyone did say this should be a sine wave, and that's for obvious reasons, because it's easy to keep a sine wave fairly clean in terms of EMI problems.

Item six said utility power, or utility-type regulations should be provided for the space station at the interface. And to get back to the point that I was making earlier, is that if you don't know what the user requirements are, it's hard to know how to regulate, and this goes back to some experiences we've had at Goddard as we've grown into high power systems. Goddard came out of an era where we design typically 28-volt regulated systems plus or minus 2 percent. But invariably by the time you got around to half a kilowatt, one kilowatt, or 2 kilowatt spacecraft, we found that the user had to put a pre-regulator in, and it's not because he can't live with a 2 percent regulation, it's because when you threw all the other has on the bus (turn-on transits, disturbances on the bus, EMC requirements) you find out in order for him to be able to survive those type of electrical disturbance he's got to put additional regulation in anyway. So, it is concensus of the group that attended the workshop at JSC that you really didn't want to try to give him very tightly regulated voltage at that interface.

And then, finally, in Item Seven, which deals with automation. There are two rationales listed. Functional requirements for automation of the power systems control and management must be developed. What it says is 'well we've been automating power systems to a large degree for some years now, but the automation was to the extent that you would usually put the power system in a failsafe mode, and then allow man intervention to reconfigure, or to perform the diagnostic functions that had to be done to know what caused you to go into failsafe mode. Basically in a system as versatile as the space station power system must be, you really have to be able not only to do the diagnostic, but you have to reconfigure, automatically, and that really is what this is addressing (the overall strategy of how you do that, how you provide the necessary protection in reconfiguring the power system, and how to ensure that you don't switch yourself into a short circuit). So this is in a very simplified form, the seven items that came out of the workshop at JSC.

In summary I'd like to (let me find the viewgraph) put up what I feel are the three biggest technical challenges we as power system people face with multiple-kilowatt power systems, more spefically with power systems in the 25-50-100 kilowatt class. Provisions for large power growth from the initial station. Jerry mentioned that the first element will be somewhere in the 50-75 kilowatt, but it had to be designed to grow to the neighborhood of 250 kilowatts over some timeframe. That's new to most of us, we usually design a system from scratch saying we know what it's going to do, we know what the requirements are, and we go build it that way. In this case, we're going to be asked to make considerations for growth, in terms of power level and power qualities, that we can't even define at the time we start cutting the first hardware. The second part, which is also a real big one, is accommodate new technology as it evolves. Jerry mentioned a term called 'focus technology,' which is within NASA a program that is geared towards the technology for the next generation of space station (not meaning as the space station evolves) what technologies can we enhance it with).

This morning you're going to hear about solar dynamics, you're going to hear about fuel cell, electrolysis fuel cell, you're going to hear about nickel hydrogen batteries. All these are in contention for the initial station, but also you can envision that with growth, particularly to the 250 kilowatt class, you're going to need to be able to take advantage of technology that comes into acceptability in that timeframe. And finally, the third one, which I feel as a major challenges is build Jerry mentioned it too . . . is that you're talking about a very large structure and very large system that has to be integrated in orbit. They have to be verified and maintained. We have to change our payloads as a normal course of action. SMM recovery went up and replaced a module, that was one time. If you look at the top of that power tower where the payloads are going to sit, and say 'well the scientists are going to be wanting to put different types of instruments up there over a 20-year period, (if you're talking about an electrical connector,) you can envision that connector being mated and demated at least in the neighborhood of twice a year (maybe more) depending on what the scenario is for the particular science involved. So, over a 20-year period, you're going to envision a lot of wear and tear on connectors. And, how do you replace a connector that's part of the initial design. In summary, I think we have lot of challenges facing us; I see it as in the next several years, quite an exciting time.

POWER MANAGEMENT AND DISTRIBUTION WORKSHOP

HELD AT NASA/JSC APRIL 24-27, 1984

OVERVIEW

BY

FLOYD E. FORD
GSFC

SUMMARY OF PMAD WORKSHOP

1. NO MAJOR TECHNOLOGY OBSTACLES WERE IDENTIFIED, BUT ADVANCED DEVELOPMENT IS REQUIRED.

2. CONVENTIONAL 28-VOLT POWER SHOULD NOT BE CONSIDERED FOR THE MAIN DISTRIBUTION BUS.

3. VOLTAGE LEVEL SHOULD BE AS HIGH AS PRACTICAL WITH LOCAL ENVIRONMENT CONSIDERATIONS.

4. THERE IS NO SIGNIFICANT COST DISCRIMINATOR BETWEEN AC AND DC HIGH VOLTAGE DISTRIBUTION.

5. AN AC SINE WAVE AT A STANDARDIZED TBD FREQUENCY AND VOLTAGE SHOULD BE PROVIDED AT THE USER (PAYLOAD) INTERFACE.

6. "UTILITY"-TYPE REGULATION SHOULD BE PROVIDED BY THE SPACE STATION PMAD TO THE INTERFACE.

7. FUNCTIONAL REQUIREMENTS FOR AUTOMATION OF THE POWER SYSTEM CONTROL AND MANAGEMENT MUST BE DEVELOPED.

ITEM 1.

A. SOLID STATE DEVICE AND OTHER ELECTRONIC COMPONENT TECHNOLOGY FOR POWER CONVERSION AND SWITCHING EXIST.

B. TRANSMISSION LINE TECHNOLOGY EXIST.

C. AUTOMATION AND MANAGEMENT TECHNOLOGY EXIST.

D. THREE TO FOUR YEARS IS REQUIRED TO DEVELOP COMPONENTS TO AN ACCEPTABLE QUALITY, RELIABILITY, AND COST LEVEL.

ITEM 2.

A. MAGNITUDE OF CURRENT AT 28-VOLT PROHIBITIVE.

B. SYSTEM LOSSES UNACCEPTABLE BECAUSE OF I^2R LOSS.

C. TRANSMISSION LINE AND DISTRIBUTION WEIGHT WOULD BE PROHIBITIVE.

D. TRANSMISSION AND DISTRIBUTION WIRES ARE UNACCEPTABLY COMPLEX.

ITEM 3.

A. REDUCES CURRENT MAGNITUDE TO A MANAGEABLE RANGE.

B. EXISTING SYSTEM COMPONENTS ARE COMPATIBLE WITH THIS VOLTAGE LEVEL.

C. 200 VOLTS REPRESENTS A VIABLE COMPROMISE.

ITEM 4.

A. MAJOR COST DRIVER IS GOING TO HIGHER POWER LEVEL; I.E., DEVELOPING QUALIFIED COMPONENTS AND ENGINEERING THEM INTO A HIGH POWER SYSTEM.

B. POWER CONDITIONING COMPONENT TECHNOLOGY REQUIREMENT IS THE SAME FOR BOTH SYSTEMS.

C. SELECTION OF AC OR HIGH VOLTAGE DC FOR PRIMARY DISTRIBUTION SHOULD BE EVALUATED DURING THE PHASE B STUDIES.

ITEM 5.

A. SUPPLYING EVERY USER WITH CONDITIONED/REGULATED POWER WOULD NOT BE COST EFFECTIVE.

B. AN AC SINE WAVE AT THE INTERFACE IS SIMPLE AND COST EFFECTIVE WITH AVAILABLE HARDWARE.

ITEM 6.

A. SUPPLYING HIGHLY REGULATED POWER TO ALL USERS IS NOT COST EFFECTIVE.

B. A LARGE PERCENTAGE OF USERS DO NOT REQUIRE HIGHLY REGULATED POWER.

C. COST EFFECTIVE, TIGHT REGULATION IS MORE EASILY ACCOMPLISHED AT EACH INDIVIDUAL LOAD.

ITEM 7.

A. AUTOMATION LEVEL, LEVEL OF SPACE STATION DATA MANAGEMENT SYSTEM (FACILITIES MANAGEMENT SYSTEM) CONTROL, AND REDUNDANCY MANAGEMENT WILL ALL HAVE A SIGNIFICANT INFLUENCE ON THE SYSTEM DESIGN CONCEPT, AND HARDWARE AND SOFTWARE IN THE PMAD SYSTEM.

B. EARLY DEVELOPMENT OF A COHERENT AND INTEGRATED MANAGEMENT APPROACH WITH DEFINITE GOALS IS ESSENTIAL TO PRECLUDE POWER SYSTEM MANAGEMENT INCOMPATIBILITIES. A CONSISTENT DATA BASE IS REQUIRED FOR INCLUSION IN THE PMAD SYSTEM TRADE STUDIES.

MAJOR DESIGN CHALLENGES

- PROVISIONS FOR LARGE POWER GROWTH FROM INTIAL STATION
- ACCOMMODATION OF NEW TECHNOLOGY AS IT EVOLVES
- ON-ORBIT INTEGRATION, VERIFICATION, MAINTENANCE, AND PAYLOAD CHANGE OUT

REGENERATIVE FUEL CELL SYSTEMS FOR SPACE STATION

Mark A. Hoberecht and Dean W. Sheibley
Lewis Research Center

ABSTRACT

Regenerative fuel cell (RFC) systems are one of the leading energy storage candidates for Space Station. Key design features include its advanced state of technology readiness and high degree of system level design flexibility. Technology readiness has been demonstrated through extensive testing at the single cell, cell stack, mechanical ancillary component, subsystem, and breadboard levels. Design flexibility characteristics include independent sizing of power and energy storage portions of the system, integration of common reactants with other Space Station systems, and a wide range of various maintenance approaches. These design features have led to selection of a RFC system as the sole electrochemical energy storage technology option for the Space Station Advanced Development Program.

INTRODUCTION

The RFC program was initiated in 1979 by OAST to bring fuel cell and electrolysis technology to a level of flight readiness by 1987. The program has been a joint effort by NASA Lewis Research Center (LeRC) and NASA Johnson Space Center (JSC). The LeRC program has been directed toward development of alkaline technology, with fuel cell work being conducted at United Technologies Corp. (UTC) and electrolysis work at Life Systems, Inc. (LSI). The program at JSC has been directed toward both acid SPE fuel cell and electrolysis technology, the work conducted at General Electric Company (GE). More recently, the work sponsored out of LeRC has been aimed at alkaline cell component technology, specifically in the areas of electrode catalysts, unitized electrode assemblies, cell frames, separator matrices, feed-water cavity matrices, electrolyte reservoir plates (ERP's), and decay modeling. The JSC work has focused on both alkaline and acid SPE system technology, mainly in the areas of mechanical ancillary components and breadboard demonstrations.

A detailed in-house design study has been performed at LeRC to investigate the merits of the alkaline and acid SPE technology options. The results of this study have shown the alkaline fuel cell - alkaline electrolysis RFC to be the best option for further development; in terms of system complexity, performance, development cost, and risk. The end-item deliverable of this program will be a 10 KW alkaline engineering model system (EMS) by 1987. The system shall be capable of demonstrating full integration with autonomous control, high voltage operation ($\geq$ 100 Vdc) and good overall round-trip electrical efficiency ($\geq$ 55 percent).

TECHNOLOGY READINESS

FUEL CELL

Alkaline fuel cells are a flight-qualified aerospace technology. An extensive data base has been generated through the Shuttle-Orbiter program, both in qualification testing and in actual mission performance. Improvements to this technology, in the electrochemical and mechanical ancillary component portions of the system, are already under way.

In the electrochemical cell component area, key items are the cell frame, separator matrix, ERP, and anode catalyst. Replacing the present fiberglass/epoxy frame with polyphenylene sulfide (PPS) and the current asbestos matrix with potassium titanate (PKT) are both aimed at carbonate reduction, which will lower the degradation rate of the cell by an order of magnitude and extend life. Substitution of graphite for the present nickel ERP will reduce cell weight almost in half, while utilizing a platinum-on-carbon anode catalyst in place of platinum/palladium will also reduce degradation and extend life. Ongoing endurance test results for a six-cell stack and four-cell stack at UTC are shown in Figures 1 and 2, respectively. The six-cell stack incorporates a platinum-on-carbon catalyst, while the four-cell stack is composed of a PKT matrix, graphite ERP, and platinum-on-carbon catalyst. PPS frames in varying combinations with these other electrochemical cell component improvements are being tested under Navy and UTC IR&D programs.

Key items in the mechanical ancillary component area are the dual pressure regulator, thermal control valve, coolant pump, and hydrogen pump/separator. Reduction of internal wear to those components with moving parts is the major activity. Specifically, improved bearing lubricant seals and advanced bearing concepts are under investigation. Endurance testing will verify feasibility.

ELECTROLYSIS

Alkaline electrolyzers are not flight-qualified. However, a substantial data base exists for life support and terrestrial hydrogen production applications. As with alkaline fuel cells, improvements to the electrochemical and mechanical ancillary component portions of the system are under way.

In the electrochemical cell component area, key items are unitized electrode assemblies and the feed-water cavity matrix. Unitized core construction improves cell sealing reliability and reproducibility. Replacing the current asbestos feed-water cavity matrix with a porous hydrophobic sheet will allow passage of any evolved gaseous hydrogen from the feed-water cavity to the hydrogen cavity. Ongoing performance of present aerospace technology has already been demonstrated, as can be seen in Figure 3. Test results for a six-cell stack incorporating unitized electrode assemblies are shown in Figure 4. Successful scale-up of cell active area has been verified in a DOE program at LSI.

Key items in the mechanical ancillary component area are the coolant control assembly, fluids control assembly, and fluids pressure controller. Each of these components combines several functions (valves, sensors, etc.) in order to simplify the subsystem. Successful endurance testing continues at LSI under a NASA Ames Research Center (ARC) program.

DESIGN FLEXIBILITY

SEPARATE SUBSYSTEMS

A simple RFC system schematic diagram is shown in Figure 5. The system consists primarily of three subsystems; fuel cell, electrolysis, and reactant storage. The power portion of the system is the fuel cell and electrolysis subsystems, both separate units. The energy storage portion is the reactant storage subsystem. Because of the separate nature of these subsystems, independent sizing for a particular mission application is possible. This is not true of battery systems, where reactants are stored in the electrodes themselves. The RFC system is thus very adaptable to different peak and emergency power conditions, where power loads (KW) and energy storage loads (KW-hr) may not be directly related and could vary substantially for the Space Station.

INTEGRATION WITH OTHER SYSTEMS

The RFC system is amenable to both closed loop (internal reactant supply/demand) and open loop (external reactant supply/demand) operation. The former is typical of battery systems, while the latter type of operation allows for integration with other Space Station systems through sharing of common reactants. The other systems include life support, propulsion, and possibly space manufacturing. Water can therefore be the logistic fuel for all these systems, either used directly or readily converted to gaseous hydrogen and oxygen through electrolysis. Scavenging of residual Shuttle-Orbiter cryogenics may be another form of integration possible with an open loop system.

MAINTENANCE APPROACHES

Separate subsystems also make possible various maintenance schemes. The mechanical ancillary components as opposed to the electrochemical portions of the system are generally regarded as the least reliable items. Depending on redundancy requirements, packaging of system elements can be performed in such a way as to minimize the impact of a failure. For those items with the least reliability, parallel plumbing with multiple mechanical ancillary components may be the optimum approach. The orbital replacement unit (ORU) philosophy will dictate which grouping of system elements is the most advantageous. Any arrangement from an entire system to an individual component is possible. Replacement and introduction of new technology in both the electrochemical and mechanical ancillary component portions of the system thus becomes more likely as well.

CONCLUDING REMARKS

Regenerative fuel cell systems offer many advantages over other competing energy storage systems for the Space Station application. Technology readiness has been demonstrated through partial flight qualification and a significant endurance test data base for the fuel cell and electrolysis subsystems. The integrated system offers an inherent design flexibility due to the separate nature of the reactant storage subsystem. These design features have led to selection of an alkaline RFC as the electrochemical energy storage system technology option for the Space Station Advanced Development Program.

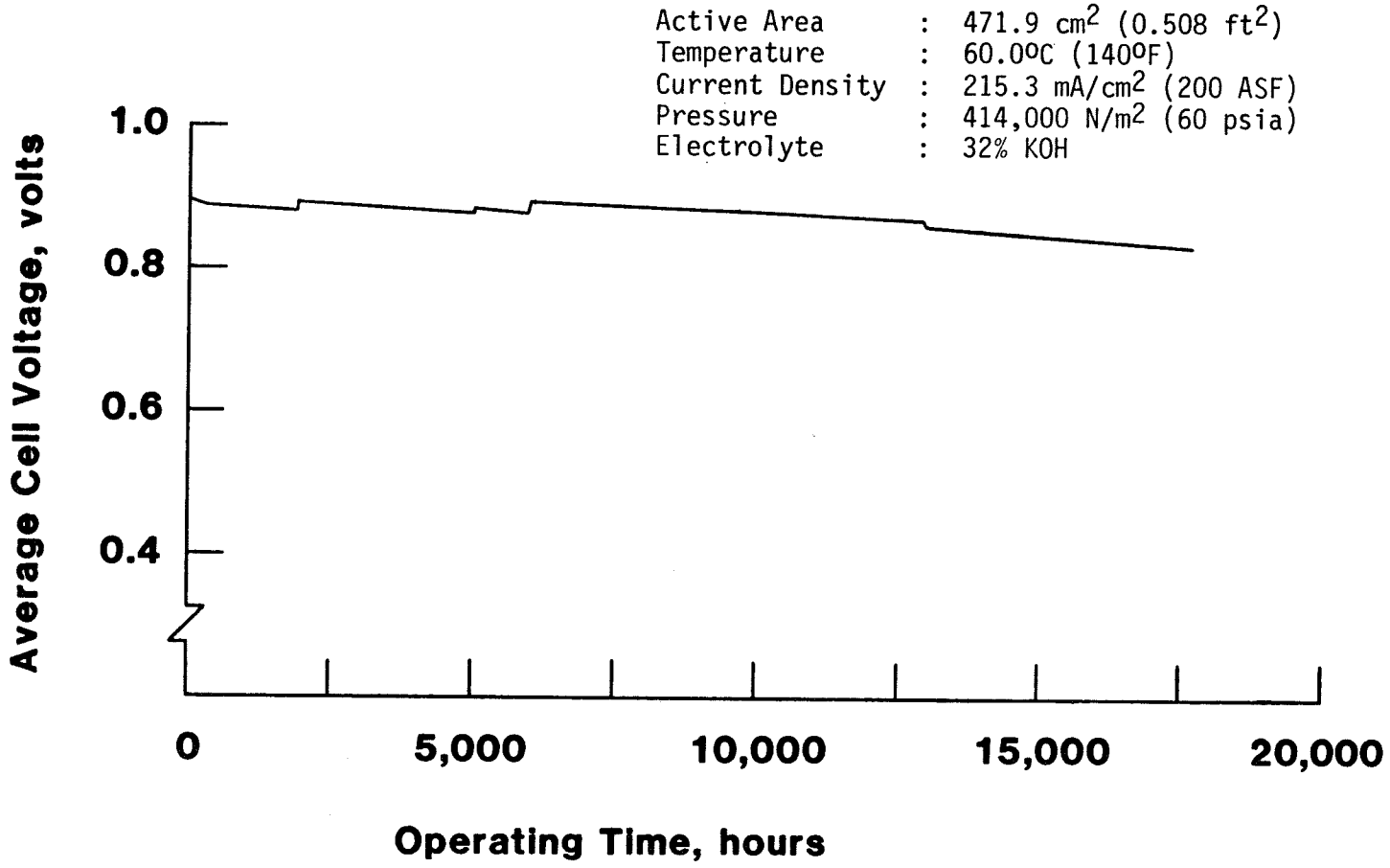

Figure 1. UTC six-cell stack endurance test

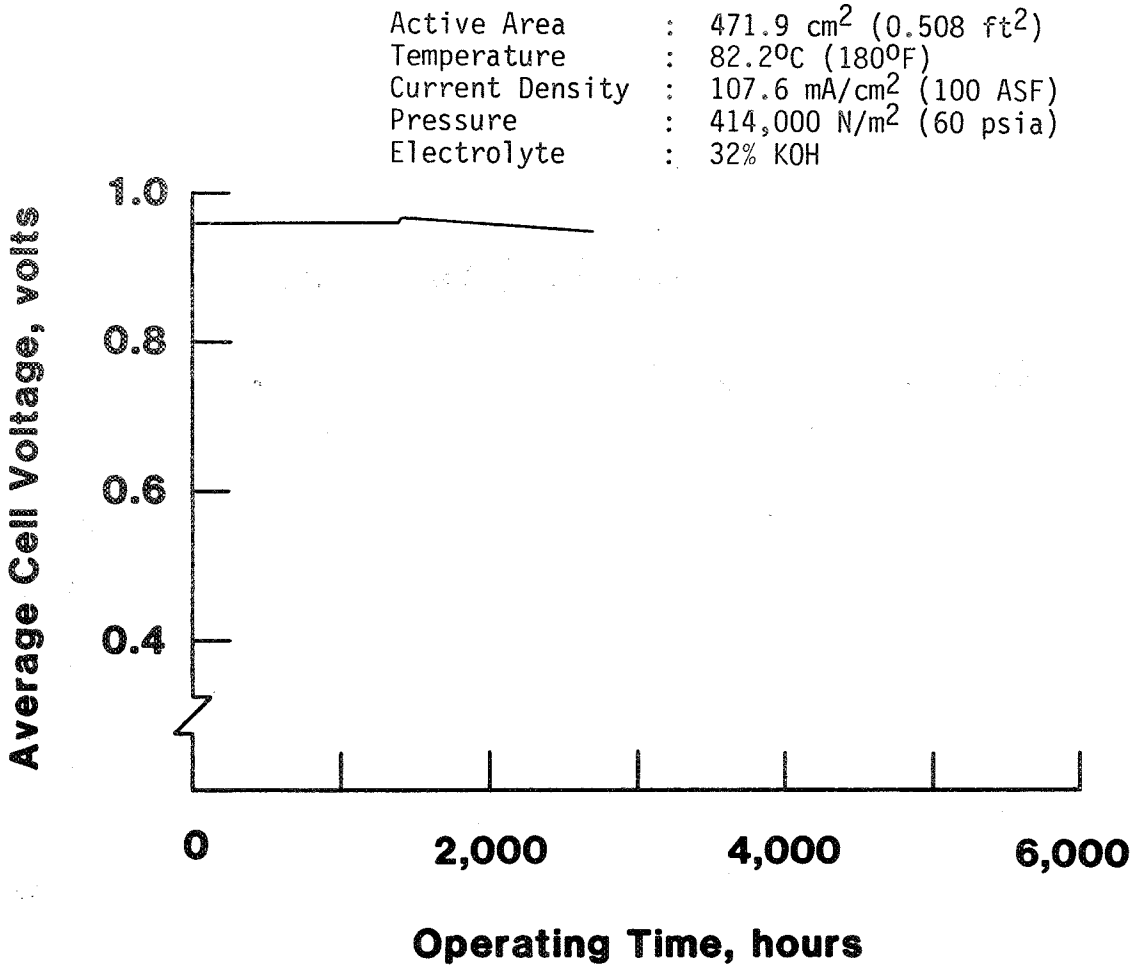

Figure 2. UTC four-cell stack endurance test

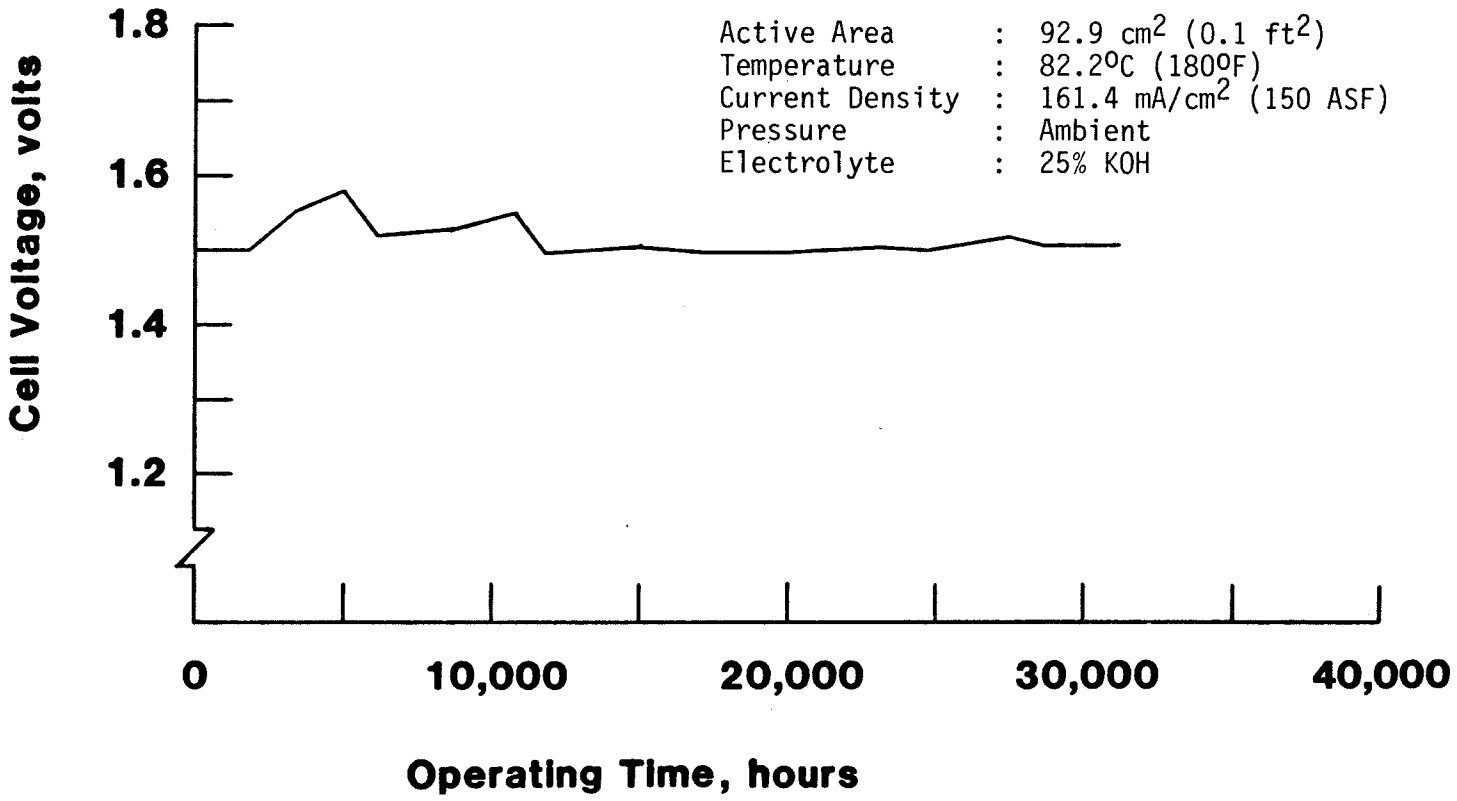

Figure 3. LSI single cell endurance test

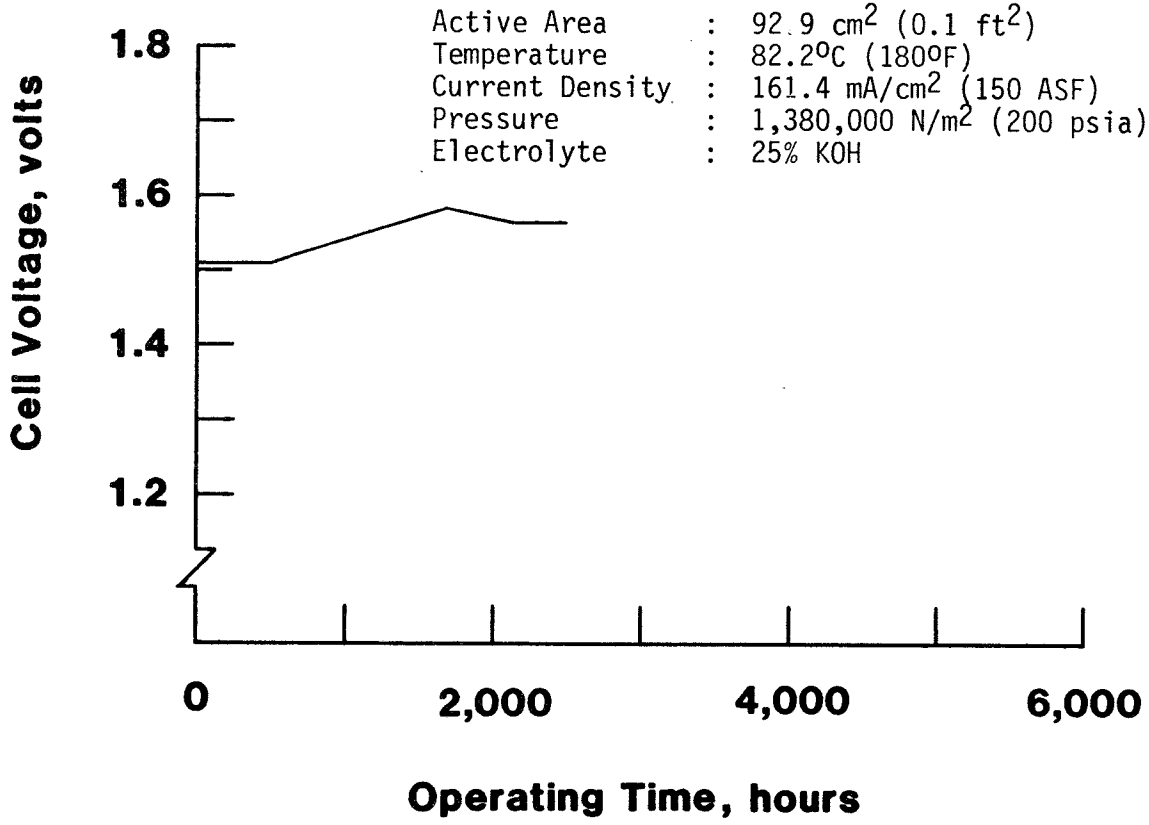

Figure 4. LSI six-cell stack endurance test

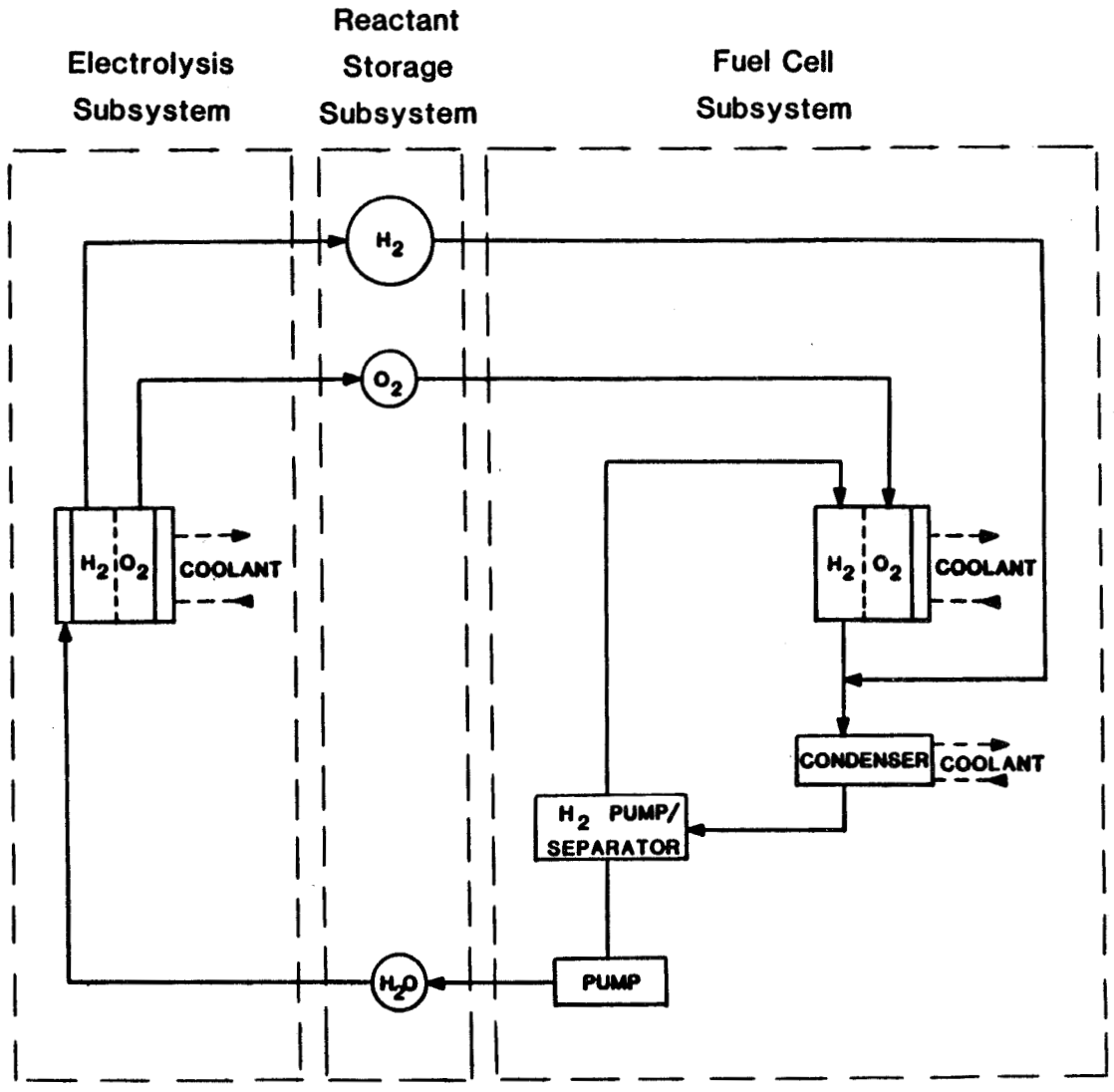

Figure 5. RFC system schematic diagram

MULTIKILOWATT HYDROGEN-NICKEL OXIDE BATTERY SYSTEM*

James D. Dunlop
COMSAT Laboratories
Clarksburg, MD 20871

INTRODUCTION

A new development program has resulted from a favorable assessment (ref. 1) of the potential of the H_2-NiO battery for terrestrial applications. This program uses a multicell design approach that differs significantly from the aerospace individual pressure vessel design. A number of experimental 100-Ah cells were built to evaluate the new design concepts and components. Results from these experimental cells provided the input needed for a multicell battery design. Several experimental 100-Ah cells and one 6-cell battery were delivered to Sandia National Laboratories for life testing.

This new multicell H_2-NiO battery has a number of potential advantages for aerospace applications such as the manned space station. Thes advantages are discussed, and a design concept is presented for a multikilowatt battery in a lightweight pressure vessel.

AEROSPACE HYDROGEN-NICKEL OXIDE BATTERIES

Aerospace H_2-NiO cells and batteries have been developed to replace Ni-Cd batteries as the energy storage subsystem for commercial communications satellites (refs. 2-4). These batteries increase cyclic life and calendar lifetime, improve reliability, and reduce battery mass. Figure 1 shows the INTELSAT V aerospace battery.

AEROSPACE FLIGHT PROGRAMS

Programs using or planning to use aerospace H_2-NiO batteries are outlined in table I. The NTS-2 satellite launched in June 1977 was the first satellite to use H_2-NiO batteries in space. The INTELSAT V program was the first commercial communications satellite series to use H_2-NiO batteries. To date, three satellites in this series (F-6, F-7, and F-8) have been launched with H_2-NiO batteries on board, and the remaining seven satellites in the series are scheduled to use H_2-NiO batteries. All of the H_2-NiO battery systems in space are performing well.

*This paper is based on work performed at COMSAT Laboratories under the sponsorship of Sandia National Laboratories.

EXPERIMENTAL TERRESTRIAL 100-Ah CELLS

For the Sandia-sponsored program, the design approach departed from the cylindrical individual pressure vessel (IPV) aerospace cell, and instead used a prismatic multicell design approach. Cost reduction was a major incentive for using the prismatic arrangement. The challenge was to produce a workable design in this geometry. A number of experimental 100-Ah cells were designed, fabricated, and tested to evaluate new concepts and different electrode stack components.

DESCRIPTION OF 100-Ah CELLS

Figure 2 shows an assembled 100-Ah cell with the following key features:

a. The electrodes are sized at 14 cm x 12 cm x 0.76 mm.

b. The polypropylene container is one section of a standard, 6-cell, injection-molded battery container such as that employed in a 54-Ah lead-acid battery (Johnson Controls, Inc.*).

c. Threaded negative and positive nickel post terminals are employed, with nickel hex nuts.

d. The cover is heat-sealed to the case, and a gas-permeable plug is provided for hydrogen flow into and out of the cell.

e. A total of 21 or 22 positive electrodes were used to build one 100-Ah cell.

Table II describes the nine 100-Ah experimental cells fabricated to date. Reference 5 describes these cells and their performance data in detail.

PERFORMANCE

Test data were collected for these 100-Ah cells, with emphasis on the data which were most relevant to the battery design. The platinum/carbon electrode with reduced platinum loading generally performed well. Above 20°C, the positive electrodes with cadmium additive performed better than those with cobalt additive. Cells with the back-to-back electrode stack design performed best.

*Johnson Controls, Inc. (JCI) is a subcontractor to COMSAT Laboratories on the Sandia program.

Platinum/Carbon Electrode

This electrode was developed to reduce cost. The platinum content of the electrode was reduced by more than an order of magnitude, from 7 to 0.4 mg/cm^2, with no degradation in performance (see fig. 3). Cell 1 had the aerospace negative electrodes, and Cell 2 had the carbon/platinum negative electrodes. Otherwise, the components in these two cells were the same.

Self-Discharge

At 10°C, the self-discharge data for Cells 1 and 2 were identical, as shown in figure 4. The time constant was 1,748 hr.

Back-to-Back Design

Cells 3 and 9, with cadmium additive in the positive electrodes, asbestos separator material, and back-to-back design, gave the best performance. Figure 5 gives performance data for Cell 3 at 10°C. This cell completed 89 cycles at COMSAT Laboratories, and then was shipped to Sandia National Laboratories. Sandia currently has Cells 3 and 9 on a life test.

6-CELL, 7.5-V, 100-Ah BATTERY

From the experimental development effort, Cell 9 evolved as the most advanced cell design. The 6-cell stacks for the H_2-NiO battery were built to this design.

BATTERY ASSEMBLY INTO POLYPROPYLENE CONTAINER

The H_2-NiO battery, shown in figure 6, has the following salient features:

a. a standard, polypropylene, injection-molded container to house the six cell stacks;

b. a cover which was heat-sealed on the assembly line;

c. negative and positive nickel post terminals injection-molded into the cover;

d. cell interconnects within the polypropylene case; and

e. individual voltage-sensing leads to monitor the individual cell voltages, with individual caps for each of the six cells.

BATTERY ASSEMBLY INTO PRESSURE VESSEL

Figure 7 shows the battery being assembled into the pressure vessel. Note that a heat exchanger is placed around the battery case to allow temperature control of the battery during testing. The completely assembled battery is shown on test in figure 8. Also note that a gas cylinder is connected to the battery to allow for external storage of hydrogen gas. During long periods of stand, hydrogen gas can be stored externally by closing a valve, thus preventing self-discharge.

PERFORMANCE DATA

After activation, the first sealed discharge produced the voltage and pressure profiles displayed in figure 9. The capacity measured when the first cell reached 1 V was 103.7 Ah. The maximum pressure reached on charge was 332 psig without external hydrogen storage, and 230 psig with external hydrogen storage. Precharge in this battery was set at 70 psig.

COST

The battery shown in figure 6 was assembled by JCI at their lead acid battery pilot plant. All of the assembly steps followed established semiautomatic procedures. A detailed cost study is underway for a multikilowatt H_2-NiO energy storage system based on this new multicell battery. Significant cost reductions (over 30/1) are projected for this system, as compared with present aerospace IPV batteries.

SANDIA NATIONAL LABORATORIES BATTERY TEST RESULTS*

The H_2-NiO cell being cycled at room temperature (ID 351, Cell 3), has accumulated 681 cycles at 80-percent depth of discharge, and the capacity is stable at 88.5 Ah, as presented in table III. The other cell (ID 373, Cell 9), and the battery (ID 385, Battery 2), were also deep cycled, but the amount of overcharge was controlled based on the slope of the pressure-time curve. Different values of $\Delta P/\Delta T$ were used to terminate charge. The 6-cell battery has over 100 cycles at Sandia and is performing well (table III). The cell voltages are very uniform; the end-of-discharge and end-of-charge voltages for the last cycle of the set are presented in table IV.

MULTIKILOWATT BATTERY SYSTEM

This 6-cell, 7.5-V, 100-Ah battery will be the building block for a multikilowatt battery system. Ten to fifteen of these batteries could readily be connected in series and installed into one common pressure vessel, as shown

*Data courtesy of D. Bush, Program Manager, Sandia National Laboratories.

in figure 10. This configuration would provide approximately 10 kWh of stored energy (100 Ah at 100 V).

Figure 11 shows a lightweight pressure vessel version of this multikilowatt battery system. The potential advantages of this battery system for multikilowatt aerospace applications are presented in table V.

CONCLUSIONS

To date, performance data for the H_2-NiO prismatic multicell battery design approach have been very encouraging. Many of the design concepts demonstrated in the multicell 100-Ah battery are suitable for both terrestrial and aerospace applications.

REFERENCES

1. Clifford, J. E.; and Brooman, E. W.: "Assessment of Nickel-Hydrogen Batteries for Terrestrial Solar Applications: Final Report," NTIS No. SAND-80-7191, 1981.

2. Dunlop, J.: "Nickel-Hydrogen Batteries," Handbook of Batteries and Fuel Cells, David Linden, ed., New York: McGraw-Hill, 1984, p. 22-1.

3. Dunlop, J.; and Stockel, J.: "Nickel-Hydrogen Battery Technology--Development and Status," Journal of Energy, Vol. 6, No. 28, 1982, pp. 28-33.

4. Dunlop, J.; Stockel, J.; and van Ommering, G.: "Sealed Metal Oxide-Hydrogen Secondary Cells," Power Sources 5, D. H. Collins, ed., London and New York: Academic Press, 1974, p. 315.

5. Dunlop, J; Vaidyanathan, H.; Sindorf, J.; and Earl, M.: "Design and Development of a Sealed 100-Ah Nickel-Hydrogen Battery," Contract Report SAND-84-7155, August 1984.

TABLE I. AEROSPACE PROGRAMS USING H_2-NiO BATTERIES

Spacecraft Program	Spacecraft Manufacturer	Cell Capacity (Ah)	Design	Cell Manufacturer	No. of Cells Per Spacecraft	Satellite Orbit
INTELSAT V	FACC[a]	35	IPV-COMSAT[b]	EPI[c]	54	Synchronous
A	RCA[d]	30	IPV-COMSAT	EPI	66	Synchronous
B	RCA	40	IPV-COMSAT	EPI	66	Synchronous
C	RCA	50	IPV-COMSAT	EPI	66	Synchronous
D	RCA	35	IPV-COMSAT	EPI	44	Synchronous
INTELSAT VI	HAC[e]	48	IPV-HAC	HAC	64	Synchronous
SDS (Military)	HAC	25	IPV-HAC	HAC	36	Synchronous
MMBI (Military)	HAC	25	IPV-HAC	HAC	36	Synchronous

[a]Ford Aerospace Communications Corporation.
[b]COMSAT Laboratories.
[c]Eagle Picher Industries.
[d]Radio Corporation of America.
[e]Hughes Aircraft Corporation.

TABLE II. EXPERIMENTAL CELLS

Cell Number	Positive[a]		Negative[b]		Separator[c]	Design
	Number	Type	Number	Type		
1	22	JCI	22	Platinum	W. R. Grace	Back-to-back
2	22	JCI	22	10% Platinum/carbon	W. R. Grace	Back-to-back
3	22	JCI	22	10% Platinum/carbon	Asbestos	Back-to-back
4	22	255 JCI	22	10% Platinum/carbon	Asbestos	Back-to-back
5	21	255 JCI	22	10% Platinum/carbon	Asbestos	Recirculating
6	21	255 JCI	22	10% Platinum/carbon	Asbestos	Recirculating
7	21	JCI*	22	10% Platinum/carbon	Asbestos	Recirculating
8	21	255 JCI	21	10% Platinum/carbon	Asbestos	Back-to-back
9	21	JCI	21	10% Platinum/carbon	Asbestos	Back-to-back

[a]Positive Electrodes

JCI : 0.76-mm-thick wet slurry plaque, aqueous impregnation process with cadmium additive.

255 JCI : 0.76-mm-thick dry sinter plaque, aqueous impregnation process with cobalt additive.

JCI* : 0.76-mm-thick wet slurry plaque, aqueous impregnation process with cobalt additive.

[b]Negative Electrodes

Platinum : Standard aerospace platinum catalysts with 6 to 8 mg Pt/cm^2 surface area.

10% Platinum/Carbon : Carbon/platinum catalyst with 0.4 mg Pt/cm^2 surface area.

[c]Separator

W. R. Grace : Inorganic/organic composite consisting of non-woven polyolefine with inorganic filler material.

Asbestos : Quin-T fuel cell grade asbestos.

TABLE III. ACTIVE H_2-NiO BATTERY TEST SUMMARY
(SEPTEMBER 1984)

ID Number	Nominal Rating		Test Condition*	Cycles	Capacity (Ah)
	V	Ah			
Cell 3: 351	1.25	90	NEMA	681	89
Cell 9: 373	1.25	100	NEMA	272	88
Battery 2: 385	7.5	100	NEMA	108	98

*80-percent depth of discharge based on National Electric Manufacturers Association (NEMA) standard.

TABLE IV. BATTERY VOLTAGES

Cell Number	End-of-Discharge Voltage	End-of-Charge Voltage
1	1.199	1.524
2	1.201	1.521
3	1.200	1.520
4	1.201	1.522
5	1.194	1.521
6	1.199	1.523

TABLE V. COMSAT/JCI H_2-NiO BATTERY: POTENTIAL ADVANTAGES FOR AEROSPACE

Advantage	Description
High Energy Density	65 Wh/kg
High Power Density	600 W/kg
Improved Energy per Unit Volume	64 Wh/L Two times better than battery fabricated from present IPV H_2-NiO cells.
Advanced Design Concepts for a Multikilowatt Energy Storage System	Multicell design, activation procedures, etc., represent a significant advancement over present state-of-the-art IPV cells.
High Watt-Hour Efficiency	$\geq$85%
Background Data Base	100-Ah battery and cells on test.
Building-Block Concept	1-kWh modules can be connected to make multikilowatt systems.
Manufacturing Reliability	JCI has applied proven and reliable manufacturing processes to the assembly of these batteries.
Cost Reduction	30/1 reduction compared with IPV cell technology.

Figure Captions

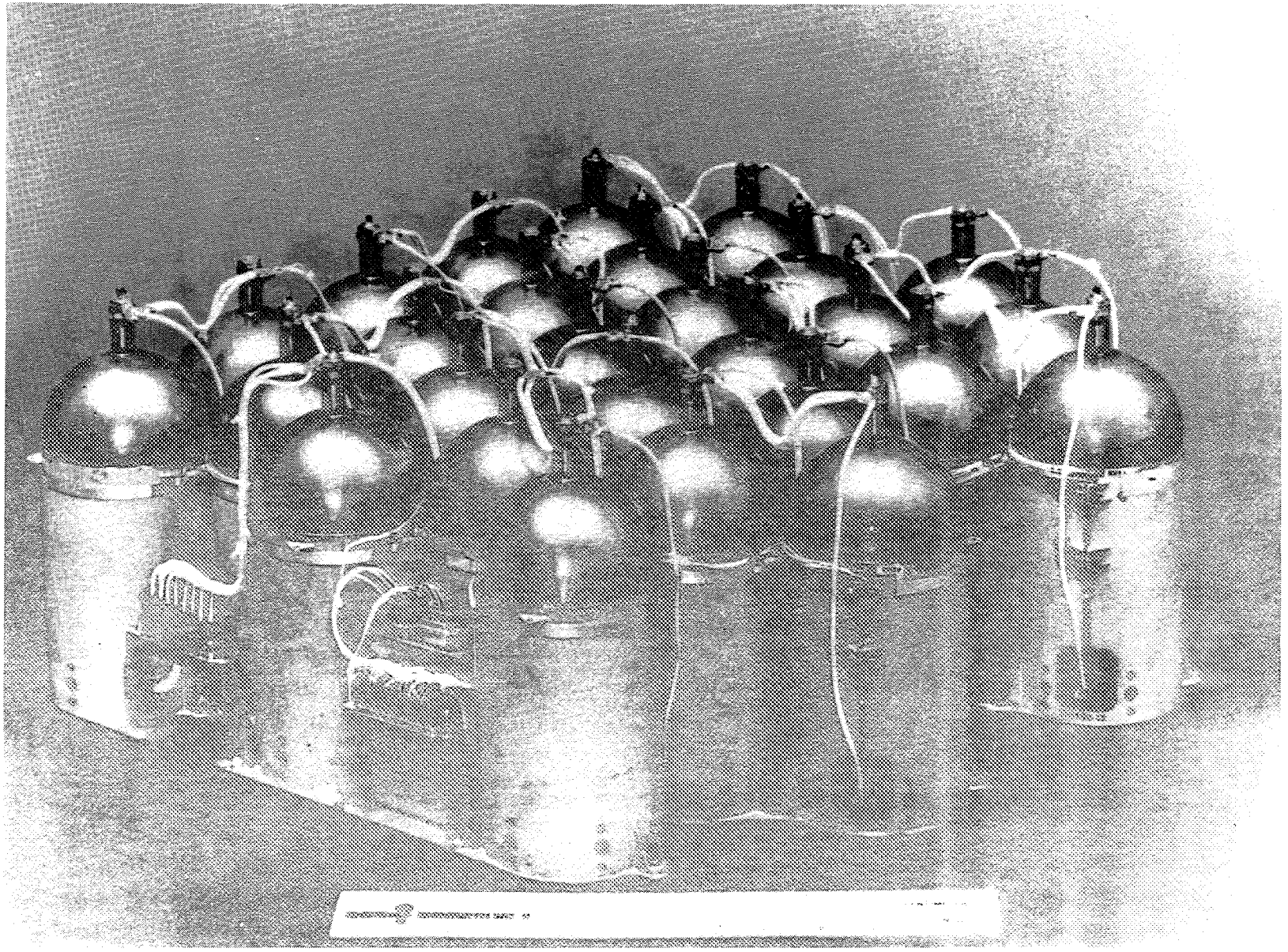

Figure 1. INTELSAT V H_2-Ni0 Battery

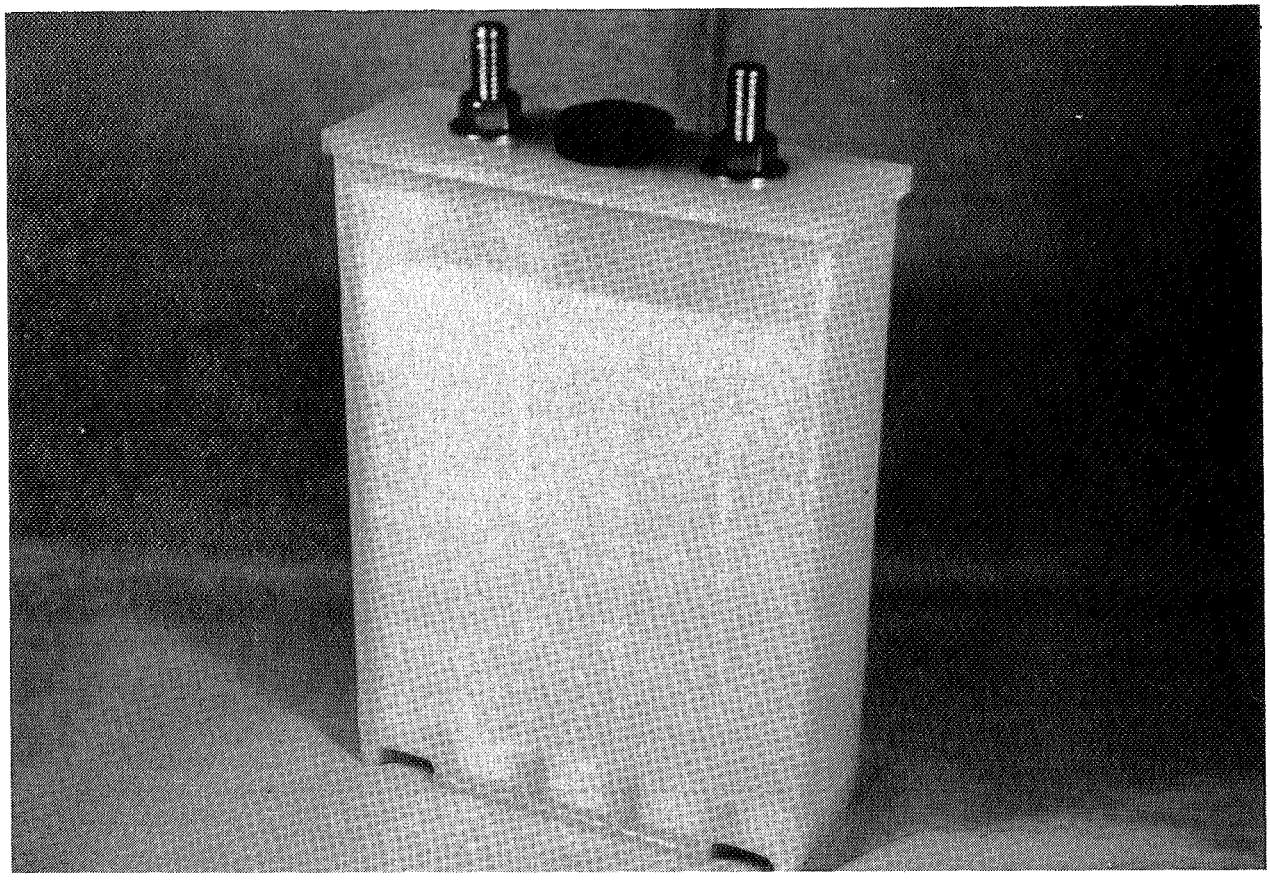

Figure 2. 100-Ah Experimental Cell

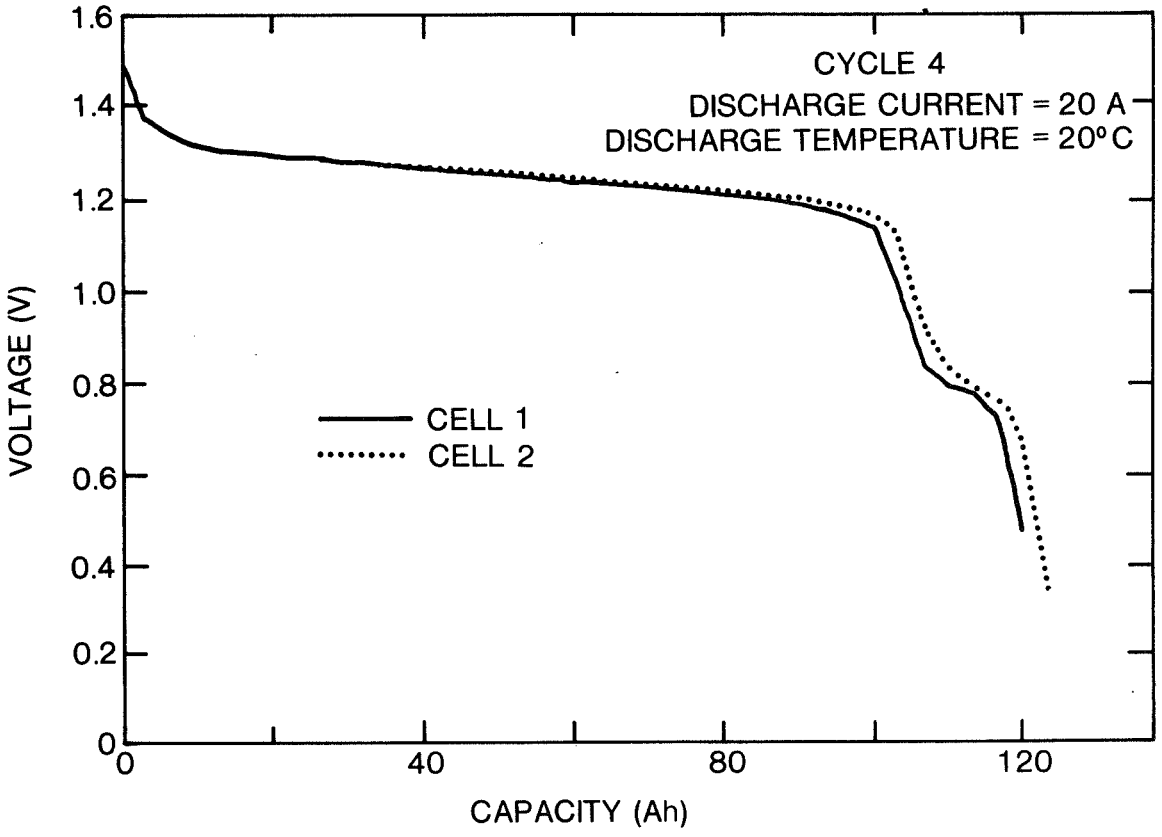

Figure 3. Voltage on Discharge for Cells 1 and 2

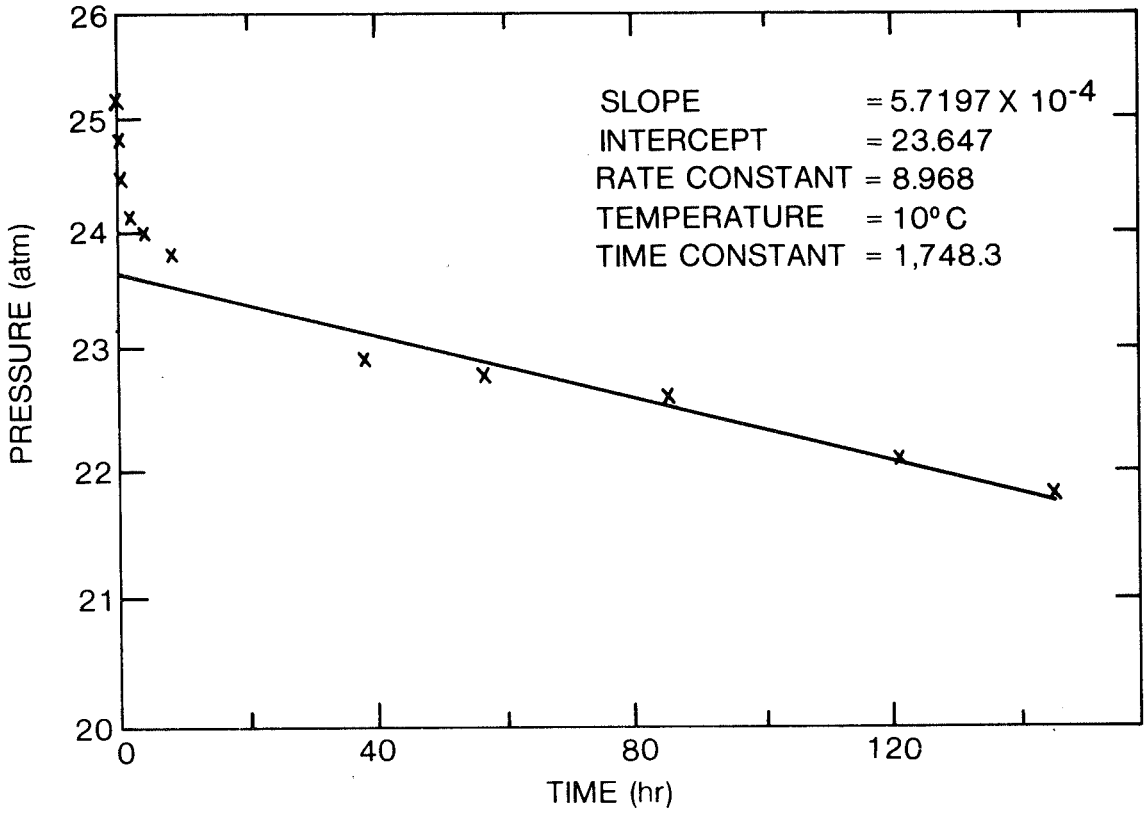

Figure 4. Self-discharge for Cells 1 and 2

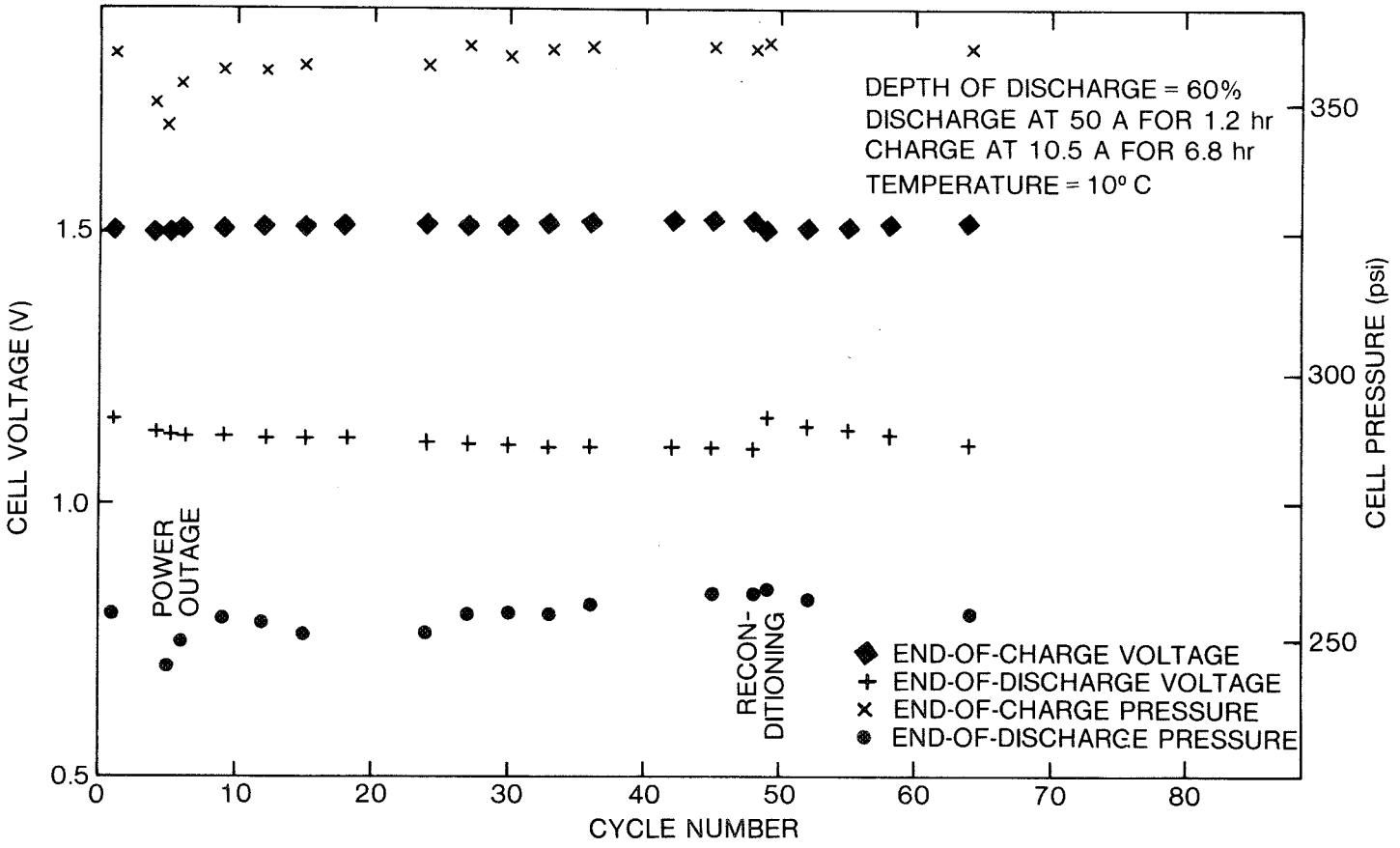

Figure 5. 8-hr Cycle Test Data for Cell 3

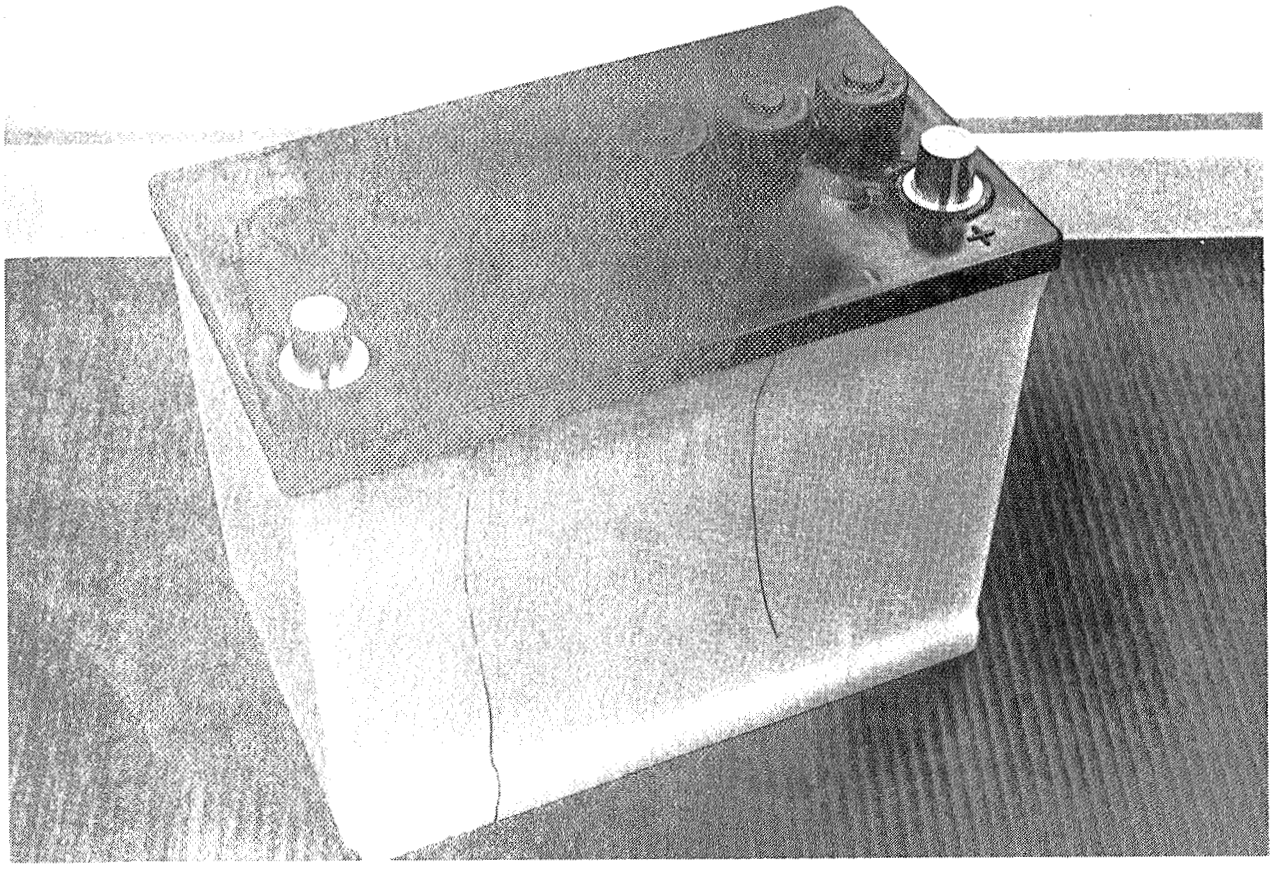

Figure 6. 6-cell, 7.5-V, H_2-Ni0 Battery

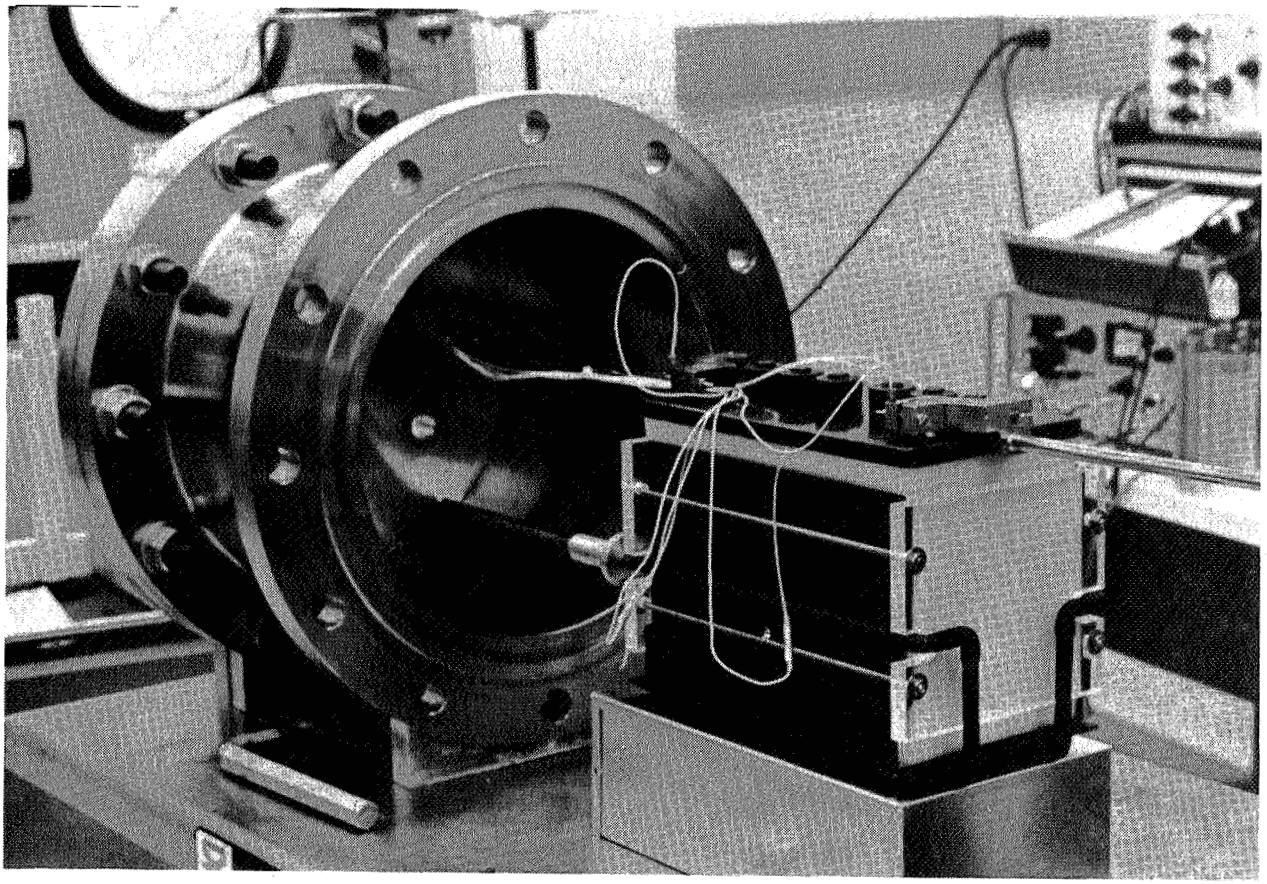

Figure 7. H_2-Ni0 Battery Assembly in Pressure Vessel

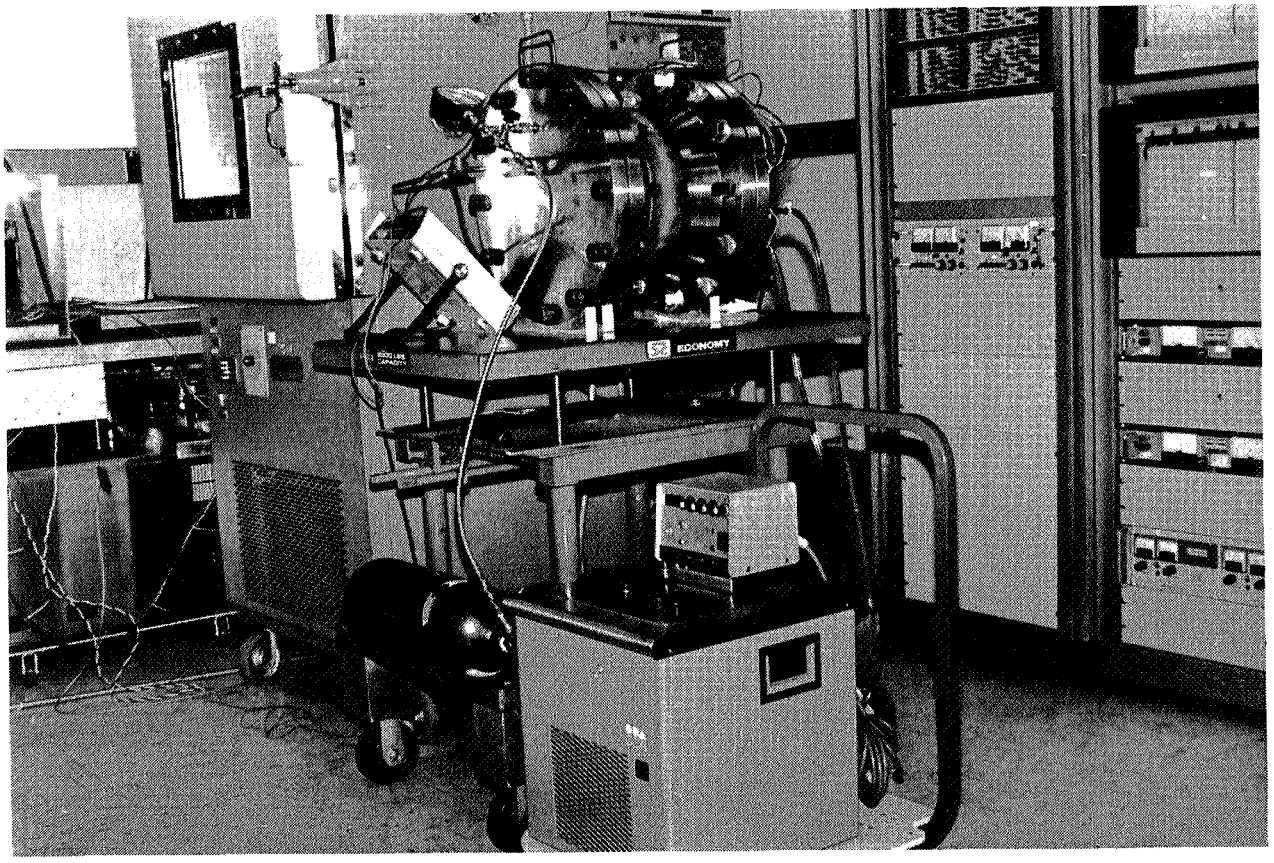

Figure 8. H_2-Ni0 Battery on Test

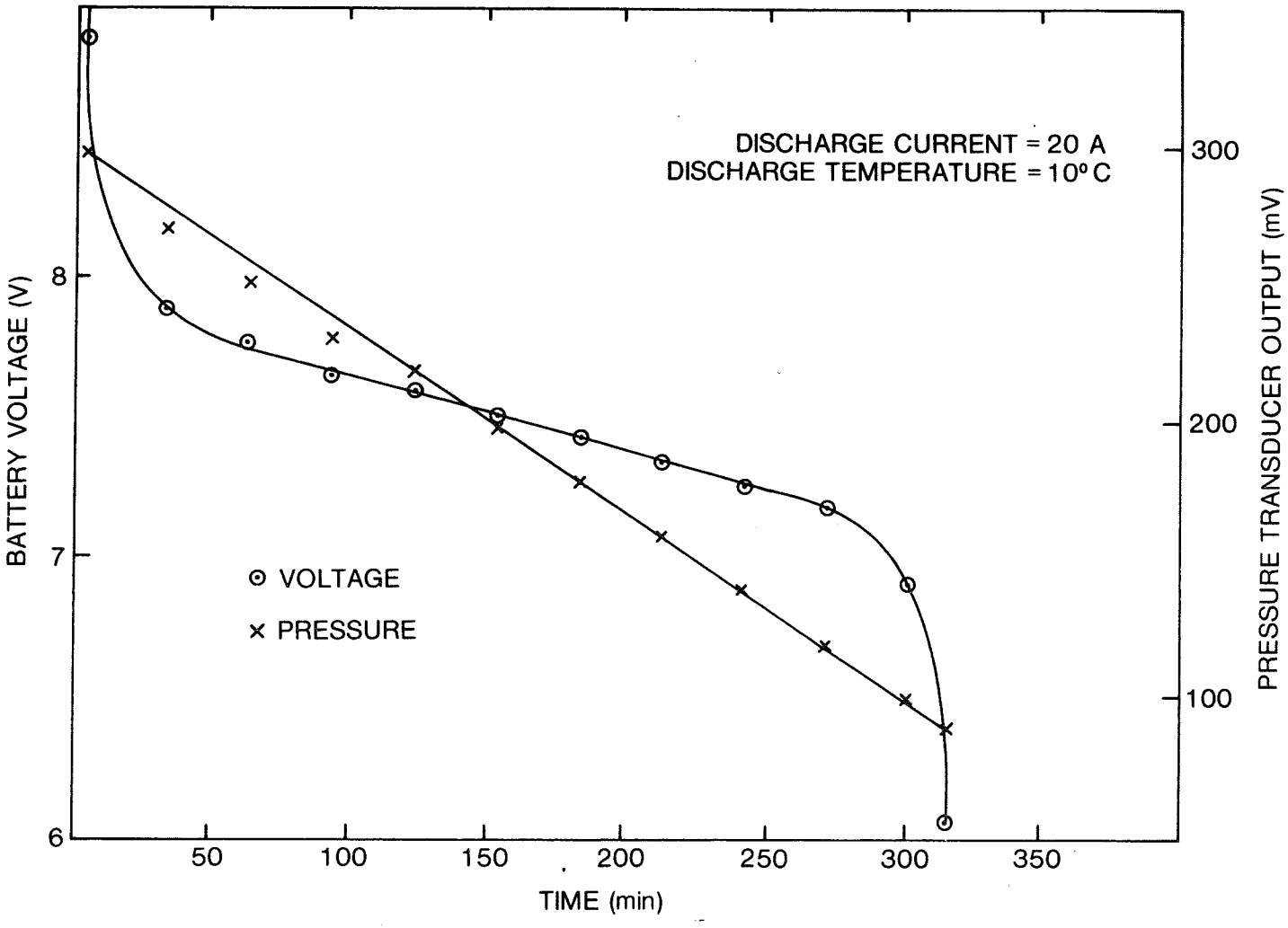

Figure 9. Discharging Profiles for Battery Voltage and Pressure

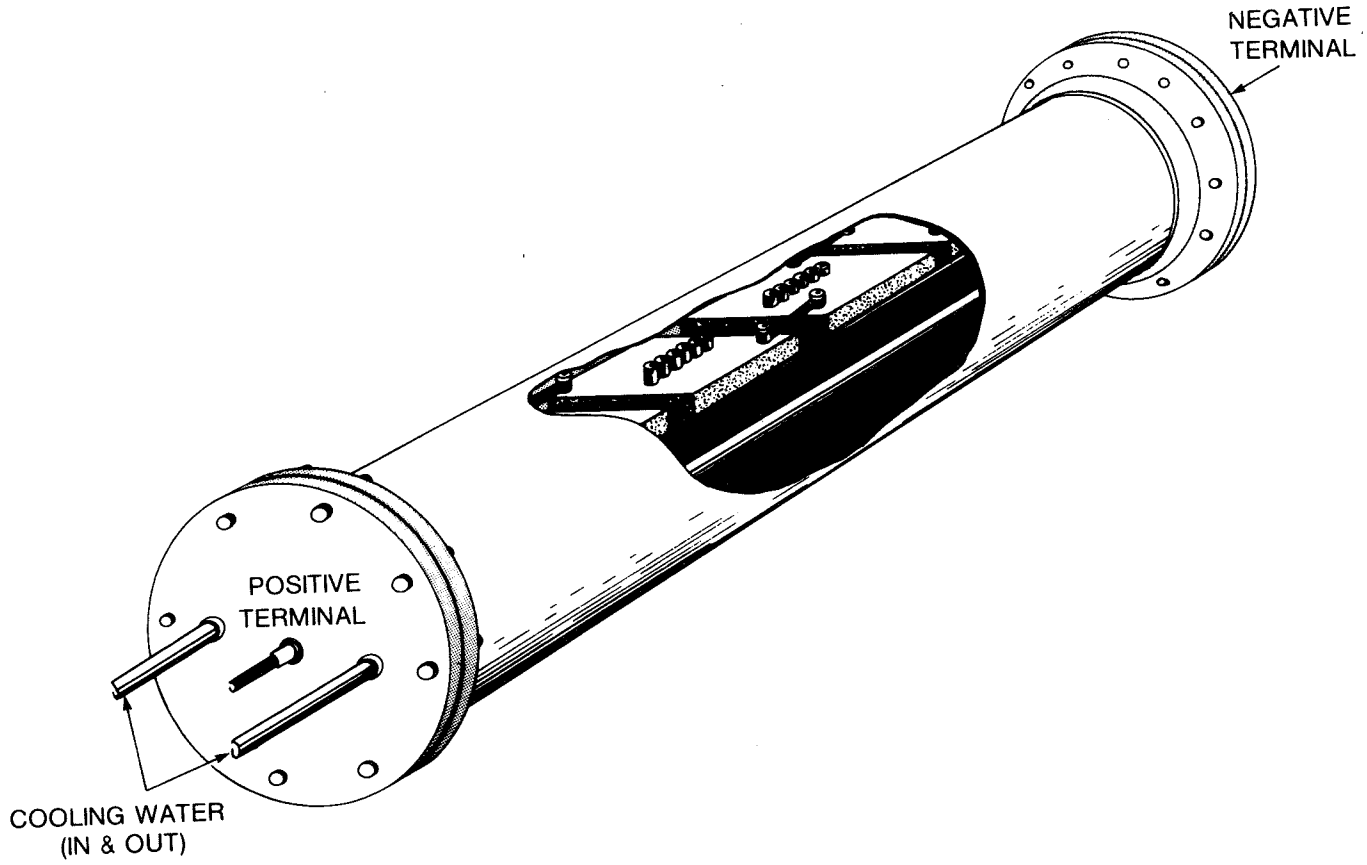

Figure 10. Conceptual Drawing of a 15-kWh H_2-NiO Battery System

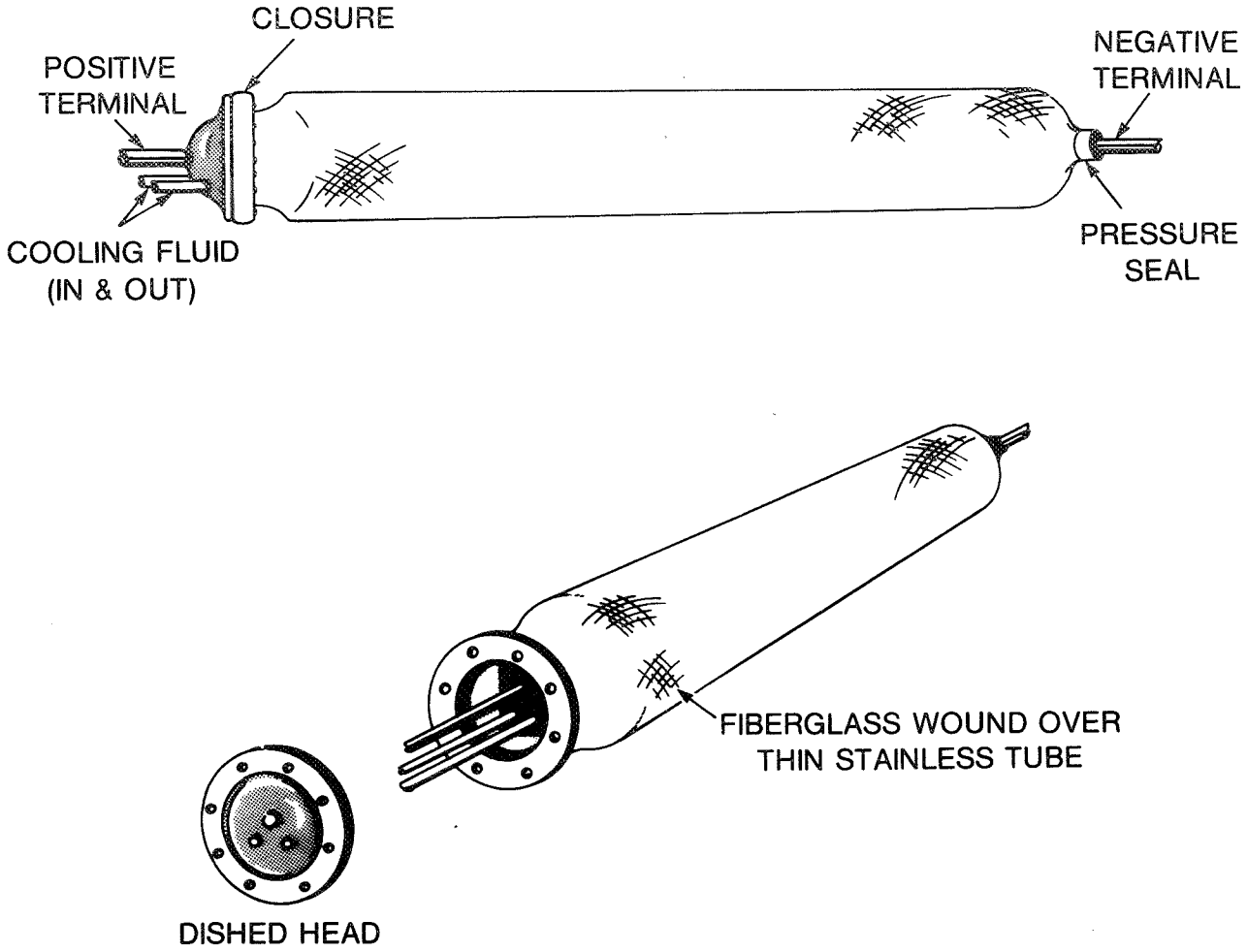

Figure 11. Lightweight Pressure Vessel

SPACE STATION DEVELOPMENT WORK

SOLAR DYNAMIC SYSTEMS

BY

MILES O. DUSTIN

LEWIS RESEARCH CENTER

NOVEMBER 13, 1984

SOLAR DYNAMIC SYSTEMS

WHAT IS IT?

WHY ARE WE INTERESTED?

WHAT ARE THE BENEFITS?

WHAT IS THE SOLAR DYNAMIC DEVELOPMENT PROGRAM?

SYSTEM CONCEPT

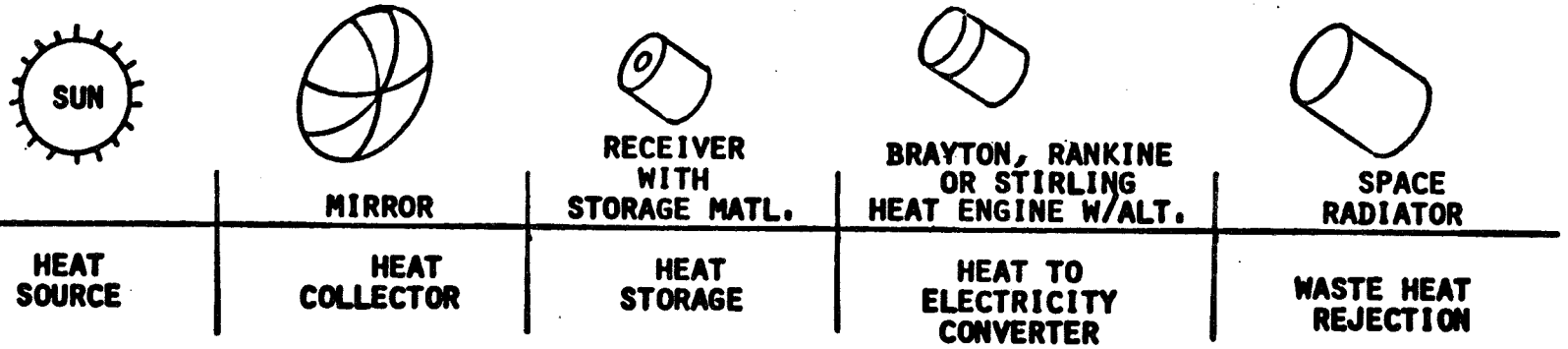

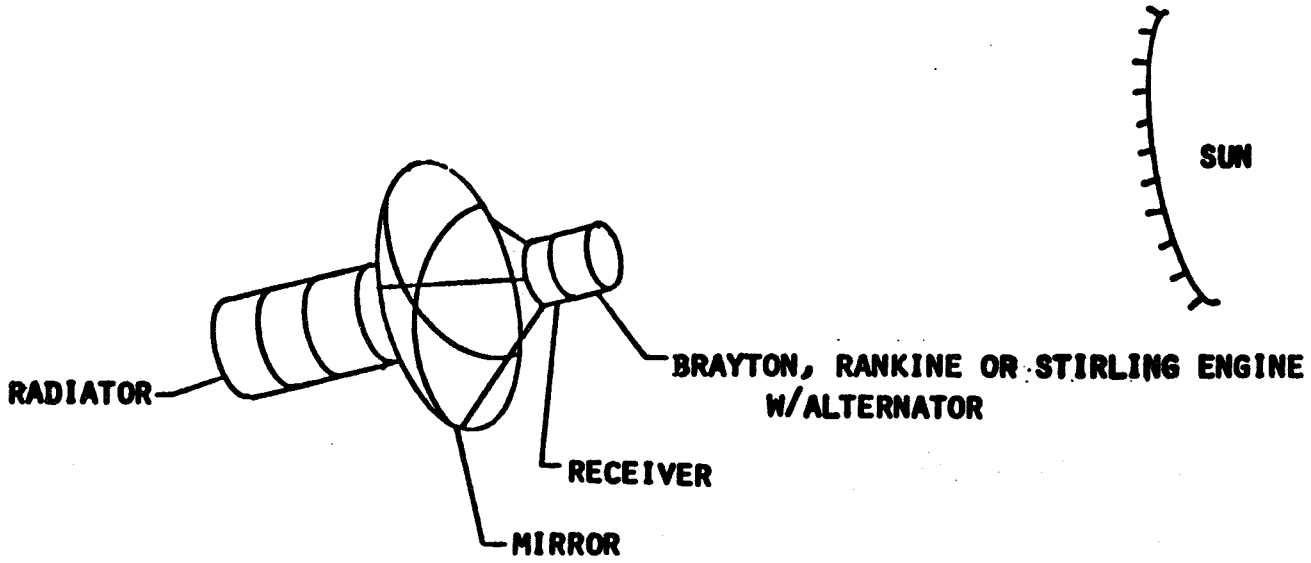

Organic Rankine Cycle

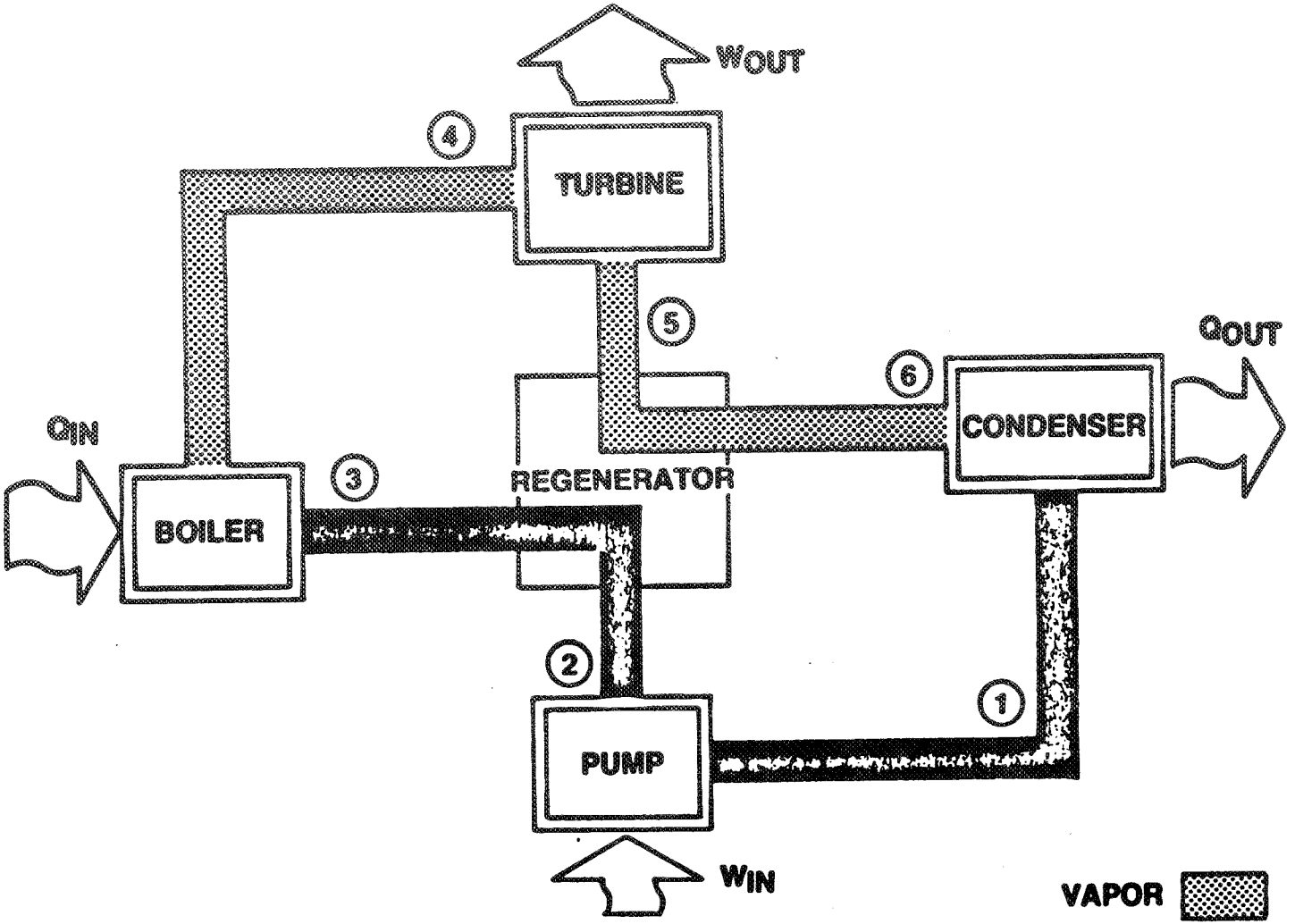

BRAYTON CYCLE SPACE POWER SYSTEM

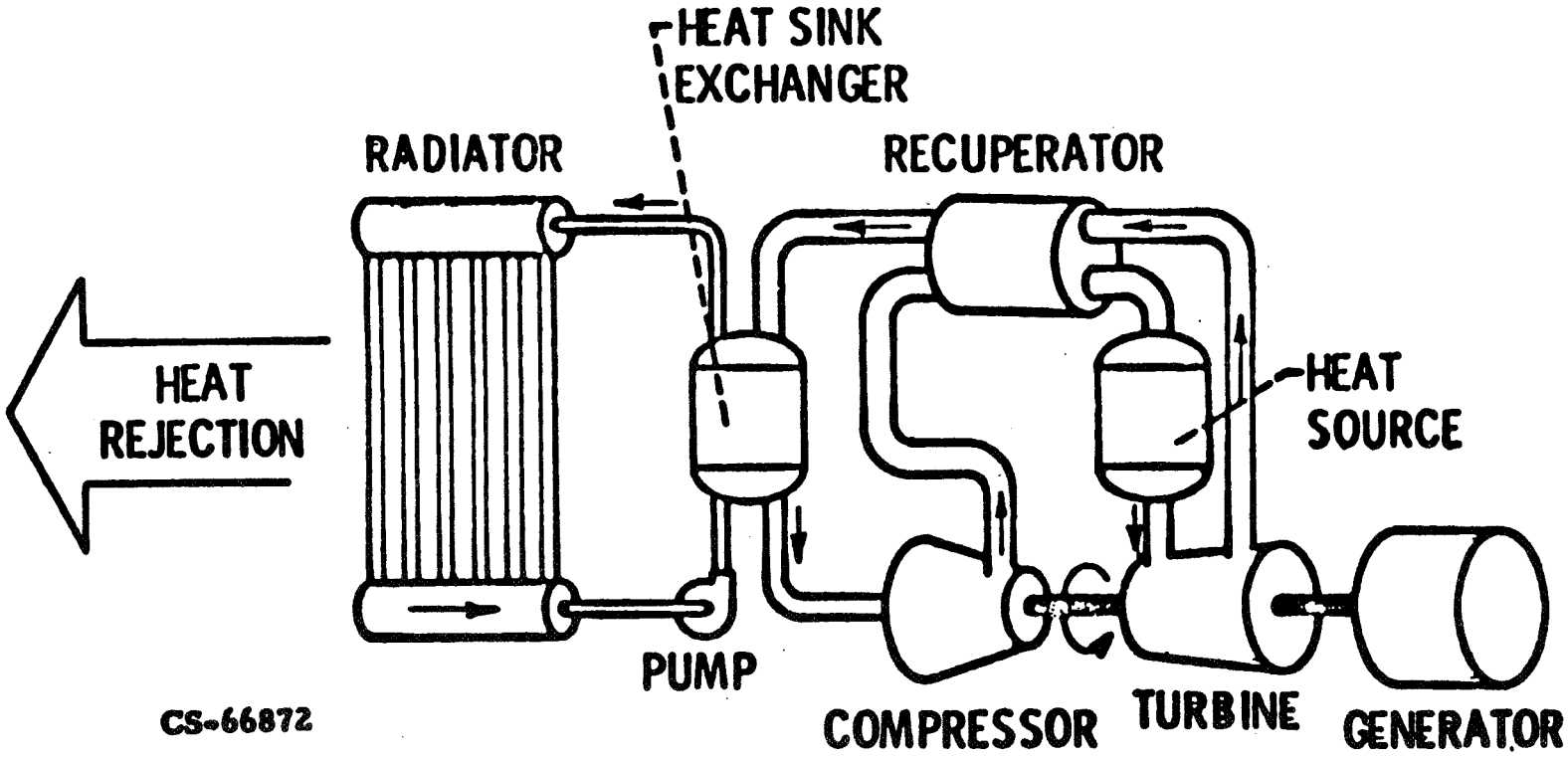

SOLAR DYNAMIC RADIATOR REQUIREMENTS

20 KW_E

	ORGANIC RANKINE		BRAYTON			
TURBINE INLET TEMP	670K	(750F)	730K	(855F)	1080K	(1490F)
CONCENTRATOR DIA. AREA	14.6M		14.8M		12.6M	
	$167M^2$		$170M^2$		$125M^2$	
HEAT REJECTION RATE	105 KW		115 KW		80 KW	
PRIME RADIATOR AREA	$150M^2$		$220M^2$		$60M^2$	
RADIATOR TEMP	355K	(180F)	376K	(220F)	451K	(350F)
	344K	(160F)	296K	(70F)	324K	(120F)

BENEFITS OF SOLAR DYNAMIC SYSTEMS OVER PV SYSTEMS

PRIMARY

SMALLER AREA

- DRAG
- ORBIT ALTITUDE
- VIEW ANGLE
- STABILITY AND CONTROL
- ACCESSIBILITY

SECONDARY

LOWER MASS

LOWER COST

HIGHER RELIABILITY

75 KW SPACE STATION
PHOTOVOLTAIC

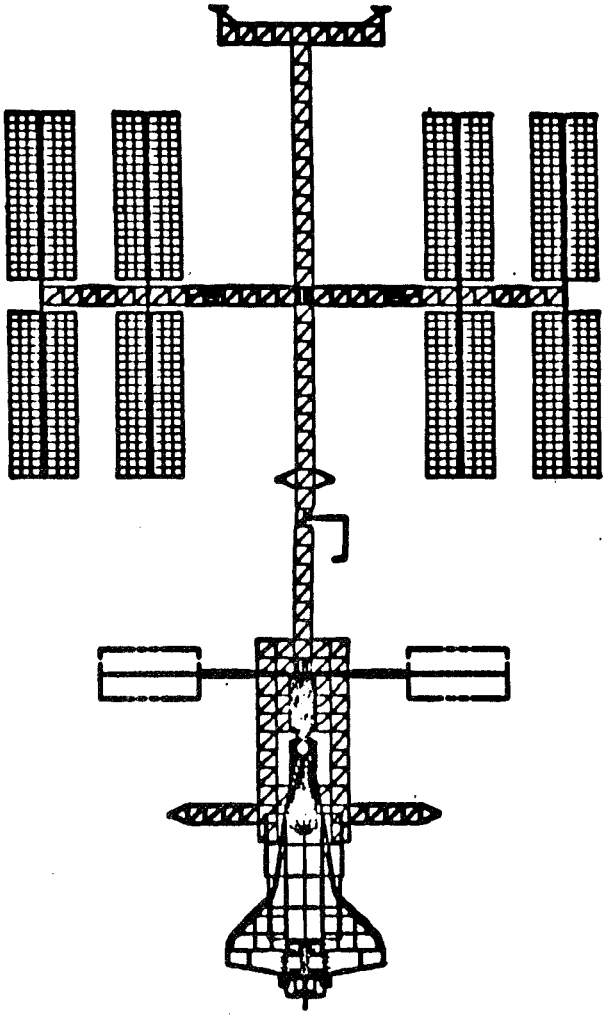

75 KW SPACE STATION

SOLAR DYNAMIC

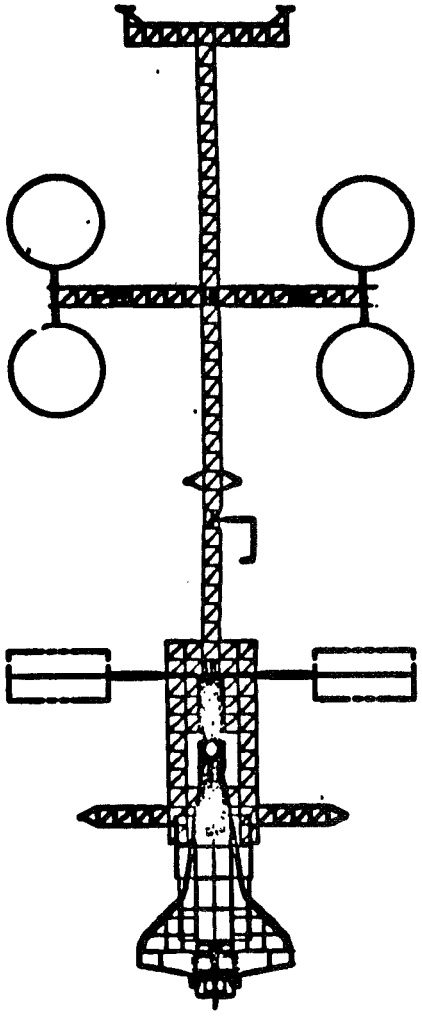

300 KW SPACE STATION
PHOTOVOLTAIC

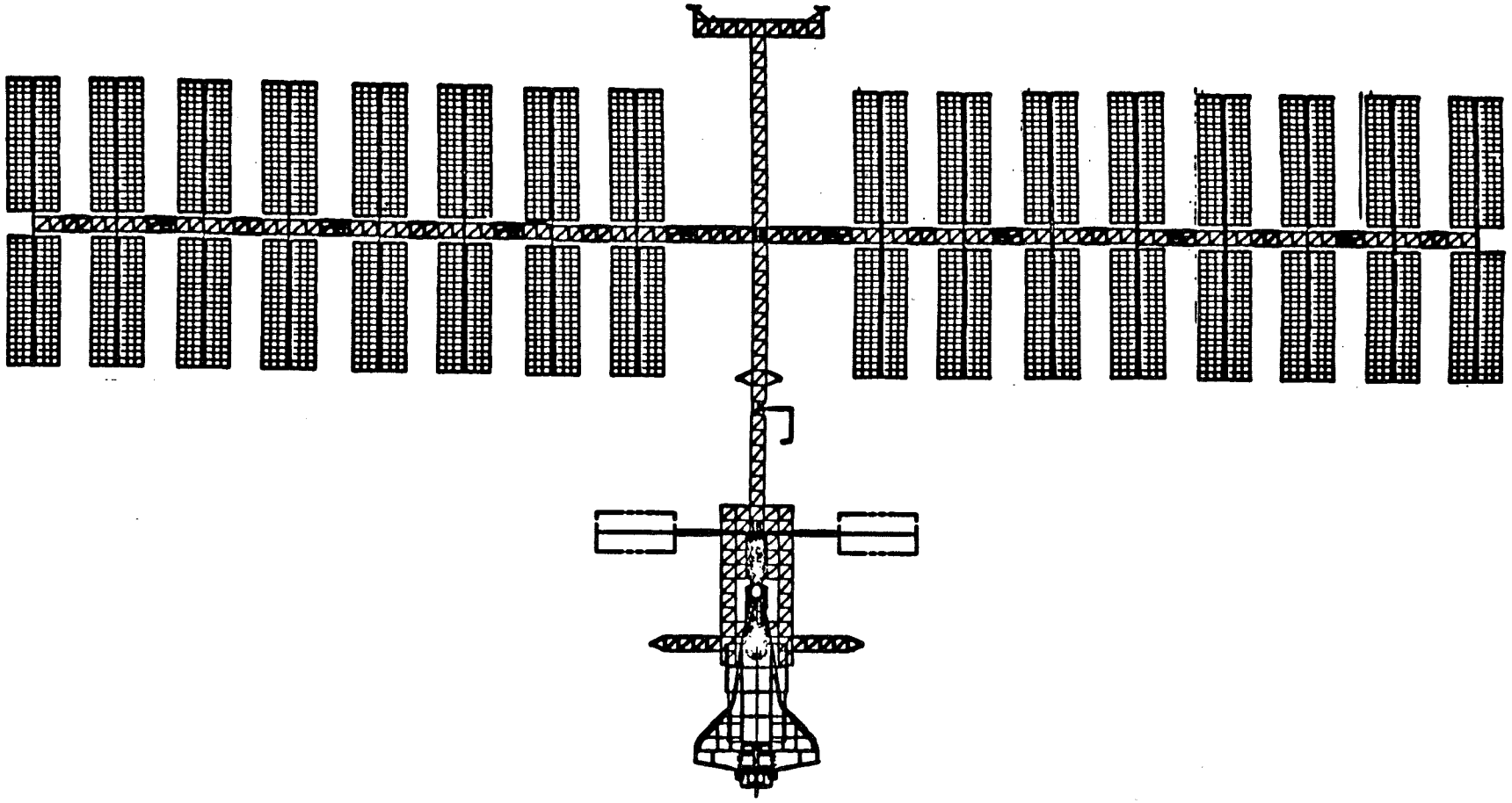

300 KW SPACE STATION
SOLAR DYNAMIC

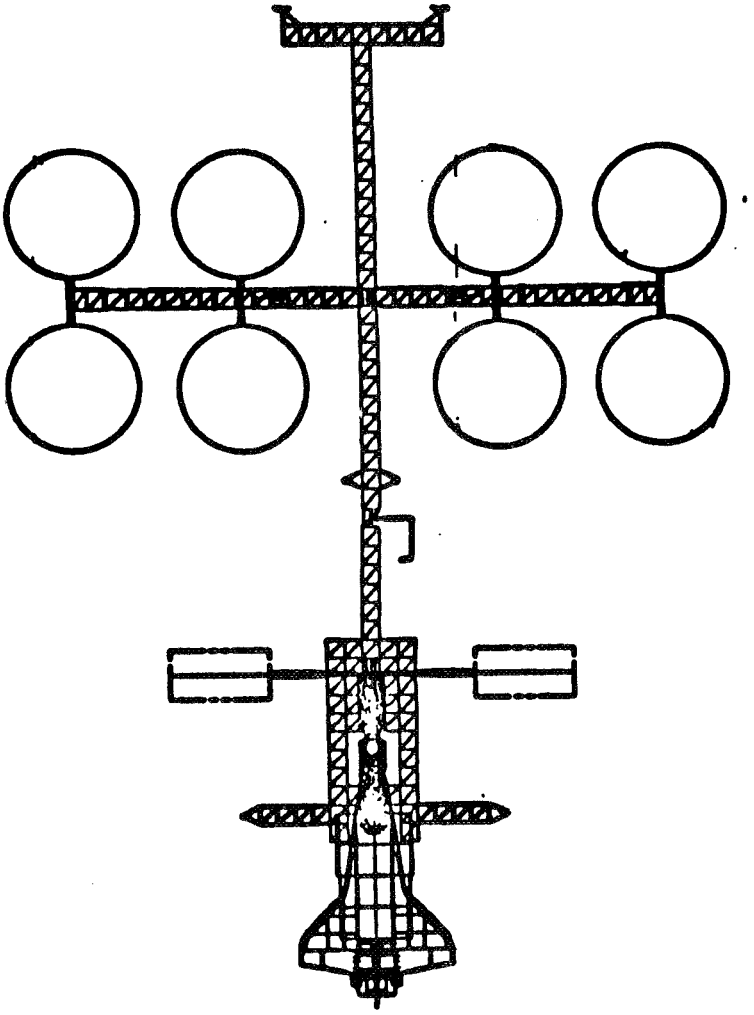

SPECIFIC MASS AND AREA OF SEVERAL SPACE STATION POWER SYSTEMS
Net Power Output = 75 kWe

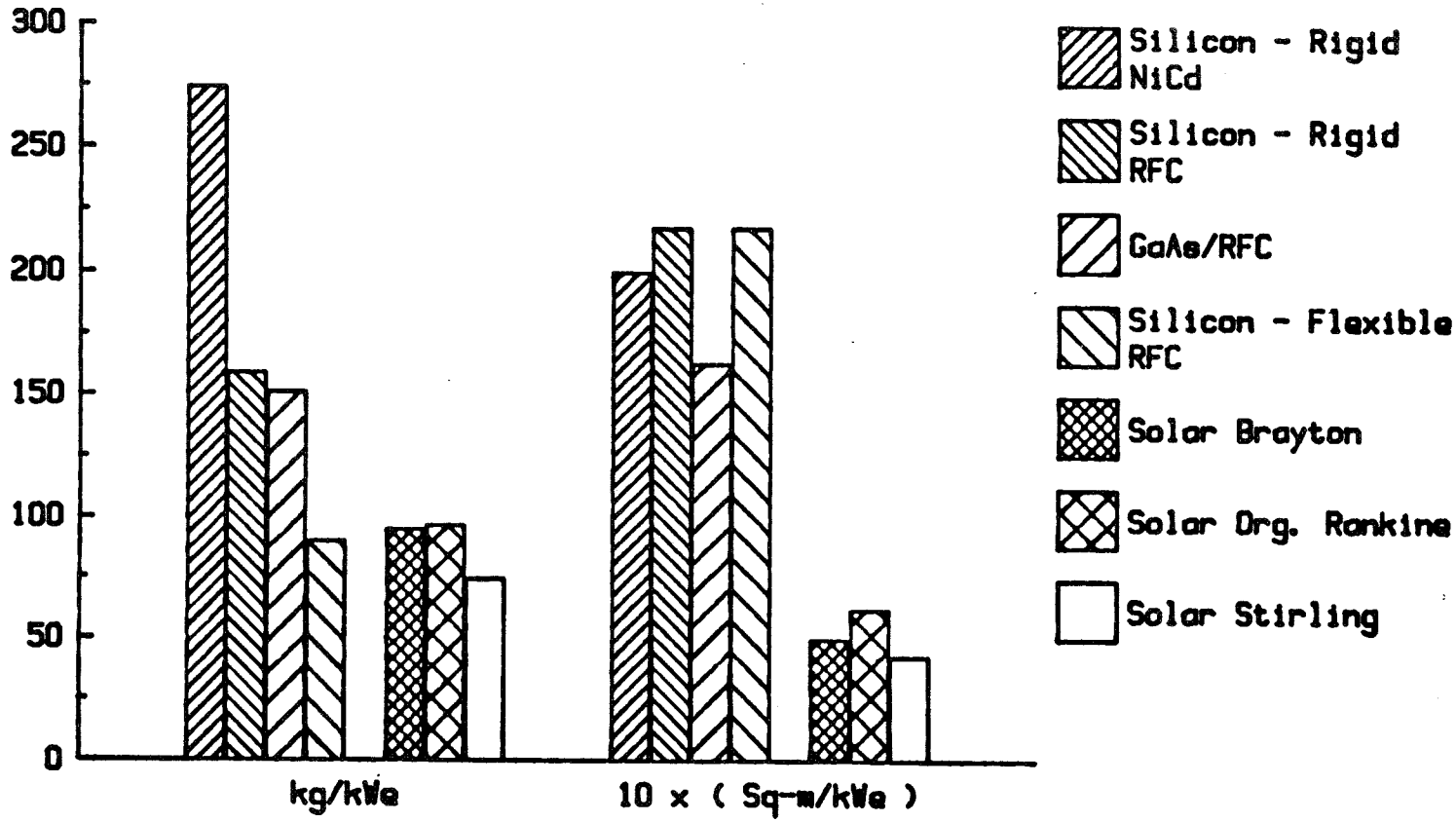

LeRC Space Systems Office

SOLAR DYNAMIC DEVELOPMENT HISTORY

- SEVERAL SPACE CONCEPTS ACTIVELY PURSUED BY NASA AND USAF IN 1960's AND 70's
  - RANKINE
  - BRAYTON — 1 - 15 KW_E LEVELS
  - KINEMATIC STIRLING
- GREATEST EFFORT EXPENDED ON RANKINE AND BRAYTON POWER CONVERSION SUBSYSTEMS
- LESS EFFORT EXPENDED ON CONCENTRATORS AND RECEIVERS
- SYSTEMS DESIGNED FOR EXPENDABLE BOOSTER LAUNCH
- NO SYSTEMS HAVE FLOWN
- DEVELOPMENT DISCONTINUED IN EARLY 70's FOR LACK OF SUITABLE MISSIONS
- DOE DEVELOPING LOW COST CONCEPTS FOR TERRESTRIAL APPLICATIONS SINCE APPROX. 1977

SOLAR DYNAMIC ADVANCED DEVELOPMENT

PURPOSE:

PROVIDE A BASE OF DATA ON THE CRITICAL TECHNOLOGY OF SOLAR DYNAMIC SYSTEMS FOR SPACE STATION

- TO ASSESS VIABILITY OF THE SOLAR DYNAMIC OPTION FOR IOC
- TO PROVIDE BASIS FOR SYSTEM DESIGN

APPROACH:

- o ADDRESS PRIMARY CRITICAL TECHNOLOGY AREAS
  - RECEIVER/STORAGE
  - CONCENTRATOR
  - SOLAR DYNAMIC SYSTEM INTEGRATION WITH SPACE STATION
- o EMPLOY CONSERVATIVE DESIGN APPROACHES
- o FABRICATE AND TEST CRITICAL COMPONENT FUNCTIONS

SOLAR DYNAMIC ADVANCED DEVELOPMENT

CRITICAL CONCENTRATOR TECHNOLOGY

CENTERS: LeRC, JPL

- DEFINE CONCENTRATOR REQUIREMENTS
- DEVELOP SEVERAL DESIGN CONCEPTS FOR 12-18 M. DIAMETER CONCENTRATORS
  - FAB TECHNIQUES
  - ACCURACY
  - DISTORTION
  - SINGLE VS. CASSEGRAINIAN
  - COATINGS
  - POINTING REQUIREMENTS
  - SHUTTLE REQUIREMENTS
  - STOWAGE
  - DEPLOYMENT/ERECTION
- FABRICATE AND TEST ELEMENTS OF SELECTED DESIGNS
- TEST REFLECTIVE SURFACE SAMPLES IN SPACE

SOLAR DYNAMIC ADVANCED DEVELOPMENT

CRITICAL HEAT RECEIVER TECHNOLOGY

CENTER: LeRC

- o DEFINE HEAT RECEIVER REQUIREMENTS
- o DEVELOP SEVERAL DESIGN CONCEPTS FOR RECEIVERS IN THE RANGE OF 75-160 KW_T AND TEMPERATURE NEAR 700K AND PERHAPS TO 1100K)
  - THERMAL STORAGE MATERIAL
  - CONTAINMENT OF STORAGE MATERIAL
  - MOVEMENT OF STORAGE MATERIAL
  - HEAT PIPES
  - TEMPERATURE CONTROL
  - FABRICATION METHODS
  - COATINGS
  - APERTURE MATERIAL
- o FABRICATE AND TEST DESIGNS OF ALTERNATE APPROACHES
- o CAPSULE TESTS OF STORAGE AND CONTAINMENT MATERIALS

SYSTEM LEVEL ELECTROCHEMICAL PRINCIPLES

Lawrence H. Thaller
National Aeronautics and Space Administration
Lewis Research Center
Cleveland, OH 44135

INTRODUCTION

The high power applications that are appearing on the horizon will require a considerable change in the approach taken in spacecraft design. This is particularly true in the area of energy storage. These projected applications are not only seen to require higher voltages and powers but coincidently will require higher heat rejection rates. For many years the function of energy storage was to make up for the dark portion of the orbit when the solar array could not supply the required power. This meant that a few hundred watts were required for periods of time up to 1.2 hours at a voltage level of about 28 volts. In the past few years the power requirements have increased to where several kilowatts are now required during the dark portion. Some of the projected applications will not only require significant increases in the power but the energy storage function may be used to supply peaking power during light as well as dark portions of the orbit. Copper loss considerations will dictate the use of significantly higher operating voltages; possibly in the range of 100 to 200 volts as the output of the energy storage device. As the power requirements are increased, the heat rejection requirement will also increase.

Traditionally, batteries are made up of series connected strings of individual elements called cells. These cells are usually individually monitored and may be individually controlled. Heat may be rejected passively by judicious placement in selected locations within the spacecraft or semiactively by being placed upon a cold plate. The heat rejection requirements limit the peak power outputs of traditional batteries to a greater degree than the actual electrochemistry. The adverse effects on cell life caused by operation at elevated temperatures has the effect of restricting the maximum rates of power output to rather modest levels. Aside from the limitations related to rates of power that can be withdrawn, the energy density of the more traditional batteries based on nickel-cadmium or IPV nickel-hydrogen cells place an upper limit on the size of the energy storage system. This is a consequence of total launch capability of the current or future space transportation system. To meet this challenge presented by high power application, several alternative energy storage concepts are being considered. Figure 1 depicts a generic overall system for such an application. The size of the solar array and the radiator are functions of the operating characteristics of the energy storage and power conditioner characterstics. Since this short paper is to consider the energy storage portion of the overall system, the power management and distribution portion with its own temperature and efficiency characteristics will not be considered.

The size of the solar array (per unit of power out of the storage subsystem) will depend upon the round-trip efficiency of the storage portion of the power system. In like manner the size (weight) of the radiator will be very much a function of the operating temperature of the storage device. The usual figure of merit of a storage device is its energy density (Whr/Kg). Another very important characteristic of a storage device is its power density (W/Kg). These numbers can be misleading when comparing one device against another. The most meaningful number is related to the entire system. It is only as the power system is considered as a whole can different devices and technologies be properly compared. Overall system weights would be favored by a high round trip efficiency device to reduce the solar array areas as well as by a high heat rejection temperature to reduce the weight associated with the radiator.

It is only fair to point out that storage systems based on non-electrochemical devices are currently being considered for these more advanced, higher powered missions. The major problems associated with traditional battery concepts that are based on the connecting together of series strings of individual cells are related to difficulties in maintaining intercell and/or intracell balance of the state of charge of the active materials within the cells. The challenges are being presented by concepts based on flywheels, solar dynamic systems, as well as newer electrochemical concepts. So besides abandoning electrochemical concepts entirely, there are several suggested solutions to this problem that are being investigated. Electronic sensing and control of the grouping of cells is a very attractive approach that has reached a high degree of sophistication. Cell sensing, control and switching; charge protocols; reconditioning techniques; etc. might be viewed as an electrical engineer's approach to the problem. This paper will confine itself to electrochemical concepts and principles, and within that framework, suggest ways of addressing the problem. Electrochemical approaches to this problem have addressed the use of active materials that are more amenable to electrochemical rebalancing techniques (sometimes called reconditioning) as well as the more recent approach of using electrochemistries that lend themselves to the common storage of reactants as fluids. These fluids are common to all the cells of a separate power producing assembly of electrochemical cells. The regenerative fuel cell (RFC, Ref. 1) is an example of this type of storage system which might truly be called an electrochemical system.

BATTERY PACK APPROACHES

Table 1 represents one way of classifying the single cell electrochemistries that have found various degrees of acceptance for aerospace applications. Also noted in this table is a nonexhaustive list of difficulties that have been associated with batteries made from groupings of these cells or simply cells by themselves. Common to all but sodium sulfur batteries is the problem of the gradual dispersion of the intercell and intracell electrochemical capacities of the individual cells caused by a certain degree of randomness associated with the charge and discharge efficiencies among the cells. Sodium

sulfur cells experience their own type of capacity dispersion resulting from the stochastic nature of the individual cell resistance. One of the apparent attractive features of the nickel hydrogen electrochemistry is the ability to safely overdischarge the cells. By comparison, nickel cadmium cells can not tolerate a very high rate of overdischarge (possibly c/20), Ref. 2. Antipolar mass, signal electrodes, reconditioning cycles are all words associated with the art of keeping a multi-cell battery in proper balance and to correct for the cumulative effects of very minor differences among cells within a battery pack. An alternative approach to keeping all of the cells in balance is to use fluids as the reactive materials and have these fluids be common to all the cells of the battery. These devices tend to be somewhat more complicated than traditional battery packs. They will be referred to as electrochemical systems.

ELECTROCHEMICAL SYSTEMS

As a point of clarification, Figure 2 describes very briefly three different classes of batteries. On the top is illustrated the traditional type of battery where a cell string is placed in contact with a cold plate. In the center of that figure is illustrated a fully contained battery where an actively cooled stack of cells is employed. At the lower part of the figure a battery is illustrated where the actively cooled cell stack and the storage portions of the complete system may be treated somewhat independently. The stack of cells, complete with internal cooling passages, can be sized in terms of cell area and number of series connected cells to best meet the load requirements. In like manner, storage tanks for the electrochemical reactants are sized according to the requirements of the particular mission.

The use of active cooling is new to the more traditional battery industry but let the electrochemical aspects of these latter two battery concepts be described in more detail before that aspect is covered. Figure 3 is a simplified schematic of an RFC. It is seen that in reality it consists of a water electrolysis section and a fuel cell section along with the water storage and gas storage portions of the system. In principle, one cell (or stack of cells) could be used for both the charging portion (electrolysis of water) and discharging portion (consumption of hydrogen and oxygen) of the cycle. Then it would more closely resemble the type of cell it is meant to replace; namely, the more traditional type of cell wherein the active materials are contained in a completely sealed container. The containment of the reactive materials is a significant difference between the more traditional electrochemical cell and the RFC. It should be obvious that they both perform the function of a rechargeable electrochemical cell. This difference becomes more evident when one makes the transition between thinking about a single cell and thinking about a multicell battery. With the more usual battery, it is made up of a number of individual units each containing a sealed set of active materials. The fuel cell battery is also made up of a number of individual cells. The reactants however, being fluids, are stored in a common set of tanks; one containing all the hydrogen and the other all the oxygen. Storage of reactants in this manner permits all of the cells to always be at the same state of charge.

Another significant difference exists between RFC and traditional batteries. This is related to the method that groups of cells are assembled together to form the battery. Traditional cells being completely independent entities are wired together electrically, binding post to binding post. Fuel cells and water electrolysis stacks are grouped together in a more or less integral manner with appropriate manifolds for the distribution or collection of the gases and liquids. Since the reactant gases are stored outside of the stack of cells, the cells themselves are rather thin. This facilitates the interleaving of coolant plates in among the electrochemical cells. Usually a dielectric material serves as the heat transfer medium. It is hard to say whether the use of active cooling techniques or the commonality of reactants are the most significant difference between the RFC concept and the traditional battery pack.

Although a hydrogen oxygen RFC was used as an example in describing a large actively cooled bipolar battery, there is ongoing research and development being carried out on other electrochemical systems as well. Hydrogen bromine and hydrogen chlorine are examples of concepts where the storage portion of the system and the power producing portion of the overall system can be independently sized. Bipolar nickel hydrogen battery systems (Ref. 3) represent an example of a fully contained actively cooled electrochemicl system. In this case the hydrogen is common to all the cells whereas the nickel oxide cathode material is unique to each individual cell. The special attributes of these actively cooled bipolar batteries can be summarized as follows: 1) In the case of the fully decoupled power section and storage section (H_2-O_2, H_2-Br_2, H_2-Cl_2) cell to cell capacity dispersion can be eliminated, 2) active cooling permits scaling up or down in cell size without undesirable consequences upon the thermal characteristics of the basic electrochemical cell, 3) active cooling permits a very wide range of peak and base power output, 4) the cell-to-cell stochastic characteristics that result in capacity dispersion and performance decay can be designed for as part of the battery design process. It is probably this last point that may be the one that is most difficult to understand, comprehend, and internalize, yet at the same time, it may well be the most significant.

Capacity dispersion usually stems from competing electrochemical reactions that take place on recharge. The nickel electrode, for example, evolves oxygen during recharge at a rate that depends on the type of additive in the nickel electrode, the state of charge, the temperature, the current density and possibly other factors. During any one recharge, the oxygen evolved will most likely be a random variable that causes the individual cell capacities to diverge. This divergence can be corrected for by using a reconditioning cycle in the case of traditional IPV nickel hydrogen cells or nickel cadmium cells. In the case of the electrolysis of alkaline (KOH) or hydrobromic acid (HBr) solutions, the contribution from spurious side reactions is all but nonexistent. In the case of large bipolar nickel hydrogen devices techniques as described in reference 4 address that system. In brief, cell designs are described that render the battery less susceptable to minor cell to cell

variations. The design of the cell and battery components in regard to pore size, pore size distribution, chemical compatability, compression strength, etc. is very important to minimize the performance decay phenomenon that take place during operation. By more fully understanding these processes, certain design modifications can be made.

SUMMARY

In summary, it can be stated that the traditional electrochemical storage concepts are difficult to translate into high power, high voltage multikilowatt storage systems. The increased use of electronics, as well as the use of electrochemical couples that minimize the difficulties associated with the corrective measures to reduce the cell to cell capacity dispersion, have already been adopted by battery technologists. However, these concepts can become quite complicated and heavy. Actively cooled bipolar concepts are described which represent some attractive alternative system concepts. In general, they are projected to have higher energy densities lower volumes than current concepts. Furthermore, they should be easier to scale from one capacity to another and most definitely will have a closer cell-to-cell capacity balance. These newer storage system concepts will be easier to manage since they are designed from the start to be a fully integrated battery. Grouped together, these ideas are simply referred to as system level electrochemistry. The hydrogen-oxygen RFC is probably the best example of the integrated use of these principles. These principles in part should be recognized to be to a certain degree ex post factor from the perspective of people familiar with fuel cell technology while at the same time they may appear to be somewhat avant-garde from the point of view of one steeped in the details of single cell electrochemical technology.

REFERENCES

1. Hoberecht, M. A., Miller, T. B., Reiker, L. L., Sanabria, O. D.: Design Considerations for a 10-kW Integrated Hydrogen-Oxygen Regenerative Fuel Cell System. Proceedings of the 19th IECEC, Vol. 1, Aug. 1984, pp 240-246.

2. Ritterman, P. F.: Hydrogen Recombination in Sealed Nickel-Cadmium Aerospace Cells. Proceedings of the 14th IECEC, Vol. 2, Aug. 1979, pp 1288-1291.

3. Cataldo, R. L.: Design of a 1-kWH Bipolar Nickel Hudrogen Battery. Proceedings of the 19th IECEC, Vol. 1, Aug. 1984, pp. 264-269.

4. Thaller, L. H.: Design Principles for Nickel Hydrogen Cells and Batteries. Proceedings of the 1984 NASA/GSFC Battery Workshop.

5. Abbey, K. M. and Thaller, L. H.: Pore Size Engineering Applied to Starved Electrochemical Cells and Batteries. Proceedings of the 17th IECEC, Vol. 2, Aug. 1982, pp 757-764.

Table 1

DIFFICULTIES WITH SPECIFIC ELECTROCHEMISTRIES AS THEY RELATE TO MULTICELL BATTERY PACKS

	NICKEL HYDROGEN	NICKEL CADMIUM	SILVER HYDROGEN	SILVER CADMIUM	SILVER ZINC	SODIUM SULFUR (350° C)	LITHIUM IRON SULFIDE (450° C)
CELL TO CELL CAPACITY DISPERSION	X	X	X	X	X		X
POOR OVERDISCHARGE CHARACTERISTICS		X		X	X	X	X
POOR OVERCHARGE CHARACTERISTICS					X	X	X
INDIVIDUAL CELL CONTROL REQUIRED					X		X
CADMIUM MIGRATION		X		X			
SILVER SOLUBILITY			X	X	X		
SHAPE CHANGE					X		
RANDOM SOFT SHORTS						X	X

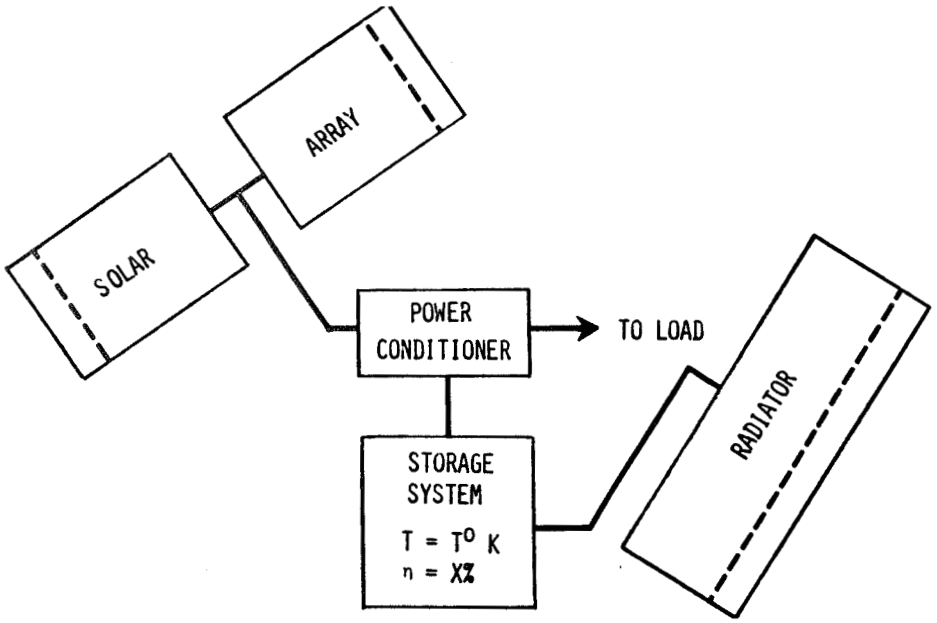

Figure 1. Components of a Large Space Power System

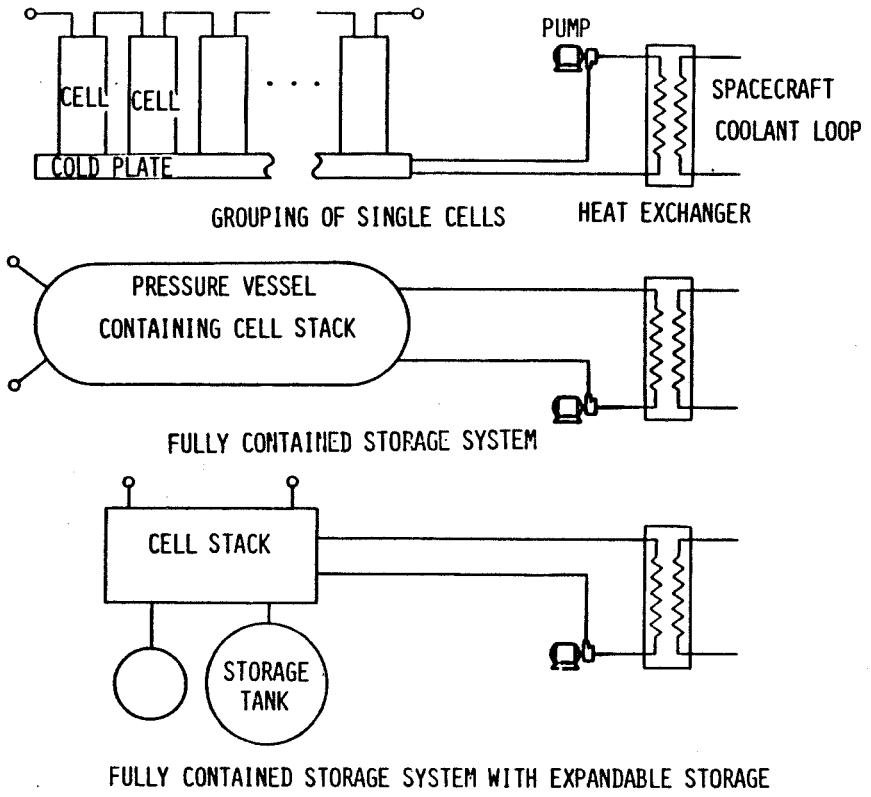

Figure 2. Three Different Classes of Electrochemical Storage Systems

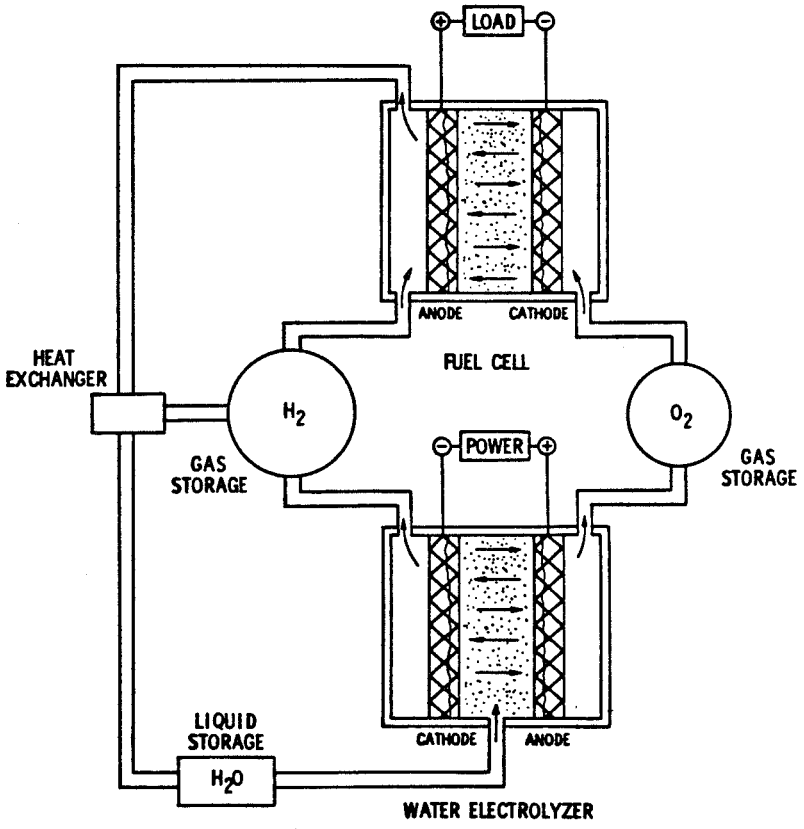

Figure 3. Schematic Diagram of a Hydrogen Oxygen Regenerative Fuel Cell

SESSION II

LITHIUM CELL TECHNOLOGY AND SAFETY

Chairman: G. Halpert
Jet Propulsion Laboratory

ADVANCES IN RECHARGEABLE LITHIUM MOLYBDENUM DISULFIDE BATTERIES

K. Brandt and J.A.R. Stiles
Moli Energy Limited
3958 Myrtle Street
Burnaby, B.C.
Canada V5C 4G2

INTRODUCTION

Considerable effort has been focused in recent years on the development of rechargeable ambient temperature lithium batteries. This effort has been spurred by the expectation that such batteries would have many of the desirable characteristics associated with non-rechargeable lithium batteries. These characteristics include high gravimetric energy density (energy per unit weight) volumetric energy density (energy per unit volume) and long charge retention times (10 years or more).

The major obstacle to overcome in the development of secondary lithium batteries has been the development of a reversible anode. A secondary obstacle has been the development of a low cost, high discharge rate cathode. Significant progress has been made in overcoming these obstacles with the development by Moli Energy Limited of the lithium molybdenum disulfide system.

The energy density of the lithium molybdenum disulfide system as manifest in practical cells is substantially higher than that of other rechargeable systems. In the first state of development the volumetric energy density of the lithium molybdenum disulfide system is approximately 50% higher than that of state-of-the-art Nicad and proportionately higher than that of sealed Pb-acid. With recent advances of the system, the energy density can be improved to the point where the volumetric energy density advantage over Nicad is greater than 100%. The charge retention capability of the system has also proven to be excellent, with a charge retention time in excess of 8 years.

The characteristics of the lithium molybdenum disulfide system are ideally matched to the power requirements of devices where light weight and low volume are of concern, particularly where they are subject to intermittent use with long interspersed standby periods when the device is not connected to a primary power source.

In this paper are presented some of the advances in the performance characteristics of 'C' size cells that have been made during the past year with a new electrolyte formulation. The characteristics of 'C' cells with the previous electrolyte formulation have been published elsewhere [1] and can be summarized as follows:

HIGH ENERGY DENSITY

The energy density of a 'C' size cell is in the range of 60 to 65 watt hours per kilogram at a discharge rate of 800 milliamperes. At rates of less than 100 milliamperes, the energy density is increased to about 70 watt hours per kilogram.

HIGH RATE CAPABILITY

Sustained drain rates of 5 amperes at a cell voltage between 2.3 volts and 1.3 volts can be obtained at 21° C.

INHERENT SAFETY BELOW 110° C

Electrical, mechanical and thermal abuse tests have shown the 'C' size cell to be resistant to venting or rupture for cell temperatures below 110° C. These tests are described in a separate article [2].

WIDE AMBIENT TEMPERATURE OPERATING RANGE

Sustained drain rates of at least 1 ampere, with a cell voltage above 1.3 volts, can be maintained at temperatures from -12° C to 70° C.

CHARGE RETENTION CAPABILITY

The 'C' size cells have a charge retention time in excess of 8 years.

STATE OF CHARGE INDICATOR

The open circuit voltage of a cell decreases approximately linearly with increasing depth of discharge. This provides a simple and reliable state-of-charge indication.

HIGH ELECTRICAL EFFICIENCY

The overall round trip energy efficiency for a 'C' size cell at a discharge rate of 800 milliamperes and a charge rate of 250 milliamperes is in excess of 90%.

LEAKPROOF CONSTRUCTION

The 'C' size cells are hermetically sealed and no leakage or gassing should occur during either storage or normal usage. The cell contents are unpressurized.

CELL CHEMISTRY AND DESIGN

The lithium molybdenum disulfide system utilizes a lithium metal anode and a molybdenum disulfide cathode. The molybdenum disulfide, obtained

as a naturally occurring mineral is processed so as to alter its crystal structure to allow reversible intercalation, or dissolution of lithium within the crystal lattice. The discharge reaction for the system is thus represented as follows:

$$x \cdot Li + MoS_2 \longrightarrow Li_xMoS_2$$

The ratio of lithium in the cathode material, denoted by x, can vary from about 0.2 to about 1.0.

Proprietary concepts have been developed at Moli Energy Limited which allow the recharge reaction

$$Li_xMoS_2 \longrightarrow x \cdot Li + MoS_2$$

to proceed whereby the lithium dissolved in the cathode material is extracted and lithium is plated, in a smooth fashion, back on to the lithium metal anode. The advanced cell chemistry utilizes a new electrolyte formulation which improves lithium plating and the kinetics of discharge and charge reaction over cells with the previous electrolyte formulation.

The 'C' size lithium molybdenum disulfide cell is constructed in a spirally wound format. The cathode is electrically connected to a central mandrel which in turn is attached to the centre terminal of the cell. The electrodes are separated by a microporous polymeric separator. The total geometrical surface area of each electrode is about 750 square centimeters.

The cell is hermetically sealed utilizing welded construction and a glass-to-metal seal. Two safety vents are incorporated into the cell to allow for the controlled release of excessive pressure should the cell be subject to extreme abusive conditions. The vents are coined at both ends of the cell case.

DYNAMIC PERFORMANCE OF 'C' CELLS

A number of standard tests have been devised to evaluate the performance of the 'C' size and other molybdenum disulfide cells. These include a charge and discharge profile test, standard cycling tests and discharge rate capability tests. Test results of advanced 'C' cells are given in this paper.

A typical charge/discharge voltage profile is shown in Figure 1. In this case the 'C' cell was discharged at 840 milliamperes to a voltage cutoff of 1.3 volts and charged immediately following the discharge at 280 milliamperes to a voltage cutoff of 2.4 volts. This charge/discharge sequence defines one standard cycle. The profile

given is for the tenth such cell cycle. Under these conditions the voltage profile is independent of the two electrolyte formulations used. The round trip energy efficiency as calculated from the results shown in Figure 1 is about 92%.

A standard cycling test is defined by a sequence of standard cycles which are performed without time lag. This test is continued until the cell capacity falls to a preselected capacity value.

Generally the delivered capacity falls gradually with increasing number of cycles: there is no precipitous loss in capacity which defines end of life. The failure mode of the cells is a gradual increase in cell impedance with an increasing number of cycles. The capacity of a typical 'C' cell as a function of cycle number under the standard test conditions is shown in Figure 2. The cycle life of cells with advanced electrolyte formulation is twice or more that of cells with the previous electrolyte formulation.

Figure 3 shows the capacity of 'C' cells as a function of cycle number for two different depths of discharge. The depth of discharge is reduced by narrowing the voltage range on cycling. Data presented here are of cycling tests which are still in progress.

The standard discharge rate capability test is conducted as follows. A cell is charged at 280 milliamperes until the cell voltage reaches 2.4 volts. The cell is then discharged at the highest discharge rate at which the delivered capacity of the cell is to be measured. The discharge is terminated when the cell voltage on discharge falls to 1.3 volts. The cell is then rested on open circuit for a time equal to that of the just completed discharge. The cell is then further discharged at a discharge rate, equal to one half of the rate on the previous discharge again until the cell voltage falls to 1.3 volts. The delivered cell capacity at this lower rate is then taken to be the sum of the discharge capacities for the two discharges. The cell is then rested again for a period of time equal to the total elapsed time from the beginning of the first discharge, and the cell is discharged at one quarter of the initial discharge rate. The delivered cell capacity at this rate is then taken to be the sum of the capacities of the cells for all discharges undertaken since the cell was charged. The process is repeated until the discharge rate has been reduced successively by one half until the realized capacity at the lowest rate desired has been measured. This procedure has been found to give equivalent results to those obtained when the cell is fully charged before each discharge at the desired rates or to those obtained when matched fully charged cells are discharged at different rates. The deliverable 'C' cell capacity as a function of drain rate for environmental temperatures of 22°C, -20°C, and -30°C is shown in Figure 4. The cell is capable for sustained discharge currents in excess of 5

amperes at room temperature, in excess of 1 ampere at -20°C, and .5 amperes at -30°C, respectively. This represents a substantial increase in low temperature rate capability over cells using the previous electrolyte formulation.

The advanced electrolyte formulation enables a larger capacity to be realized from the 'C' cells because the cells can be charged to a higher voltage, and discharged to a lower voltage than can cells with the previous electrolyte. This is possible because of the improved kinetic stability of the electrolyte. During discharge, the open circuit voltage varies between 2.5 volts for a fully charged cell and 1.1 volts for a fully discharged cell. The 'C' cell will deliver 3 ampere hours on its initial cycle when cycled in this way, and will deliver in excess of 2 ampere hours even after 150 deep cycles. A modified cycle life test similar to the standard cycle life test was performed on these cells, but where the voltage for termination of charging is 2.6 volts rather than 2.4 volts as it is for the standard test, and the voltage for termination of discharge is 1.1 volts rather than 1.3 volts as it is for the standard tests. The charge and discharge currents used were identical to those used in the standard test. The realized capacity of a cell as a function of cycle number for the modified test is shown in Figure 6. The energy density of the 'C' cell with improved electrolyte using the extended voltage range is about 90 watt hours per kilogram.

The effect of environmental temperature on discharge voltage profiles for cells cycled over the extended voltage range is shown in Figure 7. At a temperature of -10°C, a capacity in excess of 2 ampere hours can be achieved when the cell voltage is allowed to drop to .9 volts.

The effect of various discharge currents on the cell voltage profile is shown in Figure 8. Discharge currents of 10 amperes can be sustained for more than 9 minutes corresponding to a cell capacity of 1.6 ampere hours before the cell voltage drops to .9 volts. This increased rate capability is due to the charge in electrolyte which has caused the a.c. impedance of the cell measured at a frequency of 1 Hertz to drop from a value of 80 milliohms to about 60 milliohms.

OTHER PERFORMANCE ATTRIBUTES

The lithium molybdenum disulfide cells with the improved electrolyte formulation have proven to be very stable on open circuit stand. Although direct measurements of charge retention times have not yet been completed, microcalorimetric techniques have been used to compare charge loss rates of cells with the advanced electrolyte formulation with cells of the previous chemistry. The charge loss rate is projected to be less than 8% per year.

Electrical, mechanical, and thermal abuse tests, are being performed to establish the range of safe operation for cells with the advanced electrolyte formulation and the improved vent system. Experiments conducted so far show improved safety characteristics.

CONCLUSION

The lithium molybdenum disulfide system as demonstrated in a 'C' size cell, offers attractive performance characteristics for applications where light weight and low volume are important. A gravimetric energy density of 90 watt hours per kilogram can be achieved in a 'C' size cell package. The combination of excellent charge retention capabilities, high energy density and a state-of-charge indicator in a rechargeable cell provides an ideal power package for a wide range of devices. The system overcomes the 'memory' effect in Nicads where the full capacity of the battery cannot be utilized unless the full capacity of the battery was utilized on previous cycles. The development of cells with an advanced electrolyte formulation has led to an improved rate capability especially at low temperatures and to a significantly improved cycle life.

REFERENCES

1) J.A.R. Stiles, Lithium - Molybdenum Sulfide Secondary Cells, Progress in Batteries and Solar Cells, Volume 5, 1984, page 52.

2) K. Brandt, D. Fouchard, J.A.R. Stiles, Safety Aspects of a Rechargeable Lithium C Cell, Proc. 31st Power Sources Symposium, May 1984, Cherry Hill, N.J. (in press)

FIGURE CAPTIONS

Figure 1 - Charge/discharge profile for a 'C' cell cycled in the standard voltage range. Charge current 280 mA, discharge current 840 mA. Cell at cycle number 10.

Figure 2 - Capacity vs. cycle number for a 'C' cell cycled in the standard voltage range. Charge current 280 mA, discharge current 840 mA.

Figure 3 - Capacity vs. cycle number for 'C' cells cycled to different depths of discharge.
1: Cell cycled between 2.2V and 1.6V
2: Cell cycled between 2.2V and 1.8V

Figure 4 - Capacity vs. discharge current for three different temperatures. 'C' cell at cycle number 10.

Figure 5 - Charge/discharge profile for a 'C' cell cycled over the extended voltage range. Charge current 280 mA, discharge current 840 mA. Cell at cycle number 1.

Figure 6 - Capacity vs. cycle number for a 'C' cell cycled in the extended voltage range. Charge current 280 mA, discharge current 840 mA.

Figure 7 - Discharge profiles for 'C' cells at three different temperatures at a current of 840 mA. Charged at 280 mA to 2.6 V. Cell at cycle number 1.

Figure 8 - Discharge profiles for 'C' cells for various discharge currents. Charged at 280 mA to 2.6 V. Cell at cycle number 1.

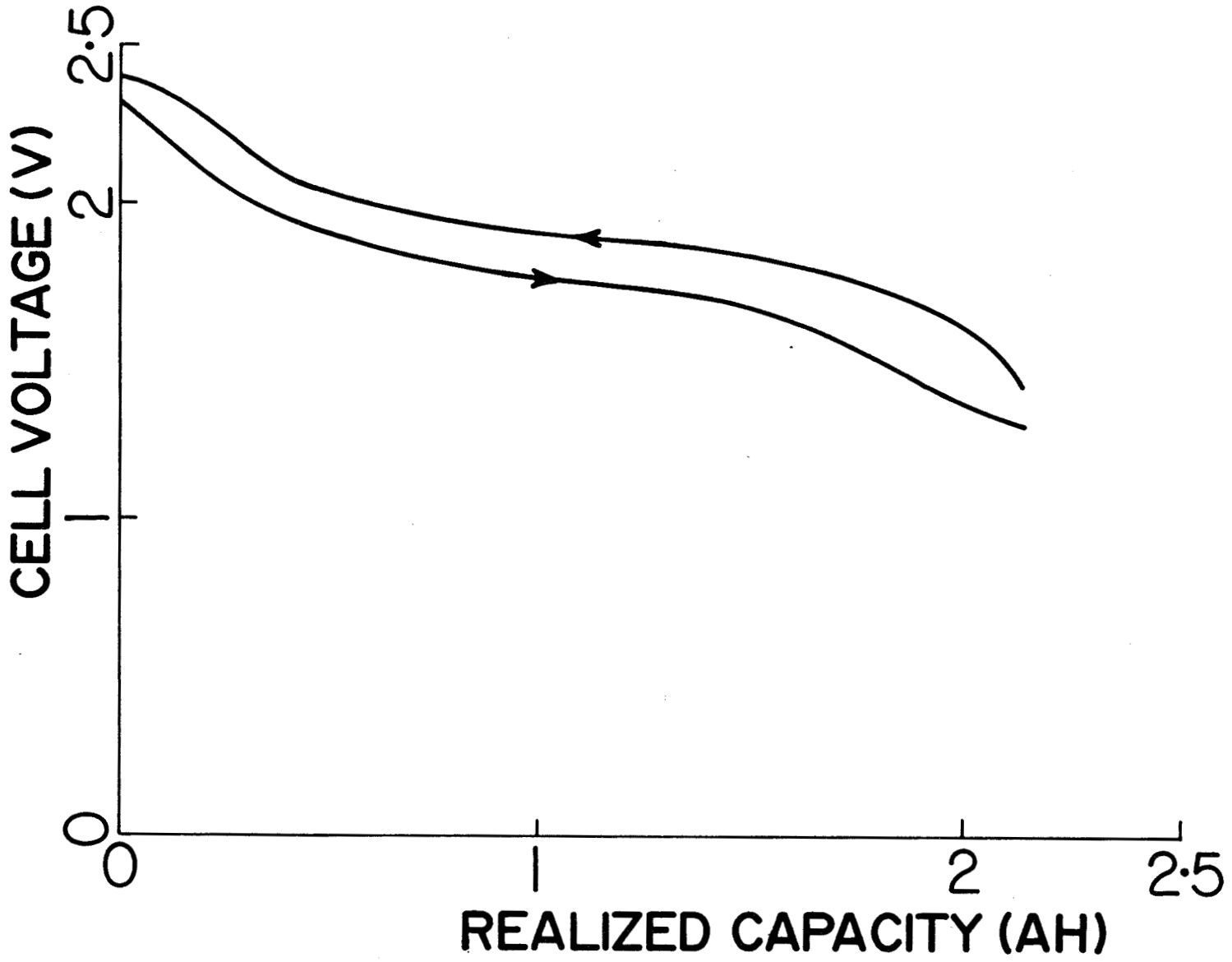

Figure 1 - Charge/discharge profile for a 'C' cell cycled in the standard voltage range. Charge current 280 mA, discharge current 840 mA. Cell at cycle number 10.

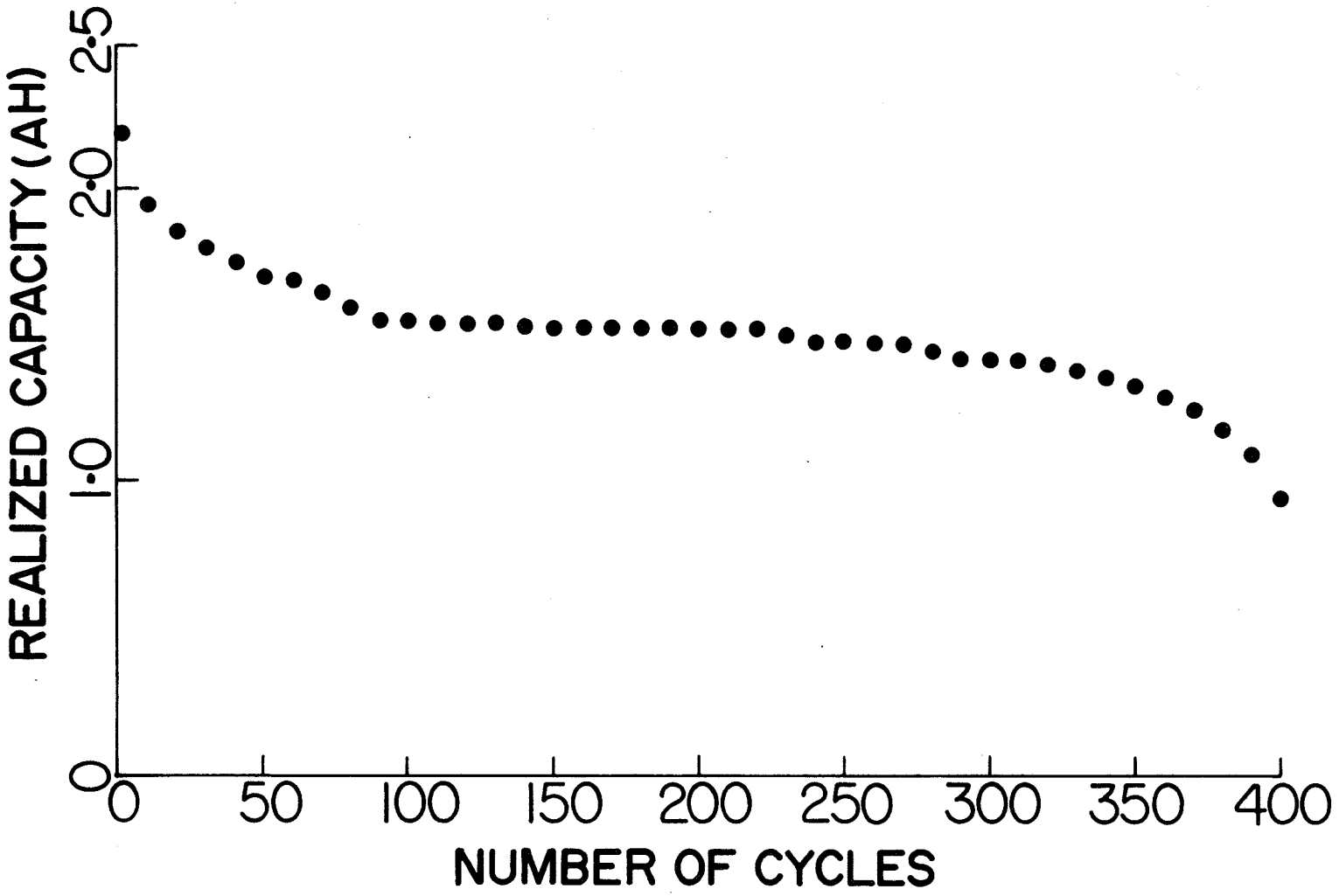

Figure 2 - Capacity vs. cycle number for a 'C' cell cycled in the standard voltage range. Charge current 280 mA, discharge current 840 mA.

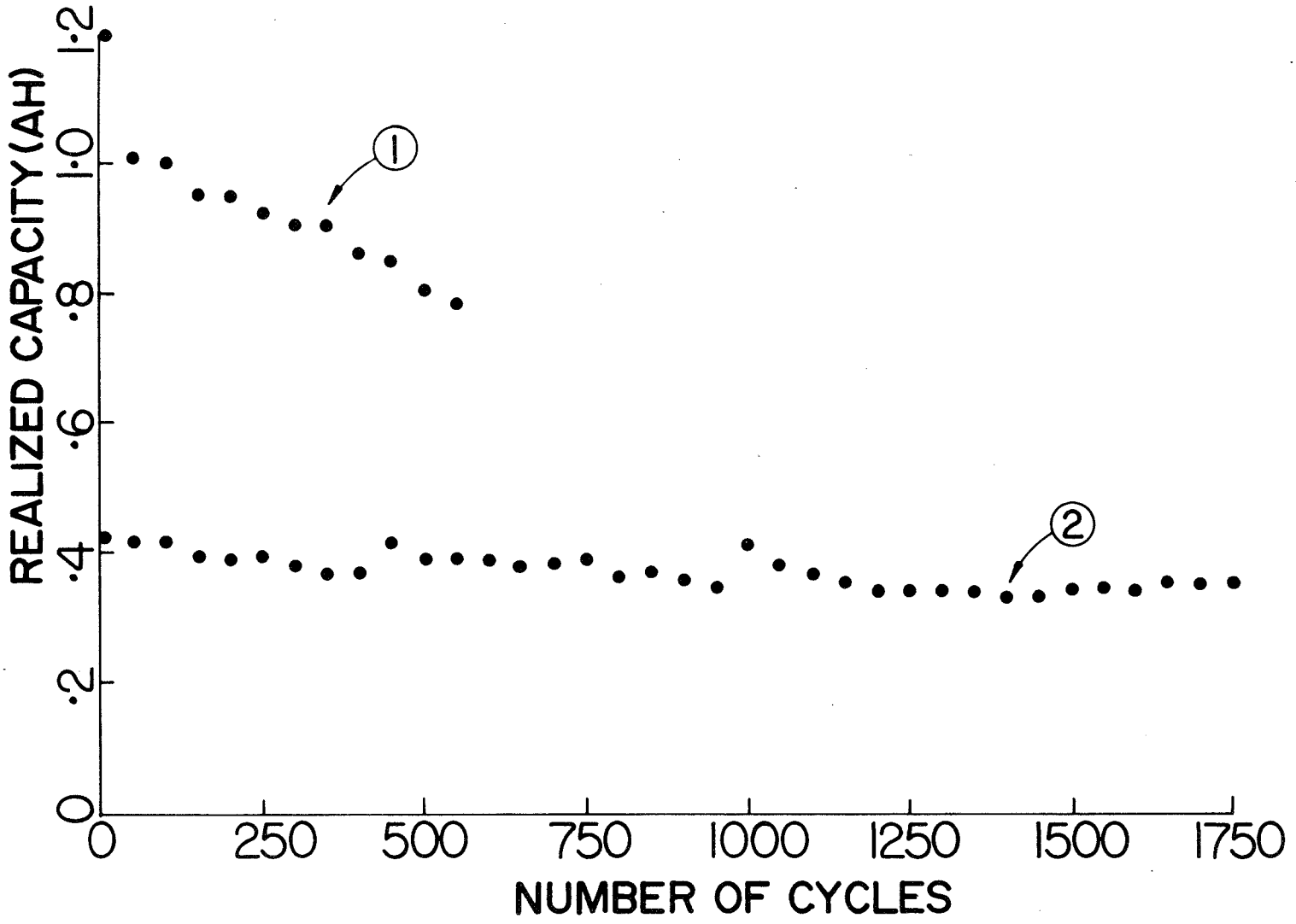

Figure 3 - Capacity vs. cycle number for 'C' cells cycled to different depths of discharge.
1: Cell cycled between 2.2V and 1.6V
2: Cell cycled between 2.2V and 1.8V

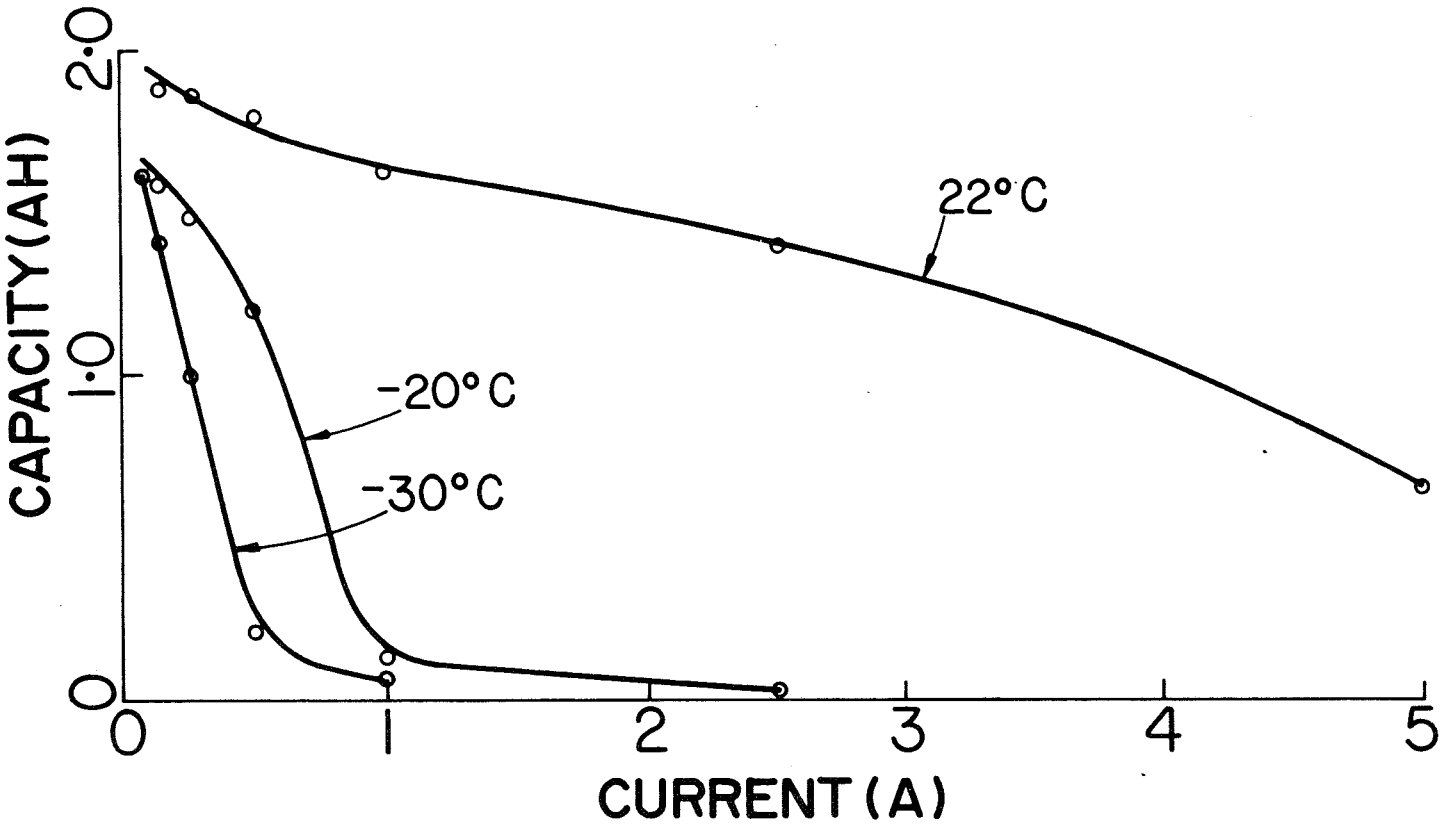

Figure 4 - Capacity vs. discharge current for three different temperatures. 'C' cell at cycle number 10.

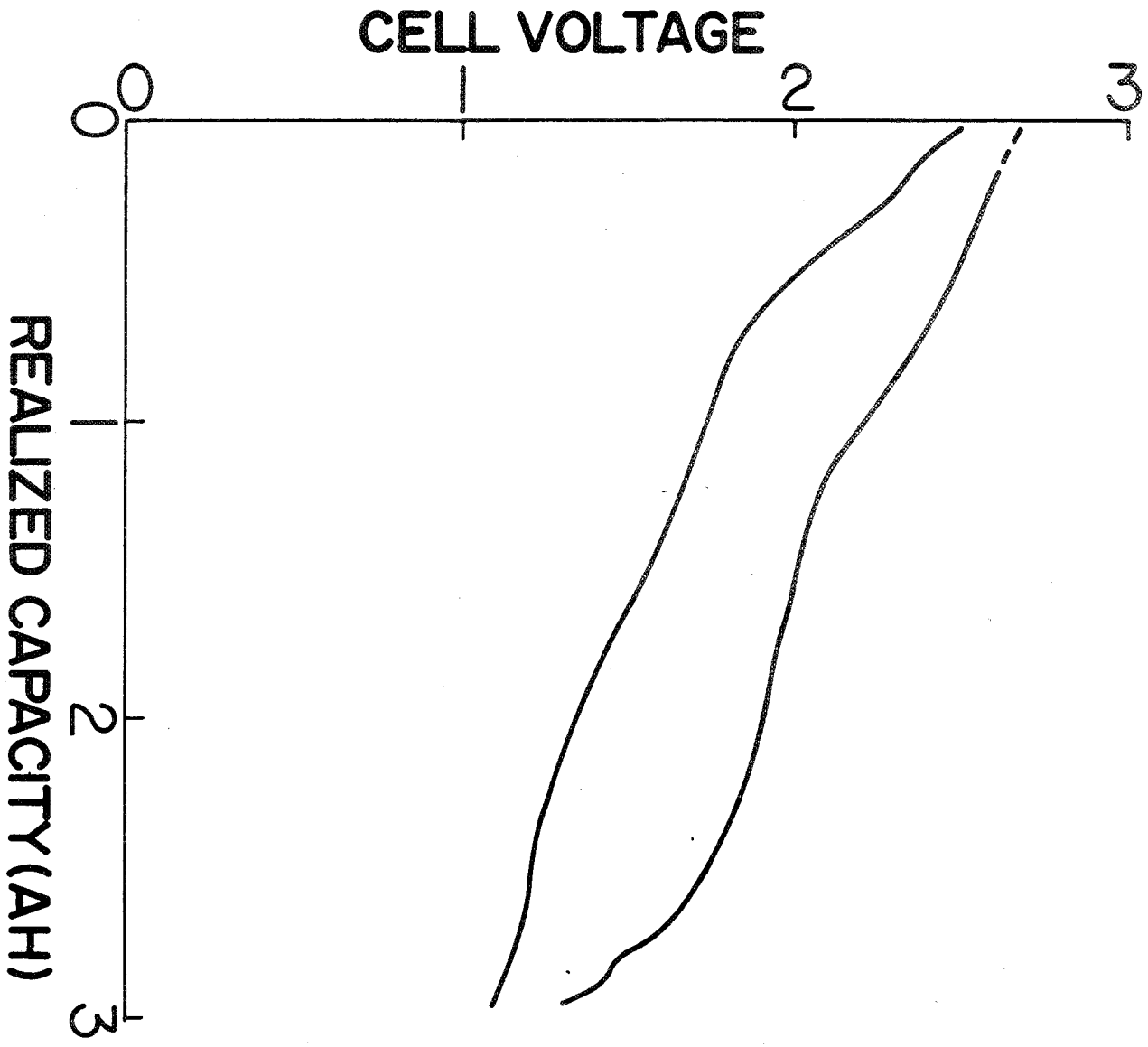

Figure 5 - Charge/discharge profile for a 'C' cell cycled over the extended voltage range. Charge current 280 mA, discharge current 840 mA. Cell at cycle number 1.

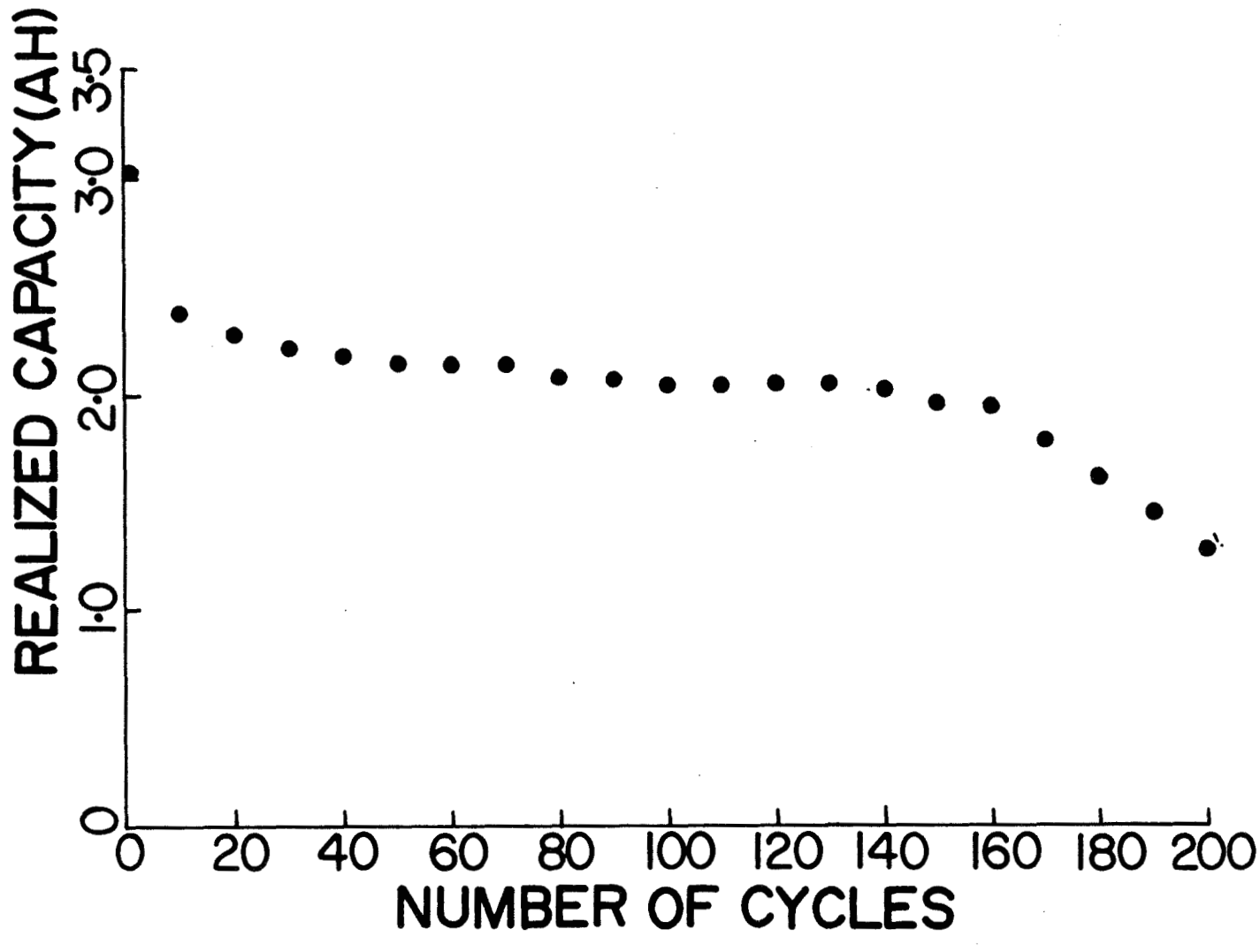

Figure 6 - Capacity vs. cycle number for a 'C' cell cycled in the extended voltage range. Charge current 280 mA, discharge current 840 mA.

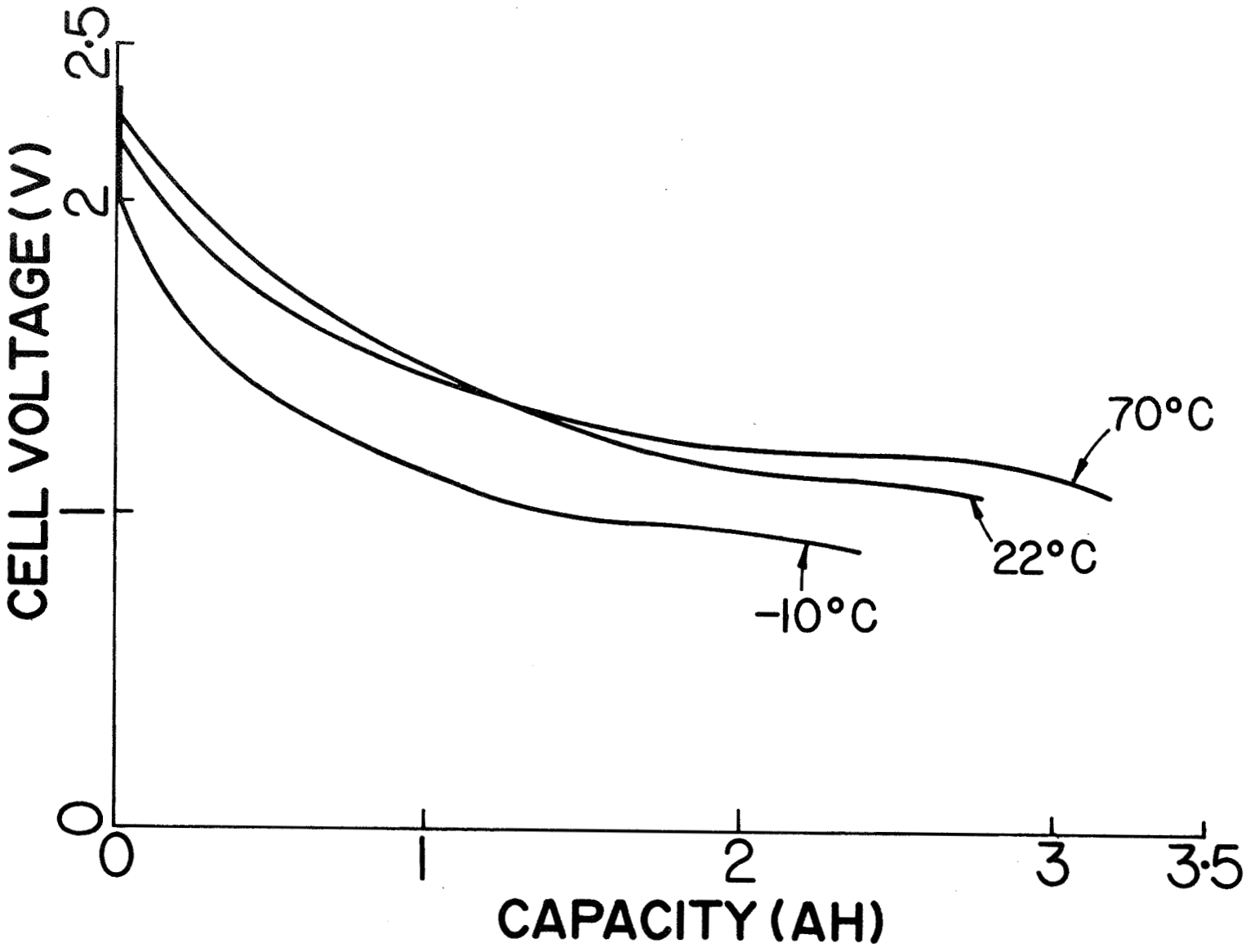

Figure 7 - Discharge profiles for 'C' cells at three different temperatures at a current of 840 mA. Charged at 280 mA to 2.6V. Cell at cycle number 1.

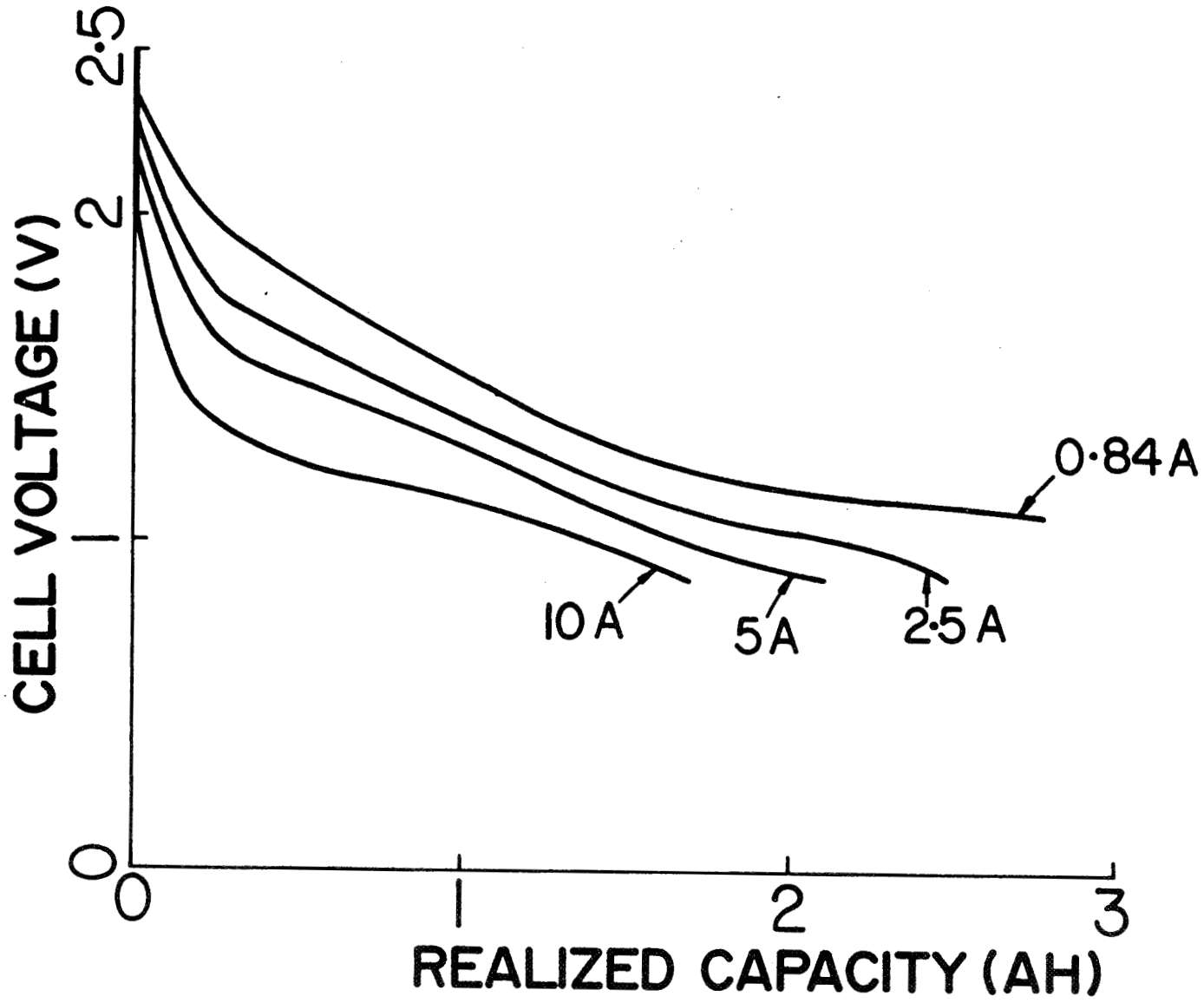

Figure 8 - Discharge profiles for 'C' cells for various discharge currents. Charged at 280 mA to 2.6V. Cell at cycle number 1.

GEOSYNCHRONOUS PERFORMANCE OF A LITHIUM-TITANIUM DISULFIDE BATTERY

Burton Otzinger
Rockwell International

ABSTRACT

An ambient temperature rechargeable Lithium-Titanium disulfide ($Li-TiS_2$) five cell battery has completed the first orbital year of accelerated synchronous orbit testing. A novel charge/discharge, state-of-charge (SOC) control scheme is utilized, together with taper current charge backup to overcome deleterious effects associated with high end-of-charge and low end-of-discharge voltages. The results indicate that ten orbital years of simulated synchronous operation may be achieved. Preliminary findings associated with cell matching and battery performance are identified.

INTRODUCTION

Ambient temperature rechargeable lithium cells hold promise as advanced energy sources for future space application. The $Li-TiS_2$ couple, with nonaqueous electrolyte, is the best known ambient temperature system. A battery of this type is of interest due to its expected high energy density (greater than 100 Wh/Kg) and long life (greater than 10 years). However, $Li-TiS_2$ cell research and technology are in an early development stage with only hand or custom made cells available.

An accelerated synchronous orbit life test of a five cell, $Li-TiS_2$ battery was initiated using advanced JPL designed and fabricated cells and a novel Rockwell charge/discharge, SOC-control method. This first test in the industry of these advanced rechargeable Lithium cells as a battery was initiated to obtain the following results:

1. Determine if the battery performance goal of ten orbital years of synchronous operation, established by NASA (RTOP), can be achieved, on an accelerated life test basis.

2. Gain an early look at battery related problems that arise in the selection and performance of cells to assist JPL in their cell development program.

3. Evaluate the capability of the Rockwell SOC-control method to extend the cycle life of a $Li-TiS_2$ battery.

This paper summarizes the results of the first orbital year of accelerated life testing.

METHOD OF INVESTIGATION

In a paper presented last year (Ref. 1), it was concluded that the rechargeable Lithium battery had good potential for synchronous satellite application. It was decided to explore this potential further by conducting an accelerated synchronous orbit life test on a 5 cell Li-TiS_2 battery. The Li-TiS_2 cells were fabricated at JPL and the cell design details are described in Table I.

The synchronous orbit life test was accelerated by reducing each solstice period between eclipse seasons to two weeks. The battery was charged after the last eclipse of each season and placed on open circuit stand during the two week period. Charged open circuit status was selected since this condition should result in minimum battery degradation during stand periods. The battery was also given a "top-off" charge at the end of the two week period to restore any stand losses. All charges were conducted within the selected SOC-control cut-off and rate limits.

A simulated 46 day eclipse season was used in this synchronous orbit life test and was conducted on a real time basis. The simulated eclipse period values are shown in Table II. The diagram in Figure I shows the test parameters and typical performance of the battery during a maximum eclipse day. All discharges were started at 9:00 A.M. and all charges started at 2:00 P.M. to make it possible to observe critical test events during normal work-day hours. The battery was allowed to stand open circuit after charge until the next morning to maintain the 24 hour real-time test basis.

The charge duration values shown in Table II and Figure I are approximate values since the charge was terminated based on the return of 100% of the capacity (Ah) removed during the prior discharge. This charge termination function was accomplished by the (Ah) integration and comparison capability of the test control computer. The discharge rate of 150 mA was selected to provide a maximum DOD (72 minutes) of 45% based on the 0.4 Ah rated battery capacity. Prior cell characterization testing indicated that extensive cycle capability could be expected at 45% DOD. The extended test time should expose any time dependant as well as cycling failure mechanisms.

The control of charge/discharge SOC was set to operate the battery between 90% and 45% SOC during the maximum (72 minutes) eclipse period. During other eclipse periods the recharge returned the SOC to approximately 90% in each case. This SOC positioning was accomplished prior to the first eclipse season by a discharge to 45% SOC from full charge and subsequent recharge to 90% SOC with a return of 45% of rated capacity. The charge voltage at 90% SOC is approximately 2.53 volts per cell and should remain constant with successive cycles until degradation of capacity exceeds 45% of rated. After capacity degradation in excess of 45%, the charge voltage during maximum eclipse must increase to allow the SOC to increase above 90% and eventually to full charge at 2.64 volts per cell. Degradation beyond 55% of rated capacity will cause battery failure/test termination at maximum DOD. The charge supply is set to provide a constant charge rate of 77.5 mA until a constant/clamp voltage of 2.64 volts per cell is reached with subsequent current taper. The constant voltage/taper charge feature is a back-up to prevent an excessive charge voltage across the cells. Charge to 2.64 volts/cell has been shown to result in full charge of the battery.

RESULTS

Two important variables used to evaluate battery performance during a synchronous cycle life test are the end-of-discharge voltage (EODV) and end-of-charge voltage (EOCV). The end-of-discharge voltage versus eclipse cycle is shown in Figure 2 for the first two eclipse seasons or first orbital year of operation. The ordinate in Figure 2 is provided with an equivalent average cell voltage scale to make it convenient to visualize the battery voltage value in terms of cell voltage. It can be seen in Figure 2 that, battery operation is well above an average of 2 volts per cell. The eclipse durations during the first eclipse season did not conform with the Table II values for all cycles due to computer program errors. Direct comparison of season 1 and 2 EODV is therefore not possible for cycles 19, 25 and 26. The Li-TiS_2 couple typically loses capacity and voltage performance during the early cycles of operation. This characteristic is evident in a comparison of season 1 and 2 EODV values from cycle 1 thru 18. After the non-uniform initial cycling losses, the relative performance in cycles 27 thru 46 indicate stable operation at a nearly fixed voltage performance loss. The character of this voltage degradation can be better seen in Figure 3. Note in Figure 3 that the voltage versus time characteristics during cycle 24 for the two seasons run parallel showing a nearly constant polarization factor from season 1 to season 2. It appears that, the polarization factor acts the same as the insertion of a pure resistance would to the discharge characteristic.

The range of EOCV values is shown in the following table:

Season	EOCV Range
1	12.55 to 12.69
2	12.65 to 12.79

The range is actually not as great as indicated due to a computer program deficiency that has been corrected prior to season 3. The EOCV trend has not shown any sign of degradation through the first two eclipse seasons.

The continuing good match of cell characteristics is reflected in the cell EODV and EOCV for cycle 24 of season 2 shown in the following table:

Cell No.	EOCV	EODV
1	2.548	1.994
2	2.557	1.963
3	2.546	1.998
4	2.547	2.010
5	2.550	1.965

The system under-voltage limit for the purposes of the life test is 8 volts. When the battery voltage drops to less than 8 volts (1.6 volts/cell) the test will be terminated. The voltage during season 2, maximum DOD, was about 9.93 volts. The difference (1.93 volts) between 9.93 and 8.00 volts equals the loss margin available prior to test termination. Assuming an average loss in battery voltage at maximum DOD of 0.1 volt per season, there are then approximately 19 seasons remaining. This estimate supports the possibility of demonstrating a ten orbital year (20 season) life.

CONCLUSIONS

The results of this life test support the estimate that ten orbital years of simulated synchronous operation can be achieved by a Li-TiS_2 battery. It was found that cells with capacities within a 6% range provided satisfactory battery operation while a 14% range did not. It was shown that the Li-TiS_2 couple performs well within a battery providing a real 2 volt/cell system under load to 45% DOD.

REFERENCES

1. Otzinger, B.M., Somoano, R.B.: Charge Control Investigation of Rechargeable Lithium Cells. Proceedings of The Goddard Space Flight Center Battery Workshop, November 1983, NASA Conference Publication 2331, pp. 45-63.

2. Yen, S.P.S., Shen, D.H., and Somoano, R.B.: Elastomeric Binders for Electrodes. Electrochem. Soc., Vol. 130, No. 5, May 1983, pp. 1107-1109.

Table I. DESCRIPTION OF JPL Li-TiS_2 CELL

Configuration	Cylindrical - plates spiral wound
Capacity	
Analytical	0.47 Ampere-hours
Rated	0.40 Ampere-hours to 1.7 volts
Voltage	
Open Circuit	2.7 Volts
Load (Ave.)	2.0 Volts at C/3 rate
Number of Plates	2
Plate Area	77.4 square cm
Positive Plate	TiS_2 on Ni Exmet-Elastomeric binder (0.020 in.) (Ref. 2); no conductive diluent
Negative Plate	Li Foil pressed on Ni Exmet (0.012 in.)
Electrolyte	(1.5M) $LiAsF_6$-2Methyl THF
Separator	2 Layers of Celgard 2400
Case Material	Stainless Steel
Size	2.3 cm diameter by 6.4 cm long
Weight	85 Grams

Table II. SIMULATED ECLIPSE SEASON PARAMETERS

ECLIPSE DAY	150 Ma DISCHARGE DURATION (MINUTES)	CHARGE 77.5 Ma CUT-OFF AT (HRS.) (MIN.)
1 46 2 45	12	0 23.2
3 44 4 43	30	0 58.1
5 42 6 41 7 40 8 39	45	1 27
9 38 10 37 36	53	1 43
11 35 12 34 13 33 14 32	60	1 56
15 31 16 30 17 29 18 28 19 27	66	2 8
20 26 21 25 22 24 23	72	2 19

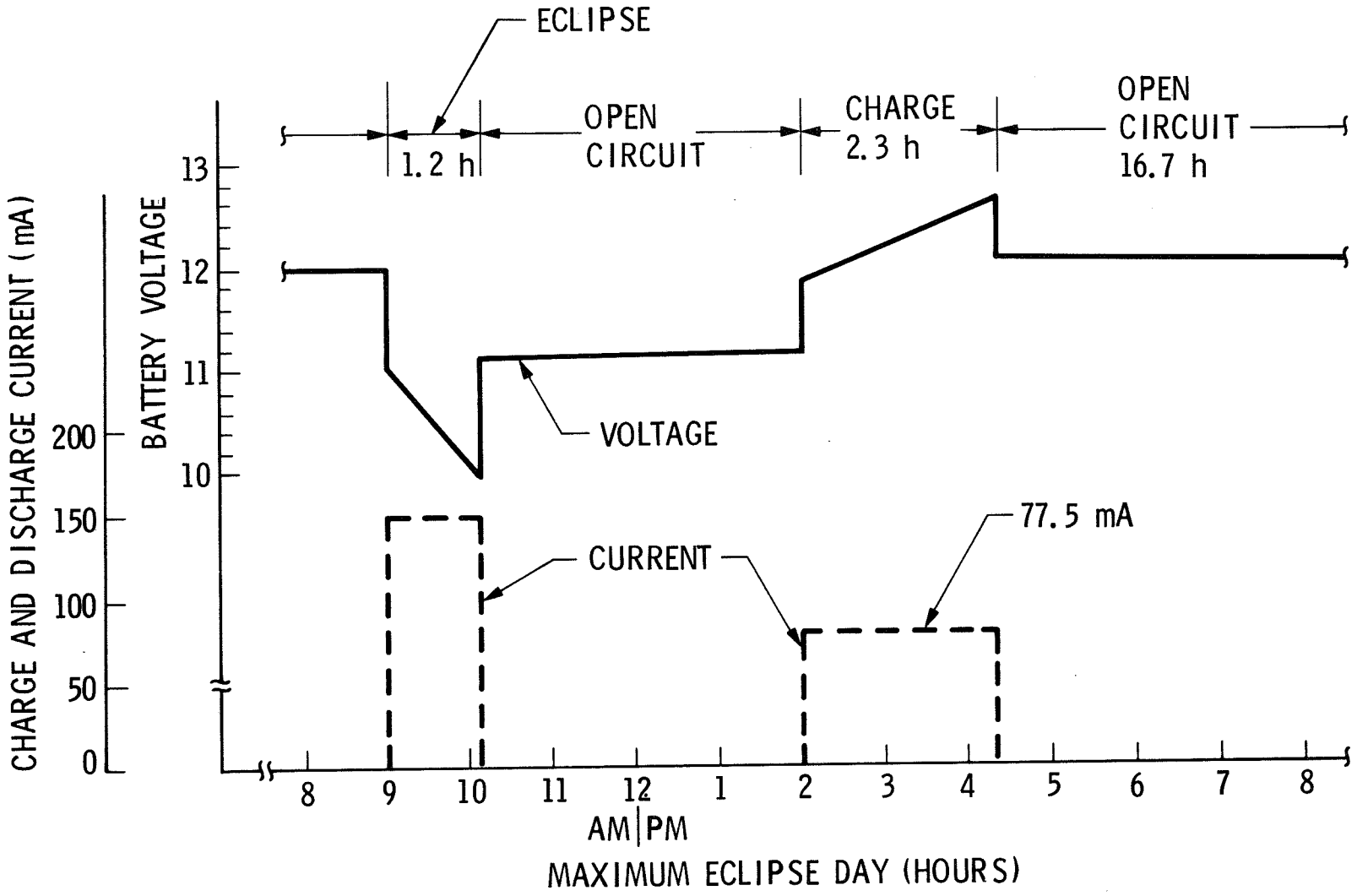

Figure 1 - Simulated Real-time Eclipse Season Test Parameters and Performance for Maximum Eclipse Day.

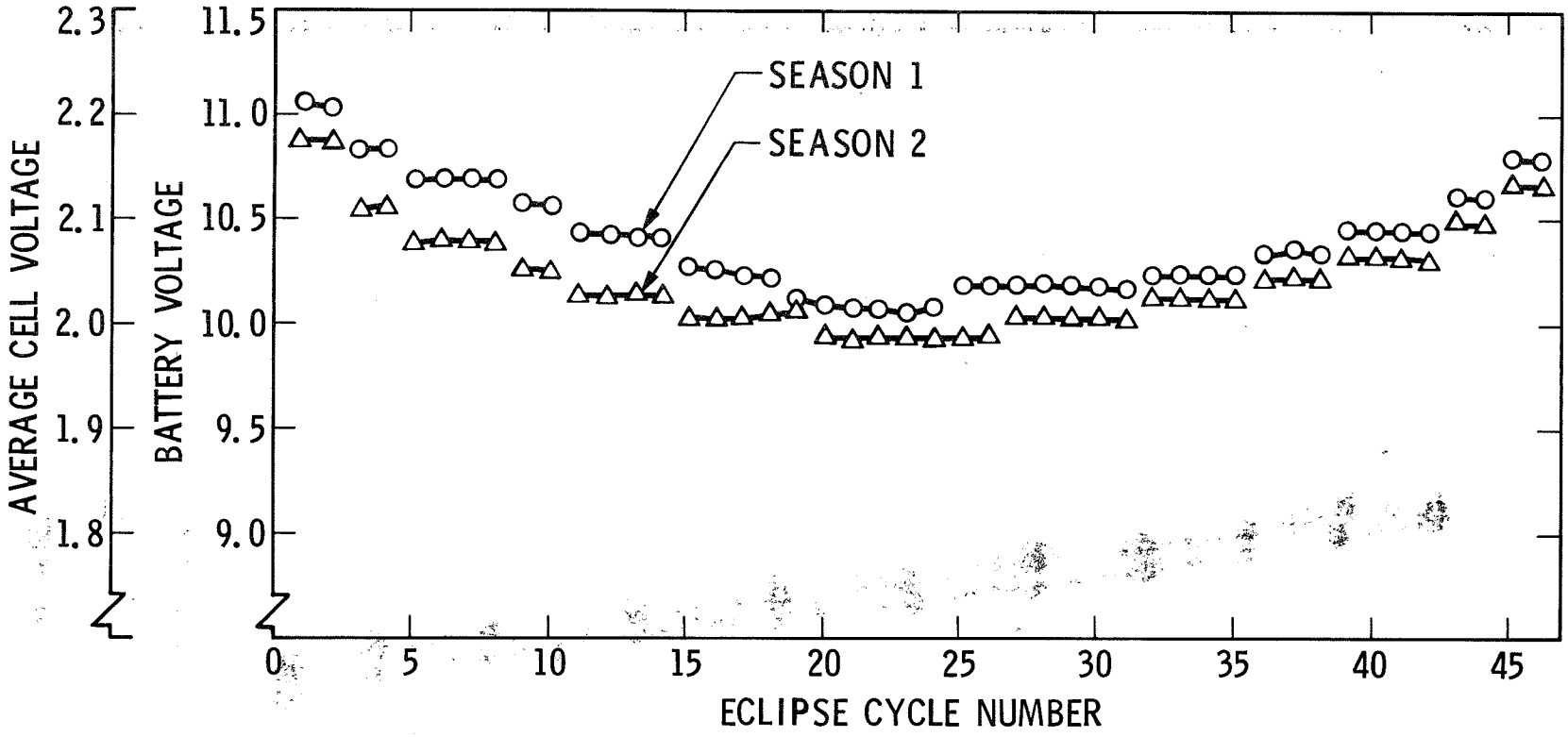

Figure 2 - End of Discharge Voltage Versus Cycle During Simulated Real-time Eclipse Seasons for 5 Cell Li-TiS_2 Battery.

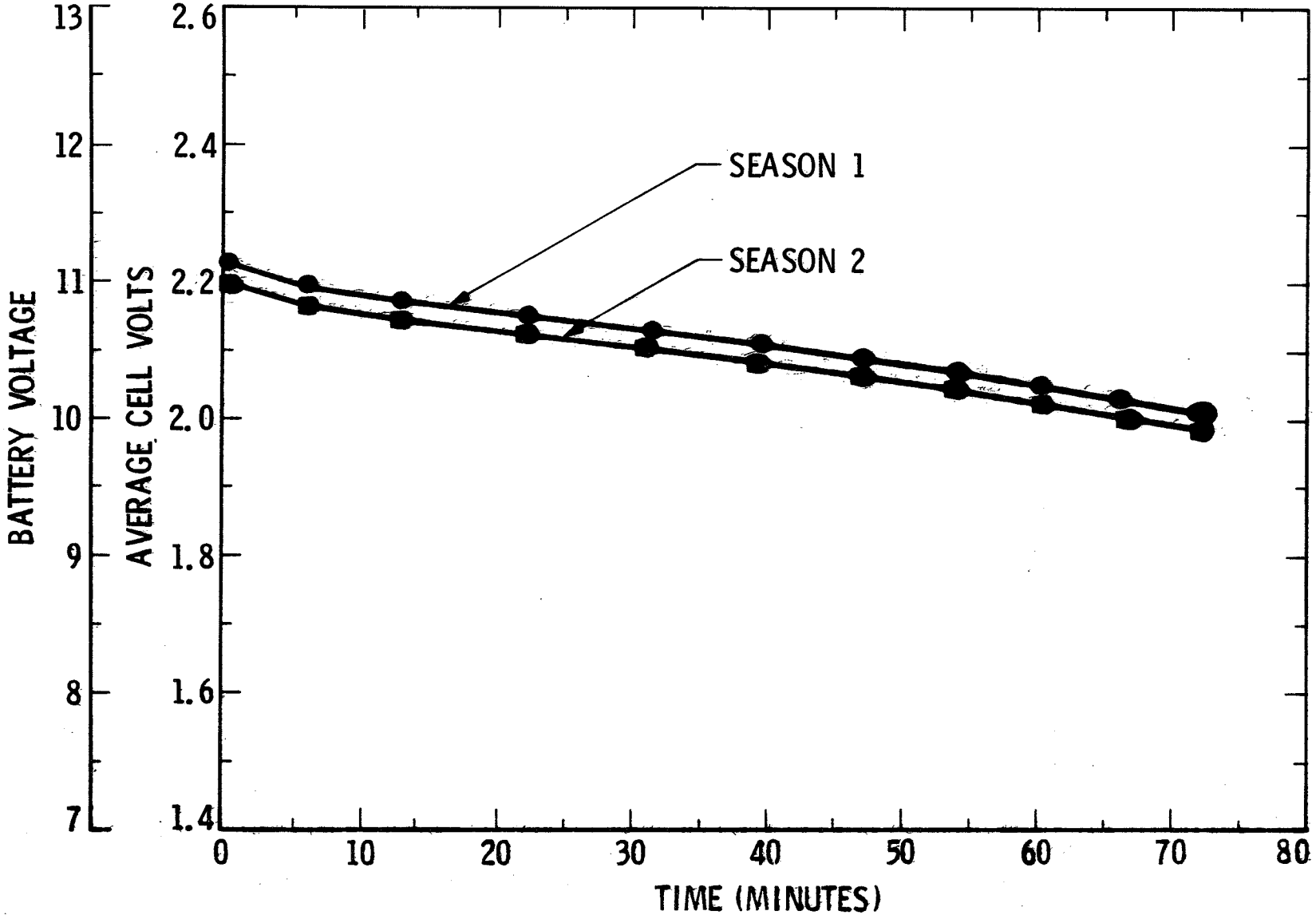

Figure 3 - Discharge Voltage Versus Time During Simulated Real-time Eclipse Seasons for Cycle 24.

DEVELOPMENT OF A LITHIUM SECONDARY BATTERY SEPARATOR*

J. A. Moore and Roice Willie
Rensselaer Polytechnic Institute

ABSTRACT

A non-porous membrane based on the polymerization of 2,3-dihydrofuran followed by crosslinking in situ has been prepared. The material is compatible with rechargeable Li battery components and, when swollen with an appropriate solvent such as tetrahydrofuran, exhibits separator resistance and Li^+ transport equivalent to Celgard.

INTRODUCTION

Efforts to develop light-weight batteries have lead to the production of ambient temperature, lithium metal-chalcogenide secondary cells (Li, TiS_2) containing ionic conductors (lithium hexafluoroarsenate) in aprotic, inert solvents such as tetrahydrofuran (THF).[1] The development of these batteries will be aided by improvements in separator technology which should significantly enhance cell performance and cycle life. Among the problems which exist with microporous separator materials (such as Celgard) is the formation of Li dendrites which penetrate through the pores of the separator from the anode to the cathode and ultimately short circuit the cell. Thus, a non-porous membrane which selectively transports solvated Li^+ cations from one electrode to the other may well outperform a microporous separator in terms of enhancing cell life during charge and discharge.

Among the requirements for such separators are that the material be insoluble in, but wettable by the solvent-electrolyte solution, that it be unreactive with metallic lithium and the cathode and that it be capable of ion transport. Because a large mass of data indicates that tetrahydrofuran and its derivatives are stable under normal battery conditions and fulfill all of the above criteria, it is reasonable to believe that incorporation of tetrahydrofuran units into a polymer chain will yield a material which will be an effective separator. Such a polymer would be completely compatible with the electrolyte solvent systems in use and could be made insoluble by appropriate crosslinking reactions. Extensive literature documents the activity of ether groups in general, and THF rings, in particular.

---

*This work was supported under a grant from the National Aeronautics and Space Administration, Lewis Research Center, NAG 3-199.

It has been reported that vinyl ethers such as 2,3-dihydrofuran can be polymerized to high molecular weight, processable materials.[3a,b] Such materials could fulfill the requirements for a useful separator and therefore we have undertaken a reinvestigation of this, and related systems.

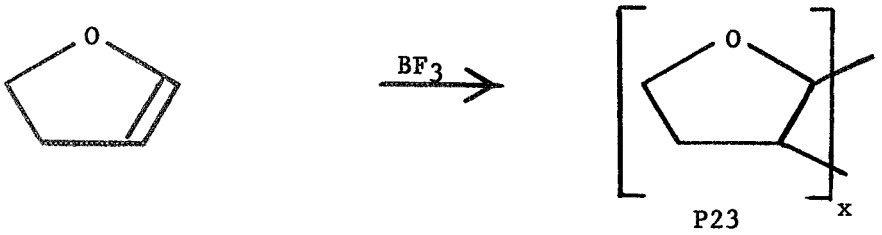

P23

This work describes the preparation and preliminary study of poly(2,3-tetrahydrofurandiyl) (P23) separator. This material was subjected to a series of compatibility experiments with rechargeable Li battery components as well as other physicochemical measurements. The results were compared to those from a Celgard 2400 standard.

EXPERIMENTAL

GENERAL

Electrochemical and transport properties were measured by Covalent Associates, Inc., Woburn, MA. All electrochemical experiments were conducted at 28°C. Compatibility tests were conducted in an oven thermostatted at 70±2°C. Atomic absorption (AA) analyses were accomplished with a Perkin Elmer Model 403 spectrometer. Optical microscopy was conducted with an American Optical binocular zoon instrument to 40X. Scanning electron microscopy (SEM) was run by Photometrics, Inc., Woburn, MA. The P23 Separator, shipped under N_2 in sealed vials, was opened in an Ar filled glovebox and not exposed to air unless otherwise indicated. Infrared spectra were recorded on a Perkin Elmer Model 237 spectrometer, ultraviolet spectra were recorded on a Perkin Elmer Model 552 spectrometer and ^{13}C and ^{1}H nuclear magnetic reonance spectra were obtained with a 200 MHz Varian Model 200XL spectrometer.

MEMBRANE PREPARATION

The polymerization of 2,3-dihydrofuran in bulk and in solution has been effected using $BF_3 \cdot Et_2O$ as initiator. Typically, a solution of $BF_3 \cdot Et_2O$ in CH_2Cl_2 was added to the monomer in bulk and in CH_2Cl_2 solution at -78°C. Anhydrous conditions and a N_2 atmosphere were maintained. At the completion of the reaction the initiator was deactivated with $MeOH/CH_2Cl_2$ solution, and the white, ropey polymer was precipitated into methanol.

Membranes were prepared by dissolving the reprecipitated polymer [reduced viscosity = 0.77dL/g] in chlorobenzene at a concentration of about 30% and adding 1% triphenyl phosphite and 5% benzoyl peroxide. Films were cast on a Teflon block with a draw knife to the nominal dimensions and, after drying for 9 hr at room temperature under N_2, then heated in an oven under vacuum at 78°C for 12 hr. After cooling under vacuum, the films were peeled from the casting surface, solvent extracted to remove byproducts, cut to size and stored under N_2.

COMPATIBILITY TESTS

Measurements of physical dimensions were made on two 1.0 cm x 2 mil P23 pieces cut from the membrane as received and after a 2 hr soak in tetrahydrofuran [(THF) Burdick and Jackson] and 2-methyltetrahydrofuran [(2-MeTHF) Aldrich] distilled from CaH_2 under Ar. Additional 1 cm x 4 cm x 2 mil P23 samples and 1 cm x 4 cm x 1 mil Celgard 2400 samples were cut for the compatibility tests. Weight changes of P23 were assessed after 7 days storage at 70°C in both 2-MeTHF and 1.4M $LiAsF_6$ (U.S. Steel Agrichemicals)/2-MeTHF.

All compatibility tests were conducted in duplicate in Teflon-taped screw cap vials. The components comprised Li foil (Lithcoa, 10 mil), TiS_2 (Cerac, battery grade), as well as 2-MeTHF and 1.4M $LiAsF_6$/2-MeTHF prepared at dry ice temperature followed by pre-electrolysis between 2 Li electrodes.

The following quantities of materials were used:

Li foil: 1 cm x 4 cm

TiS_2: 1.0 g

Celgard 2400 or P23: 1 cm x 4 cm

Solvent or electrolyte: 5.0 ml

A series of 20 vials was prepared and numbered as follows:

Vial Number	Contents
1	solvent, P23
2	electrolyte, P23
3	electrolyte, P23, Li
4	electrolyte, P23, Li, TiS_2
5	solvent, Celgard
6	electrolyte, Celgard
7	electrolyte, Celgard, Li
8	electrolyte, Celgard, Li, TiS_2
9	electrolyte
10	electrolyte, Li
11	duplicate of 1

12	duplicate of 2
13	duplicate of 3
14	duplicate of 4
15	duplicate of 5
16	duplicate of 6
17	duplicate of 7
18	duplicate of 8
19	duplicate of 9
20	duplicate of 10

CYCLIC VOLTAMMETRY AND INFRARED ANALYSIS

Cyclic voltammetry (CV) was conducted directly in Vials 2, 3, and 6 after the 7 day storage period. A 3 mm dia. polished vitreous C working electrode along with Li counter and reference electrodes were inserted into the vial inside the glovebox. Voltammograms were generated by a BAS CV-1B instrument and recorded on an HP 7015B XY recorder. Infrared spectroscopy was conducted in sealed matched and polished KCl cells (Wilmad) with a 0.1 mm path length.

RESISTIVITY MEASUREMENTS

A two-compartment polypropylene cell (designed by Covalent Associates) was used for all resistance measurements. The membrane was supported by Viton "O"-rings which sealed the cell and fixed the area exposed to the electrolyte at 6.0 cm^2. Resistivity data was taken with a GenRad Model 1650A impedance bridge.

LI ION TRANSPORT STUDY

The flux of Li^+ through the P23 membrane was conducted in the same cell used for resistivity measurements. One compartment contained 2.0M $LiClO_4$/THF while the other contained 2.0M $NaClO_4$/THF. Because the P23 material swelled to a much greater degree in THF than in 2-MeTHF (vide infra), THF was the solvent of choice. The cell was filled and allowed to equilibrate. Subsequently, 1.0 ml aliquots were removed from the $NaClO_4$/THF compartment and analyzed for Li^+ content with AA spectroscopy. This experiment was then repeated with Celgard 2400 separator material.

RESULTS AND DISCUSSION

COMPATIBILITY TESTS

The sealed tubes were opened inside the glovebox and the 2 mil and 5 mil P23 membranes were measured for uniformity of thickness. The normal 2 mil membrane ranged from 1.5 to 2.5 ml in thickness, while the 5 mil membrane

ranged from 2.0 to 3.0 mil in thickness. Both samples were flexible and cellophane-like in mechanical behavior. The P23 samples could be folded and unfolded many times without structural damage.

Under the 40X microscope, neither bubbles nor cracks were evident in either the 2 mil or the 5 mil sample. Two pieces of P23 were deliberately exposed to air for 3 days. Microscopic examination revealed no visible structural changes nor was any embrittlement detected.

All of the 70°C compatibility tests employed 2 mil P23. All visual observations were identical for their corresponding duplicates. No loss of solvent volume was detected over the 7 day storage period.

After 20 hr of storage at 70°C, a yellowing of the P23 membrane in vials containing $LiAsF_6$ was observed. The yellowing was enhanced in vials containing $LiAsF_6$ and Li foil.

In Vial 1 containing only 2-MeTHF, the P23 sample was clear and colorless. but in the presence of $LiAsF_6$ (Vial 2), P23 turned uniformly yellow. Vial 13 revealed an amber color permeating the membrane with the edges being the most intensely colored. It is important to note that the electrolyte solutions in Vials 2 and 13 were clear and colorless. Only the membrane was affected. Similarly, the Celgard 2400 samples in Vials, 5, 6, and 7 were unchanged as were the blanks (Vial 19 and 20).

Experience with this membrane suggests that the yellowing may be caused by oxidation of the polymer by residual O_2, and that this oxidation is exacerbated by the presence of halide. Over the following 6 days no further changes were noted with the exception of a slight yellowing of the electrolyte in contact with P23.

At the end of the 7 day storage tests the samples were removed from the vials and examined. As the samples dried they shriveled to a form which makes microscopic examination or dimensional measurements difficult. P23 from vial 12 seemed to be markedly yellow when compared to P23 from vial 11. The Celgard 2400 standard was unchaged after storage for 7 days at 70°C. When rinsed with methanol to remove small particles of TiS_2, the P23 membrane from Vials 4 and 14 was as yellow in color as the P23 from Vials 3 and 13. Even after solvent evaporation in the glovebox, the membranes retained their plasticity -similar to commercial Saran Wrap rather than cellophane. None of the P23 samples manifested any sign of brittleness.

Infrared scans on 2-MeTHF from Vial 11 and 1.4M $LiAsF_6$/2-MeTHF from Vial 12 were obtained and compared to electrolyte from Vial 16 which contained Celgard 2400. All spectra were identical. The spectrum of electrolyte from Vial 12 compared to the spectrum of electrolyte from Vial 16 showed no extraneous absorbances. Thus the spectral evidence indicates that P23 is not dissolving in the solvent or solvent-electrolyte solutions. Attempts by reweighing the test samples to determine if dissolution was occuring were inconclusive.

To probe further the possibility of P23 degradation, cyclic voltammetry scans were made on electrolyte from Vial 6 (Celgard 2400), Vial 2 (P23), and Vial 3 (P23 + Li). With the exception of a slight increase in cathodic current from electrolyte in Vial 3, no large quantities of electroactive materials are present between 0.8 and 4.4 V vs. Li. A slightly enhanced current from Vial 3 may well be caused by small amounts of electrolyte-Li reaction products.

RESISTIVITY MEASUREMENTS

A 2 mil sample of P23 was placed in the resistivity cell after which the cell was filled with 1.4M $LiAsF_6$/2-MeTHF electrolyte. After 5 min, the total cell resistance was 41,000 ohms; after 30 min, 2150 ohms; after 1.5 hr, 520 ohms; after 3 hr, 204 ohms; after 5 hr, 170 ohms. The total cell resistance stabilized at this last value. In the absence of the P23 separator, the cell manifested a resistance of 165 ohms. Thus, the separator resistance multipled by the 6 cm^2 geometric area gave a value of 30 ohm cm^2.

When Celgard 2400 was substituted for P23, the cell resistance was found to be below the sensitivity of the impedance bridge after just 5 minutes. Thus, the P23 separator resistance is at least 30 times greater than that of Celgard in 2-MeTHF.

To ascertain whether the P23 might swell more readily in THF rather than in 2-MeTHF and thereby become less resistive, the resistance of a P23 separator in 1.4M $LiAsF_6$/THF was measured. After 5 min, the total cell resistance was essentially equivalent to the cell resistance without P23 as in the case for Celgard 2400. This result clearly demonstrates that P23 is a good Li^+ transporter when it can be made to swell by an appropriate solvent.

LI ION TRANSPORT STUDY

Based on the results with THF, it was decided to conduct this experiment with 2.0 M $LiClO_4$/THF and 2.0 M $NaClO_4$/THF electrolytes. Over a 3.6 hr period the average rate was found to be 2.2×10^{-1} mmole $Li^+/h/cm^2$. Under exactly the same conditions, Celgard 2400 was also found to give a rate of 2.2×10^{-1} mmole $Li^+/hr/cm^2$. This result corroborates the resistivity data acquired in $LiAsF_6$/THF for P23 and Celgard 2400. It should be noted that because of the propensity of P23 to swell in THF (vide infra), the geometric area and actual swollen area may differ by up to 100%. However, this uncertainty should not prevent P23 from being used as an effective battery separator.

MISCELLANEOUS TESTS

P23 Wetability and Swelling Measurements. It was found that methanol, 2-MeTHF, and THF readily wet P23 while H_2O does not. In 2-MeTHF (7 days), P23 went from 2-3 mil to 3-3.5 mil in thickness. In THF (5 min) P23 went from 2-3 mil to 3-4 mil in thickness. These numbers are grossly approximate because of the difficulty of measuring thickness accurately on a gelatinous material.

Dimensional changes for P23 in THF and 2-MeTHF were roughly assessed in their respective vials because removing the membranes from the solvent resulted in rapid shrinkage. Thus, P23 in 2-MeTHF increased in length and width by about 13% after 2 hr at 28°C. But in THF, P23 appeared to undergo a 90% increase in length and width within 5 min of contact with THF at 28°C. No further changes were noted with time.

Heat Sealing. A sample of P23 was heat sealed to itself satisfactorily with a jaw impulse heater at a setting of 5. P23 requires more heat than Celgard 2400, but this fact presents no problem in suitably bagging battery electrodes with P23.

SEM Study of P23 Structure. All attempts at obtaining SEM images of the THF-swollen membrane failed because of the shriveling phenomenon as the solvent evaporated. The dry membrane surface (shiny side) is remarkably smooth and featureless at 11,000X. To obtain a cross section free of distortion from a cutting implement, a sample of 2 mil P23 was fractured at liquid N_2 temperature. The cross section is amorphous and pinhole-free at 4,440X.

CONCLUSIONS

P23 is pliable, insoluble in 2-MeTHF and in THF, and manifests adequate conductivity in THF-electrolyte systems. Further work and extended compatibility studies in THF-based electrolytes would be fruitful. Indeed, the latest EIC electrolyte (50:50 THF:2-MeTHF plus 2-methylfuran) is an obvious choice. Finally, P23 must be tested as a separator in rechargeable Li cells to ascertain its resistance to dendrite penetration and long term chemical and electrochemical stability. The very promising results obtained from these initial efforts bode well that continued study of novel polymers containing heterocyclic rings may lead to separator systems which are superior to those currently in use.

REFERENCES

1. "Status of the DOE Battery and Electrochemical Technology Program", Mitre Corp., report #MTR-8026, September, 1979.

2a. C. J. Pedersen and H. K. Frensdorff, Angew. Chem. Int. Ed. Engl. 11, 16 (1972).

2b. J. J. Christensen, D. J. Eatough and R. M. Izatt, Chem. Rev. 74, 351 (1974).

2c. W. J. Schultz, M. C. Etter, A. V. Pocius and S. Smith, J. Am. Chem. Soc. 102, 7981 (1980).

2c. W. J. Schultz, M. C. Etter, A. V. Pocius and S. Smith, J. Am. Chem. Soc. 102, 7981 (1980).

3a. D. A. Barr and J. B. Rose, J. Chem. Soc. 1954, 3766.

3b. G. J. Schmitt and C. Schuerch, J. Polym. Sci. 49, 287 (1961).

TOTAL CELL RESISTANCE

Membrane

	THF					2MTHF				
	5 min.	30	90	180	300	5 min.	30	90	180	300
P23	~0	–	–	–	–	41,000Ω	2150	520	204	170
Celgard 2400	~0	–	–	–	–	~0	–	–	–	–

Electrolyte = 1.4M $LiAsF_6$

Li^+ TRANSPORT

2.0 M $LiClO_4$/THF//2.0 M $NaClO_4$/THF

Membrane	Average Rate (MMole Li^+/hr/Cm^2)
P23	2.2×10^{-1}
Celgard 2400	2.2×10^{-1}

IMPROVEMENTS IN SAFETY TESTING OF LITHIUM CELLS

Russell C. Stinebring and Paul Krehl
Wilson Greatbatch Ltd.

ABSTRACT

A systematic approach has been developed for evaluating the basic safety parameters of high power lithium soluble-cathode cells. This approach consists of performing a series of tests on each cell model during the design, prototype and production phases. Abusive testing is performed in a facility where maximum protection is given to test personnel.

INTRODUCTION

Lithium cells with spirally-wound anodes are used extensively in applications where high power is required. These cells have the capability of delivering high current densities as a function of the anode surface area. In designing and fabricating high-power cells, considerable attention must be given to the evaluation of safety.

While all of the cells of this type manufactured at our facility are protected by external fuzes against short-circuiting, consideration must also be given to the behavior of the cells under a variety of abusive conditions.

A system has been established for evaluating new cell models during the design, prototype and production phases. Cells are subjected to some abusive conditions which may possibly be encountered during usage. In addition, cells are also evaluated under conditions of severe abuse which may cause rupturing and release of the cell contents. In some cases, the sudden release of energy may be of considerable force.

All of the abusive tests on our cells are done in a special facility that was designed to give maximum protection to the test personnel and equipment.

DISCUSSION

I. FACILITY DESCRIPTION

The abusive test facility consists of several test bays which have reinforced concrete walls, heavy steel entry doors, blow-out walls and high volume exhaust systems.

Feed-through ports are provided for cables and sensor wires so that measuring equipment can be located outside of the test bay. Alarm beepers are also activated to signal that a test is in progress and to warn personnel about entering the test bay.

In addition, eacy bay has a thick laminated glass window which permits direct viewing and video recording as the test is being conducted.

Severe abusive tests, where the full energy of the cell or multi-cell battery pack may be released, are readily and safely contained in these test bays.

Some of the types of severe abuse tests which are conducted are:

- puncture
- crush
- incineration or rapid heating with electrical heat tape
- charging at high rates
- forced overdischarge at high rates

II. SYSTEMATIC APPROACH TO SAFETY TESTING

A. DESIGN PHASE

The evaluation of safety parameters and margins starts during the design phase of new models.

After cells are fabricated by the Research and Development scientists, they are subjected to short-circuit testing using shunts that apply a resistive load of less than .01 ohms. Current and temperature are monitored during the test to characterize behavior. In addition, cells are discharged at high and moderate rates, while current, voltage and temperature are monitored. Initial force discharge tests are also performed to (prove/evaluate) the basic cell design.

The results of these tests are used to evaluate the safety of the basic design and to determine if the cells are essentially qualified to build and handle. At this stage, the results of the tests may be used to change or improve the design (TABLE I). Also, preliminary sketches of cell components are made and transferred to engineering.

B. ENGINEERING PROTOTYPE PHASE

After the design of the model has been established, Engineering prototypes are fabricated. These units are built with production equipment and tolerances and the safety testing at this phase consists of:

- maximum current discharge at maximum operating temperature
- short-circuiting with and without fuzes
- DOT-E-7052 requirements of altitude simulation, thermal stability, vibration testing
- force-discharge at moderate rates
- drop testing (five feet onto a metal plate)
- full drawing packages are prepared at this time

The results of this series of tests determine if the unit is qualified to ship and to be used safely under the conditions described on the cell label.

Standard discharge tests at several rates are also done to determine the normal cell performance, but a primary focus of all testing is to establish the safety of the design.

During this phase, severe abusive tests such as crushing, incineration or high rate heating, puncture and charging may be done to further characterize the safety tolerance of the design (TABLE II).

C. PRODUCTION PHASE

The safety parameters and margins were studied during the design and engineering phases for the particular models which were made by well defined sets of processes and specifications.

In order for the safety test results to be valid, it must be determined that cells are made consistently and that processes do not vary inordinately. In our system, statistical quality control techniques are used. These techniques incorporate trend charts and other analyses to assure that processes are not subtly changing, thereby resulting in cells that deviate from the design which had been thoroughly characterized during the previous phases.

In some cases, processes may be deliberately changed in order to effect cost improvements, efficiencies etc. When changes are made or contemplated it becomes a responsibility of the Engineering and Reliability groups to qualify the change. This often requires that safety tests be repeated and a new safety assessment be made before the change is incorporated or cells are put into use.

In addition to the standard discharge tests, cells are stored for various periods of time and under varying environmental conditions. Periodically the stored cells are tested under conditions of normal and abusive tests to evaluate behavior and sensitivity over an extended period of time (TABLE III).

SUMMARY

Lithium soluble cathode cells go through extensive safety assessment using a systematic approach. This approach has resulted in cells and designs which are well characterized in terms of safety and performance.

Abusive tests are performed in a special facility where a maximum amount of protection is given to the test personnel. This facility permits testing to be done on cells and battery packs where they are deliberately abused beyond their limits thereby releasing their full energy.

By analyzing the results of the normal and severe abusive tests safety margins can be established and design improvements can be made.

The test results also form a base line of data so that comparisons can be made periodically between the production cells and their prototypes.

In addition, quality and process control techniques are used in the production phase to assure that the basic design and processing is being maintained. As a result, the safety and performance testing results remain valid throughout the production phase.

Where changes are introduced in the processing of cells and components, they are qualified by repeating safety tests and updating the baseline.

Table I. DESIGN PHASE FOR NEW MODELS

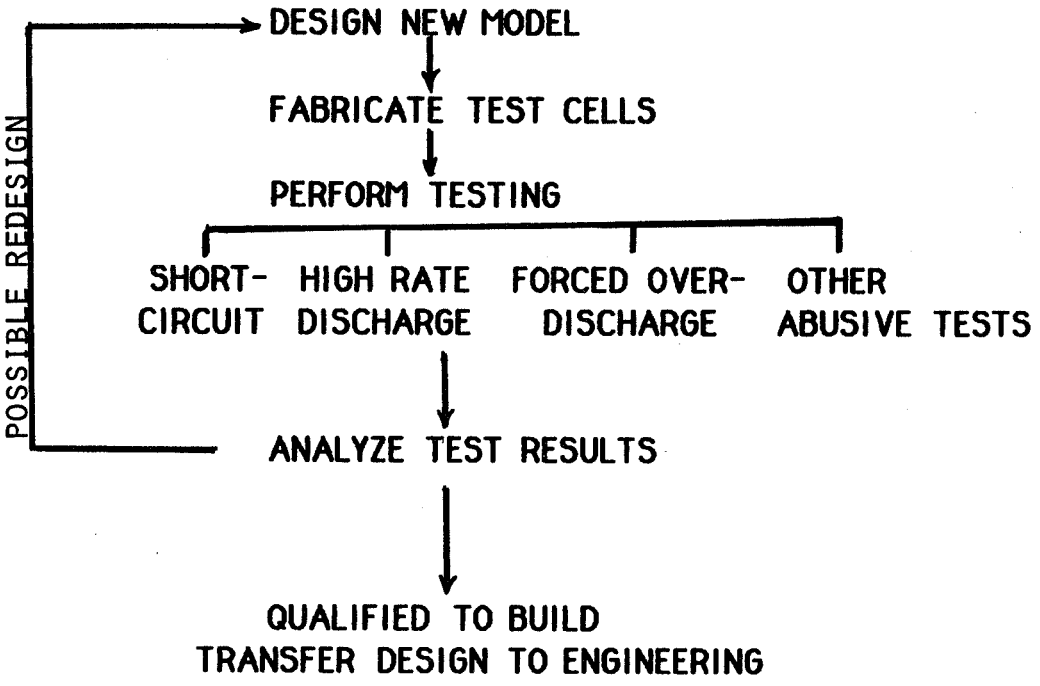

Table II. ENGINEERING PHASE FOR NEW MODELS

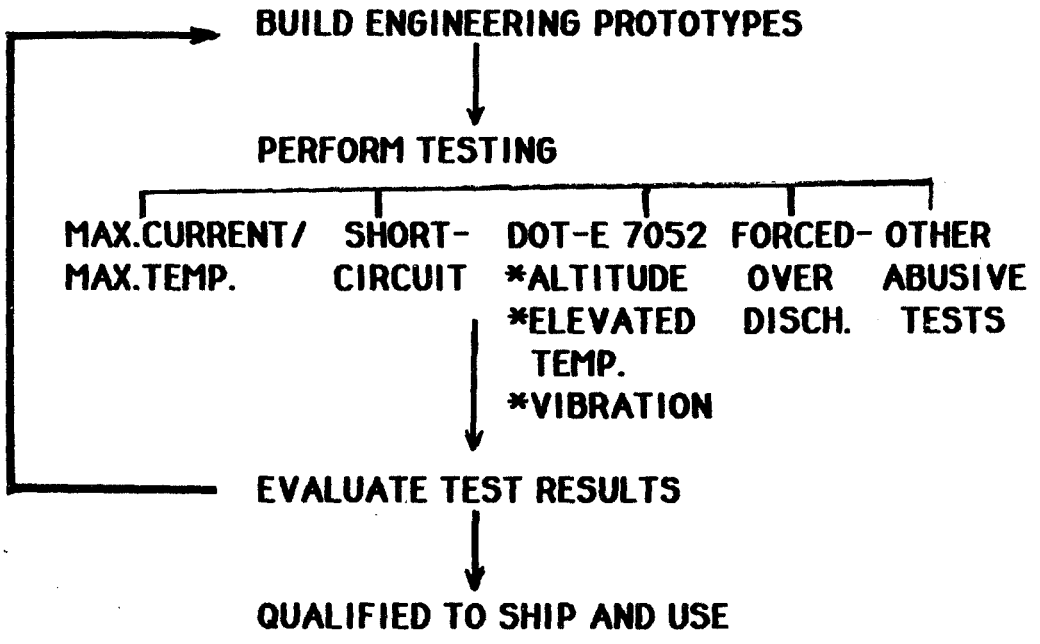

Table III. PRODUCTION PHASE OF NEW MODEL

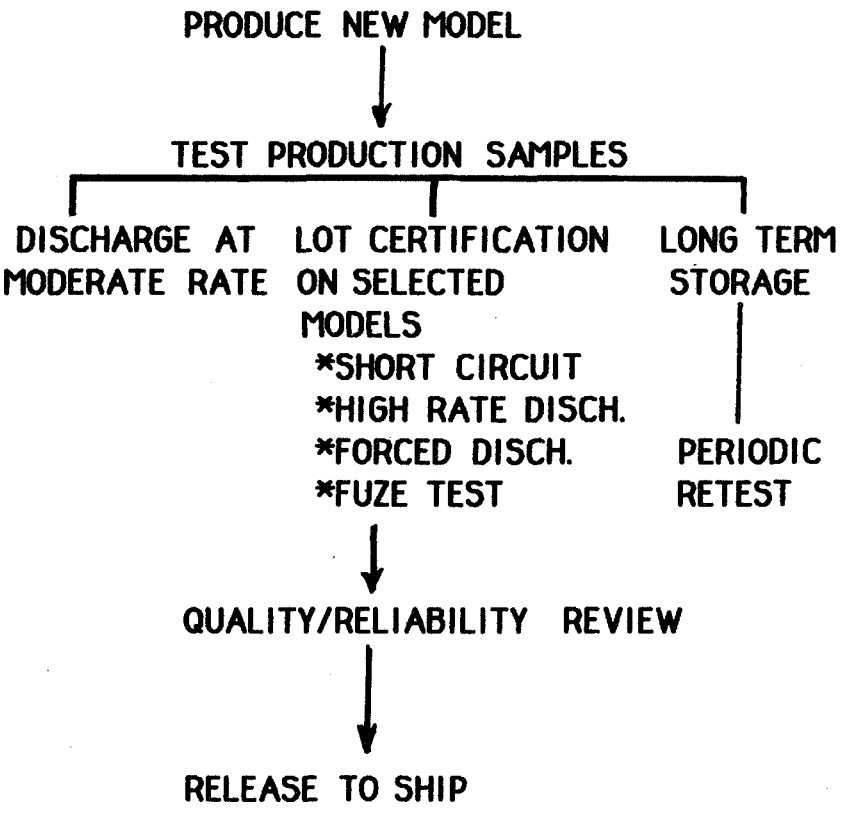

DESIGN EVALUATION OF HIGH RELIABILITY LITHIUM BATTERIES

Richard C. Buchman,
William D. Helgeson
and Naim S. Istephanous

Energy Technology, Division of Medtronic, Inc.

INTRODUCTION

High reliability batteries are required not only for space applications but also for implantable medical devices as well. In this paper, I will be discussing the techniques used by Medtronic to evaluate high reliability lithium batteries for implantable applications.

Medtronic, Inc., through its Energy Technology division, began manufacturing lithium batteries for implantable device applications in 1977 with the introduction of its lithium-iodine system. Manufacture of lithium-thionylchloride batteries for use in higher current drain applications such as implantable drug pumps and pain control devices began several years later. Because of these applications, the evaluation of each battery design is very important and it is performed with a high reliability goal in mind.

BACKGROUND

Once a new battery design has been established and assembly procedures finalized through prototype test builds, the design must successfully complete a three stage evaluation program. The first stage, design qualification, involves a large battery build intended as the qualification set for the final battery design. Within the next year, production qualification tests begin on actual production batteries. Concurrent with these qualification programs, real time or long term discharge tests are also initiated. The data, along with the qualification program results, are then used to project battery longevity and generate reliability data for each battery design. By utilizing this evaluation sequence, a lithium battery can be verified as capable of meeting the high reliability requirements demanded in applications such as space or implantable medical devices.

TEST METHODS AND RESULTS

The typical design qualification program consists of accelerated discharge tests, calorimetry measurements, environmental exposure, destructive analysis and materials compatibility

and corrosion resistance testing. Accelerated discharge is performed at 37°C under various constant current conditions in large walk-in ovens with the batteries positioned in various orientations. Figure 1 shows the voltage behavior of a lithium-iodine battery at current drains of 50-400μA as a function of delivered capacity. The data are then used to construct a mathematical model to project battery longevity at application rates.

During the accelerated discharge tests, several cells from specific tests are periodically monitored for heat output on a Tronac model 315RA calorimeter. The heat output, corrected for polarization effects, for a lithium-iodine battery and a lithium-thionylchloride battery are shown in Figures 2 and 3 respectively. Assuming the heat output is self-discharge related, and after correcting for the entropic heat effect, the capacity loss can be determined and included in the longevity projection calculations.

Environmental exposure tests are performed on all battery designs to simulate worst case conditions the battery might experience during shipping and handling. These tests include subjecting batteries to various combinations of +60 and -40°C temperature extremes combined with mechanical shock and vibration testing, followed by electrical discharge. Abuse tests such as over-discharge, charge, short circuit and shock are also performed on the thionylchloride batteries to determine safety characteristics. Destructive analysis tests are completed to verify the batteries are constructed according to the design engineer's specifications.

The compatibility of all battery components with the reactive electrode and electrolyte materials is best determined by accelerated and actual temperature exposures over the projected battery lifetime. At pre-determined time intervals, several batteries are removed from application rate discharge at 60 and 37°C and the various components shown in Table 1 are examined for signs of corrosion and chemical degradation utilizing scanning electron microscopy, Auger electron spectroscopy, X-ray spectroscopy and other metallurgical and chemical techniques.

Of the indicated phenomena of interest, degradation of the glass in the feedthrough is important, particularly in liquid electrolyte systems. Figure 4 shows a scanning electron micrograph of a typical glass seal from a fresh battery, while Figure 5 shows a glass seal from a liquid electrolyte lithium battery from another manufacturer after approximately 3.6 years exposure. The exposed feedthrough shows extensive glass fragmentation across its entire surface.

This phenomenon has led to premature battery failure in various liquid electrolyte systems. To test for this problem, several of my colleaques have recently developed a technique that examines glass degradation in a matter of weeks instead of years. This technique, detailed at the Fall ECS meeting in New Orleans, involves sputtering nickel onto glass slides, discharging them in the electrolyte of interest and monitoring the current during discharge. SEM/x-ray spectra techniques can then be used to characterize the reaction products.

The last step in the design evaluation involves real time or long term discharge tests. The batteries required for these tests originate from the design qualification build and time samples of production battery builds. Figure 6 compares the real time discharge results for a lithium-iodine battery to the longevity projection. The real time data are tracking the projected curve very well, just as other lithium-iodine battery designs have tracked their projected curves during the past eight years of using this technique. We therefore believe battery lifetime can be reliably forecast after one year of testing instead of the five to ten years typically required to discharge the battery at the application rates.

One method of examining the reliability of batteries at application rate is the calculation of the random failure rate. A summary of random failure rate data for three general lithium-iodine battery designs are indicated in Table 2. Nearly 4400 Type A batteries on laboratory test have accumulated 230 million hours at a random failure rate of 0.0023%/month at a 90% confidence level. With this low rate, this battery design is exhibiting a reliability comparable to silicon transistors and diodes. Type B and C batteries are also accumulating significant device hours with similar low random failure rates.

CONCLUSIONS

Within one year, a lithium battery design can be qualified for device use through the application of accelerated discharge testing, calorimetry measurements, real time tests and other supplemental testing. Materials and corrosion testing verify that the battery components remain functional during expected battery life. By combining these various methods, a high reliability lithium battery can be manufactured for applications which require zero defect battery performance.

Table 1. MATERIALS AND COMPONENTS PERFORMANCE ASSESSMENT.

COMPONENT	PHENOMENA OF INTEREST
METALLIC	• CORROSION — TYPE AND EXTENT (IF ANY)
NON—METALLIC	• CHEMICAL STABILITY AND STRUCTURAL INTEGRITY, INSULATION PROPERTIES
FEEDTHROUGH	• GLASS DEGRADATION • SEAL HERMETICITY
WELD JOINTS	• LOCALIZED CORROSION • INTEGRITY • PENETRATION AND FUSION

Table 2. RANDOM FAILURE RATES FOR LITHIUM IODINE BATTERIES

BATTERY	INITIAL SAMPLE	MAX. YEARS	DEVICE-HOURS	RANDOM FAILURE RATE (%/MO.)
TYPE A	4350	8.9	230×10^6	0.0023 *
TYPE B	1887	5.9	84×10^6	0.0034
TYPE C	1355	5.4	37×10^6	0.0045
SILICON TRANSISTORS				0.0028
SILICON DIODES				0.0011

*LOWEST RFR PRIOR TO NATURAL END-OF-LIFE.

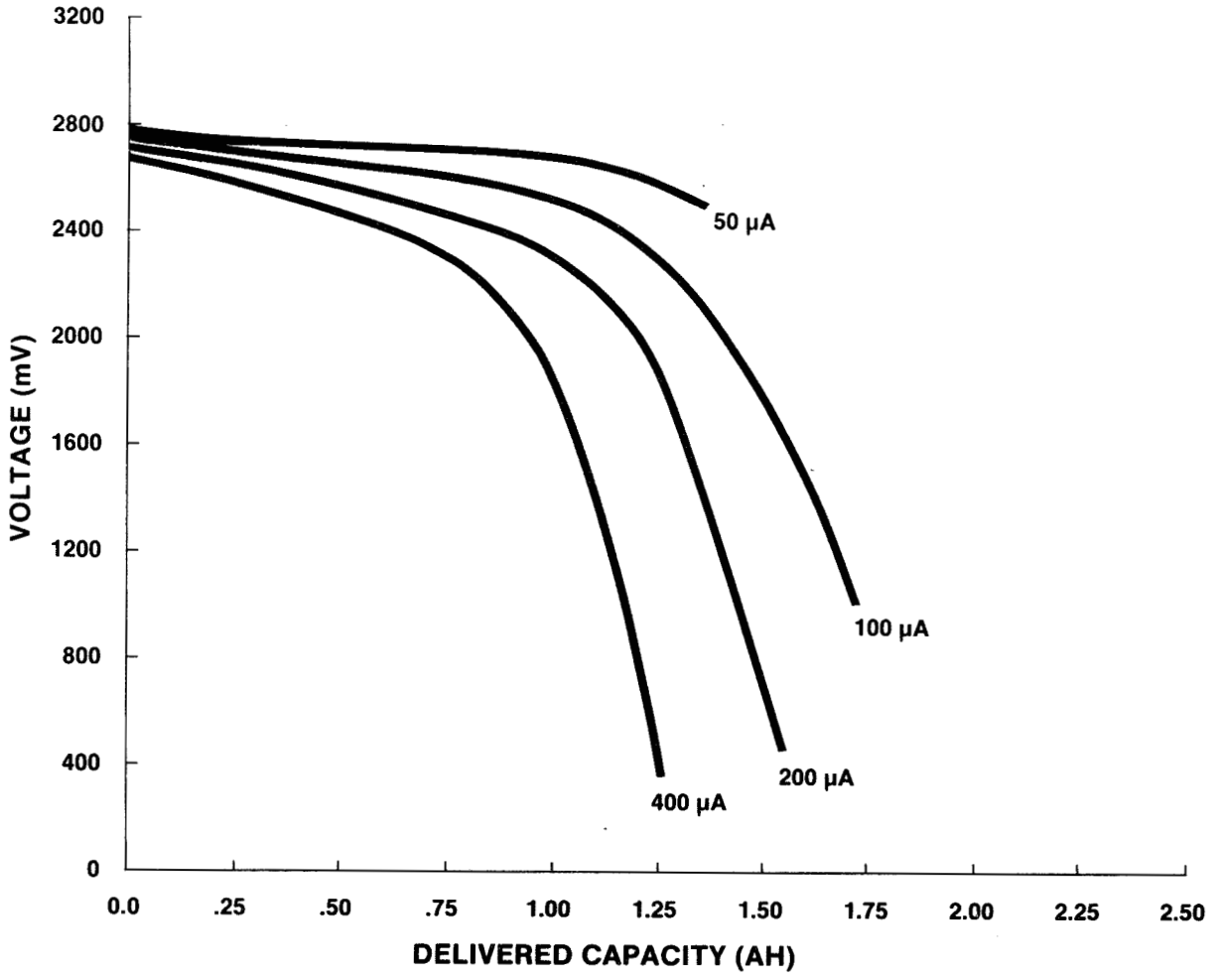

Figure 1 - Accelerated Discharge of a Lithium Iodine Battery.

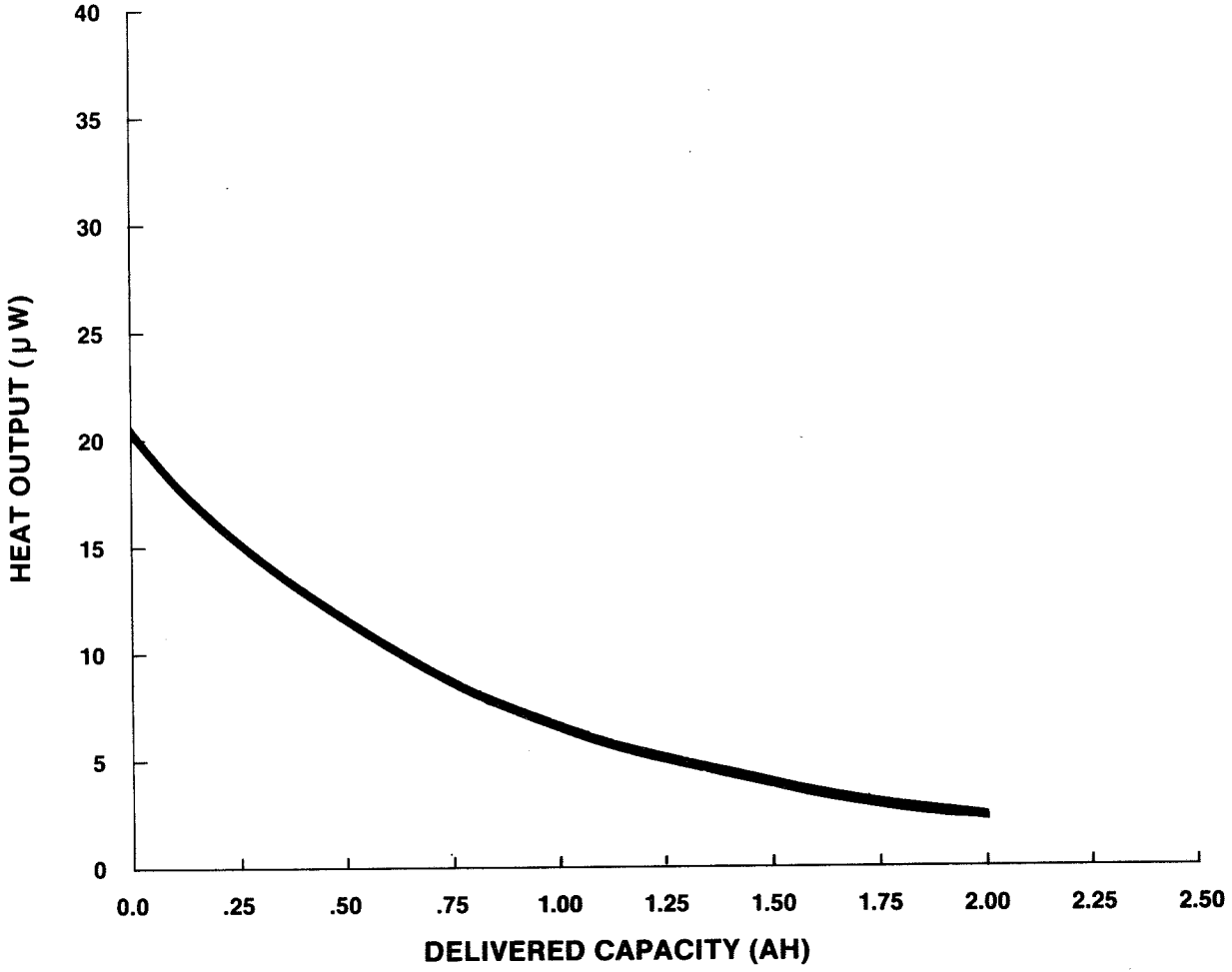

Figure 2 - Heat Output vs. Delivered Capacity-Lithium Iodine Battery.

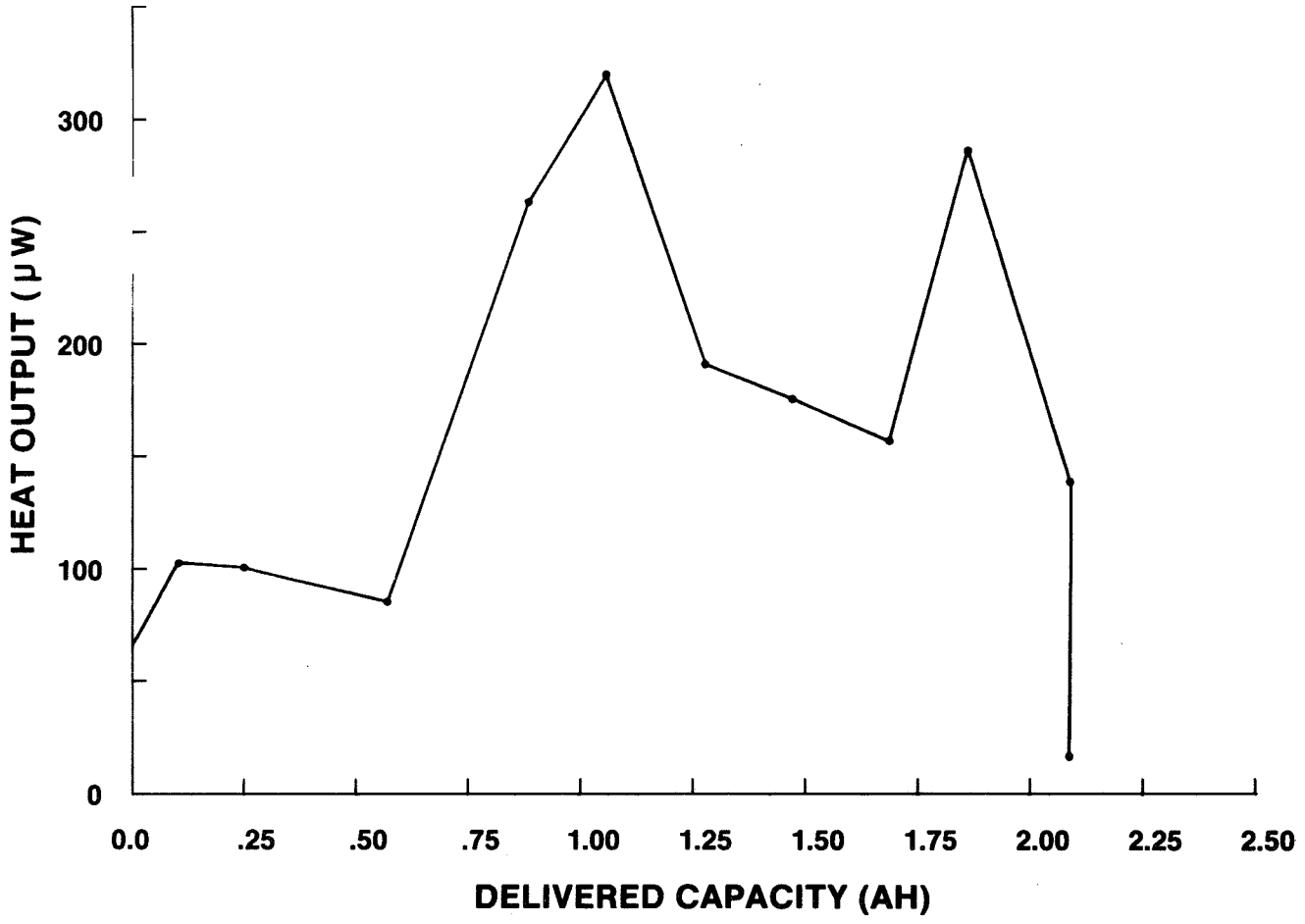

Figure 3 - Heat Output vs. Delivered Capacity-Lithium Thionyl Chloride Battery.

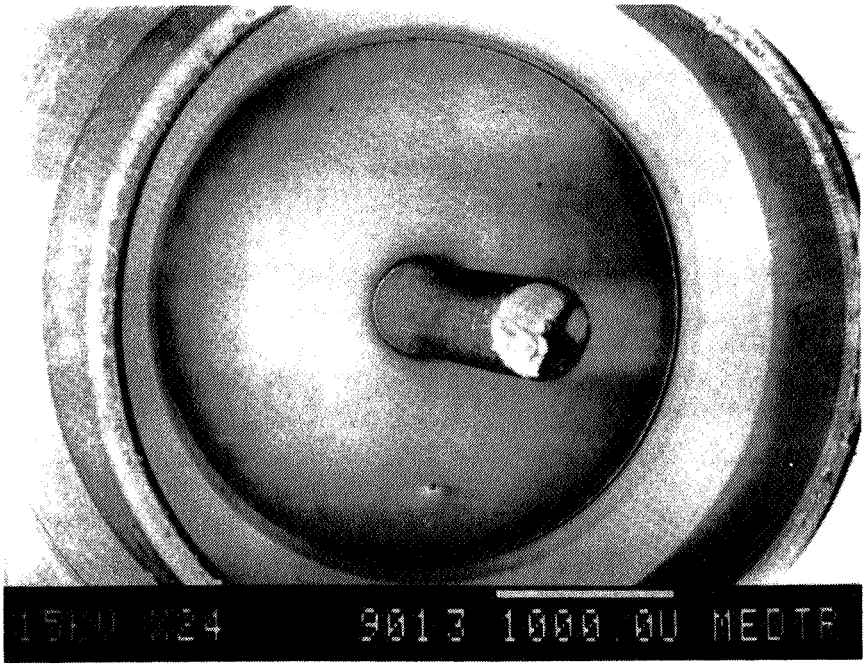

Figure 4. Glass Seal From Fresh Battery

Figure 5. Glass Seal After Exposure to Liquid Electrolyte

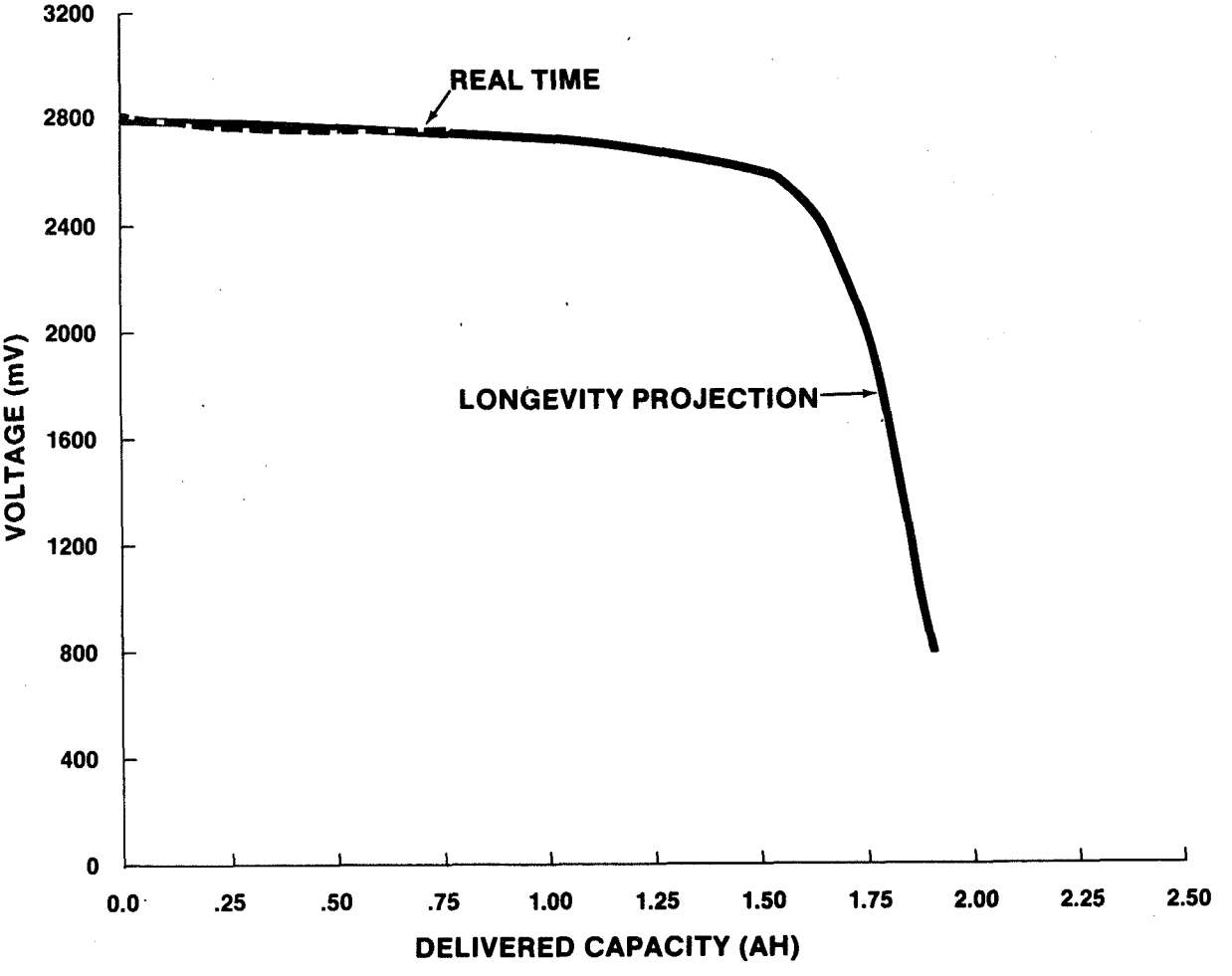

Figure 6 - Realtime Discharge Results For a Lithium Iodine Battery.

GALILEO BATTERY TESTING

AND THE IMPACT OF TEST AUTOMATION

Walter T. Pertuch and C. Thomas Dils
Honeywell Power Sources Center

ABSTRACT

Test complexity, changes of test specifications, and the demand for tight control of tests led to the development of automated testing used for Galileo and other projects at Honeywell. The use of standardized interfacing, i.e., IEEE-488, with desktop computers and test instruments, resulted in greater reliability, repeatability, and accuracy of both control and data reporting. Increased flexibility of test programming has reduced costs by permitting a wide spectrum of test requirements at one station rather than many stations.

INTRODUCTION

Throughout the 1960's and early 1970's, battery testing was frequently done with some rather basic equipment, such as the VTVM (Vacuum Tube Voltmeter), source current driven recorders, carbon and wire-wound resistors, and bulky constant current power supplies. Precision and accuracy were somewhat limited and often cost prohibitive.

The more complex test parameters and high accuracy requirements were usually met with the design and build of dedicated test stations. These custom stations would include the use of hybrid circuits composed of vacuum tube, transistor, early generation integrated circuit, and mechanical designs, such as cams, relays, and stepping switches. Profile discharge testing required the use of multiple load elements--constant current supplies, resistors, etc. The resulting test station yielded more accurate data and improved test repeatability.

The disadvantages to such systems were as follows:

- Could be cost prohibitive except in certain production applications
- Major test specification changes frequently required major hardware changes (timing control, load profile sequencing, or the addition/deletion of loads)
- Reuse of test station subassemblies is limited

Rapid advances in electronics technology have created the need to have more exacting test techniques. Military, space, commercial, and bio-medical electronics continue to demand self-contained power sources, i.e., batteries. Consequently, the testing of these batteries must closely approximate the application for which they are designed. One such application is that of the

battery designed for powering the instrumentation contained in the Jupiter probe of the Galileo Project. Developing a suitable testing method became an immediate challenge.

THE MODULAR TEST STATION

THE LOAD SIMULATOR

A load simulator is an electronic instrument which is designed to simulate electrical loads to test power supplies, batteries, and other similar power sources. Many commercially available units can synthesize the load parameters of both constant current and fixed resistance which may be varied over a wide range determined by the specification limits of each design. The power is dissipated by a bank of parallel connected power transistors. For constant current, regulation is achieved by feedback circuits which sample current. In the case of fixed resistance, feedback circuits sample current and load voltage.

REMOTE PROGRAMMING

In practice, load simulators can be programmed to change loads by means of an external input from a variable precision voltage source. For example, a programming input of 0-10 Vdc could correspond to 0-50 Adc or 5 amps/volt as a programming sensitivity. The load simulator can thus be used to replace multiple loads if programming voltages and timing are properly sequenced.

EARLY GALILEO PROFILE TESTING

A multi-segment (8 independent output levels) function generator was calibrated to drive the load simulator at current levels similar to those shown in Table I. With the aid of a clock, the test operator manually sequenced profile changes. A second simulator and voltage source was used to load the pyro bus (the pyrotechnic load tap on the Galileo battery).

Advantages were as follows:

- Equipment usually required no extensive modification if load or timing specifications changed.
- Equipment could be used on a larger variety of tests (multi-device).
- The need for custom control circuits was reduced.

Disadvantages were as follows:

- Most load changes were done manually. The prototype module discharge tests required 17 manual load switching operations and 42 manual logging functions.

- The function generator was complicated--instructions were a translation to English from another language.
- The risk of error from set-up and control was high.
- Instrumentation drift approached tolerance limits.

ASSESSING THE TEST SITUATION

The use of manual control and the load simulator/function generator test set-up presented problems in conducting many discharge tests over a period of many months. These problems were identified as operator-related and set-up or equipment failures.

THE DESKTOP COMPUTER AND THE IEEE-488 INTERFACE

SEARCHING FOR A BETTER METHOD

After much consideration, Honeywell decided to purchase a desktop computer system and instrumentation that could be controlled by the IEEE-488 interface bus or GPIB (General Purpose Interface Bus). This standard has been accepted internationally and many test instrument manufacturers offer this capability as an option.

APPLICATION DEVELOPMENT

The desktop computer system and instrumentation was initially used for data acquisition. The new system capabilities expanded to not only acquire data, but also to control events, and by adding a power supply programmer (a precision GPIB controlled voltage source) and other instrumentation, we could eliminate the function generator and manual control.

MOST RECENT IMPROVEMENTS TO TEST CAPABILITIES

EQUIPMENT

The Test Group has recently added interface capability to a previously purchased datalogger and increased the number of available load simulators giving a wide range of current and power handling ability. Our most recent capital item was a GPIB compatible digital storage scope for recording high speed, high resolution transient data, and used on the most recent Lot 4 module descent test in July 1984.

OTHER APPLICATIONS

Similar equipment is being used internally for low frequency analysis in cell storage studies and dynamic impedance measurements on the same tests. Virtually all groups within our organization are using desktop systems and special instruments or peripheral equipment to improve work efficiency and to help maximize the repeatability of certain critical operations.

IMPACT ON THE GALILEO PROGRAM

The benefits to the Galileo Program are as follows:

- Testing personnel was reduced from 4 to 2 to conduct descent tests; one to observe and one to adjust a chamber to follow a specified temperature profile which is not yet automated.
- Manual load operations were reduced from 17 to 2; main bus connect and pyro bus connect.
- There is flexibility to changing specifications.
- Test reliability is high with no significant deviations in eight major tests; test duration is 150 days from background loading to the descent profile.
- Methods and equipment contribute to tight control of test parameters.
- In the Galileo cell storage program, we are using some of the same test equipment to log voltage and AC impedance on over 1000 cells each month.
- The test equipment and techniques are understood by Honeywell Power Sources Center and the customer.

SUMMARY AND CLOSING STATEMENTS

Facing the challenge of the Galileo program allowed us the opportunity to develop a better method which grew out of the concept of modular testing systems. We maintain full coverage of environmental chambers through an alarm system and communication by way of a terminal and modem whereby we can determine the nature of the alarm and take corrective action. We now use uninterruptible power supplies to provide backup to computers in the event of power outages.

Table I. DESCENT SEQUENCE–BATTERY LOAD PROFILE

Start Time	Duration	MOD #1	MOD #2	MOD #3	Pyro Tap
-10.115 sec	15 msec*	← (1)	75Ω	→	N/A
-10.100 sec	100 msec*	600Ω	600Ω	600Ω	N/A
-10.000 sec	10 sec	9.66Ω	9.66Ω	9.66Ω	N/A
0 sec	10 sec	←	1.44A**	→ (2)	N/A
+10 sec	5.527 hrs	←	0.35A**	→	N/A
+ 5.53 hrs	0.72 hr	←	1.52A**	→	N/A
+ 6.24 hrs	35 msec	←	1.52A	→	6.3A
+ 6.25 hrs	0.875 hr	←	9.6A**	→	N/A
+ 6.32 hrs	35 msec	←	9.6A	→	6.3A
+ 6.40 hrs	35 msec	←	9.6A	→	6.3A
+ 6.48 hrs	35 msec	←	9.6A	→	6.3A
+ 6.56 hrs	35 msec	←	9.6A	→	2.5A
+ 6.64 hrs	35 msec	←	9.6A	→	2.5A
+ 6.72 hrs	35 msec	←	9.6A	→	2.5A
+ 6.80 hrs	35 msec	←	9.6A	→	2.5A
+ 6.88 hrs	35 msec	←	9.6A	→	2.5A
+ 6.96 hrs	35 msec	←	9.6A	→	4.5A
+ 7.04 hrs	35 msec	←	9.6A	→	2.5A
+ 7.06 hrs	N/A	Specified End of Mission			N/A

* Pulse duration tolerances

15 msec	15 to 35 msec
100 msec	90 to 110 msec

Pulses to be overlapped to prevent "load gap"

** ← n →
Indicates load n applied across battery through isolation diodes (Constant Current).

(1) Place 75Ω across battery, add 600Ω to each module, add 9.8Ω in parallel to 600Ω. Remove resistance, then initiate 1.44 Amps.

(2) Maximum of 1 sec OCV between 9.66Ω and 1.44 Amps.

NOTE: Specification taken from Descent Test Procedure, GAL-H-0014.

RAY-O-VAC BR2325
LITHIUM CARBON MONOFLUORIDE
CELL PERFORMANCE

Joseph K. McDermott
Martin Marietta Denver Aerospace
Denver, Colorado

ABSTRACT

RAY-O-VAC currently markets a 160 mAH lithium cell recommended for usage in watch and calculator products. The lithium carbon monofluoride cell offers an extended shelf life with no reduction in performance effectiveness. The BR2325 cell has aerospace applications for memory devices and telemetry systems. Over one-hundred thirty (130) cells were purchased and tested for evaluation purposes. This paper reviews the test statistics and overall cell performance of the RAY-O-VAC BR2325 lithium carbon monofluoride cell.

INTRODUCTION

The RAY-O-VAC BR2325 lithium monofluoride cell is a commercially available product recommended for usage in watch and calculator products. The cell has a nameplate capacity of 160 mAH (13,000 Ohms at 21°C to 2.0 V), a volume of 1.04 cc and a weight of 3.1 grams. The button cell dimensions, depicted in Figure 1, comply with the proposed industry standard sizes for lithium cell utilized for watch and calculator products (ref 1). Figures 2 and 3 depict advertised discharge characteristics for varying loads and temperatures.

The RAY-O-VAC BR2325 cell has possible applications for memory backup and telemetry systems. The most important features of any battery power system are first, reliability, and second, the ability to deliver energy with a good volumetric efficiency. Most lithium cells, including the BR2325, fulfill the second requirement but have not clearly demonstrated the first. Therefore, a goal of the test program was to establish a reliability data base for consideration of the monofluoride cell for future aerospace usage. Another important feature of a lithium power system, due to the historical backgound of lithium couples, is the safety considerations associated with the lithium battery. The fact that not all lithium cells/batteries are hazardous is demonstrated by the existence of certain lithium batteries, such as the BR2325, in the commercial market (ref 2).

The procurement of 130 BR2325 cells specified the cells be manufactured from the same lot and on the same day. The cells were manufactured 08 April 1983 at the RAY-O-VAC Corporation in Madison, Wisconsin. The testing facilities, test plan and test statistics are reviewed in the following paragraphs.

TEST FACILITIES

The evaluation testing of the RAY-O-VAC BR2325 cells was conducted at the Experimental Battery Test Facility (EBTF), a dedicated facility for performing testing and evaluation on experimental battery types such as high energy density lithium batteries. The facility is equipped with seven temperature test chambers and a dedicated data acquisition system. Each of the test chambers is capable of maintaining temperatures of minus 40°F to plus 350°F. The chambers have been modified to accommodate six modular test fixtures designed for cells such as the BR2325. The chamber test patch panel, mounted externally, is the interface point for the Data Acquisition System and the mounting location for the test load resistors.

The EBTF Data Acquisition System consists of a 420 channel Fluke Model 2240C Data Logger, a Commodore PET computer and a Texas Instrument Silent 700 Electronic Data Terminal. This system, depicted in Figure 4, is controlled by the test monitoring software resident in the 32K PET computer. All test data, including cell voltages and chamber temperatures, is monitored approximately every two minutes. When a data recording is required, as determined by cell voltage rate of change or prescribed data record interval, the data record is transmitted to the electronic data terminal where it is recorded on cassette magnetic tape and printed on hardcopy.

TEST PLAN

The test plan for the RAY-O-VAC BR2325 cells is summarized in Table 1. The cells were tested at six discharge rates and five temperatures. Twelve cells were placed in ambient storage for 6 months and six cells for 12 months to measure the effect of long term storage on the BR2325 cell.

TEST SUMMARY

The average capacities for the BR2325 cell as a function of temperature and discharge rate are summarized in Tables 2 and 3. Typical discharge curves for the five test temperatures at the 30 day discharge rates are provided in Figures 5 through 9. Figure 5 illustrates the voltage sensitivity of the BR2325 cell to test temperature changes for the low temperature ($-10^{o}F$) test. The voltage sensitivity versus test temperature changes was not as pronounced for the other test plan temperatures. As expected, the RAY-O-VAC BR2325 cell generally provided the greatest capacity at the $+75^{o}F$ test temperature. The capacities obtained at the various discharge rates and temperatures generally agreed with the RAY-O-VAC literature on the lithium carbon monofluoride cell.

The effect of long term storage on the cell performance of the BR2325 cell is negligible. Figure 10 depicts the discharge profile for the median cell from the 12 month storage test group. The cell performance was nearly identical to the performance of a cell not subjected to long term storage.

CONCLUSIONS

The overall cell performance of the RAY-O-VAC BR2325 lithium carbon monofluoride cell was acceptable from a statistical viewpoint. The coefficient of variation was generally below 5% and the standard deviation was generally less than 10 milliampere-hour for the five cell test groups. The statistical uniformity is attributed partly to the fact the cells came from the same manufacturing lot.

The low capacities at $-10^{o}F$ can be attributed to the rate reductions of the energy producing chemical reactions within the lithium carbon monofluoride cell. The voltage stability at the low temperature was excellent provided the test temperature of $-10^{o}F$ was stable. The voltage sensitivity to test temperature changes for the high temperature tests was minimal. The reduced capacities at the high temperature are attributed to the speed up in battery deterioration.

The BR2325 cell appears to be a viable candidate for aerospace applications for memory devices and telemetry systems. The cells tested were "off the shelf" hardware which uniformally supported the resistive loads. A special build of the RAY-O-VAC BR2325 cell for a particular aerospace application should provide a reliable energy storage system.

REFERENCES

1. Crompton, T. R., Small Batteries Primary Cells Volume 2, John Willey and Sons, Inc., New York, 1983.

2. Smith, J. J., "Research Issues in Future Navy Lithium Inorganic Electrolyte Batteries for Navy Application", Naval Undersea Center TP 564, February 1977.

Table 1. RAY-O-VAC BR2325 LITHIUM CARBON MONOFLUORIDE TEST PLAN

Discharge Rate	Resistive Load (Ohms)	Discharge Current (mA)	Test Temperature
53 Hrs	905	3.0	+ 32°F
53 Hrs	905	3.0	+ 75°F
53 Hrs	905	3.0	+ 120°F
80 Hrs	1330	2.0	+ 32°F
80 Hrs	1330	2.0	+ 75°F
80 Hrs	1330	2.0	+ 120°F
160 Hrs	2745	1.0	+ 32°F
160 Hrs	2745	1.0	+ 75°F
160 Hrs	2745	1.0	+ 120°F
30 Days	12 K	0.22	- 10°F
30 Days	12 K	0.22	+ 32°F
30 Days	12 K	0.22	+ 75°F
30 Days	12 K	0.22	+ 120°F
30 Days	12 K	0.22	+ 160°F
90 Days	36.4 K	0.074	- 10°F
90 Days	36.4 K	0.074	+ 32°F
90 Days	36.4 K	0.074	+ 75°F
90 Days	36.4 K	0.074	+ 120°F
90 Days	36.4 K	0.074	+ 160°F
180 Days	75 K	0.037	- 10°F
180 Days	75 K	0.037	+ 32°F
180 Days	75 K	0.037	+ 75°F
180 Days	75 K	0.037	+ 120°F
180 Days	75 K	0.037	+ 160°F
Storage 8 months	36.4 K	0.074	+ 75°F
Storage 10 months	36.4 K	0.074	+ 75°F
Storage 12 months	36.4 K	0.074	+ 75°F

Table 2. AVERAGE CAPACITY TO A 2.0 VOLTAGE CUTOFF

Discharge Rate	Test Temperature °F				
	-10	32	75	120	160
53 Hrs (3.0 mA)		081	110	170	
80 Hrs (2.0 mA)		087	122	165	
160 Hrs (1.0 mA)		098	142	155	
30 Days (0.22 mA)	043	146	173	168	141
90 Days (0.074 mA)	086	155	137	146	102
180 Days (0.037 mA)	093	169	171	130	104

Table 3. AVERAGE CAPACITY TO A 0.2 VOLTAGE CUTOFF

Discharge Rate	Test Temperature °F				
	-10	32	75	120	160
53 Hrs (3.0 mA)		149	149	172	
80 Hrs (2.0 mA)		152	158	172	
160 Hrs (1.0 mA)		152	167	169	
30 Days (0.22 mA)	073	171	174	170	148
90 Days (0.074 mA)	103	172	174	149	127
180 Days (0.037 mA)	130	171	172	142	136

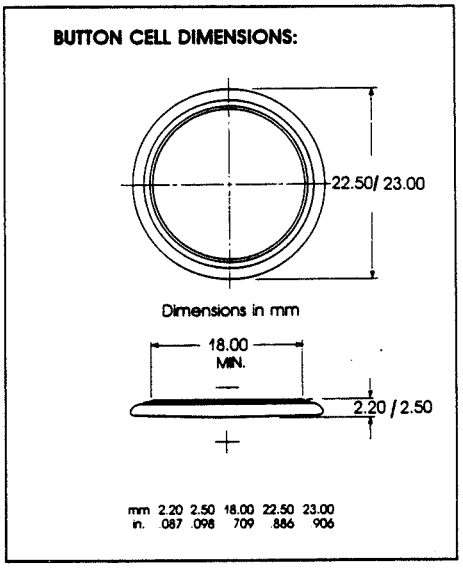

Figure 1. Ray-O-Vac BR2325 Cell Dimensions

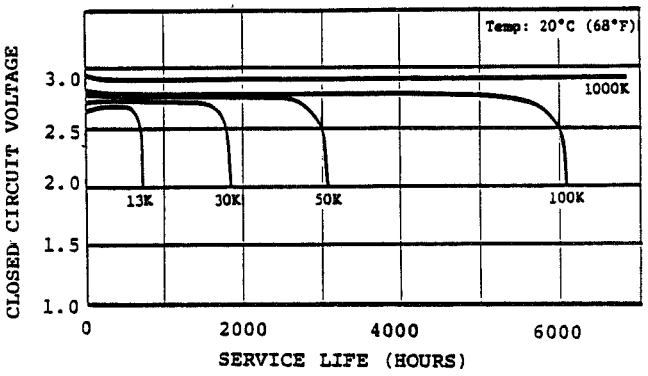

Figure 2. Ray-O-Vac BR2325 Service Life Versus Load

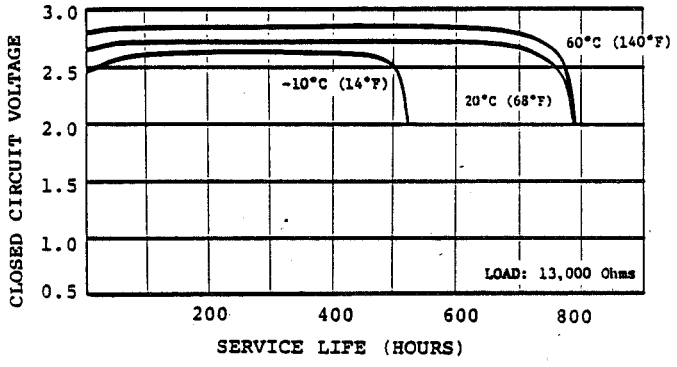

Figure 3. Ray-O-Vac BR2325 Service Life Versus Temperature

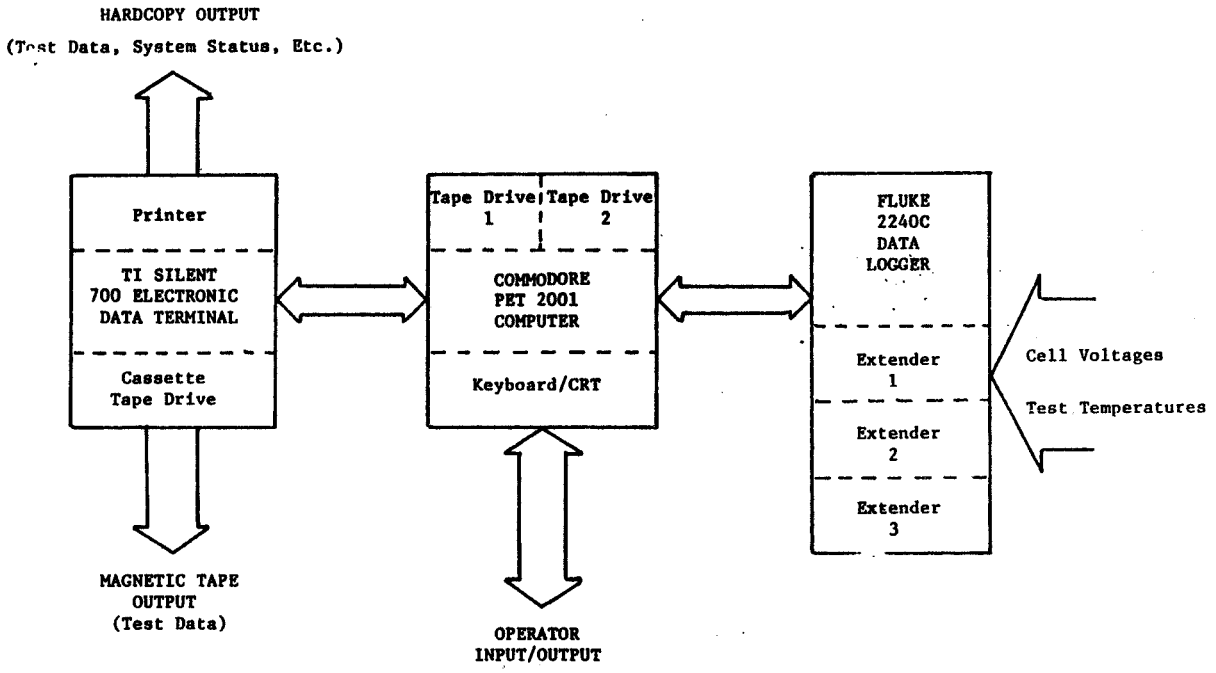

Figure 4. EBTF Data Acquisition System

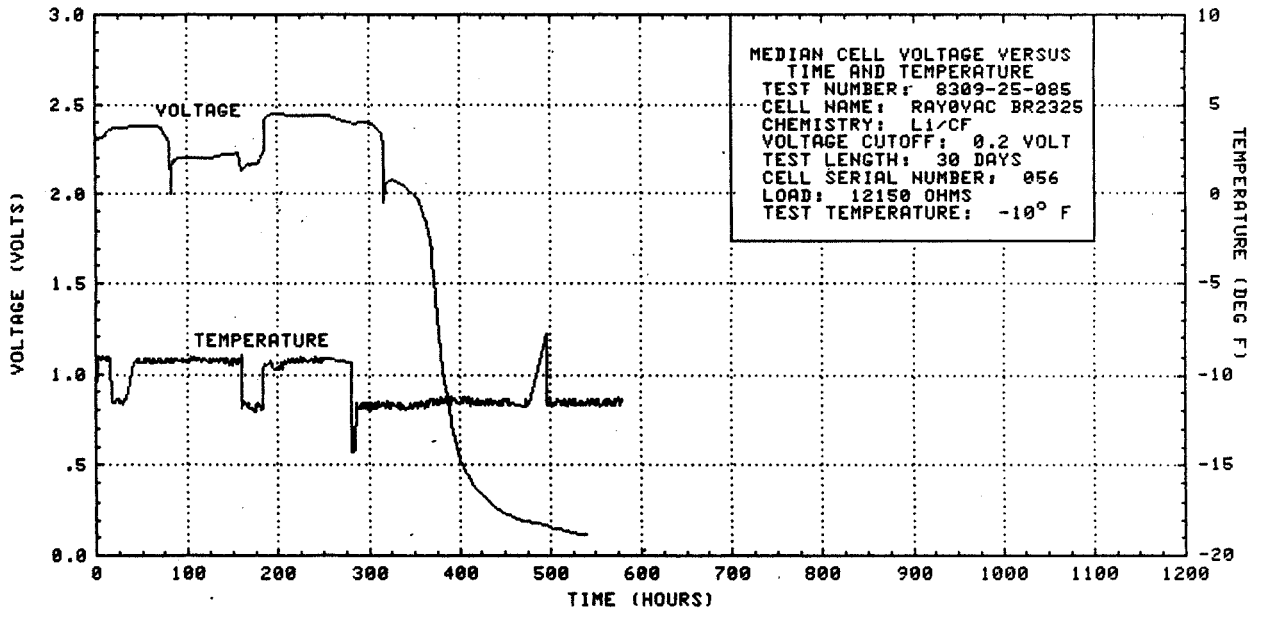

Figure 5. Median Cell Voltage Versus Time and Temperature, -10°F

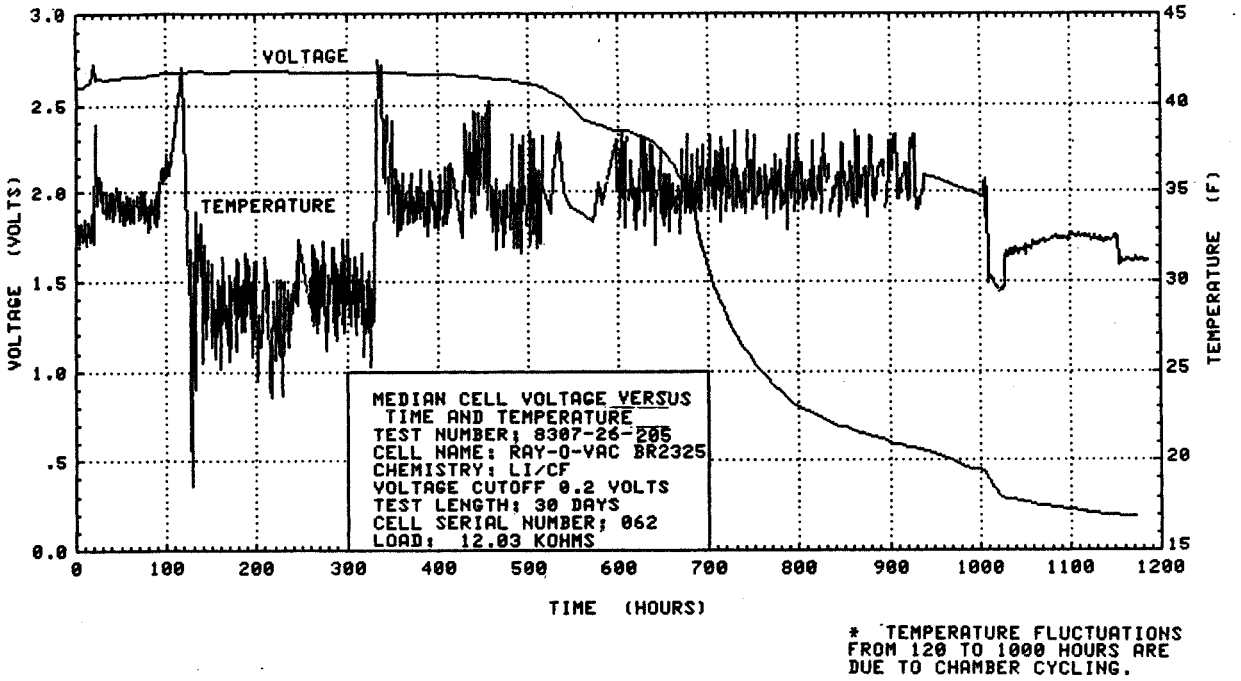

Figure 6. Median Cell Voltage Versus Time and Temperature, 32°F

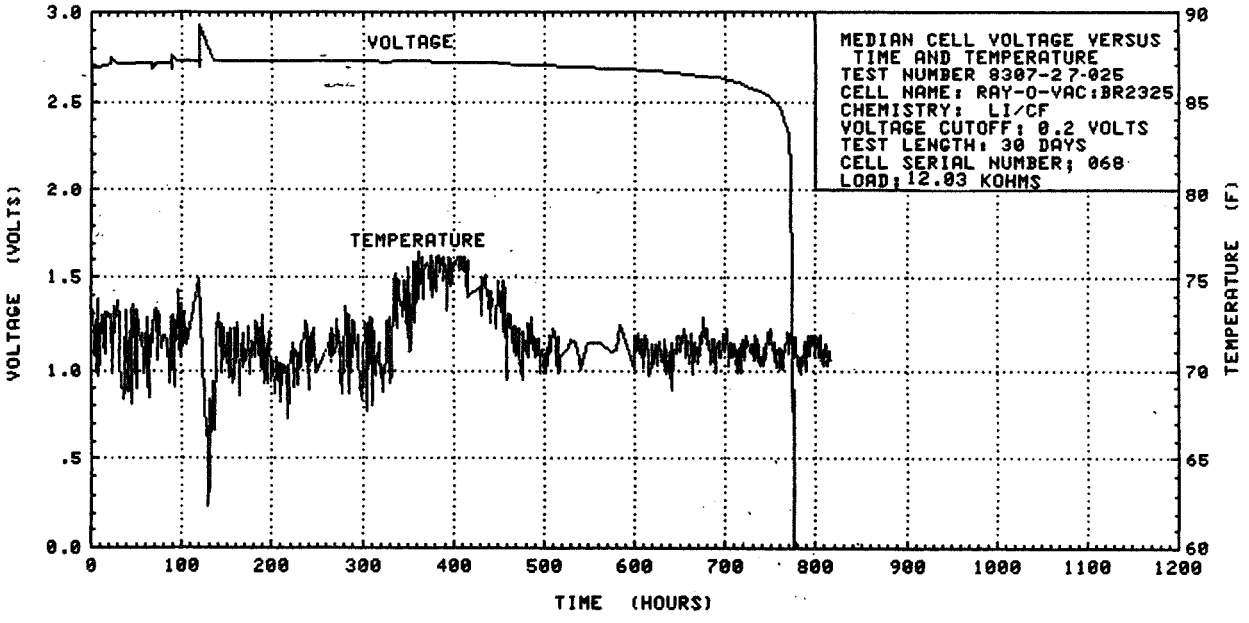

Figure 7. Median Cell Voltage Versus Time and Temperature, 75°F

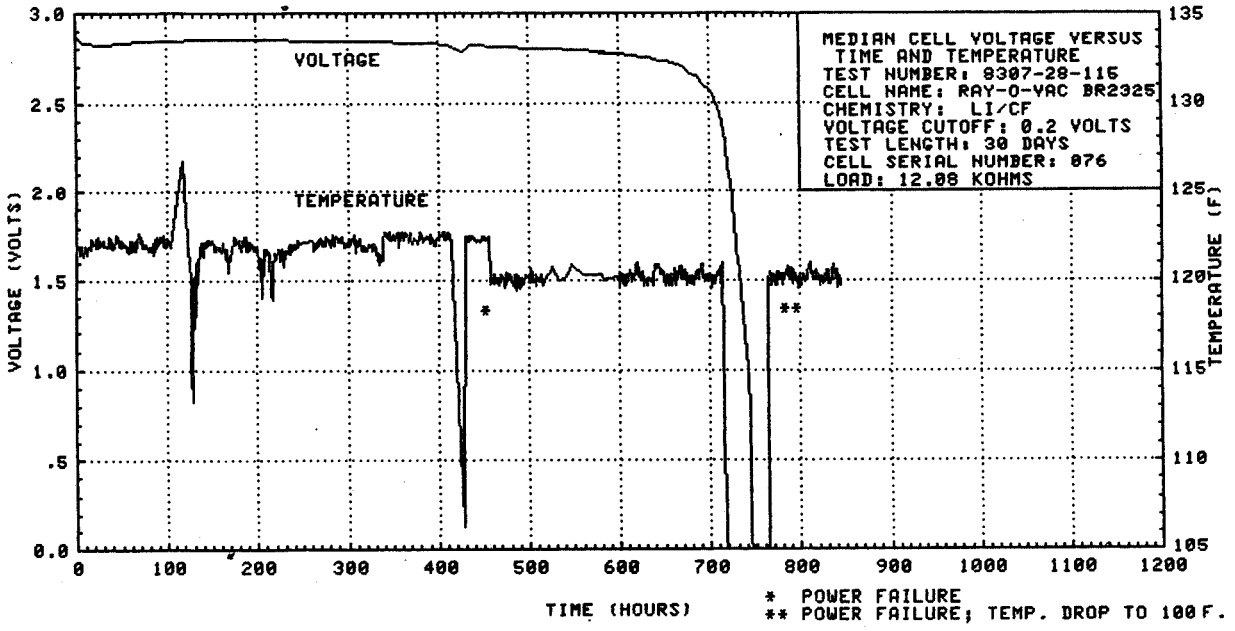

Figure 8. Median Cell Voltage Versus Time and Temperature, 120°F

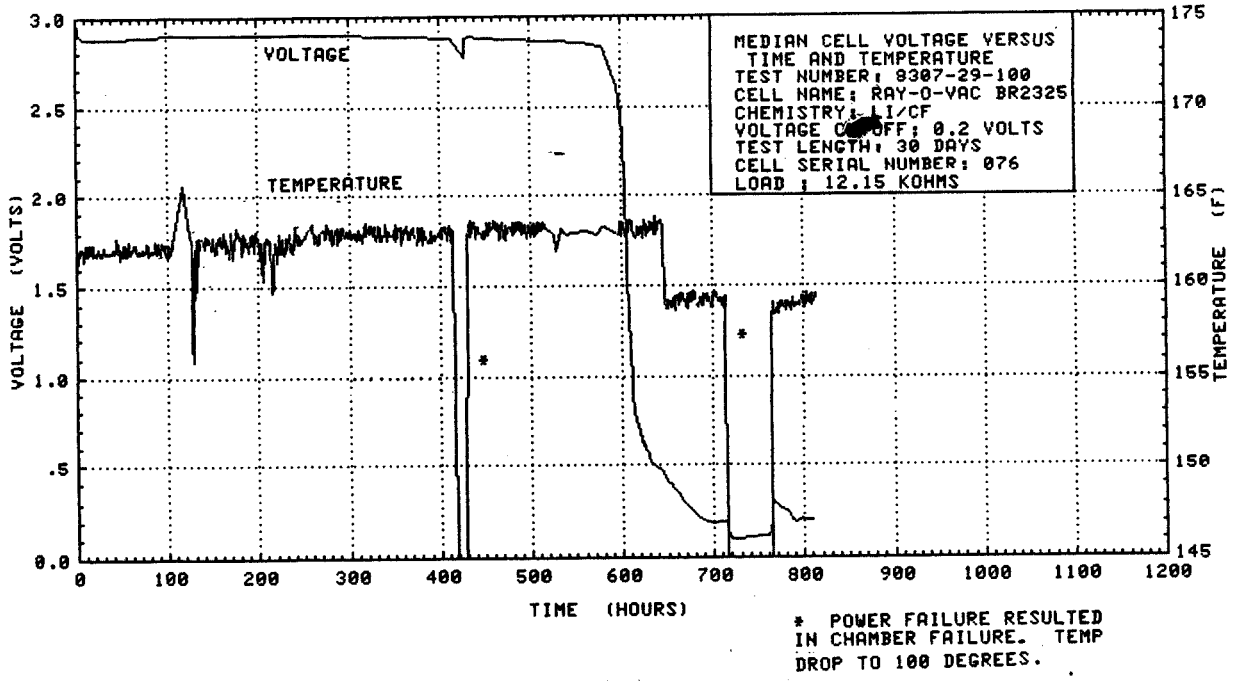

Figure 9. Median Cell Voltage Versus Time and Temperature, 160°F

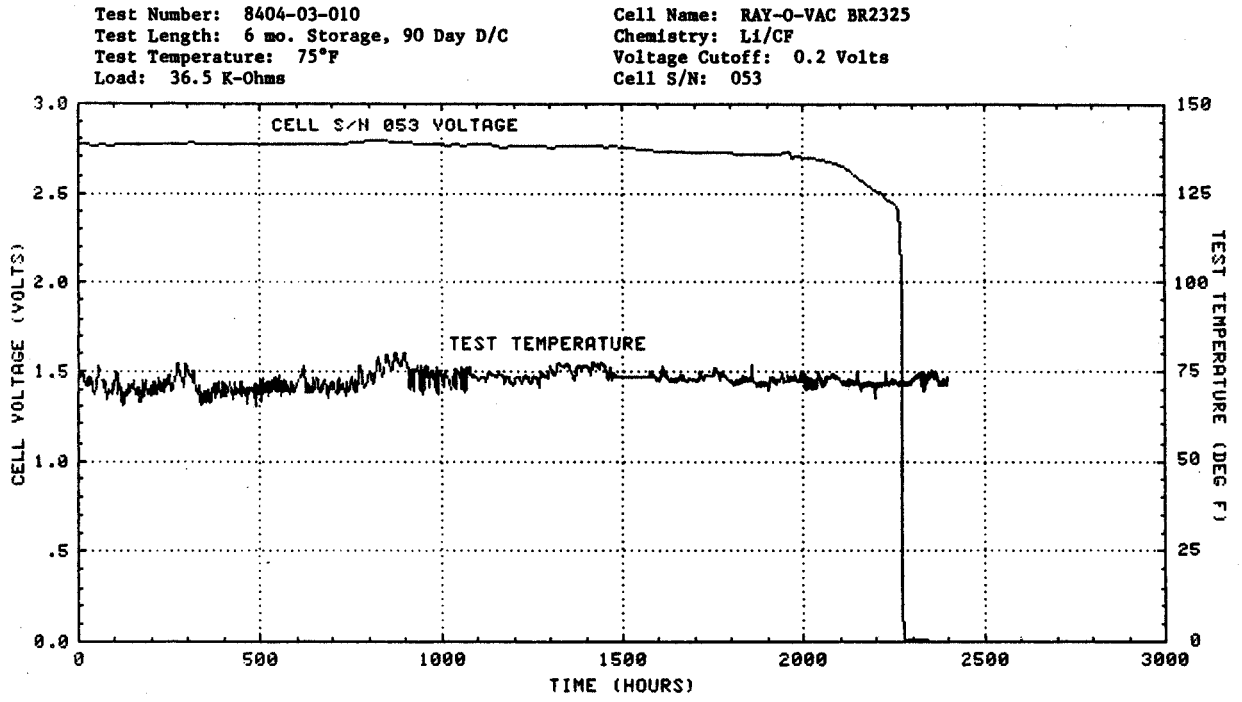

Figure 10. Median Cell Voltage Versus Time and Temperature, 6 Month Storage

Safety of Li-$SOCl_2$ Cells

S. Subbarao
G. Halpert

Jet Propulsion Laboratory

The safety of lithium thionyl chloride cells has been a concern of JPL for some time in our development of these cells for NASA's use. Because the safety problems are complex and several issues are interrelated it was decided that it would be best to put together an organized review of the safety issues. This paper is intended to address these issues.

Figure 1

In the first viewgraph we point out that we are aware of certain problems that limit the use of Li-$SOCl_2$ cells. These include the unsafe behavior, poor performance at high rates and the fact that at the present time the cells do not meet the reliability requirements for space use.

Figure 2

Generally, hazards can be classified in three broad categories; 1) cell leakage - a problem dealing with construction or materials, 2) venting of toxic gases through seals and welds - considered a mild hazard in which electrolyte and gas is released and 3) the unfortunate violent rupture or controlled rupture of cell with the possibility of explosion of the materials inside.

Figure 3

The next two viewgraphs are an overview of the areas by which hazards can occur. The first is the user-induced type which as you see from the figure involves the operation of the cell or its equipment. There are also two types of abuse:

1. Electrical
2. Mechanical/physical

As you can see the electrical and mechanical/physical type are considered hazardous.

Figure 4

In the next viewgraph we summarize the conditions for which the manufacturer has responsibility. These are in two areas which are referred to as cell design and/or quality control. We will be talking about these as we go along further in this paper.

Figure 5

The next viewgraph is quite simple in that it merely relates the fact that heat is generated, by drawing current out of the cell or battery; new chemical reactions are initiated and both add to the involvement of the potential hazards.

Figure 6

Here we present the influence of discharge rate on cell performance. First of all we know that the cell can be discharged at the C/10 discharge rate safely provided it is in an environment where the heat can dissipate. Secondly, we note that cell performance decreases as the discharge rate increases. This is seen in both capacity and voltage. The problem arises when we

start to discharge at higher rates and here the cells, if not designed properly and especially without adaquate thermal dissipation, can undergo venting or explosion.

Figure 7

In this chart we break down the influence of discharge rate on safety. As you can see at less than the C/10 rate the cells are safe. At rates of C/10 - C/2 there is a probability of heat buildup as temperature increases, and if temperature increases the pressure increases. Both SO_2 gas and $SOCl_2$ vapor increase thus increasing the possibility of venting if the heat is not adequately dissipated. At very high discharge rates, e.g. > C/2, heat is obviously generated rapidly. The temperature increases, there is a greater possibility of lithium melting and reacting with the $SOCl_2$ and thus there is high probability of venting and violent rupture.

Figure 8

The various explanations reported for the unsafe behavior of Li-$SOCl_2$ cells during discharge fall into three categories. They are pressurization, thermal runaway and hazardous intermediates. The discharge rate causes the internal cell temperature to rise. The gaseous products and $SOCl_2$ vapor expand rapidly, thereby raising the internal pressure of the cell. Secondly, the thermal runaway mechanism is based on the fact that new exothermic reactions can occur at elevated temperatures resulting in a cell rupture or even explosion. Presently it is believed that thermal runaway of a Li-$SOCl_2$ cell is due to the reaction between molten lithium (MP > 191°C) and $SOCl_2$. It has been reported that hazardous

intermediates such as SO, (SO)n, OCLS or Li_2O_2 are formed during discharge which may be responsible for the unsafe behavior of these cells. Many previously discussions have been held on these issues.

Figure 9

What is the affect of temperature? We see that at temperatures of -20 to 60°C cells operate safely as long as the current is less than the C/10 rate. They do lose capacity on storage, particularly at higher temperatures. They can undergo venting or even explosion if they are discharged at temperatures higher than +80°C. They may also exhibit poor performance at lower temperatures.

Figure 10

This chart breaks down the effect of temperture on safety. At low temperatures, conductivity and mass transport in the electrolyte decrease, resulting in increased cell internal impedance (polarization loss) and carbon electrode passivation (capacity loss). Safety problems have not been reported thus far for low temperature operation. For ambient temperature conditions, refer to figure 8. At the higher temperatures (> +80°C), even at low rates , gas expands, pressure increases and venting is probable. At +130°C, sulfur can react with $SOCl_2$ to give extra heat, again the pressure increases and venting probable. At +181°C or greater we know that the lithium melts and can react with the constituents of the cell, especially thionyl chloride. It is possible that there could be a violent

rupture.

Figure 11

In this figure we summarize the causes for unsafe behavior at low and high temperatures. At low temperatures, it suggests that an increase in polarization due to IR and an increase in stability of hazardous intermediates are possible which at high rates can lead to hazardous conditions. At high temperatures, higher pressures leading to venting is possible. Thermal runaway is also possible when violent reactions,such as molten lithium reacting with $SOCl_2$ occurs.

Figure 12

Here we address the subject of the effect of an external short-circuit on cell safety. In Bobbin type construction which has limited surface area, the rate is self limiting and there is little possibility for a short circuit to result in a serious problem. Spiral wound construction cells have been found to vent, or even explode in a short-circuit.

Figure 13

At high rates of discharge such as that occuring in a cell under a short-condition, cells experience large I^2R heating due to the relatively poor conductivity of the electrolyte. The increase in internal cell temperature can lead to melting of lithium, which in turn can react with $SOCl_2$.

Figure 14

The subject of the effect of forced overdischarge on safety is addressed in this figure. We know that venting or explosion can

occur if a cell is reversed. This has been one of the more serious problems. During discharge one cell in a series string which is either not operating properly or has lower capacity can be forced into reversal by the other cells in the series. Certain results indicate that after a cell has been driven into reversal and allowed to stand for a time that it may be sensitive to shock as well.

Figures 15

The effect of forced overdischarge reversal on cell safety depends to significant extent on cell design which determines whether a cell is lithium limited, carbon limited, or $SOCl_2$ limited. The three different mechanisms are discussed in this figure. For the lithium limited cell, lithium is depleted first, resulting in substitute reactions taking place at the anode. The predominant reaction is the oxidation of the electrolyte ($SOCl_2$) producing Cl_2. SO_2Cl_2, SCl_2, and $AlCl_3$. Reducion of Cl_2 produced takes place at the cathode prefentially to $SOCl_2$ reduction resulting in the formation of LiCl. The LiCl reacts with $AlCl_3$ and $SOCl^+AlCl_4^-$ resulting in the formation of $LiAlCl_4$ and $SOCl_2$. These reactions being exothermic in nature, produces heat which raises the cell temperature during the reversal process. If reversal currents are very low the cell can be considered safe.

In carbon-limited cells, the end of cell life is brought about by the passivation of the carbon electrode. During reversal oxidation of lithium continues to take place at the anode while at the cathode the reduction of lithium ions (Li^+) is favored. Two possibilities exist relative to cell safety. It is possible

for the lithium deposited by the carbon electrode to react with $SOCl_2$. If this occurs, depending on the reversal current, heat is generated and the temperature of the cell increases. At low rates the cells can be considered safe. An alternative mechanism that can occur in the carbon-limited cells is the formation of internal short-circuits formed by lithium dendrite bridging. In such a case the dendrites can carry the short-circuit current directly to the anode thus avoiding chemical and/or electrochemical reaction and I^2R heat generation. On open-circuit stand, it is reported that these dendrites are responsible for the observed shock sensitivity.

In the $SOCl_2$-limited cells the end of cell life is brought about by the depletion of $SOCl_2$. In such cells the I^2R heating results in an increased temperature of the cell. At elevated temperatures exothermic reactions are possible resulting in cell thermal runaway.

Figure 16

The various theories for unsafe behavior of Li-$SOCl_2$ cells on reversal are summarized in this viewgraph.

Figure 17

On the matter of the effect of charging on safety and performance, cells gain little or no additional capacity during the charge period. However, there is some increase in temperature and one would expect also some increase in pressure so that there could be some venting.

Figure 18

The problems associated with physical and mechanical abuse are shown here. We note that crushing or puncturing can either lead to venting or internal shorts which are a serious concern. Intense heat can generate undesirable reactions as we noted before with melting lithium reacting with sulfur and/or thionyl chloride. Obviously, these are of concern to us and care must be exercised in cell handling, storage and transportation.

Figure 19

Vibration and shock requirements must be considered for NASA missions. Cells must meet these requirements in order to be considered for use. Before use testing would be required to verify the structural integrity of the cell and battery over a range of vibration and shock regimes.

Figure 20

This is a look at the manufacturer-induced factors. In general, the cells are optimized for performance, not for safety. They may not have an adequate amount of electrolyte and current distribution may not optimized. The extremely important thermal dissipation requires improvement, additional "cell-overhead" volume to maintain the extra thionyl chloride would be desireable, and there is a possibility that redundant terminal connections could be an enhancement. In terms of Quality Control, material purity is always a concern, especially in performance, but sometimes in safety. Contamination by moisture and other constituents during the assembly of the components can occur.

The handling and assembly process itself needs to be better controlled.

Figures 21 & 22

The conclusions are summarized in the following two viewgraphs. With regard to fundamental issues there are a number of items listed that require further attention to explain what is happening in the cell. We consider the fact that the cell design may not be optimized for the application at high rate and we need to better involve ourselves in the actual design whether it be thermal, structural or the most significant one, the optimization of the ratio of lithium, carbon and thionyl chloride.

Figure 23

Finally, the processing and Quality Control of materials require adequate consideration. Material purity and handling of quality control is important to us as well as the use of some nondestructive methods to determine the health of the cell. The last item is one that we feel is extremely important. Education is an extremely important facet of this effort. We believe that it is important that all people that come in contact with these cells or the materials, whether it be on the assembly line, quality control, operation, test, the user or the equipment designer be aware of the safety issues and that all understand fully the problems associated with these devices. This may be relatively straight forward for a NASA mission which is a controlled activity but more difficult for other applications. However, educating all those involved can enhance the safety and

reliability of cells in the future. We need to better understand the chemistry and the safety issues as they develop and we believe, as we have indicated in this particular discussion, that the lithium thionyl chloride cell can be built safely and operate safely when all of the concerns are addressed. Further, the design is such that the hazard conditions described will not be reached in the applications. Thank you

Present Limitations of $Li\text{-}SOCl_2$ Cells

CELLS REPORTEDLY:

- EXHIBIT UNSAFE BEHAVIOR UNDER CERTAIN CONDITIONS
- EXHIBIT POOR PERFORMANCE AT HIGH RATES OF DISCHARGE
- DO NOT MEET THE RELIABILITY REQUIREMENTS OF NASA

Figure 1.

Classification of Hazards of $Li\text{-}SOCl_2$ Cells

- LEAKAGE OF ELECTROLYTE THROUGH SEALS AND WELDS
- VENTING OF TOXIC GASES AND ELECTROLYTE THROUGH SEALS AND WELDS
- VIOLENT OR CONTROLLED RUPTURE OF CELL WITH EXPULSION OF TOXIC MATERIALS SOMETIMES EXPLOSIVELY WITH FIRE

Figure 2.

Analysis of the Factors Responsible for Unsafe Behavior of Li-$SOCl_2$ Cells

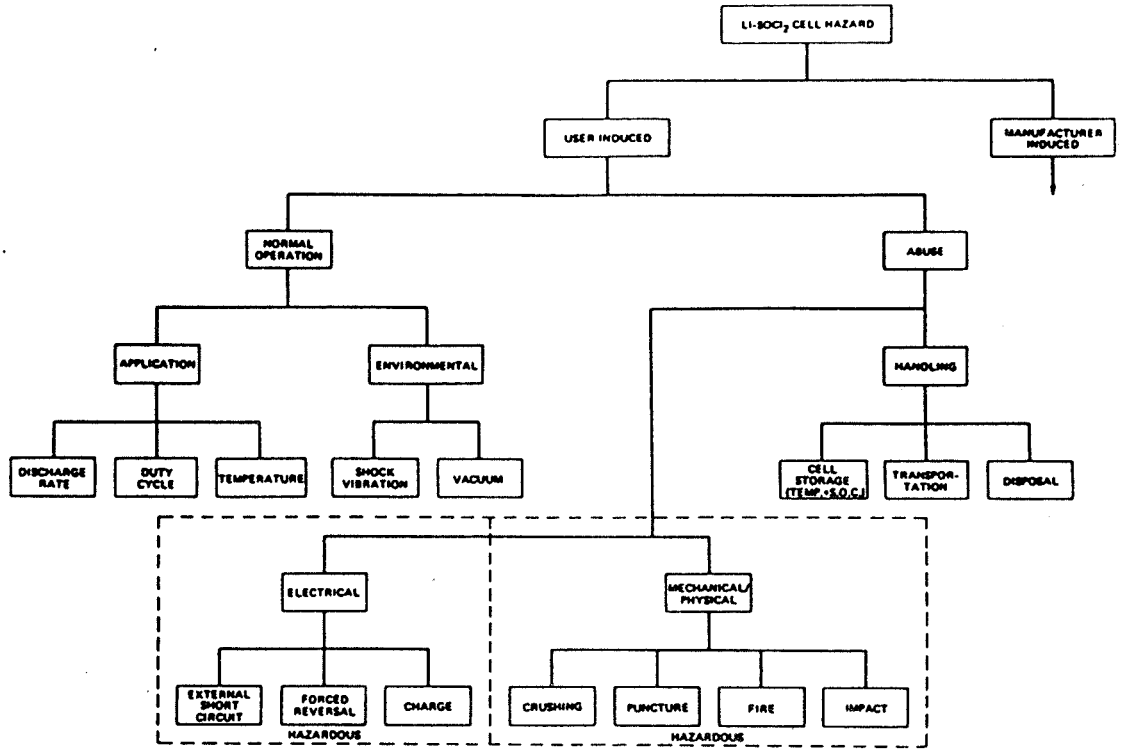

Figure 3.

Analysis of the Factors Responsible for Unsafe Behavior of Li-$SOCl_2$ Cells

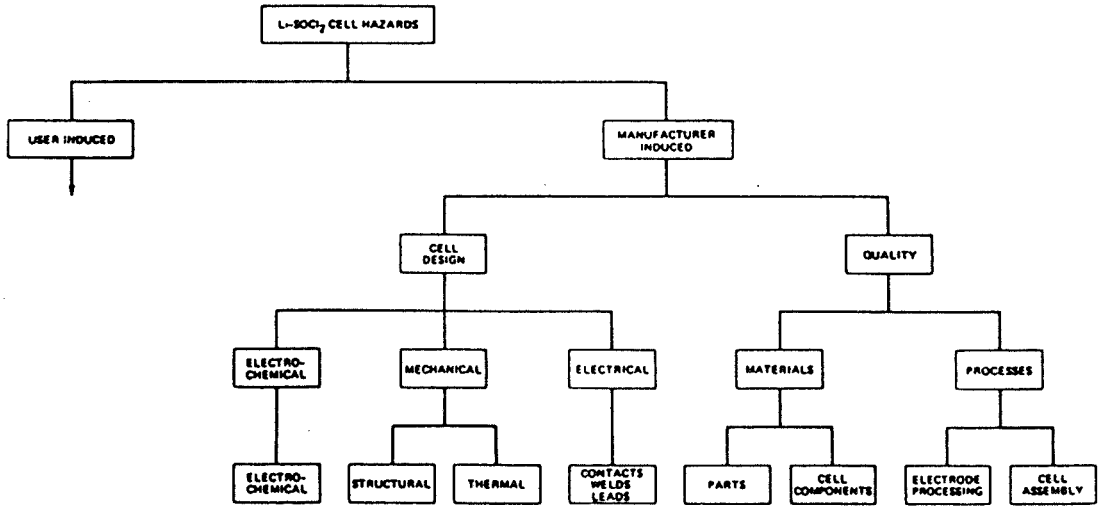

Figure 4.

Proposed Mechanism for the Unsafe Behavior of Li-$SOCl_2$ Under High Rates of Discharge/Short Circuit/Forced Over Discharge

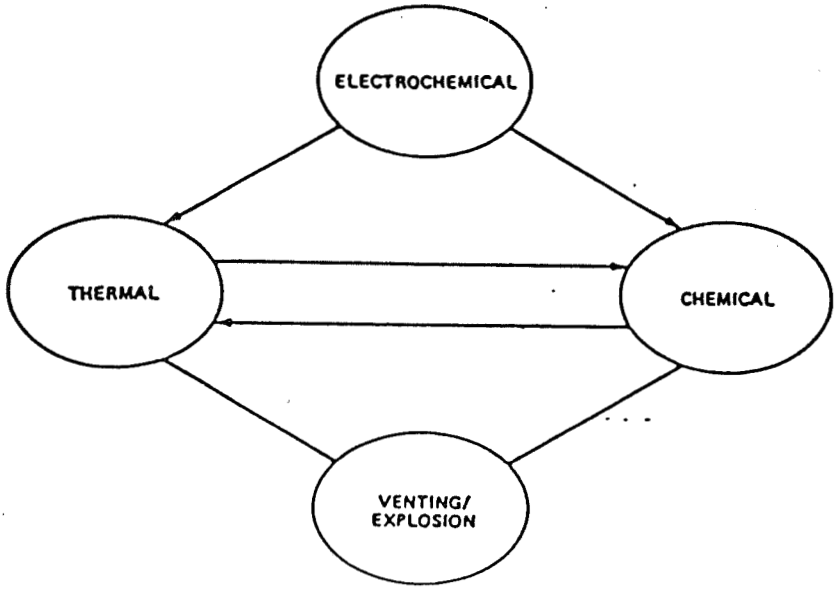

Figure 5.

Effect of Discharge Rate

- CELL CAN BE USED SAFELY UP TO C/10 DISCHARGE RATES
- CELL PERFORMANCE DECREASES (CAPACITY AND OPERATING VOLTAGE) WITH THE INCREASE OF DISCHARGE RATE
- CELLS MAY VENT OR EXPLODE IF DISCHARGED AT RATES HIGHER THAN C/3

Figure 6.

Influence of Discharge Rate on Safety

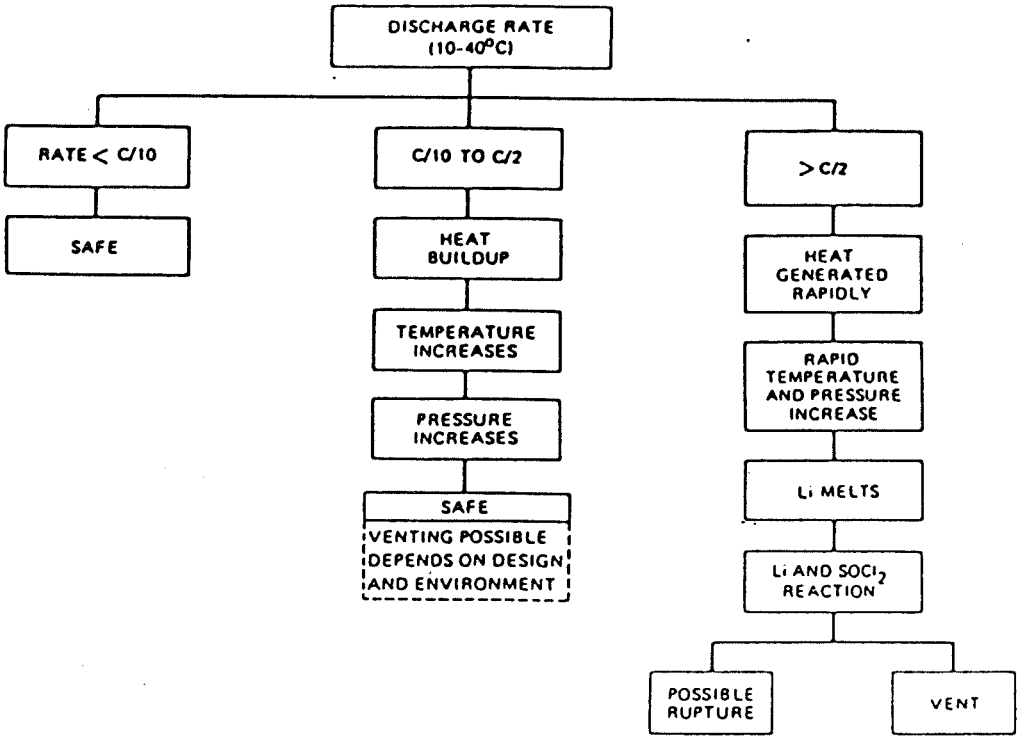

Figure 7.

Proposed Theories to Explain the Unsafe Behavior of Li-$SOCl_2$ Cells During Discharge

PRESSURIZATION

- o CELL PRESSURE INCREASES DUE TO $SOCl_2$ VAPORIZATION AT HIGHER TEMPERATURES AND FORMATION OF GASEOUS DISCHARGE PRODUCTS

THERMAL RUNAWAY

- o ELECTROCHEMICAL AND OTHER PARASITIC CHEMICAL REACTIONS RAISE THE CELL INTERNAL TEMPERATURE
- o AT ELEVATED TEMP EXOTHERMIC REACTIONS POSSIBLE (Li + S, S + $SOCl_2$, MOLTEN Li + $SOCl_2$)
- o FORMATION OF GASEOUS PRODUCTS AND TEMPERATURE LEAD TO CELL VENTING/EXPLOSION

HAZARDOUS INTERMEDIATES

- o SO, $(SO)_N$ OCIS, AND Li_2O_2 ARE REPORTED TO BE FORMED DURING DISCHARGE AND THEY MAY LEAD TO UNSAFE BEHAVIOR

Figure 8.

Effect of Temperature

- CELLS CAN BE DISCHARGED SAFELY AT RATES < C/10 AT -20 TO 60°C
- CELLS LOSE CAPACITY ON STORAGE AT TEMPERATURES HIGHER THAN 45°C
- CELLS MAY VENT OR EXPLODE IF DISCHARGED AT TEMPERATURES HIGHER THAN 80°C
- CELL EXHIBIT POOR PERFORMANCE AT LOWER TEMPERATURES
- CELLS KEPT AT LOWER TEMPERATURES WERE REPORTED TO VENT (OR EXPLODE) WHEN WARMED UP

Figure 9.

Influence of Temperature on Safety

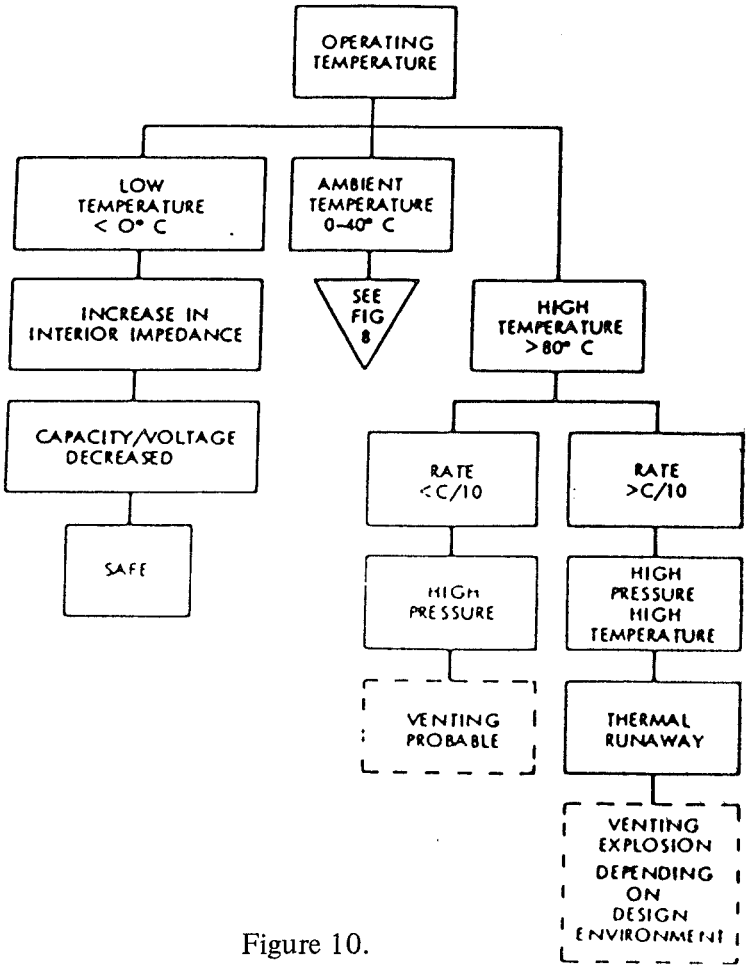

Figure 10.

Proposed Theories to Explain the Unsafe Behavior of Cells at Low and High Temperatures

LOW TEMPERATURE

- THE INCREASE IN IMPEDANCE LEADS TO POLARIZATION AND EARLY FAILURE
- INCREASE IN STABILITY OF HAZARDOUS INTERMEDIATES MAY LEAD TO UNSAFE BEHAVIOR

HIGH TEMPERATURE

- INCREASE IN INTERNAL PRESSURE
- > 80°C VENTING
- THERMAL RUNAWAY DUE TO
  - (S + $SOCl_2$ REACT EXOTHERMICALLY (130°C)
  - (MELTED Li REACTS WITH $SOCl_2$ (190°C)

Figure 11.

Effect of Short Circuit on the Safety of Li-$SOCl_2$ Cells

- CELLS OF BOBBIN TYPE CONSTUCTION POSE NO PROBLEMS UPON SHORT CIRCUIT
- CELLS OF SPIRAL WOUND CONSTUCTION WILL VENT/EXPLODE UPON SHORT CIRCUIT

Figure 12.

Causes for the Unsafe Behavior of Li-$SOCl_2$ Cells Under Short Circuit Conditions

- POOR ELECTRICAL CONDUCTIVITY OF THE ELECTROLYTE
- LOW MELTING POINT OF LITHIUM
- POOR THERMAL DISSIPATION

Figure 13.

Effect of Forced Over Discharge on the Safety of Li-$SOCl_2$ Cells

- CELLS MAY VENT OR EXPLODE
- CERTAIN RESULTS INDICATE THAT CELLS DRIVEN INTO REVERSAL ARE SENSITIVE TOWARDS SHOCK

Figure 14.

Influence of Cell Reversal on Safety

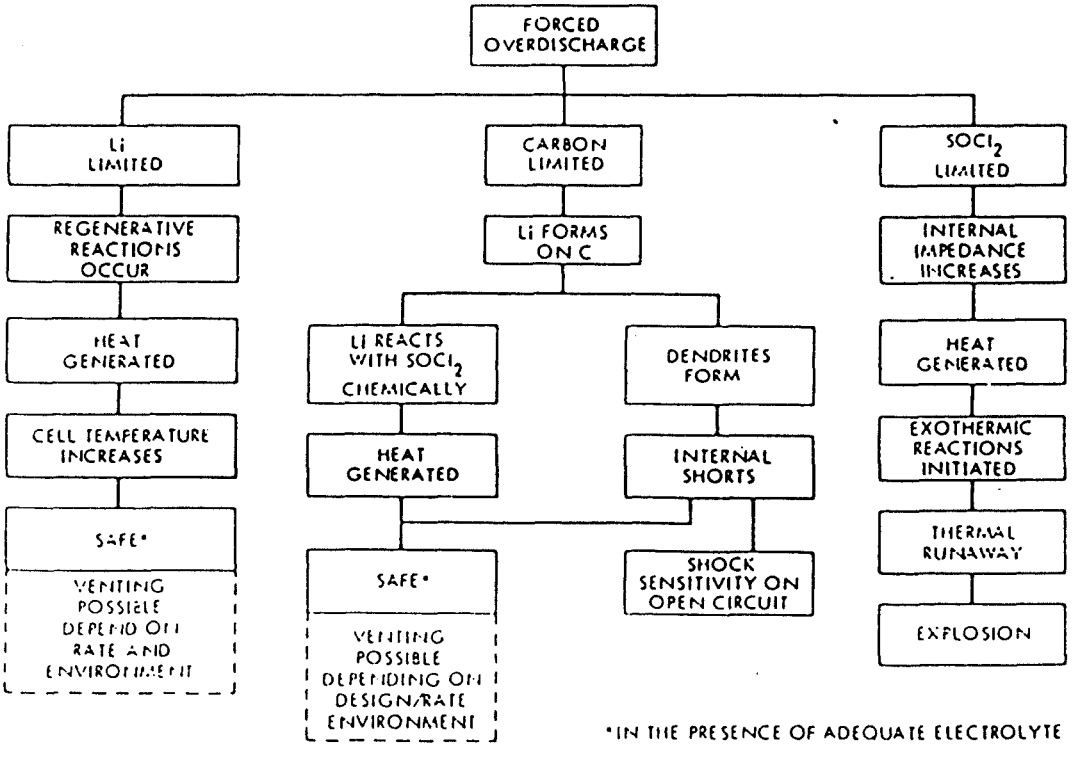

Figure 15.

Proposed Theories to Explain the Unsafe Behavior of Li-$SOCl_2$ Cells During Forced Over Discharge

CARBON LIMITED CELLS

- HIGH REACTIVITY OF Li DENDRITES WITH $SOCl_2$ AT THE CARBON ELECTRODES
- FORMATION HAZARDOUS INTERMEDIATES (Li_2O_2)

LITHIUM LIMITED CELLS

- FORMATION OF HAZARDOUS INTERMEDIATES (Cl_2))
- COMPLEX CHEMICAL REACTIONS

$SOCl_2$ LIMITED CELLS

- FORMATION OF DRY SPOTS
- MANY EXOTHERMIC REACTIONS POSSIBLE (EX Li + S, Li + GLASS PAPER ETC.)

Figure 16.

Effect of Charge Rate on the Performance and Safety of Li-$SOCl_2$ Cells

- LITTLE OR NO ADDITIONAL CAPACITY
- MARGINAL INCREASE IN CELL TEMPERATURE
- CELLS WITH CRIMPED SEALS MAY VENT

Figure 17.

Causes for the Unsafe Behavior of Li-$SOCl_2$ Cells During Physical/Mechanical Abuse

- o CRUSHING OR PUNCTURING LEADS TO
  - RELEASE OF TOXIC MATERIALS
  - INTERNAL SHORTING - VENTING
- o INTENSE HEATING WITH FLAME
  - PRESSURE INCREASE DUE TO VAPOR PRESSURE OF Li-$SOCl_2$
  - EXOTHERMIC REACTIONS BETWEEN ..
    Li, S, AND $SOCl_2$ (AT 130°C)
    Li AND $SOCl_2$ (AT 190°C)

Figure 18.

Influence of Vibration, Shock and Spin on the Performance and Safety of Li-$SOCl_2$ Cells

- o CELLS CAN MEET THE REQUIREMENTS OF MOST LAUNCH ENVIRONMENTS
- o CELLS DRIVEN INTO REVERSAL ARE REPORTED TO BE SENSITIVE TOWARDS SHOCK

Figure 19.

Analysis of Manufacturer-Induced Factors on the Safety of Li-$SOCl_2$ Cells

DESIGN

- o NOT OPTIMIZED FOR SAFETY
- o INADEQUATE QUANTITY OF ELECTROLYTE
- o NON-UNIFORM CURRENT DISTRIBUTION
- o POOR THERMAL DESIGN
- o INSUFFICIENT OVERHEAD VOLUME
- o NO REDUNDUNCY OF TERMINAL CONNECTIONS

QUALITY CONTROL

- o IMPURE MATERIALS
- o CONTAMINATION OF ELECTRODES AND OTHER COMPONENTS DURING STORAGE AND/SPACE HANDLING
- o INEFFECTIVE OF QUALITY CONTROL PROCEDURES

Figure 20.

Conclusions

SAFE Li-$SOCl_2$ CELLS CAN BE DEVELOPED FOR NASA APPLICATION

FUNDAMENTAL ISSUES: TO BE ADDRESSED

- o CHEMISTRY OF THE OELLS DURING DISCHARGE AND REVERSAL AT VARIOUS TEMPERATURES AND DISCHARGE RATES
- o ROLE OF INTERMEDIATES (OCIS, LI_2O_2 ETC.) IN CELL SAFETY
- O CHEMISTRY OF ELECTROLYTE LIMITED CELLS
- o THERMAL ANALYSIS OF Li-$SOCl_2$ CELLS DURING REVERSAL
- o CORRELATION OF CARBON ELECTRODE CHARACTERISTICS AND ITS PERFORMANCE
- o INVESTIGATION OF NEW ELECTROLYTES WITH IMPROVED CONDUCTIVITY
- o INFLUENCE OF ADDITIVES/CATALYSTS FOR IMPROVING PERFORMANCE AND SAFETY

Figure 21.

Conclusions (Con't)

CELL DESIGN: CONSIDERATIONS

- DESIGN FOR SAFETY, FIRST -- THEN PERFORMANCE
  - OPTIMIZATION OF ELECTROLYTE COMPOSITION AND QUALITY
    - TO ACCOUNT FOR NORMAL DISCHARGE
    - TO SUSTAIN CONDUCTIVITY DURING DISCHARGE AND REVERSAL
    - TO KEEP DISCHARGE PRODUCTS IN SOLUTION
- OPTIMIZATION OF ELECTRODE CAPACITY (Li/C) RATIO
  (LITHIUM LIMITED DESIGN POSSIBLE ONLY FOR LOW RATE CELLS)
  (CARBON LIMITED DESIGN IS THE ONLY CHOICE FOR HIGH RATE CELLS)
- MINIMIZE CURRENT DISTRUBUTION PROBLEMS
- OPTIMIZE THERMAL MANAGEMENT
- UTILIZE CORROSION RESISTANT SEALS
- USE THERMAL RESISTANCE FUSES

Figure 22.

Conclusions (Con't)

- PROCESSING AND QUALITY CONTROL: CONSIDERATION
  - MATERIAL PURITY REQUIREMENTS
  - IMPROVEMENT OF HANDLING, PROCESSING AND ASSEMBLY TECHNIQUES
  - DEVELOPMENT AND IMPLEMENTATION OF A EFFECTIVE QUALITY CONTROL PROGRAM
  - DEVELOPMENT OF N.D.T. METHODS TO DETERMINE THE HEALTH OF THE CELL
- EDUCATION OF THE USER

Figure 23.

An Update of the JPL Program to Develop Li-$SOCl_2$ Cells

G. Halpert, V. Ang, R. Banes,
S. Dawson, H. Frank, S. Subbarao, and L. Whitcanack

JPL has been involved in a lithium thionyl chloride cell development program as I have indicated in the previous paper. It's goals are given in the first viewgraph.

Figure 1

These include 300 Wh/Kg at a 2+hour discharge rate, safely operated, with a five year storage life and a process that is well documented and controlled. This has been our goal. In this paper we will show you some of the results achieved to date.

Figure 2

We include the typical energy/power curves that one has seen before to show why lithium thionyl chloride is important to us and why we think we can meet the requirements.

Figure 3

This shows some of the applications that we are considering for space transportation, system for launch vehicles, orbiting transfer vehicles and planetary spacecraft.

Figure 4

Additional applications are given in this next viewgraph. Specific ones include the Manned Manuvering Unit (MMU), portable instruments, tools, lighting and switching among others. These are all probable applications in shuttle and space station. The main purpose in presenting this paper is to inform you of the status of the JPL Electrochemical program.

Figure 5 & 6

We are pleased to announce that we have met the goal of producing a Li-$SOCl_2$ spiral wound "D" cell. We refer to it as a First Generation Cell. Photos of the JPL lithium thionyl chloride cell are shown. We had target a goal of producing first generation cells by October 1984. We have met that goal. The cell design and electrodes, particularly the carbon cathodes were produced in-house. Also all parts were assembled, the welding performed, the electrolyte added and the cells sealed in-house.

The lithium capacity (theoretical) was 19.3 ah and that of the $SOCl_2$ in the 1.8 m $LiAlCl_4$ electrolyte, 16.4 ah (we are convinced that a greater excess of $SOCl_2$ is necessary for safe high rate operation). The electrode surface area was 452 cm^2. The carbon electrode comprised Shawinigen Black/Teflon -30 (90/10 by weight) mixture 0.020 inches thick on an expanded metal screen prepared in the JPL laboratory. There were two tab connections to the cathode. The 0.0078 inch thick lithium foil was rolled into an expanded nickel screen. The separator was Mead 934-5 figerglass material.

Figure 7

The actual results are given in this figure. As you can see we have operated at 2 amps (C/50), 1 amp (C/10), and 5 amps (C/2). The voltage curves are flat and we achieved, as you see, almost 12 amp hour at the C/50 rate over 10 amp hours at the C/10 rate, and at 5 amps (C/2) we have achieved 9 plus ampere hours. We are very pleased with these results.

Figure 8

E-I measurements were performed at 100% state-of-charge, 50% state-of-charge, and 10% state-of-charge. The power numbers are quite high, much to our pleasant surprise.

Figure 9

This is the power curve for these cells measured at different states of charge. The maximum was 48 watts at the 2C rate which is rather significant. You notice there was still almost 30 watts of power even at 90% depth-of-discharge. Another rather significant finding.

Figure 10

In summary we produced our first lithium thionyl chloride cylindrical "D" cells. The initial test results show that we were able to get up to 350 Wh/Kg at the 50 hour rate, almost 300 at the 10 hour rate, and 247 at the 2 hour rate. The power capability was 48 watts at C/2. The program and our studies on the safety are being continued in order to optimize the use of the cells. Thank you.

Lithium Thionyl Chloride Cells and Batteries Program Objectives

DESIGN, DEVELOP, AND TRANSFER TECHNOLOGY TO INDUSTRY TO MANUFACTURE FLIGHT QUALITY LITHIUM THIONYL CHLORIDE PRIMARY CELLS AND BATTERIES

- o 300 WH/KG ENERGY DENSITY
- o 2-HOUR DISCHARGE RATE
- o SAFE OPERATION
- o 5 YEAR STORAGE LIFE
- o MANUFACTURING CONTROL DOCUMENT (IDENTIFIES MATERIALS, PROCESSES, REQUIREMENTS AND QUALITY)

Figure 1.

Power and Energy Characteristics of Primary Cells

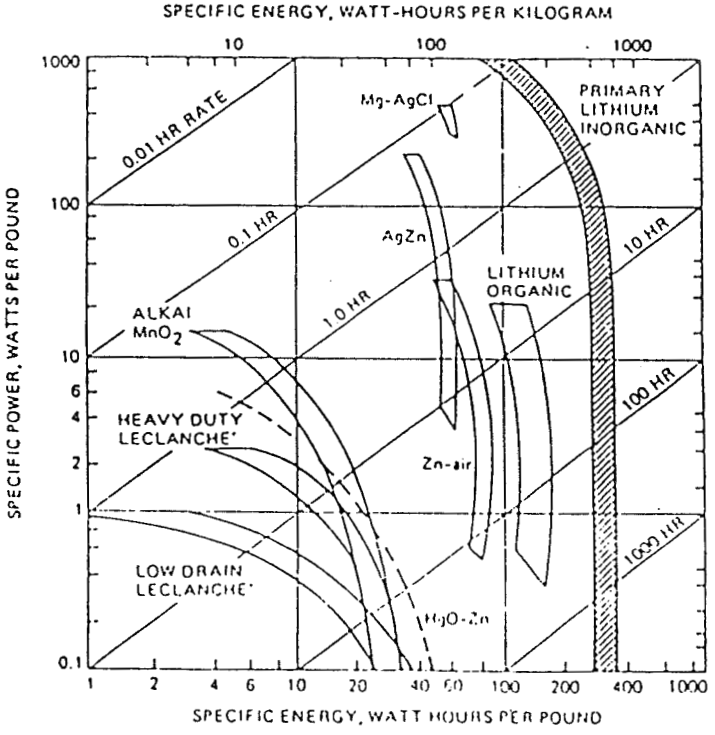

Figure 2.

Lithium Thionyl Chloride Battery Applications

- SPACE TRANSPORTATION SYSTEM (STS)
  - LIFE SUPPORT AND PROPULSION FOR ASTRONAUTS EVA
  - PORTABLE RADIOS, CAMERAS, LIGHTS, TOOLS ETC
  - DEPLOYABLE INSTRUMENTS
- LAUNCH VEHICLES
  - LOCATION AID FOR SOLID ROCKET BOOSTERS (SRB)
  - RANGE SAFETY FOR (SRB)
- ORBIT TRANSFER VEHICLES
  - POWER FOR GYROS, AVIONICS, THERMAL CONTROL, GUIDANCE, TELEMETRY, AND PROPELLENT MOTORS
- PLANETRY SPACECRAFT
  - PRIMARY POWER FOR PROBES AND LANDERS
  - PEAK POWER REQUIREMENTS FOR SPACECRAFT

Figure 3.

Lithium Thionyl Chloride Cells Applications

- MMU/EMU
- PORTABLE INSTRUMENTS
- TOOLS
- LIGHTING
- SWITCHING
- CAMERAS
- RADIO/COMMUNICATIONS EQUIPMENT
- STANDBY POWER
- STAND ALONE POWER
- DEPLOYABLE INSTRUMENTS

Figure 4.

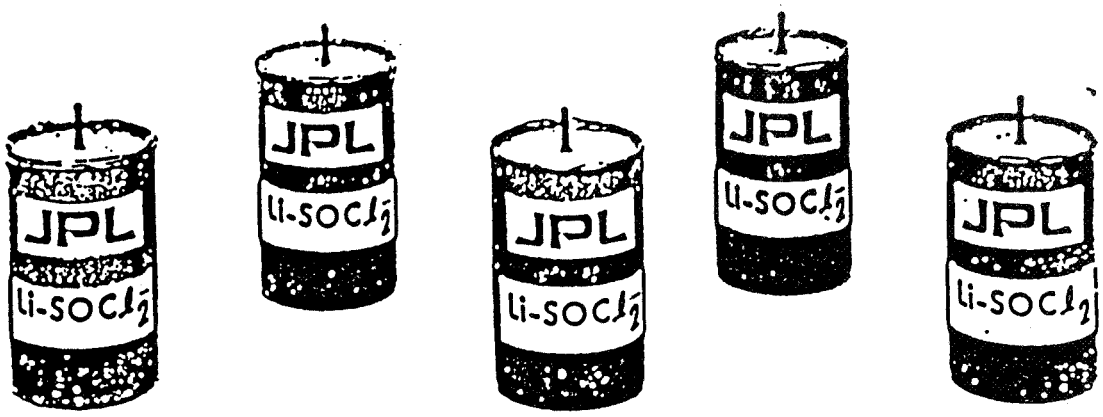

Figure 5

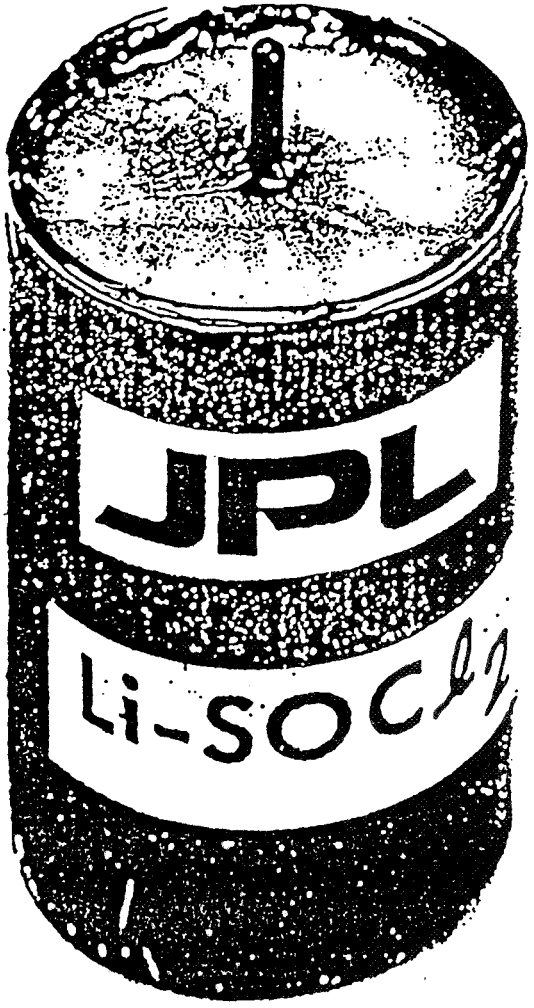

Figure 6

First Generation D-Cells: Constant Current Discharge Characteristics

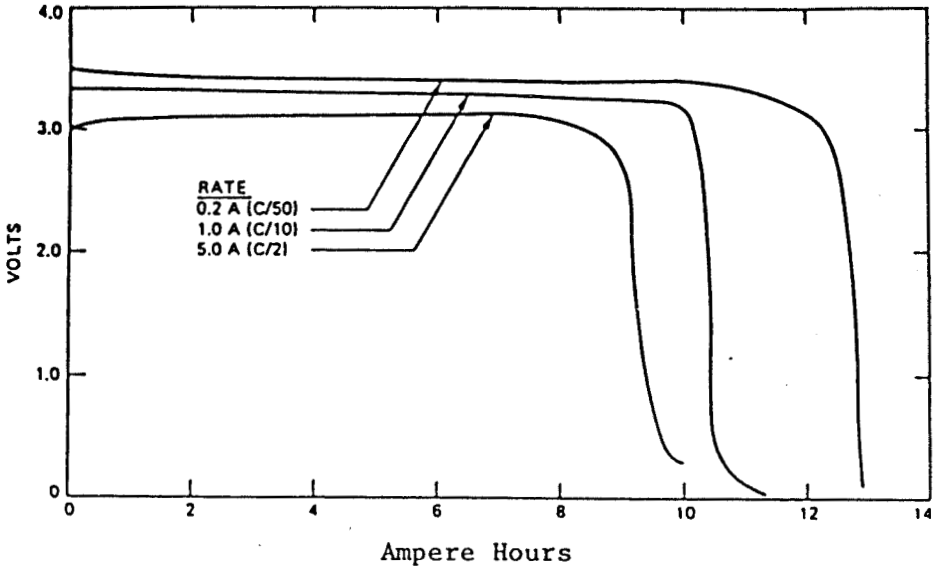

Figure 7.

First Generation D-Cells: Effect of State of Charge on Voltage-Current Characteristics

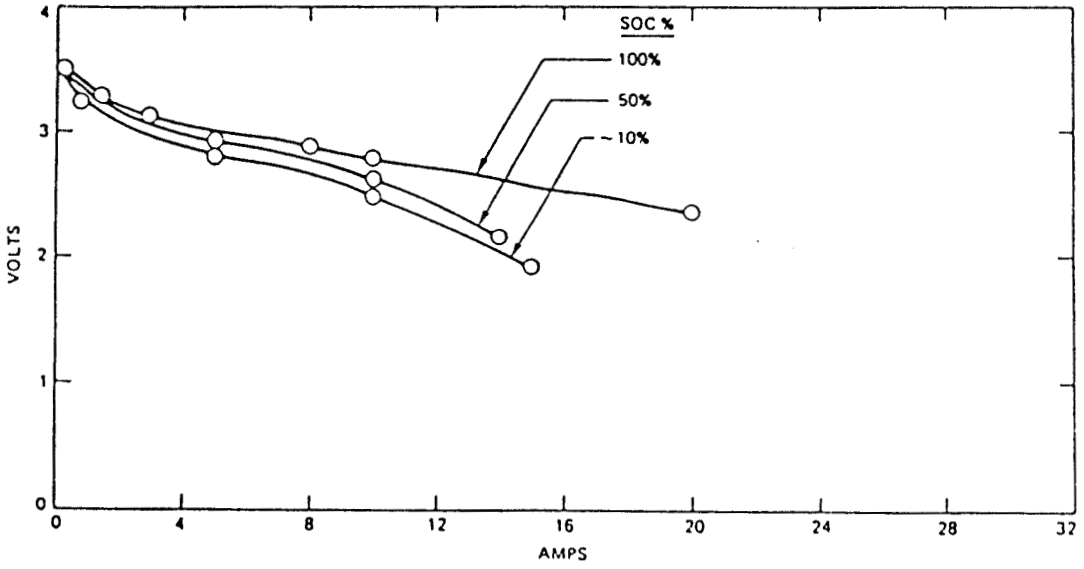

Figure 8.

First Generation D-Cells: Power Output Characteristics

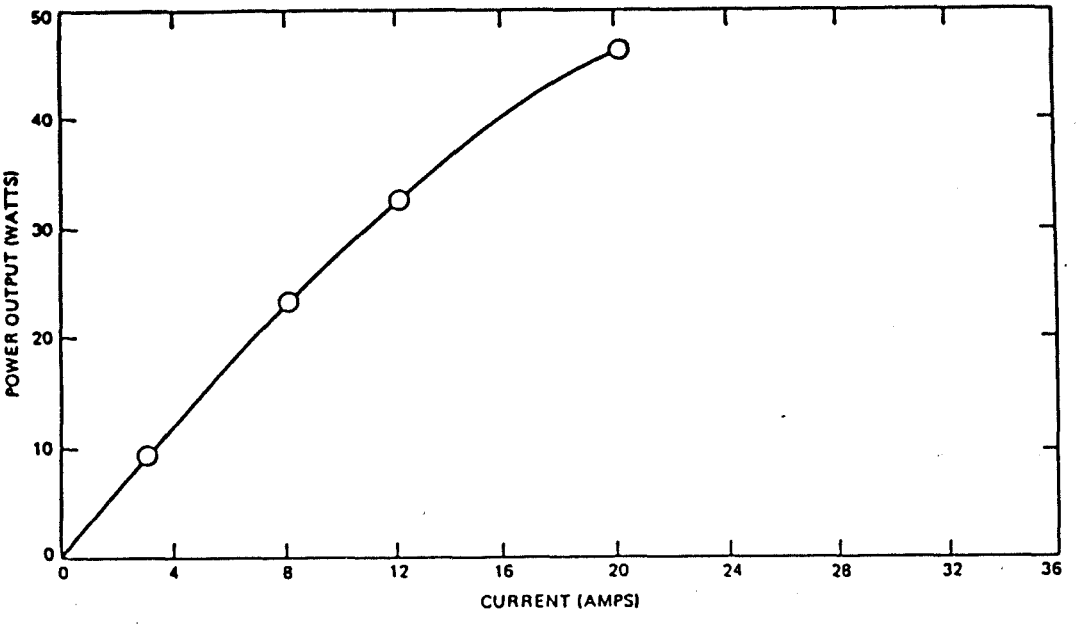

Figure 9.

Summary

- o FIRST GENERATION $Li-SOCl_2$ "D" CELLS ASSEMBLED
- o INITIAL TEST RESULTS - INDICATE TARGETS ARE WITHIN REACH

  12.6 AH AT C/50 = 350 WH/Kg
  10.4 AH AT C/10 = 299 WH/Kg
  9.2 AH AT C/2 = 247 WH/Kg

- o POWER CAPABILITY HIGHER THAN ANTICIPATED
  48 WATTS AT 2C RATE

- o DEVELOPMENT CONTINUING WITH SAFETY THE PRIMARY GOAL

Figure 10.

SESSION III

NICKEL-CADMIUM TECHNOLOGY

Chairman: C. M. Tasevoli
Goddard Space Flight Center

RCA'S PLANNED TEST PROGRAM TO COMPARE THE PERFORMANCE AND LIFE OF NiCd CELLS CONTAINING PELLON 2536 IN CONTRAST WITH PELLON 2505 SEPARATOR MATERIAL

Stephen F. Schiffer
RCA Astro-Electronics
Princeton, N.J.

ABSTRACT

RCA Astro-Electronics will be characterizing and life-testing two groups of hermetically-sealed aerospace nickel-cadmium cells to determine the effect, if any, of a separator change on cell performance. This test, designed to provide information for a specific low-earth-orbit satellite application, will also add to the overall data-base for cells with the new separator.

INTRODUCTION

The most widely used separator material for hermetically-sealed aerospace nickel-cadmium cells, Pellon Corporation's Pellon 2505 ML, is no longer being produced. Manufacture of this non-woven fabric was discontinued by Pellon Corporation in 1976. The last of the "stockpile" of this material available at General Electric Battery Business Department (G.E.), a manufacturer of aerospace NiCd cells for RCA Astro-Electronics and others, will be committed by early 1985.

General Electric and Pellon Corporation have recommended an alternate material-Pellon 2536- as a substitute aerospace NiCd battery separator. At the 1983 NASA/GSFC Battery Workshop, Martin Milden of the Aerospace Corporation reported on the joint Government program to qualify the new separator material for aerospace NiCd cells (ref. 1). Cells have been procured for that program and testing will begin in 1985 at the Naval Weapons Support Center (NWSC), Crane, Indiana, to qualify the new material for aerospace applications.

It is also necessary to characterize existing cell designs with the new separator for specific mission requirements and compare these results to known data with Pellon 2505 ML. RCA-Astro uses 26.5 ampere-hour (nameplate) nickel-cadmium cells procured from G.E. (G.E. P/N 42B030AB10) in low-earth-orbit satellites for both NASA and U.S.A.F. programs. RCA has been funded by these customers to run characterization and life tests on the 26.5 Ah cells under their simulated mission conditions. This test is designed to determine the effects, if any, of the separator change on cell performance related to the power subsystems and charge controllers for these satellites.

Two groups of 11 cells each of one manufacturing lot, with separator being the only variable, have been procured from G.E. and will be tested side-by-side in the sequence listed below. The test is scheduled to begin in January, 1985.

TEST FLOW SEQUENCE

1. Acceptance testing at G.E.
2. Physical inspection, impedance measurements at RCA.
3. Conditioning (25°C).
4. Capacity determination (25°C, 10°C, 5°C, 0°C, -5°C)

   2 cycles at C/2 discharge, 1 cycle at C-rate discharge at each temperature.
5. Voltage recovery test.
6. Open circuit stand test.
7. Constant-current overcharge test

   Determine stabilized overcharge voltages at 0°, 5°, 10°, 25°, -5°C.
8. V-T charge control test (5°C, 10°C, 25°C)* 6 cycles each at each V-T limit at each temperature under low-earth-orbit cycling conditions. Charge at C/4 rate until voltage limit, then taper current for a total charge time of 69 minutes. Discharge at constant power, for 33' to 25% depth-of-discharge. After 6 cycles at each V-T limit at each temperature, measure capacity by discharging until the first cell in the group drops to 1.15 volts.

8a. V-T charge control test with C/5 charge rate, 25% depth-of-discharge, at 5°C

8b. V-T charge control test with C/4 charge, 15% depth of discharge at 5°C.

8c. V-T charge control test using 2 selected curves as in '8' above, at 0°C and at -5°C.

9. Simulated orbital life test @ 5°C, real-time cycling. V-T taper charge for 69 minutes, C/4 maximum charge rate. Constant power discharge for 33 minutes to 25% depth-of-discharge. Adjust V-T limits during cycling to provide 1.04 recharge ratio (subject to later adjustment if required).

MATERIALS EVALUATION

The specified characteristics of the 2505ML separator and the 2536 separator are shown in Table 1.

One goal of this program is to determine whether any differences develop in the other cell components, as well as the separator, after electrical cycling.

Two dry sealed cells and two filled cells will be retained for future reference of starting material characteristics, one each containing the Pellon 2505ML and the second containing the Pellon 2536 separator.

Every 6 months during the life test, a cell will be removed from each test group and the charge and discharge voltage limits for the remaining cells will be adjusted accordingly.

Cells removed from the life test will be tested as follows, with the data compared to early-life data:

Measure AC impedance
Determine overcharge voltage values
Determine full capacity at 10°C
Perform voltage recovery test at 25°C
Perform 72 hour stand test at 10°C
Perform electrolyte leak check and internal resistance test

* V-T charge control is voltage-limited battery charging with pre-selected voltage limits. The battery is charged at a constant current until a pre-determined voltage(temperature-dependent) is reached. The voltage is limited at that value and the charging current tapers as charging continues.

Determine negative electrode precharge
and excess negative capacity

The cells shall then be physically dissected and the internal components examined. As a minimum, the following characteristics will be checked:

Positive and negative electrode thickness
Separator degradation and cadmium penetration
Positive and Negative flooded capacity

Materials from the dry sample cells will be used as a basis for comparison for these material tests.

CONCLUSIONS

This test will provide timely data to establish V-T charge control limits and power-balance predictions for RCA's specific low-earth-orbit satellite applications. It will also provide a direct comparison under low-earth-orbit test conditions of charge and discharge characteristics and, eventually of life, of identical cells containing Pellon 2536 separator in contrast with Pellon 2505 ML, for which there is a sizable data base.

With the testing scheduled to begin in January, 1985, sufficient data should be available in advance of Flight use of these cells to provide confidence in their behavior.

REFERENCES

(1) Milden, M.J.: Separator Qualification for Aerospace Nickel-Cadmium Cells. Presented at the 1983 NASA Goddard Space Flight Center Battery Workshop.

(2) Milden, M.J. and Harkness, J.: Separator Qualification for Aerospace Nickel-Cadmium Cells. Proceedings of the 19th Intersociety Energy Conversion Engineering Conference, 1984 pp. 108-110.

Table 1. BRIEF COMPARISON OF NiCd SEPARATOR (Ref. 2)

ITEM	2505ML	(2536 TENTATIVE)
GENERAL DESCRIPTION	STABILIZED ZINC CHLORIDE BONDED NYLON	HOT INERT GAS BONDED NYLON
WEIGHT	60+8 g/m^2	80+7 g/m^2
THICKNESS (UNDER 7.28 KG/CM^2	0.007-.010 INCH	0.007-0.009 INCH*
TENSILE STRENGTH		
(MACHINE DIRECTION)	3 LBS.	5 LBS. MINIMUM
(CROSS DIRECTION)	5 LBS.	5 LBS. MINIMUM
ELECTROLYTE RETENTION (31% KOH)	400% MINIMUM	300% MINIMUM*
SHRINKAGE (31% KOH, 70°C, 200 HRS)	1% MAXIMUM	1% MAXIMUM
WETABILITY (31% KOH)	5 MINUTES MINIMUM	5 MINUTES MINIMUM

*FROM GE SPECIFICATION A50-PB-168

RCA'S PLANNED TEST PROGRAM TO COMPARE THE PERFORMANCE AND LIFE OF Ni Cd CELLS CONTAINING PELLON 2536 IN CONTRAST WITH PELLON 2505 SEPARATOR MATERIAL

STEPHEN F. SCHIFFER
RCA ASTRO ELECTRONICS

BRIEF COMPARISON OF NICD SEPARATOR

ITEM	2505ML	(2536 TENTATIVE)
GENERAL DESCRIPTION	STABILIZED ZINC CHLORIDE BONDED NYLON	HOT INERT GAS BONDED NYLON
WEIGHT	60+8 g/m^2	80+7 g/m^2
THICKNESS (UNDER 7.28 KG/CM^2	0.007-.010 INCH	0.007-0.009 INCH*
TENSILE STRENGTH		
(MACHINE DIRECTION)	3 LBS.	5 LBS. MINIMUM
(CROSS DIRECTION)	5 LBS.	5 LBS. MINIMUM
ELECTROLYTE RETENTION (31% KOH)	400% MINIMUM	300% MINIMUM*
SHRINKAGE (31% KOH, 70°C, 200 HRS)	1% MAXIMUM	1% MAXIMUM
WETABILITY (31% KOH)	5 MINUTES MINIMUM	5 MINUTES MINIMUM

*FROM GE SPECIFICATION A50-PB-168

TYPICAL V-T LIMIT CURVES

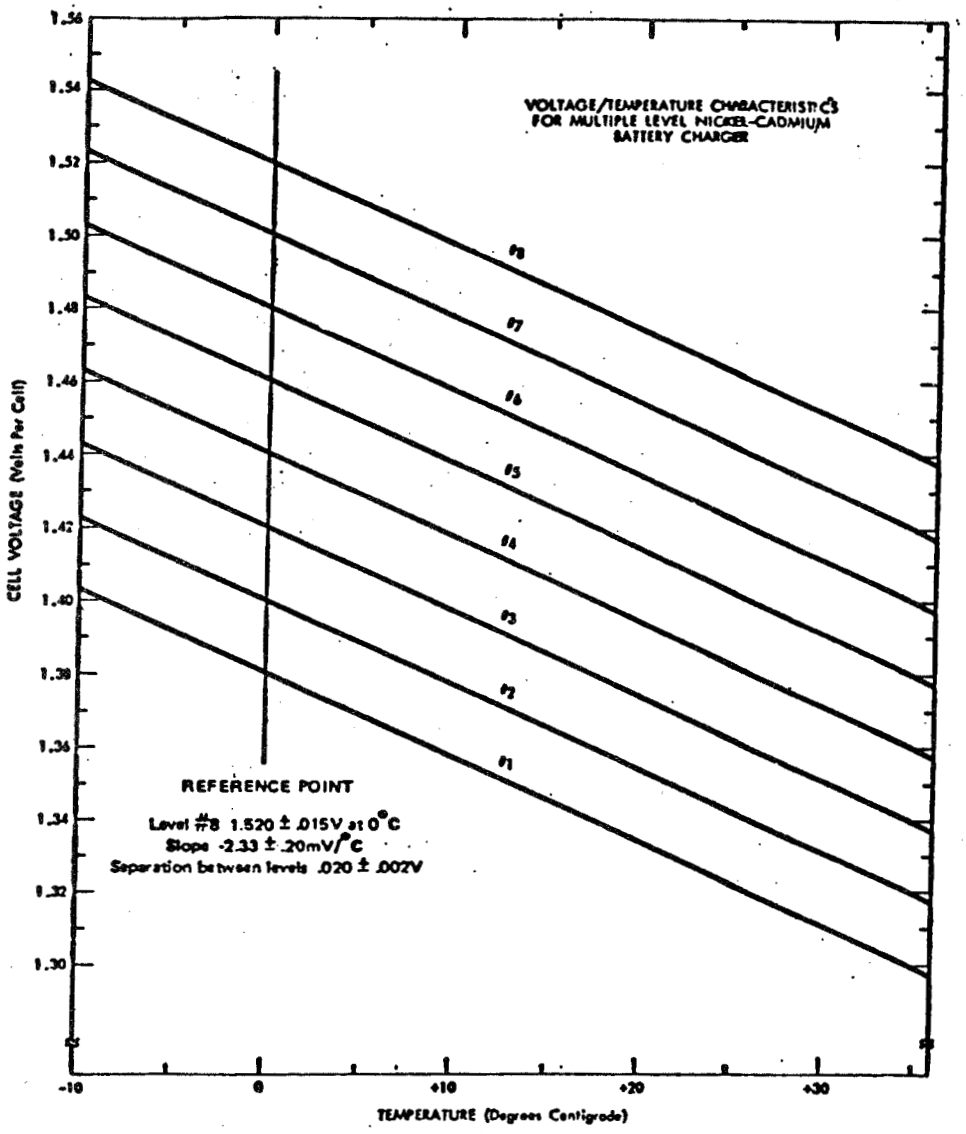

Cell Voltage Limit versus Temperature

ELECTRICAL TESTS, PRE-LIFE CYCLING
(11 CELLS OF EACH SEPARATOR TYPE)

- IMPEDANCE
- CONDITIONING
- CAPACITY DETERMINATION
  25°C, 10°C, 5°C, 0°C, -5°C
- VOLTAGE RECOVERY TEST @ 25°C
- OPEN CIRCUIT STAND - 72 HOURS @ 10°C
- CONSTANT CURRENT OVERCHARGE
  25°C, 10°C, 5°C, 0°C, -5°C
- V/T LIMIT CHARGE CONTROL EVALUATION
  25°C, 10°C, 5°C
  6 CYCLES AT EACH LIMIT, 69' CHARGE, 33' DISCHARGE
  25% DOD. 2 CHARGE RATES - C/4, C/5.
  CAPACITY DETERMINATION AFTER EACH 6 CYCLES.
  ADDITIONAL TESTS AT 0°C, -5°C.

LIFE-CYCLING

- REAL-TIME, LOW-EARTH-ORBIT, 5°C
- V-T TAPER CHARGE FOR 69 MINUTES, C/4 MAX. CHARGE RATE
- CONSTANT-POWER DISCHARGE FOR 33 MINUTES TO 25% DOD
- RECHARGE RATIO: 1.04
- REMOVE ONE CELL EVERY 6 MONTHS FOR ANALYSIS
- TEST FOR THREE YEARS OR UNTIL VOLTAGE < 1.0 VOLT/CELL

POST-CYCLING TESTS

- REMOVE ONE CELL EVERY 6 MONTHS
  - MEASURE AC IMPEDANCE
  - DETERMINE OVERCHARGE VALUES
  - DETERMINE FULL CAPACITY AT 10°C
  - PERFORM VOLTAGE RECOVERY TEST AT 25°C
  - PERFORM 72 HOUR STAND TEST AT 10°C
  - DETERMINE NEGATIVE ELECTRODE PRECHARGE AND EXCESS NEGATIVE CAPACITY
  - ELECTROLYTE LEAK CHECK
  - DISSECT

POST DISSECTION ANALYSIS

- POSITIVE AND NEGATIVE ELECTRODE THICKNESS
- SEPARATOR DEGRADATION AND CD PENETRATION
- POSITIVE AND NEGATIVE FLOODED CAPACITY

FAILURE MODES EXPERIENCED ON SPACECRAFT NiCd BATTERIES

Sidney Gross
Boeing Aerospace Company
Seattle, Washington 98115

ABSTRACT

A review has been made of failures and irregularities experienced on nickel cadmium batteries for 31 spacecraft. Only rarely did batteries fail completely. In many cases, poorly performing batteries were compensated for by a reduction in loads or by continuing to operate in spite of out-of-voltage conditions. Low discharge voltage was the most common problem observed in flight spacecraft (42%). Spacecraft batteries are often designed to protect against cell shorts, but cell or battery shorts accounted for only 16% of the failures. Other causes of problems were high charge voltage (16%), battery problems caused by other elements of the spacecraft (10%), and open circuit failures (6%). Problems of miscellaneous or unknown causes occurred in 10% of the cases.

INTRODUCTION

Information on battery problems can be useful in guiding research to improve battery technology. Problems that are serious or reoccur are the obvious ones to concentrate on. Observed problems can be caused by more than one phenomenon, however. It is the function of research programs to define these wearout and failure phenomena, to learn about their causes, and to attempt improvements. A survey was made, therefore, to document observed problems on spacecraft, with the scope limited to U,S. spacecraft. The survey was also limited to the information that could be obtained in a relatively short period of time.

A survey of problems on spacecraft nickel cadmium batteries cannot easily be a thorough or highly accurate undertaking. Up to December 31, 1975, a total of 725 U.S. satellites were placed in Earth orbit, posing an immense task for an accurate survey. The task is made even more difficult by the fact that only seldom are spacecraft performance and problems documented.

The approach taken in this survey was to rely primarily on the knowledge of battery specialists within the industry. Operating problems, especially major ones, are significant events that are not easily forgotten. There are important difficulties in this approach, however, including faulty or incomplete memory, transfer or relocation of cognizant personnel, poor communication between spacecraft users and battery specialists, and unwillingness to be candid. Only rarely can information be obtained on classified spacecraft.

RESULTS

Spacecraft having identified failures or irregularities with nickel cadmium batteries are listed in Table 1. Not included are those spacecraft where battery problems occurred but were caused by another subsystem or power system element. For example, the NRL 160 series spacecraft had serious thermal problems with the batteries, and the ATM Skylab module lost some batteries temporarily due to stuck relays.

Table 1 includes thirteen spacecraft which have experienced discharge voltage degradation. There are very likely many more such instances which have not been listed, for that kind of behavior is common and is a major shortcoming in nickel cadmium technology.

Descriptions of identified battery problems are given in Table 2. Quantitative information was used when available, but in some cases only qualitative information was available. No attempt was made to eliminate from this listing those occasions when problems occurred after the design lifetime had been passed, for that information can also be useful.

For convenience, battery problems have been coded on Table 2 into categories from 1 to 6. Table 3 identifies the codes and lists the number of occasions each type of problem was experienced. Low discharge voltage was the most common problem, followed by shorts and high charge voltage.

CONCLUSIONS

Nearly all the kinds of nickel cadmium battery problems seen during laboratory testing also have been observed in spacecraft. Most of the problems have been degradation displayed as low discharge voltage; only rarely have batteries failed completely. In many cases, poorly performing batteries have been countered by a reduction in loads, compromising on requirements to avoid undervoltage conditions.

There have been enough problems that it is clear that nickel cadmium battery technology needs improvement. Spacecraft experience is thus in agreement with laboratory experience, which also suggests improvement is desirable. The need for improvement is further emphasized when it is considered that greater reliability, longer life, and deeper depths of discharge are desired for many future spacecraft.

Table 1. SPACECRAFT WITH IDENTIFIED NICKEL CADMIUM BATTERY PROBLEMS

SPACECRAFT	ORBIT	LAUNCH	BATTERY	REFERENCES
Transit 4A	Near Earth	June 29, 1961	34 cells, Sonotone 4 AH	1
Navigation Satellite 1B	Near Earth	April 1960	?	2
OAO-1	Near Earth	April 1966	22 cells, Gulton 20 AH, 2 batteries + 1 standby battery	3, 4
OAO-2	Near Earth	December 1968	Some cells with auxiliary electrodes	3, 4
OAO-3	Near Earth	August 1972	Some cells with auxiliary electrodes	3, 4
SAS-A	Near Earth	December 1970	8 (?) cells, Gulton 6 AH	5
SAS-B	Near Earth	November 1972	8 cells, G.E. 6 AH, teflonated negatives	5, 6, 7, 8
SAS-C	Near Earth	May 1975	12 cells, Gulton 9 AH	5, 6, 7, 8
Intelsat 3 (Five S/C)	Geosynchronous	December 1968 to April 1970	22 cells, Gulton 12 AH	9, 10, 11
Intelsat 4, F-2	Geosynchronous	January 1971	25 cells, 15 AH, LiOH in KOH, no Ag in neg.	9, 11, 12
Intelsat 4A	Geosynchronous	January 1971?	25 cells, 24 AH, Ag in neg.	9, 11
Unspecified	---	---	---	---
Classified	Geosynchronous	---	---	10, 12
72-1	Near Earth	October 1972	18 cells, G.E. 15 AH	14
Landsat-1	Near Earth	July 1972	23 cells, G.E. 6 AH, 8 batteries	15
SMS-1	Geosynchronous	May 1974	20 cells, E.P. 3 AH, 2 batteries	16, 17
TETR-2	Near Earth	November 1968	?	4
171	Near Earth	December 1971	22 cells, Sonotone 5 AH, polypropylene, 2 batteries	18

Table 1. (Continued)

SPACECRAFT	ORBIT	LAUNCH	BATTERY	REFERENCES
172	Near Earth	December 1971	Battery used cylindrical F cells	19
173	Near Earth	December 1971	Battery used cylindrical F cells	19
174	Near Earth	December 1971	Battery used cylindrical F cells	19
CTS	Geosynchronous	January 1976	24 cells, G.E. 5 AH, polypropylele, 2 batteries	20
ATS-6	Synchronous	May 1974	19 cells, Gulton 15 AH, 2 batteries	21
ITOS	Near Earth	January 1970	12 AH, ?	22
VELA 1	Near Earth	October 1963	Gulton 6 AH, 2 batteries	23
VELA 2	Near Earth	October 1963	Gulton 6 AH, 2 batteries	23
DODGE 1	Near Earth	July 1967	Battery used cylindrical F cells	24, 25

Table 2. FAILURES AND IRREGULARITIES IN SPACECRAFT NICKEL CADMIUM BATTERY APPLICATIONS

SPACECRAFT	FAILURE OR IRREGULARITY	CODE
Transit 4A	After five years of satisfactory operation, the battery was unable to support the mission. Cause of failure is unknown.	6
Navigation Satellite 1B	This battery contained a thermostat to turn off battery charging if temperature became too high. The thermostat setting drifted to a lower value with time, eventually reaching the normal battery temperature. As a result, the battery charger system was permanently disconnected.	5
OAO-1	The OAO-1 had sequential charging between three batteries. The sequencer failed, causing the charger to stay on only one of the batteries. Since there was no override or disable possible, the battery got very hot, approximately 150°F. As a result, the system had to be turned off. This failure was caused entirely by the charge controller.	5
OAO-2	The OAO-B and -C had a number of commandable temperature-biased voltage levels for charge, plus an alternate end of charge signal from an oxygen sensing auxiliary electrode. After three years, the auxiliary electrode gave erroneous signals, but the cause is not known. No compromise to the battery has occurred.	6
OAO-3	Though the spacecraft was designed for only six months operation, the spacecraft still continues to be used after 4½ years. As a result, low battery voltage problems are occurring. When the spacecrafts voltage limit of 1.18 V/cell is reached, the battery goes into a protective mode. A second level voltage limit of 1.12 V/cell is also used, and this limit too is exceeded at times.	1
SAS-A	Excess solar array power on this spacecraft is shunted using a transistor switching circuit. Thermal cycling of the transistors caused them to eventually fail open, putting the full excess array current on the battery. After one year of high temperature and high voltage, the battery failed. This failure was caused by failed electronics.	5

Table 2. (Continued)

SPACECRAFT	FAILURE OR IRREGULARITY	CODE
SAS-B	This spacecraft operated in an equatorial orbit, resulting in repetitive battery cycling at 22% DOD; the charge was temperature-biased voltage limit with 4 a max and a trickle rate of C/20. Battery voltage deteriorated with time, and within six months the voltage was below 1.1 V/cell. Reconditioning was tried but had only a temporary helpful effect. Increasing charge by removal of the coulometer did not help. Lowering temperature by restraint of spacecraft attitude helped a little. Though the spacecraft eventually failed due to a converter failure, such poor battery performance so early in its life may justifiably be viewed as a battery failure.	1
SAS-C	This spacecraft operated in an equatorial orbit, similar to SAS-B, resulting in repetitive battery cycling at 22% DOD; the charge was temperature-biased voltage limit with a 6 a max and a trickle rate of C/80. Battery voltage deteriorated with time, and within five months the voltage was below 1.1 V/cell. Reconditioning was tried but had only a temporary effect. Increasing charge by removal of the coulometer did not help. Lowering temperature by restraint of spacecraft attitude helped a little. The spacecraft is still functioning, but the reduced capability imposes operation limitations on the spacecraft. Such poor battery performance so early in its life may be viewed as a battery failure.	1
Intelsat 3	The Intelsat 3 series of five spacecraft had battery problems. Battery voltage during charge increased with operational life, causing early trip to trickle charge. As a result, the battery could not be fully charged and so there was a loss in capacity and inability to supply the load. In some flights, loads had to be reduced after about two years operation to make the spacecraft survive. The battery problem was determined to be due to the lack of enough overcharge protection and the use of wetting agent in the separator. The negative/positive ratio was only about 1.3. A more flexible charge control system would possibly have lengthened battery life.	1

Table 2. (Continued)

SPACECRAFT	FAILURE OR IRREGULARITY	CODE
Intelsat 4 F-2	After six years of the required seven years operation, one of the seven Intelsat 4 spacecraft went below the 1.15 V/cell limit, and loads had to be reduced. A voltage limit of 1.1 V/cell would probably have been a more realistic requirement, but it is unlikely that even this would have fully avoided the voltage problems. The spacecraft appears to have met its contractual load requirements in spite of this problem.	1
Intelsat 4A	Discharge voltage on one of the two spacecraft is within requirements, but with relatively little margin to spare. This fact, plus the fact that negative limited cells have been observed in ground tests, reduces confidence in the future performance of this battery.	1
Unspecified Spacecraft	Information on this unclassified spacecraft and its battery behavior are not publicly available. It has had low battery voltage anomalies, however.	1
Classified Spacecraft	A sudden open circuit occured on one of three batteries in a spacecraft. This was diagnosed as probably the opening of an intercell connector, caused by mechanical stress during cycling.	4
72-1	The design requirement for this was two years. After approximately three years, a short developed across one cell in each of two batteries. For a short while, there were two cells shorted on one of the batteries, but one of those two shorts opened. The battery and their charge control system were able to function properly in spite of these anomalies. This spacecraft has been working all right for five years.	3
Landsat-1	Eight batteries are parallel in this spacecraft. One of the batteries failed due to low discharge voltage and has been disconnected. Additional information on cause of failure is not available.	1
SMS-1	High voltage, in excess of 1.52 V/cell were reached during charge following discharge to 60% DOD. This problem was not observed during accelerated ground testing of a similar battery.	2

Table 2. (Continued)

SPACECRAFT	FAILURE OR IRREGULARITY	CODE
TETR	A flight failure on this spacecraft occurred when the case of one cell apparently shorted to the battery frame. Cell case and frame were separated by mylar. It is believed that constant pressure on the mylar eventually caused breakthrough. An internal cell short could also have caused this problem.	3
171	After 4.3 years trouble-free operation, one of two active batteries suddenly open circuited. It could not be determined whether the problem was with a cell, a solder joint, or a connector. One of two spare batteries was subsequently switched on to take the place of the failed battery and performed all right.	4
172, 173, 174	After a number of years operation, the batteries exhibited an increase in charge voltage and a decrease in discharge voltage. Spacecraft operation was unaffected, however.	1, 2
CTS	After two eclipse seasons on this geosynchronous spacecraft, battery voltage and capacity dropped below 1.15 V/cell at 50% DOD and capacity dropped to 70% of its initial value. Two reconditioning cycles gave a temporary improvement on ground tests. Ground test cells were found to be dry when opened.	1
ATS-6 (formerly called ATS-F)	Though the spacecraft design requirement was for two years, it has completed three years service. Voltage at 50% DOD point has degraded to 1.13 V/cell, and capacity has dropped to 12.4 AH from an initial value believed to be from 16 to 18 AH. End of charge battery voltage has been increasing with time, giving problems obtaining a full charge, since only one charge voltage level is used in the charger.	1, 2
ITOS	After several successful flights with this series of spacecraft, a problem of high charge current developed at high temperature, giving charge currents of about C/5 or C/6. This problem is believed to have been primarily a charger problem, and on subsequent spacecraft the voltage-temperature curve was lowered. Changes in battery characteristics probably also have contributed to this problem, however.	6

Table 2. (Continued)

SPACECRAFT	FAILURE OR IRREGULARITY	CODE
VELA 1	Within six months of spacecraft operation, several cells shorted in the battery. This is believed caused by silver used in the ceramic seal braze migrating across the ceramic.	3
VELA 2	Within six months of spacecraft operation, several cells shorted in the battery. This is believed caused by silver used in the ceramic seal braze migrating across the ceramic.	3
DODGE 1	After operating approximately 3½ years, a flight malfunction occurred which is believed to have been due to one cell shorting in the battery.	3

Table 3. CODE FOR BATTERY PROBLEMS

CODE	PROBLEM	NUMBER OF EVENTS	PERCENTAGE
1	Discharge voltage low	13	42%
2	Charge voltage high	5	16%
3	Short, cell or battery	5	16%
4	Open, cell, battery or circuit	2	6%
5	Problem not caused by cell performance	3	10%
6	Miscellaneous or unknown cause	3	10%

REFERENCES

1. L. A. Gibson, "Long-Life Ni-Cd Battery Evaluation", Aerospace Corp., memo 72.5113.17-3, 18 February 1972

2. R. E. Fischell, "Solar Cell Power Systems for APL Satellites", Sixth Photovoltaic Specialists Conference, March 28-30, 1967.

3. S. J. Faston, Private communication, March 22, 1977.

4. D. Baer, Private communication, April 14, 1977.

5. R. M. Sullivan, Private communication, March 28, 1977

6. W. M. Ray, "Results of SAS-B Battery Diagnostic Tests", APL memo S4S-5-030, 28 August 1973.

7. R. M. Sullivan, "Preliminary Look at Low Battery Voltage on SAS-C", APL memo S4S-5-155, September 18, 1975.

8. R. M. Sullivan, in The 1975 GSFC Battery Workshop, November 1975, Goddard Space Flight Center, pp. 161-169.

9. G. Van Ommering, Private communication, March 29, 1977.

10. W. R. Scott, Private communication, April 12, 1977.

11. J. Dunlop, Private communication, May 6, 1977.

12. S. J. Krause, Private communication, April 4, 1977.

13. J. Kettler, Private communication, March 30, 1977.

14. J. M. Graham, Private communication, April 27, 1977.

15. H. Thierfelder, Private communication, April 1, 1977.

16. J. D. Armantrout, Private communication, April 13, 1977.

17. J. D. Armantrout, in The 1975 FSFC Battery Workshop, November 1975, Goddard Space Flight Center, pp. 137-142.

18. F. Betz, Private communication, April 14, 1977.

19. J. Winkler, Private communication, May 4, 1977.

20. J. Lackner, in The 1976 GSFC Battery Workshop, November 1976, Goddard Space Flight Center, pp. 191-197.

21. T. A. LaVigna, Private communication, April 29, 1977.

22. G. Halpert, Private communication, April 18, 1977.

23. L. A. Gibson, "Secondary Battery Long Life Experience", Aerospace Corp. memo ATM 69(4129-01)-58, February 25, 1969.

24. W. Allan, Private communication, April 30, 197I.

25. L. Wilson, Private communication, April 26, 1977

NICKEL-CADMIUM CELL DESIGN

VARIABLE PROGRAM

DATA ANALYSIS

George W. Morrow
Goddard Space Flight Center
Greenbelt, Maryland 20771

ABSTRACT

A program was undertaken in conjunction with the General Electric Company to evaluate eight of the more important nickel-cadmium cell designs that are currently being used or that have been used during the past 15 years. Design variables tested in this program included teflonated negative plates, silver treated negative plates, light plate loading level, no positive plate cadmium treatment, plate design of 1968 utilizing both old and new processing techniques, and electrochemically impregnated positive plates. The data acquired from these test packs in a low earth orbit cycling regime is presented and analyzed here. This data showed conclusively that the cells manufactured with no positive plate cadmium treatment outperformed all other cell designs in all aspects of the program and that the cells with teflonated negative electrodes performed very poorly.

INTRODUCTION

A review of the design history of nickel-cadmium aerospace cells indicates that present cells bear only a slight resemblance to those used in the first satellite applications. The changes that have occurred in the cells can be attributed to a number of factors. The desire to improve energy density, the need for longer life, the need to improve production yield, the desire to enhance cell performance and the competitive drive to meet customer's requirements. Many of the changes have been tested and evaluated by the various users but there has been no systematic approach to compare to relative merits of each design. Consequently, a program was undertaken in conjunction with the General Electric (G.E.) to evaluate eight of the more important designs that are currently being used or have been used in the space program during the past 15 years. The objective of this paper is to present the test results and conclusions drawn from the Design Variable Program.

APPROACH

A cell with a proven heritage and a physical design similiar to that of other widely used aerospace cell sizes was a necessity in order to assure the validity of the data collected in this program. For these reasons the

G.E. 12Ah cell was selected as the Design Variable test cell. It had been used in the past with much success, therefore, its behavior was well documented and because its design is much like that of the 6 and 20Ah cells, the data collected could be adapted with confidence to those cells.

Eight of the most frequently used designs during the past 15 years were selected as the design variables to be used in this program. A specification was written for these designs and was incorporated into a G.E. manufacturing control document. After acceptance testing by G.E. and review and acceptance by the Goddard Space Flight Center (GSFC), the cells were shipped to the NASA Battery Test Facility at the Naval Weapons Support Center (NWSC) in Crane, Indiana were the Design Variable Test Program was carried out.

The test program consisted of two segments (Figure 1). First, an initial evaluation program was conducted. These tests were preformed in order to characterize each cell, to compare initial behavior, and to look for any manufacturing defects overlooked during acceptance testing. These tests were repeated on one cell from each design after 1 year and on all cells remaining from each group at the end-of-cycling. The two repetitions were carried out in order to compare degradation and performance based on the same criteria at different points during the life of the cells.

The second segment and principal part of the Design Variable Program was extended cycling in the low earth orbit (LEO) regime (Figure 2). This cycling regime utilized a higher than normal depth-of-discharge (DOD) of 40 percent in order to accelerate the cell degradation and therefore the test results. Data from this testing will indicate whether each variable is detrimental or beneficial to Ni-Cd cell performance in normal LEO orbit.

DESCRIPTION OF DESIGN VARIABLES

Using 12Ah cells, a control group and eight design groups of six cells per group were manufactured with the design paramenters as shown in Figure 3. A discussion of each group is as follows:

1. Control: This group represents G.E.'s basic aerospace design and processes as of 1978. The positives of these cells were subjected to cadmium treatment (PQ) as is indicative of G.E.'s process since 1970. The loading was somewhat lighter than normally used by G.E. during this time-frame. These lighter levels were chosen because the GSFC had recently procured two flight lots (IUE) with this design. The cells were manufactured with nonwoven nylon separator (Pellon 2505) and all cells recieved decarbonation treatment.

2. Teflon: These cells are identical to the control with the exception that the negatives were treated with teflon. As a result these cells also contain slightly more KOH than the Control.

3. Silver: This group is identical to the Control except the negatives had silver treatment and, as with Teflon, slightly more KOH.

4. Light Loading: The plates of this group have lighter loading (less active material) than those of the previous three groups. These plates are from the same impregnation post as the Control but are from different spirals. The purpose of this group was to evaluate a further reduction of plate loading with respect to initial and life benefits. Though no teflon or silver treatments were used, these cells contain 5cc more electrolyte than the Control cells.

5. No PQ: This group is identical to the Control except that the positives were not subjected to the PQ treatment. The positive plates are from the same impregnation post as the control but from different spirals. The negative plates are from the same spiral as the Control.

6. Polypropylene: This group contains all of the design parameters of the Control except that GAF polypropylene separator material was used in place of nylon.

7. A.K.-Old Process: This design is indicative of cells made during the middle sixties, i.e., the cells are made with the plate design and processes of that era. Specifically, no PQ treatment was used, the negatives were not depleted during the flooded cell test, and there was no decarbonation. Also, the plate design was different than the control and there was no precharge adjustment made to the cells.

8. A.K.-Present Process: This group contains the same plate lot as the A.K.-Old Process. However, these cells were processed using the same aerospace procedures and practices as the Control.

9. Electrochemical: This design contains electrochemically impregnated positives. All other variables are identical to the Control. This was an early attempt by G.E. to use electrochemical impregnation in cell manufacture.

It is noted that the amount of KOH varies from group-to-group. The criteria for determining the amount of KOH was to obtain the maximum KOH allowable in each group consistent with reasonable overcharge pressures. The overcharge pressure design goal was 30 to 76 PSIA.

The cell procurement specification requires the precharge to be set to 40 $\pm$ 5 percent of the excess negative. Since 4.6 ampere-hours of precharge on Group 1 through 6 represents between 38 and 41 percent of the excess negative, it was decided to precharge all cells in these 6 groups the same. As stated previously the A.K.-Old Process group not was precharged. The A.K.-New Process was precharged to 1.8 ampre-hours which represents 37 percent of the excess negative. The Electrochemical group was precharged to 5.8 ampere-hours which is essentially the same percentage that was used in groups 1 through 6.

INITIAL EVALUATION TEST RESULTS

Initial evaluation tests were carried out at NWSC-Crane before the start of LEO cycling, after 1 year on one cell from each group, and all remaining cells in each group at the end of cycling. All evaluation tests were performed at room ambient pressure and temperature with discharge at the 2-hour rate unless otherwise noted. The tests consisted of the following:

a. Phenolphthalein leak test.

b. Three capacity tests, the third at 20°C and internal resistance measurements made during the second.

c. Charge retention test, 20°C.

d. Internal short test.

e. Charge efficiency test, 20°C.

f. Overcharge tests at 0°C, 25°C, and 35°C.

g. Phenolphthalein leak test.

The room ambient capacity test, the 25°C overcharge test, and the 0°C overcharge test proved to be the most benefical for behavior comparison between the groups.

ROOM AMBIENT CAPACITY TEST RESULTS

The room ambient capacity test consisted of a charge at the 20-hour rate for 48 hours followed by a discharge at the 2-hour rate to 0.7 volts per cell. The initial, 1 year, and end-of-cycling capacities are shown in Figure 4.

This data indicates that the capacity loss for most groups to the end-of-cycling (3 to 4 years) was between 24 percent and 35 percent excluding only the Polypropylene, Electrochemical and No PQ groups.

Thirty-nine precent of the initial tested capacity of the Polyropylene group was gone within the first year under the LEO cycling regime. This first year capacity loss was the greatest among any of the groups as was the total capacity loss of 49 percent at the end of 3 years of cycling. Conversely, the Electrochemical group appears to have lost the least capacity with a loss of only 2 percent at the end-of-cycling. This is misleading, however, because this group remained on test for only 2.5 years (14000 cycles), and there was no 1-year test point available for comparison.

The No PQ group remained on test for 4 years (23300 cycles) and had lost the least amount of capacity of any group at the 1 year point, only 6 percent, but could not be recharged after the end-of-cycling and, therefore, no capacity data point was obtained. The other groups that remained on test for 4 years, Control and A.K.-Old Process, showed average capacity performance not only to the 1 year point showing 21 percent and 16 percent capacity losses respecitvely, but also to the end-of-cycling as was mentioned above.

25°C OVERCHARGE TEST RESULTS

The 25°C overcharge test consisted of a constant current charge at the 10-hour rate for 24 hours. The initial, 1 year, and end-of-cycling, end-of-charge (EOC) voltages reached during this test for all design groups are presented in Figure 4. Groups 1, 2, 3, 5, 6, and 9 showed little or no change in the EOC test voltage levels during life. The voltages reached by these groups were in the normal range for aerospace Ni-Cd cells and ranged from 1.454 volts to 1.465 volts. Of the groups mentioned above, the Control group showed the highest voltage each time tested followed by Polypropylene and the A.K.-Old Precess group.

Group 4, Light Loading, initially has an average EOC test voltage of 1.458 volts but when the test was repeated at the 1-year point the test voltage had risen to 1.477 volts. However, the EOC test voltage at the end-of-cycling was in the normal range. Group 8, A.K.-Present Process, also showed an EOC test voltage rise at the 1-year point with a voltage of 1.520 volts causing the charge to be stopped prematurely. Unlike Light Loading, however, an abnormally high EOC test voltage remained at the end-of-cycling indicating that these cells were "negative limited" and had been so since before the 1 year retest. The A.K.-Old Process group, even though it was made with the same plate as Group 8, surprisingly showed no signs of being "negative limited" until the remaining cells were tested at the end-of-cycling (4 years). This difference, therefore, has to be due to the differences in the plate processing techniques used on each group. Both groups initially had a lower negative to positive ratio than the other groups because of the 1968 design and so from the beginning possessed a strong tendency to becoming "negative limited." In addiiton to this, the plate forming or ECT processes of the present process, because of a longer reversal time and additional precharge adjustment, caused the amount of excess negative in the group to be reduced to a much greater extent than in the old process group. The effect of less excess negative is a rise in voltage during overcharge, a condition in which cells are said to be "negative limited." This is exactly the effect shown during this test.

0°C OVERCHARGE TEST RESULTS

The 0°C overcharge test consisted of a constant current charge at the 20-hour rate for 60 hours. The initial EOC voltages, and the 1 year, and end-of-cycling EOC and peak voltages are presented in Figure 5.

The overcharge test produced contrasts of a much greater magnitude between the groups on test than did the 25°C test. It showed that by the 1 year retest the Light Loading, No PQ, Polypropylene, A.K.-Old Process, and A.K.-Present Process groups all had higher than normal peak and EOC test voltages which indicated they had become "negative limited." In fact, the charge was stopped prematurely on each of these groups because of high voltage or pressure. By contrast, the Teflon group showed the lowest peak test voltage of any group, at 1 year, at 1.529 volts followed by Silver at 1.546 volts, and the Control at 1.551 volts.

At the end-of-cycling only the A.K.-Present Process and A.K.-Old Process groups had high EOC test voltage and therefore, were the only groups which appeared to be "negative limited" at the end-of-cycling. This agreed with the results obtained during the 25°C overcharge test. The Teflon group showed many intermittent shorts during this test at the end-of-cycling and thus, the data obtained is not valid and, in fact, represents on one of the four cells; the others could not be charged. The No PQ group formed internal shorts prior to the start of the end-of-cycling evaluation tests as was discussed previously.

LOW EARTH ORBIT CYCLING TEST RESULTS

The data analysis to be presented will concentrate on the 6 design groups that performed the best during the test program and that provided the most pertinent information with regard to the application of aerospace Ni-Cd cells. The 6 groups are the Control, Teflon, Silver, No PQ, A.K.-Old Process, and Electrochemical.

A comparison of the capacity performance of each of the groups during cycling is very beneficial to the evaluation of each design variable. Therefore, capacity checks were performed on different cells in each group at 6 month intervals through 2 years and then yearly to the end-of-cycling. These capacity checks consisted of a discharge at the nominal cycling discharge rate (9.6 amps) to a voltage of approximately 0.75v.

The 1, 2, and 3 year capacity plots for the 6 groups are shown in Figures 6, 7, and 8 respectively. A 4-year capacity plot for the Control, No PQ, and A.K.-Old Process group is shown in Figure 9. These plots indicate that the above 3 groups consistently maintained a greater capacity than any of the other groups tested and of those 3, the No PQ performed better than the other 2.

A more accurate representation of this behavior is presented in Figure 10, where the precent of the initial actual capacity versus cycle number is plotted for each group. This plot decisively shows that the No PQ group, from the beginning, lost the least amount of capacity on a precentage basis than any other group. This group lost only 15 percent of its initial capacity during 3 years of cycling and 55 percent by the end-of-cycling.

This is compared to the Control group loss of 35 percent in 3 years and 60 percent by the end-of-cycling, and the A.K.-Old Process group loss of 40 percent in 3 years and 52 percent when taken off test. The Teflon and Silver groups lost 65 percent and 59 percent of their initial capacities in 3 years and the Electrochemical group lost 22 percent of its capacity in 2.5 years. The capacity loss percentages do not necessarily agree with the capacity loss percentages presented for the evaluation tests. The discrepancies resulted from differences in the discharge current used in each of the tests. All discharges during the evaluation tests were at the 2-hour rate while those performed during the cylcling capacity checks were at the 1.3-hour nominal cycling rate. Also, a partial reconditioning took place before the evaluation test each time.

Another parameter that provides a good indication of the performance of a cell during LEO cycling is the end-of-eclipse (EOE) voltage. A comparison of the EOE voltages throughout life for the 6 groups selected is found in Figure 11. The figure again shows that the No PQ group outperformed the other groups by maintaining an EOE voltage of 1.14 volts from 7500 through 19000 cycles after slowly declining from a beginning-of-life EOE voltage of 1.21 volts and before beginning a sharp decline at the end-of-cycling. The A.K.-Old Process group performed better than the No PQ group at the beginning-of-life but leveled off at a lower EOE voltage of 1.12 volts. The Control group also provided adequate performance after a sharp decline at the beginning-of-life but maintained an EOE average voltage of only 1.03 volts throughout most of its cycle life.

The Silver, Teflon, and Electrochemical groups did not perform as well as the others. The Silver group parallelled the Control group until approximately cycle 11000 then it began a steady EOE voltage decline ending with an EOE voltage of 0.94 volts at the end-of-cycling (17300 cycles). The Electrochemical group began life by making a very sharp EOE voltage drop to 1.06 volts at 1500 cycles. It then maintained approximately this voltage until the end-of-life. The Teflon group performed worse than any other group showing a steady voltage decline throughout life. The EOE voltage of this group was 0.89 volts at the end-of-cycling (17300 cycles) the lowest end-of-cycling voltage of any of the 6 groups.

A plot of the percent recharge for each group throughout life is presented in Figure 12. A nominal percent recharge of 115 percent was to be maintained throughout life by adjusting the charge voltage limit of each pack. A percent recharge of 115 percent was not maintained. However, this plot shows that all groups maintained a recharge percentage high enough to assure that full charge was being achieved and the delta between the groups was less than 5 percent with few exceptions. Therefore, all groups were maintained in approximately the same state throughout life which indicates that all data collected during the LEO cycling test was valid.

CONCLUSIONS

The No PQ group outperformed all other Design Variable Program groups in both the area of capacity and end-of-eclipse voltage. This performance was rivaled only by the Control group that had PQ but no other treatment and the 1968 A.K.-Old Process group which did not have PQ. The failure of the No PQ group to accept charge at the end-of-cycling did leave a question mark by its performance. Inability to accept charge is an indication that hard shorts had developed between the plates in all cells, a condition that is caused by excessive cadmium migration.

The Electrochemical group showed a capacity loss lower than most other groups, especially during the evaluation tests, and enhanced active material utilization. It did not perform at the same level as the No PQ group, however, and had a very low beginning-of-life capacity as a result of the low positive plate loading levels it possessed. Undoubtedly, the cause of these low positive loading levels was that this was an early attempt by G.E. to use electrochemical impregnation in cell manufacture. Because of the indications of decreased capacity loss and enhanced active material utilization, and in light of the advances made in this area in the past 6 years, this process should be reevaluated with respect to the aerospace energy storage program.

The Teflon and Silver treatments enhance the rate of oxygen recombination and thus allow a greater amount of electrolyte to be added to the cells. One or the other of these treatments is strongly recommended by the manufacture and previous acceptnace and life test data indicated that these treatments improved cell performance. On the contrary, these groups showed the poorest performance of any of the 6 groups analyzed. The Teflon group, which is the currently accepted GSFC design, consistently gave the poorest performance of any group in all aspects of the design variable test program. This group had the highest capacity loss and the lowest end-of-eclipse voltages of any group tested. It also had intermittent shorts at the end-of-cycling (17300 cycles) which indicates excessive cadmium migration. A condition the Teflon supposedly prevents. The merits of this design should clearly be reevaluated in light of its poor performance and the strong performance of other designs.

References

1. Baer, D. and Ford, F., Proceedings of the Symposium on Battery Design and Optimization, the Electrochemical Society, Inc., 1979, page 114.

2. Baer, D., 1978 GSFC Battery Workshop, NASA CP 2088, pages 49-56.

- INITIAL EVALUATION TEST*
  - LEAK TESTS
  - CAPACITY TESTS
  - INTERNAL RESISTANCE AND SHORT TEST
  - CHARGE RETENTION TESTS
  - CHARGE EFFICIENCY TEST
  - OVERCHARGE TESTS
  - PRESSURE VERSUS CAPACITY TESTS
- LOW EARTH ORBIT CYCLING

* TESTS REPEATED AFTER 1 YEAR CYCLING AND AT END OF PROGRAM

Figure 1. Design Variable Test Program

o TEMPERATURE	20°C
o DEPTH-OF-DISCHARGE	40 PERCENT
o ORBIT PERIOD	90 MINUTES
o CHARGE CURRENT	9.6 AMPS TO A VOLTAGE LIMIT (1.453 V/CELL TYPICAL)
o DISCHARGE CURRENT	9.6 AMPS

Figure 2. Leo Cycling Test Regime

	VARIABLE	PACK NO.	POS LOADING G/DM^3 OF SINTER	NEG LOADING G/DM^3 OF SINTER	FINAL KOH QUANTITY, CC	PRECHARGE[1] ADJUST AH
1.	CONTROL	3D	2095	2180	40	4.6
2.	TEFLON	3E	2095	2180	48	4.6
3.	SILVER	3F	2095	2180	43	4.6
4.	LIGHT	3G	1840	1833	45	4.6
5.	NO PQ	3H	2113	2180	40.3	4.6
6.	POLYPROYLENE	3I	2095	2180	39	4.6
7.	AK-OLD PROC	3J	2130	2542	38	0.0
8.	AK-PRES PROC	3K	2130	2542	39	1.8
9.	ELECTROCHEM	3L	1276[2]	2280	48	5.8

[1] BASED ON 228 CC O_z/Ah

[2] BY HYDRATE PICK-UP, NOT HYDRATE REDUCTION

Figure 3. Design Variable Program—Cell Manufacturing Information

			EOC VOLTAGE C/10 CHARGE FOR 24 HOURS AT 25°C			25°C CAPACITY TO 0.7V (AMP HOURS)		
	VARIABLE	PACK NO.	INITIAL	1 YEAR	EOL	INITIAL	1 YEAR	EOL
1.	CONTROL	3D	1.462	1.465	1.461	15.3	12.1	10.6 (4 YEARS)
2.	TEFLON	3E	1.455	1.457	1.447	14.7	12.5	10.1 (3 YEARS)
3.	SILVER	3F	1.456	1.458	1.450	15.2	12.1	11.5 (3 YEARS)
4.	LIGHT	3G	1.458	1.477	1.455	13.9	11.6	10.1 (3 YEARS)
5.	NO PQ	3H	1.454	1.452	--	16.0	15.1	-- (4 YEARS)
6.	POLYPROPYLENE	3I	1.459	1.457	1.450	15.6	9.5	8.0 (4 YEARS)
7.	AK-OLD PROC	3J	1.459	1.419	1.520[1]	17.7	14.9	11.5 (4 YEARS)
8.	AK-PRES PROC	3K	1.458	1.520[2]	1.522[3]	17.4	18.0	12.5 (3 YEARS)
9.	ELECTROCHEM	3L	1.456	--	1.480	10.8	--	10.6 (2.5 YEARS)

[1] TEST TERMINATED AT 17 Ah IN DUE TO HIGH VOLTAGE

[2] TEST TERMINATED AT 23.4 Ah IN DUE TO HIGH VOLTAGE

[3] TEST TERMINATED AT 15 Ah IN DUE TO HIGH VOLTAGE

Figure 4. Design Variable Probram, Initial Evaluation Test Results
Initial, After 1 Year, End of Program

	VARIABLE	INITIAL EOC	AFTER 1 YEAR EOC	AFTER 1 YEAR PEAK	END-OF-CYCLING EOC	END-OF-CYCLING PEAK
1.	CONTROL	1.496	1.508	1.552	1.510	1.537
2.	TEFLON	1.486	1.496	1.529	1.433[3]	1.433[3]
3.	SILVER	1.494	1.494	1.546	1.496	1.527
4.	LIGHT	1.492	1.567	1.577[1]	1.512	1.542
5.	NO PQ	1.508	1.599	1.600[1]	---[4]	---[4]
6.	POLYPROP	1.497	1.578	1.583[1]	1.509	1.540
7.	AK-OLD PROC	1.575	1.585	1.583[2]	1.602	1.610[1]
8.	AK-PRES PROC	1.578	1.572	1.585[2]	1.608	1.611[1]
9.	ELECTROCHEM	1.495	---	---	1.506	1.539

[1] TERMINATED DUE TO HIGH VOLTAGE (VOLTAGE EXCEEDED 1.56V FOR 2 HOURS)

[2] TERMINATED DUE TO HIGH PRESSURE, > 100 PSIA.

[3] ALL CELLS IN TEFLON GROUP SHOWED INTERMITTENT SHORTS.

[4] ALL CELLS IN NO PQ GROUP SHORTED.

Figure 5. Design Variable Program, Initial Evaluation Test Results (Continued)

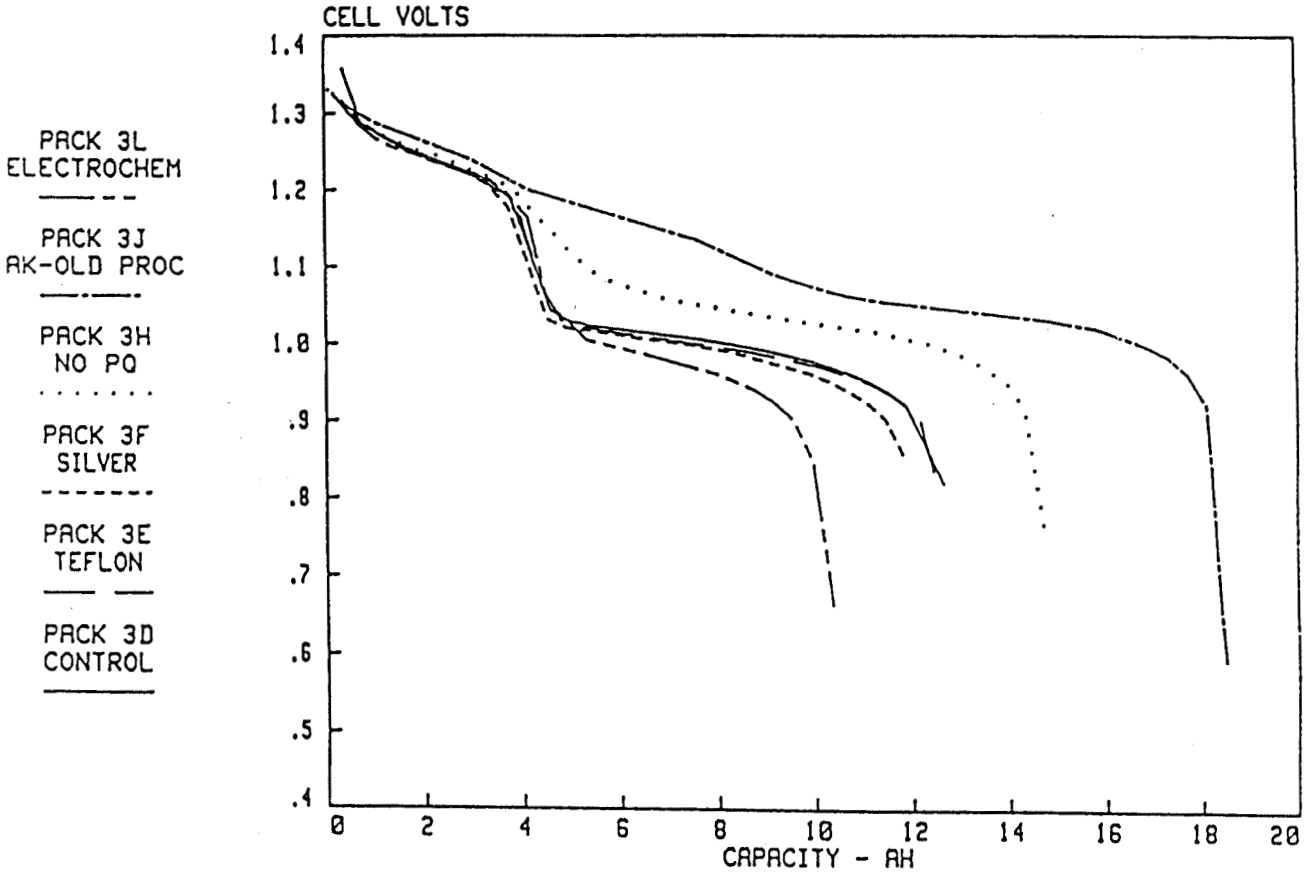

Figure 6. Design Variable Program
1 Year Capacity Comparison—9.6 Amp Discharge

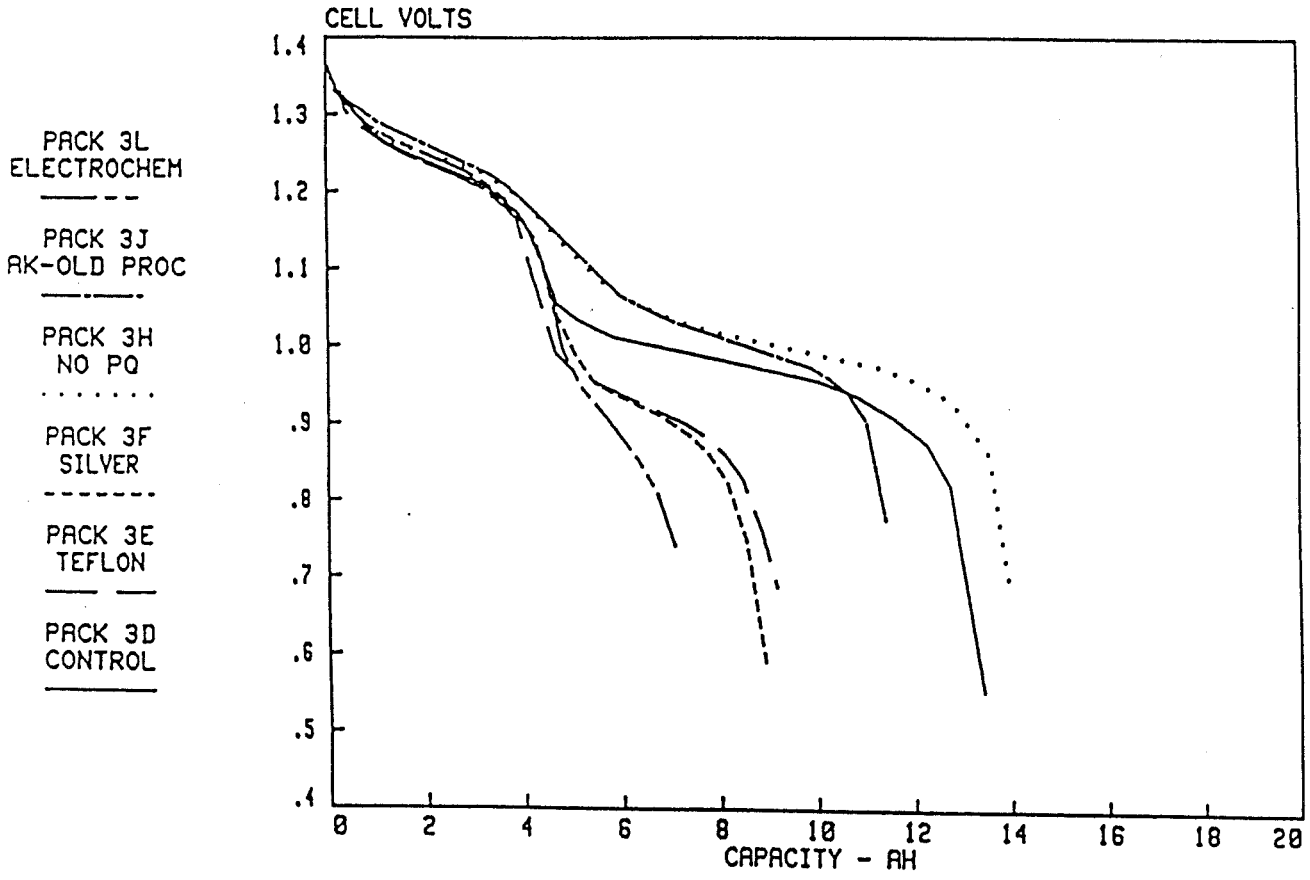

Figure 7. Design Variable Program
2 Yr Capacity Comparison–9.6 Amp Discharge

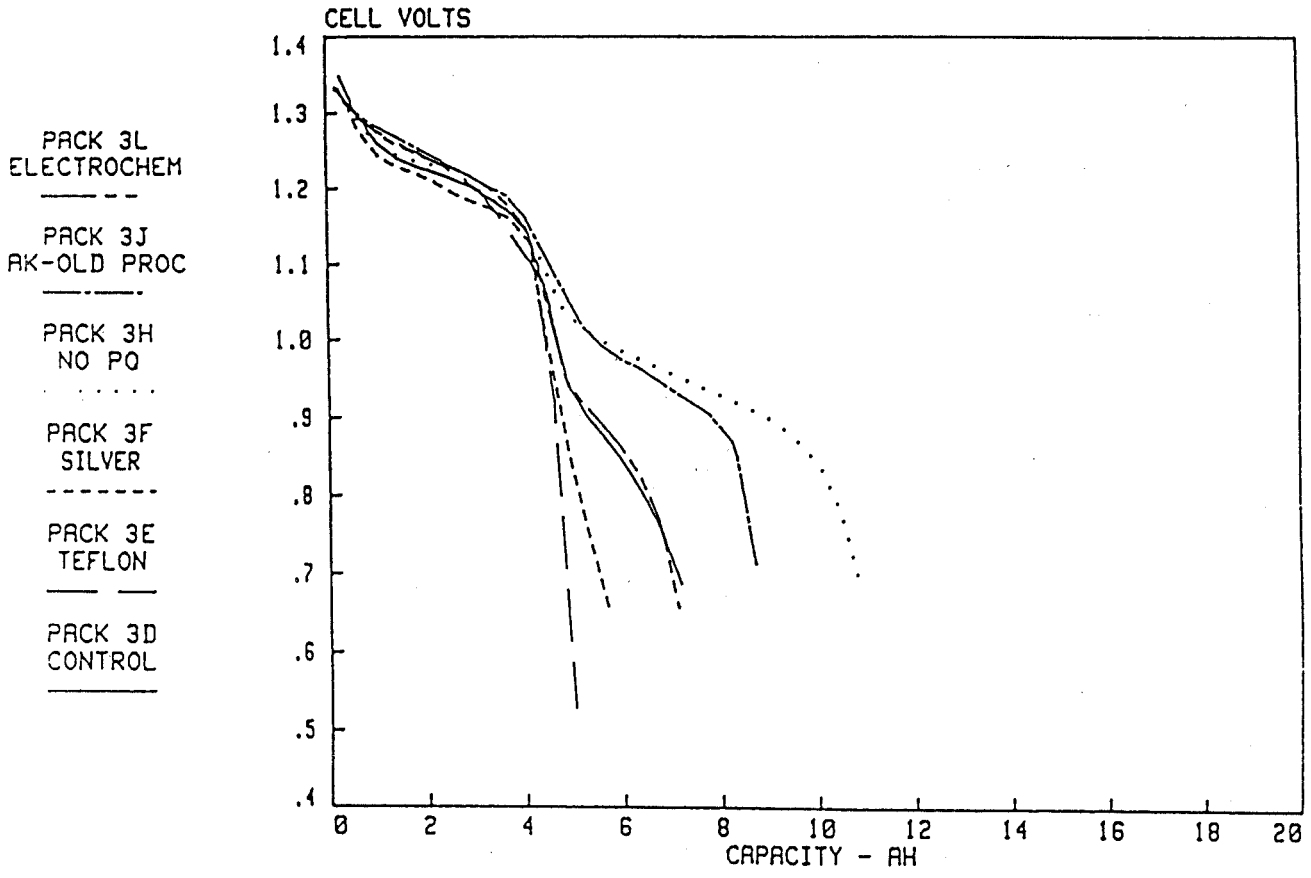

Figure 8. Design Variable Program
3 Yr Capacity Comparison–9.6 Amp Discharge

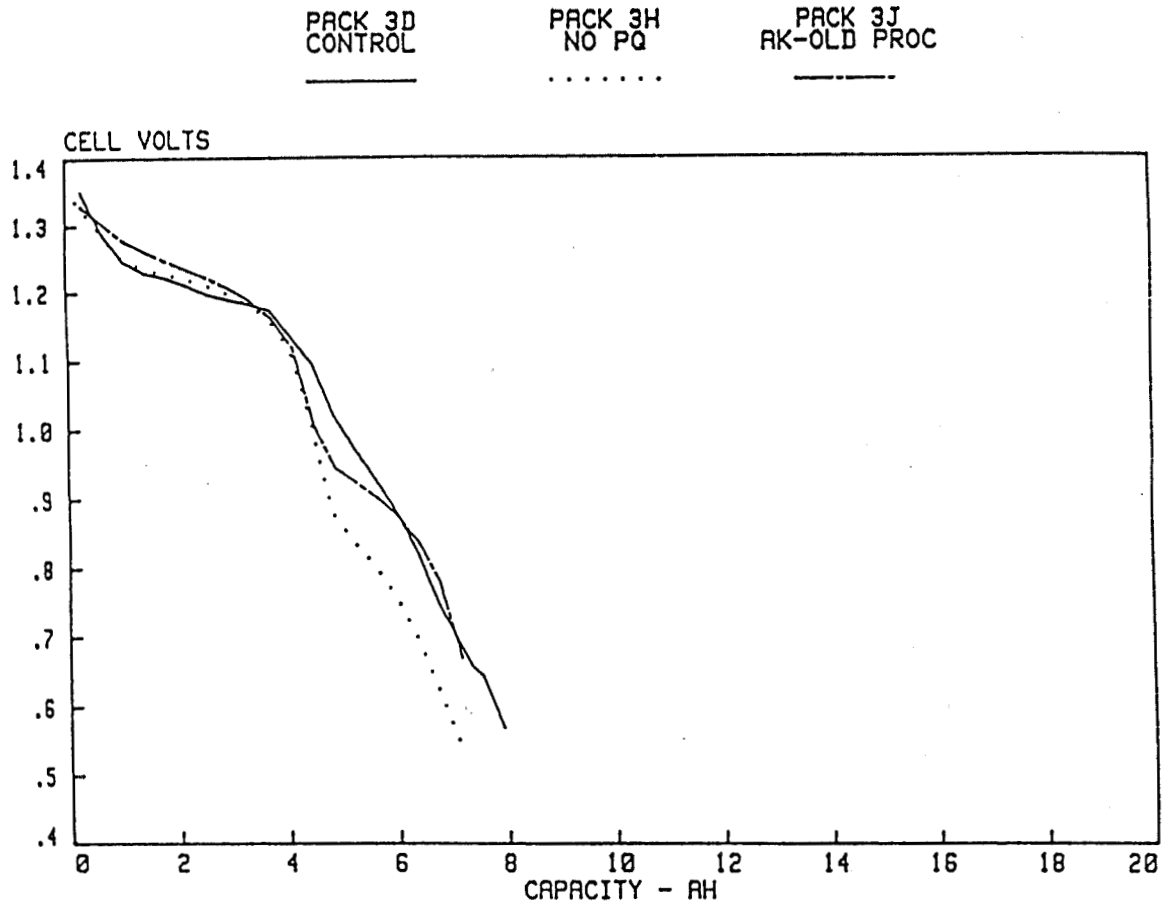

Figure 9. Design Variable Program
4 Yr Capacity Comparison–9.6 Amp Discharge

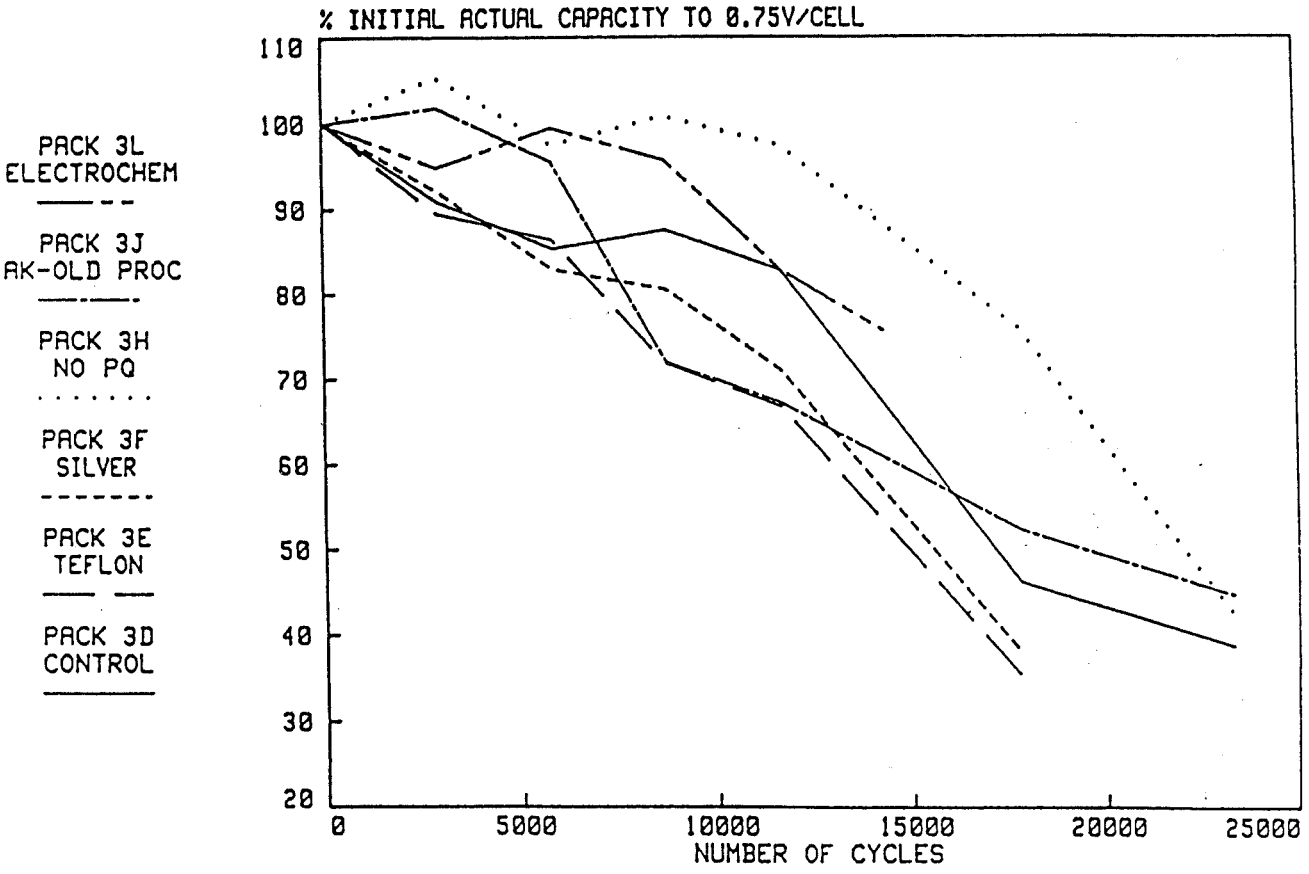

Figure 10. Design Variable Program
Percent of Initial Actual Capacity Comparison

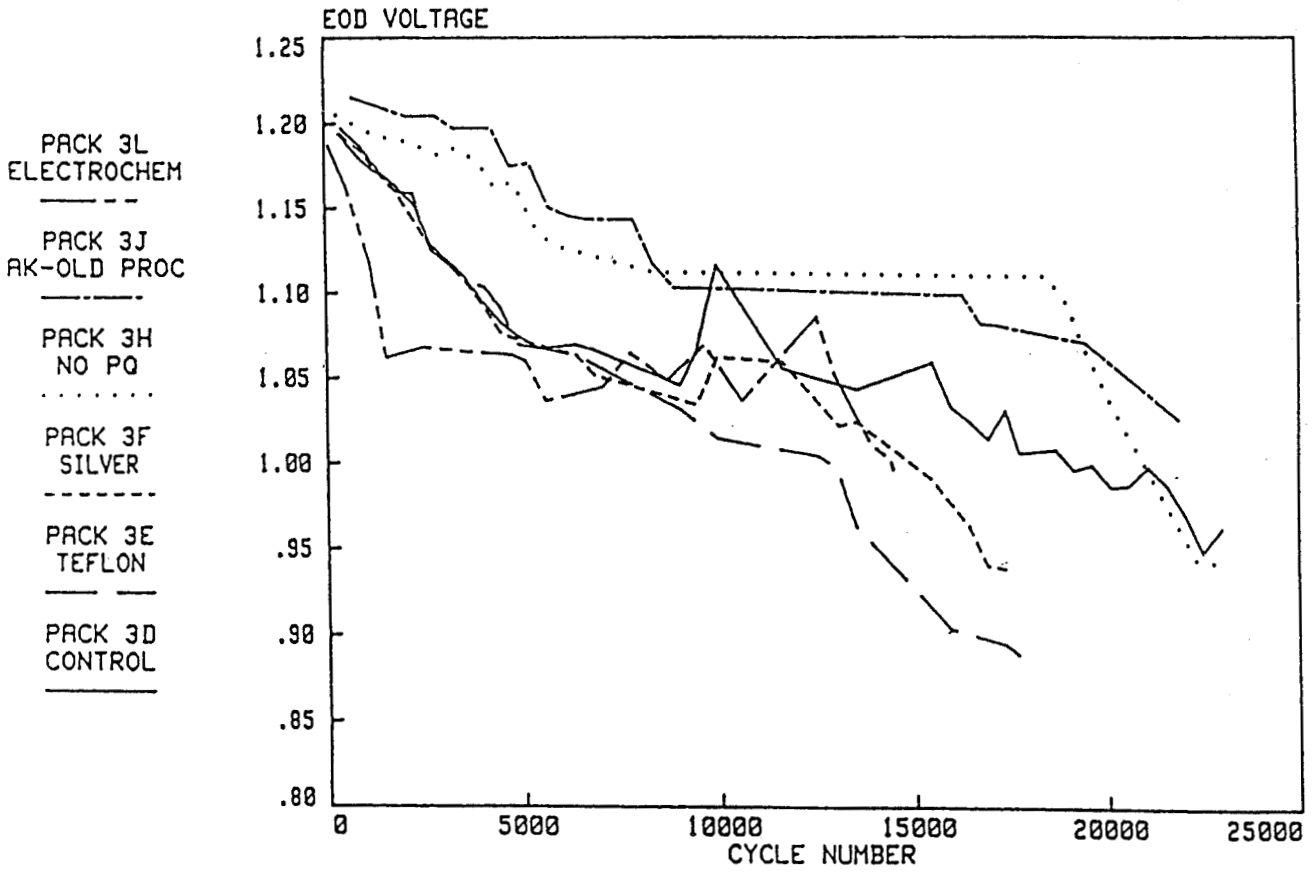

Figure 11. Design Variable Program
End of Eclipse Voltage Comparison

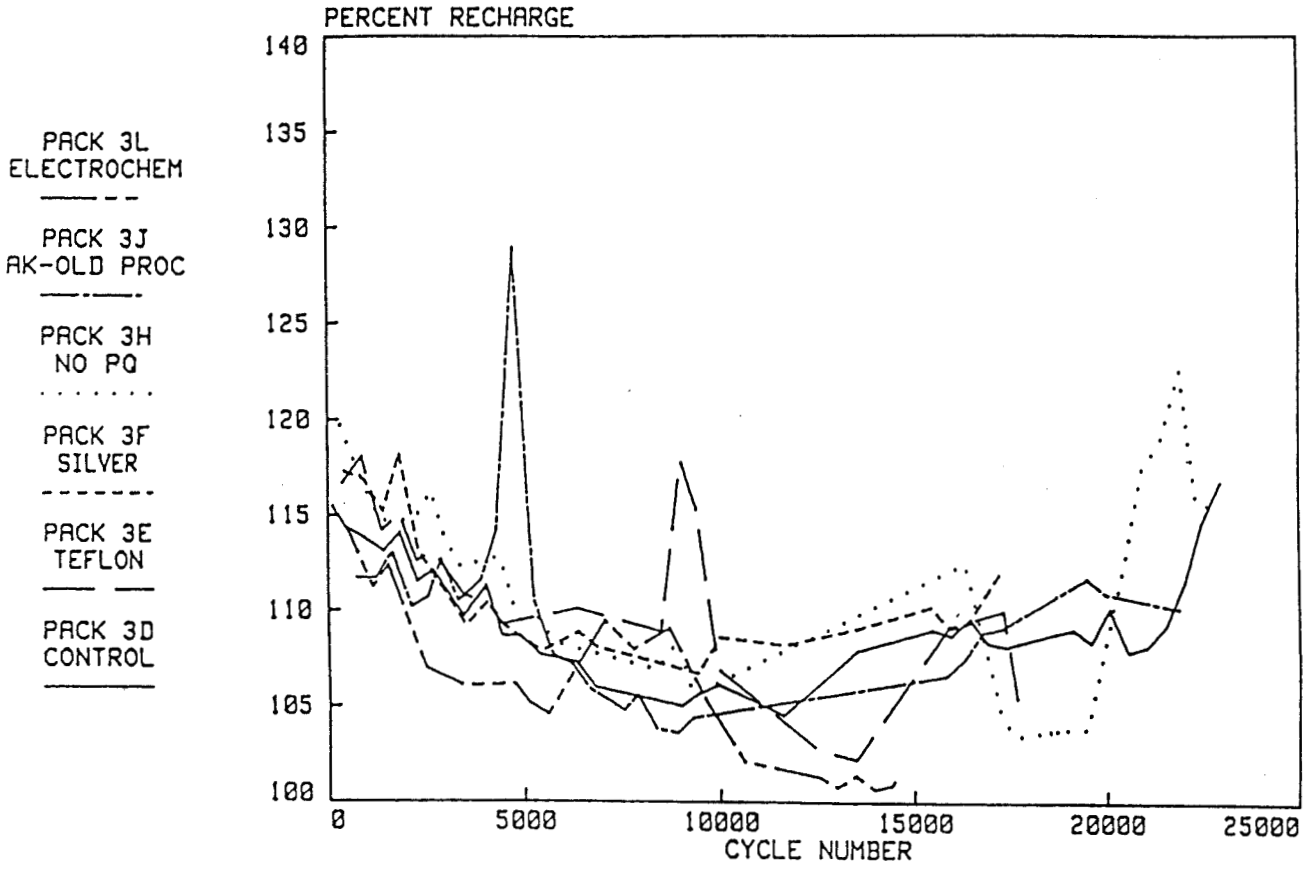

Figure 12. Design Variable Program
Percent Recharge Comparison

RESULTS OF ANALYSIS ON THE DESIGN VARIABLE CELLS

KUNIGAHALLI L. VASANTH
BOWIE STATE COLLEGE

INTRODUCTION

Sealed Nickel-Cadmium aerospace cells play a very important role in the mission of the satellite. There has been a constant effort to improve the cycle life, energy density, and reliability of these cells by many manufacturers and users. The Design Variable Cell Program is one systematic approach started by NASA in collaboration with General Electric (GE) towards that goal. Nine important designs were selected for evaluation.

Fifty-two nickel-cadmium cells each of 12AH nominal capacity manufactured by GE were sent to the Naval Weapons Support Center for evaluation of different design variables with which these cells were built. Figure 1 shows the different plate treatments and designs of the cells. The evaluation test procedure and the results of evaluation have been documented by Jim Harkness in the report WQEC/C 79-114 in December 1979 [1]. These cells were then life cycled in a Low-Earth Orbit (LEO) regime.

In February 1979 eight 5-cell packs, pack 3D through 3K corresponding to Group 1 to 8, were put on life test. The life test parameters were:

Temperature	20°C
Cycle Period	90 Minutes
Depth-of-Discharge	40 Percent
Charge Rate	9.6 Amps
Discharge Rate	9.6 Amps
Voltage Limit Per Cell	1.453
Percent Recharge	110 to 115

Cells of Group 9, Pack 3L, were put on life test in August 1979 with the same test regime.

A brief description of the design variables for each group of cells is given by George Morrow in his paper in the present proceedings, and, hence will not be repeated here.

After 1 year of cycling, one cell from each pack was removed and the initial evaluation tests were repeated. An update of the results of evaluation test and performance of these cells was presented by David Baer in the 1981 Battery Workshop [2]. The results of chemical and electrochemical analysis of the cells that were pulled out were presented by Kunigahalli Vasanth [3].

The purpose of this presentation is to give an update on the performance of the design variable cells along with the results of chemical, electrochemical analysis and capacity checks performed on cells that were cycled 3 to 4 years.

Experimental Approach

The experimental techniques that have been followed in this investigation are:

- o Visual Inspection
- o Physical Measurements
- o Chemical and Electrochemical Analysis
- o SEM Examination

A teardown analysis of each cell was carried out according to the analysis procedures given in the NASA Document X-711-74-279 Revision A.[5].

Visual Examination

On opening the cells, it was found that the cell pack was usually moist with electrolyte, the extent varying from one cell to another. With the exception of one or two groups, the separators were deteriorated very much and invariably were stuck to the surface of the negative electrode. In other words, the separator bags could not be taken out in one single piece as in the case of uncycled cell. The separator that came off the electrodes had dark to light gray patches due to different extents of cadmium migration. The polypropylene separator group cell showed very heavy cadmium migration although the separators came off in one piece (Figure 3). Strong adherence of the thin film of separator material on the negative electrode is common to all the other groups (Figure 4). The positive electrode could be easily separated from the separator.

One of the cells of Group 2 was found to have a short. The short as one can see from Figure 5 is extended to a couple of plates on either side in the stack. The SEM's in and around the short on the positive plate shows the presence of large crystals of $Cd(OH)_2$ which obviously must have migrated from the neighboring negative plate and pierced the separator material thus causing the cell failure. This particular cell was identified in the life test regime to be one that was not accepting charge. Figures 6 and 7 show the short and crystals on the negative and positive plate, respectively.

Physical Measurement

Each design variable 12AH cell consists of 11 positive and 12 negative plates. The positive plates were housed in a bag of separator material. Physical measurements involve the recording of the weight and thickness of each plate and are given in Table 1. The thickness is measured in three separate places (top, middle, bottom) and later averaged. These measurements were done after the positives, negatives, and the separators were soxhleted separately in order to extract the electrolyte and further dried in an oven at $45^{o}C$ overnight in a nitrogen atmosphere.

For all the groups, the thickness of the positives is plotted versus the number of cycles in Figure 8. The general behavior that can be seen in these curves is that the positive swelling takes place linearly during the first 6,000 cycles finally tending to taper off to a limiting value. In

the case of positives of cells of Groups 2, 3, 4, and 6, the flat part of the curve after about 18,000 cycles indicates that the thickness is reaching a limiting value. As the cell ages, swelling of the positive plate occurs leading to the squeezing of the deteriorated separator material and electrolyte loss between the plates. The dryness of the plates may result in cell failure.

P. McDermott and E. Sommerfeldt [6] reported in the analysis of data from the Accelerated Test Program on 6.0AH aerospace nickel-cadmium cells, that there was a strong negative correlation between interelectrode separation and number of cycles. They also have shown that as the separation decreases, so does the amount of electrolyte in the separators. Our results are in agreement with their observations (see Table 2). Electrolyte decreases in the separator as the positive swells due to cycling. H. Lim [7] has reported that the nickel electrode expands during discharge and that there is a linear relationship between the bending rate (expansion) and depth-of-discharge. The results of nearly 4 years of cycling of the design variable cells shows that at a fixed rate of DOD (40%) the positive swelling is linear with respect to the first few thousand cycles (4000) and is likely to reach a limiting value later on.

Electrolyte Analysis

The results of the electrolyte analysis for all the design variable groups are given in Table 2. Within a given group, the carbonate content generally increases as a function of the number of cycles. This should be expected since the Pellon separator material is a polyamide of the formula $(-NH-(CH_2)_5-CO)_n$. The amide groups (-CONH-) that link the hydrocarbon react slowly with the hydroxyl ions of the electrolyte increasing the wetability and ultimately leading to the decomposition of the separator thus increasing the carbonate level. This also leads to the degradation of the properties of the separator. The results also show that the electrolyte distribution follows the same order for all the groups considered and seem to be independent of the number of cycles.

The electrolyte distribution order is NEG>POS>SEP.

Capacity and Utilization (See Table 3)

For purposes of comparison, it may be necessary to divide the groups into three categories:

(1) Groups 2, 3, 4, 6, and 8 that underwent approximately 17,300 cycles
(2) Groups 1, 5, and 7 that underwent approximately 23,000 cycles
(3) Group 9 that underwent approximately 14,827 cycles

Considering the first category the polypropylene group (Group 6) is the one that is hard hit. It not only shows very heavy cadmium migration, but low positive and negative plate capacity and utilization. Among the other groups in this category, Teflon (Group 2) and Light Loading (Group 4) show equal performance with regard to capacity and utilization. But the visual examination of cells show that the teflonated cell separators have cadmium migration higher than that in the case of cells with light loading (Group 4). In addition, one of the teflonated cells failed at 16,150

cycles due to severe shorting which can be related to cadmium migration.

In the second category, the Control (Group 1) and No Pq (Group 5) groups performed better than the A.K. Plate Old Process and the other groups as well. SEM's of the sample electrode plates from Group 1 and Group 5 are shown in Figures 13-16. Analysis by George Morrow shows that the No Pq lost only 15% of initial capacity in 3 years of cycling and about 55% by the end of cycling, i.e., 4 years. A first look at the capacities and utilization in Table 4 for the cells in category 2, shows that all three groups seem to have performed equally. However, the A.K. Old Plate Process has large carbonate content compared to control and No Pq groups. But the positive swelling is small (refer to Table 1 and Table 2). Analysis of electrical test results show that the No Pq group lost only 15% of initial capacity in 3 years of cycling, and about 55% by the end of cycling. Further, a comparison of the end-of-eclipse voltages for these design variable groups have shown that the no pq group performed better than the rest of the groups.

It is rather difficult to choose between the Control and No Pq group, in that, the chemical analysis and electrochemical results are almost similar and group 1 shows a higher percent of utilization. A closer analysis between these two groups now becomes necessary to decide one way or the other.

NOTE: The baseline capacity test is designed to determine the actual plate capacity after a 100% overcharge based on the manufacturer's nominal cell capacity.

Cycling test is designed to determine the steady state cycling capacity. The duration of each charge cycle assures an input of 120% of the baseline capacity. The capacity of each cycle is measured at C/2 rate of discharge. The capacity obtained on the third cycle is defined as the steady-state capacity.

The author expresses his appreciation to Sher Khan, Angelie McNair, and Dr. M. Rock of Bowie State College for their help in the analysis, to Diane Kolos and Brad Parker of the Goddard Space Flight Center for pictures and SEM's, and to NASA/Goddard Space Flight Center for the award of Grant NSG-5009.

FIGURES

REFERENCES

1. J. Harkness, "Initial Evaluation Tests of GE 12AH Nickel-Cadmium Spacecraft Cells with Design Variables," WQEC/C 79-114, December 1979

2. D. Baer, "Comparisons of Different Plate Treatments and Designs - An Update," GSFC Battery Workshop Proceedings, NASA CP 2217, p. 435, November 17-19, 1981

3. V. Kunigahalli, "Comparisons of Different Plate Treatments and Designs Analysis," GSFC Battery Workshop, NASA CP 2217, p. 443, November 17-19, 1981

4. G. Morrow, "Nickel-Cadmium Cell Design Variable Program Data Analysis," GSFC Battery Workshop Proceedings, November 13-15, 1984.

5. G. Halpert and V. Kunigahalli, "Procedure for Analysis of Nickel-Cadmium Cell Materials," X-711-74-279, Revision A, December 1980

6. E. Sommerfeldt and P. McDermott, "Analysis of Data from the Accelerated Test Program on Aerospace Nickel-Cadmium Cells," X-711-77-193, July 1977

7. H. Lim, "Expansion of the Nickel Electrode," GSFC Battery Workshop, NASA CP 2177, p. 175, November 18-20, 1980

CELL DESIGN VARIABLES - GE 12 AH CELL

VARIABLE	GROUP #	TYPICAL POSITIVE THICKNESS cm	TYPICAL NEGATIVE THICKNESS cm	POSITIVE LOADING gm/dm^3 OF SINTER	NEGATIVE LOADING gm/dm^3 OF SINTER	FINAL KOH QUANTITY cc N/V3rd**	PRECHARGE ADJUST*** Ah
CONTROL*	1	0.069	0.079	2095	2180	40/40	4.6
TEFLON TREATMENT	2	0.069	0.079	2095	2180	48/49	4.6
SILVER TREATMENT	3	0.069	0.079	2095	2180	43/44	4.6
LIGHT LOADING	4	0.069	0.079	1840	1833	45/46	4.6
NO P.Q. TREATMENT	5	0.069	0.079	2113	2180	40.3/41.5	4.6
POLYPROPYLENE SEPARATOR	6	0.069	0.079	2095	2180	39/40	4.6
A.K. PLATE-1968 DESIGN, NO PQ OLD ECT PROCESS, NO DECARB PROCESS	7	0.081 (UNSIZED)	0.066	2130	2542	38/39	0
A.K. PLATE-1968 DESIGN, NO PQ PRESENT AEROSPACE CELL PROCESSES	8	0.081 (UNSIZED)	0.066	2130	2542	39/40	1.8

*CONTROL CELL REPRESENTS PRESENT AEROSPACE DESIGN AND PROCESSES WITH NO EXTRA TREATMENTS: NONWOVEN NYLON SEPARATOR, P.Q. TREATED POSITIVES, DECARBONATION PROCESS, IUE LOADING LEVELS, 31% KOH.

**TWO CELLS IN EACH GROUP CONTAINED SIGNAL ELECTRODES.

***BASED ON 228 cc O^2/Ah.

Figure 1. Different Plate Treatments and Designs

EXPERIMENTAL TECHNIQUES:

1. VISUAL INSPECTION
2. PHYSICAL MEASUREMENTS
3. CHEMICAL ANALYSIS
4. ELECTROCHEMICAL ANALYSIS

Figure 2. Experimental Techniques

CELL MATERIALS FROM S/N 005, GROUP 6, 17,632 CYCLES, SHOW HEAVY CADMIUM MIGRATION

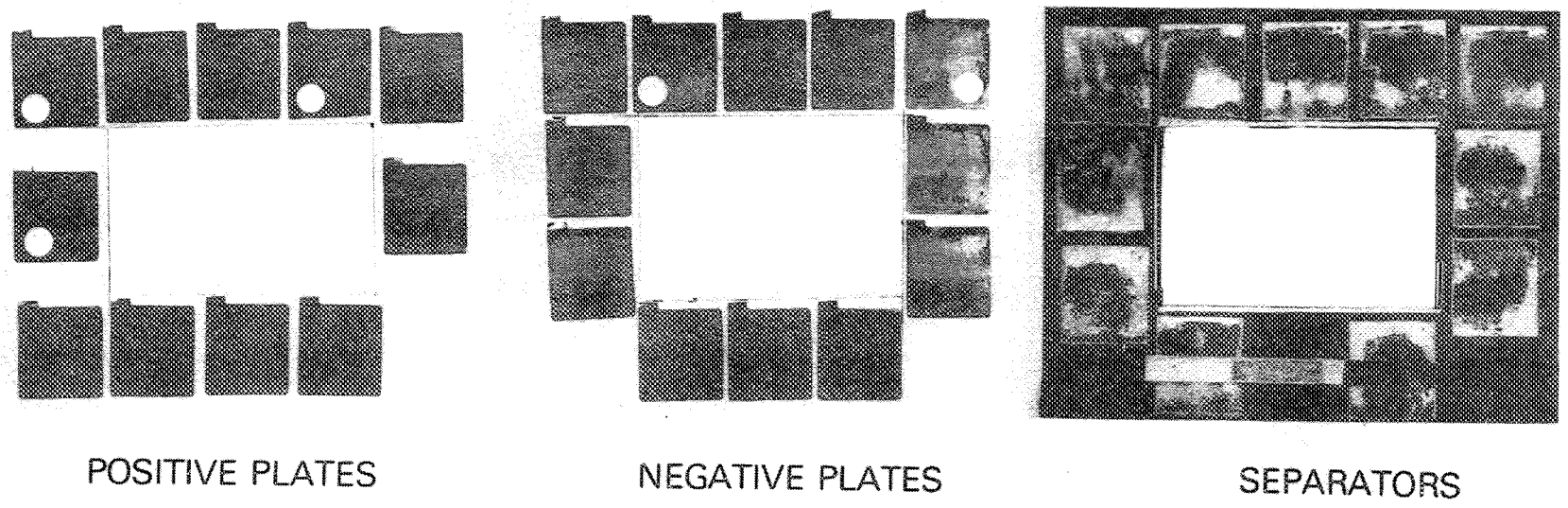

Figure 3. Heavy Cadmium Migration in Polypropylene Group Cell

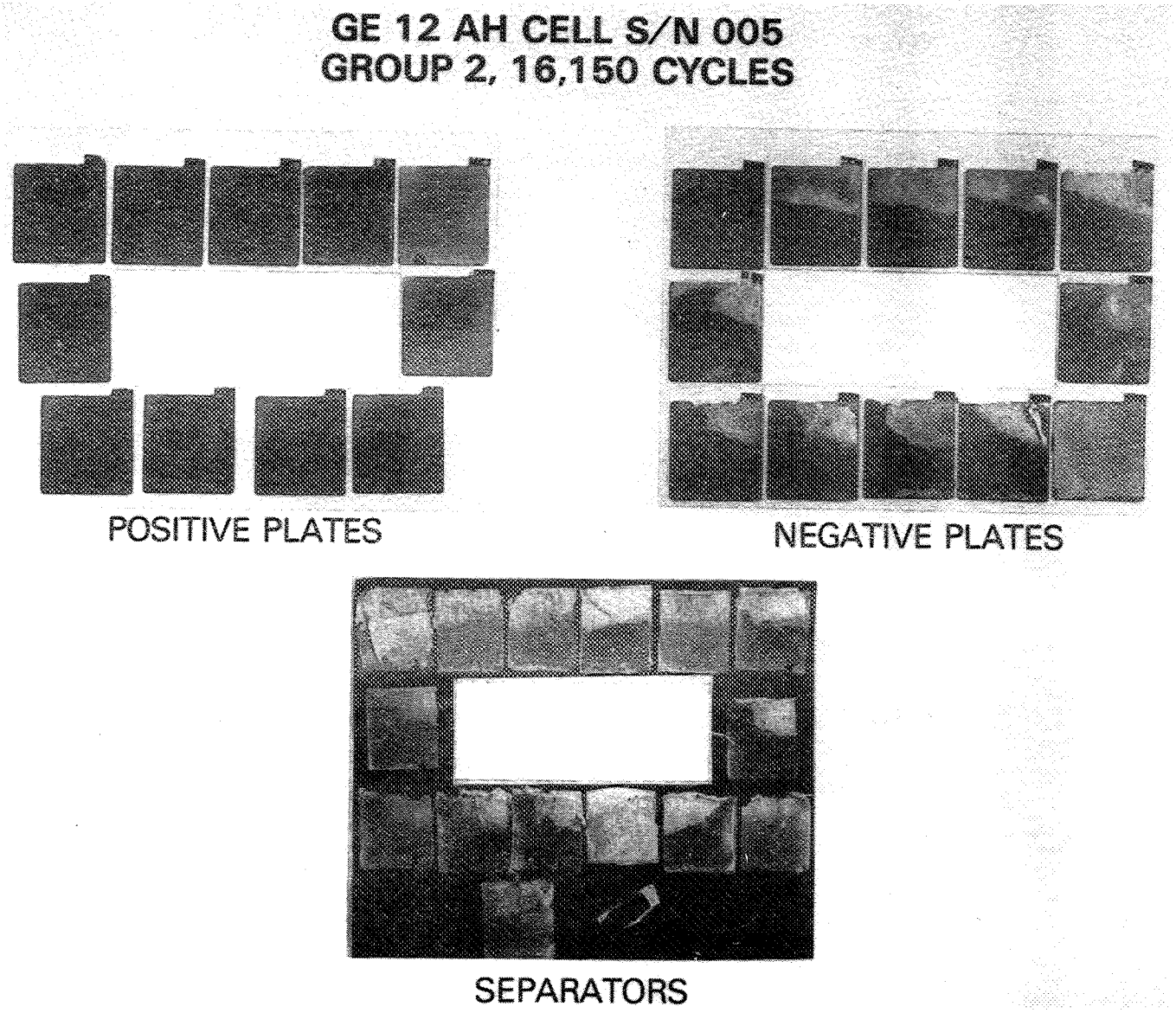

Figure 4. Example of Cell Materials from Teflon Group Show SEP Adhering to NEG

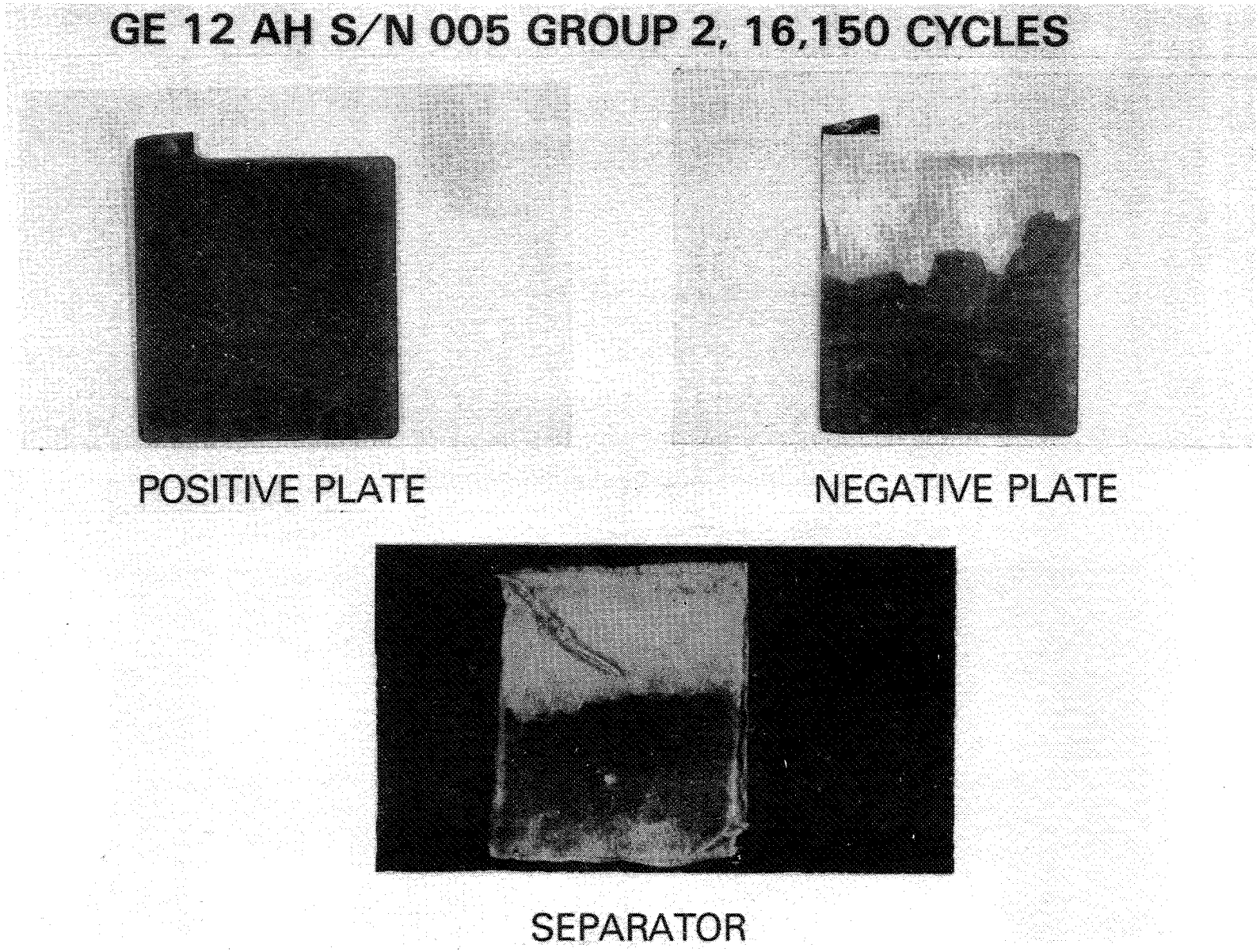

Figure 5. Close-up View of POS, NEG, and SEP in Teflon Group Cell

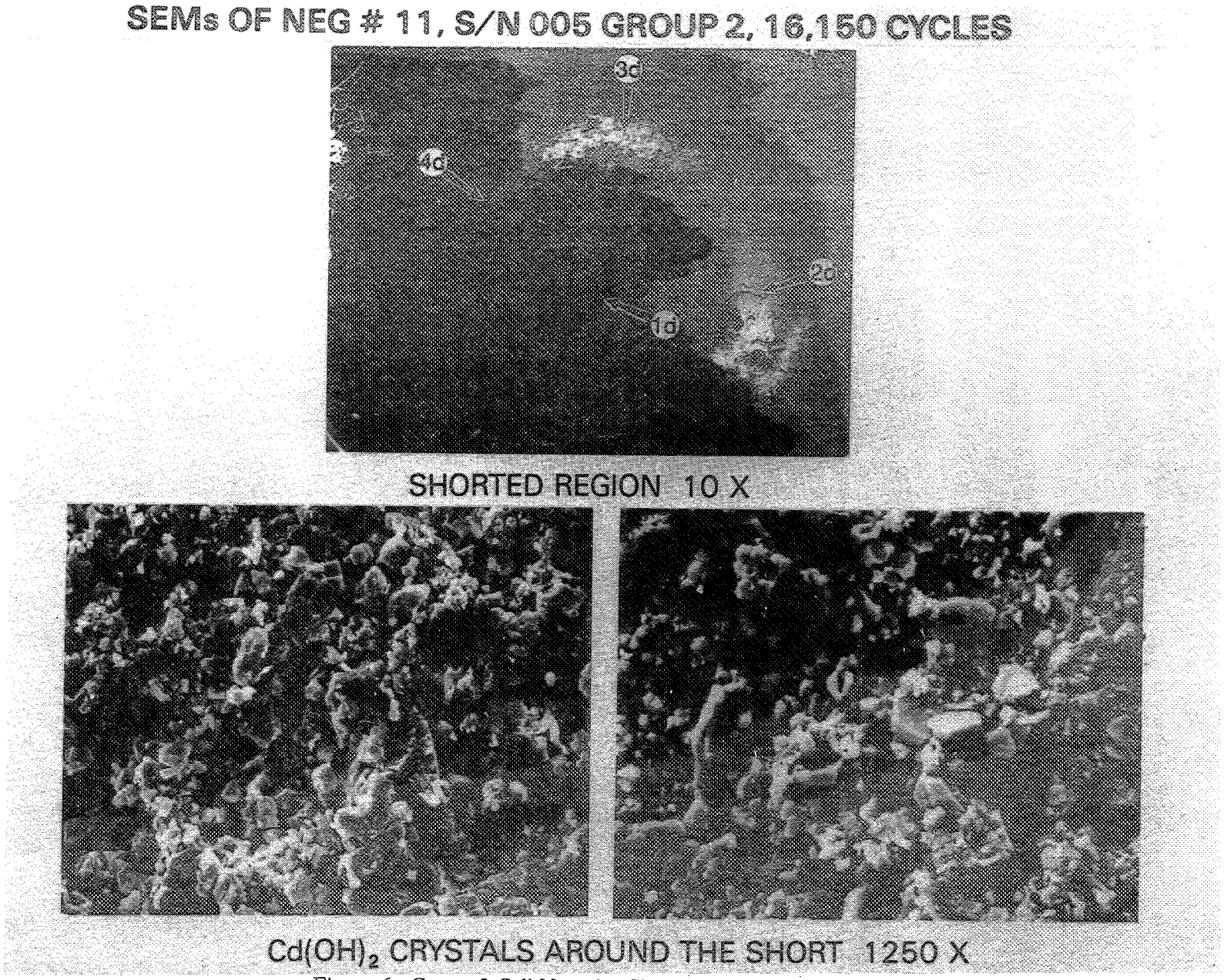

Figure 6. Group 2 Cell Negative Showing the Short and Crystals

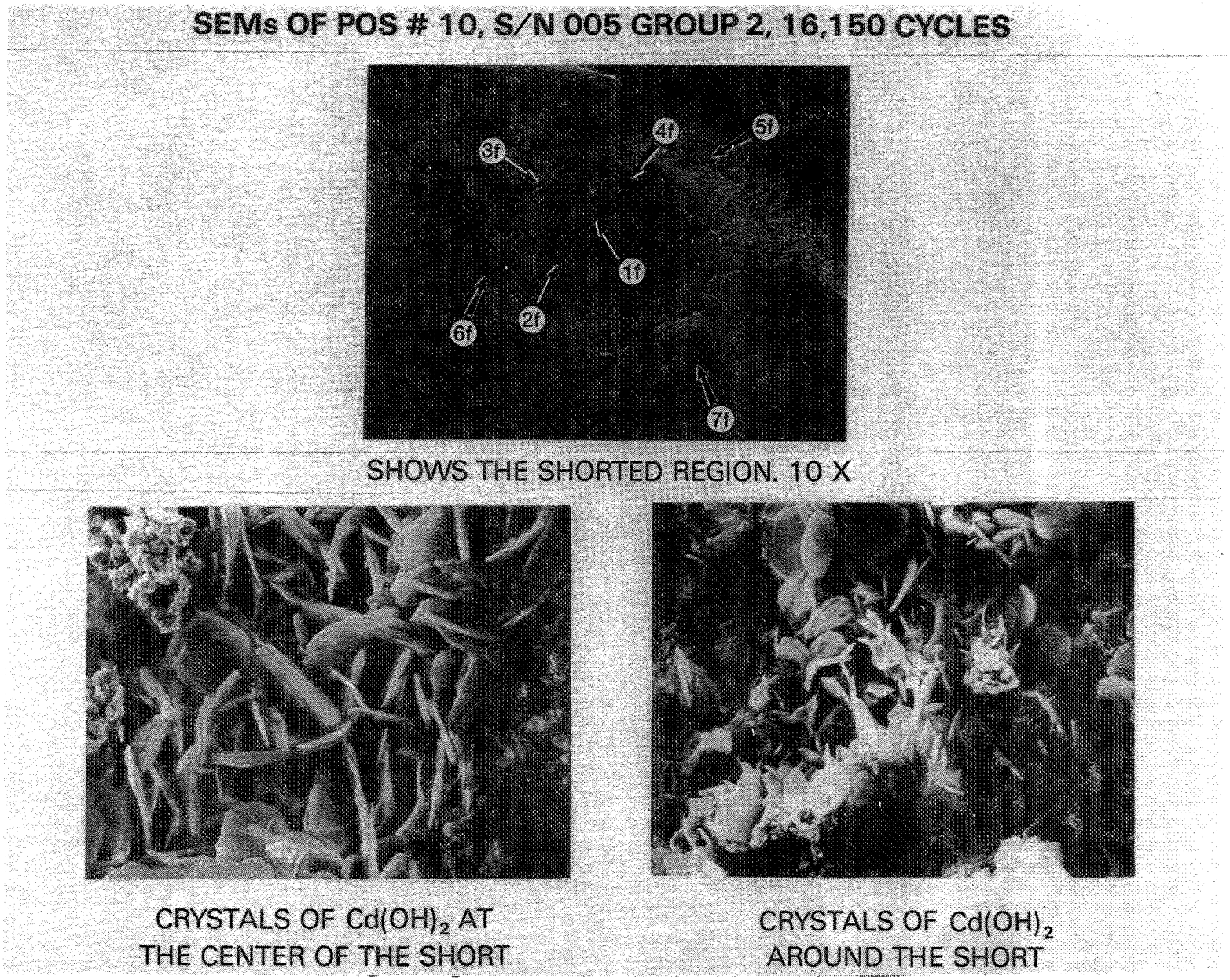

Figure 7. Close-up View of Positive Showing the Short and Crystals

POS. THICKNESS VS NO. OF CYCLES FOR DESIGN VARIABLE CELLS

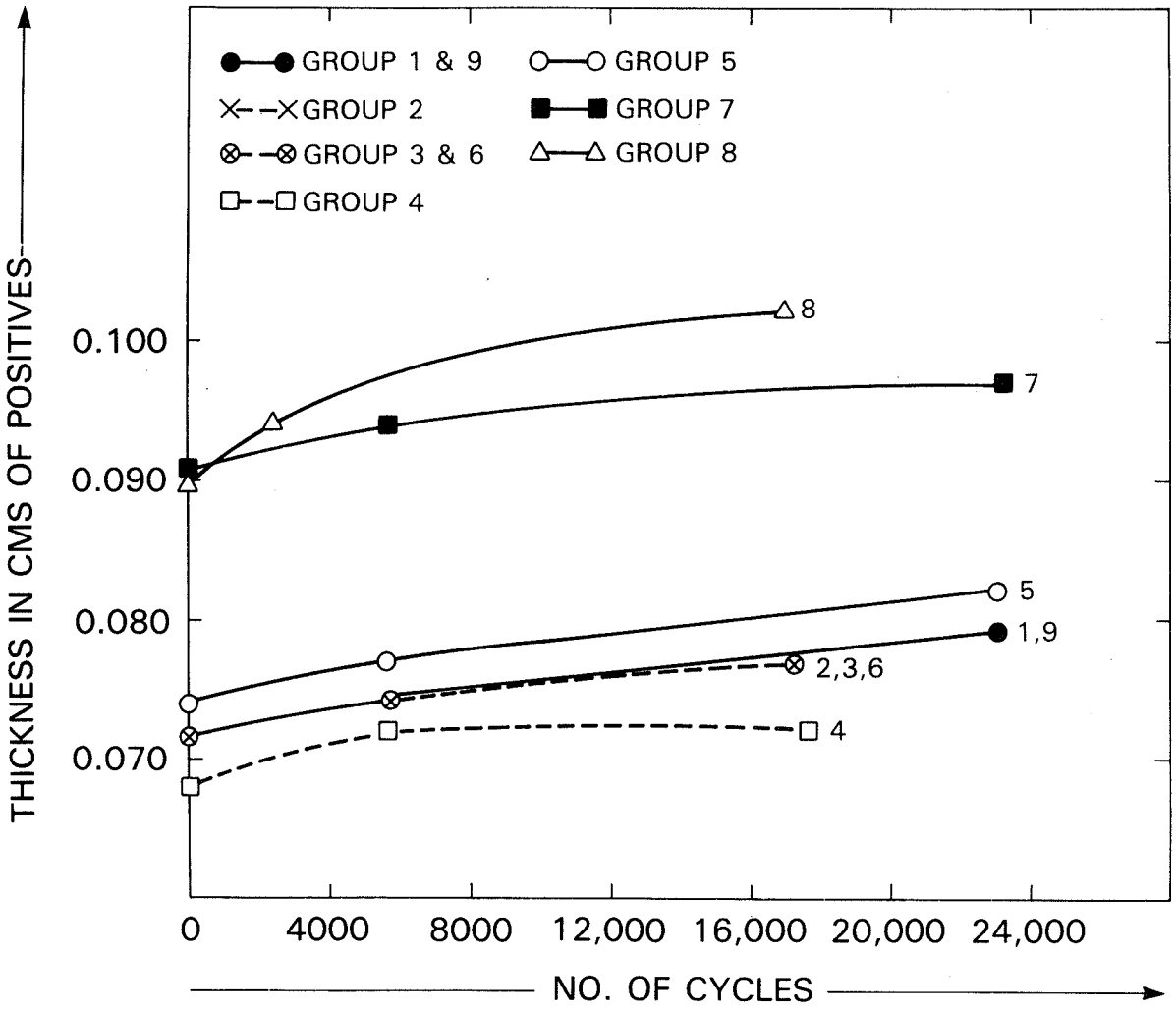

Figure 8. Curves – POS Thickness vs. Number of Cycles

Table 1. THICKNESS AND WEIGHT OF CELLS

GROUP #	S.N. OF CELL	PACK #	NO. OF CYCLES	PLATE THICKNESS (cm) POSITIVE	PLATE THICKNESS (cm) NEGATIVE	PLATE WEIGHT WITH TAB (Gms) POSITIVE	PLATE WEIGHT WITH TAB (Gms) NEGATIVE
1	04	3D	UNCYCL	0.072	0.079	13.69	15.46
	01		5833	0.074	0.080	13.97	14.83
	06		23,468	0.079	0.083	13.79	15.82
2	04	3E	UNCYCL	0.072	0.080	13.85	15.87
	01		5841	0.074	0.079	14.00	14.87
	03		17,760	0.077	0.081	13.97	14.96
3	01	3F	5844	0.074	0.083	14.03	14.82
	03		17,781	0.077	0.083	13.97	15.46
4	01	3G	UNCYCL	0.068	0.079	13.02	14.71
	02		5844	0.072	0.079	13.31	13.83
	05		17,855	0.074	0.080	13.11	14.41
5	01	3H	UNCYCL	0.074	0.079	13.32	15.43
	02		5840	0.077	0.080	13.65	14.92
	03		23,282	0.082	0.083	13.87	15.15

Table 1. (Continued) THICKNESS AND WEIGHT OF CELLS

GROUP #	S.N. OF CELL	PACK #	NO. OF CYCLES	PLATE THICKNESS (cm) POSITIVE	PLATE THICKNESS (cm) NEGATIVE	PLATE WEIGHT WITH TAB (Gms) POSITIVE	PLATE WEIGHT WITH TAB (Gms) NEGATIVE
6	02	3I	UNCYCL	0.072	0.079	13.65	15.59
	01		5833	0.074	0.083	13.88	15.38
	05		17,632	0.076	0.082	13.97	13.68
7	05	3J	UNCYCL	0.091	0.074	15.34	14.13
	06		5834	0.094	0.073	15.68	13.68
	01		23,335	0.097	0.079	15.95	13.88
8	02	3K	UNCYCL	0.090	0.071	15.35	14.02
	06		2008	0.093	0.072	15.56	13.66
	05		2459	0.094	0.073	15.57	13.62
	03		17,300	0.102	0.079	16.01	13.74
9	02	3L	14,827	0.076	0.072	13.10	15.42

Table 2. RESULTS OF ELECTROLYTE ANALYSIS

GROUP #	NO. OF CYCLES	Gms Electrolyte NEG	POS	SEP	TOTAL	% KOH	% K_2CO_3	ML KOH FOUND	ML KOH ADDED
1	–	22.55	15.69	13.56	51.80	21.64	9.21	39.85	40/40
	5833	29.32	16.14	9.09	54.55	23.94	6.76	41.42	
	23,468	30.48	20.60	3.06	54.14	22.86	11.83	41.65	
2	–	20.91	15.99	24.63	61.53	26.82	6.49	47.33	48/49
	5841	26.68	16.16	22.42	65.26	25.26	6.91	50.20	
	17,760	29.34	19.40	14.87	63.61	21.03	9.88	48.93	
3	5844	31.03	15.86	9.95	56.84	25.69	6.87	43.72	43/44
	17,781	31.18	19.67	4.77	55.62	19.94	8.36	42.79	
4	–	24.14	16.49	18.17	58.80	25.25	6.45	45.23	45/46
	5844	31.51	16.36	14.70	62.57	19.65	4.71	48.13	
	17,855	37.28	19.51	6.80	63.59	18.40	12.54	48.91	
5	–	23.38	17.77	9.84	50.99	25.40	8.97	39.22	40.3/41.5
	5840	28.15	18.12	4.64	50.91	23.53	10.45	39.16	
	23,282	30.61	20.19	0.0	50.80	25.00	11.73	39.08	

Table 2. (Continued) RESULTS OF ELECTROLYTE ANALYSIS

GROUP	NO. OF CYCLES	Gms Electrolyte NEG	POS	SEP	TOTAL	% KOH	% K_2CO_3	ML KOH FOUND	ML KOH ADDED
6	–	21.80	15.41	8.16	45.37	29.41	7.36	34.90	39/40
	5833	29.84	16.73	3.42	49.99	26.20	9.63	37.45	
	17,632	32.06	18.14	3.64	53.84	17.82	13.71	41.41	
7	–	22.78	20.11	7.63	50.52	22.01	13.35	37.87	38/39
	5834	25.54	21.47	3.70	50.71	20.47	16.08	37.82	
	23,335	24.72	22.38	1.87	48.97	15.72	17.02	37.67	
8	–	21.42	20.10	9.25	50.77	22.50	14.94	37.95	29/40
	2008	27.92	15.47	6.46	49.85	23.43	15.47	37.22	
	2459	22.69	20.58	7.40	50.67	22.15	16.08	37.79	
	17,300	24.60	21.75	1.21	47.56	22.14	13.60	36.59	
9	14,827	29.49	24.37	5.74	59.60	21.41	11.73	45.85	40/40

- $CO_3^{=}$ INCREASES AS A FUNCTION OF NO. OF CYCLES
- GROUP 7 AND GROUP 8 CELLS CONTAIN LARGE AMOUNTS OF $CO_3^{=}$
  - GROUP 7 CELLS NOT DECARBONATED
  - GROUP 8 CELLS HAVE THICKER POSITIVES
- ORDER OF ELECTROLYTE DISTRIBUTION: NEG > POS > SEP

Table 3. CAPACITIES: CHEM AND BASELINE

NAME	GROUP #	S.N. OF CELL	PACK #	NO.OF CYCLES	CAPACITY ON CELL BASIS (AH) CHEMICAL POS	CHEMICAL NEG	BASELINE POS	BASELINE NEG	% UTILIZATION POS	% UTILIZATION NEG
CONTROL	1	04	3D	–	22.64	34.02	15.54	25.60	68.87	75.25
		01		5833	21.22	30.30	14.63	18.52	58.92	61.30
		06		23,468	16.74	25.25	11.49	20.16	68.64	79.84
TEFLON	2	04	3E	–	21.74	36.28	16.39	25.56	75.39	70.45
		01		5841	22.90	30.77	15.99	18.67	69.82	60.69
		03		17,760	25.08	26.75	12.70	18.94	50.66	70.80
SILVER	3	01	3F	5844	20.86	32.80	15.55	20.14	74.54	61.05
		03		17,781	23.03	31.84	12.89	19.86	55.97	62.37
LIGHT LOADING	4	01	3G	–	20.02	30.48	14.43	23.83	72.07	78.17
		02		5844	21.44	26.17	13.98	14.47	65.21	55.30
		05		17,855	21.52	28.09	11.33	19.44	52.65	69.21
NO PQ	5	01	3H	–	22.69	34.65	16.91	28.11	74.55	81.11
		02		5840	22.44	32.11	17.02	23.54	75.85	73.31
		03		23,282	22.83	28.82	12.08	20.01	52.91	69.43

Table 3. (Continued) CAPACITIES: CHEM AND BASELINE

NAME	GROUP #	S.N. OF CELL	PACK #	NO.OF CYCLES	CAPACITY ON CELL BASIS (AH) CHEMICAL POS	CHEMICAL NEG	BASELINE POS	BASELINE NEG	% UTILIZATION POS	% UTILIZATION NEG
POLYPROPYLENE	6	02	3I	–	22.36	36.62	15.89	28.14	71.06	76.83
		01		5833	23.20	31.35	16.66	19.07	71.81	60.83
		03		17,632	25.10	27.83	11.86	14.73	47.25	52.92
A.K. PLATE	7	05	3J	–	25.23	32.54	19.61	24.99	77.70	76.81
OLD PROCESS		06		5834	26.85	28.83	18.85	23.00	70.20	79.78
		01		23,335	29.46	27.53	16.20	19.51	54.99	70.87
A.K. PLATE	8	02	3K	–	25.63	32.93	16.52	24.86	64.46	75.52
NEW PROCESS		06		2008	26.97	31.69	19.02	23.47	70.50	74.06
		05		2459	27.90	30.92	18.78	22.96	67.30	74.26
		03		17,300	28.68	27.08	14.85	18.51	51.78	68.35
ELECTROCHEM	9	02	3L	14,827	21.19	30.31				

Table 4. Co, Cd, Ni IN THE PLATES

NAME	GROUP	S.N. OF CELL	PACK #	NO. OF CYCLES	% $Cd(OH)_2$ IN POSITIVE	% $Co(OH)_2$ PLATE	AH CHARGED Cd IN NEG	% $Ni(OH)_2$ IN NEG
CONTROL	1	04	3D	UNCYCL	10.74	2.81	0.59	4.04
		01		5833	12.17	2.78	0.75	5.39
		06		23,468	8.57	2.82	0.09	5.57
TEFLON	2	04	3E	UNCYCL	9.49	3.77	1.17	4.14
		01		5841	11.48	2.98	1.20	5.39
		03		17,760	10.12	2.95	1.35	6.06
SILVER	3	01	3F	5844	12.38	3.14	1.84	4.46
		03		17,781	8.91	2.81	2.58	5.82
LIGHT LOADING	4	01	3G	UNCYCL	11.52	3.12	0.71	4.23
		02		5844	13.27	2.70	0.35	4.14
		05		17,855	8.15	2.11	1.21	4.37
NO PQ TREATMENT	05	01	3H	UNCYCL	6.46	3.20	0.71	4.29
		02		5840	7.31	3.06	1.16	4.32
		03		23,282	8.73	2.31	1.08	4.62

Table 4. (Continued) Co, Cd, Ni IN THE PLATES

NAME	GROUP	S.N. OF CELL	PACK #	NO. OF CYCLES	% $Cd(OH)_2$ IN POSITIVE	% $Co(OH)_2$ PLATE	AH CHARGED Cd IN NEG	% $Ni(OH)_2$ IN NEG
POLYPROPYLENE SEPARATOR	6	02	3I	UNCYCL	8.39	3.22	1.02	4.08
		01		5833	9.63	2.98	0.03	5.06
		05		17,632	9.23	2.30	2.60	6.53
AK PLATE OLD PROCESS NO DECARB	7	05		UNCYCL	2.75	3.56	0.87	4.41
		06		5834	4.92	3.15	0.65	5.40
		01		23,335	7.22	2.92	0.42	6.14
AK PLATE NEW PROCESS	8	02	3K	UNCYCL	4.71	3.79	0.91	4.45
		06		2008	5.36	2.57	0.89	4.37
		05		2459	4.55	2.53	0.78	4.47
		03		17,300	9.26	2.57	0.13	4.71
ELECTROCHEM	9	02	3L	14,827	–	1.87	1.23	3.59

GE 12 AH S/N 006 GROUP 1
23,468 CYCLES

NEG # 3 WITH LAYER OF SEPARATOR (320 X)

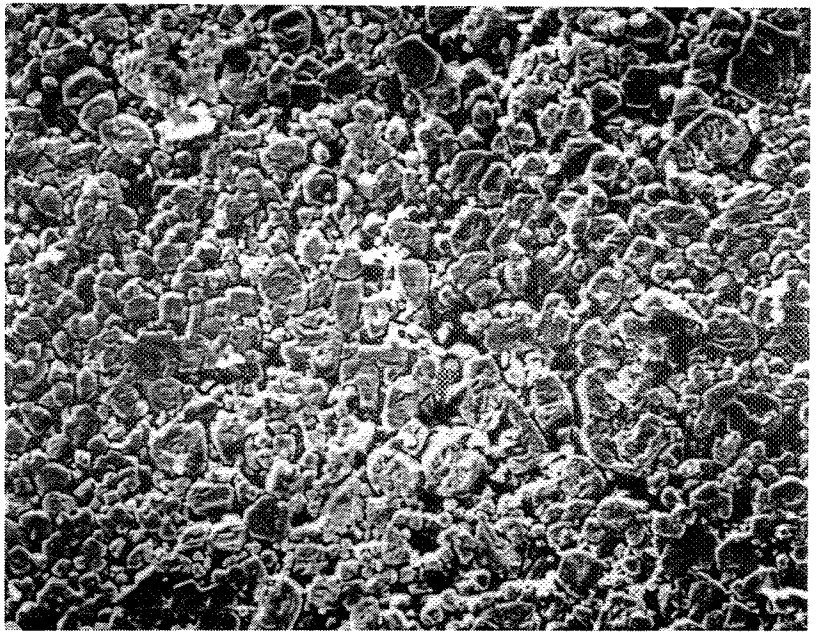

NEG # 1 LARGE CRYSTALS OF $Cd(OH)_2$ (320 X)

Figure 9. SEMs of NEG from Group 1 Cell

S/N 006 GROUP 1 NEG #1 23,468 CYCLES
HEXAGONAL CRYSTALS OF $Cd(OH)_2$

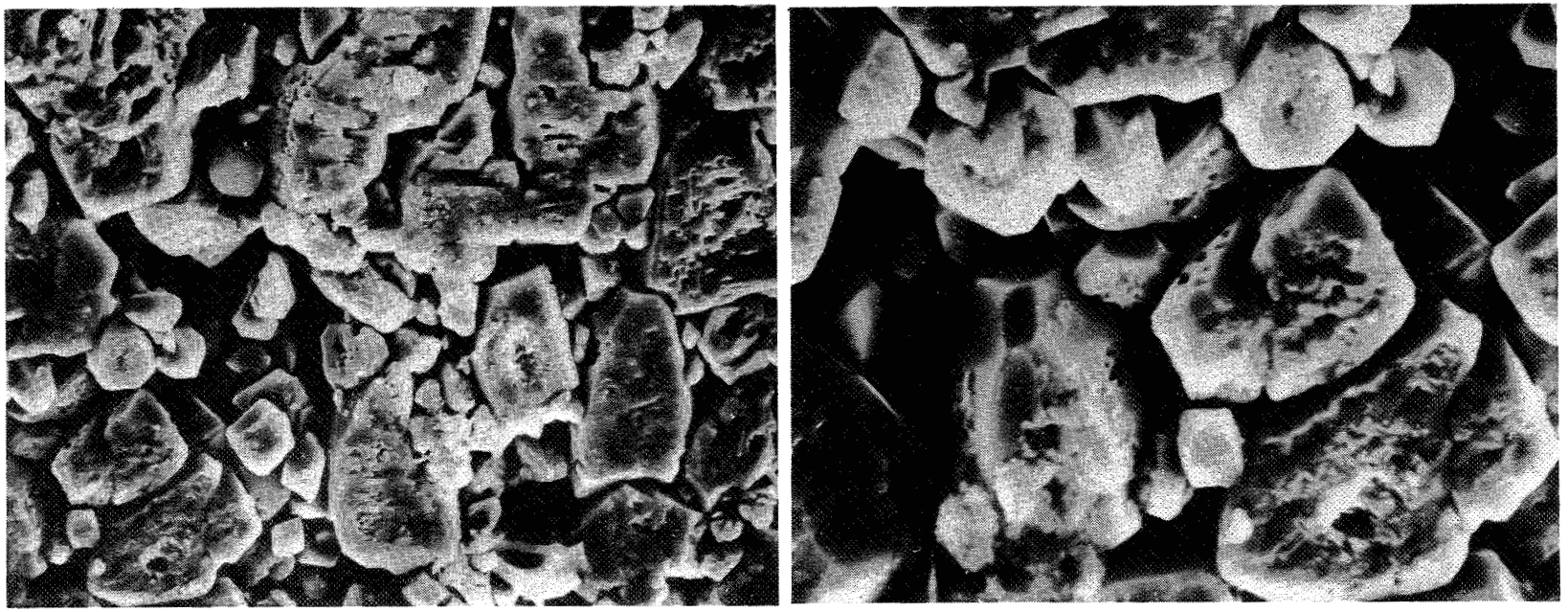

1250 X

2500 X

Figure 10. SEMs of NEG from Group 1 Cell Showing Large Crystals of Cd $(OH)_2$

GE 12 AH, S/N 003, GROUP 5
23,282 CYCLES

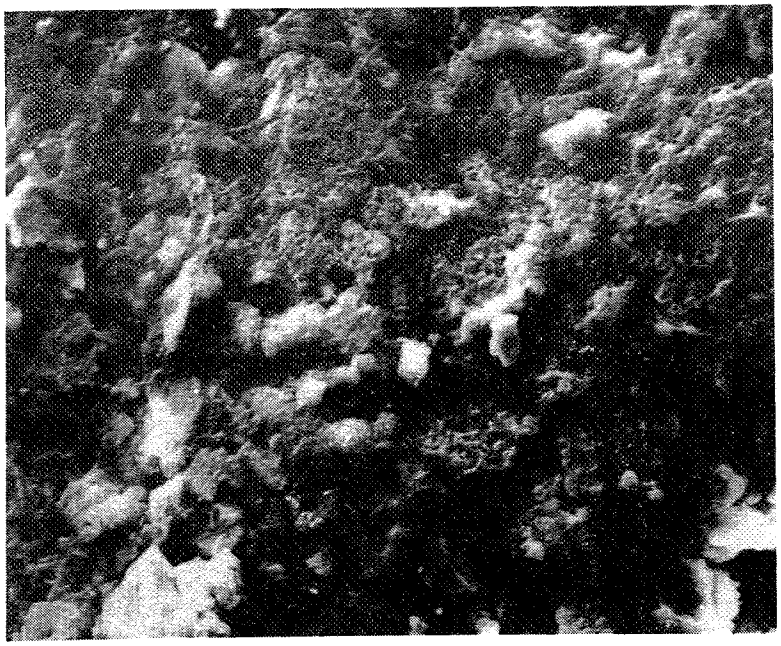

SEM OF POS. # 2 320 X

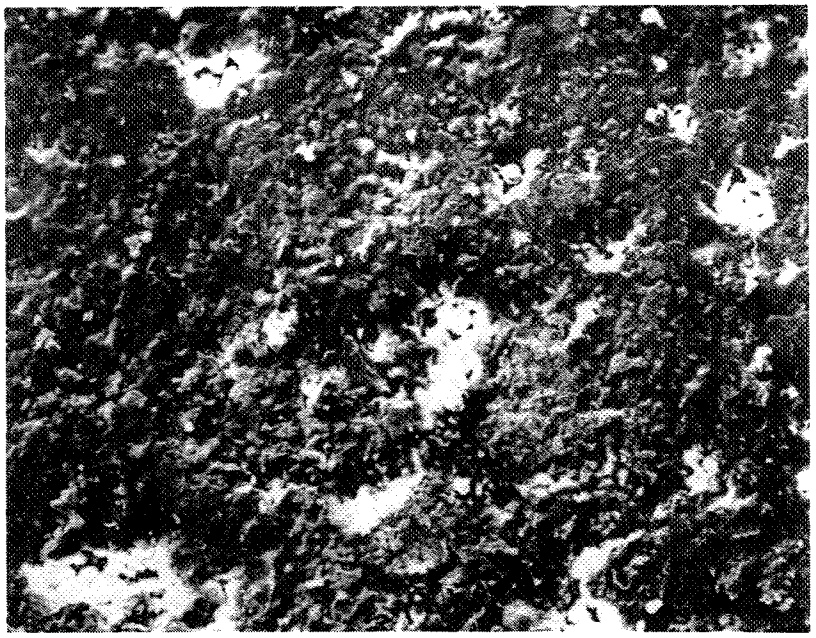

SEM OF POS. # 2 1250 X

Figure 11. SEMs of POS from Group 5 Cell

GE 12 AH S/N 003, GROUP 5
23,282 CYCLES

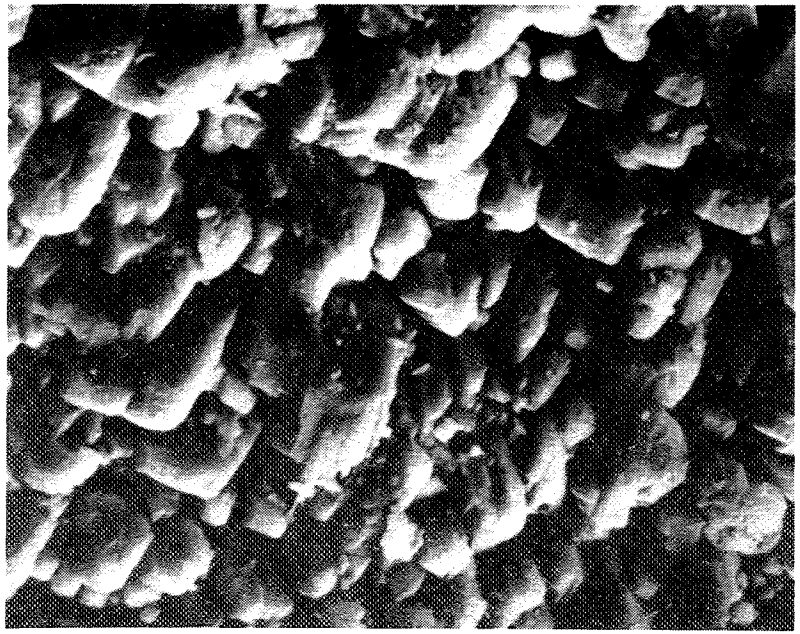

SEM OF NEG # 1 —
LARGE CRYSTALS 2500 X
OF $Cd(OH)_2$

SEM OF NEG # 3 WITH
SEPARATOR 320 X

Figure 12. SEMs of NEG from Group 5 Cell

FUNDAMENTAL ALGORITHMS OF THE GODDARD BATTERY MODEL

James M. Jagielski

NASA/Goddard Space Flight Center

ABSTRACT

The Goddard Space Flight Center (GSFC) is currently producing a computer model to predict Nickel Cadmium (NiCd) performance in a Low Earth Orbit (LEO) cycling regime. The model proper is currently still in developement, but the inherent, fundamental algorithms (or "methodologies") of the model are defined. At present, the model is closely dependant on emperical data and the data base currently used is of questionable accuracy. Even so, very good correlations have been determined between model predictions and actual cycling data. A more accurate and encompasing data base has been generated to serve dual functions: show the limitations of the current data base, and be inbred in the model proper for more accurate predictions. This paper will describe the fundamental algorithms of the model, describe the present data base and its limitations, and give a brief preliminary analysis of the new data base and its verification of the model's methodology.

INTRODUCTION

Nickel Cadmium cells have long been used as energy storage devices for photovoltaic-based satellite power systems. They have also long been the subject of many modelling efforts and discussions. A great many models have been produced to predict NiCd performance and all have their inherent weak and inherent strong points along with their own particular methodology of prediction. This is due to the fact that NiCd cells are simply not easy to model. To draw an analogy, a meteorologist may know that with the atmospheric conditions being a certain way, rain should result. Yet he is quite unable to really accurately predict how much rain will fall, how long the rain will last, or even if it will rain at all. Not only does the sheer number of variables complicate the prediction process, but the system itself (in this case, the atmosphere) is quite complex of itself. Thus, the

meterologist speaks of "probability" or "the chance of rain". So it must be with any model. The measure of a good model is how great the probability is that the model is correct. Conversely, this could be looked at as how small the error between what the model predicts and what is seen or measured in the "real world".

THE PRESENT DATA BASE

The data utilized for modelling cell performance was obtained on the NASA 20 ampere-hour (amp-hr) standard cell, manufactured by General Electric, during the Standard Cell Simulated LEO cycling (4 packs) (30 minutes discharge and 60 minutes charge) and General Performance tests (1 pack) conducted at NWSC, Crane. The desired end result was a family of charge and discharge matrices for various temperatures, voltage-temperature (VT) charge limits, and depth of discharge (DOD).

The data used was from all four LEO packs: one pack was run at 25 percent DOD at 20oC (0.5C charge and discharge rate), the other three at 40 percent DOD at 10, 20 and 30oC (0.8C charge and discharge rate). This resulted in only a few data curves for the compilation of the matrices. In order to "fill in" the empty cells of the matrices, the data generated by the General Performance testing was analysed to reveal or discover various trends or relationships in the data. The results of the General Performance testing were used to extrapolate other data curves for matrix compilation. It is this use of the General Performance testing data and the extrapolation from it which results in this data base being of questionable accuracy. Even so, the desired end result (see above) was achieved. Figure 1 is a typical charge/discharge matrix.

As can be seen, the matrices are such that each column represents a constant State of Charge (SOC) for various currents, whereas each row represents a constant charge or discharge current as the SOC of the cell varies. From this type of matrix, it is therefore possible to generate two types of battery performance curves: Voltage versus Current with SOC as a third variable, or Voltage versus SOC with Current as a third variable. (Of course, cell temperature and DOD are also variables, but are not inherent in the matrices themselves. In other words, temperature and DOD vary from matrix to matrix, not from "inside" the matrix.)

METHODOLOGY

The approach currently used by the model is to have the data from the corresponding DOD and cell temperature matrix represented as a family of curves relating cell voltage to current with SOC as the third variable. The curves themselves are represented as polynomial equations with cell current as the independent variable and cell voltage as the dependent variable. Each different curve corresponds to a different SOC. Figure 2 shows a typical family of curves.

The model at present has two major functions. The first is to predict cell voltage when cell current is known (the model keeps track of the cell SOC, so this value also is "known"). This is the normal mode of operation. The second function or mode is to predict the cell current needed to maintain a constant cell voltage. This mode is used whenever any sort of voltage-clamping charge control is used. This is the taper-charge mode of operation.

NORMAL MODE OPERATION

In calculating cell voltage, the values of normalized cell current (charge or discharge) and the SOC of the cell are known. The model proceeds to find the closest upper and lower bounding curves relative to the cell'c actual SOC. For example, if the data base has curves for the SOC's of 100, 97, 90, 85, and 80 (percent) and the cell SOC is 95 (percent), the model determines that the 97 (percent) curve is the closest upper bounding curve whereas the 90 (percent) curve is the closest lower bounding curve. This process is accomplished by using a standard binary search algorithm. The model then calculates the cell voltage relating to the (known) cell current for the upper and lower SOC curves. This, in essence, provides the model with two cell voltages at a particular cell current: one voltage refers to a cell slightly more fully charged than the simulated cell, the other voltage refers to a cell slightly less charged. The cell voltage for the simulated cell is then determined through a linear interpolation of the two bounding voltages. The linear interpolation introduces little error if the number of SOC curves is large.

Figure 3 is a graph comparing the model predicted voltage curve actual cycling data. The cell temperature was 20oC, 40% DOD, 20 ampere-hour rated capacity, 16 amp discharge (30 minutes), 16 amp charge (60 minutes), with a GSFC VT limit of 7. As can be seen, the discharge voltage correlates very highly. The charge voltage also correlates but not as well. It should be noted that the cycling data being compared was not the data used to generate the data base. Also, it should be noted on figure 3 that the actual cycling data does not hit a hard voltage clamp, but "creeps" up to it. This makes the model appear to be more in error than it actually is.

TAPER-CHARGE MODE OPERATION

This mode of operation calculates the amount of charge current needed to maintain a cell at a constant voltage. Since, as is the case in voltage clamping charge control schemes, the current exhibits an exponential-like downward taper as the voltage remains clamped and the SOC increases, this charge current is generally known as the Taper Charge Current. The approach used by this method is somewhat different than the previous mode, although, as it will be seen, it actually uses the methodology of the Normal Mode Operation.

In calculating cell current, the cell voltage is known as is the cell SOC. However, the structure of the data base curves does not directly allow the model to calculate cell current. To circumvent this problem, the model uses a search approach to determine the taper charge current. The search approach is based on the Binary Search Algorithm.

The model begins by setting up two bounds for the taper charge current. These bounds represent the upper and lower limits of the possible values for the current. Since these values are initially unknown, they are set to reflect a wide range. (At present, the lower bound is set at 0 amps, the upper at 60 amps.) In essence, this means that the model assumes that the value for taper charge current needed to maintain the voltage clamp falls between these two bounds. The model then proceeds to calculate the median value between the two bounds. This median value is the Taper Charge Estimate (TCH). Using this value, the model, using the exact same method as the Normal Operation Mode, calculates the cell voltage corresponding to the TCE and compares this with the voltage clamp. If the calculated voltage is greater than the

voltage clamp, the TCE was too high. In this case the model resets the upper bound to the TCE since it is now known that the actual taper charge current must be less than the TCE and does not fall between the TCE and upper bound (the taper current is no greater than TCE). Conversely, if the calculated voltage is less than the voltage clamp, the TCE was too small (the current was insufficient to maintain the cell at the voltage clamp). In this case the model resets the lower bound to the TCE since it is now known that the actual taper charge current must be greater than the TCE. The process then continues by calculating a new TCE with the adjusted bounds. In this way, as the bounds are constantly being adjusted, the model "zeroes in" on the actual taper charge current. Figure 4 shows a comparision between actual cycling data and model predicted data for the taper charge current. Once again it should be noted that the cycling data depicted is not the data used in the data base.

MODEL LIMITATIONS

When the cycling scheme of the data base correlates with the cycling scheme to be modeled, the model gives accurate results. As the modeled cycling scenario deviates from the data base specifications, the model becomes less accurate.

To further test model accuracy, the model was utilized in such a fashion as to predict various battery characteristic trends (such as "Charge Time to VT vs. DOD) and compare these model predicted trends to actual data trends. In all cases examined, the model predicted trends which very highly correlated to actual data trends. In many cases (such as "DOD vs. End of Charge Current", "DOD vs. Charge Time to VT", and "C/D Ratio vs. VT Limit") not only did the model exhibit the same trends, but the slopes of the model and data curves were very similar.

THE NEW DATA BASE

As stated earlier, the model is in early developement. To further enhance the model's accuracy, and to reduce its dependence on an empirical data base, another data base was generated at GSFC. Through the analysis of the new data base, it will be possible to detect, investigate, and quantify the effects of environment and history on battery performance. In

this way, by concentrating on the effects rather than the results, a more comprehensive, self-contained battery model will be achieved (By knowing WHY and HOW the voltage changes, the need to know actual values of the voltage is redundant and unnecessary).

The new data base was generated by cycling 5 NASA standard 50 ampere-hour cells under various VT limits, DOD's, temperatures, and charge/discharge rates as defined in the following table.

Data Base Voltage-Temperature (VT) Limits (GSFC):	3, 5, 7
Cell Operating Temperatures (degrees C):	0, 10, 20
Charge Rates (Amps):	10, 25, 30, 40
Discharge Rates (Amps):	5, 10, 25, 40
Discharge Time (minutes):	30
Charge Time (minutes):	60

Since the discharge time is 30 minutes, the discharge rates of 5, 10, 25, and 40 (amps) correspond to a DOD of 5, 10, 25, and 40 (percent) respectively. Additionally, cases where the cell would not be recharged after a cycle (for example, a discharge rate of 40 amps for 30 minutes and a charge rate of 10 amps for 60 minutes) were not run. Therefore, the data base has data according to the table below.

5 Amp Discharge Rate		36 test cases
VT	3, 5, 7	(3)
Temp	0,10,20	(3)
Charge	10,25,30,40	(4)
10 Amp Discharge Rate		36 test cases
VT	3, 5, 7	(3)
Temp	0,10,20	(3)
Charge	10,25,30,40	(4)
25 Amp Discharge Rate		27 test cases
VT	3, 5, 7	(3)
Temp	0,10,20	(3)
Charge	25,30,40	(3)
40 Amp Discharge Rate		18 test cases
VT	3, 5, 7	(3)
Temp	0,10,20	(3)
Charge	30,40	(2)

The model was tested against the new data base. There was good correlation between the taper charge current and Charge/Discharge (C/D) ratios. The model showed significant error in predicting cell voltage but this error was later determined to be caused mainly by the age of the cells in the new data base. The present data base was on new cells.

The data from the new data base was analysed in order to determine any functional relationships between data values and the cycling environment. The findings are quite interesting and will be discussed below.

PRELIMINARY ANALYSIS OF THE NEW DATA BASE

The first data matrix generated and analysed corresponded to the 10 deg C, VT 5 discharge test cases. Using the actual data, the matrix in figure 5 was constructed. As can be seen, the matrix has a few "empty" cells. In trying to determine a method to fill in these empty cells, an interesting functional relationship was exposed.

For each column in the matrix (in other words, each set of data with constant SOC), it was found that the cell voltage in linearly dependant on the cell voltage according the the formula:

$$Vcell = (Msoc * Icell) + Bsoc$$

where Msoc and Bsoc refer to the slope and y-intercept for each particular SOC, respectively. Figure 6 is a table containing the values of Msoc and Bsoc for each SOC set.

Upon further investigation, it was determined that the value for Msoc varies linearly with Bsoc according to the formula:

$$Msoc = (M1 * Bsoc) + B1$$

where M1 = 0.011576 and B1 = -0.013757. Hence, by knowing Msoc one can easily calculate Bsoc, and vice-versa. Knowing these values, one can easily calculate Vcell or Icell knowing the value of the other. The only restraining factor is a functional relationship between SOC and either Msoc or

Bsoc. The relationship is linear (correlation factor of 0.94) but this does not offer enough accuracy. Therefore a polynomial equation was used to relate SOC with Bsoc.

The result of this is that one can completely describe the discharge matrix, and therefore the discharge characteristics, by two real numbers (M1 and B1) and the coefficients of the polynomial equation relation SOC to Bsoc. This is a total of 6 numbers (assuming one uses a cubic equation having 4 coeficients) that the model must recall. This greatly reduces the storage requirements of the program. Additionally, since only two equations need be evaluated, the efficiency and speed is greatly increased.

Further analysis is underway to determine if the values of B1 and M1 are dependant on cell temperature and VT limit. Preliminary results point to a linear relationship but this has not been fully worked out. It will also be desired to relate the coefficients of the polynomial equation to temperature and VT limit. This has not been started as of yet.

CONCLUSION

The Goddard Space Flight Center is currently producing a LEO Battery Model for performance calculation. At present the model is in its early stages but already has shown very good correlation with cycling data which is close in history and environment to the model's data base. A new data base was generated to suppliment the model and upon analysis exposed some interesting and useful functional relationships concerning battery performance. Analysis is continuing in order to determine other relationships, if they exist, and determine their usefulness.

The author would like to thank Mr. Floyd E. Ford, Mr. G. Ernest Rodriguez, Mr. C. Michael Tasevoli, Mr. George W. Morrow (all of GSFC) and Mr. David A. Baer (of Hughes Aircraft Co.) for their help and knowledge in the area of NiCd performance.

20 AH GE 20 DEG C LEO 25%DOD [C.PALANDATI]

	0.75	0.80	0.85	0.90	0.95	1.00
-40.0	1.186	1.194	1.211	1.235	1.264	1.294
-20.0	1.228	1.237	1.252	1.278	1.305	1.335
-16.0	1.238	1.247	1.262	1.286	1.314	1.344
-10.0	1.252	1.262	1.275	1.298	1.330	1.360
- 4.0	1.273	1.283	1.300	1.325	1.350	1.380
- 2.0	1.278	1.286	1.303	1.328	1.355	1.385
- 1.0	1.281	1.289	1.306	1.331	1.358	1.388
- 0.5	1.284	1.292	1.309	1.334	1.361	1.391
0.0	1.289	1.302	1.323	1.349	1.374	1.401
0.5	1.294	1.311	1.338	1.364	1.387	1.412
1.0	1.297	1.314	1.342	1.369	1.393	1.416
2.0	1.303	1.320	1.349	1.376	1.400	1.423
4.0	1.310	1.327	1.357	1.385	1.410	1.434
10.0	1.332	1.350	1.379	1.407	1.433	1.458
16.0	1.349	1.368	1.398	1.427	1.453	1.479
20.0	1.361	1.380	1.411	1.440	1.467	1.492
40.0	1.407	1.426	1.458	1.487	1.513	1.538

Figure 1. Leo Test Data at Beginning of Life (Cycle 12)

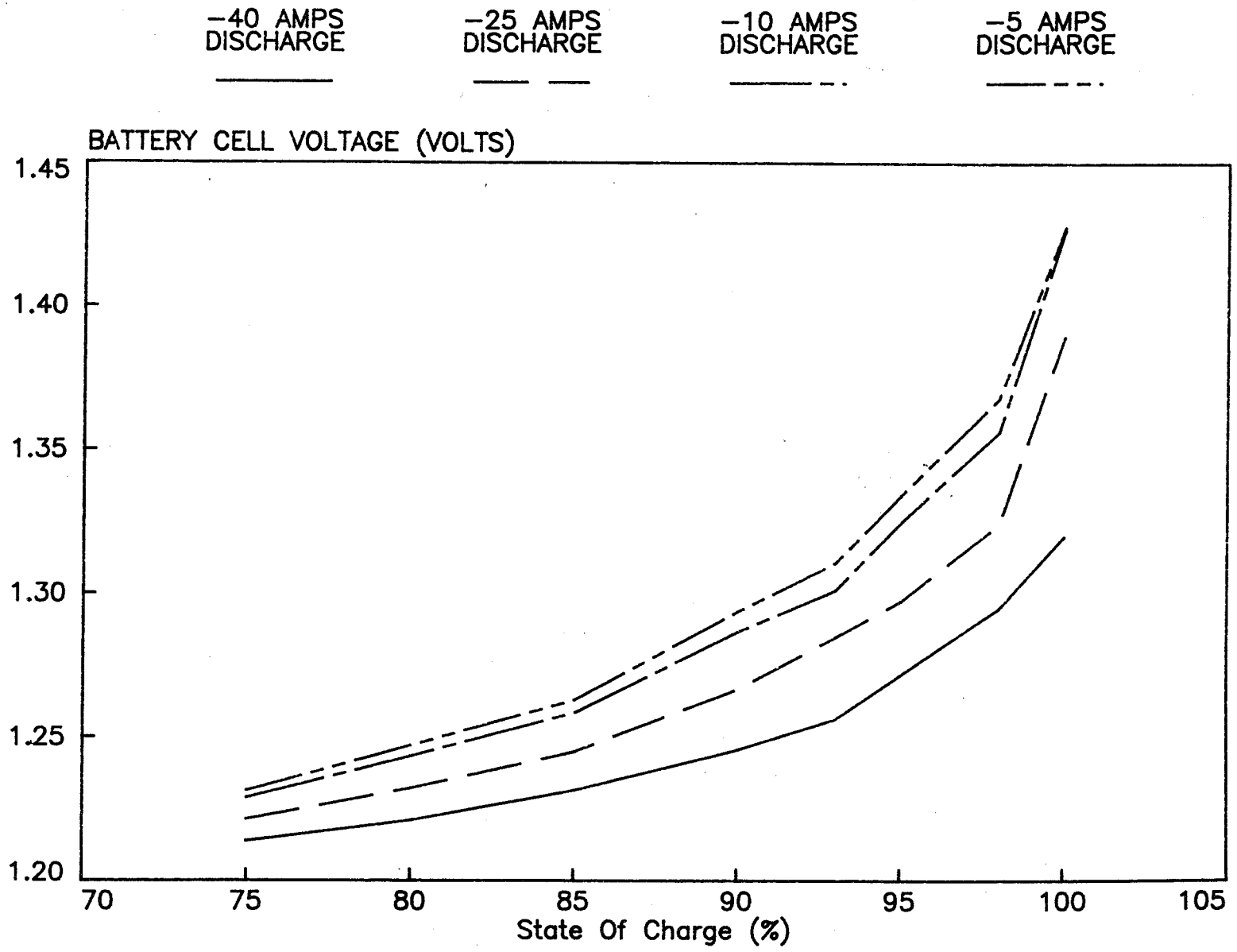

Figure 2. Discharge Curves for 10 deg C and VT 5

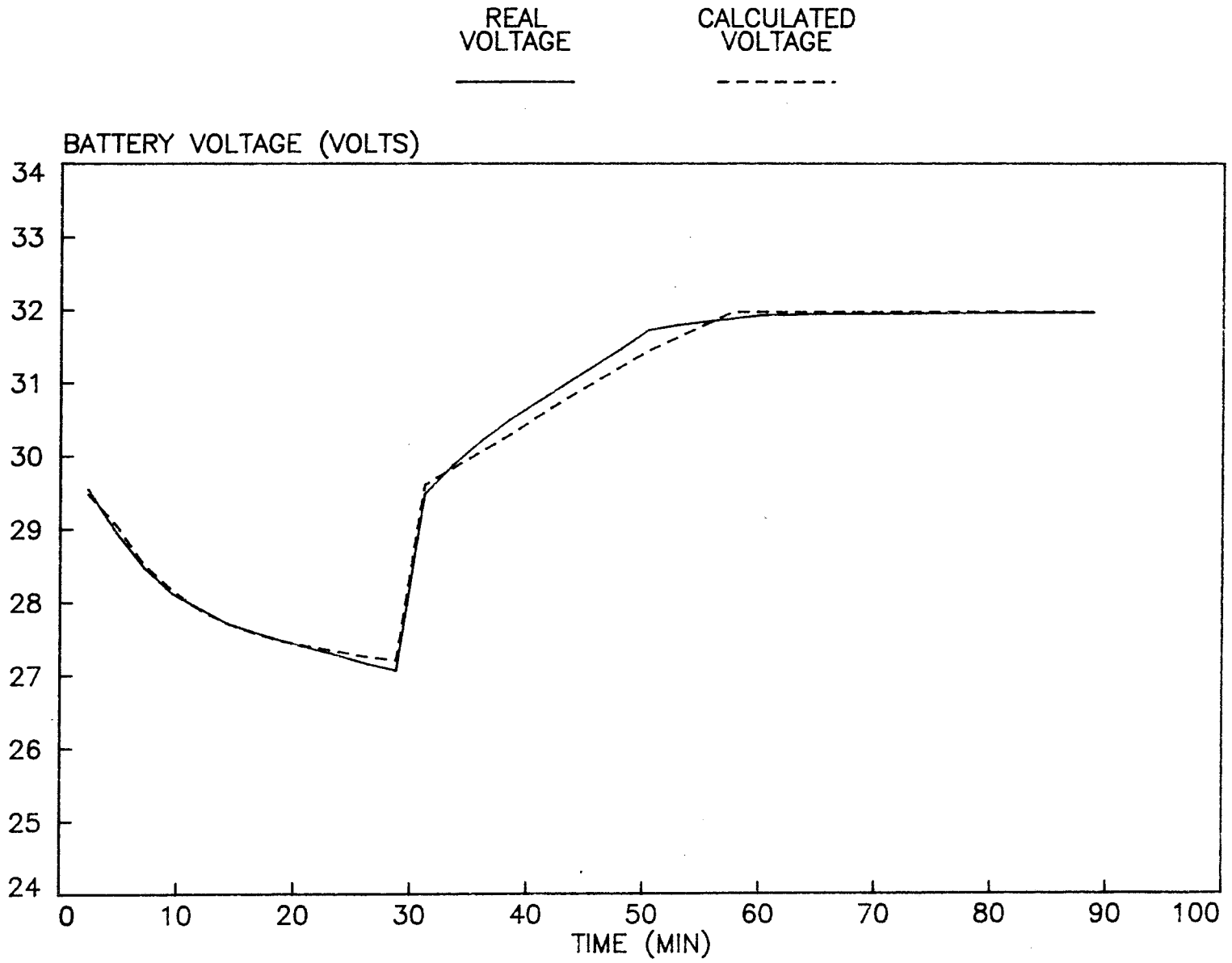

Figure 3. Modeling Study for Battery Workshop: Cycle 15, 20 C, 40% DOD, 16A Chg, 16A Disch

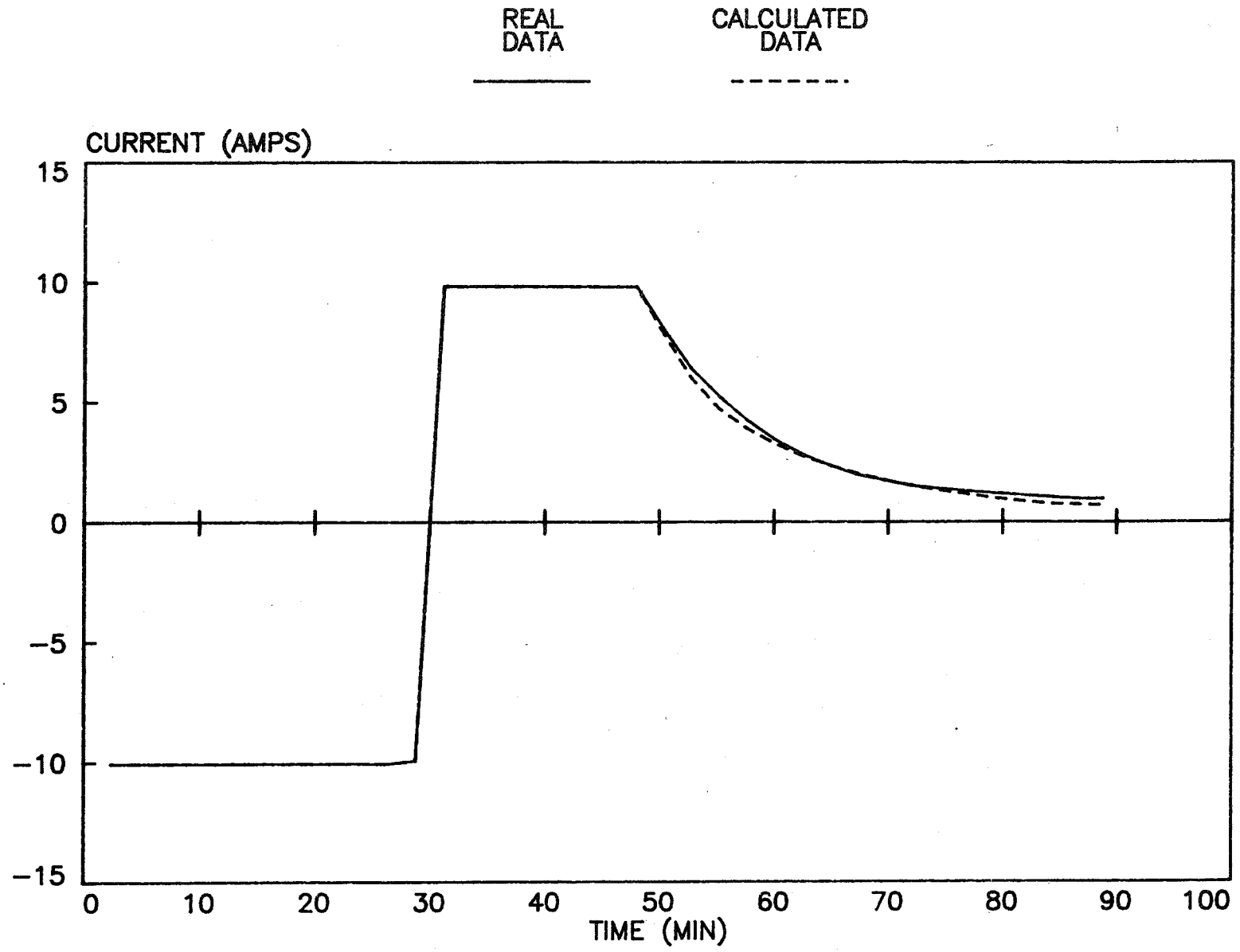

Figure 4. Modeling Study for Battery Workshop: Comparison—Real and Calculated Current Data

CURRENT AMPS	SOC 75	80	85	90	93	95	98	100
-40 :	1.2138	1.2209	1.2314	1.2455	1.2562	1.2717	1.2948	1.3200
-25 :	1.2213	1.2321	1.2449	1.2667	1.848	1.2974	1.3241	1.3895
-10 :				1.2866	1.3012	1.3248	1.3563	1.4266
- 5 :						1.3341	1.3679	1.4276

Figure 5. Data Matrix for 10 deg C, VT5, 50 Ahr, Leo

SOC		
100	Bsoc	: 1.453125
	Msoc	: 0.003110
98	Bsoc	: 1.377508
	Msoc	: 0.002087
95	Bsoc	: 1.343698
	Msoc	: 0.001785
93	Bsoc	: 1.318233
	Msoc	: 0.001500
90	Bsoc	: 1.300517
	Msoc	: 0.001370
85	Bsoc	: 1.267400
	Msoc	: 0.000900
80	Bsoc	: 1.250770
	Msoc	: 0.000747
75	Bsoc	: 1.233800
	Msoc	: 0.000500

Figure 6. Values of 'Bsoc' and 'Msoc' for Various SOCs. Data from Figure 5.

MODELING TAPER CHARGE WITH A NON-LINEAR EQUATION

Patrick P. McDermott, Ph.D.
B-K Dynamics, Inc.
Rockville, Maryland

Introduction

This is a report of work which has been in progress for six months aimed at modeling the charge voltage and current characteristics of nickel-cadmium cells subject to taper charge. Work reported at previous NASA Battery Workshops has shown that the voltage of cells subject to constant current charge and discharge can be modeled very accurately with the equation:

$$\text{Voltage} = A + \frac{B}{C - X} + De^{-Ex}$$

where A, B, D, and E are fit parameters and x is amp-hrs of charge removed during discharge or returned during charge. In a constant current regime, x is also equivalent to time on charge or discharge.

The present study is aimed at deriving equations for fitting the charge taper portion of the charge curve since the previously derived equations are not appropriate for this application. Figure 1 shows a typical current vs time plot for a cell in constant current discharge with a constant current charge to some predetermined voltage limit (VL). The current is held at -16 amps for 30 minutes during the discharge portion and then jumps to +16 amps for approximately 20 minutes of charge. At this point, the voltage hits the limit, and the current drops rapidly over the next 10 minutes flattening out to around 2 amps by the time the charge terminates at approximately 90 minutes. As we shall see in this report, the shape of the taper current will vary widely depending on the test conditions. The slope at which the current drops initially is quite variable as is the current when the charge curve flattens out at the end of the charge.

Test Matrix

Data for this study is taken from a test of 50 amp-hr cells being conducted at the Goddard Space Flight Center. This test is unique in the sense that the same group of cells in the cell pack are being tested under various conditions of charge, discharge, temperature and voltage limit. The cells are cycled under one set of conditions (8 cycles) to reach equilibrium, then returned to baseline cycling regime before being subjected to a new set of environmental test conditions. The data for the study is taken from the eighth-cycle at each test condition.

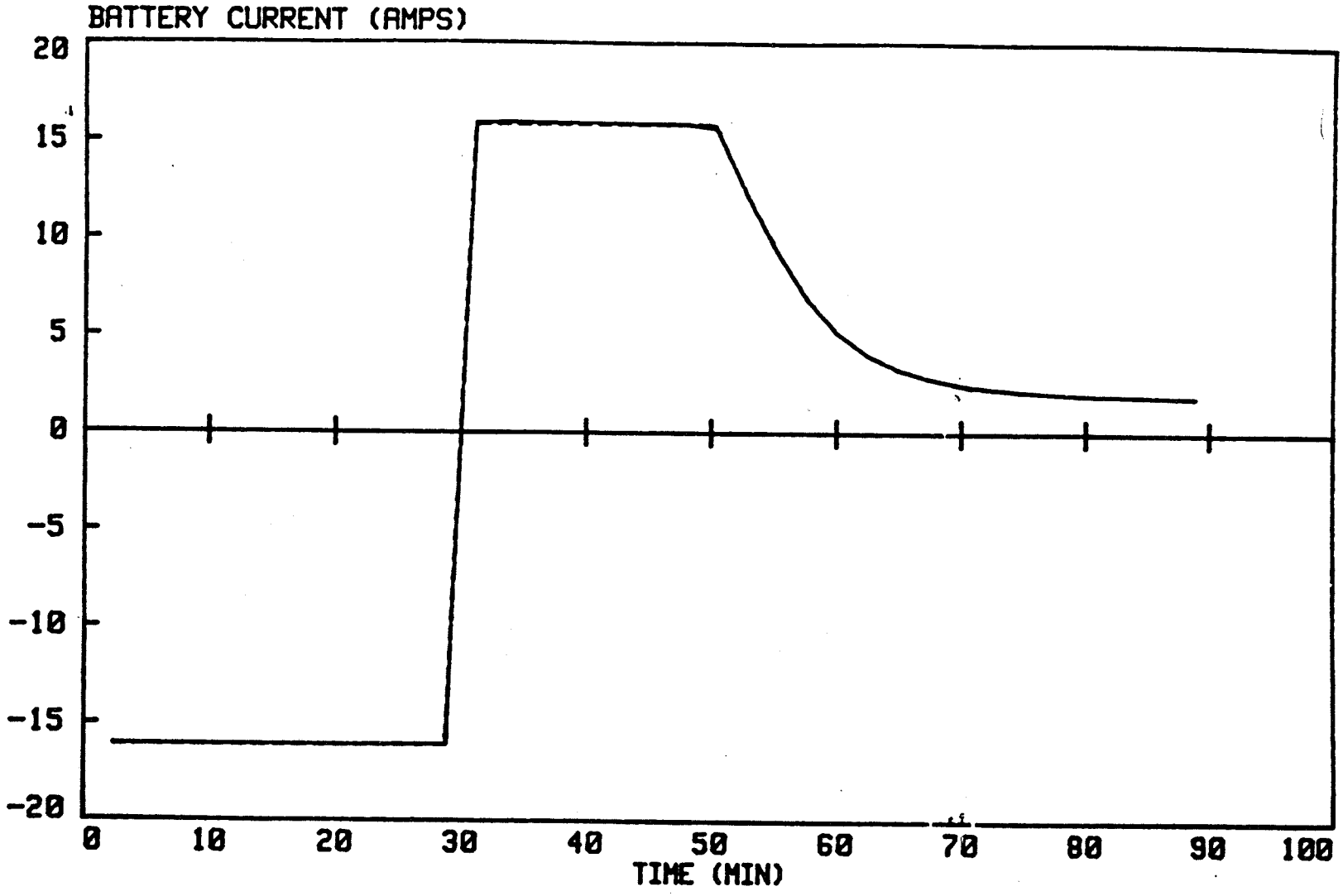

Figure 1. Typical Current Profile

Figure 2 shows the test matrix for this study. There are essentially four conditions of discharge (.1C, .2C, .5C, and .8C), four conditions of charge (.2C, .5C, .6C and .8C), three temperatures (0°C, 10°C, and 20°C), and three voltage limits (VL 3, VL 5, and VL 7). The box in the figure shows the voltage at which the cell goes into taper for the three voltage limits at the three different test temperatures. Depth of discharge (DoD) could also be considered a test variable which is totally dependent on discharge current since discharge time is always 30 minutes. DoD ranges from 5% at the .1C discharge rate to 40% for the .8C discharge rate.

The 4 x 4 matrix in Figure 2 shows all of the combinations of charge and discharge which were employed in the test. Note, however, that three of the combinations were not tested (see boxes which are crossed out) because of extreme conditions. The charge rates were not sufficient to return the amount of charge required at the 25% and 40% DoD levels.

Each box in the 4 x 4 matrix represents an additional set of nine test conditions which are the various combinations of the temperature (three levels) and voltage limit (three levels). All told, there are 117 possible combinations of these variables in the testing scheme.

Time to Voltage Limit

The various combinations of charge and discharge rates had a significant impact on the time in which the cell remained in constant current charge before hitting the voltage limit. Figure 3 shows the time to voltage limit for the various combinations of charge and discharge rate. The very short times (less than 2 minutes) are seen to occur at the high charge rates for those cells which were subjected to lower discharge rate, and, therefore, lower depths of discharge (5% and 10%).

The longer times to voltage limit occur for various combinations of charge rate and discharge rate along a diagonal from the lower left hand side of each matrix to the upper right hand side. A maximum of 30 minutes, one half of the total time in discharge, is observed at VL 7 for cells at .8C discharge and .6C charge.

The shape of the current taper, as will be seen later in the report, is roughly correlated to the amount of time that the cell stays in constant current charge before hitting the taper limit. The drop-off in current is much sharper for the cells which have a short time to voltage limit, especially those at less than 2 minutes. The parameters of the fit equations for this portion of the charge curve are highly dependent on this initial rate of drop in the current after hitting the voltage limit.

Percent of Charge Returned During the Charge Cycle

Figure 4 shows the percentage of charge returned to the cells during the charge portion of the cycle. As with the time to voltage limit, there is a significant variation in the percent return based on the

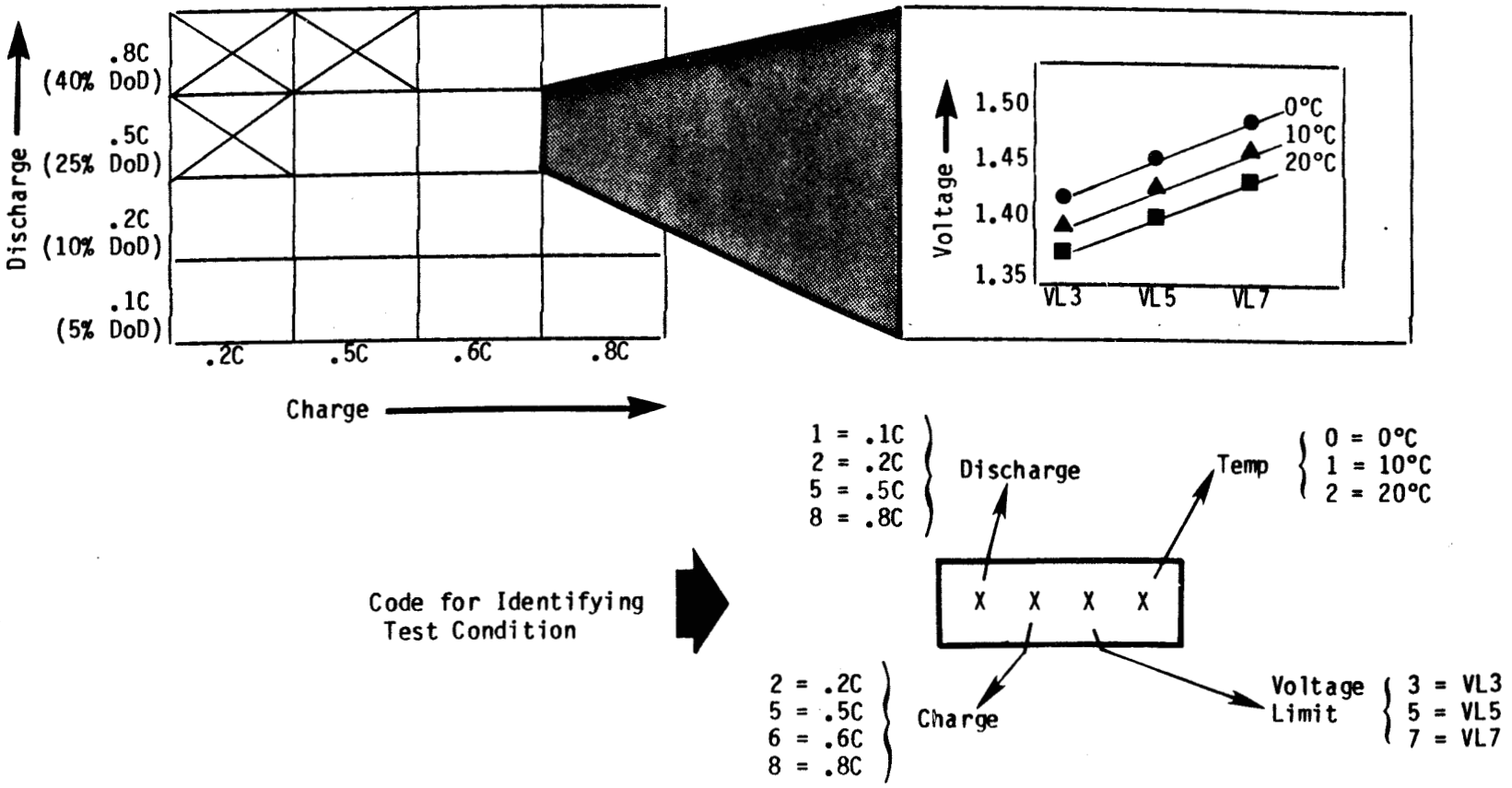

Figure 2. Text Matrix

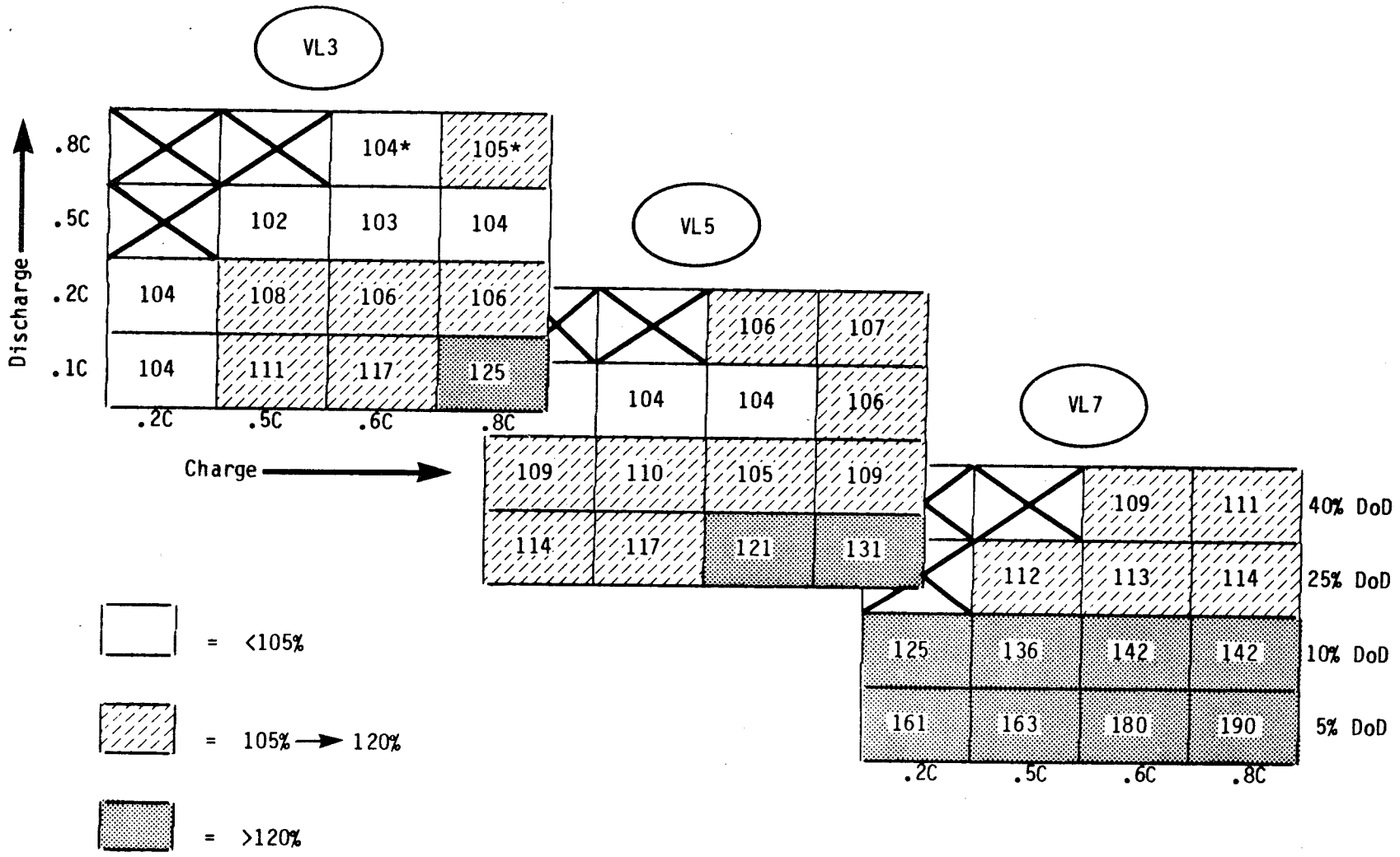

Figure 3. Percent Returned During Charge (Advantage of All Temperatures)

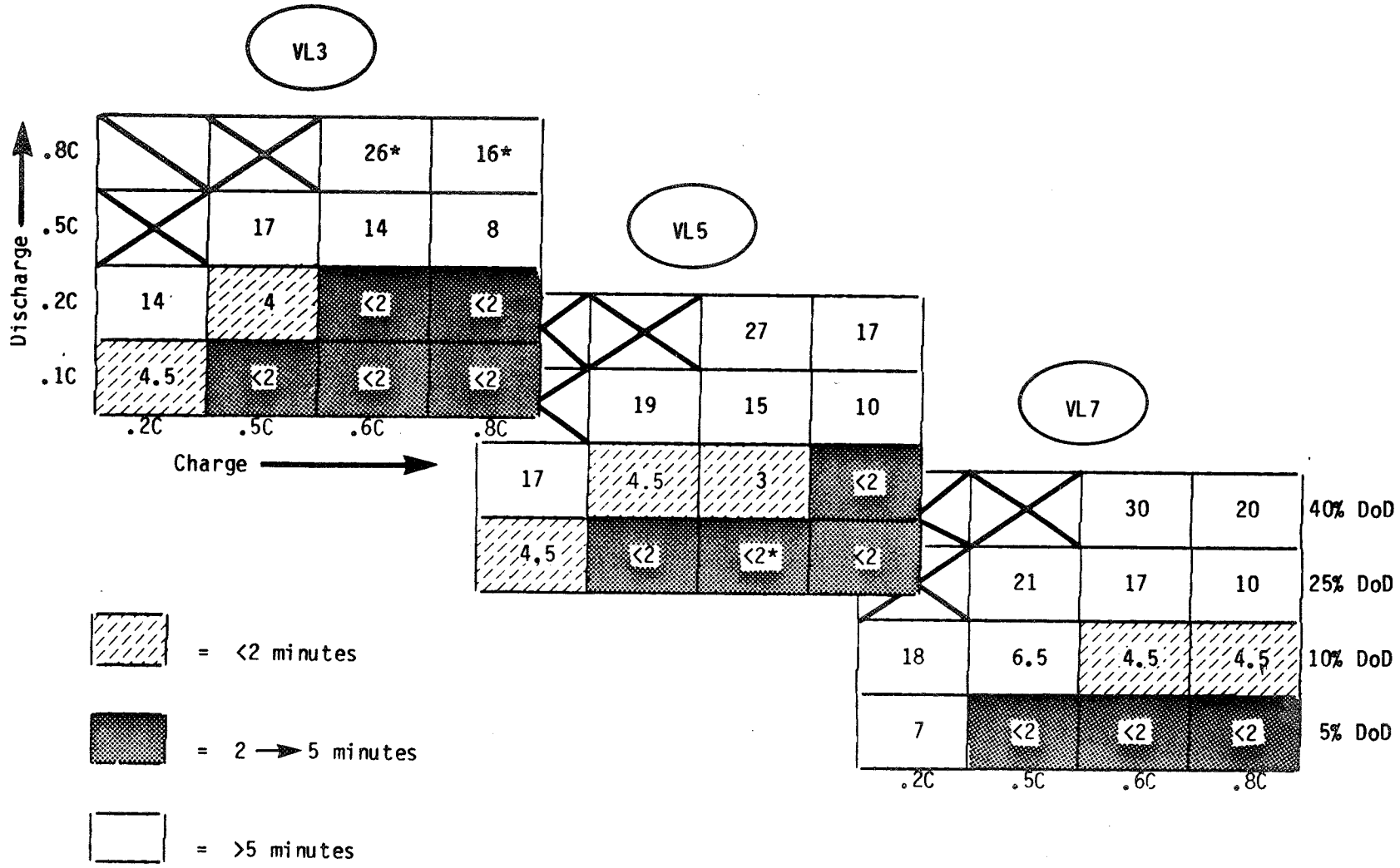

Figure 4. Time to Voltage Limit (Averages of All Temperatures)

differences in charge and discharge rates, and on the variation in voltage limit. For the matrices shown in Figure 4, the temperatures are averaged together for each specific test condition. At VL 3, the percent returned is less than 110% for most of the conditions. At VL 7, on the other hand, most of the test conditions show a percent return greater than 110%, with over half of the test conditions showing greater than 125%, at the lower DoDs. Again, there is a rough correlation between the time that the cells remain in charge before hitting the voltage limit and the percentage of charge returned to the cell. The cells at the high charge rates but modest DoDs show very short times to voltage limit, but, also, much higher percentages of return.

Fitting the Taper Portion of the Charge

It was noted by trial and error that the slope of the current in taper plotted against the current yielded a curve which was approximately linear. It was also noted that the linearity was improved if a constant term was subtracted from the current. The constant term in many cases was close to the current at the end of taper charge, suggesting that the constant was related to the value of current to which the experiment current was approaching as a limit. This observation suggested that the phenomenon could be fit by a first order differential equation of the form:

$$\frac{dI}{dt} = k\,(I - a)$$

where I is current and k and a are constants. The solution to this equation was then used in a non-linear regression fitting program to calculate fit parameters in the equation: $I = (1)\exp^{(2)t} + (3)$ where I is current and (1), (2), and (3) are the fit parameters.

This equation worked quite well in fitting data such as that shown in Figure 5a, the taper charge of the cell at .5C discharge, .5C charge, VL 7 and 0°C (Fit 5570 -- See Figure 1 for code). Parameter 3, as suggested above, is close to the point where the current is leveling off, and Parameter 3 plus Parameter 1 are approximately equal to 25 amps, the current for the cell as it hit the voltage limit.

The three parameter fit equation did not work so well, however, for curves where there was a sharp drop in current immediately after the cell hit the voltage limit. This is readily seen in Figure 6a which is a three parameter fit of the cell at .1C discharge, .5C charge, VL 3, and 20°C. As was mentioned earlier, many of the test conditions where the cell hits the voltage limit quickly demonstrated this sharp initial drop in current. It was also noted that a plot of dI/dt vs I for test conditions like those shown in Figure 6 would yield not one but two linear portions with different slopes. This suggested that there were two first order effects being demonstrated during taper charge which required a more complex equation in order to adequately fit the data.

Four and Five Parameter Fit Equations

In order to accommodate the two effects mentioned above, a four parameter equation with two exponential terms and a five parameter equation with two exponential terms and a constant were used with the non-linear regression program to fit the data. These equations are shown below:

$$\text{Four Parameter Equation:} \quad I = (1)\exp^{(2)t} + (3)\exp^{(4)t}$$

$$\text{Five Parameter Equation:} \quad I = (1)\exp^{(2)t} + (3)\exp^{(4)t} + (5)$$

where (1), (2), (3), (4), and (5) are the fit parameters.

These four and five parameter equations were able to fit both the sets of data shown in Figures 5 and 6 more accurately than the three parameter fit equation. Figures 5b and 6b are the fits obtained with the four parameter equation and Figures 5c and 6c are the fits obtained with the five parameter equation. The sum of squared residuals decreases (from 1.0 to 0.15 to 0.026) for fits 5a, 5b and 5c, suggesting that there is an increasing accuracy with the four and five parameter equations.

Tables 1 and 2 show parameters for the three fit and the five fit equations, for many of the test conditions in the test matrix. There are some trends evident as one reads from left to right (increasing VL) for any particular charge/discharge combination, or reads from top to bottom (increasing temperature). There is, however, no strong pattern as yet which suggests strong correlation with the environmental parameters.

Other Characteristics of the Taper Charge

Figure 7 shows an interesting correlation between the current at the end of charge and the percent of charge returned. When one plots one against the other, the data points cluster along straight lines, with the slope of the lines increasing the decreasing discharge rate or DoD. The currents at the end of charge are significantly higher for the cells with 40% DoD (4.0 to 5.0 amps) than for the cells at 5% DoD which range from 2.0 to 3.0 amps. What is more striking, however, are the differences in percent return. The 5% DoD cells range from 130% to over 200% charge return whereas the 40% DoD cells cluster around 110% charge return. It is interesting to note that the ln slope of the lines drawn through the data points when plotted against DoD (ln scale) yields a straight line as shown in the insert to Figure 7.

Another interesting effect is shown in Figure 8 where percent recharge is shown vs. temperature for each combination of charge and discharge. For the higher DoDs there is little or no temperature effect (40% and 25% DoD). The effect of temperature is more dramatic for the 5% and 10% DoD test conditions with increasing impact from left to right with increasing charge rate. The greatest difference, for example, is shown for the .1C discharge rate/.8C charge rate combination where percent recharge ranges from 140 to 200%.

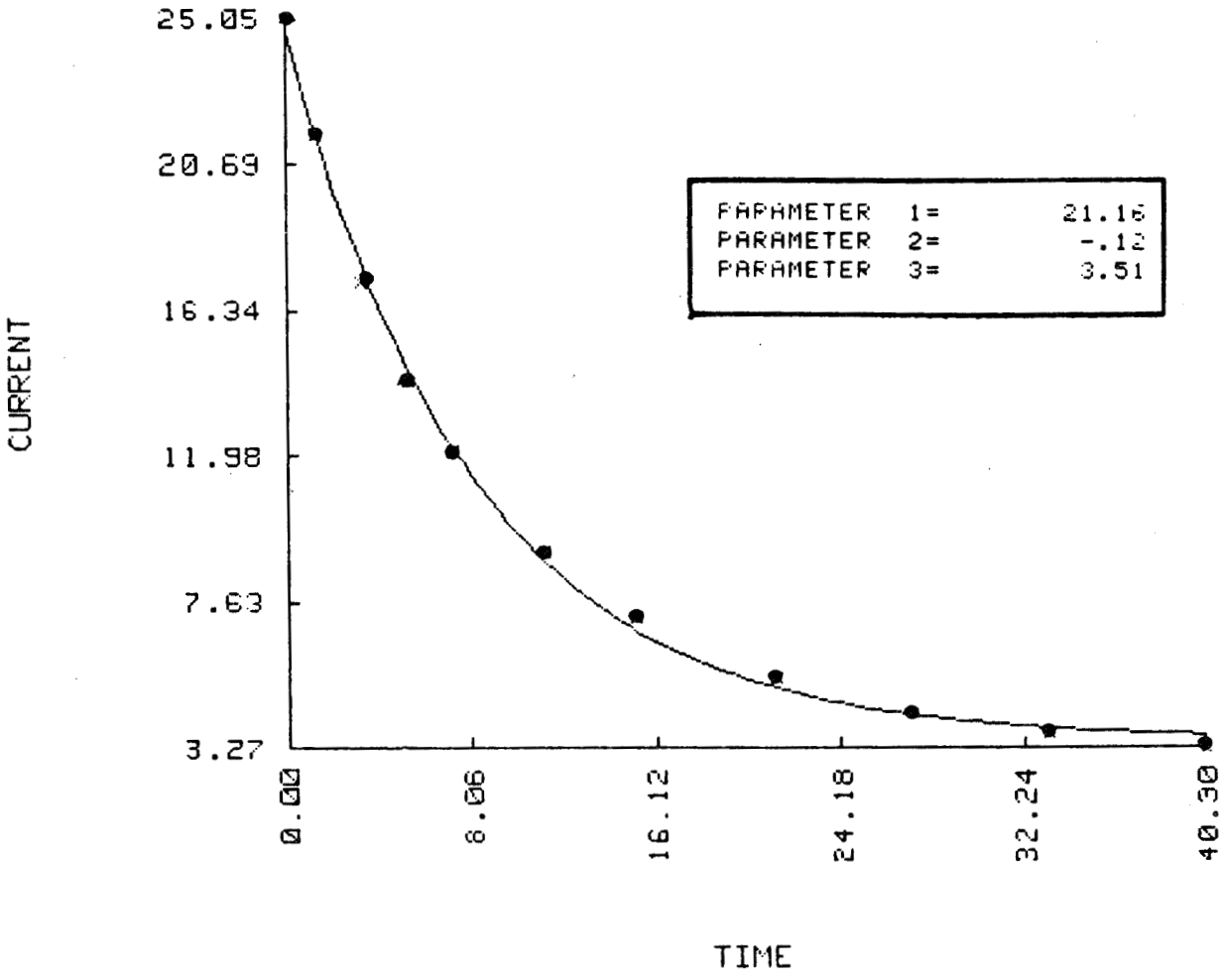

Figure 5a. Three Parameter Fit for .5C Discharge, .5C Charge, VL 7 and 0° C

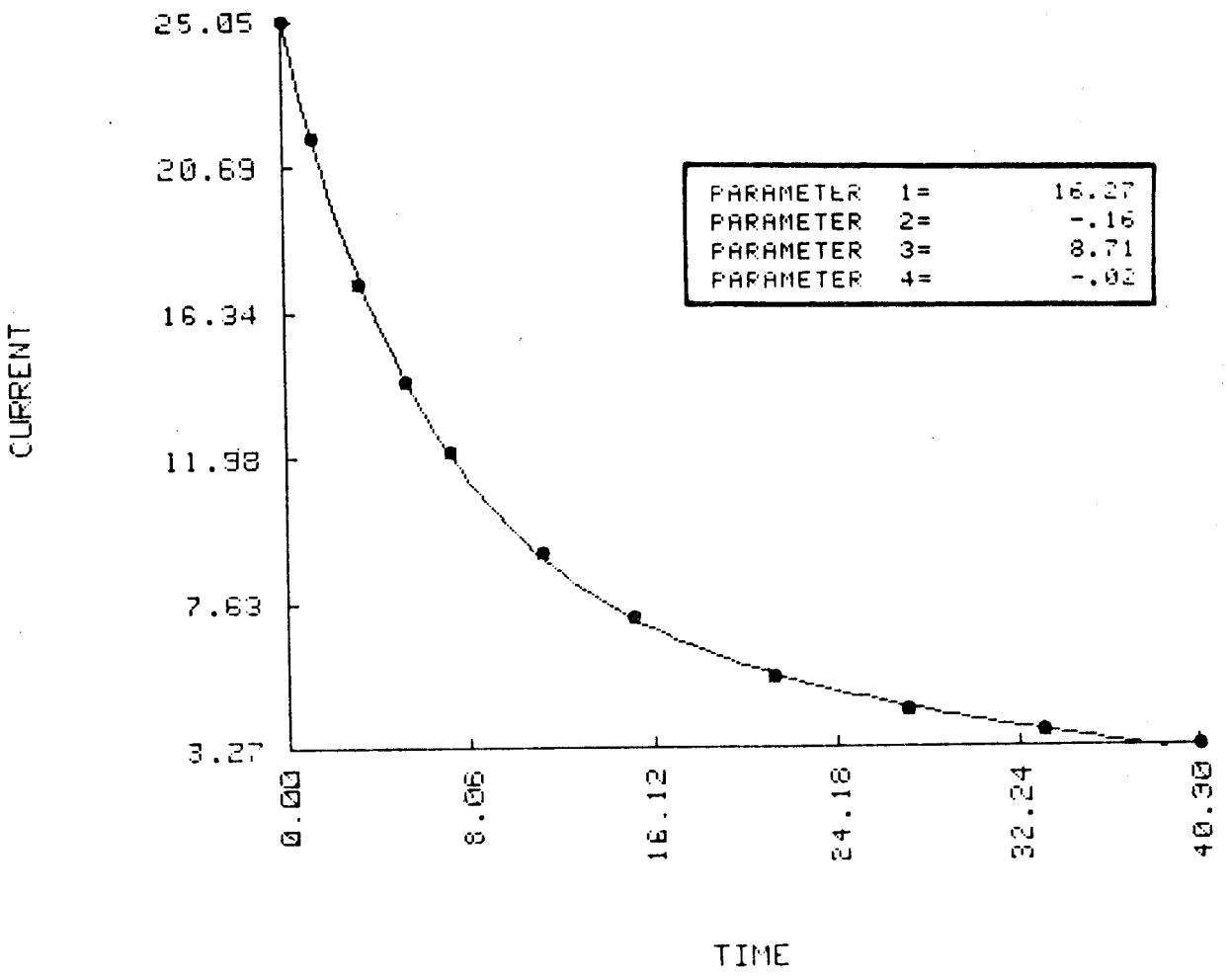

Figure 5b. Four Parameter Fit for .5C Discharge, .5C Charge, VL 7 and 0° C

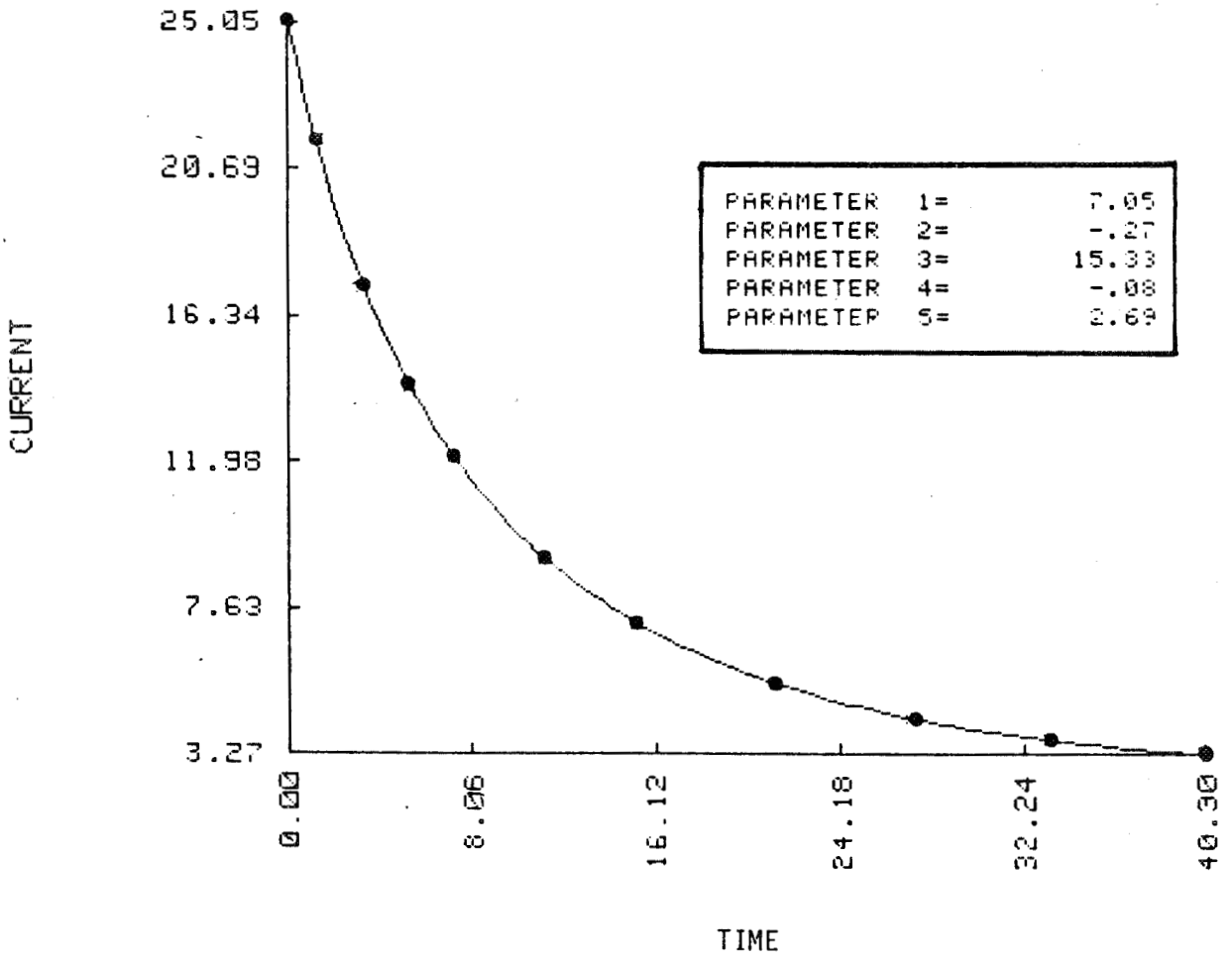

Figure 5c. Five Parameter Fit for .5C Discharge, .5C Charge, VL 7 and 0°C

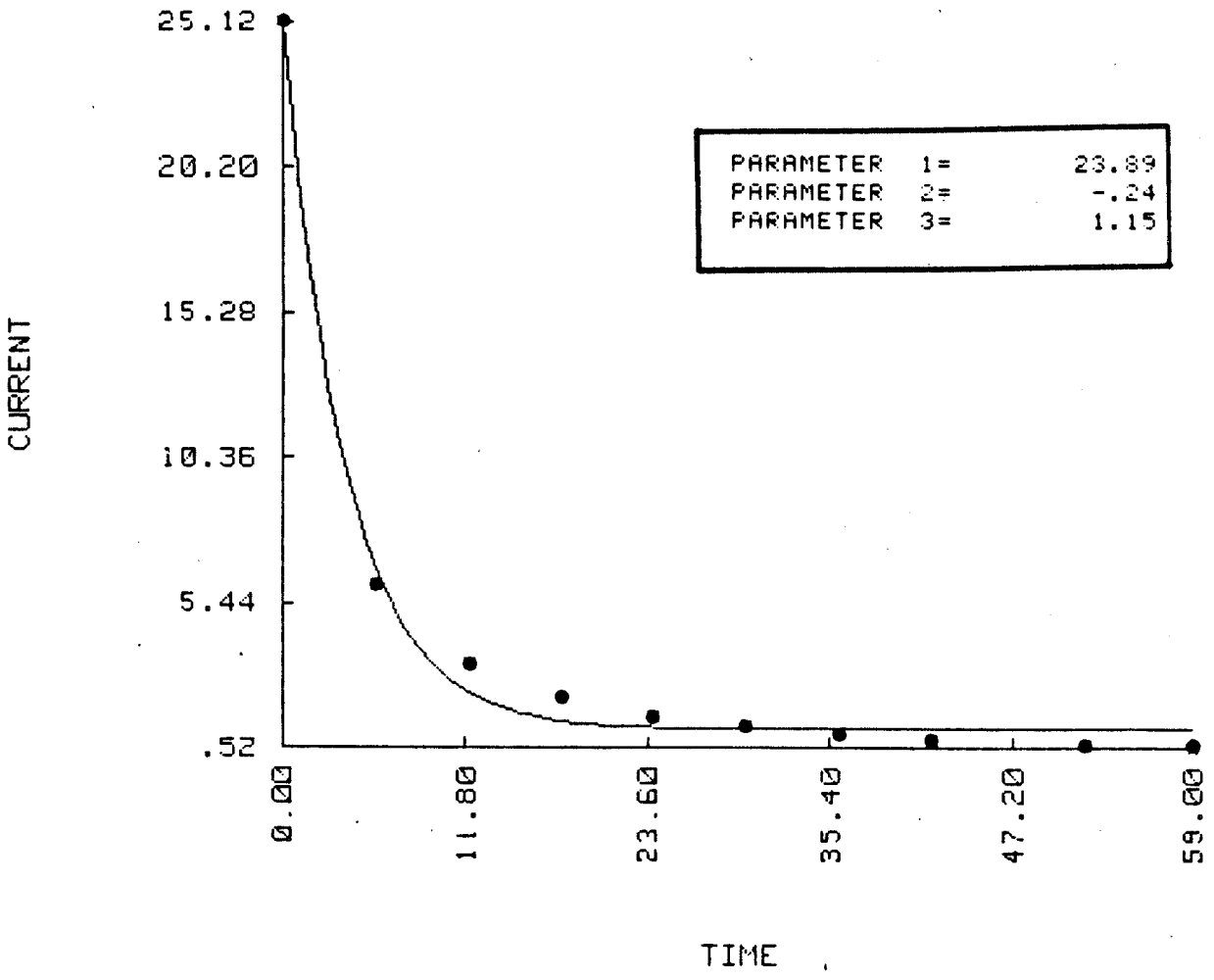

Figure 6a. Three Parameter Fit for .1C Discharge, .5C Charge, VL 3 and 20° C

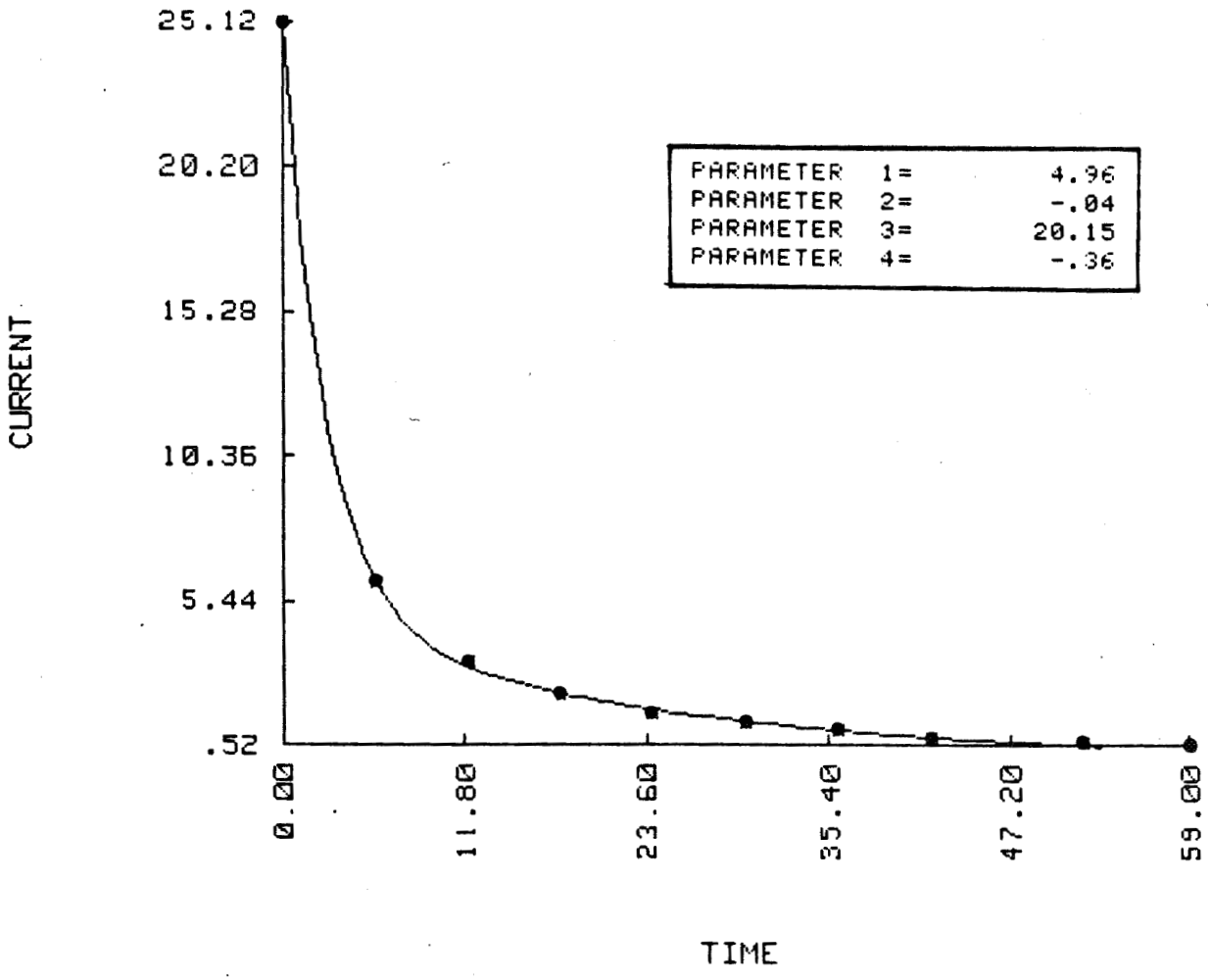

Figure 6b. Four Parameter Fit for .1C Discharge, .5C Charge, VL 3 and 20° C

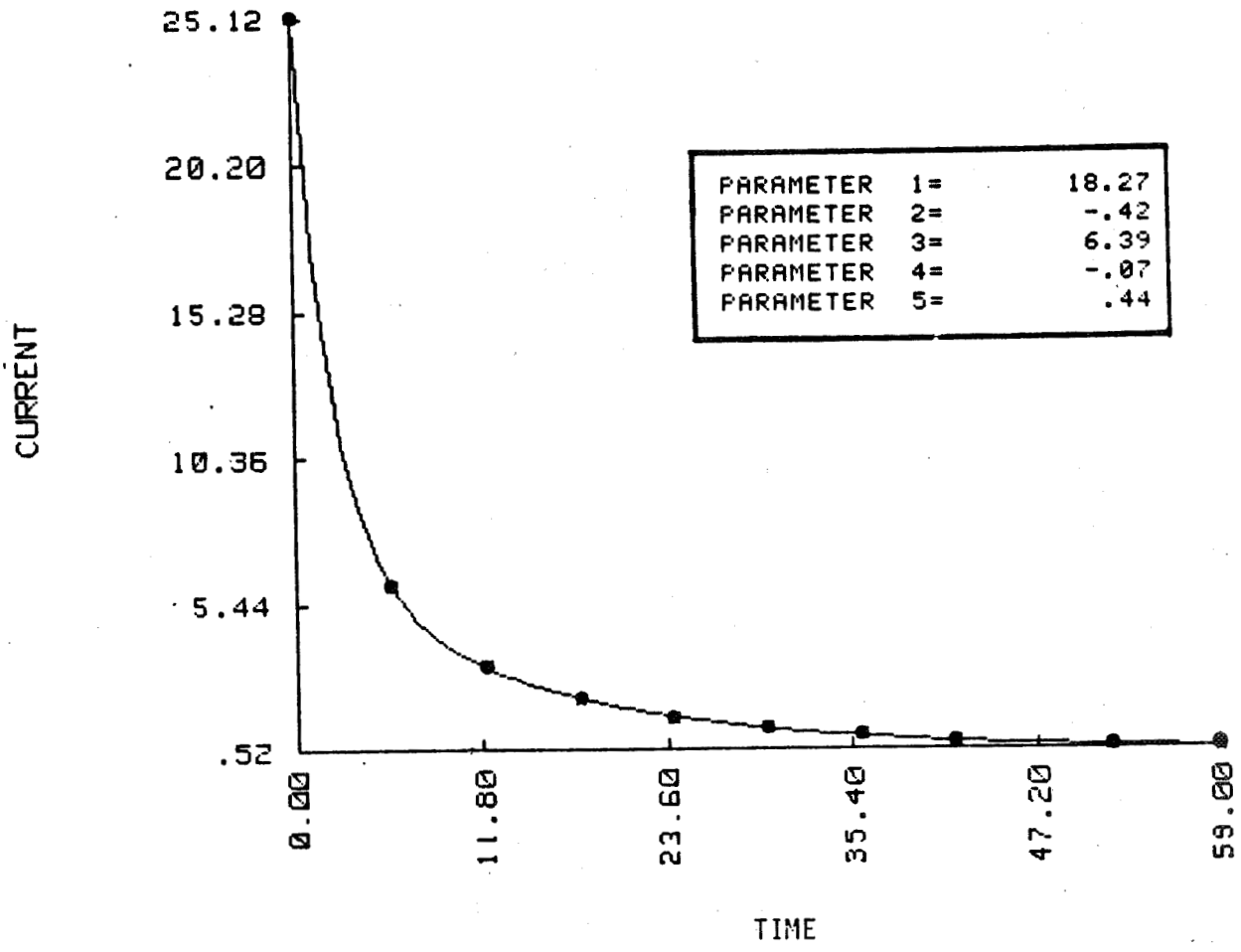

Figure 6c. Five Parameter Fit for .1C Discharge, .5C Charge, VL 3 and 20° C

Table 1. PARAMETERS FOR 3 PARAMETER FIT EQUATION

TEST CONDITION	1230	1250	1270	1830	1850	1870
Parameter 1	9.07	9.63	8.04	37.7	38.3	36.5
Parameter 2	-.137	-.103	.144	-.85	- .695	-.69
Parameter 3	1.117	.895	1.96	2.14	2.18	3.16
TEST CONDITION		**1251**	**1271**	**1831**	**1851**	**1871**
Parameter 1		9.087	7.66	37.9	37.08	36.36
Parameter 2		-.103	-.127	- .908	- .778	- .591
Parameter 3		.982	2.42	1.85	2.68	3.20
TEST CONDITION	**1232**		**1272**		**1852**	**1872**
Parameter 1	8.75		7.5		39.16	36.07
Parameter 2	-.134		-.173		- .489	- .41
Parameter 3	1.149		2.64		1.82	4.01
TEST CONDITION	**5532**	**5552**	**5572**	**8830**	**8850**	**8870**
Parameter 1	20.85	23.00	20.82	39.93	36.62	33.84
Parameter 2	- .096	- .116	- .132	- .066	- .088	- .12
Parameter 3	2.75	1.55	4.016	1.24	3.608	4.20
TEST CONDITION				**8831**	**8851**	**8871**
Parameter 1				38.68	36.7	39.09
Parameter 2				- .062	- .089	- .084
Parameter 3				1.03	3.67	3.51
TEST CONDITION				**8832**	**8852**	**8872**
Parameter 1				34.97	39.901	39.19
Parameter 2				- .068	- .066	- .085
Parameter 3				5.32	1.80	2.81

Table 2. PARAMETERS FOR 5 PARAMETER FIT EQUATION

TEST CONDITION	5530	5550	5570
Parameter 1	9.15	7.6	7.06
Parameter 2	- .02	- .27	- .27
Parameter 3	16.95	15.7	15.34
Parameter 4	- .17	- .056	- .08
Parameter 5	- .98	1.12	2.69

TEST CONDITION	5531	5551	5571
Parameter 1	9.7	6.72	7.38
Parameter 2	- .013	- .28	- .11
Parameter 3	18.1	17.7	17.14
Parameter 4	- .16	- .05	- .11
Parameter 5	-2.84	.651	3.47

TEST CONDITION	5532	5552	5572
Parameter 1	9.8	5.24	5.33
Parameter 2	- .04	- .062	- .14
Parameter 3	13.5	18.51	15.019
Parameter 4	- .14	- .134	- .148
Parameter 5	1.56	1.15	4.2

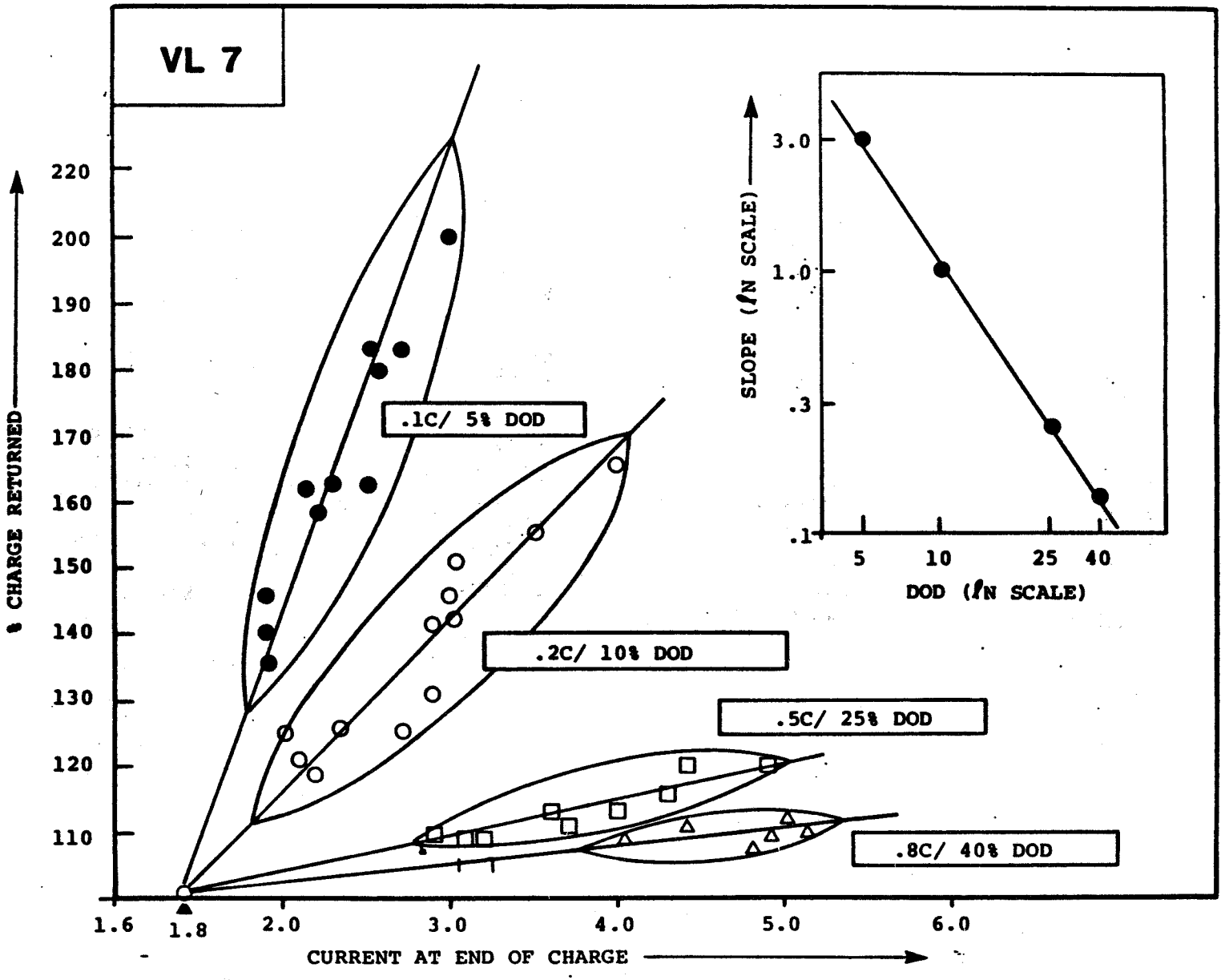

Figure 7. Correlation of Charge Returned with End of Charge Current

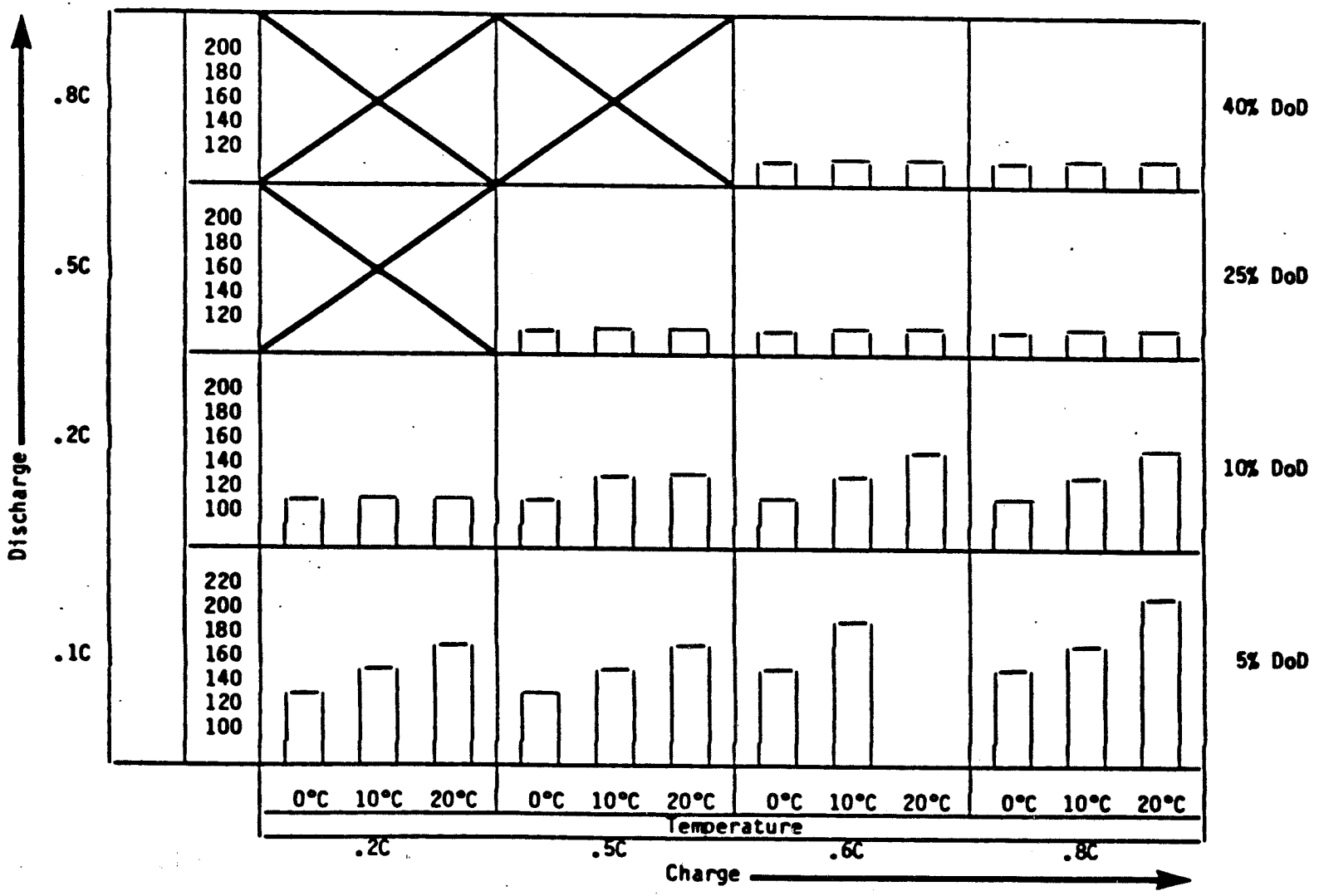

Figure 8. PERCENT RECHARGE VS TEMPERATURE FOR VL 7 TEST CONDITION

Summary and Conclusions

This study has shown that taper charge current profiles of all the environmental test conditions used in this test can be fit very accurately by a five parameter fit equation (Figures 5c and 6c). The study did not progress to the point where these parameters could then be correlated to the environmental test conditions. However, there were certain trends evident which could be pursued in future modeling efforts.

1. Percent charge returned and time to voltage limit show a distinct character which can be related to charge/discharge rate combinations and the level of voltage limit (Figures 3 and 4).

2. Cells with very modest DoDs (5% and 10%) and higher rates of charge generally showed a very short time to voltage limit, higher percentage of charge returned, a very steep drop in current after hitting the voltage limit and more modest currents toward the end of charge.

3. Cells with higher DoDs and charge rates showed, as might be anticipated, longer time to the voltage limit, lower percent of charge returned, a more modest rate of drop in current after VL, and greater currents at the end of charge.

4. Percent charge return, the relationship between DoD and current at the end of charge, can be easily modeled (Figure 7).

5. The effect of temperature is observed more at the lower discharge rates (and DoDs) and increases with increasing charge rate (Figure 8)

Future work should concentrate on a more comprehensive multiple correlation of test conditions (discharge rate (DoD), charge rate, voltage limit and temperature) with the effects of these conditions on battery performance (percent charge returned, charge efficiency, end of charge current, and current taper profile).

HIGH DISCHARGE RATE CHARACTERISTICS OF NICKEL-CADMIUM BATTERIES FOR PULSE LOAD FILTERING[1]

Gregory M. Gearing and Michael B. Cimino
Air Force Institute of Technology

David H. Fritts and John F. Leonard
Air Force Wright Aeronautical Laboratories

Andrew J. Terzuoli, Jr.
Air Force Institute of Technology

ABSTRACT

This investigation consisted of several tests of specially fabricated nickel-cadmium batteries having circular disk type electrodes. These batteries were evaluated as filter elements between a constant current power supply and a five hertz pulsed load demanding approximately twice the power supply current during the load on portion of the cycle. Short tests lasting 10^4 cycles were conducted at up to a 21 C rate and an equivalent energy density of over 40 Joules per pound. In addition, two batteries were subjected to 10^7 charge/discharge cycles, one at a 6.5 C rate and the other at a 13 C rate. Assuming an electrode to battery weight ratio of 0.5, these tests represent an energy density of about 7 and 14 Joules per pound respectively. Energy density, efficiency, capacitance, average voltage, and available capacity were tracked during these tests. After 10^7 cycles, capacity degradation was negligible for one battery and about 20% for the other. Cadmium electrode failure may be the factor limiting lifetime at extremely low depth of discharge cycling. The output was examined and a simple equivalent circuit was proposed.

INTRODUCTION

This investigation consisted of several tests of specially fabricated nickel-cadmium batteries having circular disk type electrodes. These tests addressed three areas. First, would the circular electrodes increase the maximum energy density when compared to standard aircraft batteries. Secondly, what energy density could be maintained and achieve a lifetime of 10^9 cycles at 5 hertz. And finally, how does the battery influence the voltage and current waveforms to the load.

[1] The material reported herein is based on research conducted at and supported by the Air Force Wright Aeronautical Laboratories, Aero Propulsion Laboratory, Wright-Patterson AFB, Ohio.

A bi-polar geometry was considered optimum because of its lower internal resistance and inductance, enabling it to receive and deliver pulses of high current [1]. The reduced internal losses lead to greater efficiency and therefore the potential for a higher energy density. This reduction is achieved in part, by straightening and shortening the current path within the battery.

PSEUDO BI-POLAR BATTERY

Although the construction of bi-polar electrodes has been accomplished at a number of facilities, the fabrication of a bi-polar battery has been complicated by the lack of a reliable edge seal to prevent electrolyte shorting between cells. In order to take advantage of the bi-polar geometry without inheriting the edge seal problems, a pseudo bi-polar nickel-cadmium battery was designed. It resembles a monoblock type construction and consists of a stack of single cell button style batteries in which adjoining cells share a common wall and intercell connector. Figure 1 shows an exploded view of the battery design. To obtain some understanding of the effects of this design on internal losses and to be compatible with available test equipment, several four cell nickel-cadmium pseudo bi-polar batteries were constructed.

In order to further reduce internal losses, a circular electrode with a large central current tab to uniformly collect the current was selected. The electrode was a 3.3 inch diameter disc with the active material impregnated in an annular shape around the center 1.25 inch diameter current tab. Current flow within the electrode is radial and the maximum current path length from the tab to the edge of the electrode is approximately 1 inch. This is in contrast to typical nickel-cadmium aircraft batteries which have rectangular electrodes with a current tab in one corner.

Figure 2 illustrates the differences between the test battery's electrode and that of a typical rectangular battery's electrode. The cross hatched areas are the regions of highest current density. For rectangular electrodes, this area lies between the positive and negative current tabs, and has been identified as a stress point associated with sealed battery failures. An increased current density accelerates the cadmium to cadmium hydroxide to cadmium formations that occur during battery charge and discharge. With pellon or nylon as the separator material, as used in sealed nickel-cadmium cells, cadmium crystals become lodged in the separator eventually shorting out the cell [2]. Although the circular tab does not eliminate this problem, it is a step towards a bi-polar design where the peak current density is spread more uniformly over a larger area of the electrode, thereby reducing the stress and attendant failure mechanisms.

The cells are electrically connected by a 1.125 inch diameter, 0.210 inch thick nickel slug mounted in the plexiglas wall. The large cross section and relatively short intercell path length result in both a smaller internal resistance and inductance through the battery. The nickel to plexiglas seal was established by an O-ring around the nickel slug.

The positive nickel electrodes were obtained from Eagle Picher Industries. The plaque material was a standard 0.030 inch thick nickel sinter (dry sinter process) with a porosity of approximately 80%. They were electrochemically impregnated with 1.7 grams of active NiO(OH) per cubic centimeter of void. The result was an electrode with approximately a 1.4 ampere hour theoretical capacity (C). In addition, to improve the electrode/nickel slug weld, Battery 7 was constructed with nickel electrodes fabricated at AFWAL/APL using an aqueous process [3], to approximately the same 1.4 ampere hour theoretical capacity.

The negative cadmium electrodes were fabricated at AFWAL/APL using a process developed and patented by Fritts, et. al. [4]. This process used the same base plaque, 0.030 inch thick 80% porosity nickel sinter. The electrodes were loaded with 6 to 8 grams of active cadmium each for a theoretical capacity of 2.5 to 3.1 ampere hours. This combination insured that the battery cells were nickel limited.

The cells were assembled by first welding the electrodes to the nickel slug/plexiglas wall combination. Then these units were stacked and glued one by one in a plexiglas tube. A relief vent (about 8 psi) was installed in each cell. Finally a reference electrode, a 1 millimeter diameter cadmium wire, was inserted into each cell. Leads were soldered on the outside of the end cells and a plexiglas stand was attached.

To fill the cells, the vents were removed and the battery was set upside down in a beaker of electrolyte (32% by weight KOH). A vacuum of 28 inches of mercury was pulled on the entire assembly. When the vacuum was released electrolyte was drawn into the cells. The procedure was repeated several times to insure electrode saturation.

FINDING A SEAL

One of the major problems with the construction and use of bi-polar batteries is obtaining a satisfactory intercell seal, thus keeping the electrolyte from shorting out adjoining cells. The first step in the fabrication of the test battery was to evaluate a neoprene O-ring placed around a nickel slug. This assembly was then inserted in the bottom of the test container as shown in Figure 3. The bottom of this container simulated an intercell wall. There was no noticeable electrolyte leakage in 30 days, with electrolyte under approximately 8 psi of pressure. This success, elimination of electrolyte leakage between cells, overcame one of the major stumbling blocks in bi-polar nickel-cadmium battery construction.

ELECTRODE TO CURRENT TAB WELDING

During the gluing of Battery 2, one cadmium electrode to nickel slug weld was broken. Rewelding was not possible, so construction was completed by placing the electrode in its proper place and relying on the pressure of the next layer to hold it there.

On batteries 4 through 7, the smooth side of a perforated nickel foil, typical nickel-cadmium current tab material, was welded to both sides of the nickel slug before the electrodes were attached. The rough side of the tab was driven into the electrode's center area tab by the spot welder. The resulting weld connected the nickel wire within the electrode to the nickel tab material. This weld proved to be stronger. However, one nickel slug to foil weld was broken (Battery 3) during assembly.

Temperature readings of the end terminals and case of Battery 4 during the extended cycle test indicated that the nickel terminal was hotter than the case or cadmium terminal. This was attributed to higher current densities due to the few welds remaining intact. To improve this weld, nickel electrodes with unimpregnated centers were produced for Battery 7.

ELECTRODE COMPARISON

Prior to final construction, the electrodes for each battery were weighed. The weight of each assembled battery, including electrolyte, was recorded. Separate weights were taken, since the overall battery container was not optimized for weight, but rather for ease of laboratory construction. As a comparison, the electrode weight of the batteries used by Bishop and Stumpff[2] was 6.40 pounds while their total battery weighed 11.71 pounds. Therefore, the electrode accounted for 54.65% of the total weight. This ratio was used to determine the weight used in energy density calculations. It is based on the assumption that with some technological improvements, the test battery's design would result in a similar electrode to battery weight ratio.

Another important factor in battery design is the electrode surface current density. In normal parallel plate construction, each side of an electrode acts as a separate electrode, so that one half of the current flows from the center screen through each side of the electrode. Bi-polar electrodes have only a single sided electrode, since the second side is the intercell foil connector. However, rather than metal foil separating the cells, as in a true bi-polar battery, this pseudo bi-polar nickel-cadmium battery used a nickel slug and plexiglas intercell wall with "double sided" electrodes.

For Bishop and Stumpff, the current density through the electrode frontal surface area, with a total current of 100 amperes, was 0.0458 amperes/cm^2. The test electrodes, although fabricated in a double sided configuration, were used as single sided electrodes since the time of charge and discharge, 100 milliseconds, did not allow any significant current flow from the back sides of the electrodes. As a result, the current density for the test batteries, based on a single sided current flow, was 0.1365 amperes/cm^2, with a charging/discharging current of 6.36 amperes. This results in possi-

[2] Unpublished AFWAL/APL test report regarding the testing of 5 series connected 22 ah ni-cd batteries at a charge/discharge current of 100 amps for 10^7 cycles at 5 hertz in 1983.

bly greater polarization at the electrode/electrolyte interface of the test batteries.

TEST SET UP

Figure 4 shows the equipment and circuit used for these tests. Two separate circuits were set up. The first had a 0-15 ampere load and the second had a 0-60 ampere load. A 0-50 amp, constant current, constant voltage power supply, was connected in parallel, and on opposite sides of the battery, with either a 0-15 ampere solid state load, or a 0-60 ampere solid state load. A 5 hertz square wave generator switched the load, simulating a 50% duty cycle current pulse load. A blocking diode on the output of each power supply prevented an inadvertent battery discharge back through the power supply. Current shunts were inserted to measure actual power supply current (I_S), load current (I_L), and battery current (I_B). Note that for battery charging I_B is negative and for discharging I_B is positive. Figure 5 shows typical voltage and current waveforms from this test circuit.

CONDITIONING THE BATTERY

Prior to testing the batteries, several charge/discharge cycles were completed to condition the batteries, stabilize their operation, and measure the initial capacity. The theoretical C rate of these pseudo bi-polar nickel-cadmium batteries was 1.4 ampere-hours. The charging rate was 0.75 amperes for the first two cycles and 1.5 amperes thereafter, until the total voltage reached 6.2 volts (1.55 volts/cell).

The battery was then discharged at a 1 ampere rate down to a total voltage of 4 volts. This cycling continued until the capacity was stable for two successive cycles. The measured capacity of each battery, after the initial conditioning cycles and after any additional testing, is shown in Table 1.

Since this experiment used a novel battery design, which did not have any demonstrated cycle life, the first series of tests were run under the same conditions (room temperature, 5 hertz cycle rate, 0.013% depth of discharge (DOD)) as Bishop and Stumpff's test. This provided a direct comparison of battery types.

ENERGY DENSITY

The first objective was to increase the energy density of the battery when used as a capacitive filter. Energy density is a function of the current through the battery (the voltage is nearly constant) and the weight of the battery. A five hertz test was run at various charge and discharge currents starting at five amperes and increasing in five ampere steps. Each current level was maintained for 10,000 cycles with data collection occurring after approximately 5000 cycles.

Battery 4 was tested up to 25 amperes or 18 times the C rate. By incorporating a larger load, Battery 7 was tested to 35 amperes, or 21 C. At this point, the exterior case reached 60°C and further increases were not attempted. The 60°C cutoff was an arbitrary level picked to insure internal temperatures would remain well below the boiling point of the electrolyte, approximately 100°C.

The resulting battery voltage and current plots were utilized to evaluate the average capacitance during discharge, the energy density, and efficiency of the battery.

CALCULATIONS

To calculate the energy into and out of the battery and average capacitance during discharge, the battery voltage was assumed to be a step increase/decrease followed by a linear ramp. The average ramp voltage was used as a constant value for the entire charge or discharge. The initial step change was due primarily to the instantaneous series resistance of the battery. The remaining ramp change was primarily a function of the double layer capacitances and faradaic discharge. Since the solid state loads and power supplies are not ideal devices, the battery was not reacting to a perfect step increase or decrease in current during the first few milliseconds of any cycle. Therefore, the calculations started after the load and power supply currents had stabilized, i.e., approximately 1 millisecond after the start of the load switching.

Figure 5 shows a typical waveforms from the test circuit. The voltage rate of change varied from about 9 volts/second during the first 20 milliseconds to 3 volts/second for the remaining 80 milliseconds. From Figure 5, the average voltage, using a straight line approximation, is 4.90 volts, while the integral of the voltage divided by the time gives an average of 4.86 volts. This approximation results in less than a 1 percent error.

MAXIMUM ENERGY DENSITY TESTING

Figures 6 through 8 depict the average capacitance, energy density, and efficiency as functions of DOD. At the higher current levels examined with Battery 7, it was observed that as battery voltage varied, so did the other parameters, particularly average capacitance. For example, at 30 amperes discharge current the end discharge voltage dropped below 4 volts. By increasing the average battery voltage from 5.1 to 5.3 volts, this low point was raised to approximately 4.25 volts, roughly the value recorded during the 25 ampere discharge test. This point coincides with the abrupt reversal of the average capacitance and efficiency in Figures 6 and 8. At the highest current, the test battery's equivalent energy density was over 40 joules per pound. In addition, it appears that battery discharge voltage has a significant effect on the voltage regulation, or effective average capacitance, and efficiency.

CYCLE LIFE

In order to project a possible cycle lifetime for the new design, two batteries were run for 10^7 cycles. Since this is only a small fraction of the proposed lifetime and no catastrophic failures occurred, no conclusive data was obtained. Figures 9 through 13 show average battery voltage, energy density, average capacitance, efficiency, and capacity versus cycles completed at DOD's of 0.013% and 0.025%. These DOD's, which reflect the depth of capacity discharged each cycle, not necessarily the actual state of charge, were based on the theoretical battery capacity, not the rated capacity.

The relatively low measured capacity, when compared to the theoretical capacity, may be due to incomplete conditioning of the batteries prior to testing. However, the main purpose was to demonstrate energy densities above 10 Joules/pound, document performance of the batteries over 10^7 cycles, and analyze the battery influence on voltage and current when used as a filter. Incomplete conditioning did not noticeably impede any of these objectives.

Although not a failure, Battery 3 had a varying internal resistance during the 10^7 cycle test. It was found that by increasing pressure on the end of the battery, the internal resistance would drop. After completing the testing, the battery was taken apart. In addition to a broken weld during construction, several other welds were very easy to break during dissection. The varying internal resistance is attributed to these poor welds.

Figure 13 shows the relative capacity of the test batteries before and after cycling. Battery 3 was reconditioned around 4.8 million cycles and therefore has three data points. As a comparison, the relative capacity measured by Bishop and Stumpff, from their test of 5 series connected 22 ampere/hour nickel-cadmium aircraft type cells is also included in Figure 13.

After completing the 10^7 cycle test, samples of both nickel and cadmium electrodes were examined and compared with uncycled electrodes. Photographs of these electrodes are shown in Figures 14 through 18. There was no apparent change in the nickel electrode. The cadmium electrode, however, showed a significant change. After cycling there were no large cadmium crystals left, only small ones, about 500 times smaller than those crystals found in an uncycled electrode. It is possible that the cadmium electrode may be the lifetime failure mechanism, as is typical of nickel-cadmium batteries in "normal" operations. Since most nickel-cadmium batteries are designed to be nickel electrode limited, this decrease would not show up until the cadmium capacity dropped below that of the nickel electrode. Post cycling capacity testing revealed that this was, in fact, the case for Battery 3.

Figure 13 shows the measured battery capacity versus number of cycles completed at a 5 hertz rate. Assuming that any decrease in measured capacity is attributable to a cadmium loss, the abrupt change in Battery 3's capacity could be attributed to the gradual failure of the cadmium electrode, finally dropping below that of the nickel electrode. Bishop and Stumpff's batteries

also show a fairly rapid decrease in measured capacity after about 5 million cycles, which may have also been a result of cadmium electrode deterioration.

Even with this increased rate of capacity loss, the test batteries appear to have lifetimes of 10^9 cycles or more. The dashed line in Figure 13 runs through the RMS values obtained from Batteries 3 and 4 at $5x10^6$ and 10^7 cycles. It projects approximately a 50% remaining capacity at 10^9 cycles. Projecting this line back towards 1 cycle, results in a value of approximately 250% of initial battery capacity. This is roughly equivalent to about 80% of the initial theoretical cadmium capacity. However, there are still too few data points to accurately predict the lifetime of batteries when used as filters.

There were no identifiable trends or failures in energy density, average capacitance, or efficiency during the 10^7 cycles. Figures 10 through 12 only show the trends of these values through 10^7 cycles. Unless a catastrophic failure occurs, such as a complete short or open circuit, end of life performance criteria, such as effective average capacitance or efficiency, will have to be established before further testing can project an actual lifetime for these batteries when used as filter elements.

EQUIVALENT CIRCUIT

The third area of interest was to determine what effect a battery would have in a circuit when used as a filter element. During the energy density and 10^7 cycle testing, the power supply current was not constant. It appeared that the power supply output capacitors were charging and discharging faster than the battery during the first millisecond after the load switched on or off. To eliminate as many variables as possible, the battery was charged and then connected directly to the load without a power supply. The resulting voltage and current waveforms, together with those obtained during earlier testing, were used to form the basis for the proposed equivalent circuit below.

Each electrode had a volume of approximately 3.55 cm^3. Using a nickel Brunauer, Emmett, and Teller (BET) surface area to volume ratio of 70 m^2/cm^3, 2000 $\mu F/cm^2$ nickel capacitance to BET area, a cadmium BET surface area to volume ratio of 6 m^2/cm^3, and 50 $\mu F/cm^2$ cadmium capacitance to BET area ratio [5,6], the theoretical double layer capacitances were calculated. The nickel double layer capacitance is approximately 5000 farads and the cadmium double layer capacitance is approximately 11 farads.

The change in voltage due to the faradaic discharge for the batteries at a 5 C rate for 0.1 seconds at a 50% state of charge is approximately 0.14 millivolts. This term was neglected since it was over 1000 times less than observed voltage changes. Most of the discharge then, would appear to be across the cadmium capacitances since they are over 100 times smaller than the nickel capacitances.

Combining 4 cells in series gives the proposed battery equivalent circuit shown in Figure 19. E_1 is the combination of the nickel electrode voltage, resistance, and double layer capacitance. R_3 is the series ohmic resistance through the electrolyte, electrodes, and current tabs. C_2, E_2, and R_2 represent the cadmium electrode double layer capacitance, voltage across the electrode/electrolyte interface, and electrode/electrolyte ionic activation resistance respectively.

The equivalent circuit of Figure 19 results in an equation for the total battery voltage of:

$$V(t) = E_o - 4iR_3 - 4iR_2[1 - \exp(-t/R_2C_2)] \qquad (1)$$

where

$V(t)$ = Total Battery Discharge Voltage over Time
E_o = Initial Voltage before Discharge
i = Total Discharge Current
t = Time of Discharge
R_2 = Cadmium/KOH Ionic Activation Resistance
R_3 = Series Electrolytic Ohmic Resistance
C_2 = Cadmium Double Layer Capacitance

From battery voltage curves, $4R_3$ was between 20 and 57 milliohms for Battery 3 and 28 to 38 milliohms for Battery 4. Taking the initial rate of change of voltage from the discharge voltage waveform obtained during the early part of the 10^7 cycle test and using the equation $i=C(dv/dt)$, $(1/4)C_2$ was approximately 0.3 farads. After the 10^7 cycle test, it was not possible to determine C_2, although it appeared to have decreased significantly.

After determining $4R_3$ from the instantaneous change of voltage at both the beginning and end of the discharge, $4iR_2$ was assumed to be the remaining voltage drop occurring during the discharge. Solving for $4R_2$ gave a value of approximately 54 milliohms for both Battery 3 and 4.

Using these values and equation (1), V(t) was plotted against the actual voltage waveforms for Batteries 3 and 4 as shown in Figures 20 and 21. Figure 22 shows the calculated V(t) and actual voltage of Batteries 3 and 4 connected in series. The equation for V(t) then became:

$$V(t) = E_o - 8iR_3 - 8iR_2[1 - \exp(-t/R_2C_2)] \qquad (2)$$

The same values obtained before for C_2, R_2, and R_3 were used as well as the actually measured current and initial voltage. This verifies that the equivalent circuit in Figure 19 appears to be reasonable approximation for these batteries when used as a capacitive filter.

When running the maximum energy density test with Battery 7, the voltage and current waveforms were recorded to evaluate the equivalent circuit of Figure 19. However, the values obtained for R_2, R_3, and C_2 varied as the discharge current and battery voltage varied. $4R_2$ ranged from 12 to 40 milliohms, $4R_3$ ranged from 18 to 35 milliohms, and $(1/4)C_2$ varied from 0.14 to 1.66 farads. It also appeared that at discharge currents above 10 C that the nickel double layer capacitance could no longer be ignored. Furhter analysis of this, which would appear to involve a more complet equivalent circuit, was beyond the scope of this paper.

As the number of cycles on the batteries increased, the voltage curve became initially steeper and then flatter, suggesting that the cadmium double layer capacitance may be decreasing. This may be attributed to the breakdown of the cadmium crystals causing the active electrode surface area to decrease.

If this is the case, a more uniform voltage output, excluding the first 5 milliseconds or so of each pulse, may be obtained by conditioning the battery, causing the cadmium capacity and capacitance to decrease. The nickel double layer and faradaic capacitances would then dominate (after the first 10 milliseconds) giving a much higher effective capacitance over the discharge cycle for the battery. However, this will leave a larger rate of change of voltage at the beginning of each discharge period, possibly allow the battery to become cadmium electrode capacity limited more quickly, and possibly reduce the battery lifetime.

DISCHARGE WITHOUT POWER SUPPLIES

To minimize test circuit induced stray inductance and capacitance on the waveforms of the battery while cycling, the power supply was disconnected. The battery was then connected directly across the load with a minimum of test circuit wiring. The resulting waveforms showed that the test circuit induced inductance was minimal, but the power supply capacitors charged and discharged during the first millisecond of each load change. This caused the power supply current to fluctuate so that the battery was not required to supply an instantaneous change in current. After the first millisecond the power supply and load currents were essentially constant. Therefore, analysis was started after one millisecond and is an accurate indication of battery operation, even with the power supply connected to the battery.

CONCLUSION AND RECOMMENDATIONS

In summary, a maximum equivalent energy density of over 40 joules per pound was demonstrated by the specially constructed test nickel-cadmium batteries. Ten million cycles at a 5 hertz rate with a useful equivalent energy density of 14 joules per pound were completed. Capacity degradation was negligible for one battery and only a 20% decrease for the other. Cadmium electrode failure may be the factor limiting lifetime. An equivalent circuit was derived, but further testing will be required to completely evaluate the results. Internal resistances and double layer capacitances

varied with changes in either battery voltage or current, suggesting that a more complex equivalent circuit may be required.

Batteries appear to be a competitive alternate to capacitors. Further research and testing needs to be accomplished in several areas. First, begin a long term life cycle test, 10^8 cycles or more, to obtain more conclusive data on the battery's long term capability to function as a filter element. Second, construct a bi-polar battery, if necessary achieving an intercell seal at the expense of weight, to determine if a bi-polar design would significantly improve the electrical characteristics desired. If successful, this would support large scale efforts to achieve a true lightweight bi-polar design. Third, begin more detailed experimentation to investigate the relationships between SOC, DOD, energy density, efficiency, output response, average voltage, and average effective capacitance to identify optimum operating conditions and devise a control system to maintain those conditions. Fourth, in view of the dramatic change in the cadmium structure, further analysis is needed to identify exactly what changes are taking place in the electrode, and how these changes will effect the long term performance of the battery when used as a filter element.

REFERENCES

1. Bauer, P.: Batteries for Space Power Systems. Washington D.C.: NASA, 1968. (NASA SP172).

2. Fritts, D.H. and Dueber, R.E.: Inhibiting Cadmium Migration in Nickel-Cadmium Cells by the Addition of Boron Compounds. The Electrochemical Society Fall Meeting, Extended Abstracts-Battery Division 100, New Orleans, Louisiana, 7-12 October 1984.

3. Pickett, D.F.: U.S. Patent 3,827,911, 1974.

4. Fritts, D.H.; et. al.: Methods of Fabricating Cadmium Electrodes, U.S. Patent 4,242,179, December 30, 1980.

5. Amile, R.F.; Ockerman, J.B.; and Ruetshci, P.: Absorption of Hydrogen and Oxygen on Electrode Surfaces. Journal of the Electrochemical Society, 108: 377, 1961.

6. Milner, P.C.; and Thomas, U.B.: The Nickel-Cadmium Cell. Advances in Electrochemistry and Electrochemical Engineering, Vol 5. 1-86. Edited by C.W. Tobias. New York: Interscience Publishers, 1967.

Table 1. MEASURED BATTERY CAPACITY (ampere hours)

BATTERY NUMBER	INITIAL CAPACITY	FINAL CAPACITY
1	Ø.1	Ø.Ø (INTERCELL SHORT)
2	Ø.8	Ø.Ø (INTERCELL SHORT)
3	1.Ø	Ø.8
4	Ø.95	Ø.93
5	Ø.63	NOT TESTED
6	NOT USED (INTERCELL SHORT)	
7	Ø.75	1.Ø1

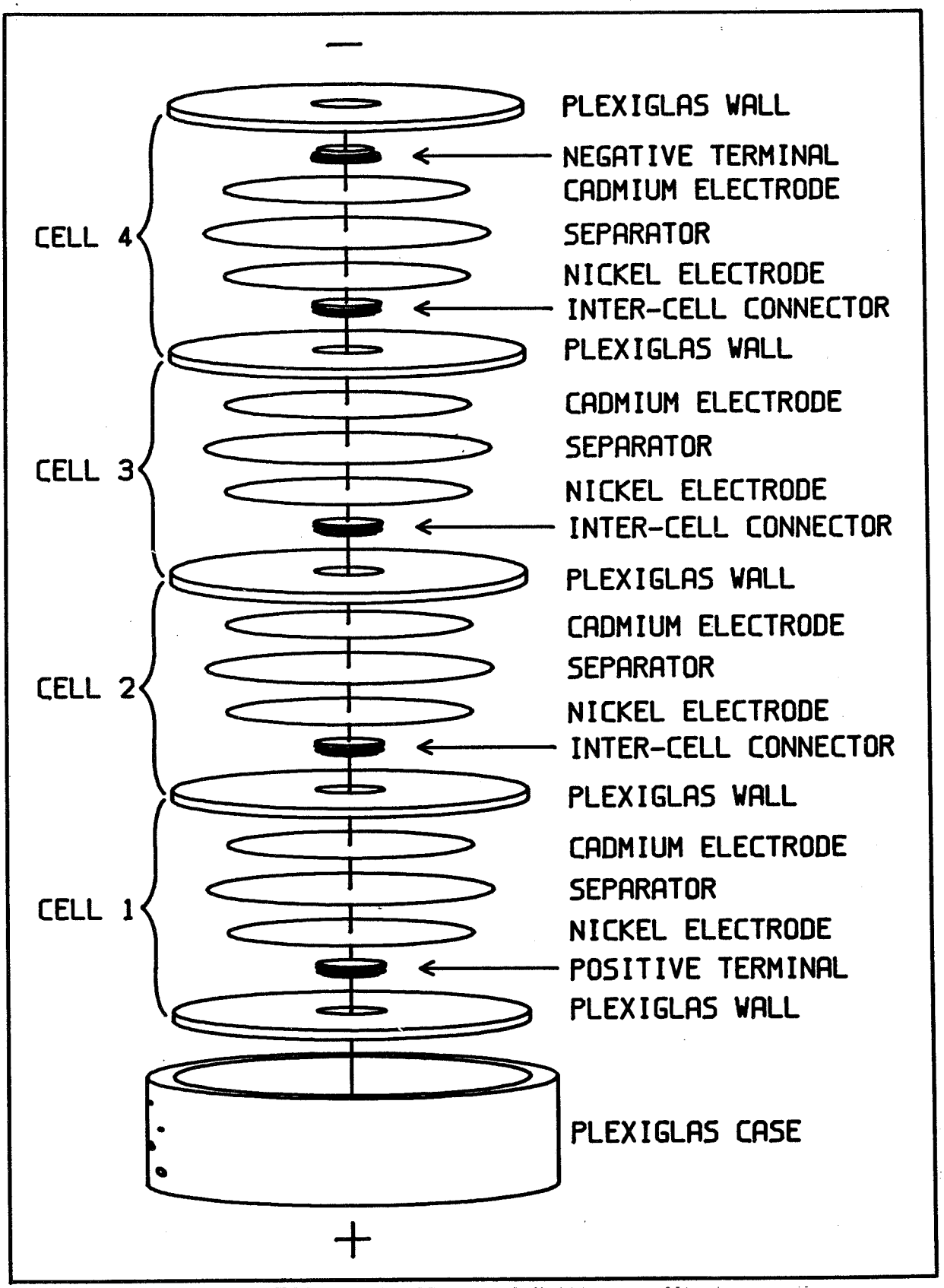

Figure 1. Expanded View of the Test Battery

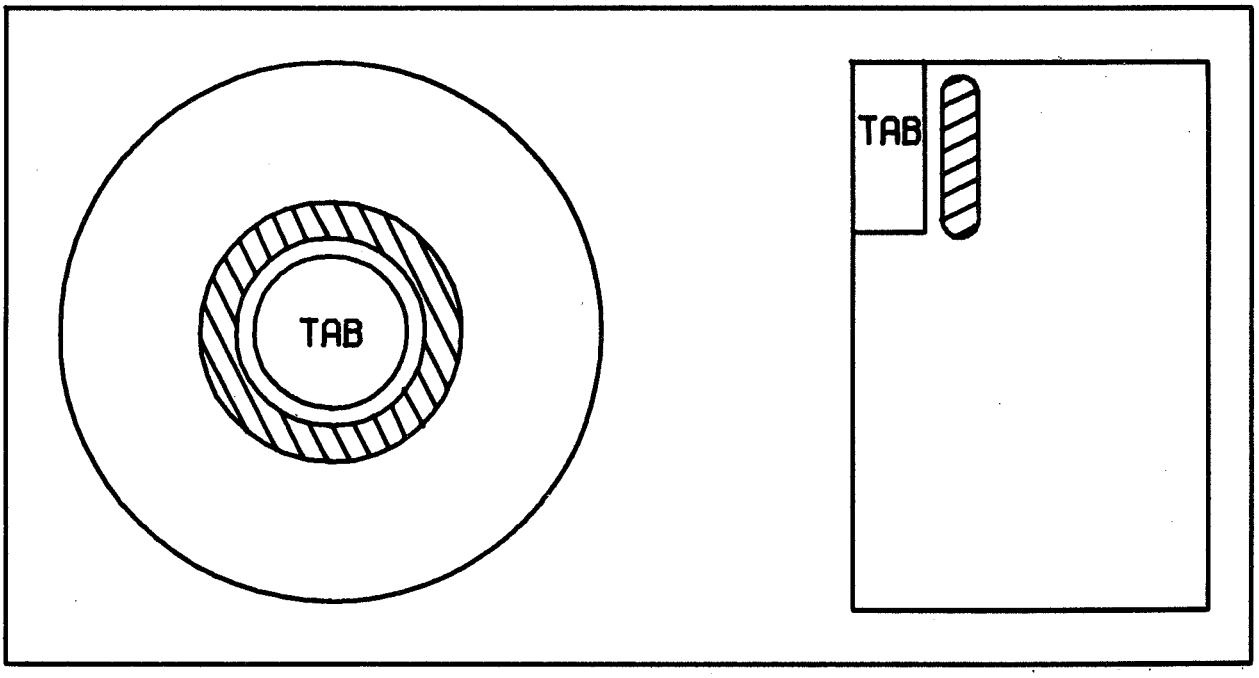

Figure 2. Circular Versus Rectangular Electrodes

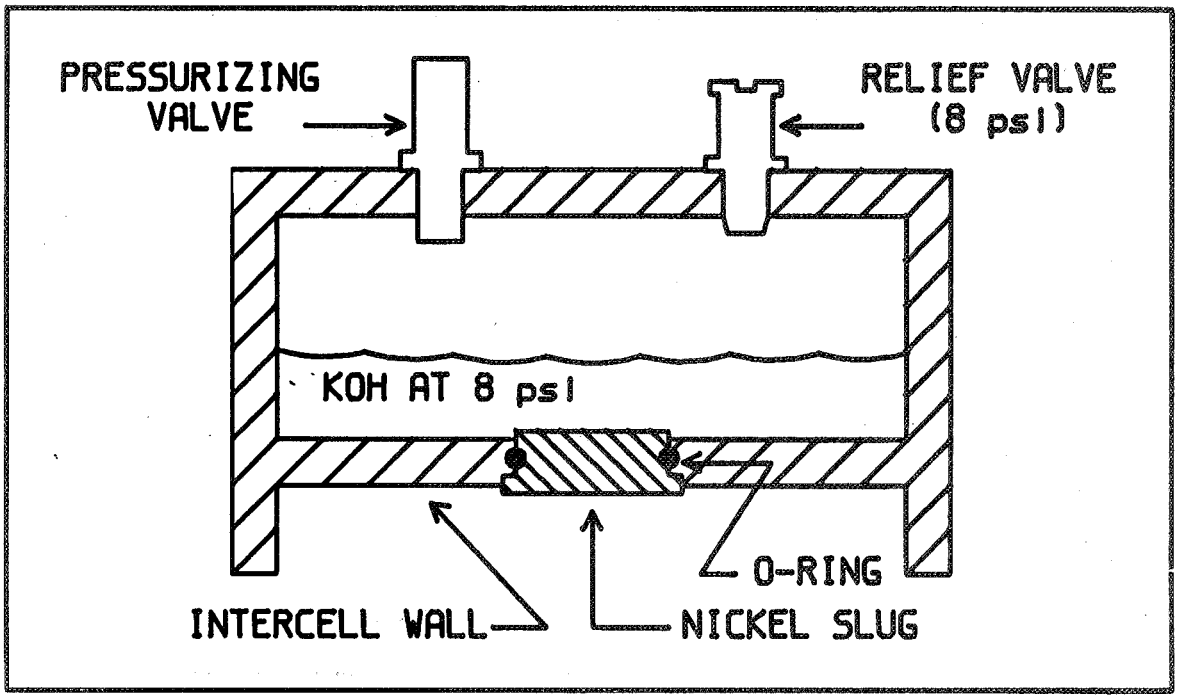

Figure 3. Cutaway of O-Ring Seal Test Container

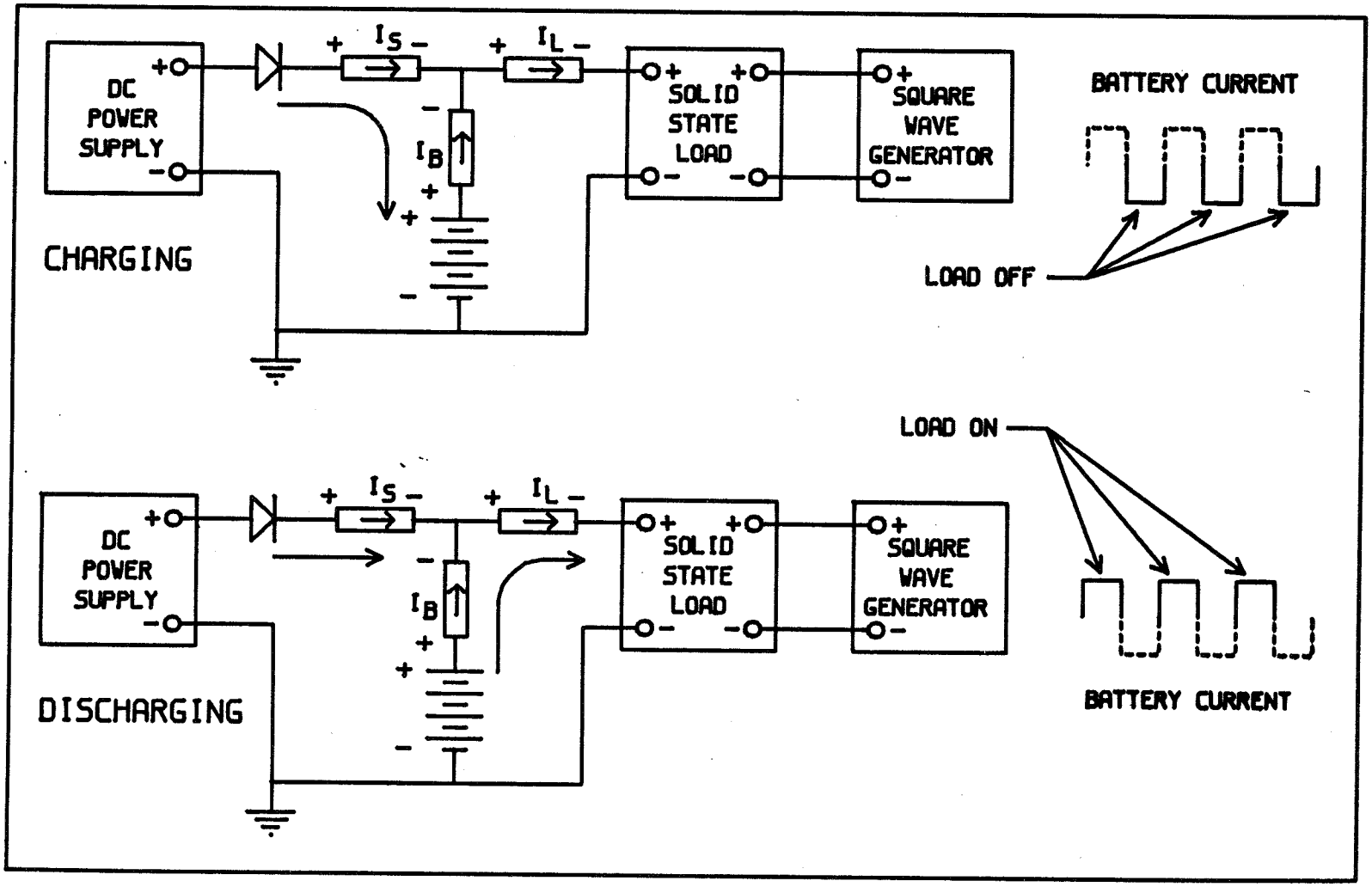

Figure 4. Test Circuit

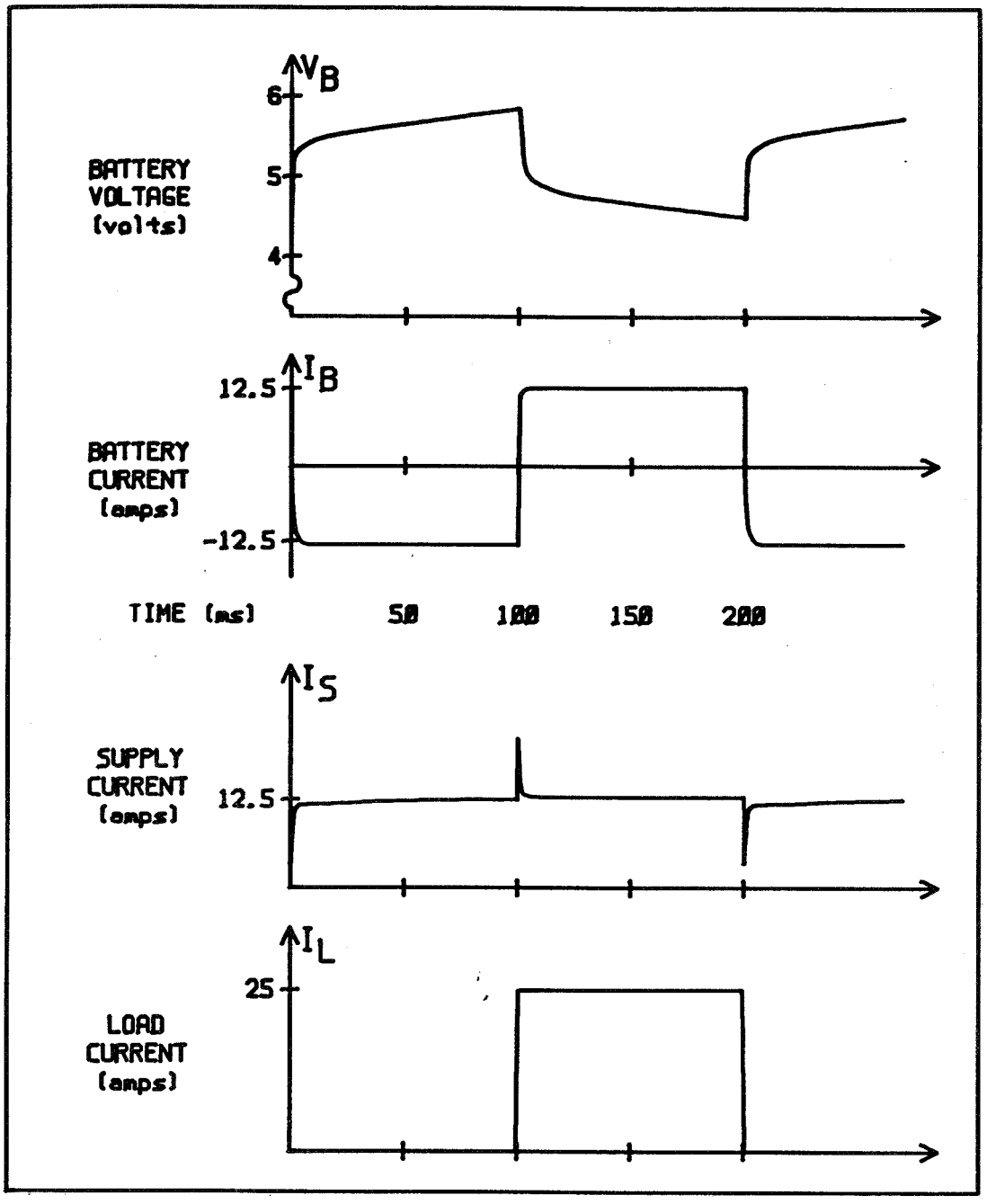

Figure 5. Typical Waveforms

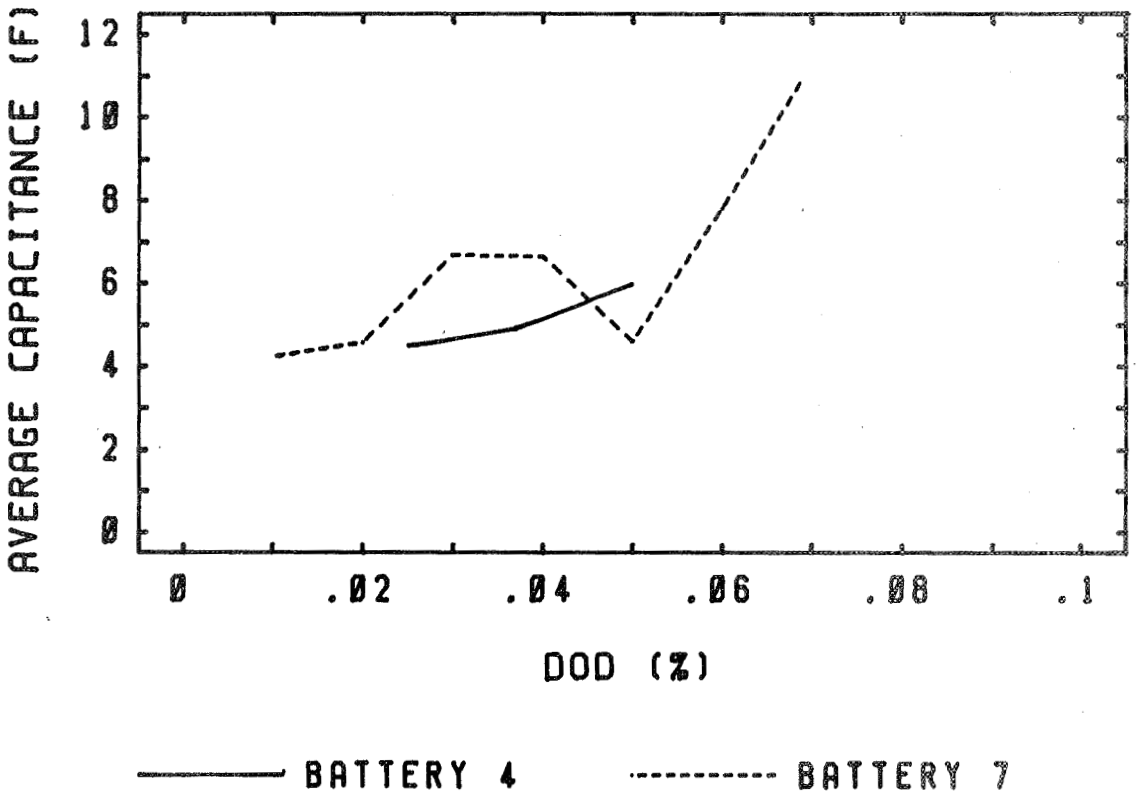

Figure 6. Average Capacitance Versus DOD

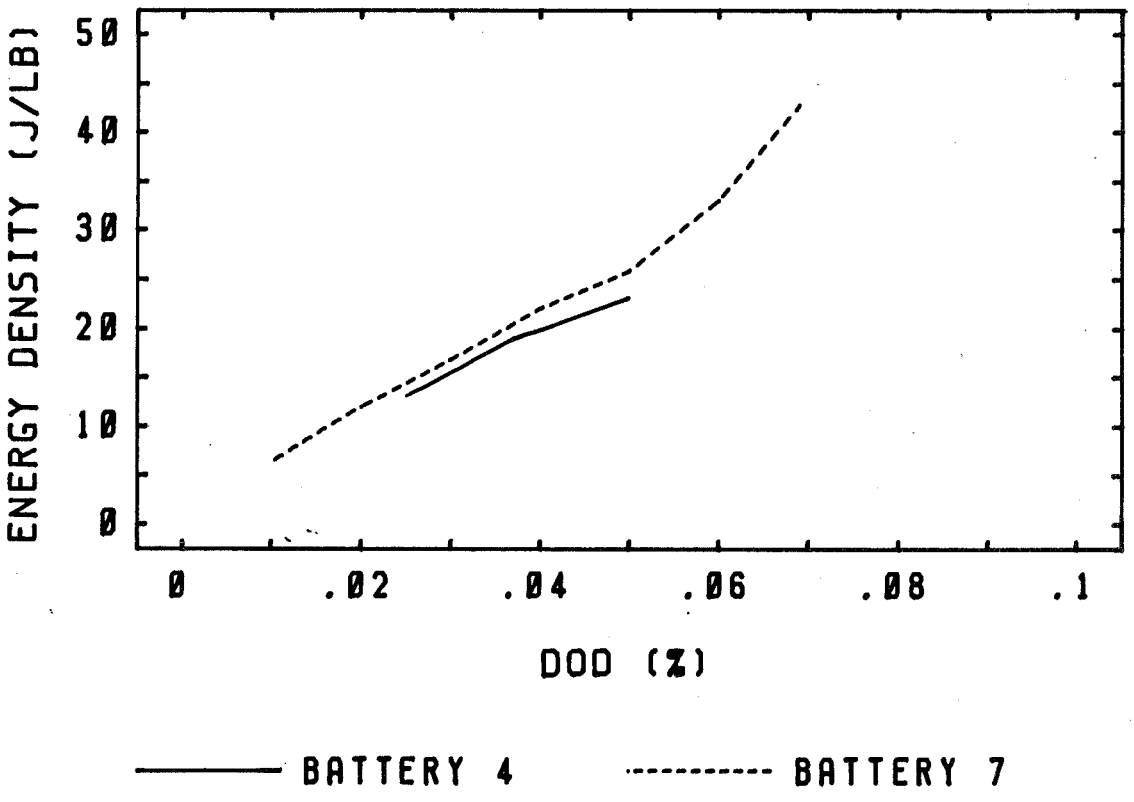

Figure 7. Energy Density Versus DOD

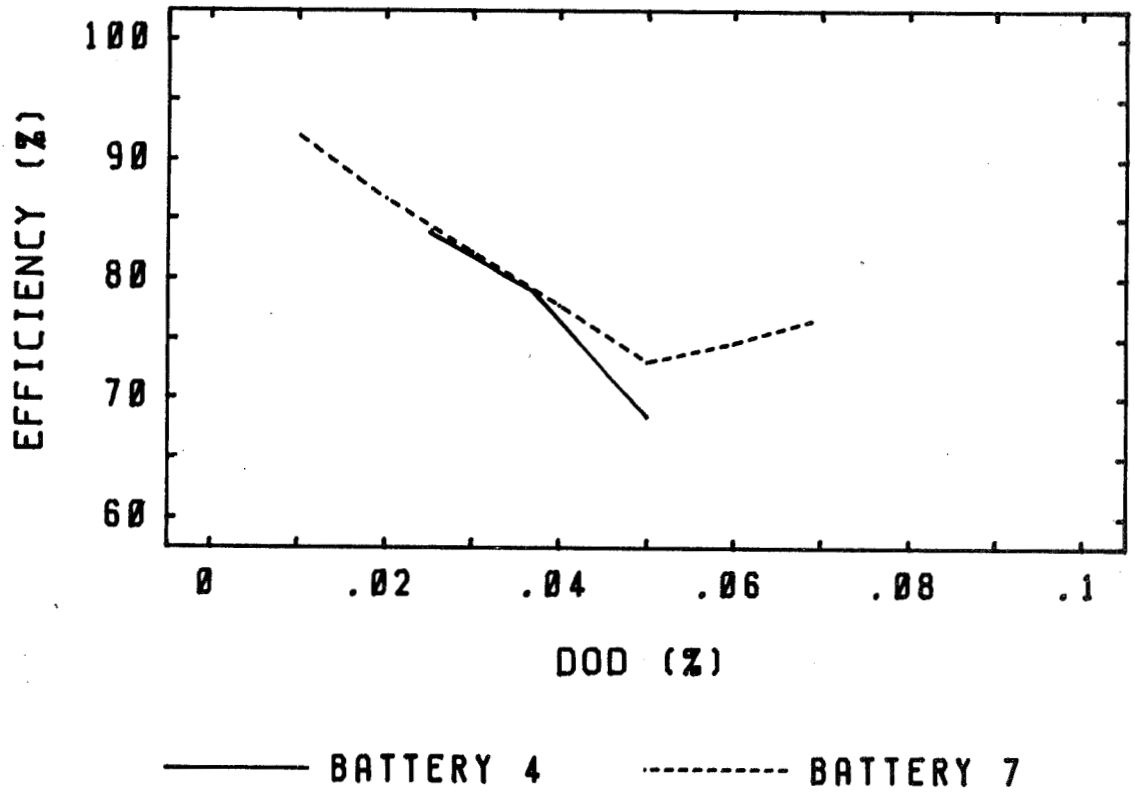

Figure 8. Efficiency Versus DOD

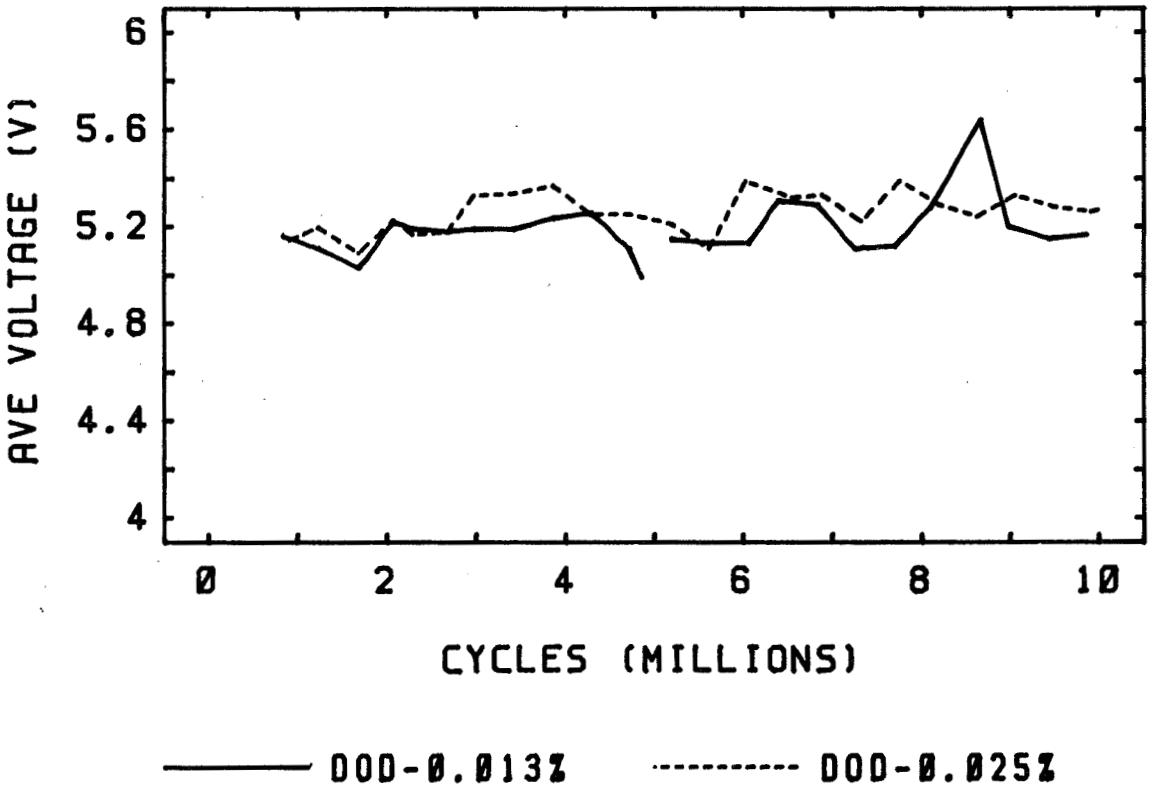

Figure 9. Average Battery Voltage Versus Cycles

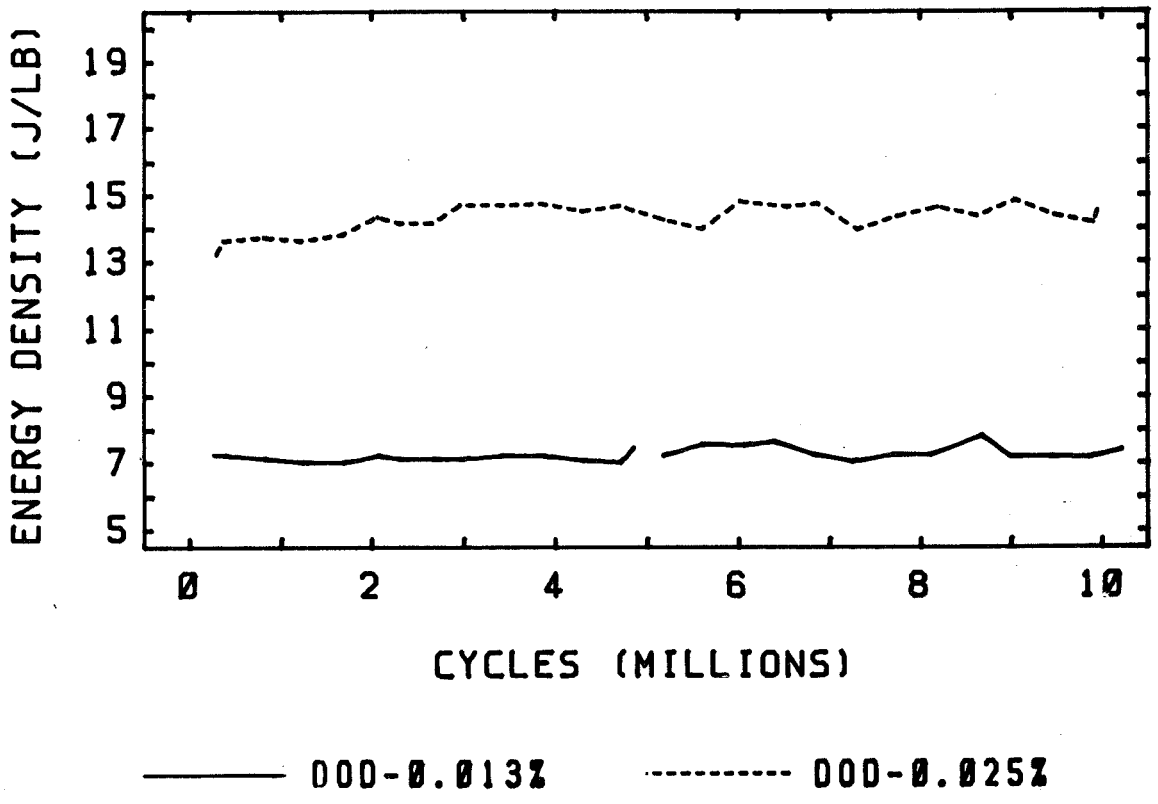

Figure 10. Energy Density Versus Cycles

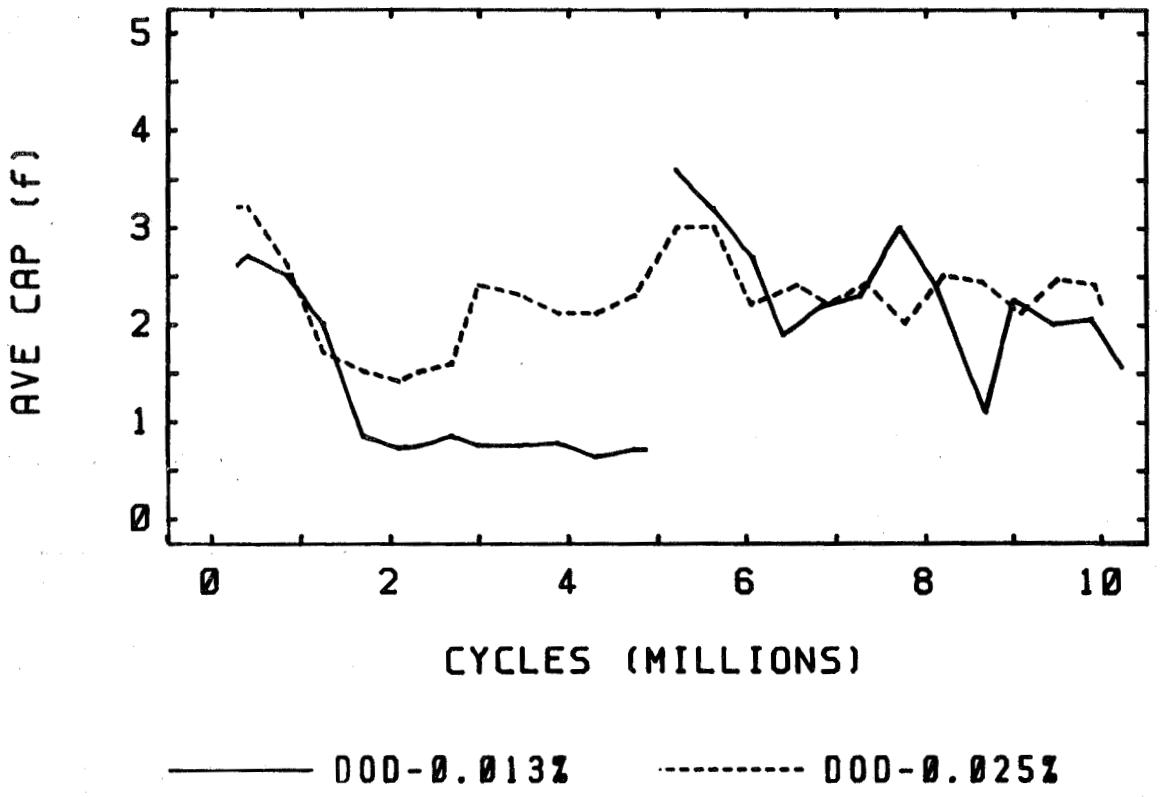

Figure 11. Average Capacitance Versus Cycles

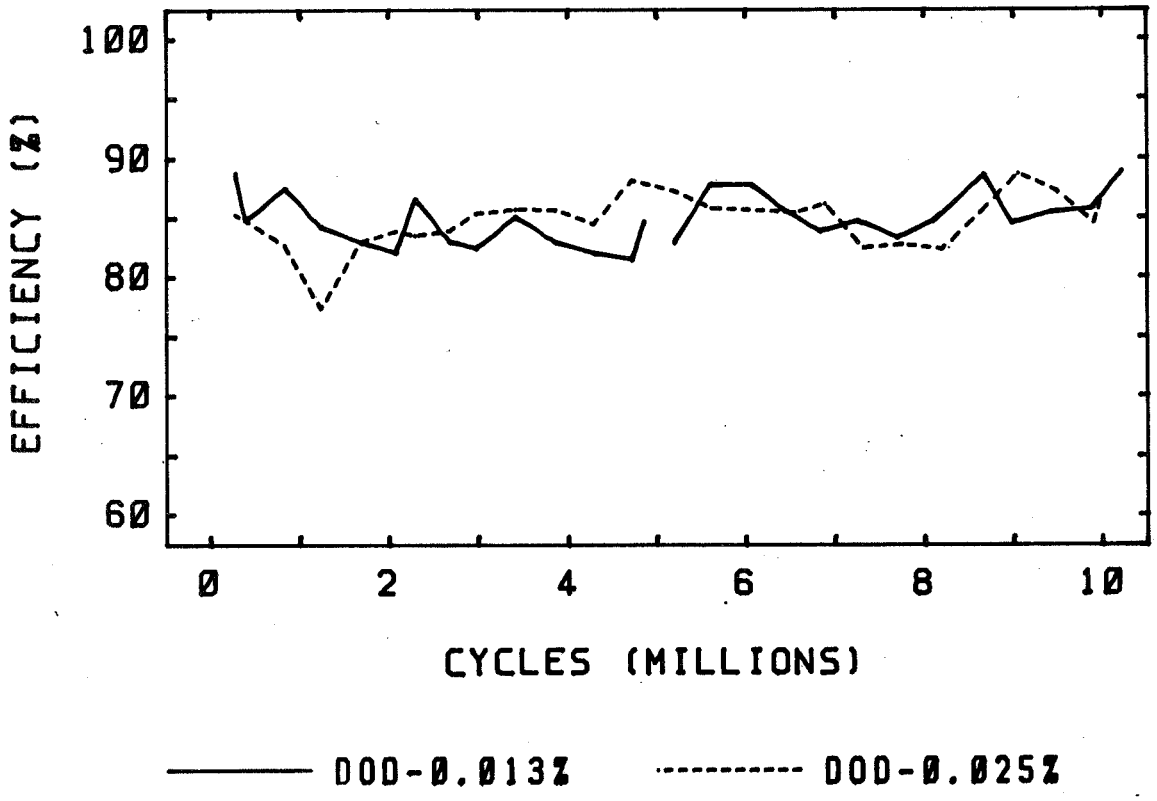

Figure 12. Efficiency Versus Cycles

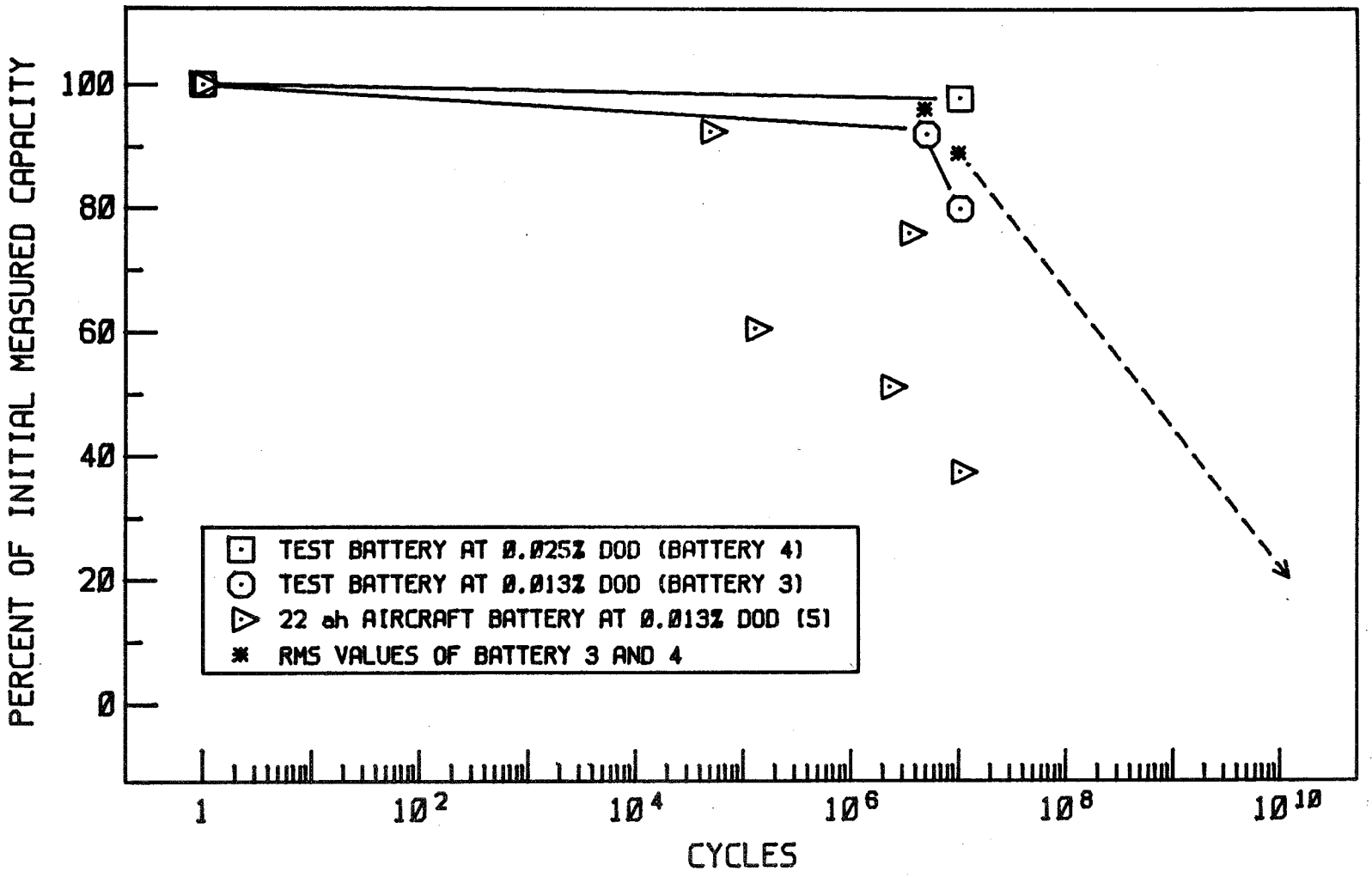

Figure 13. Percent Capacity Remaining Versus Cycles

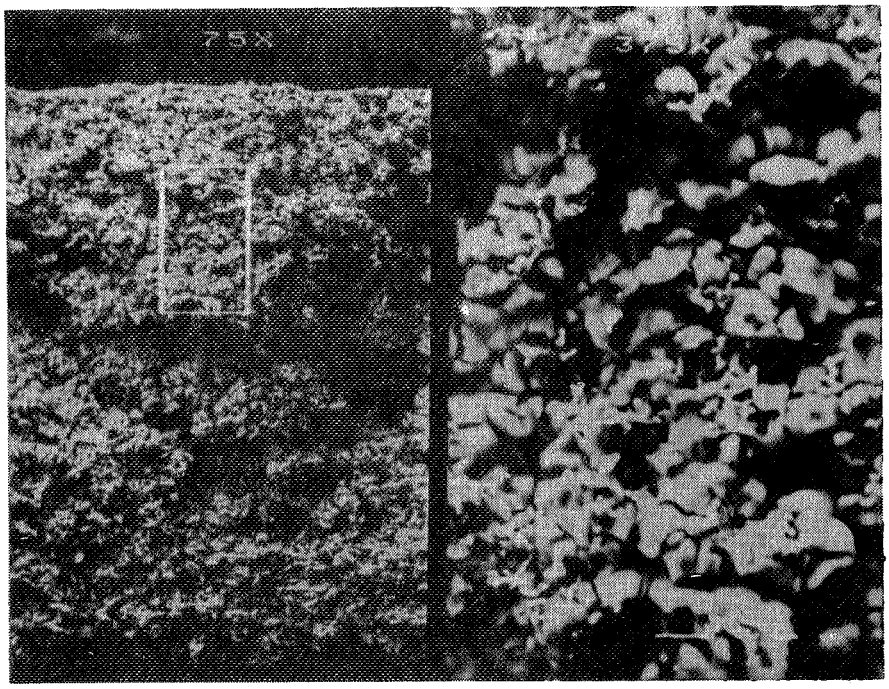

Figure 14. Uncycled Nickel Electrode (75X, 375X

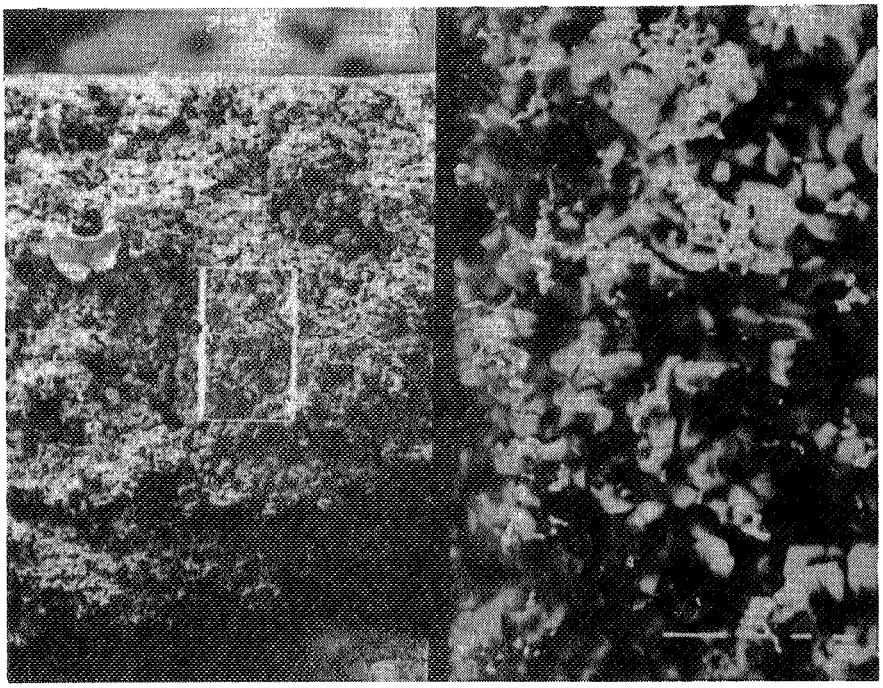

Figure 15. Cycled Nickel Electrode (75X, 375X)

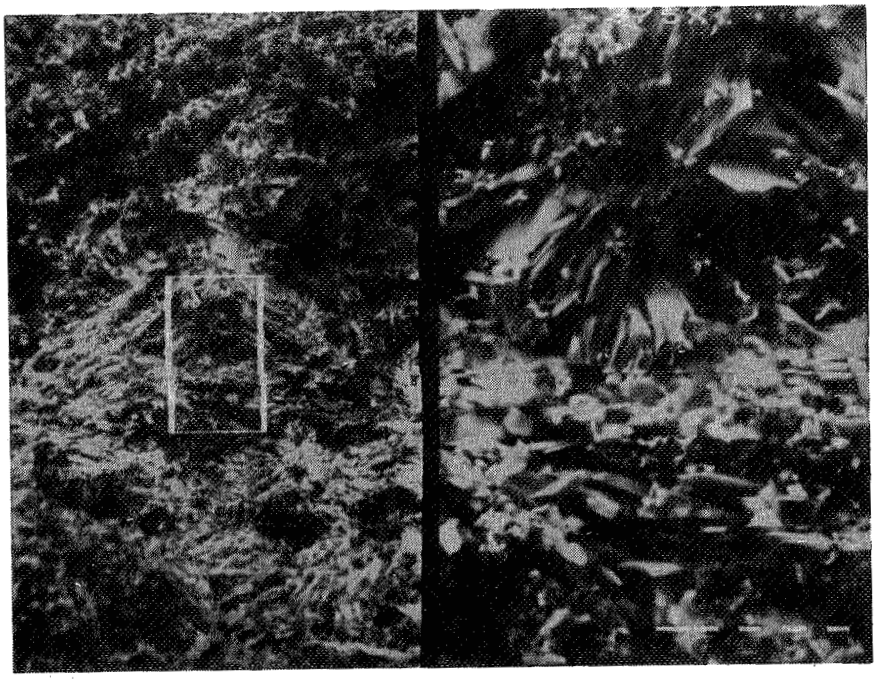

Figure 16. Uncycled Cadmium Electrode (75X, 375X)

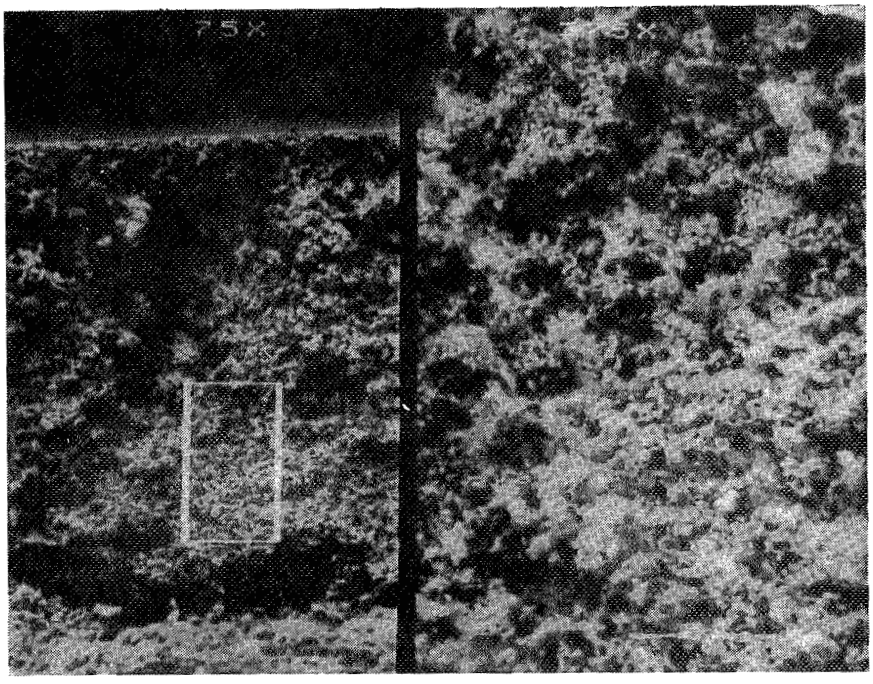

Figure 17. Cycled Cadmium Electrode (75X, 375X)

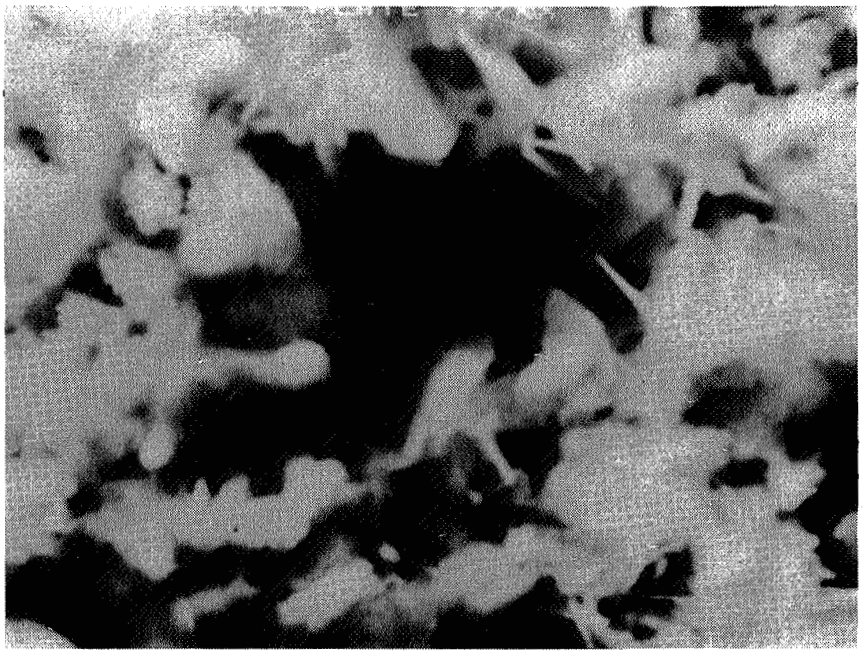

Figure 18. Uncycled Cadmium Electrode (3700X)

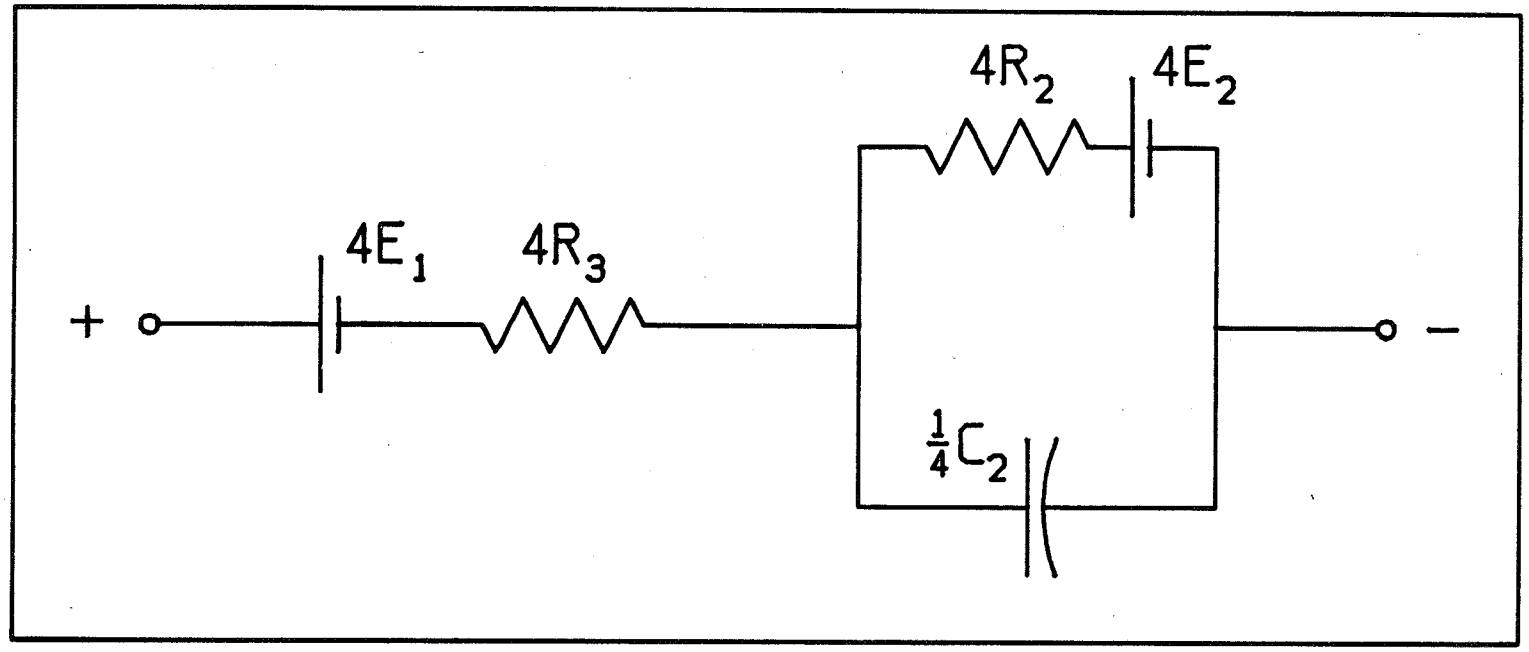

Figure 19. Simplified Nickel Cadmium Battery Equivalent Circuit

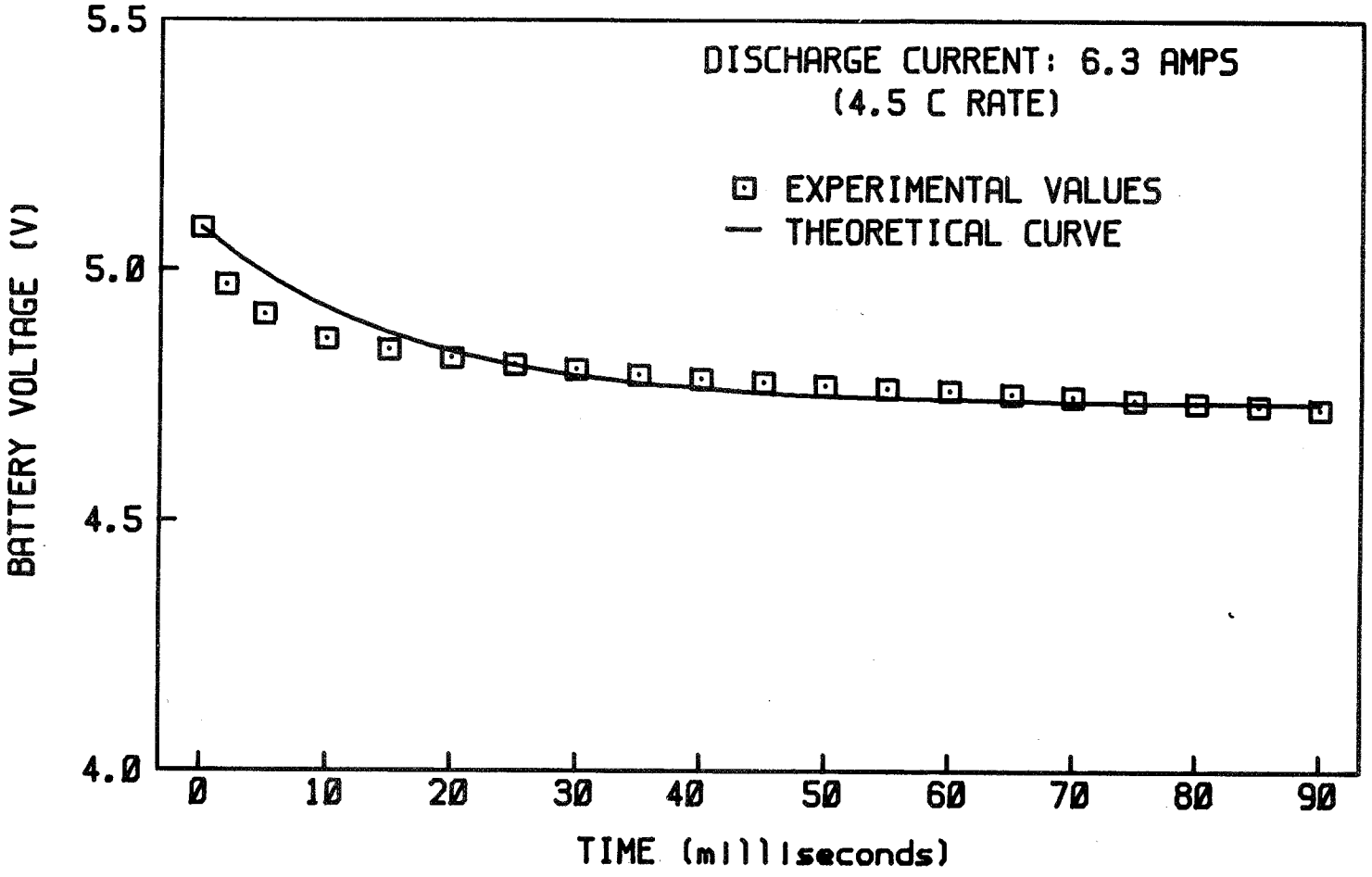

Figure 20. Battery 3 Discharge Voltage

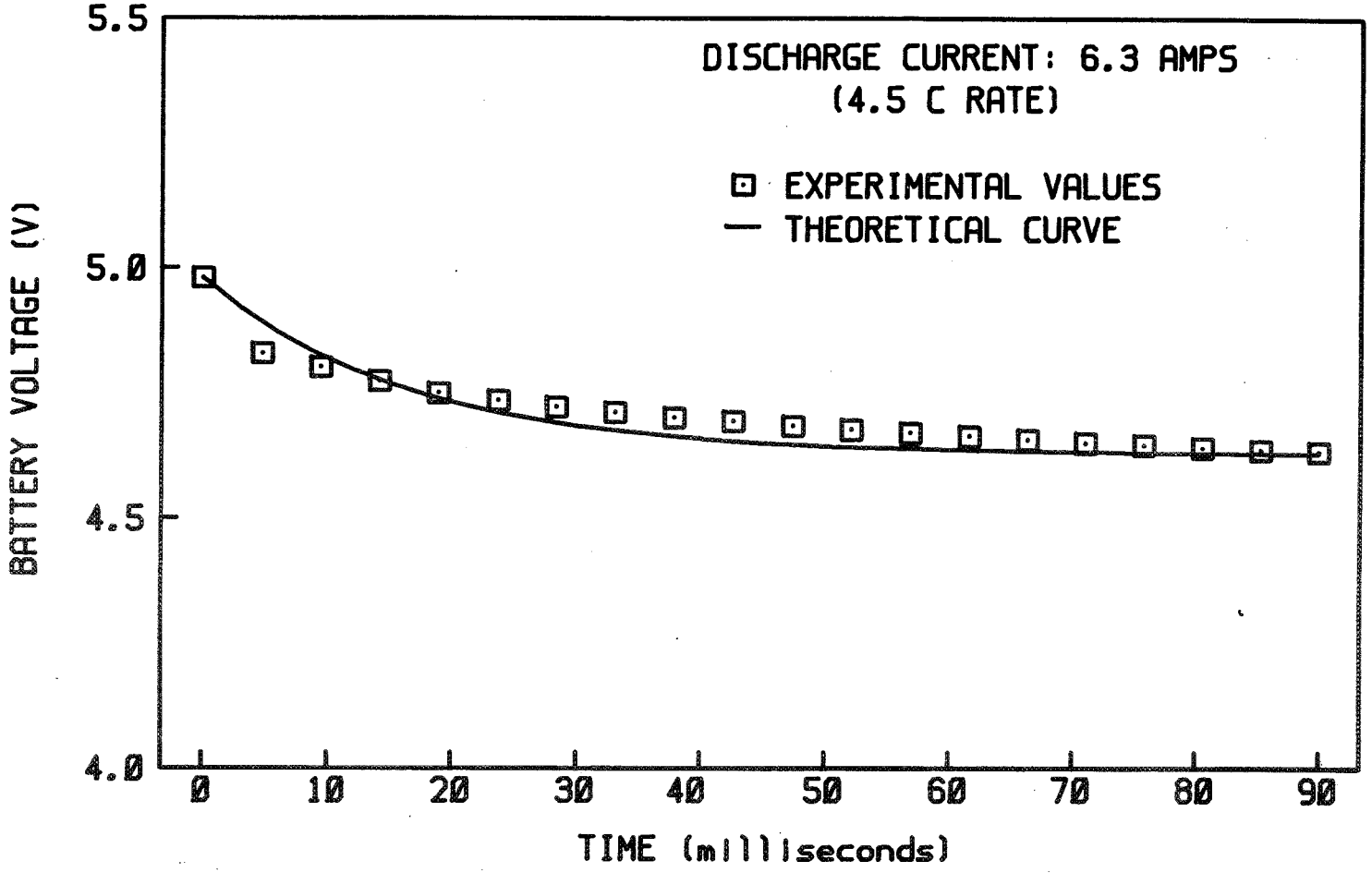

Figure 21. Battery 4 Discharge Voltage

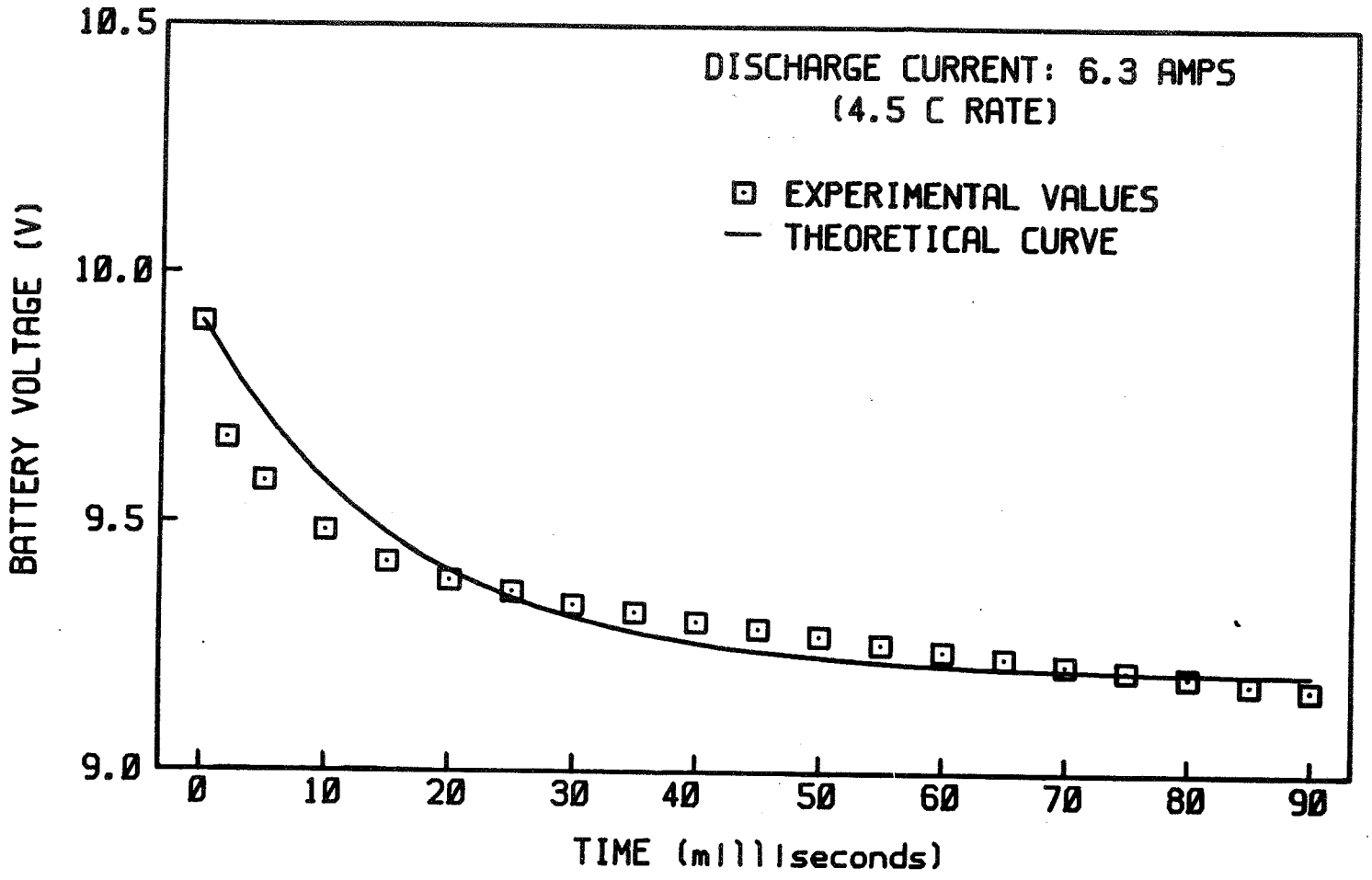

Figure 22. Battery 3 + 4 Discharge Voltage

SESSION IV

NICKEL-CADMIUM TESTING AND FLIGHT EXPERIENCE

Chairman: M. Milden
Aerospace Corporation

NICKEL-CADMIUM BATTERY CELL REVERSAL FROM RESISTIVE NETWORK EFFECTS

by Albert H. Zimmerman
The Aerospace Corporation
Los Angeles, California 90009

prepared for presentation at the
NASA Goddard Battery Workshop
Washington, D. C.
13-15 November 1984

NICKEL-CADMIUM BATTERY CELL REVERSAL FROM RESISTIVE NETWORK EFFECTS

Albert H. Zimmerman
The Aerospace Corporation
Los Angeles, California 90009

ABSTRACT

During the individual cell short-down procedures often used for storing or reconditioning NiCd batteries, it is possible for significant reversal of the lowest capacity cells to occur. The reversal is caused by the finite resistance of the common current-carrying leads in the resistive network typically generated during short-down. A model is developed to evaluate the extent of such reversal in any specific battery, and the model is verified using data from short-down of a 4-cell, 3.5 Ah battery. Computer simulations of short-down on a variety of battery configurations indicate the desirability of controlling capacity imbalances due to cell configuration and battery management, limiting variability in the short-down resistors, minimizing lead resistances, and optimizing lead and battery configurations.

INTRODUCTION

Nickel-cadmium (NiCd) battery cells are often stored during extended periods of inactivity in a totally discharged state, usually with a shorting connector across the terminals of each cell. Much evidence points to this being the optimum storage mode, particularly at reduced temperature. In addition, a growing body of data also indicates that periodic total discharge of individual cells in a battery is an extremely useful way of reconditioning and balancing cell performance, and thus extending the operational life of a NiCd battery. For a battery of series-connected cells, the process of total discharge must generally be done for each cell independently, so that the lower capacity cells will not be series driven into reversal by the higher capacity cells. A particularly simple way to accomplish an independent discharge for each cell is merely to place a resistor (typically 1 ohm) across each cell and allow the cell to discharge for an extended period of time. For batteries this is often done by attaching a shorting resistor assembly to voltage sensing wires at a battery connector.

Typical battery short-down procedures involving discharge of more than one cell at a time do not provide for totally independent discharge of each cell. This situation arises simply because of the finite resistance in the current-carrying wires common to adjacent cells. The short-down procedure actually creates a resistive network in which coupling between adjacent cells must always exist as long as any lead resistance is present, as indicated in Fig. 1.

Because of the coupling effects of lead resistances, there is a distinct possibility that the lower capacity cells will be driven into reversal by the higher capacity cells, even when individual resistors are connected across

each cell. The driving forces for such reversal should be generally minimized by maintaining capacity balance, minimum lead resistance, optimized cell configuration, and appropriate short-down procedures. In this report the network of Fig. 1 is analyzed as a function of cell characteristics, lead resistance, and shorting resistance. The extent of cell reversal that may realistically be expected is calculated for typical battery short-down configurations. Test data are also presented to support the model for a 4-cell NiCd battery consisting of 3.5 Ah "D" cells. Finally conclusions are provided to indicate how to minimize the possibility of cell reversal during individual cell short-down.

NETWORK ANALYSIS

For the network of Fig. 1, the cell currents I_n must be determined as a function of the cell voltages V_n, the shorting resistances S_n, and the lead resistances R_n. For each cell n, the application of Kirchhoff's laws shows that the current through the shorting resistor, I_n must equal the cell current. The voltage of each cell is equal to the sum of the voltage drops around each loop, i.e.,

$$V_n = I_n S_n + R_n(I_n - I_{n-1}) + R_{n+1}(I_n - I_{n+1}) \qquad (1)$$

which may be rearranged to

$$V_n = I_n(S_n + R_n + R_{n+1}) - I_{n+1}R_{n+1} - I_{n-1}R_n \qquad (2)$$

The relationships between voltage, current, and resistance are thus simply reduced to the equation

$$\underline{\mathbf{R}}\ \underline{\mathbf{I}} = \underline{\mathbf{V}} \qquad (3)$$

where $\underline{\mathbf{R}}$ is the n-by-n network resistance matrix with elements

$$r_{ij} = (S_i + R_i + R_{i+1})\delta_{ij} - R_j\delta_{i+1,j} - R_i\delta_{i-1,j} \qquad (4)$$

where δ_{ij} is the delta function. The diagonal term in Eq. 4 represents the discharge paths expected for ideal individual cell discharge. The off-diagonal terms represent the coupling of each cell through the network to other discharging cells. The current and voltage in Eq. (3) are both n-element column vectors with elements I_n and V_n, respectively. Equation (3) may be solved for either the cell voltages V_n if the currents I_n are known, or the currents may be determined if the voltages are known.

EXPERIMENTAL RESULTS

To evaluate how the analysis of the previous section can be applied to battery discharge, a 4-cell battery and resistance network were prepared having the values given in Table 1. The cells were 3.5 Ah NiCd "D" cells. The voltage and current of each cell was monitored as a function of time during the discharge through the resistors. The battery was typically charged for 16

h at C/10 following at least a 16-h short-down.

The first test involved charging cells 1 through 3 only, discharging these three cells for 2.5 h at 1 A, then resistively shorting down all four cells using the network defined in Table 1. The observed voltage behavior for the four cells is indicated in Fig. 2, where the points indicate the voltage calculated from Eq. (3) and the lines indicate the experimentally measured voltages. Cell 4, which is totally discharged, remains in reversal for about 2.5 h. The reversal current depends on the voltages of the other cells, but was as high as 94 ma (C/37) early in the reversal. The good agreement between the experimental data and the calculated points in Fig. 2 indicates that the network model of Fig. 1 can accurately describe the behavior of battery cells during individual cell short-down.

The second test involved connecting the shorting resistor to cell 4, 1 h before shorting down the other cells, thus creating about a 1 Ah lower capacity in cell 4. As indicated in Fig. 3, cell 4 was still driven into reversal for about 12 min with a maximum reversal rate of 92 ma. The third test was similar to the second test except that short-down was begun 1 h earlier on cell 3 rather than cell 4. The results are indicated in Fig. 4. The reversal rate was 172 mA at its maximum, about twice that of the previous test, presumably because during most of the reversal period the cells on each side of cell 3 had high voltages. In the third test the cell was in reversal for 32 min. These results suggest that during short-down the end cells in a series string have a much more benign environment with regard to reversal.

BATTERY SHORT-DOWN SIMULATIONS

The short-down of a battery containing n cells was simulated by a computer model. The inputs to this model consisted of shorting resistances, lead resistances, the capacity of each cell, and a current-voltage relationship as a function of residual capacity discharged from the depleted cell.

The current-voltage relationship that was used in the simulations was derived from short-down data for 3.5 Ah cells having 1 ohm short-down resistors, and is meant to provide only a representative current-voltage relationship during short-down. Each cell was assumed to have a constant voltage of 1.15 volts until its capacity was depleted, after which the voltage deceased linearly to 0.2 volts during the discharge of an additional 0.04 Ah. Thereafter each cell was assumed to have a voltage given by

$$V_n = 0.317 \times 10^{-5Q} - \Delta I(1.228\times10^{-1.226\Delta I}) \qquad (5)$$

where Q is the residual capacity discharged in Ah, and ΔI is any discharge current in excess of that anticipated from the diagonal terms in Eqs. (3) and (4). Equation (5) was obtained empirically by fitting the voltage of one cell during short-down. When the voltage is negative, a voltage limitation of $V_n = -0.06\log(I/0.00014)$ is used to give a reasonable asymptotic dependence for hydrogen evolution. While this model is only approximate, it provides a reasonable empirical representation of the short-down behavior with 1 ohm resistors, which can be used for evaluating trends in the short-down behavior.

The first computer simulation was for a 4-cell battery using the short-down parameters of Table 1, 3.5 Ah of capacity for cells 1 through 3, and 2.5 Ah for cell 4. The trends in the simulation should therefore be directly comparable to the data in Fig. 3. The results of the simulation, indicated in Fig. 5, clearly show the same features as the data in Fig. 3.

The second computer simulation was done for a 22-cell battery where 1 cell was assumed to have 1 Ah less capacity than the other 21 cells, and the position of the low-capacity cell was varied from one end to the middle of the cell string. All shorting resistors were 1 ohm and all lead resistances were 0.1 ohm. The results of this simulation, presented in Fig. 6, clearly show that the end cell should be subject to considerably less reversal than cells of equal capacity situated away from either end of the cell string.

A third simulation was done to determine the effect of varying the lead resistance on the cell reversal. An 11-cell battery was simulated, with the Ah in reversal during short-down plotted as a function of lead resistance in Fig. 7. The center cell was assigned 1 Ah less capacity than the other cells, so it is the cell being reversed in Fig. 7. All short-down resistances were 1.0 ohm. From the results in Fig. 7, approximately 0.025 ohm of lead resistance are required before reversal occurs under these conditions of simulation. The amount of reversal increases in a nearly linear fashion as the lead resistance is increased relative to the shorting resistance.

It is expected that the amount of cell reversal should increase as capacity imbalance increases. In Fig. 8 a fourth simulation is presented in which the capacity imbalance is varied and both the capacity and the time in reversal are plotted. This simulation is for an 11-cell battery whose center cell is low in capacity; shorting resistors are 1.0 ohm, and lead resistances are 0.1 ohm. Both capacity and time spent in reversal increase with increasing capacity imbalance. However, if the imbalance is near 2 Ah or higher, the low cell will stay in reversal long after the other cells are depleted, since it has been taken down far enough in capacity that even the low residual voltages present for the other cells can hold the low cell in reversal. The data in Fig. 8 clearly indicate the need to avoid conditions that can lead to large imbalances in capacity.

Capacity imbalances between the cells of a battery are generally controlled to less than 5% of the total capacity by cell matching procedures. However, extended periods of open-circuit stand, cycling, or other environmental considerations may temporarily create greater imbalances. If a normal distribution of cell capacities is assumed for an 11-cell battery, and these cells are arranged in order of increasing capacity in the battery, it was not possible to reverse any of the cells in a computer simulation where the total spread of capacities was allowed to go up to 1 Ah. This is because adjacent cells are never very different from each other in capacity. Adjacent cells would probably have to differ by 0,3 Ah or more to get reversal in this configuration. On the other hand, if the cell arrangement is changed so that high-capacity and low-capacity cells alternate without any change in the overall cell capacity distribution, extensive reversal becomes possible. This is simulated in Fig. 9, where the extent of reversal is plotted as a function of the Ah spread in an 11-cell battery, assuming a normal distribution of capacities. The cells alternate in capacity so that cells 2, 4, and 6 are the three lowest capacity cells. The results in Fig. 9 indicate that when capacity imbalances are possible, it is very likely that several cells can be driven

into reversal simultaneously.

A final situation that can lead to significant imbalance in cell capacities in a battery is the effect of unmatched short-down resistors being used to take a battery down from a high state of charge. This effect causes some cells to discharge faster than others, so that large imbalances in capacity can exist when the first cell reaches depletion, even if all the cells were closely matched at the start of discharge. The effect is simulated in Fig. 10, where both the extent of reversal and the effective cell imbalance are plotted as functions of short-down resistor imbalance. The simulation started with a fully charged 3.5 Ah battery containing 11 cells, of which the center cell has an imbalanced short-down resistor. The initial capacity spread between high and low cell was 0.3 Ah and followed a normal distribution. The cells were arranged in an alternating high-low capacity arrangement. Fig. 10 indicates that a 15 to 20% imbalance in short down resistors can add 0.7 Ah to the imbalance between cells and can cause extensive reversal. The situation of imbalance due to variations in short-down resistors can be easily managed by either using matched resistors, or by discharging battery capacity as a series cell string until the lowest cell is depleted before the short-down resistors are connected.

CONCLUSIONS

The results presented here indicate that significant reversal of the lowest capacity cells can result from individual cell short-down of a NiCd battery. A model has been presented that provides a straightforward way to evaluate the risk of cell reversal for a particular battery or a particular short-down procedure. The consequences of cell reversal are likely to be (1) some hydrogen evolution, although not enough to overpressurize the cell; and (2) significant Cd reduction at the Ni electrode, possibly leading to Cd dendrite short-circuits. Such short-circuits, if formed, will be oxidized during recharge and are not expected to have any lasting impact on performance.

This report suggests a number of points that are important in minimizing the possibility of cell reversal, as follows:

1. Minimize capacity imbalances that may arise from uncontrolled battery handling or storage. This is particularly important during integration and test procedures.

2. Do not discharge battery capacity from a high state of charge by using individual cell short down. Discharge the battery as a series string of cells until the lowest capacity cell is depleted, then apply short-down resistors to individual cells.

3. Use 1%-tolerance resistors for short-down.

4. Minimize lead resistance relative to the resistance of the short-down resistors. Lead resistance includes that of leads internal to the battery assembly, plus that of any cable used to connect the battery to a breakout box where the short-down resistors are attached. The ultimate solution to minimize lead resistance is to attach the short-down resistors at the cell terminals, or to attach separate leads at

each cell terminal.

5. The arrangement of cells within a battery is critical. The optimum arrangement for minimizing the possibility of cell reversal is to order the series string of cells in terms of capacity, from high at one end to low at the other end. This procedure makes it difficult to reverse any cell in the string during short-down as long as the spread in cell capacities does not increase significantly beyond the initial spread typically allowed in NiCd batteries.

6. The end cells in the series-connected string are always less subject to reverse discharge during individual cell short down than the other cells in the battery.

Table 1. EXPERIMENTAL BATTERY NETWORK PARAMETERS FOR 4 CELLS CONNECTED IN SERIES (3.5 A h)

Lead Resistance, Ω	Shorting Resistance, Ω
R_1 = 0.0721	S_1 = 1.045
R_2 = 0.0786	S_2 = 0.940
R_3 = 0.0878	S_3 = 0.991
R_4 = 0.0942	S_4 = 0.974
R_5 = 0.0879	

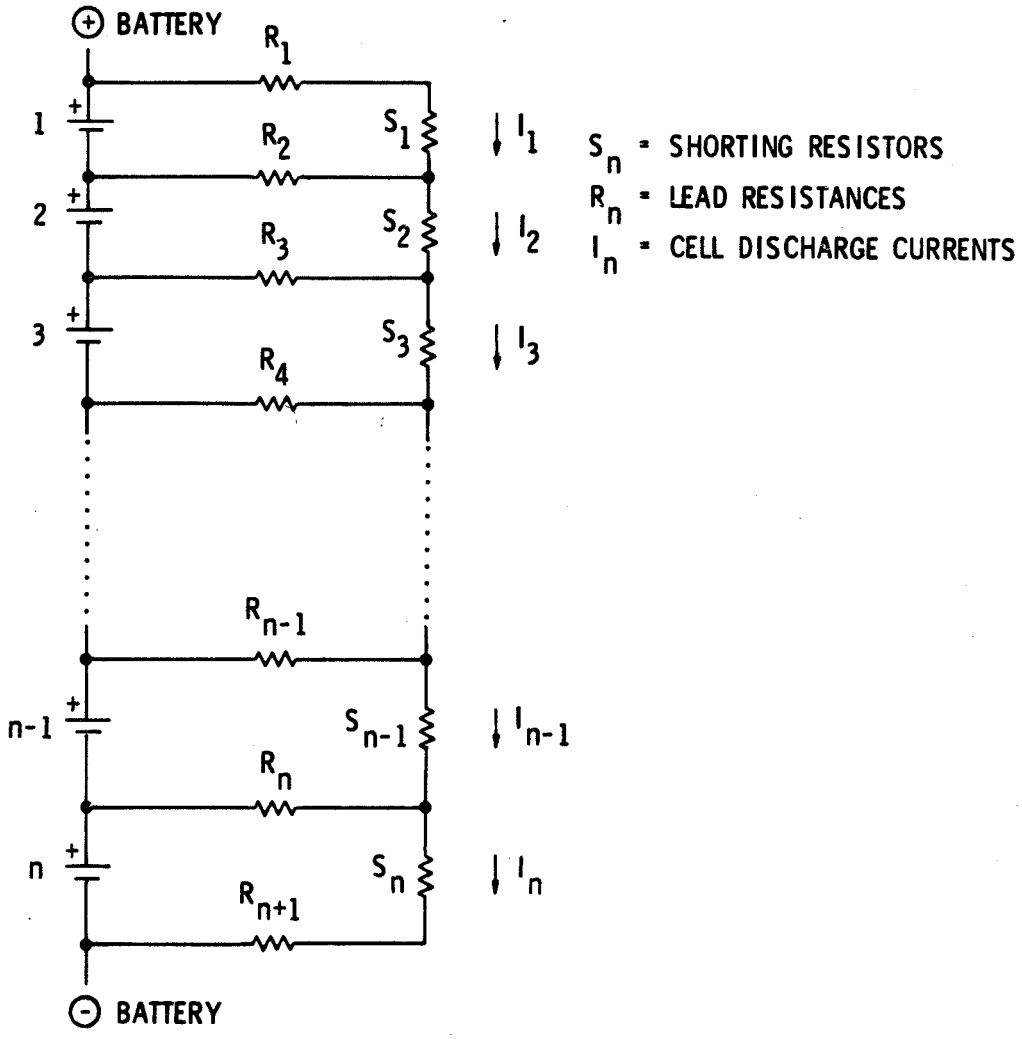

Figure 1. Resistive Network Created during Individual Cell Short-down of an N-Cell Battery

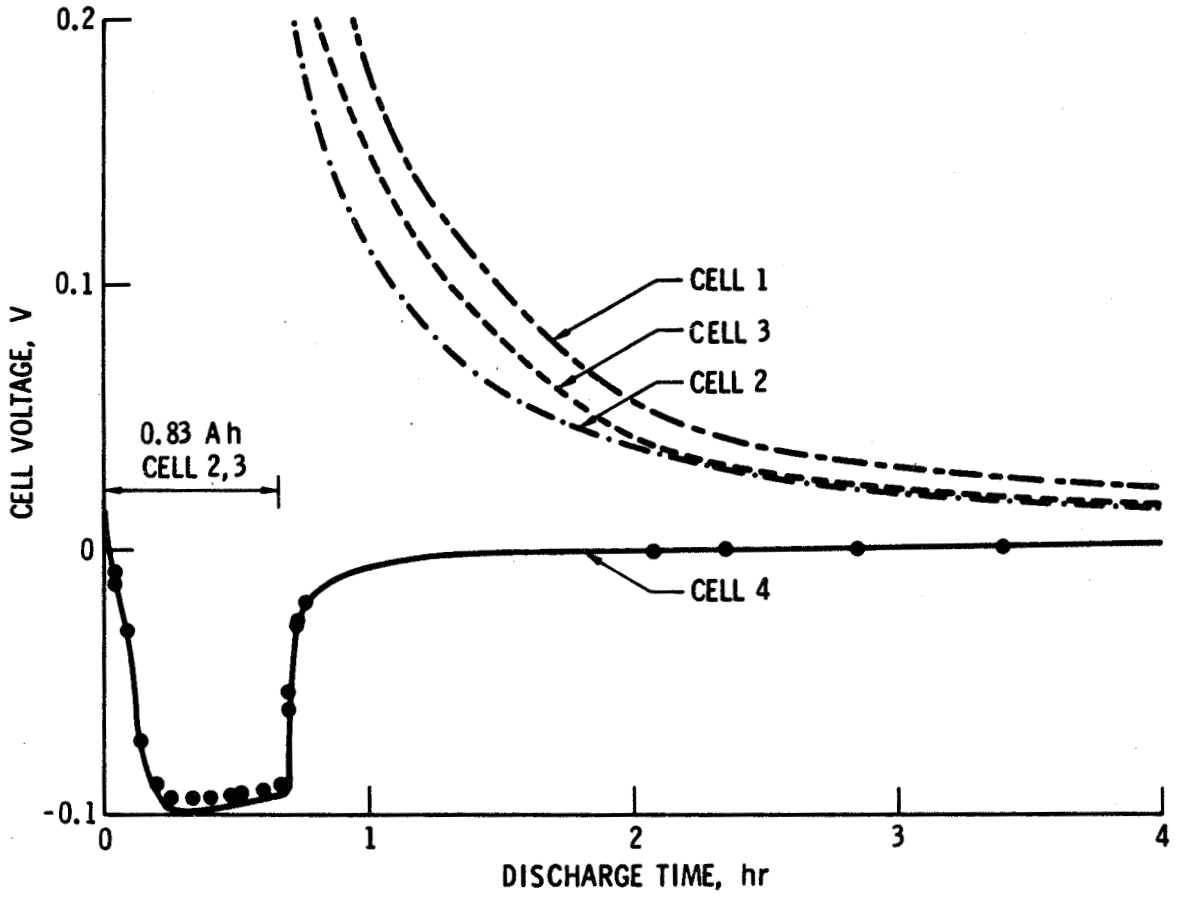

Figure 2. Short-down of a 4-Cell Battery; Cell 4 is Totally Discharged and Cells 1 Through 3 Have ∿1—A h Capacity

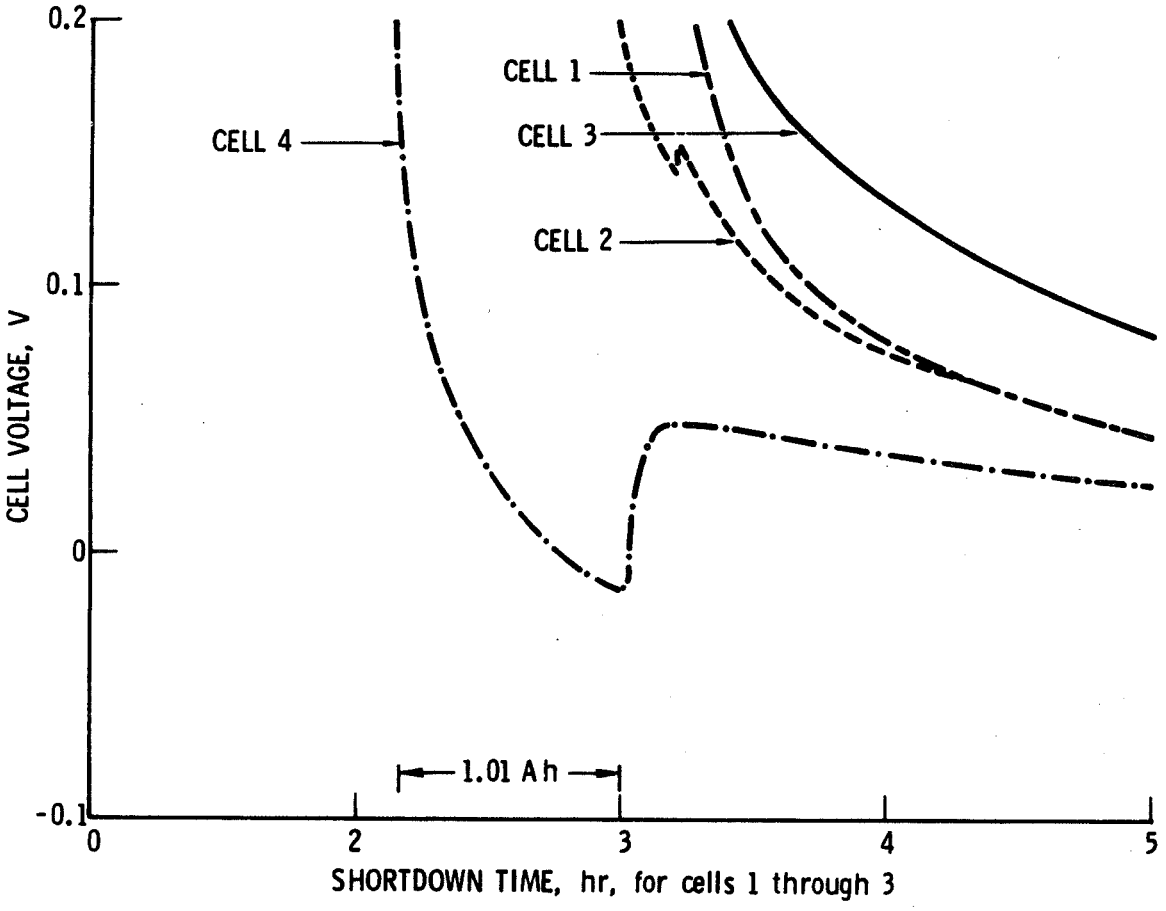

Figure 3. Short-down of a 4-Cell Battery; Cell 4 Discharge Started 1 hr Earlier Than Did That of the Other Cells

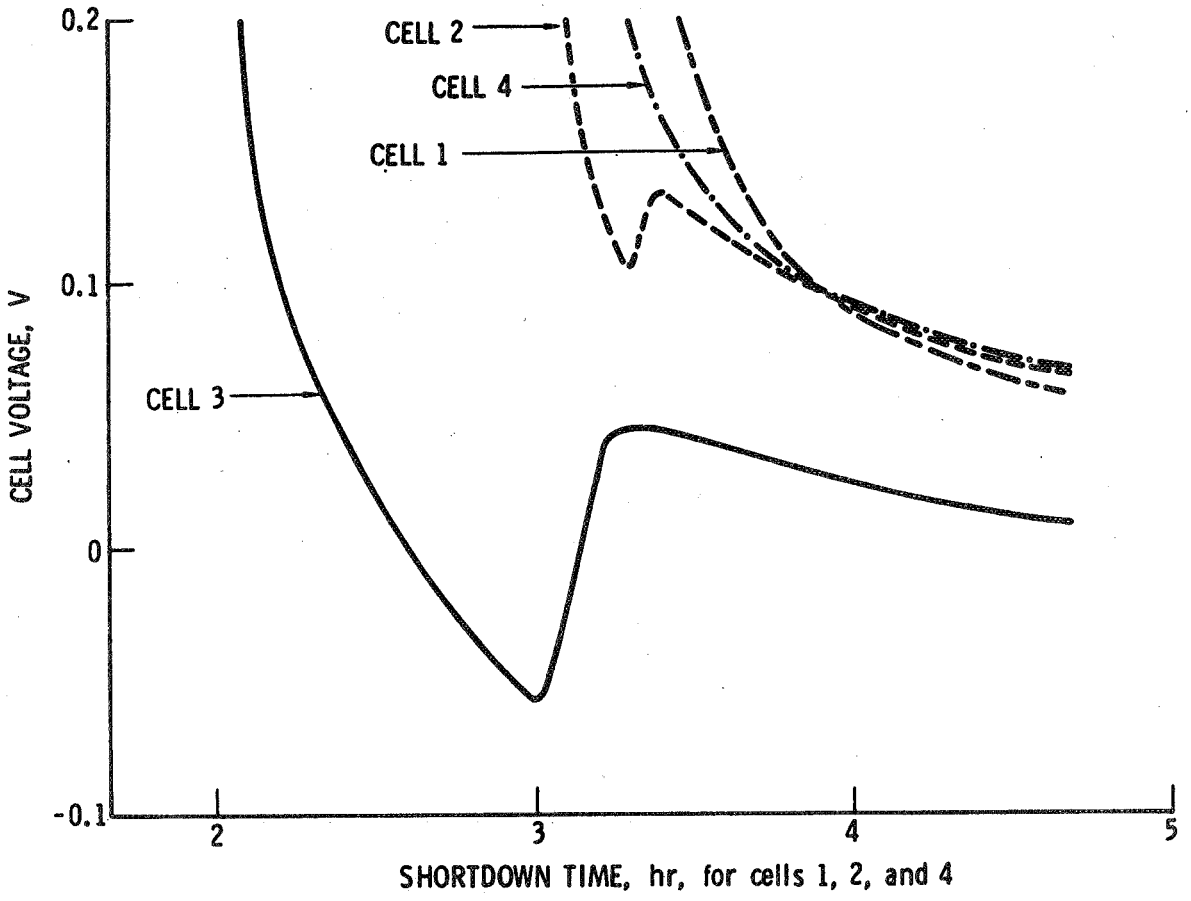

Figure 4. Short-down of a 4-Cell Battery; Cell 3 Discharge Started 1 hr Earlier Than Did That of the Other Cells

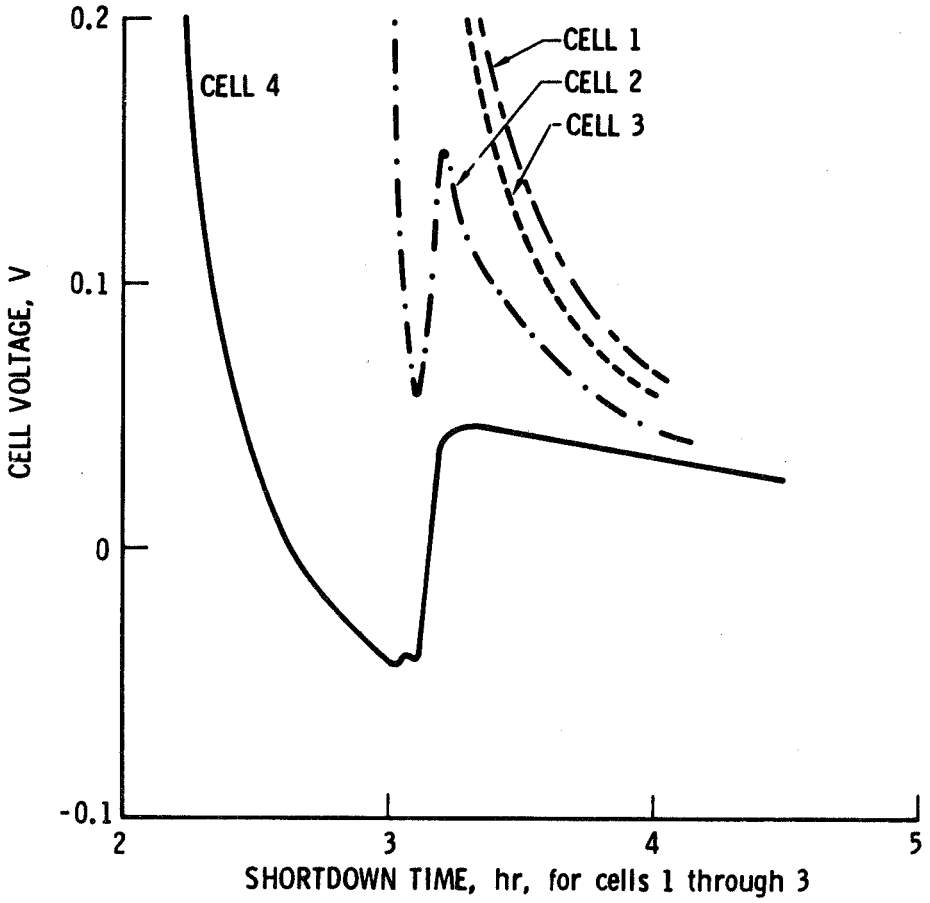

Figure 5. Short-down Simulation for a 4-Cell Battery, with 3.5 A h in Cells 1 Through 3, and 2.5 A h in Cell 4

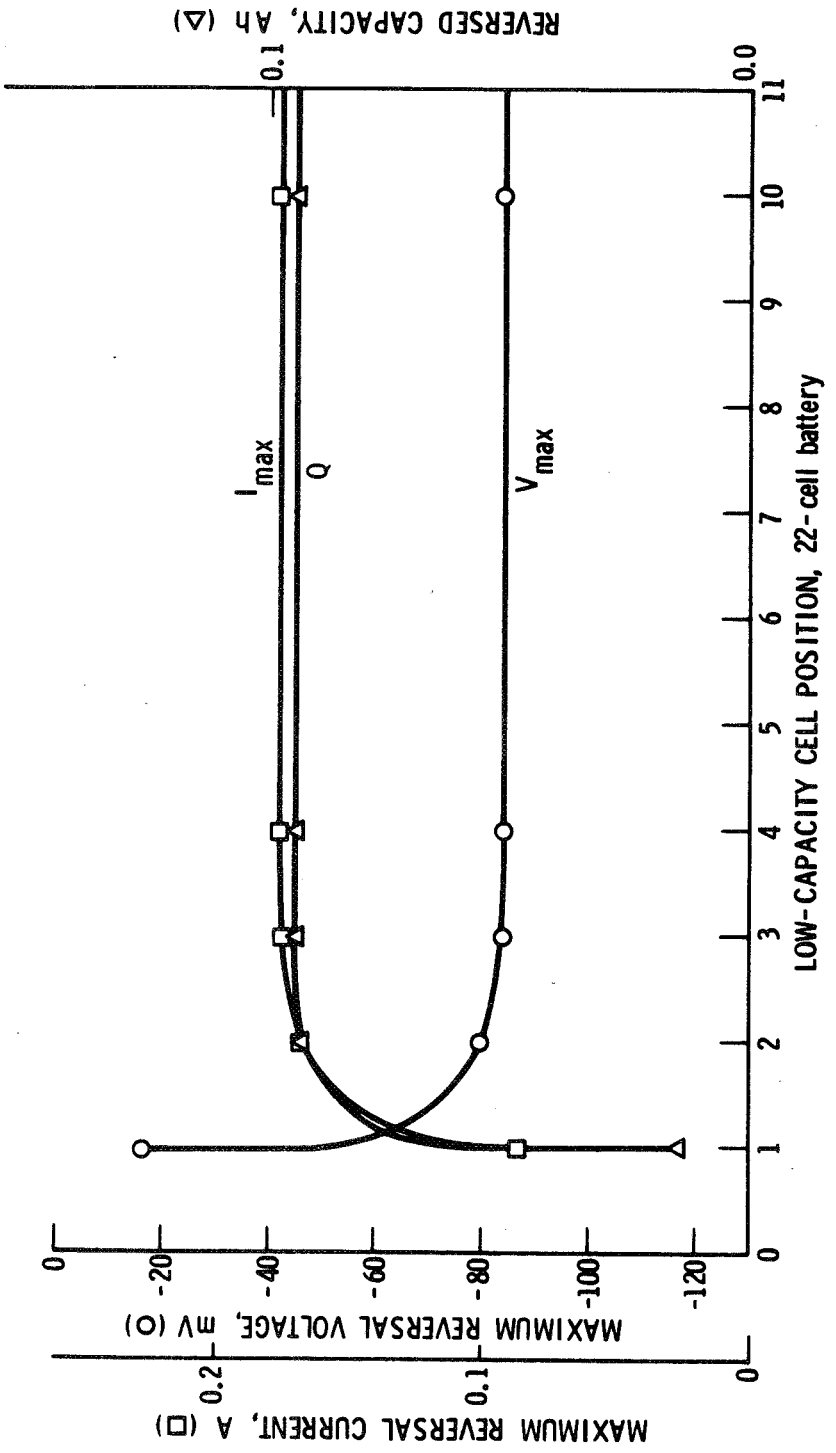

Figure 6. Dependence of the Extent of Reversal on Cell Position, for Capacity Imbalance = 1 A h, R_n = 0.1 Ω, and S_n = 1.0 Ω

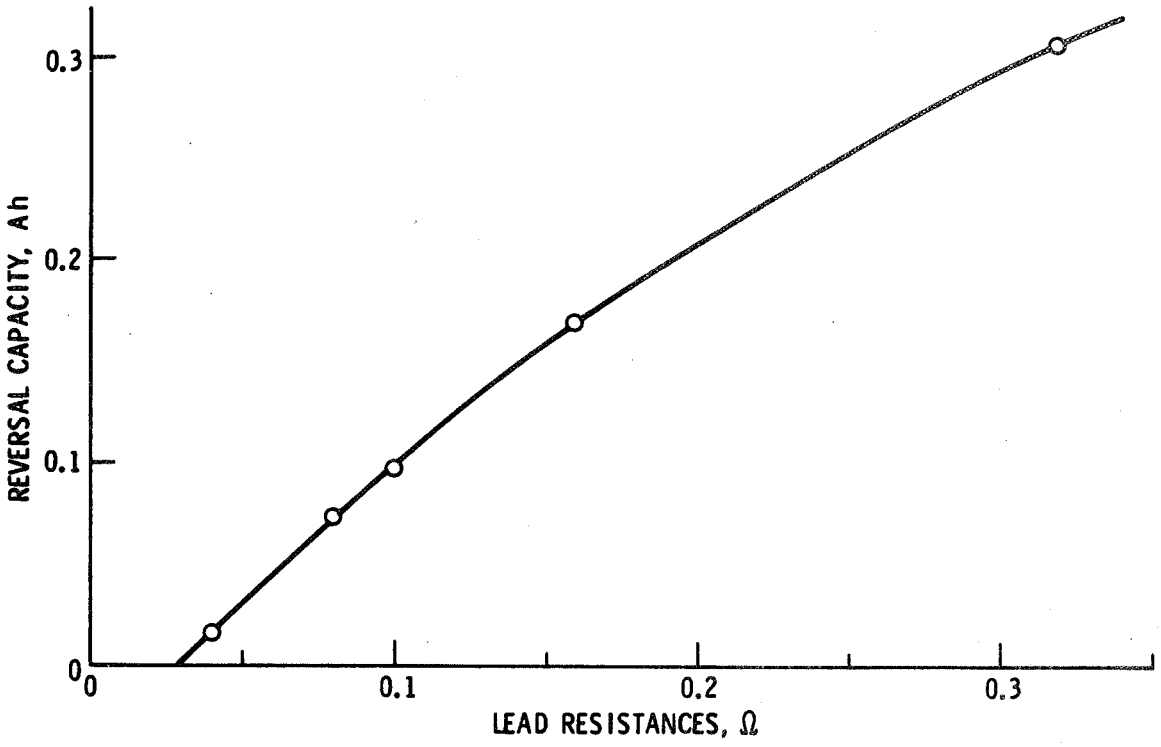

Figure 7. Extent of Reversal as a Function of Lead Resistance for the Center Cell of an 11-Cell Battery, for Capacity Imbalance = 1 A h and S_n = 1.0 Ω

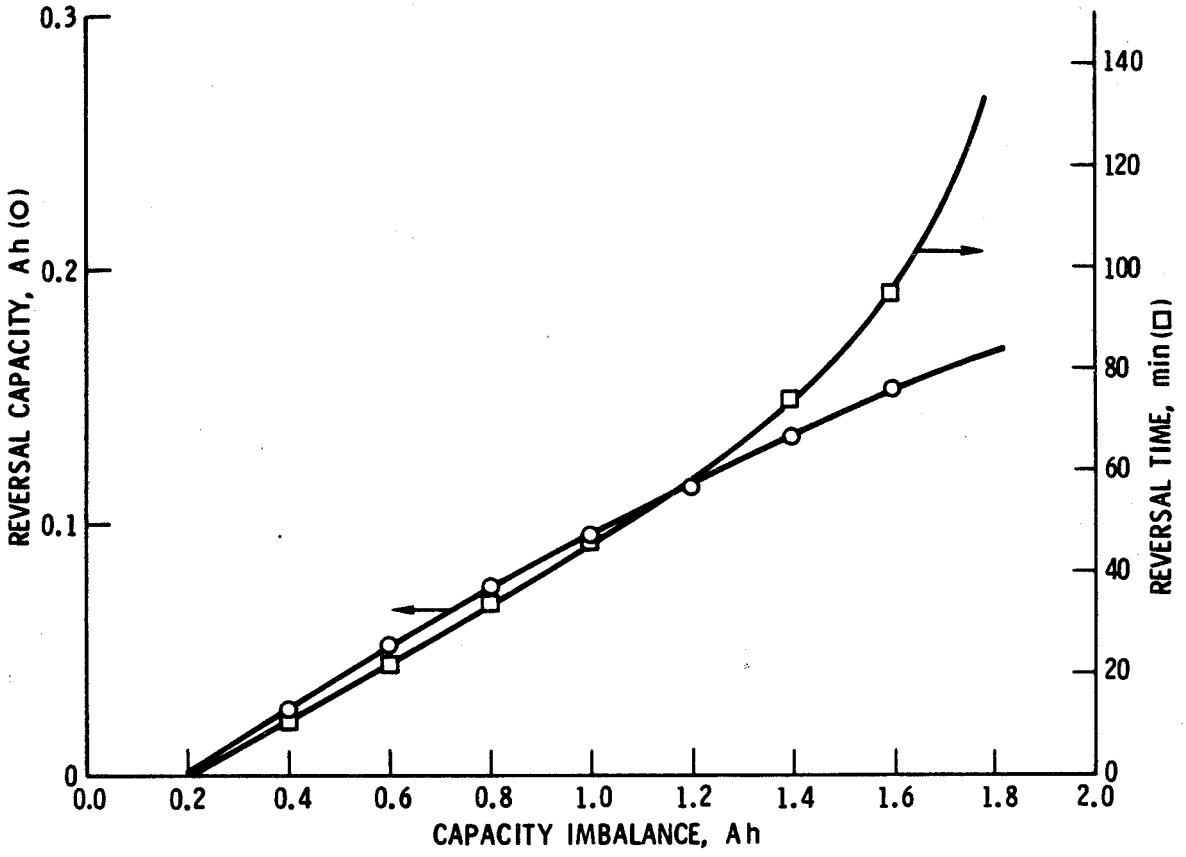

Figure 8. Extent of Reversal as a Function of Capacity Imbalance in the Center Cell of an 11-Cell Battery, for $S_n = 1.0\ \Omega$ and $R_n = 0.1\ \Omega$

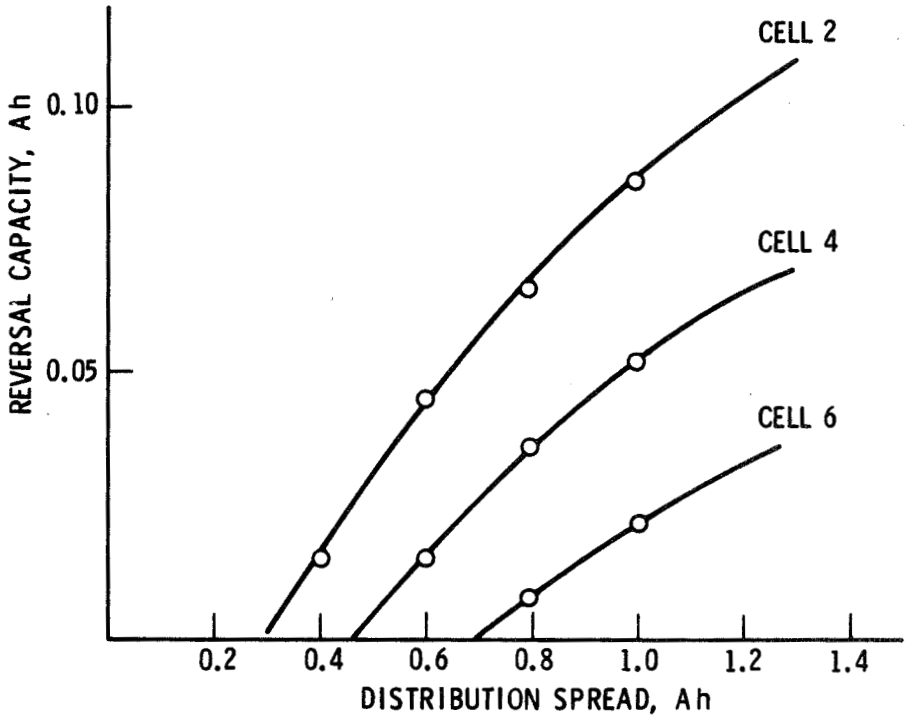

Figure 9. Extent of Reversal as a Function of Capacity Imbalance in an 11-Cell Battery Having Normal Capacity Distribution (High/Low Alternation of Cells), for $S_n = 1.0\ \Omega$ and $R_n = 0.1\ \Omega$

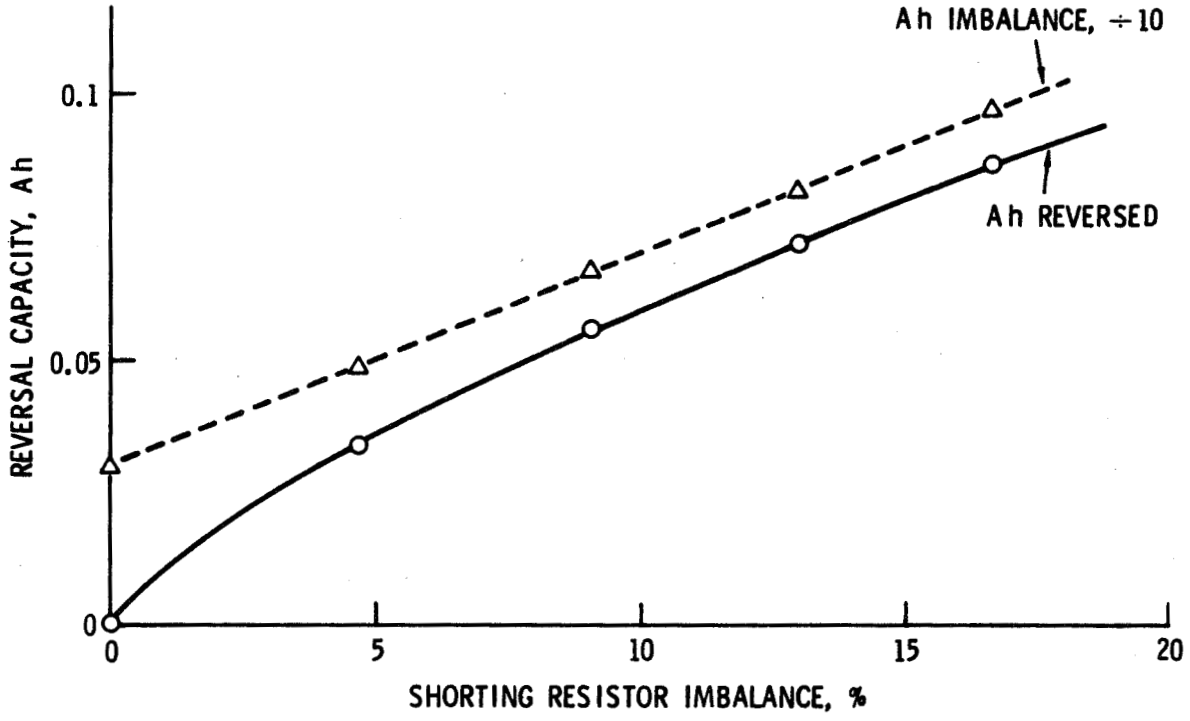

Figure 10. Short-down of Fully Charged Battery vs. Shorting-resistor Imbalance for Capacity Imbalance = 0.3 A h and $R_n = 0.1\ \Omega$

L E O LIFE TESTING WITH DIFFERENT CHARGE CONTROL

F. Baron
Energy Storage Section
European Space Research and Technology Center
European Space Agency

ABSTRACT

The effect of charge control on the performance of Nickel-Cadmium batteries is very important. The purpose of this paper is to describe the results of three tests performed in the Battery Test Centre of ESTEC. Two techniques were employed: the tapering method well known for space applications, and the temperature derivative technique (TDT) developped by ESTEC.

In addition, a comparative study has been made between the behaviour of a group of 3 batteries charged and discharged in parallel compared to an identical group discharged in parallel, but charged individually.

An approach of evolution laws for the main electrical characteristics of cells is presented, then some ageing equations will be introduced. These tests were supported by the European Space Agency project ERS-1 and analyzed by the University Paul Sabatier of Toulouse (Pr. Comtat) under ESTEC Contract (1).

INTRODUCTION

In ESA GEO Spacecraft, it has become usual to charge the Nickel-Cadmium batteries until a certain temperature-dependent battery voltage has been reached. Following this the battery voltage is held at this value and the current allowed to fall, or "taper". Since the sunlight periods are long compared to the eclipses there is no shortage of time to recharge the batteries. In Low-Earth-Orbit (LEO) the situation is very different, since the battery charging has to be completed within a period of some 65 minutes. With the larger European craft such as SPOT, ERS-1 and EURECA, requiring several kilowatts of eclipse power, it is necessary to minimise the size of the solar array so as to reduce the array and propellant load. In order to use the array power most efficiently it is therefore desirable to reduce to a minimum period of taper charge in which array power is wasted.

Indeed, the tapering method consists in a charge at constant current rate (in general C/2 or C/3) up to an applied battery voltage limit, after which remaining time of charge is performed at constant voltage, the current tapering. For the taper charge control method, eight cell voltage limits spaced 20 mv apart were defined according to the following equation (fig. 3)

$$V_{limit} = 1.372 + (n \times 0.020) - 0.0023\ T$$

Where T is the cell temperature in degree Celsius
n is the level number

The VL level (n = 5) is chosen in order to maintain the battery fully charged during the life time test; the changes of temperature are automatically compensated with the taper control unit. This method was used for the SPOT tests and the Hybrid tests. At the same time possible alternative criteria indicating battery full charge was considered.

The principle to the new battery charging technique (1) is to terminate the charge at constant current when the battery temperature starts to increase following the endothermic reaction of the first period of charge. The temperature is measured at individual battery cell level at the location of the thin metal thermal conduction plates between the isolated cells. It is thus virtually independent of environmental temperature fluctuations. This technique allows one to reduce by approximately 30% the power compared with the "tapering technique". The logic circuit (figures 4 and 5) detects end of charge during the sunlight phase of an orbit when the battery temperature starts to increase for a temperature derivative level (dT/dt) calculated from the set of thermistors which are connected to the positive input of an operational amplifier set up with a gain of about 2700. The temperature derivative level for end of charge is equal to:

$$dT/dt = dV\ \text{thermistor}/dt \times dT/dVth = 0.2\ ^{\circ}C/\text{hour}$$

The remaining part of the sunlight period is spent in open circuit mode. The figures n° 4 and 9 give an example of the relationship between battery voltage, current and cell temperature in a low earth orbit profile.

TEST PROGRAMME

Three tests were conducted as follows, each using the same discharge and available charge time.

1. ('SPOT test') 3 identical batteries charged and discharged in parallel with taper charge control.

2. ('Hybrid test') 3 identical batteries discharged in parallel but charged independently each with taper charge control

3. ('Reference test') A single battery with temperature derivative charge control.

The current passing through each battery of a group was separately measured.

The batteries consist of 14 Ni-Cd cells (SAFT type V035M) connected in series. The nominal capacity is 35 Ah.

Figure 1 shows the method of battery packaging, thermal dissipation being obtained by monitoring the batteries on the ground with an air-cooled baseplate. One cycle consisted of a charge and three steps of discharge chosen to simulate the power profile of the satellite payload (fig. 2).

SYMBOLS AND STUDIED PARAMETERS

A,B,C,D,E,F,G	key points
$\overline{Q_D}$	discharged capacity (average in Ah)
$\overline{Q_C}$	charged capacity (average in Ah)
$\overline{K}$	recharge factor = $\frac{\overline{Q_c}}{\overline{Q_d}}$
DOD	depth of discharge (percentage of nominal capacity)
I_C, I_D	charge and discharge current (A)
$\overline{U}$eoc	end of charge battery voltage (average over cycling period)
Veoc	end of charge cell voltage (Volt)
$\overline{U}$eod	end of discharge battery voltage (average over cycling period)

W	energie (KJ)
η	energie efficiency (percentage) = $\frac{W_d}{W_c}$ x 100
σ	standard variation
corr. c	correlation-coefficient

RESULTS ANALYSIS FOR THE SPOT-TESTS (9000 cycles)

A typical record of the battery parameters during one cycle is given with fig. 6. Points of interest are marked by letters.

The parameters of each battery were recorded separately in order to evaluate the parallel charge/discharge effect upon the batteries electrical behaviour.

The level n° 5 was applied with for consequence a recharge factor near to 1.05. The table 1 groups together the main results about the applied test conditions. These values are valid up to cycle 8000. After this, the depth of discharge was reduced from 27% to 23%.

The first results show that the values are reproducable from one battery to an other; secondly, the battery voltages at all the key points during a cycle stayed stable apart from the end of the second discharge stage battery voltage (point E') for the peak power simulation (SPOT load profile) where we can apply an evolution law as follows:

$$U = Uo + mN$$

with N = cycle number

Uo and m were determined by a regression method (see table 2). The end of discharge voltage (point F') varied strongly and periodically without the possibility to develop an equation expressing the trend of U_{eod} with cycle number. The energy efficiency was greater than 80% which was one of the requirements for this type of LEO missions (fig. 7).

The cell temperatures appeared nearly the same for the three batteries, but nevertheless with a great dispersion which did not allow to provide an evolution law.

RESULT ANALYSIS FOR THE HYBRID TESTS

The test conditions are summarised in the table 3. The test has performed 7000 cycles without interruption. An interesting parameter is the battery voltage dispersion and the charge time at constant current (table 4). From the test results we can determine three evolution laws giving the time in function of the cycle number. Apparently most of the key points indicated no change during the 7000 cycles, only the point F' (end of discharge battery voltage) showed a linear decrease during the cycling (fig. 8 and table 5).

The battery temperatures showed a significant variation between the three batteries, at all stages during a cycle (table 6).

RESULTS ANALYSIS FOR THE REFERENCE TEST

As mentioned below, this test used the temperature derivative technique. Two series of cycles have been achieved:

- First, two thousand cycles were performed with a very simple profile consisting of a charge at constant current until TDT detection followed by an open circuit for the end of charge period. Discharge was also at constant current (fig. 9). During this test phase, the K recharge factor has been constant and equal to 1.09. The DOD was around 26.2% and the energy efficiency fluctuated between 89 and 82%.

- A second series of cycling was later carried out with the same profile as defined for the SPOT and Hybrid tests. The DOD was of 25.8% with a recharge factor of 1.11.

During the first six hundred cycles, the battery degraded linearly until a steady state was reached. Indeed, the end of discharge voltage decreased gradually from 1.30 volt to 1.15 volt; and then remained steady. The average end of discharge battery voltage was of 16.2 V with σ equal to 0.4 volt. Furthermore, we didn't see notable evolution of the charge time at constant current for the 5000 cycles (fig. 10). The average amplitude of temperature per cycle for the Reference test was lower than for the SPOT and Hybrid tests (table 7).

Although the energy efficiency remained almost constant during the cycling, a slight decrease in both the charge and discharge energies appeared after cycle 3800.

EVOLUTION LAWS

Equations which describe the variations of voltage and temperature with the cycling time are shown below. From the first series of results of the reference test we have tried a similar approach to that used to describe chronopotentiometry. Two cases have been studied.

- "Fast" systems where the interfacial concentrations are in a balance stage, we introduce the term "T_i" transition time where the concentrations C (0, T_i) = 0;

  therefore;

$$E = E^\circ + \frac{RT}{nF} \ln \frac{D_r^{\frac{1}{2}}}{D_o^{\frac{1}{2}}} \ln \frac{RT}{nF} + \frac{T_i^{\frac{1}{2}} - t^{\frac{1}{2}}}{t^{\frac{1}{2}}}$$

Where D_o and D_r are the diffusion coefficients of oxidising and reducing species respectively and t is the redox reaction time.

- With the second case, "slow" systems, we employ the classical cinetic law:

$$E = \frac{RT}{h\ naF} \ln \frac{T_i^{\frac{1}{2}} - t^{\frac{1}{2}}}{T_i^{\frac{1}{2}}} + \frac{RT}{h\ naF} \ln \frac{nFK^\circ Co^\circ}{i}$$

  with h = transfer coefficient
  na = electron number exchanged in the redox reaction
  k° = transfer speed

Therefore, two different laws have been tried:

1) $$U = A + K \ln \frac{T_i^{\frac{1}{2}} - t^{\frac{1}{2}}}{t^{\frac{1}{2}}} \qquad \text{(model 1)}$$

2) $$U' = A' + K' \ln \frac{T'_i{}^{\frac{1}{2}} - t^{\frac{1}{2}}}{T'_i{}^{\frac{1}{2}}} \qquad \text{(model 2)}$$

The parameters have been determined with the first series of results of the reference test for which the power profile was the simplest. It appears that the first model is better adapted for the charge mode whereas the second is better for the discharge phase. (fig.11)

During the cycling, T_i and K from equation 2 were found to decrease on discharge whereas on charge using equation 1, T_i increased whilst K decreased (fig. 13). Because of the more complicated discharged profile the models were inapplicable for the second series of the reference test as well as the SPOT and Hybrid tests. Indeed, the large random variations found in T_i and K confirm that such an approach is correct only when charge and discharge are carried out at constant current.

Concerning the curves of temperature versus time, it was found that the temperature was proportional to $1/\sqrt{t}$ for the charge period, whereas it was proportional directly to time on discharge. No variations due to ageing were discernable.

CONCLUSION

The main results are summarized in table 7. The results coming from the SPOT tests showed that most of the electrical performances of the three batteries were similar. The end of discharge battery voltage fluctuations are certainly due to a thermal unbalance of the batteries during cycling. This indicated that the main factor to be considered for a parallel charging system is the thermal environment of the batteries.

The Hybrid test presented less fluctuations in the end of discharge battery voltage from cycle to cycle than the SPOT test. Charging the three batteries separately has stabilized their appropriate recharge factor.

Indeed the Hybrid-test results showed a linear decrease of the battery voltage (Point F', fig 8) during the cycling from 17 volts to 14 volts, or less for the Battery 2 where the k recharge factor was the lowest (K = 1.04). The SPOT test results showed a general fluctuation of U_{eod} between 18 and 14 volts.(fig.14). The reason for this instability seemed due to a too low applied recharge factor.

The Reference test gave for the first time, results confirming that the Temperature Derivative Technique (TDT) seems a suitable one for charging batteries in LEO. Indeed, the main criterion for a good battery management system is to maintain the end of discharge cell voltage as high as possible and with minimum variation . this situation has been observed during the cycling where the battery voltage reached the average value at end of discharge of 16 volts (fig. 15 and table 7).

It is clear that the TDT method presents some advantages in comparison with the "standard" management because its principle is directly related to the reactions occuring in the batteries at end of charge. In another hand, the TDT stops the charging where batteries are charged and avoids any overcharge whatever the DOD profile is in operation; that is a major interest for lifetime.

We can mention that a similar test is running at the Battery Test Center at ESTEC with three batteries of 14 V035M cells each charged and discharged in parallel and managed by the Temperature Derivative Technique at 15 °C. Presently about 6000 cycles have been carried without problem. The end of charge and end of discharge cell voltage remain stable with the respective values: 1.48 volt and 1.20 volt.

It is sure that all the tests described have been carried out with "commercial cells" (with the same type of electrodes used for the space cells), but nevertheless the comparison between the different charge techniques remain valid.

If the TDT method appears very attractive, it still presents some incertainties for a space application such as:

- interferences between battery dissipation and external heat sources like solar radiation, battery heaters, ...
- its behaviour under orbital conditions requiring the battery power during a part of the sunlight period, or with variable DOD and discharge at constant power instead of constant current as used in the above mentioned tests.

The use of mathematical models in order to represent the cell evolution in cycling is limited to the simple charge and discharge profiles such as the ones for the Reference test (first series).

REFERENCES

(1) ESTEC Contract n° 4999/82 - F DD

(2) ESA Patent/1.2/MM/6838 (H.J. Spruijt)

Table 1. SPOT TESTS CONDITIONS

Spot-Tests	Battery A	Battery B	Battery C
$\overline{Q}_D$ Ah	9.66	9.54	9.23
σ	0.35	0.32	0.28
$\overline{Q}_c$ Ah	10.19	9.96	9.54
σ	0.44	0.39	0.33
$\overline{K}$	1.05	1.04	1.035
σ	0.03	0.03	0.03
DOD %	27.6	27.3	26.4
σ	1	0.9	0.8

Table 2. EVOLUTION LAWS FOR THE SECOND DISCHARGE STATE BATTERY VOLTAGE (SPOT TESTS) WITH N = CYCLE NUMBER

(Volts)	COR.C
Battery A : $U_{F'A} = 17.53 - 5.7.10^{-4}$ N	- 0.624
Battery B : $U_{F'B} = 17.47 - 4.2.10^{-4}$ N	- 0.521
Battery C : $U_{F_C} = 17.42 - 3.1.10^{-4}$ N	- 0.398

Evolution Laws for the second Discharge Stage Battery Voltage (SPOT tests)

WITH N = CYCLE NUMBER

Table 3. HYBRID TESTS CONDITIONS

Hybrid Tests	Battery 1	Battery 2	Battery 3
$\overline{Q_D}$ Ah	9.42	9.48	9.72
σ	0.15	0.2	0.2
$\overline{Q_c}$ Ah	10.08	9.87	10.52
σ	0.15	0.3	0.2
$\overline{K}$	1.07	1.04	1.08
σ	0.02	0.03	0.02
DOD %	26.9	27.1	27.7
σ	0.4	0.6	0.6

Table 4. EVOLUTION LAWS FOR THE CHARGE TIME AT CONSTANT CURRENT (HYBRID TESTS)

(hour)	COR. C
Battery 1 : $t = 0{,}543 - 16{,}2.10^{-6}$ N	-0.904
Battery 2 : $t = 0{,}573 - 40{,}2.10^{-6}$ N	-0.981
Battery 3 : $t = 0{,}580 - 8{,}8.10^{-6}$ N	-0.610

Table 5. EVOLUTION LAWS FOR THE END OF DISCHARGE BATTERY VOLTAGE (HYBRID TESTS) WITH N = CYCLE NUMBER

(volt)	COR. C
Battery 1 : $UF'_1 = 16{,}66 - 2{,}4.10^{-4}$ N	-0.658
Battery 2 : $UF'_2 = 16{,}75 - 3{,}8.10^{-4}$ N	-0.981
Battery 3 : $UF'_3 = 16{,}69 - 2{,}5.10^{-4}$ N	-0.610

Table 6. AVERAGE IN CELL TEMPERATURES FOR THE HYBRID TEST

KEY POINTS	A"	B"	C"	D"	E"
	$T(°C)_\sigma$	$T(°C)\sigma$	$T(°C)\sigma$	$T(°C)\ \sigma$	$T(°C)\ \sigma$
BAT 1	24.2 0.7	24.7 0.8	27.3 0.7	27.5 0.6	24.2 0.7
BAT 2	23.8 0.8	24.2 0.8	26.9 0.7	27.1 0.7	23.8 0.8
BAT 3	24.8 0.7	25.3 0.7	28.0 0.7	28.1 0.7	24.7 0.8

Table 7. GENERAL RESULTS FOR THE THREE TESTS

TESTS	SPOT			HYBRID			REFERENCE
DOD %	27.6	27.3	26.4	26.9	27.1	27.7	25.8
K_F	1.05	1.04	1.035	1.07	1.04	1.08	1.11
V_{eoc} (volt)	1.408			1.416	1.408	1.421	1.484
$\overline{U_{eod}}$(volts)	Fluctuations between: 18 volts and 13.9 volts			From: 17 volts to 14 volts			16 volts
W_c kJ	704	693	667	709	706	765	698
W_d kJ	602	597	588	579	577	588	563
η %	86	86	88	82	82	77	81
Δ °C	3.2			3.3			2.8
BATTERIES	A	B	C	1	2	3	1 battery

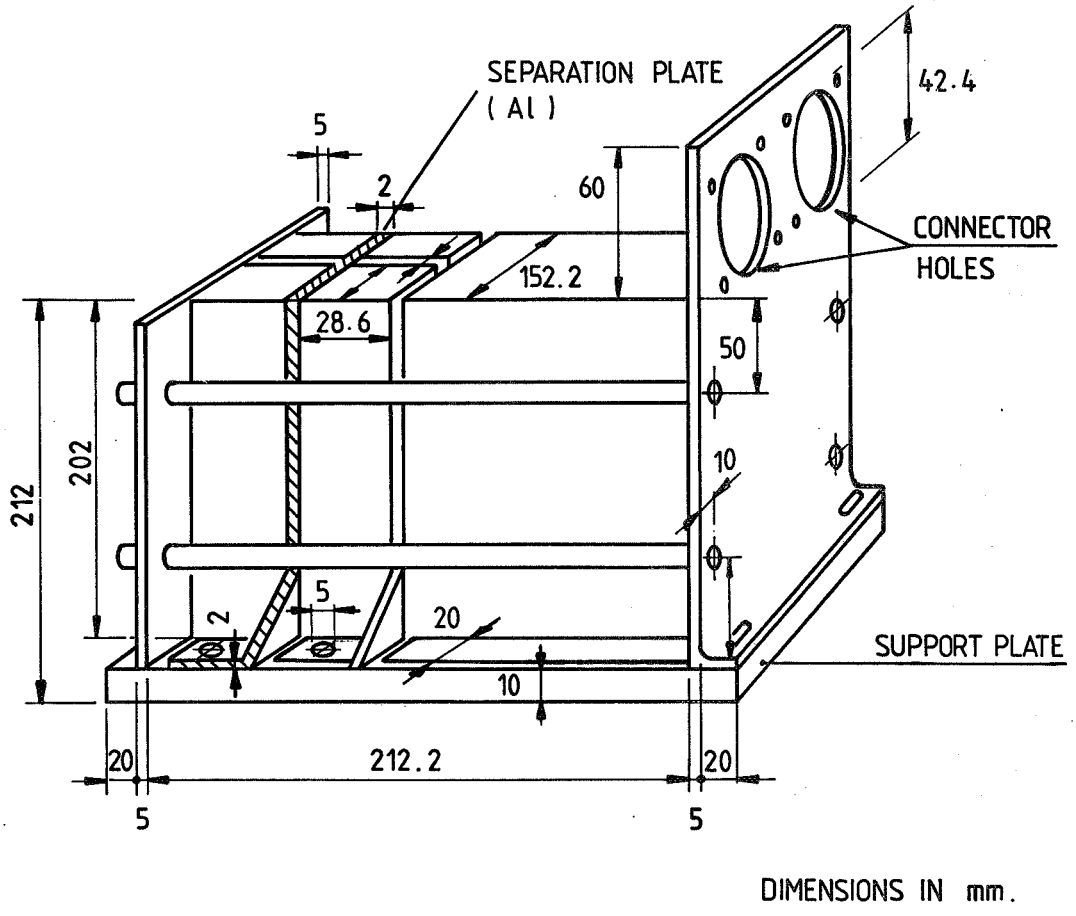

Figure 1. Diagram of the Packaging

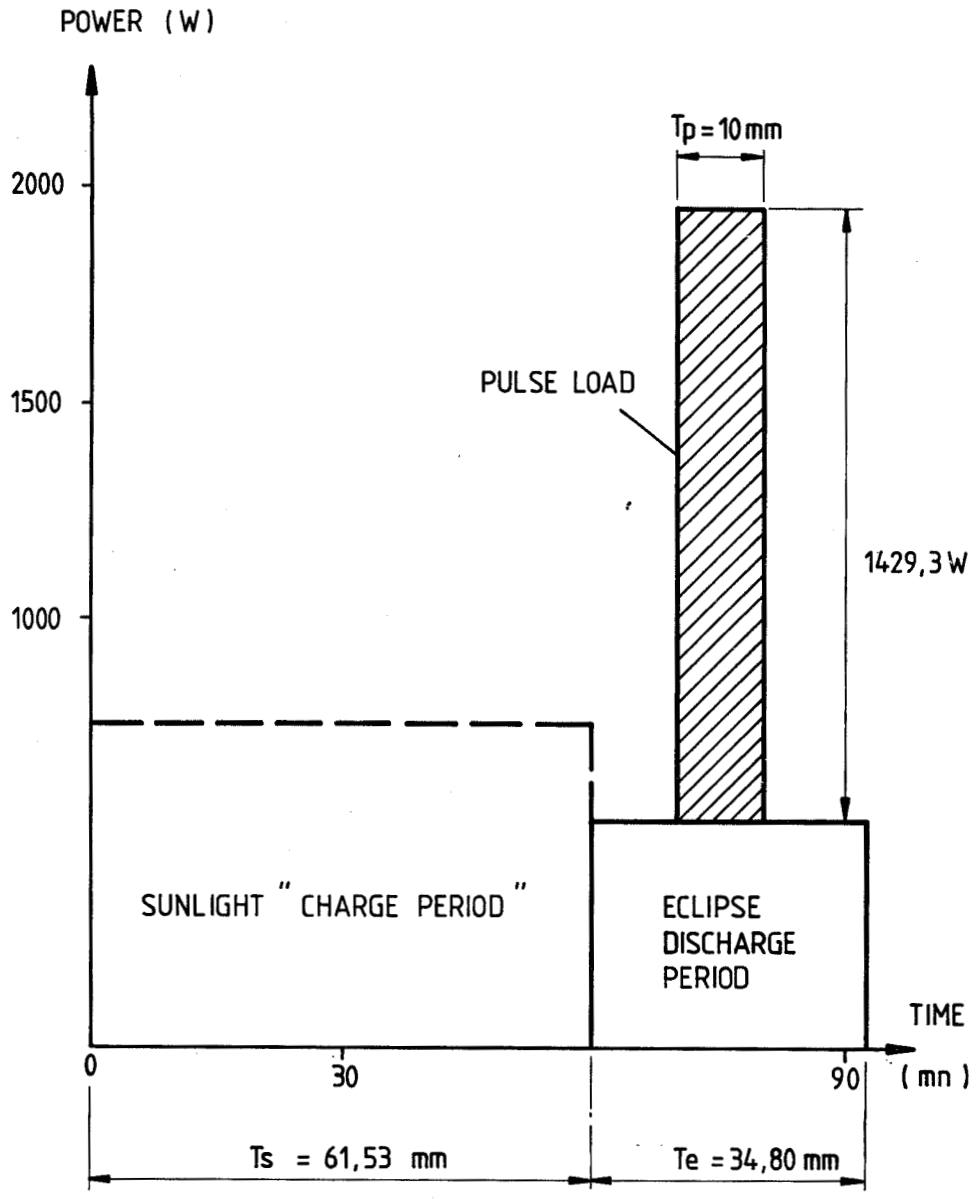

Figure 2. SPOT Power Profile

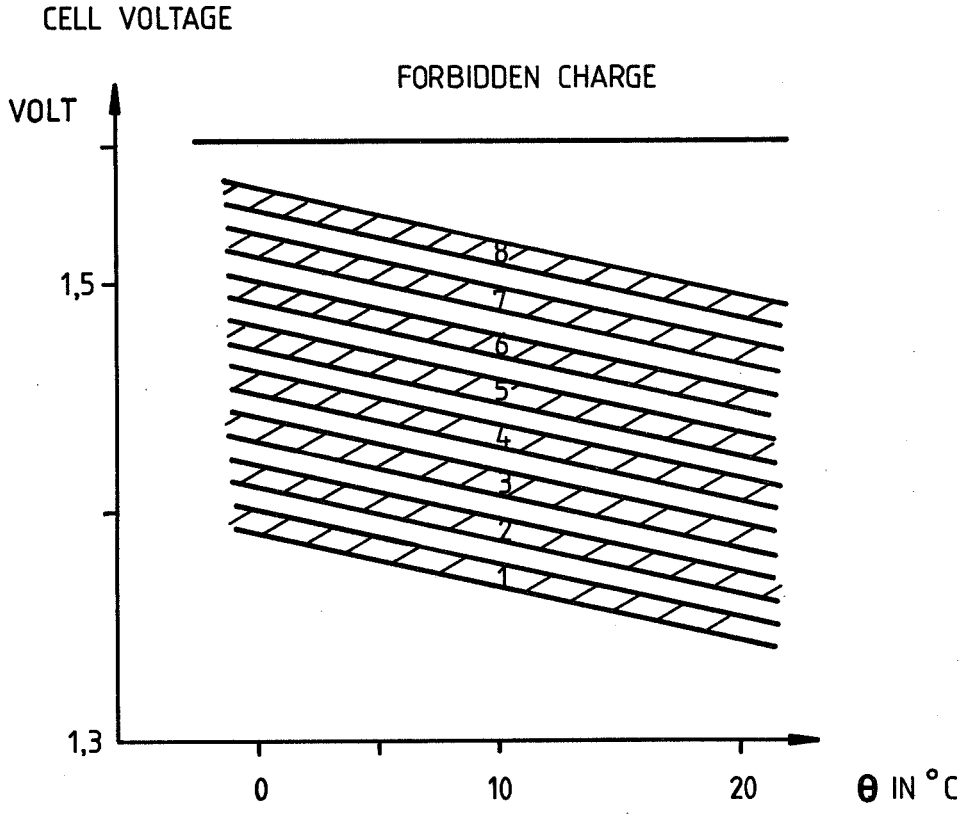

Figure 3. Voltage Limit Function of Temperature

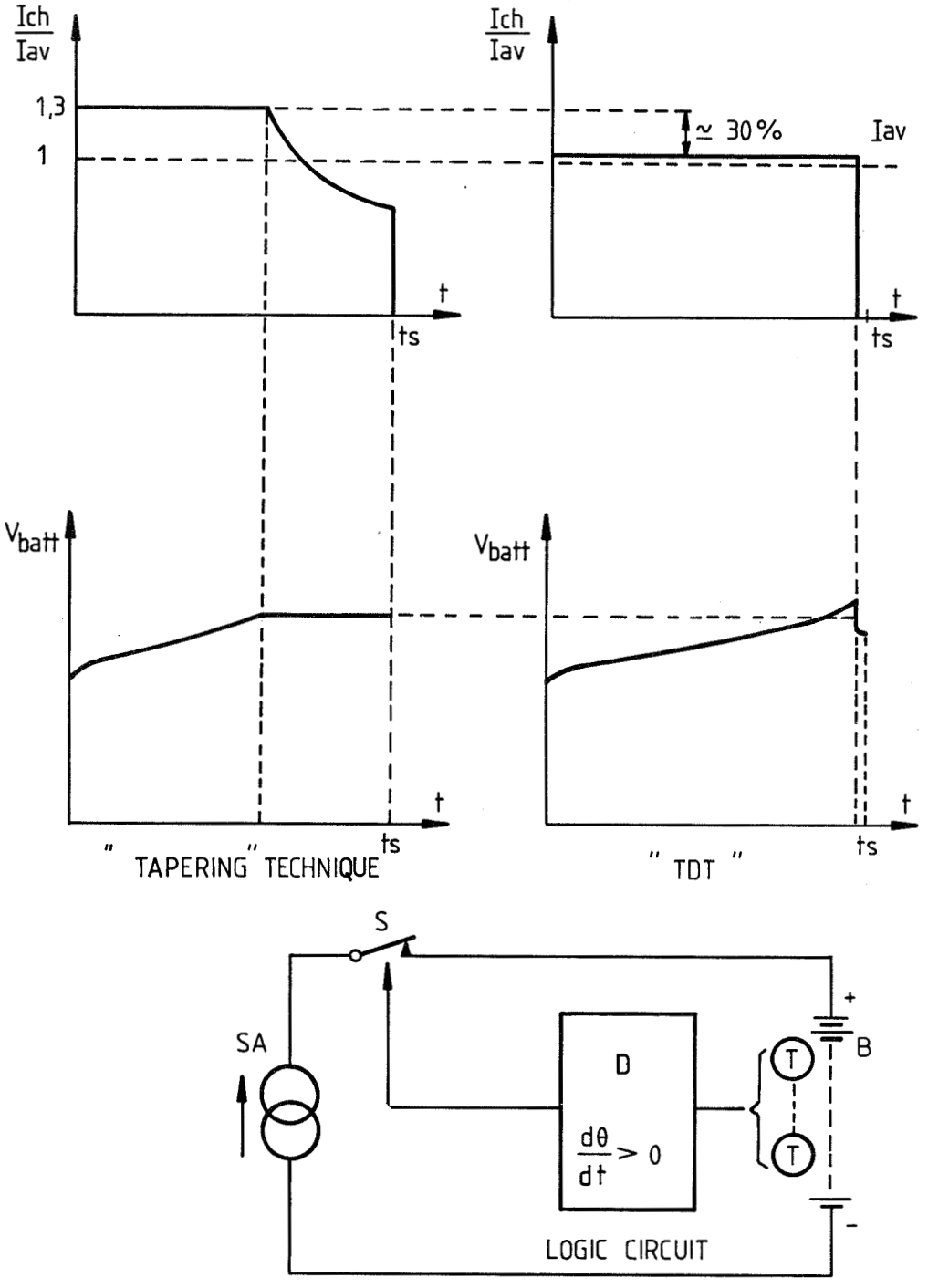
Ich
Iav
1,3
1
t
ts
Ich
Iav
≃ 30 %
Iav
t
ts
Vbatt
t
ts
" TAPERING " TECHNIQUE
Vbatt
t
ts
" TDT "
S
SA
D
dθ
dt
> 0
T
T
+
B
-
LOGIC CIRCUIT

Figure 4.

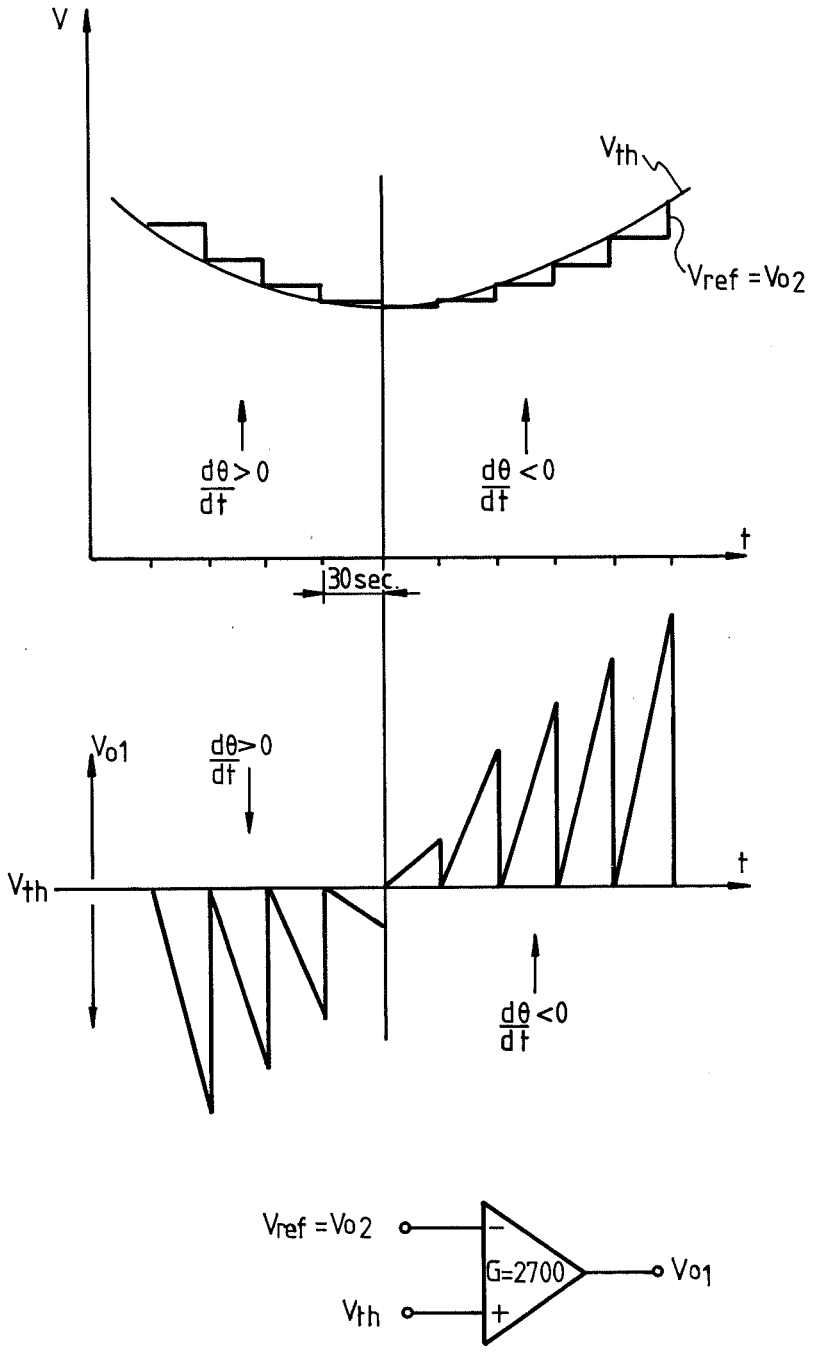

Figure 5. Temperature Derivative Technic Principle

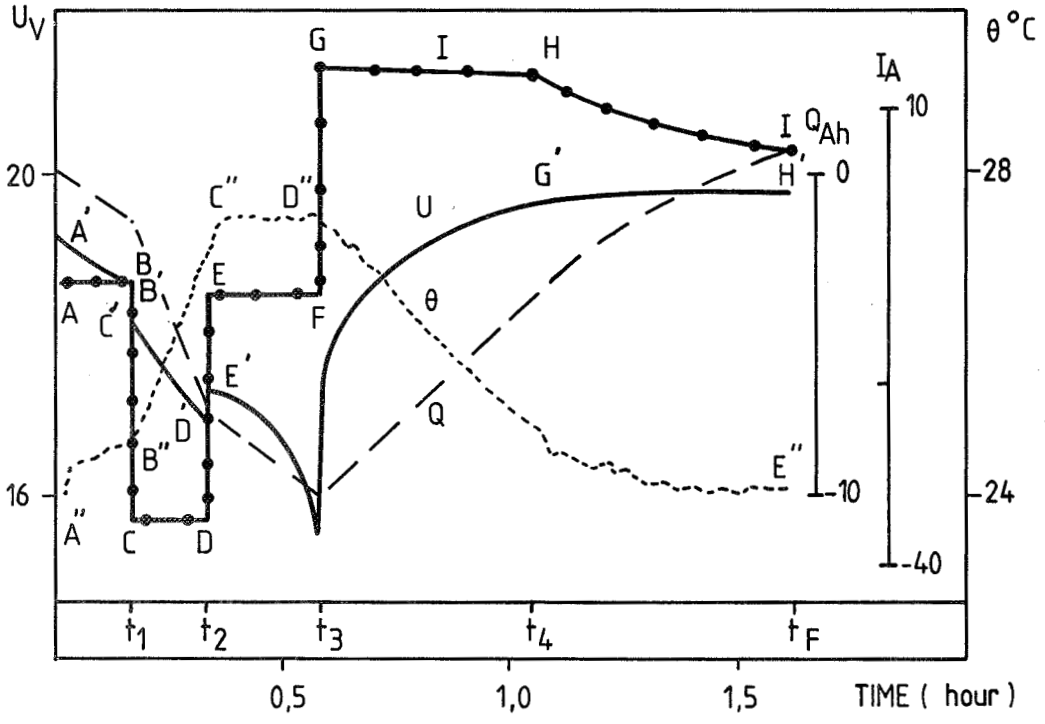

Figure 6. SPOT Tests Description

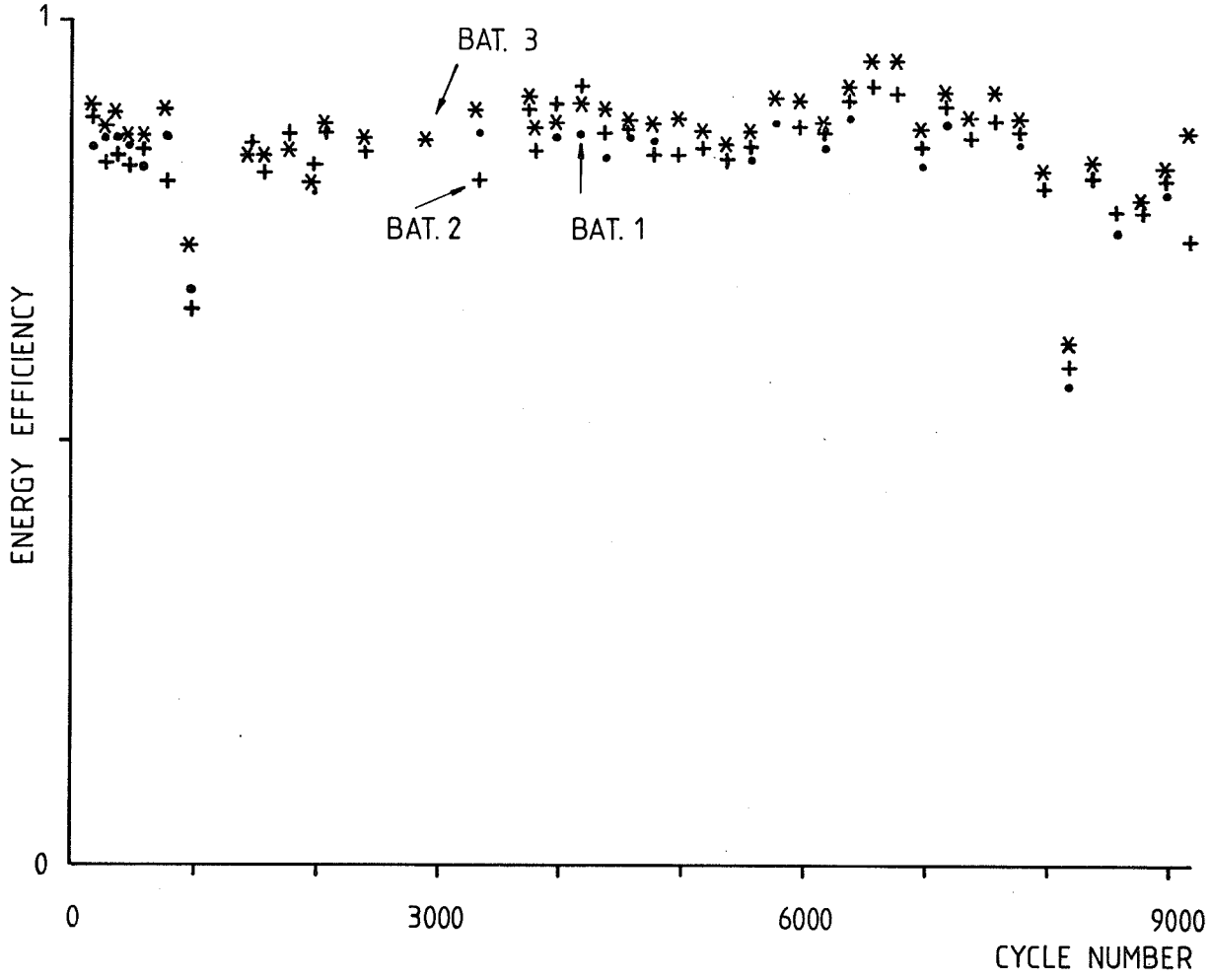

Figure 7. SPOT Tests

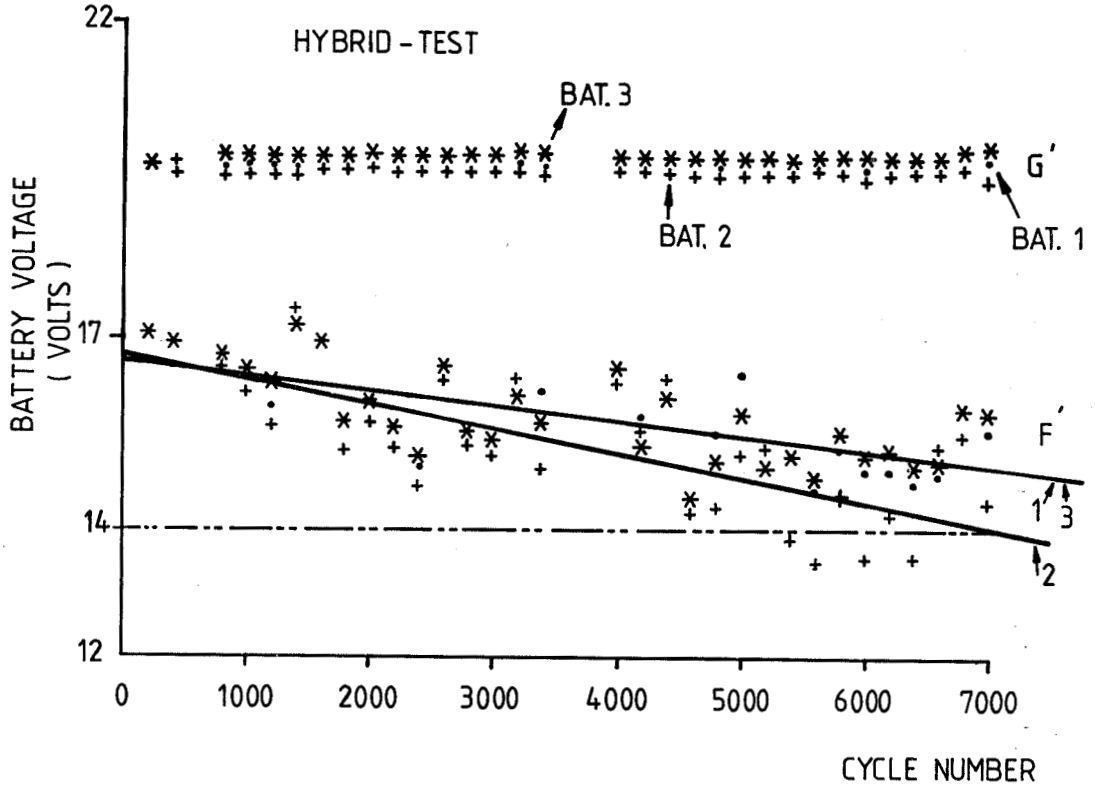

Figure 8. Battery Voltage Evolution at the End of Charge (Point G') and End of Discharge (Point F') in Function of the Cycle Number

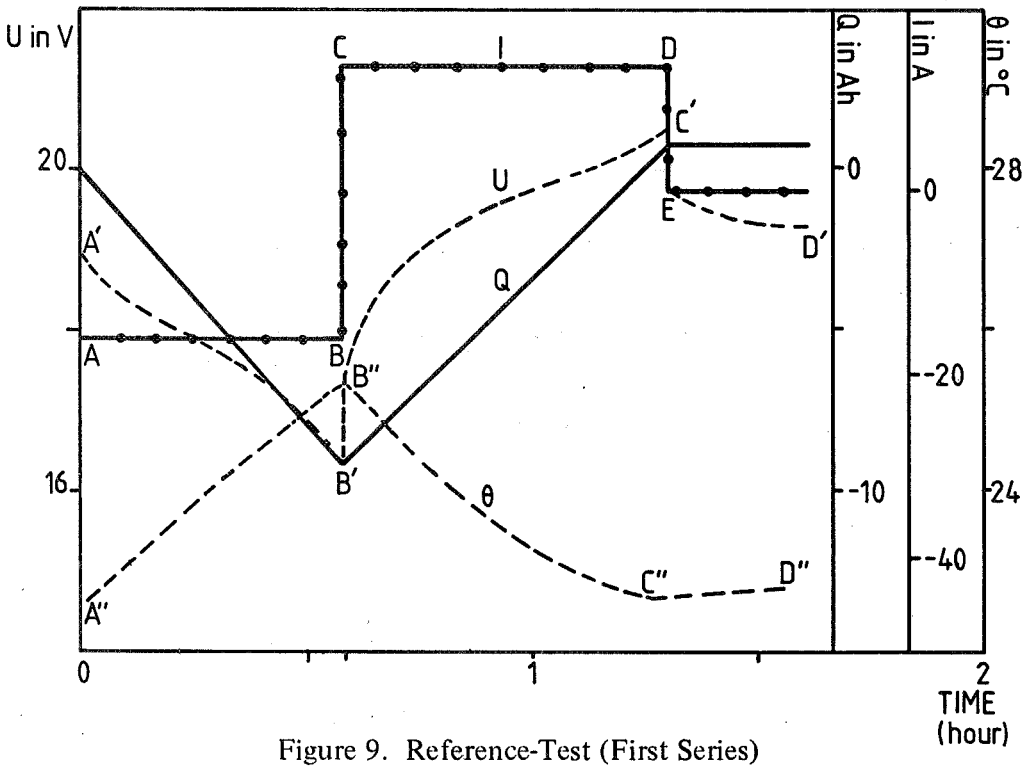

Figure 9. Reference-Test (First Series)

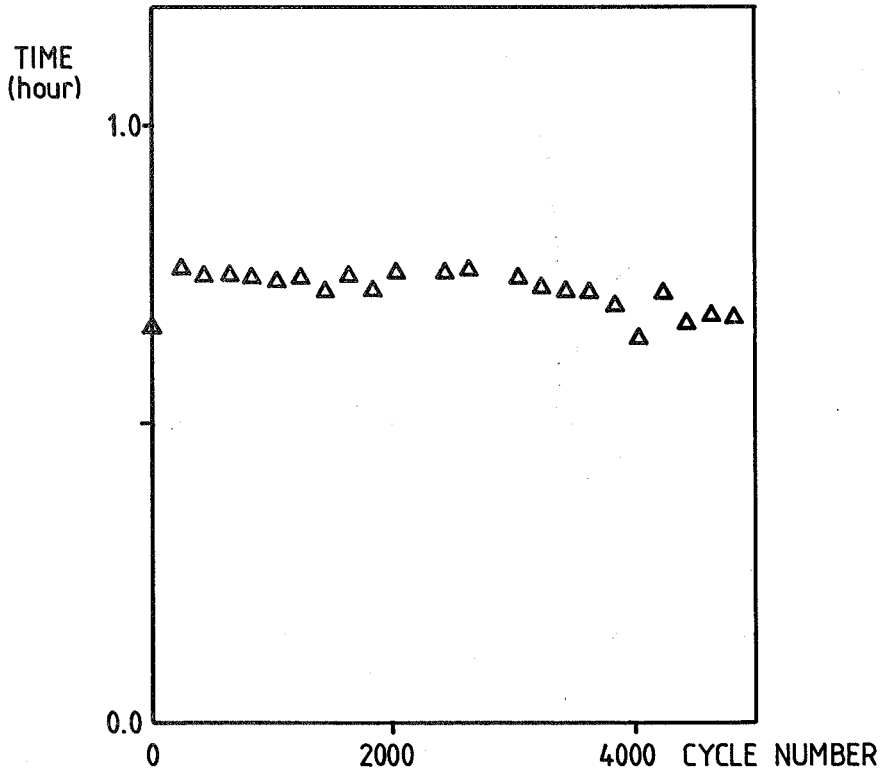

Figure 10. Reference-Test (Second Series) Charge Time at Constant Current

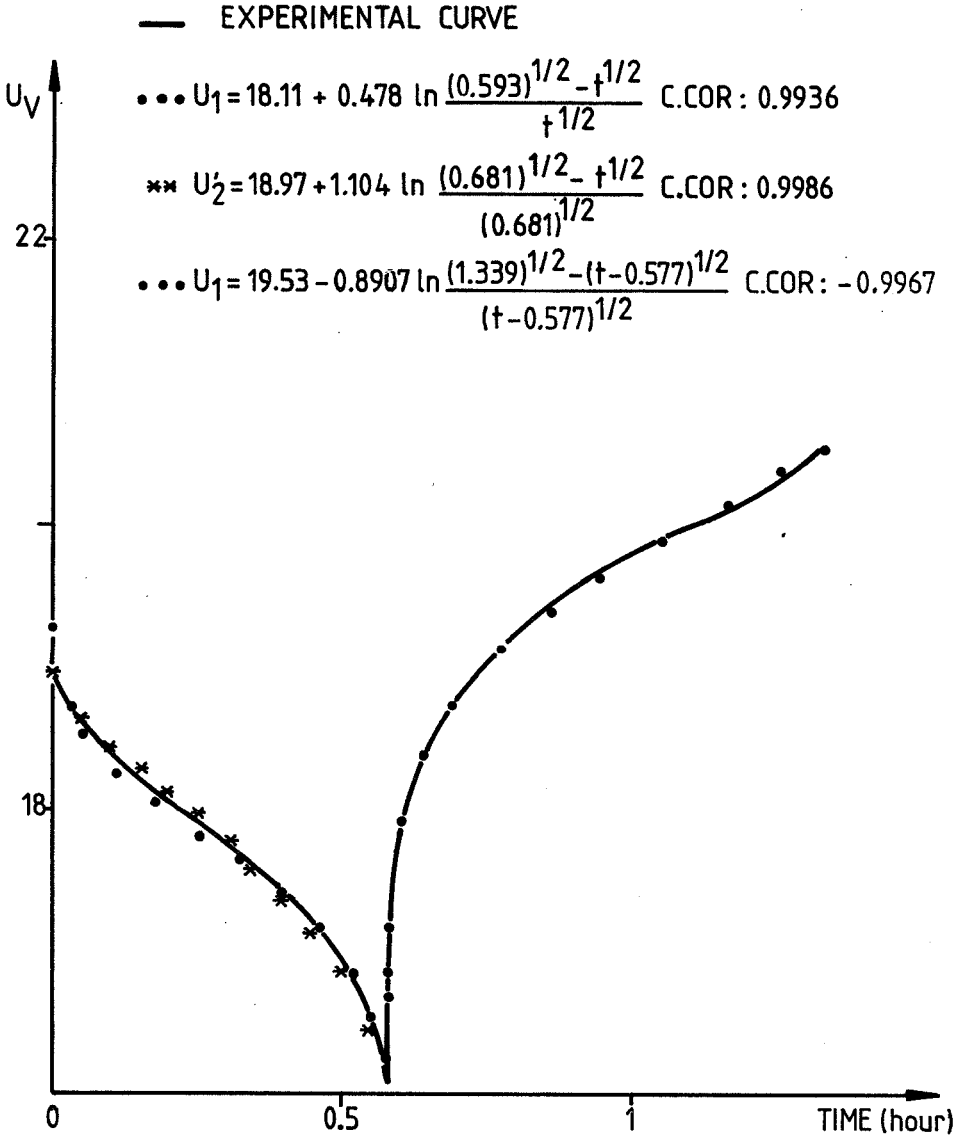

Figure 11; Reference-Test (First Series), Cycle 1000

Cronopotentiometric Models for the Battery Voltage
for Charge and Discharge Periods

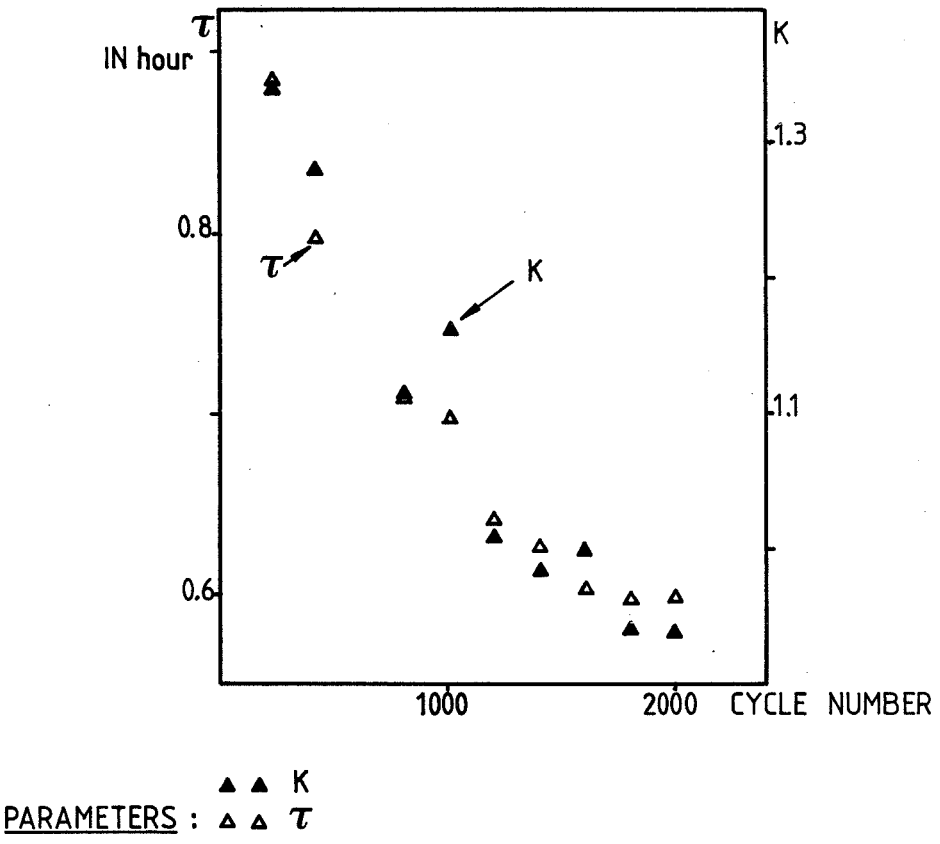

Figure 12. Reference-Test (First Series) τ and K Evolution in Function of the Cycle Number for the Discharge Period

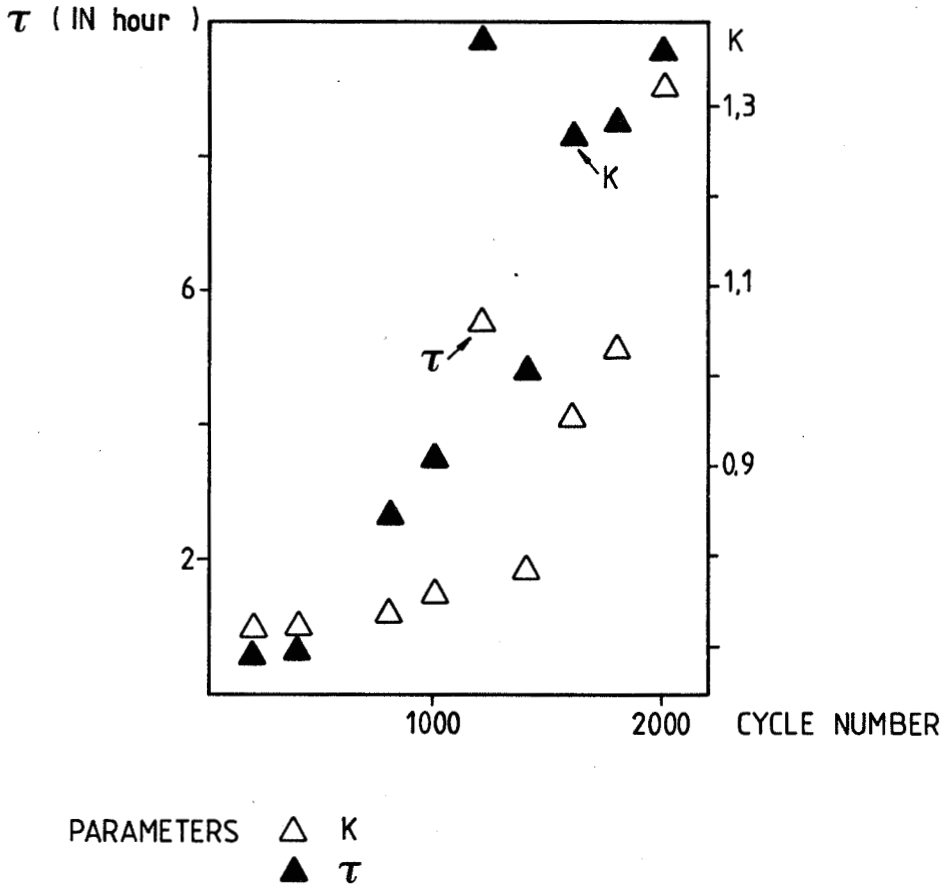

Figure 13. Reference-Test (First Series) τ and K Evolution in Function of the Cycle Number for the Charge Period

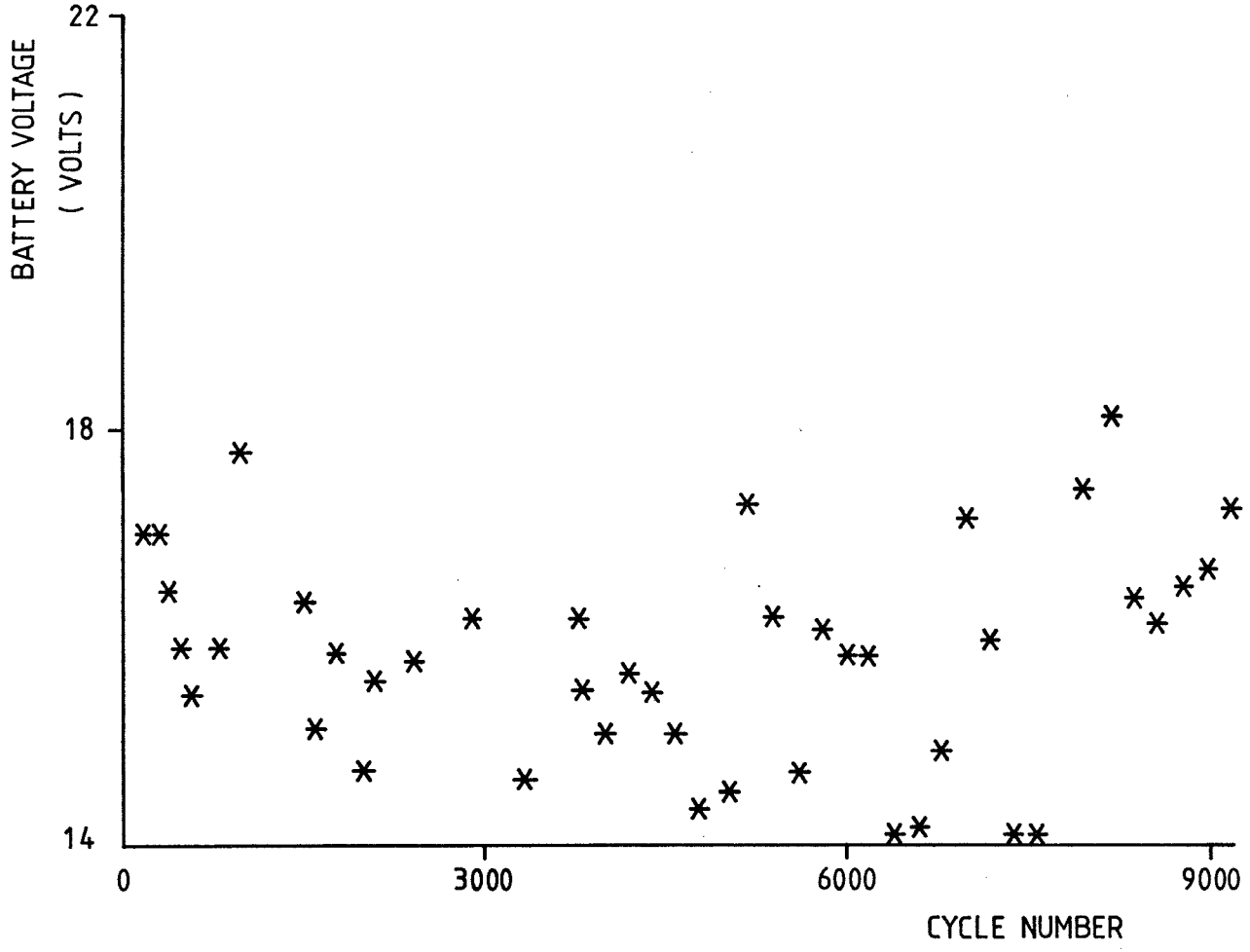

Figure 14. Spot-Test, End of Discharge Battery Voltage (Point F')

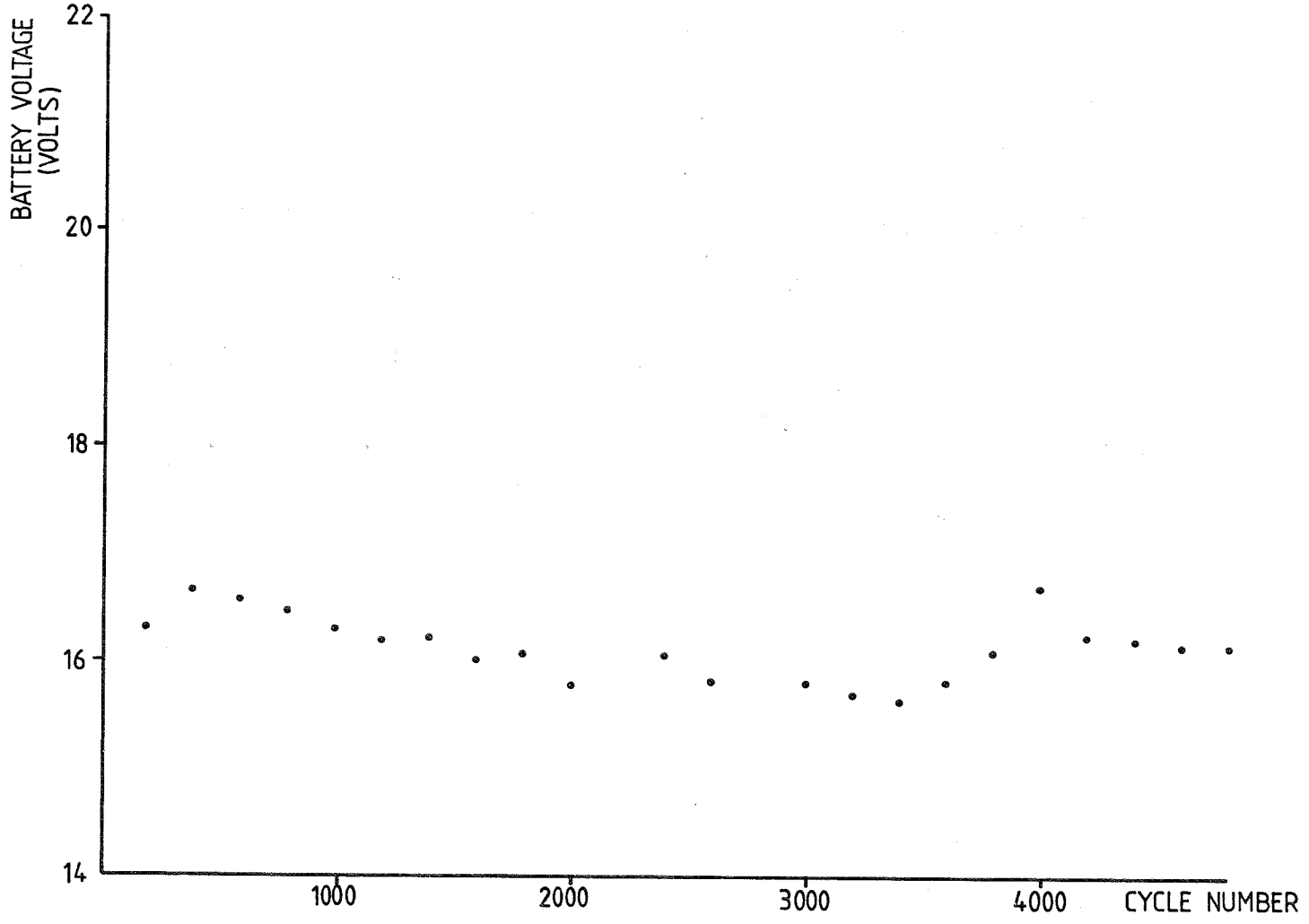

Figure 15. Reference-Test (Second Series), End of Discharge Battery Voltage Evolution

34 AMPERE-HOUR NICKEL-CADMIUM MINIMUM TRICKLE CHARGE TESTING

Paul J. Timmerman
Martin Marietta Denver Aerospace
Denver, Colorado

ABSTRACT

The current rates used for trickle charging batteries are critical in maintaining a full charge and in preventing an overcharge condition. The importance of the trickle charge rate comes from the design, maintenance and operational requirements of an electrical power system. This paper describes the results of minimum trickle charge testing performed on six, 34 ampere-hour, nickel-cadmium cells manufactured by General Electric. The purpose of the testing was to identify the minimum trickle charge rates at temperatures of 15°C and 30°C.

INTRODUCTION

Five 34 ampere-hour, nickel-cadmium cells were series connected into a cell pack and used as the test article for trickle charge testing. The pack had been used in previous developmental tests, but showed no signs of degradation that might impart a bias into the test results. The pack was instrumented for battery and individual cell voltages, and a single skin temperature measurement. Data leads were soldered to the cell terminals and a copper constantine thermocouple was attached to the top of the center cell. All instrumentation leads were interfaced to the Automatic Control and Data Acquisition System (ACDAS) depicted in Figure 1.

At each of the two test temperatures, a series of four tests were performed. The first test was a baseline capacity check. This test consisted of a 1.70 ampere charge (C/20) for forty hours, followed by a -17.0 ampere (C/2) discharge to a 1.0 volt/cell cutoff. The self-discharge test has a sixteen day (384 hour) open circuit phase between the charge and discharge phases. The results of this test are used to calculate the self-discharge rate. The next test was to do the C/20 charge, a sixteen day low rate trickle charge, using the self-discharge rate as the low rate trickle charge value, and finally the C/2 discharge to the 1.0 volt/cell cutoff. The high rate trickle charge test was similar to the low rate, except the trickle charge rate was twenty-five milliamperes above the self-discharge rate. All tests were completed by shorting the cell with one ohm resistors to below 50 millivolts.

TEST RESULTS

The voltage profiles for all tests are shown in Figures 2 through 7. The capacities of the test are given in Table 1. By comparing the capacities achieved (in the self-discharge, low rate, and high rate tests) to the baseline capacity, values for the capacity losses are calculated, as shown in Table 1. The listed capacity losses are corrected values, using methods described below.

Baseline Capacity - End of 16 Day Capacity = Capacity Loss

The rate of discharge was calculated for the sixteen day open circuit or trickle charge phases. The following method was used.

Capacity Loss/Phase Time = Discharge Rate

The discharge rates at various trickle charge rates are given in Table 2. Figure 10 shows the 15°C and 30°C plots for the trickle charge rate versus the self-discharge rate. Note that the X-intercepts provide the theoretical rates of a zero capacity loss.

The efficiencies for the tests are given in Table 3. They were calculated using the following formula.

$$\text{Efficiency} = \frac{\text{Trickle Charge Rate - Discharge Rate}}{\text{Trickle Charge Rate}} \times 100$$

The Self-Discharge Rate Profile, Figure 12, shows the projected self-discharge for a zero to forty Celsius range.

The test results were calculated in a way which minimizes all possible sources of error. The effects of test anomalies on voltage are seen in Figures 3 and 4. Figures 8 and 9 reveal that temperature is a direct cause of some of these anomalies. The temperature plots reveal a direct correlation between temperature and voltage. The effect of these anomalies upon other calculated parameters is not nearly as apparent. Using the curves for efficiency, self-discharge, trickle-charge effectiveness, and voltage, it is possible to evaluate the effect of, and often compensate for, these variations.

The sixteen day long phases of testing were sometimes punctuated with anomalies. We can talk about two types of these anomalies. The first type is the simple test abort during a self-discharge test. The down time experienced can be compensated for in an easy manner.

Discharge Rate = Capacity Loss/Phase Time + Down Time

The second type of anomaly occurred during a trickle charge phase. A method for compensating for the second anomaly was as follows:

$$\text{Corrected Capacity Loss} = \text{Measured Capacity Loss} - \text{Self-Discharge Rate} \times \text{Down Time}$$

This method yielded accurate corrections if the down time was accurate and the self-discharge rate was truly representative.

One case where the self-discharge rate was not a true representation of the changes occurring was the low rate trickle charge at 15°C (Figure 4). Figure 9 shows a 15°C temperature while the test was running. The peaks represent chamber control failures, which resulted in test aborts. The temperature while in a test abort condition were not represented. Test histories show that 30°C is a more representative temperature during the test's down time. It follows that the 30°C self-discharge rate, and not the 15°C self-discharge rate, was the correct factor to use.

The effect of changing the abort temperature is to raise the used self-discharge rate from 10 mA to 14 mA. The recomputed corrected capacity loss was affected by 4% for the low rate trickle charge test at 15°C. The measured capacity loss was -3.39 AH. With a 10 mA self-discharge rate, the correction factor for the 31.7 hours of down time was +0.32. And with a 14 mA self-discharge rate, the recomputed correction factor for the 31.7 hours of down time was 0.44 AH. Thus, the baseline and recomputed corrected capacity losses were -3.07 AH and -2.95 AH respectively. The discharge rates were 8.0 mA and 7.7 mA respectively, which also reflected a 4% delta.

The high rate trickle charge test at 15°C shows variations in voltage during the sixteen day test phase which appear unnatural (see Figure 3). Figure 8, the low rate trickle charge temperature plot, reveals an inverse relationship between the temperature and voltage which is quite sensitive. The cell characterization plots, Figures 10 through 12, demonstrate the effects of deviations and anomalies. Figure 8 depicts a temperature deviation as great as 1.5°C.

With a slope of +0.32 (mA/°C) for the Self-Discharge Rate Profile, Figure 12, the 1.5°C drop in temperature would result in a smaller self-discharge rate by 0.5 mA. Another significant factor is the efficiency's dependency on temperature. The slope depicted in Figure 11, Trickle Charge Efficiency, is +0.80 (%/°C). This results in a 1.2% decrease in the efficiency of the trickle charge.

The direct effect of the 1.5°C decrease on the 34 mA trickle charge at 15°C was to alter the effective charge rate by 6%, from 7.2 mA to 6.8 mA. This is the result of the efficiency decreasing to 19.8%, which in turn gives us a -3.2 mA discharge rate. The additional 0.5 mA decreases the discharge rate to -2.7 mA. The net change from -2.8 mA is 4%.

The 1.5°C value used was a worst case figure, which is too large for the temperature plot for test 211. A more realistic figure is a 0.5°C drop average over the length of the sixteen day test phase. This would point to an error of slightly over 1% in the calculated results.

CONCLUSION

By using the curves generated from the test results, trickle charge rates can be determined for most circumstances. A rate can be calculated after the temperature and acceptable rate of discharge have been determined. One constraint upon this is that the temperatures considered are not extremes of the range studied. The linearity of the graphs, often dictated by only two points, undoubtedly falters at the extremes. This also applies to the rates, which must also be in the normal range. The normal operating temperature for the 34 ampere-hour battery is represented by the curves in this report. The plot for trickle charge effectiveness, Figure 10, represents the most critical data for design, maintenance, and operation. With the three existing points, the linearity of the plots were supported. A linear interpolation gives us the values for zero loss trickle charge rates at 15°C and 30°C. The respective rates were determined to be 49 milliamperes and 40.5 milliamperes. It is interesting to note the lower rate necessary at the higher temperature. This can be attributed to the greater trickle charge efficiency at the higher temperature.

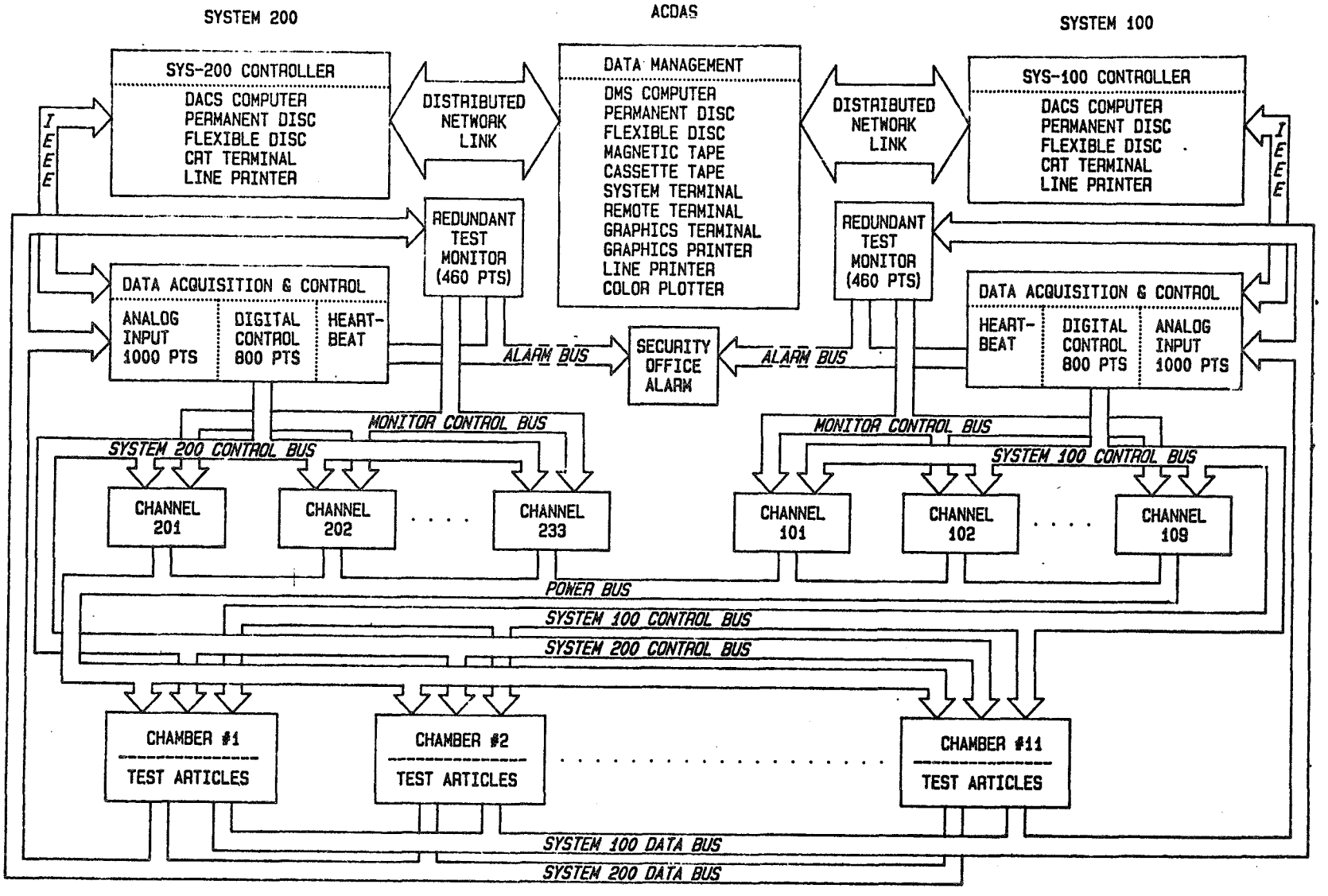

Figure 1. Block Diagram of the Automatic Control and Data Acquisition System

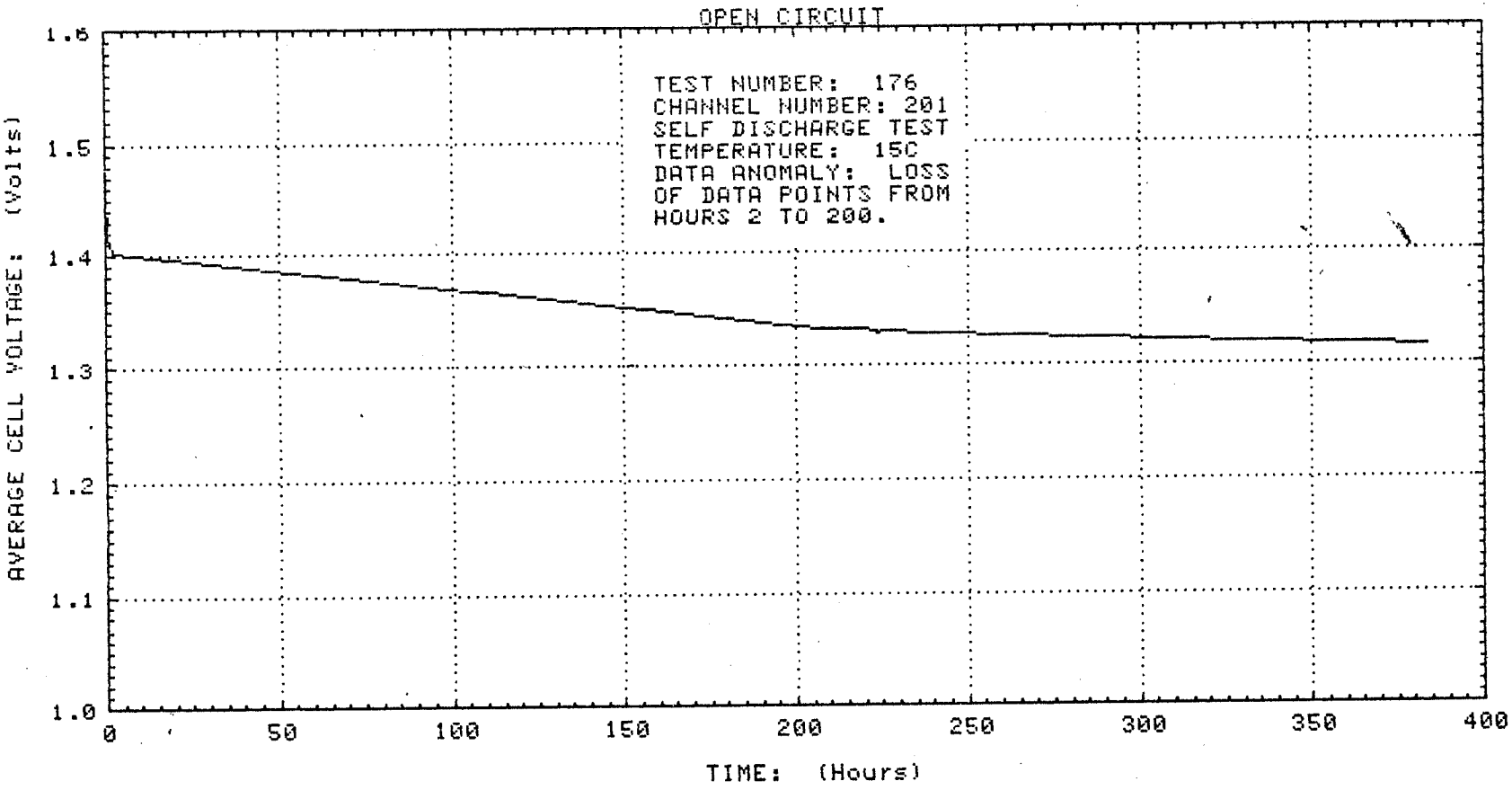
OPEN CIRCUIT
TEST NUMBER: 176
CHANNEL NUMBER: 201
SELF DISCHARGE TEST
TEMPERATURE: 15C
DATA ANOMALY: LOSS
OF DATA POINTS FROM
HOURS 2 TO 200.
AVERAGE CELL VOLTAGE: (Volts)
1.6
1.5
1.4
1.3
1.2
1.1
1.0
0
50
100
150
200
250
300
350
400
TIME: (Hours)

Figure 2.

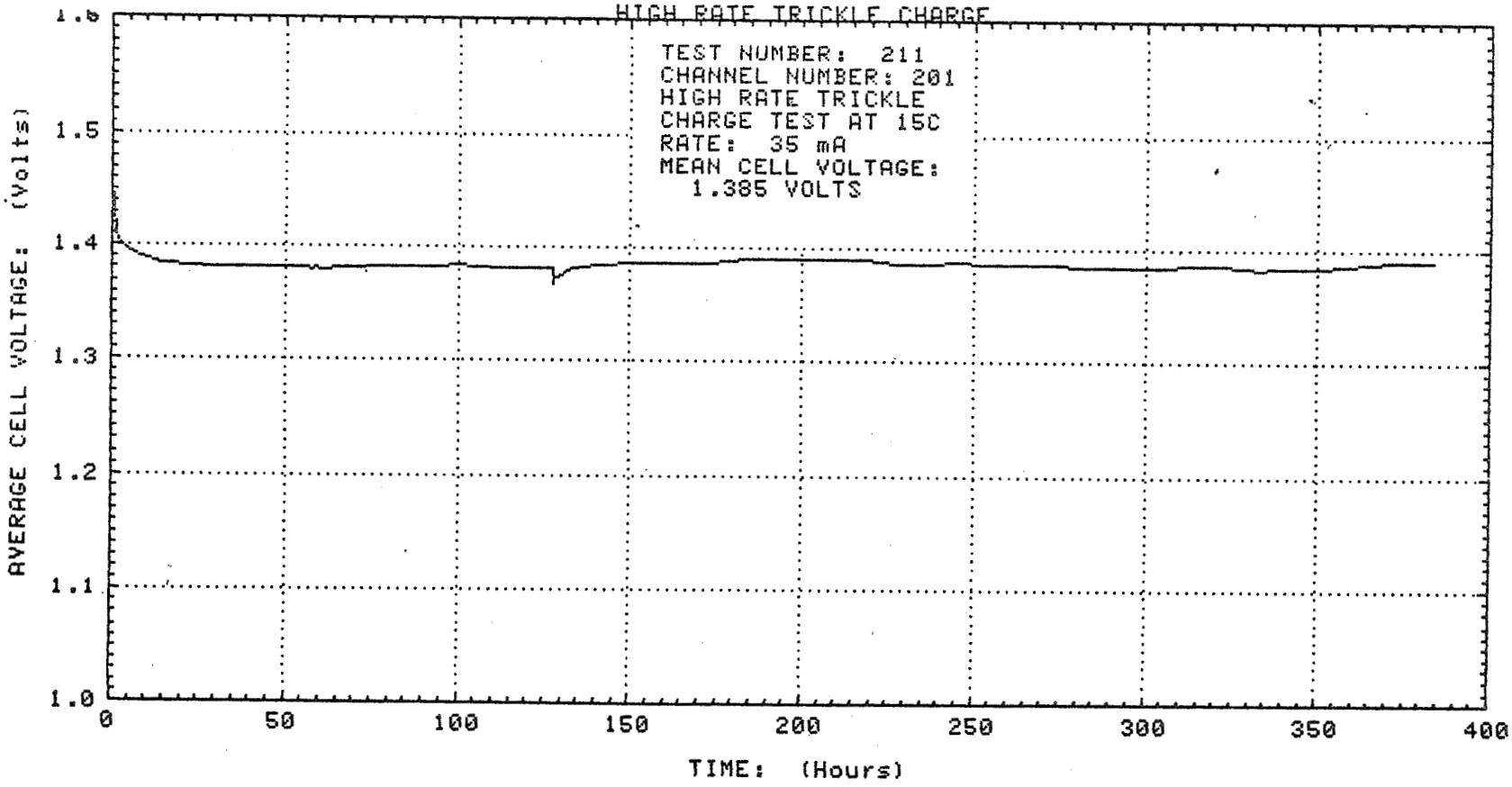
HIGH RATE TRICKLE CHARGE
TEST NUMBER: 211
CHANNEL NUMBER: 201
HIGH RATE TRICKLE
CHARGE TEST AT 15C
RATE: 35 mA
MEAN CELL VOLTAGE:
1.385 VOLTS
AVERAGE CELL VOLTAGE: (Volts)
1.6
1.5
1.4
1.3
1.2
1.1
1.0
0
50
100
150
200
250
300
350
400
TIME: (Hours)

Figure 3.

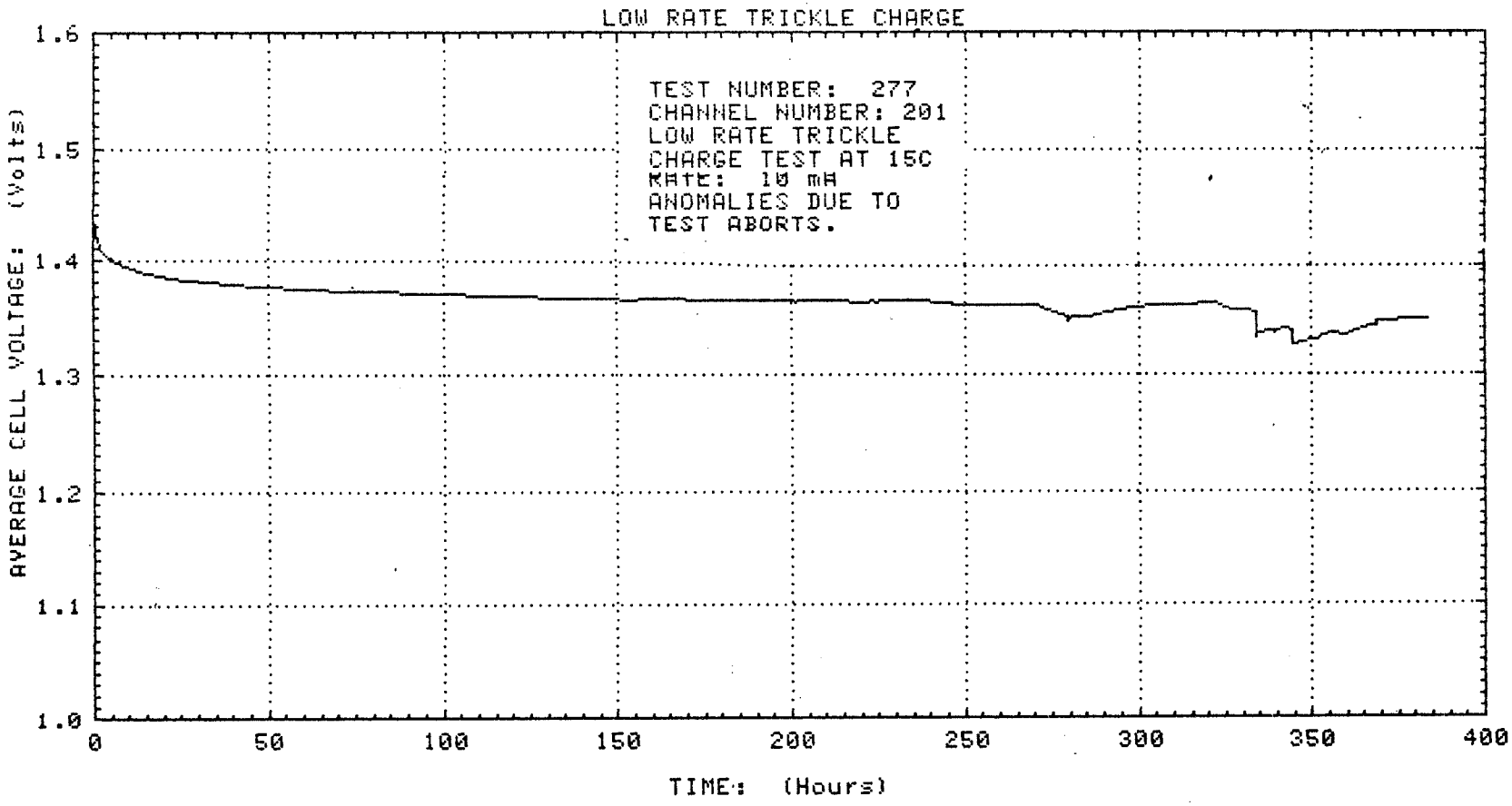
LOW RATE TRICKLE CHARGE
TEST NUMBER: 277
CHANNEL NUMBER: 201
LOW RATE TRICKLE
CHARGE TEST AT 15C
RATE: 10 mA
ANOMALIES DUE TO
TEST ABORTS.
AVERAGE CELL VOLTAGE: (Volts)
1.6
1.5
1.4
1.3
1.2
1.1
1.0
0
50
100
150
200
250
300
350
400
TIME: (Hours)

Figure 4.

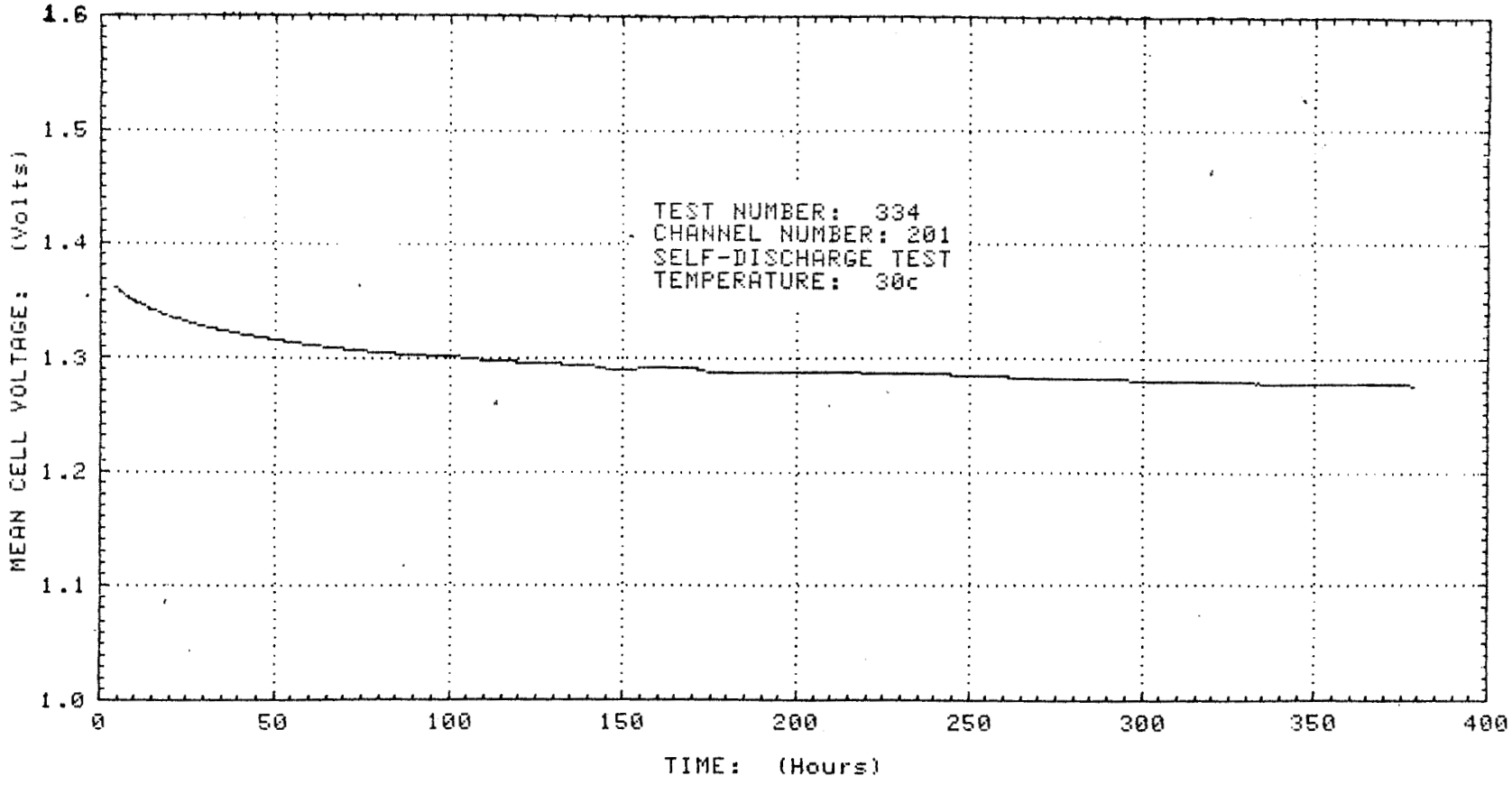
1.6
1.5
1.4
1.3
1.2
1.1
1.0
MEAN CELL VOLTAGE: (Volts)
TEST NUMBER: 334
CHANNEL NUMBER: 201
SELF-DISCHARGE TEST
TEMPERATURE: 30c
0
50
100
150
200
250
300
350
400
TIME: (Hours)

Figure 5.

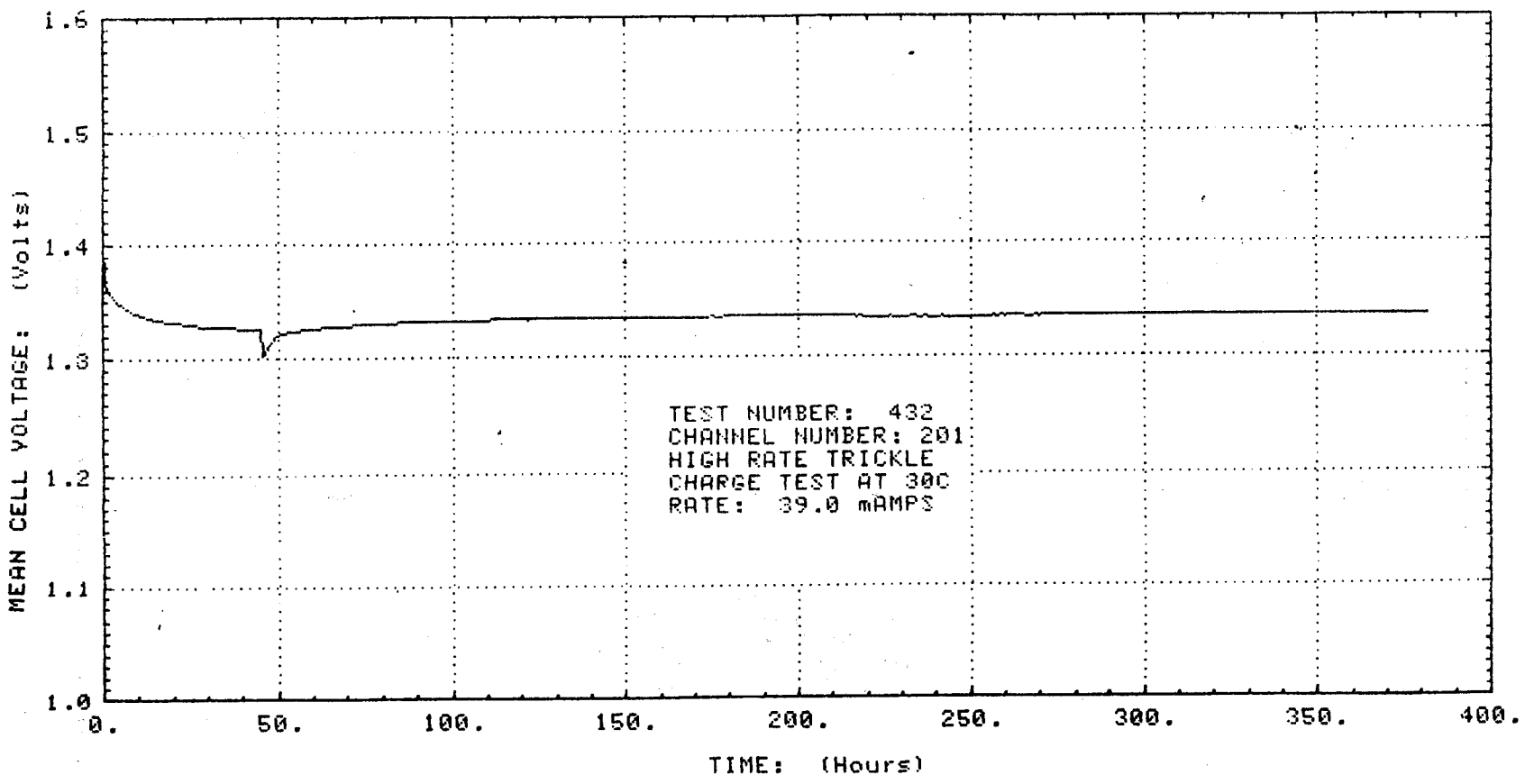
MEAN CELL VOLTAGE: (Volts)
1.6
1.5
1.4
1.3
1.2
1.1
1.0
0.
50.
100.
150.
200.
250.
300.
350.
400.
TIME: (Hours)
TEST NUMBER: 432
CHANNEL NUMBER: 201
HIGH RATE TRICKLE
CHARGE TEST AT 30C
RATE: 39.0 mAMPS

Figure 6.

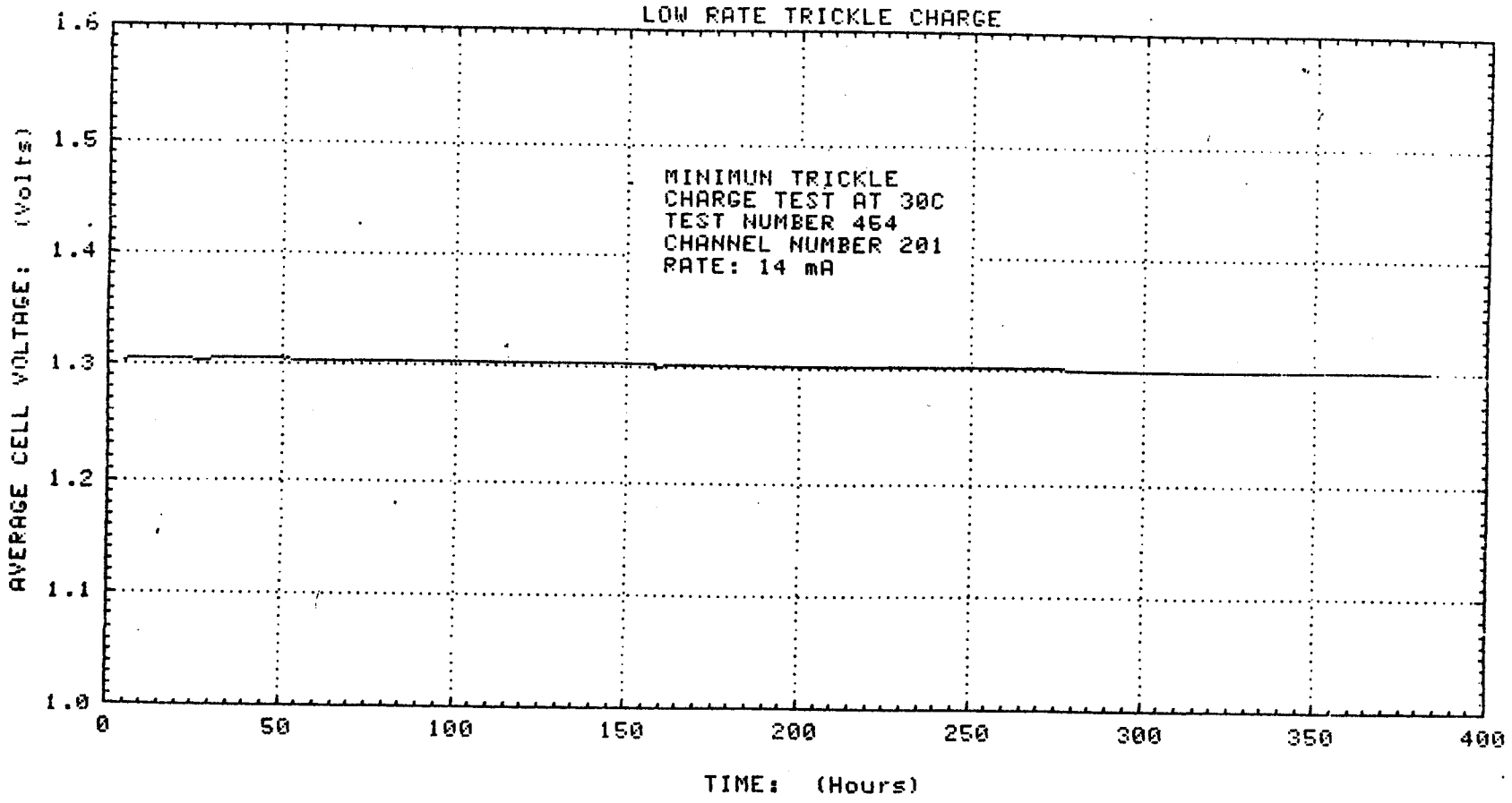
LOW RATE TRICKLE CHARGE
MINIMUN TRICKLE
CHARGE TEST AT 30C
TEST NUMBER 464
CHANNEL NUMBER 201
RATE: 14 mA
AVERAGE CELL VOLTAGE: (Volts)
1.6
1.5
1.4
1.3
1.2
1.1
1.0
0
50
100
150
200
250
300
350
400
TIME: (Hours)

Figure 7.

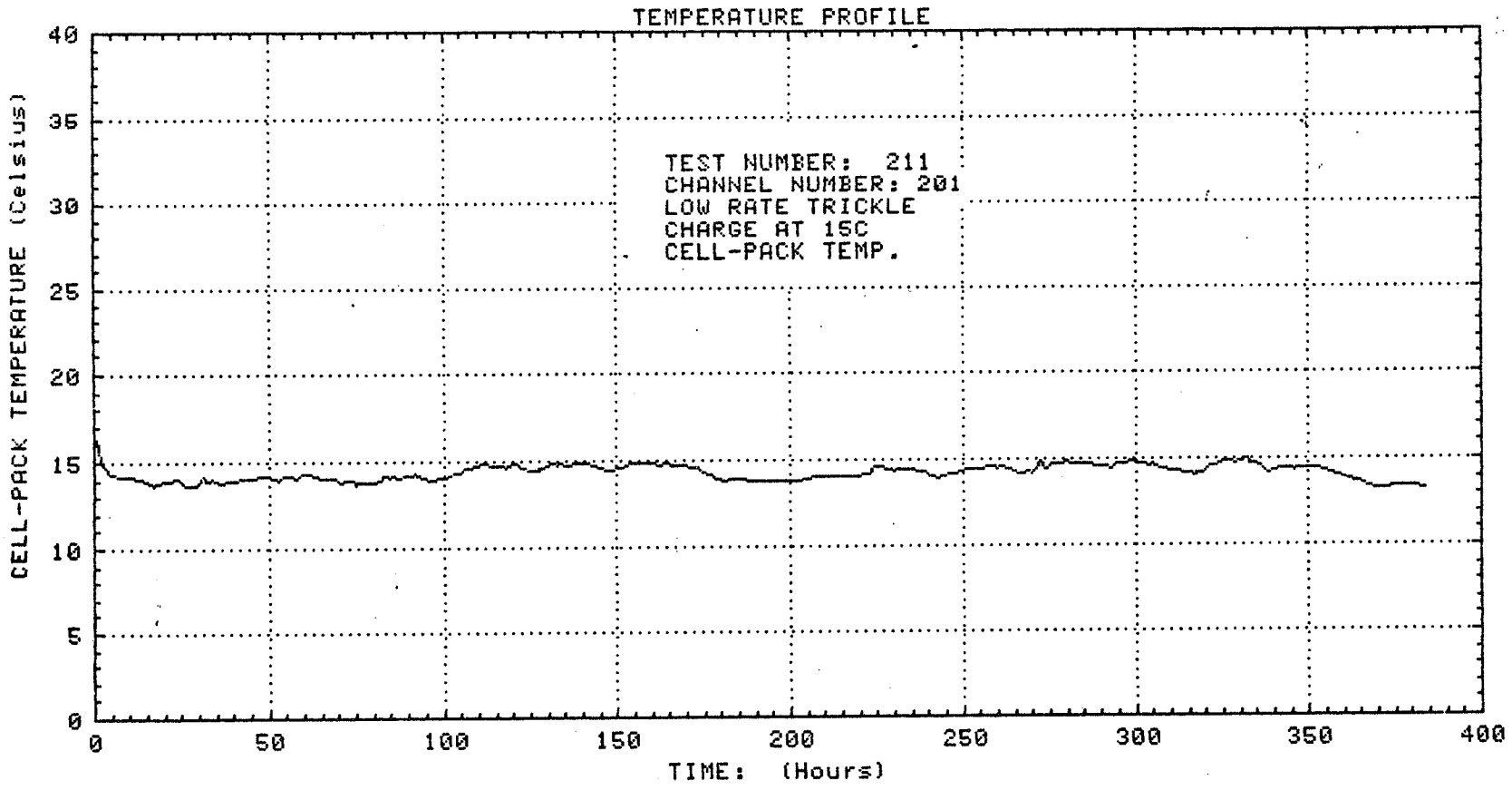
TEMPERATURE PROFILE
TEST NUMBER: 211
CHANNEL NUMBER: 201
LOW RATE TRICKLE
CHARGE AT 15C
CELL-PACK TEMP.
CELL-PACK TEMPERATURE (Celsius)
TIME: (Hours)
0
5
10
15
20
25
30
35
40
0
50
100
150
200
250
300
350
400

Figure 8.

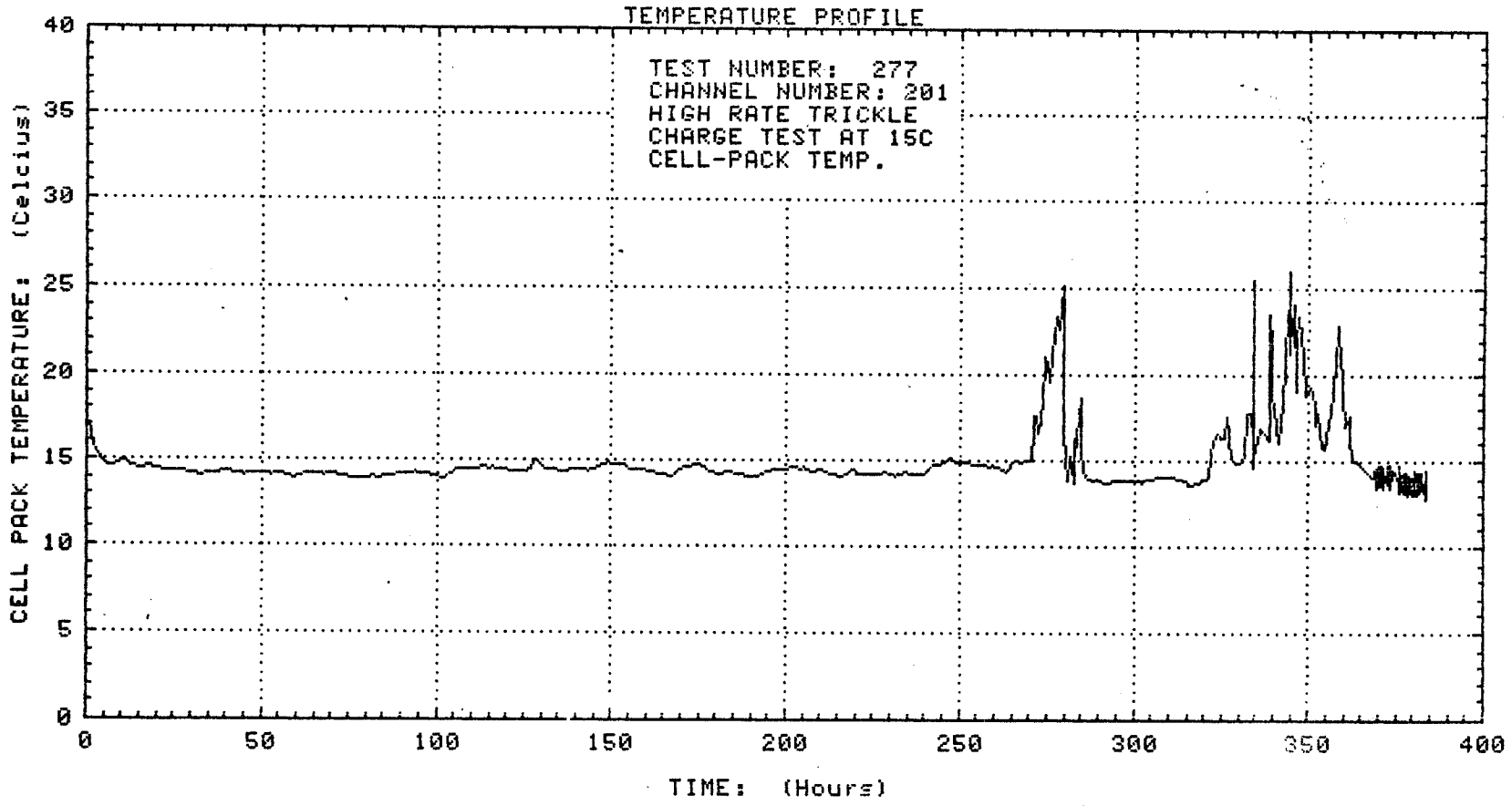
TEMPERATURE PROFILE
TEST NUMBER: 277
CHANNEL NUMBER: 201
HIGH RATE TRICKLE
CHARGE TEST AT 15C
CELL-PACK TEMP.
CELL PACK TEMPERATURE: (Celcius)
0
5
10
15
20
25
30
35
40
0
50
100
150
200
250
300
350
400
TIME: (Hours)

Figure 9.

Table 1.

CAPACITIES

TEST	15c	30c
BASELINE CAPACITY	40.68 AH	39.21 AH
SELF-DISCHARGE	36.99 AH	33.85 AH
HIGH RATE TRICKLE CHARGE	39.65 AH	38.61 AH
LOW RATE TRICKLE CHARGE	37.39 AH	35.48 AH
HIGH RATE CAPACITY LOSS	2.78 AH	0.38 AH
LOW RATE CAPACITY LOSS	3.08 AH	3.73 AH

Table 2.

TEST DESCRIPTION	15 c		30 c	
	TRICKLE RATE	DIS-CHARGE RATE	TRICKLE RATE	DIS-CHARGE RATE
SELF-DISCHARGE	0.0 mA	9.8 mA	0.0 mA	14.0 mA
LOW RATE TRICKLE	10.0 mA	8.0 mA	14.0 mA	9.7 mA
HIGH RATE TRICKLE	35.0 mA	2.8 mA	39.0 mA	0.6 mA

Table 3.

CHARGE EFFICIENCIES

TEST DESCRIPTION	15 c	30 c
LOW RATE TRICKLE CHARGE	20 %	31 %
HIGH RATE TRICKLE CHARGE	21 %	34 %

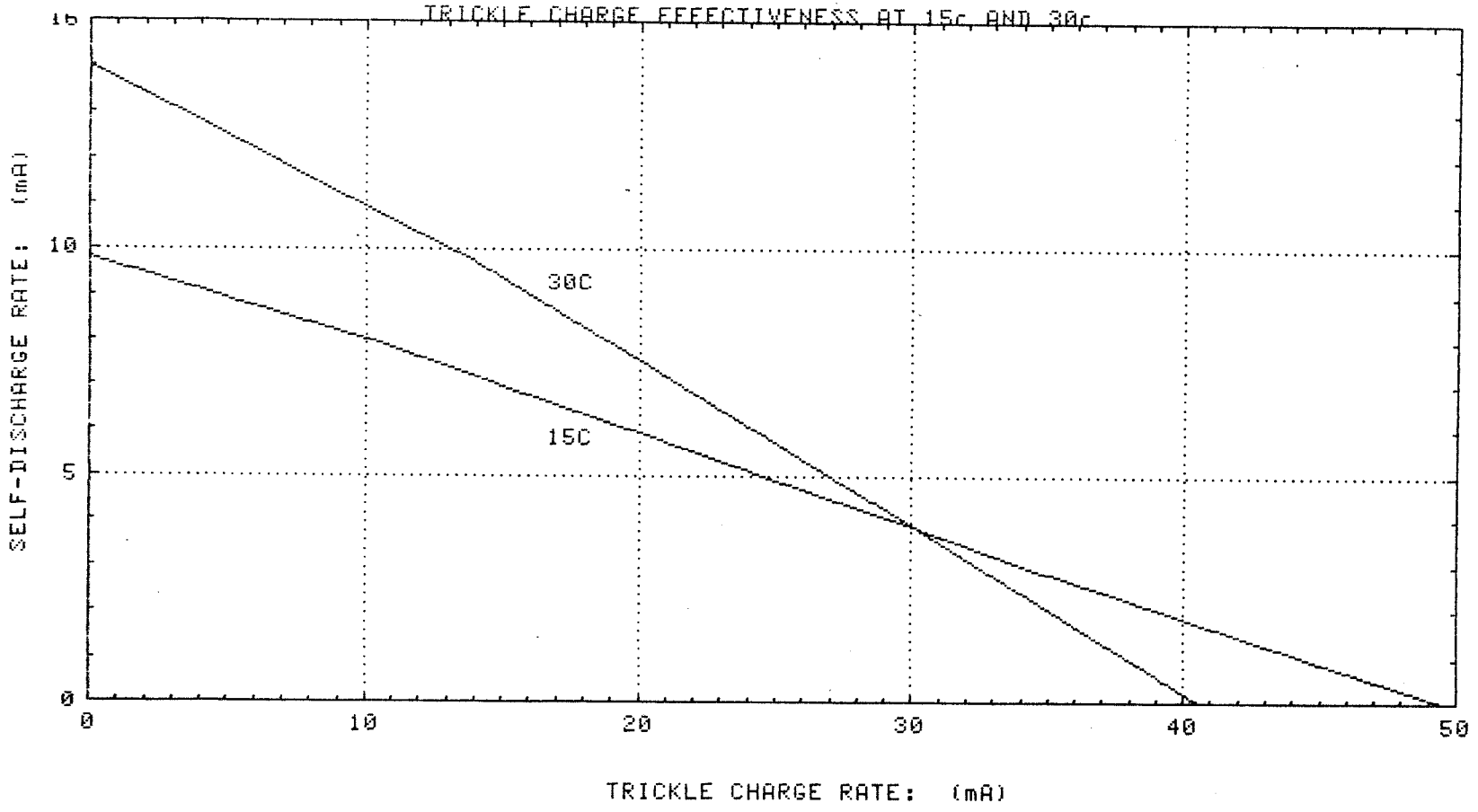
TRICKLE CHARGE EFFECTIVENESS AT 15c AND 30c
SELF-DISCHARGE RATE: (mA)
15
10
5
0
30C
15C
0
10
20
30
40
50
TRICKLE CHARGE RATE: (mA)

Figure 10.

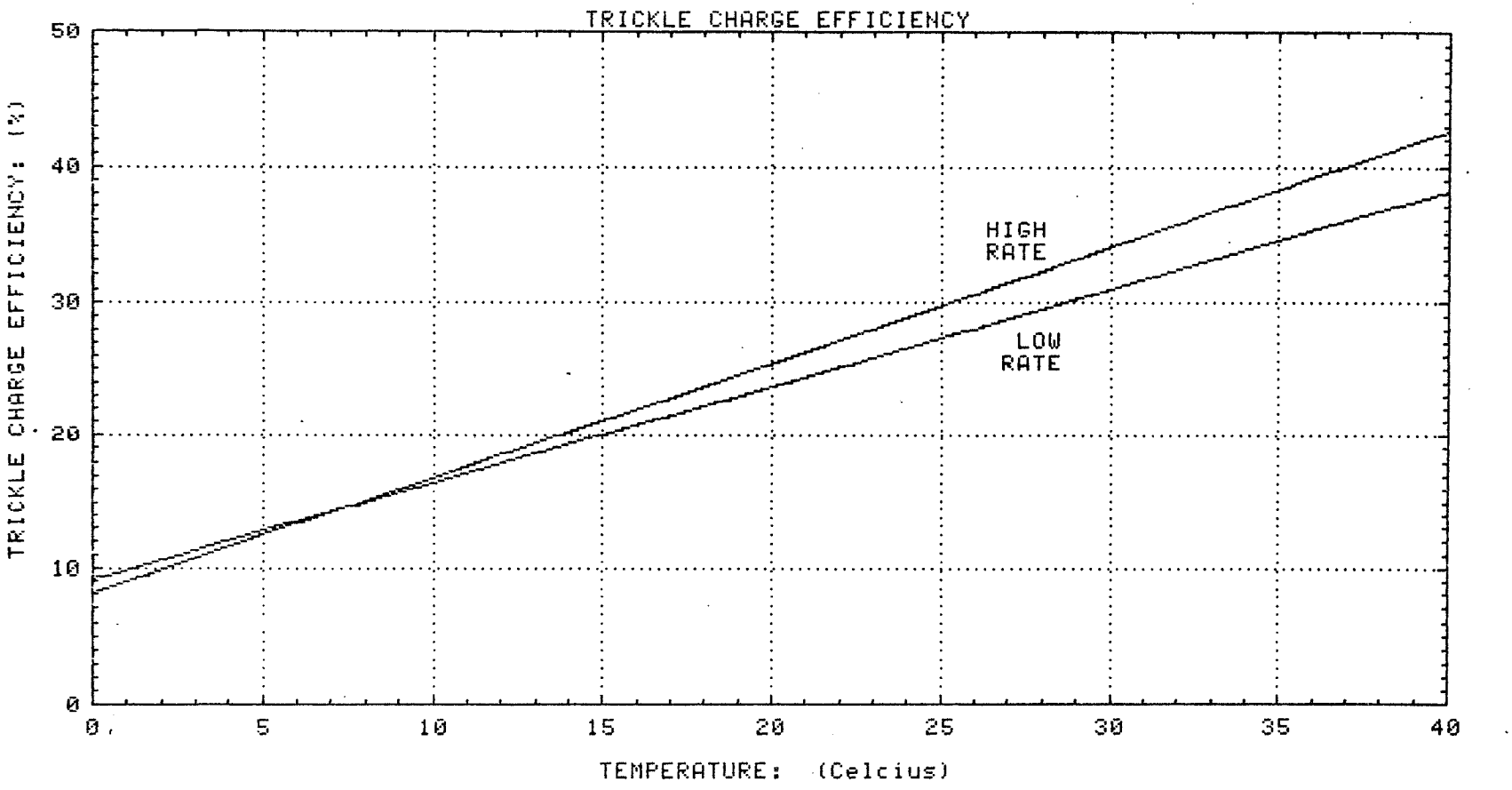
TRICKLE CHARGE EFFICIENCY
TRICKLE CHARGE EFFICIENCY: (%)
50
40
30
20
10
0
0.
5
10
15
20
25
30
35
40
HIGH
RATE
LOW
RATE
TEMPERATURE: (Celcius)

Figure 11.

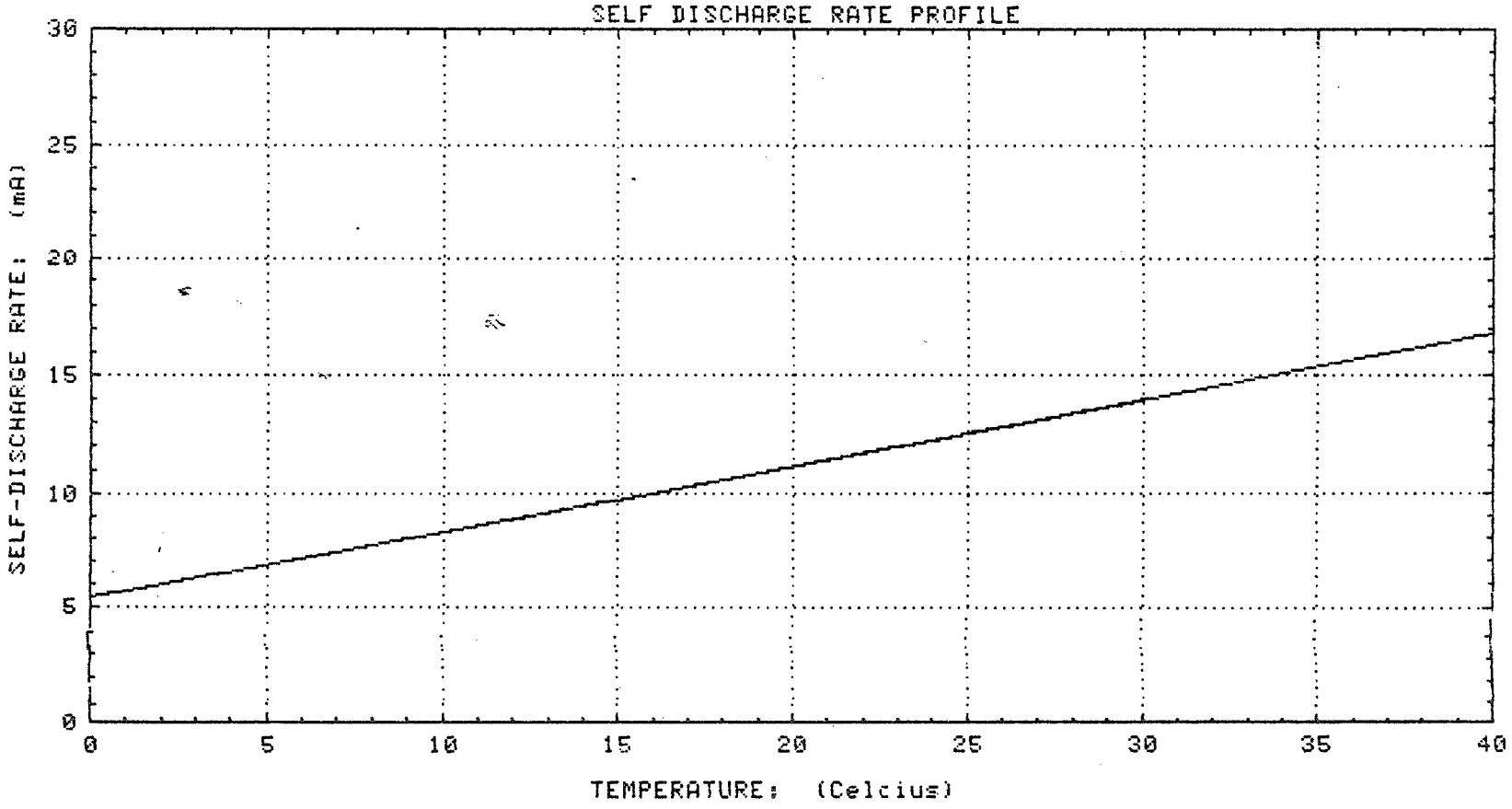
SELF DISCHARGE RATE PROFILE
SELF-DISCHARGE RATE: (mA)
TEMPERATURE: (Celcius)
0
5
10
15
20
25
30
35
40

Figure 12.

AUSSAT BATTERY LIFE TEST PROGRAM

P.W. GORIAN
Aussat Pty Ltd, El Segundo, California

D.F. PICKETT JR., R.S. BOGNER, T.I. CHAO, J.P. JORDAN, K.B. CLARK
Hughes Aircraft Company, El Segundo, California

ABSTRACT

AUSSAT Pty Ltd, the Australian National Satellite organization, has contracted with the Hughes Aircraft Company (HAC) for the construction of 3 satellites based on the now familiar HS-376 product line. As part of the AUSSAT contract, HAC is conducting an extensive NiCd battery life test program. This paper describes the life test program, its objectives and test results to date. Particular emphasis is given to the evaluation of the FS2117 separator as a future replacement for the Pellon 2505 separator of which only a very limited quantity remains.

BACKGROUND

The AUSSAT spacecraft design shown in Figure 1 is based on the standard HS-376 product line. However the unique payload requirements of the AUSSAT mission have pushed the mass and power design limits of the HS-376 bus, particularly in the power subsystem. The major features of the power subsystem are summarised on Table 1.

The spacecraft employs two 27 A-hr. NiCd batteries. Each battery contains 32 cells configured as 4 separate packs, each pack holding 8 cells. The cells themselves are a scaled up version of those previously used by HAC on the HS-376 product line, and manufactured by General Electric (GE). The major cell design parameters are listed in Table 2.

For thermal control each pack employs a radiator fin and packs are evenly located around the spun shelf. A battery heater controller actively maintains the packs above 5°C. A battery charge and reconditioning unit (BCRU) provides four selectable charge rates and two selectable reconditioning rates.

Due to power limitations it was not possible to size the medium charge string to allow parallel high rate charging of both batteries. Hence the sequential post-eclipse charging scheme illustrated in Figure 1 was proposed. In this scheme one battery would be fully charged at the high 2M+T rate, while the other battery is trickle charged at the T-rate. The charging rates would then be reversed to enable charging on the latter battery to be completed at the high rate. In order to limit any possible side effects from the long trickle charge applied to this battery before high rate charging can be applied, it was further decided to rotate the battery initially placed on trickle charge after each eclipse.

Virtually all space flight NiCd batteries have been built using the Pellon Corporations 2505 non-woven nylon fabric as the separator. Unfortunately production of the material was discontinued in 1976 and recent attempts to commercially reproduce the separator have failed. GE expects their supply of the 2505 separator to be committed by early 1985. As such it was proposed by HAC to use the opportunity presented by the AUSSAT life test program to evaluate the FS2117 material as a replacement for the Pellon 2505.

The US government agencies have also been alerted to the limited amount of Pellon 2505 available. A joint USAF/NASA evaluation program for qualifying a replacement separator is pending. USAF/NASA are negotiating with Pellon in the USA to produce a new separator similar to the FS2117. This is not a reflection on the FS2117 but a desire to have a domestic rather than a foreign source. According to reference 2, life testing on cells with the new domestic separator is scheduled to commence during May/1985 with preliminary results available a year later.

LIFE TEST OBJECTIVES

The objectives of the life test program are seen as follows:

- To adequately qualify the scaling of the Hughes third generation NiCd battery to the AUSSAT A-hr. name plate rating. The previously testing cells were 21.6 A-hr. as opposed to the 27.5 A-hr. nameplate capacity required for AUSSAT.

- To provide a check on the manufacturing processes and materials at the cell vendor (G.E.) at a point just prior to the production of the fight cells.

- To provide BOL and EOL indications of the performance to be expected from the battery.

- To verify the new sequential battery post-eclipse charging scheme proposed by HAC.

- To evaluate the performance of the FS2117 separator.

In addition the test program must provide at least a preliminary indication of flight battery performance as early in the program as possible and certainly prior to launch.

LIFE TEST DESCRIPTION

In order to meet the objectives defined above, a continuous 900 cycle throughput test and a 20 season real time GEO eclipse shortened solstice test were selected.

The throughput test is a continuous cycling test in which a 10 cell engineering pack is discharged at 14 amperes (C/2) for 1 hour to give a nominal 50% depth of discharge, and then charged at 2.8 amperes (C/10) for 7 hours to a 140% recharge return. The engineering pack is maintained at 10°C. Testing at 3 discharge/charge cycles per day is only interrupted for reconditioning and environmental chamber maintenance. Individual cell reconditioning is performed when the cell voltage on discharge falls below 1.14 volts. The test has been included in order to verify the cycle life capability of the flight batteries prior to launch, but will also enable test results to be correlated with previous testing performed on similar battery designs at HAC.

The real time eclipse shortened solstice test is a much more representative test of in-orbit conditions and, in particular, the post-eclipse sequential charging scheme. Three 8-cell qualification battery packs and a 6-cell engineering pack are subjected to 20 GEO eclipse seasons in real time, with the intermediate solstice trickle charge period shortened to 14 days. Reconditioning is performed prior to each eclipse season. The discharge and charge profiles used to simulate each GEO eclipse season are shown in Table 3. The profiles reflect the actual eclipse daily levels in terms of charge and discharge times, charge and discharge rates, and the sequential battery charging scheme.

The engineering packs have been utilized to allow gauge cells to be included for cell pressure monitoring and to enable easy addition, and removal of cells for destructive physical and chemical analysis.

For the purposes of evaluating the performance of the new separator, 2 cells with the new separator were included in each of the engineering packs, while one of the real time qualification packs was assembled totally from cells using the new separator. Two different plate lots have been used in preparing the life test cells. Half the FS2117 separator cells were assembled from each plate lot.

THE NEW SEPARATOR

A comparison of the physical and chemical properties of the 2505 and FS2117 separator is summarized in Table 4. The 2505 data is taken from the Sealed-Cell Nickel-Cadmium Battery Applications Manual (ref. 1), while the FS2117 data has been supplied by the General Electric Battery Business Department. In general, the property values quoted are typical rather than specification.

Significant property differences between the separators and the impact these may have on cell performance and design parameters are discussed below.

PHYSICAL/CHEMICAL PROPERTY DIFFERENCES

The FS2117 separator is denser as a joint result of the use of Nylon 66 and the calendaring process. The calendaring process has been used to bond and reduce the thickness of the separator. No specific data on the tensile strength and elongation was available; however these properties should be comparable.

Electrolyte absorption and air permeability are lower, as expected for the FS2117 separator. The 35% increase in density matches well with the 30% decrease in electrolyte retension and air permeability.

Impurities in the form of anti-static coatings are present on both the FS2117 materials. No information is available on these coatings however the FS2117 separator is subjected to the same wash treatments to remove these as the 2505 material. The effectiveness of the treatment is checked by a foam test. The above, while lacking any degree of technical sophisication, appears to work. The only concern here is that some residual impurities may be different and have a significant impact on cell performance; this has occured in the past where different and apparently acceptable separators have been substituted.

No specific data is available on hydrolysis reaction rates for the FS2117 separator. However, with the use of Nylon 66, the FS2117 materials breakdown rate in KOH electrolyte should be significantly less. The reaction rate is also affected by the bonding method and exposed surface area.

EXPECTED CELL PERFORMANCE DIFFERENCES

A number of flight performance differences can be expected as a result of the above physical and chemical differences in the separators. The differences in performance are expected to be minor, but they can easily be corrected in future flight battery applications of the separator. The correction would include only slight changes in the present cell design and activation procedures in order to fine tune the cell for the 2117 separator.

Precharge to overcharge levels: Second generation NiCd cells typically specified a 35 - 40% precharge level on the negative Cd plate in order to prevent voltage fading of the cell during discharge especially at beginning of life. Hydrolysis of the separator and subsequent oxidation of the products increases the precharge level at the expense of overcharge protection as the separator breaks down over life. Hence the present generation of NiCd cells now specify only 30 - 35% precharge in order to maintain a higher overcharge protection level at end of life. The lower hydrolysis rate of the 2117 separator will result in a lower overall precharge levels and will be somewhat more prone to voltage fading problems at beginning of life and, in particular, at low

temperature. This has in fact been observed with initial 0°C capacity tests. However after a 30 cycle burn-in test, no significant differences at normal operating temperatures have been recorded.

Electrolyte Retension & Redistribution: One of the major life limiting factor for NiCd cells is drying of the separator. This occurs over life as the plates swell and the electrolyte migrates out of the separator and into the plate. The lower electrolyte retension capability of the 2117 separator would have aggravated the problem on older cells. However the use of teflonated negatives and increased electrolyte quantitites (3 to 4 cm^3/A-hr) should obviate the problem at least for 7 year applications. Electrolyte redistribution will be less noticeable over short periods of time, the effect of this has already been demonstrated in the qualification cell capacity differences observed between the 2117 and 2505 separators after a 20 day stand period.

Overcharge Pressure: The higher density of the FS2117 separator will reduce the amount of free void volume for gas expansion in the cell and thus increase cell overcharge pressure unless the electrolyte level or cell free volume is suitably increased. In addition, the lower gas permeability of the 2117 separator may decrease the oxygen recombination rate and this also increase cell overcharge pressure.

LIFE TEST STATUS AND RESULTS

Life testing commenced in July 1984. The throughput test will require 10 months to complete 900 discharge/charge cycles, while the real-time eclipse shortened solstice test will need 3.5 years to complete 20 seasons. At the time of writing, 115 cycles and one eclipse season have been completed on the respective tests.

The 2505 and FS2117 separator cell end of charge and end of discharge voltages from the through-put and real-time eclipse test are shown in Figure 3 through 6. FS2117 separator cell performance, at the present early stage of testing, matches well with the 2505 separator cell performance. FS2117 separator cell voltages are, in general, bounded by the upper and lower voltage ranges observed on the 2505 separator cells.

The through-put and real-time eclipse test behaviour of the 2505 separator cells is also normal. In particular the sequential charging scheme has had no short term affect on the real-time eclipse test performance of the cells.

REFERENCES

1. Sealed-Cell Nickel-Cadmium Battery Applications Manual. NASA reference Publication 1052, December, 1979.

2. M. J. Milden; J. Harkness: Separator Qualification for Aerospace Nickel-Cadmium Cells. 1984 IECE Conference, Paper 849037.

Table 1. POWER SUBSYSTEM CHARACTERISTICS AND PERFORMANCE

Parameter/Unit	Characteristics/Performance		
Main bus voltage range	Sunlight	Eclipse	Posteclipse Transient
Spinning	30.0±0.5V	29.1±0.1V	29.0 to 42.5V
Despun	29.5±0.5V	28.5±0.1V	28.5 to 42.5V
Minimum at loads	28.15V	28.15V	-
Minimum transient (squib firing)	26.5V	-	-
Solar arrays			
Expected main array power at 29.3V		BOL	EOL
21 June solstice		1047.1W	860.0W
21 September equinox		1163.5W	943.4W
Charge array current at 50.6V			
Trickle (21 June)		0.421A	0.343A
Trickle (21 September)		0.471A	0.394A
Medium (21 September)		0.848A	0.708A
Batteries			
Number per spacecraft	2		
Cells per battery	32		
Capacity per battery	27.0A-hr		
Average eclipse voltage, BOL	39.68V		
Discharge controller	One unit with two redundant, constant power, pulse width modulated controllers.		
Input voltage	31 to 45V		
Output voltage	29.1 ±0.1V		
Charge and reconditioning unit	Configures four solar panel trickle (T) and medium (M) boost arrays and selects two reconditioning loads.		
Charge configurations	T, M, 2M, T + M, T + 2M		
Reconditioning loads	186ohm, 93ohm.		
Bus limiters	Redundant units with four individually commandable limiters per unit.		
Set and tap points			
Limiter A	29.62V at cell 23 of 69 total (aft)		
Limiter B	29.86V at cell 23 to 69 total (aft)		
Limiter C	30.10V at cell 19 to 66 total (fwd below radiator)		
Limiter D	30.34V at cell 18 to 66 total (fwd above radiator)		
Battery cell voltage monitor	One unit per battery measures cell voltage with 4 mV accuracy.		
Battery Heater Controllers	Two units, each with redundant controllers, maintain minimum battery temperature of 5°C (41°F) Nominal setpoint is 6.4°C (43.5°F).		

Table 2. AUSSAT NiCd BATTERY CELL DESIGN PARAMETERS

- 27 A-hr capacity at 10°C.
- 1.09 aspect ratio.
- 9.31 x 8.57 x 0.0647 cm coined plates.
- 15 positive/16 negative plates.
- 0.2mm inter-electrode spacing.
- 304L stainless steel case.
- GE butt geometry for positive terminal.
- Common case to negative terminal.
- Pellon 2505 separator.
- 10.2 g/dm^2 positive plate loading.
- 13.9 g/dm^2 negative plate loading.
- 5mA/cm^2 nominal current density.
- 80% nominal sinter void volume.
- 30-35% pre-charge.
- 50% excess negative overcharge protection.
- TFE negatives.
- 3.2 cc/A-hr electrolyte (31% KOH).
- Less than 3 g/l carbonate.
- -18°C to 40°C survival temperature.
- 8°C average case temperature.

Table 3. REAL TIME ECLIPSE TEST PROFILES

Eclipse Day	Discharge Time (min.)	High Rate Charge Charge Time (min.)	Total Trickle Charge Time (hours)
1-2	10	61	22.82
3-8	20	121	21.65
9-13	40	242	19.30
14-18	60	363	16.95
19-28	70 (52% dod)	423	15.78
29-33	60	363	16.95
34-38	40	242	19.30
39-44	20	121	21.65
45-46	10	61	22.82

Notes:
1. Sequential recharge scheme used.
2. High rate charge time sized to give a 100% A-hr. return.
3. Discharge rate is fixed at C/2.25 (12.0 Amperes).
4. High rate charge is fixed at C/13.5 (2.0 Amperes).
5. Trickle charge rate is fixed at C/67.5 (0.4 Amperes).

Table 4. COMPARISON OF 2505 and 2117 SEPARATOR PROPERTIES

Property	2505 Separator[1]	2117 Separator[2]
Filament Type	Nylon 6	2/3 Nylon 66 1/3 Nylon 6
Weight (gm/m^2)	60 ± 8	74
Thickness (mm)[6]	0.38 ± 0.07	0.30
Breaking Strength (kg) Parallel to machine direction Across machine direction	 2.3 3.2	 NA[5] NA
Electrolyte absorption (wt-%)	800(min)	580
Air Permeability (cfm ft^2 at 0.5 in. H_2O)	200(min)	142
Bonding method	Chemical[3]	Heat [4]
Calendaring	No	Yes[4]
Residual Impurities	Anti-static coating; both materials are treated by GE to remove these.	
Hydrolysis Reaction Rates	No quantitative data however Nylon 66 oxidation rate is less than Nylon 6.	
Shrinkage (31% KOH, 70°C, 200 hrs)	1% (max)	1% (max)
Wetability (minutes in 31% KOH)	5 (min)	5 (min)

Notes:
1. Typical measured values taken from reference -1.
2. From data supplied by G.E.
3. Stabilized zinc chloride bonded nylon.
4. Hot inert gas (argon) bonded nylon.
5. No data available.
6. Cady gauge.

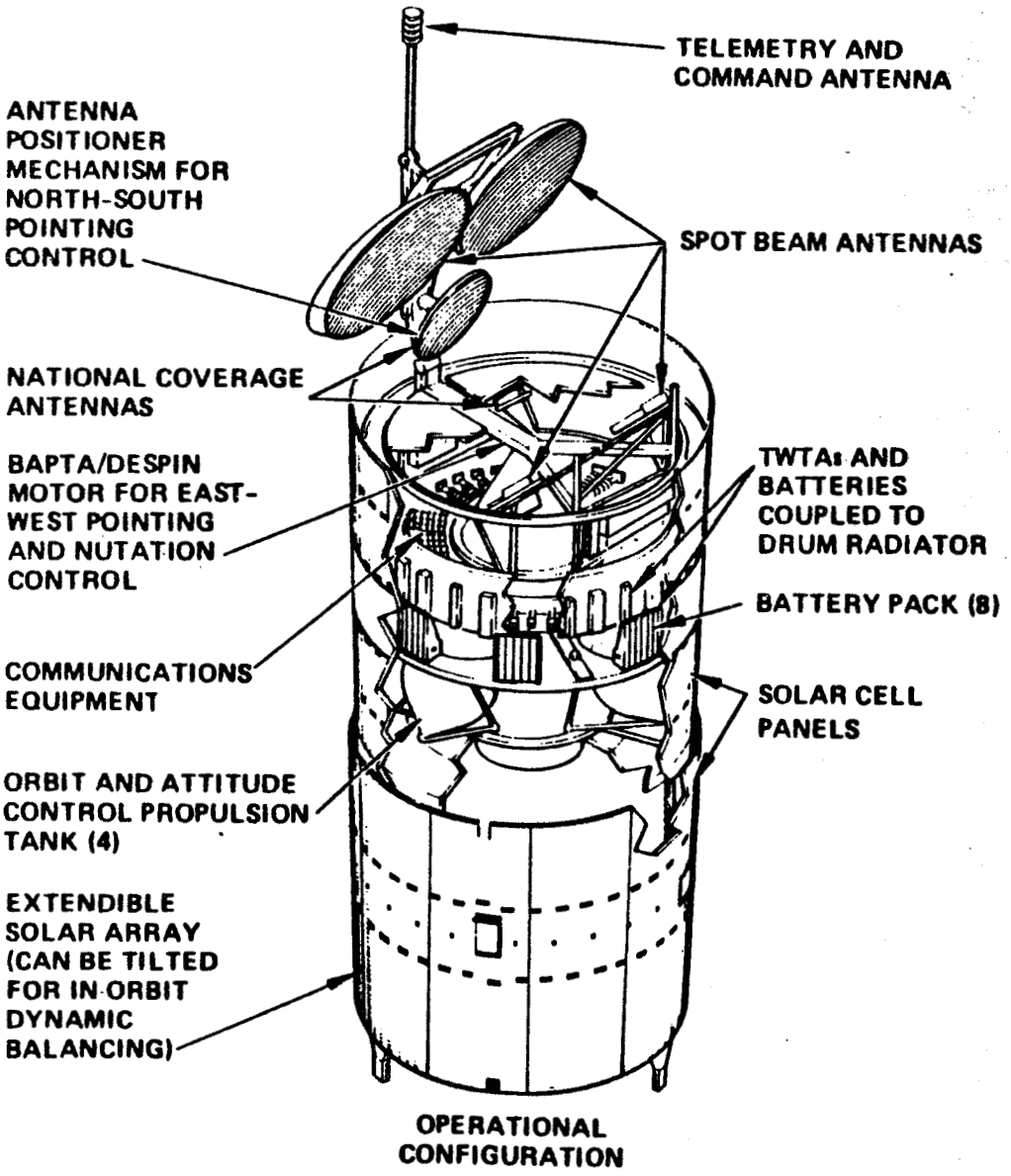

Figure 1. Aussat Spacecraft Configuration

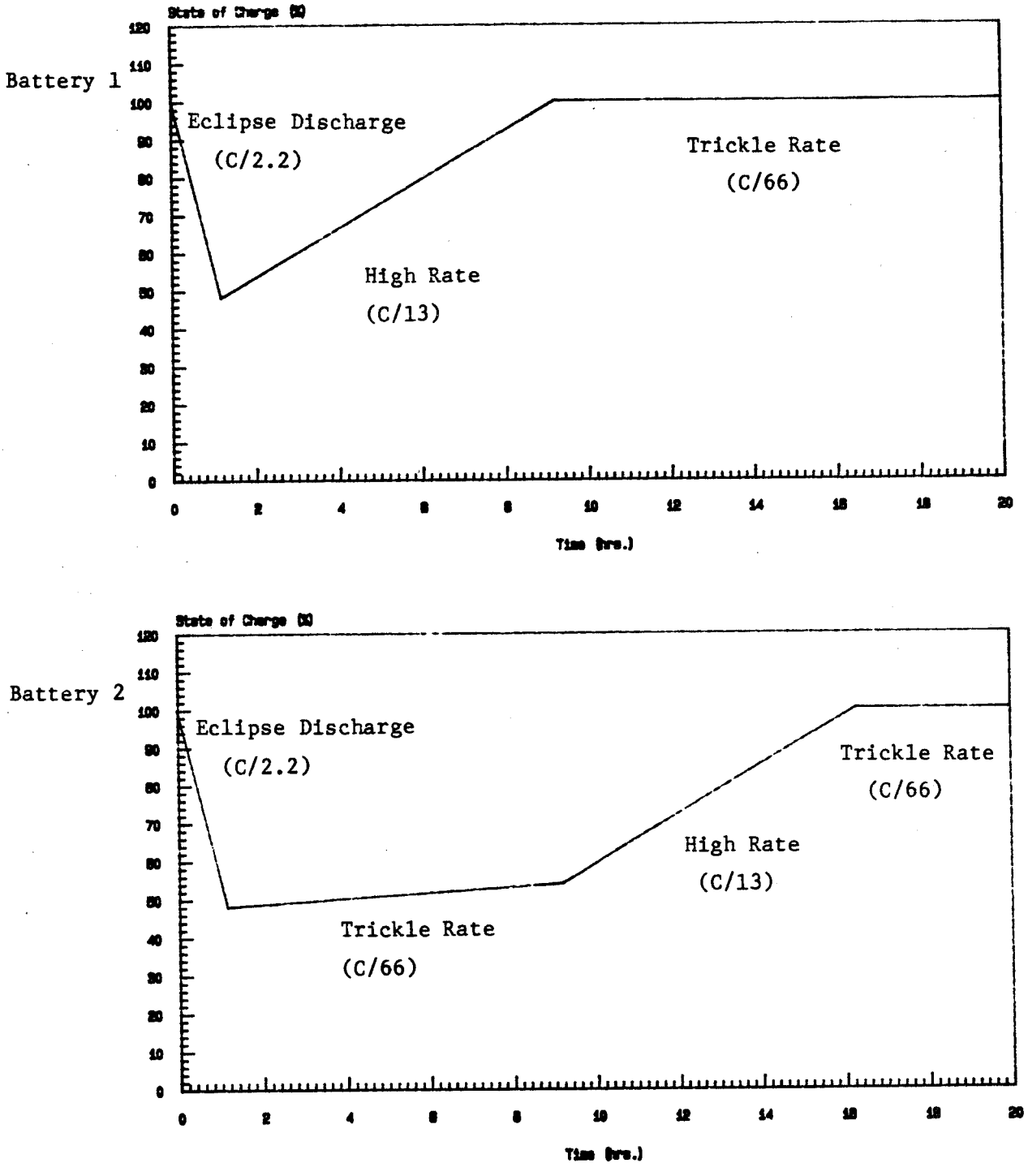

Figure 2. Aussat Battery Sequential Charging Scheme

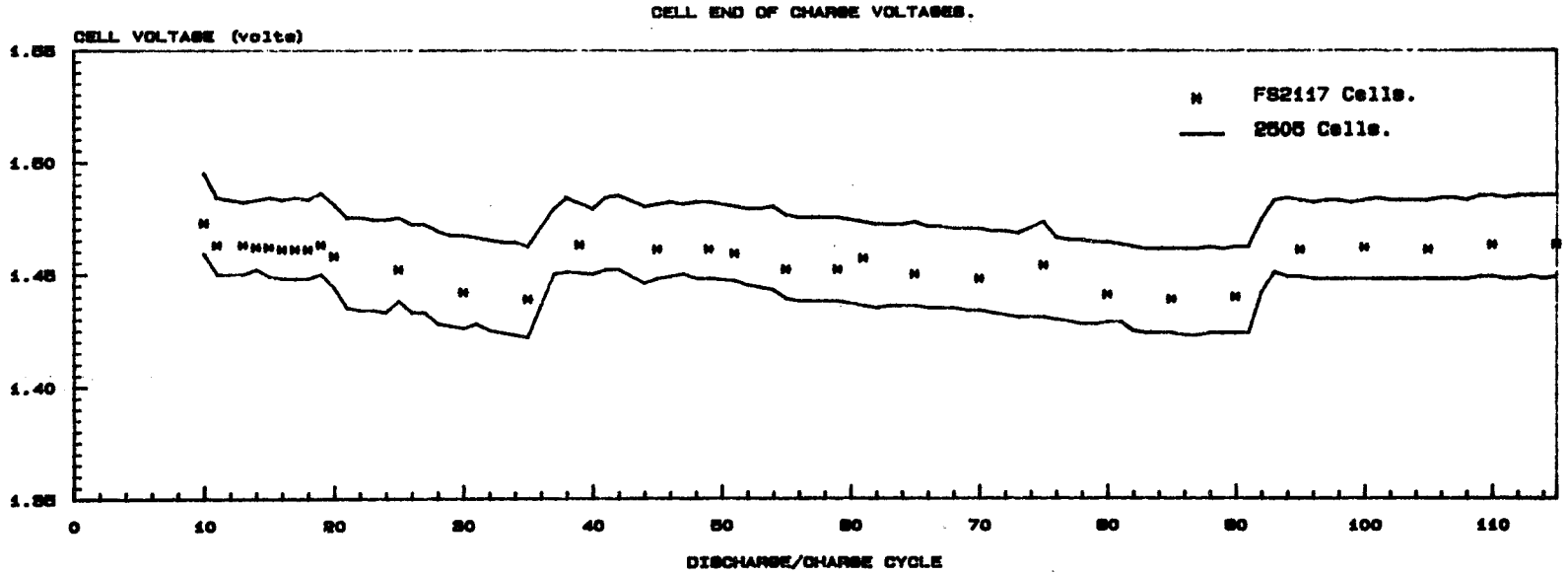

Figure 3. Through-put Test Results

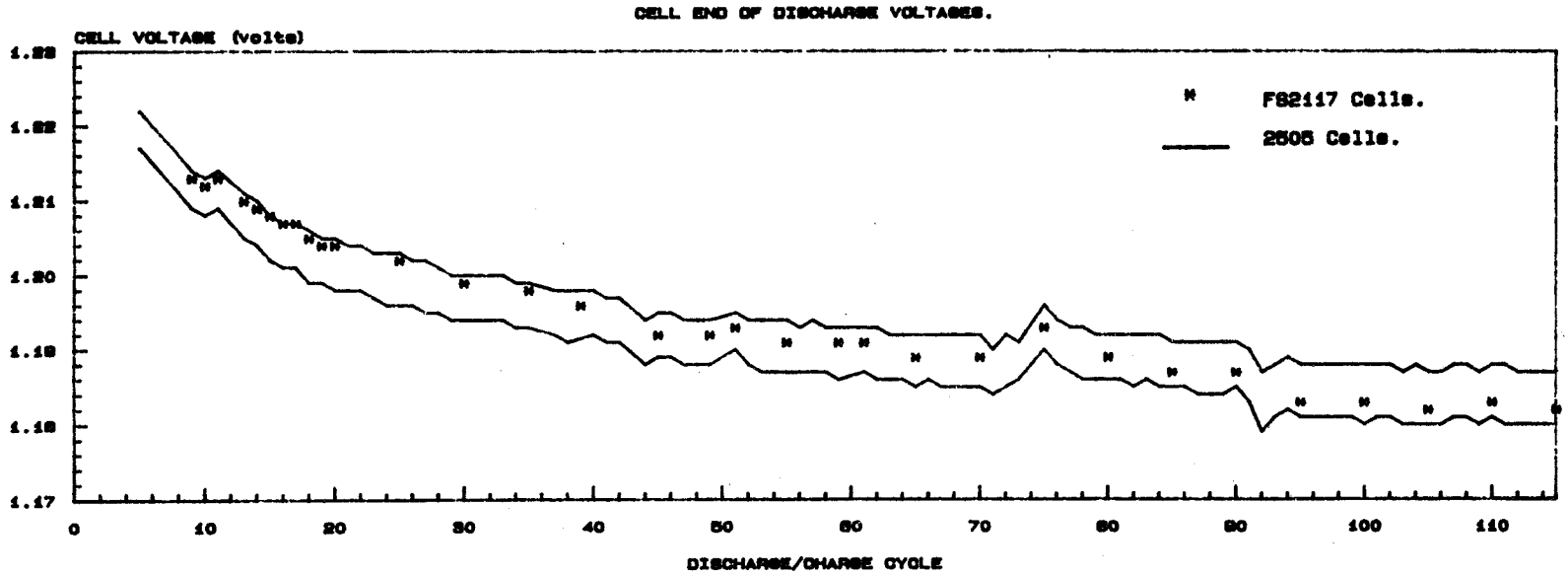

Figure 4. Through-Put Test Results

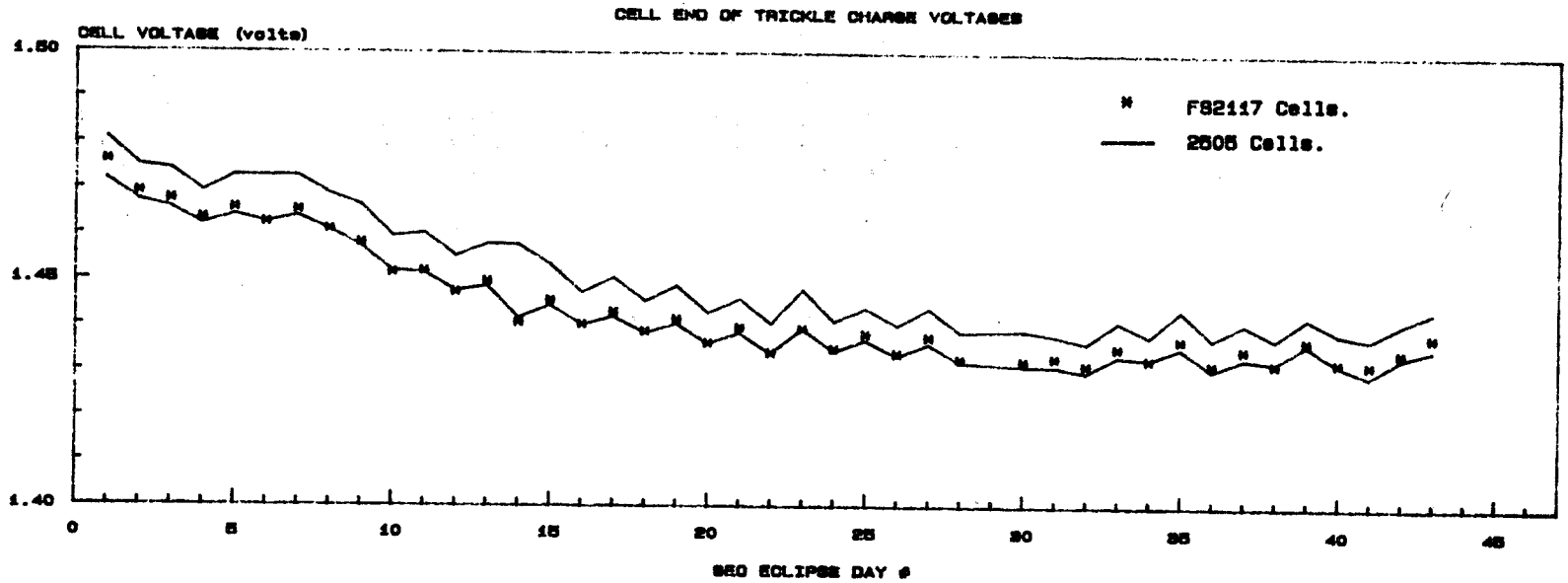

Figure 5. Real Time Eclipse Test Results

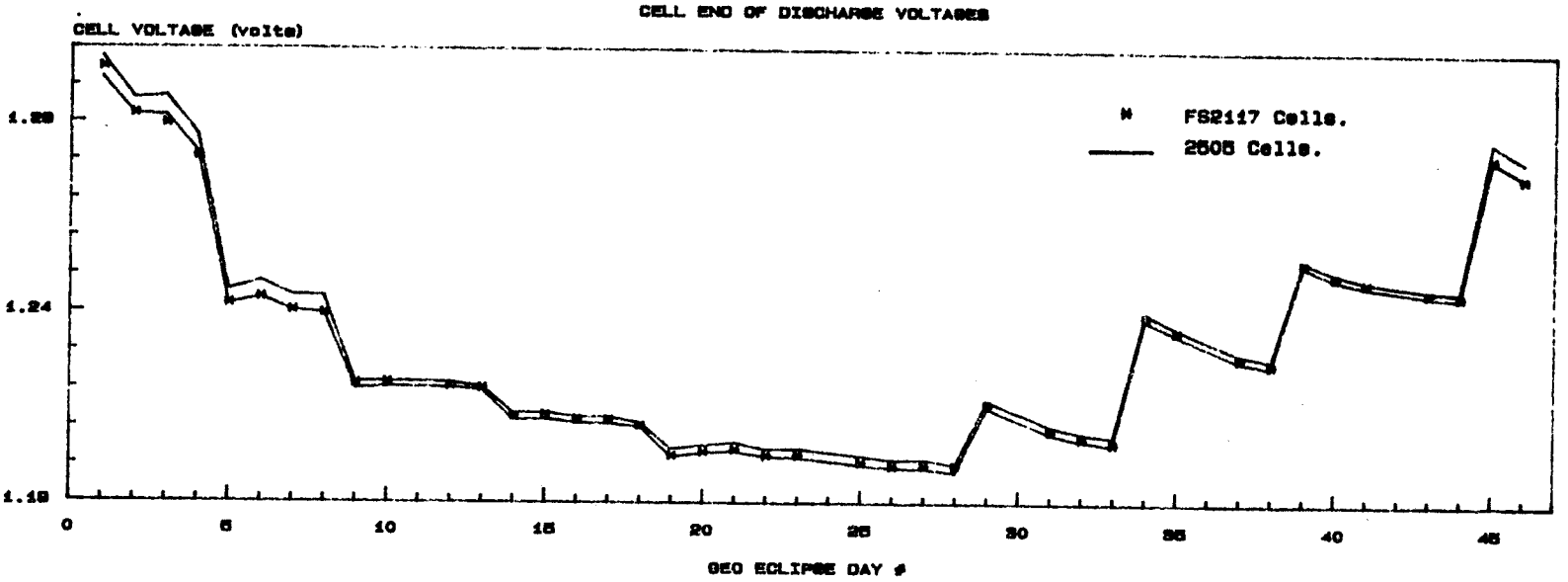

Figure 6. Real Time Eclipse Test Results

FLIGHT EXPERIENCE OF SOLAR MESOSPHERE EXPLORER'S TWO NICKEL-CADMIUM BATTERIES

Jack Faber
SME Flight Analyst
Laboratory for Atmospheric and Space Physics
University of Colorado
Boulder, Colorado

ABSTRACT

This paper summarizes the performance of the power system on the Solar Mesosphere Explorer (SME) since launch and predictions for continued operation for the rest of the projected mission. The SME satellite's power system was characterized by both insufficient loading and excessive battery charging during the first year of the mission. These conditions affected battery performance and jeopardized the long-term mission. Increased loading on selected orbits has improved battery performance. Long term projections indicate steadily increasing temperatures for the remainder of the mission.

INTRODUCTION

SME was launched 6 Oct 1981 into a nearly circular, sun-synchronous earth orbit at an altitude of 534 km. Each 95 minute orbit at launch included 65 minutes of sunlight (battery charging) and 30 min of darkness (discharging). The attitude of the spacecraft is maintained with a constant sun angle of 37 degrees.

DESCRIPTION OF SME'S POWER SYSTEM.

The main emphasis of the design was to provide a simple, highly autonomous power system (fig 1). The secondary goal was to keep cost as low as possible. This was accomplished by using flight proven technology and hardware. SME was designed to have excess power capability throughout the first 18 months of the mission.

SME has an unregulated, direct energy transfer power system. Power is generated by fourteen parallel diode protected solar array panels, three of which can be commanded on and off line. The energy is stored in two nickel-cadmium batteries containing 21 cells each. While charging to each battery can be disabled, both batteries can discharge through a diode even when commanded off line. Overcharge protection is provided by a shunt regulator

that can be commanded to shunt at one of four voltages-temperature (VT) levels (fig 2). These VT levels determine clamp voltages which are based on the desired full charge capacity and the temperature of the batteries. The spacecraft contains an automatic cell failure protection system. One of the batteries will be taken off line if the voltage of its upper ten cells deviates 190 mV from that of its lower eleven cells. Undervoltage protection is provided by logic that will turn off all non-essential loads if the voltage drops below 23.7 volts. Additional loading is provided by an internal resistive load, called the dummy load, which draws 1.4 amps.

DEFINITION OF PROBLEM AT LAUNCH

Upon launch the recharge ratios (coulombs of charge divided by coulombs of discharge) were high enough to cause cell voltage instability during the clamped portion of charge. Under ideal operating conditions the upper and lower halves of the battery would be balanced. However, the voltage in the upper cells of battery I soon became 190mV greater than the voltage in the lower cells and the automatic cell monitor took battery I off line. Because the batteries are in parallel it is undesirable to switch the batteries on and off line. To solve the problem of high cell imbalance several options were available: the automatic cell balance monitors could be disabled, battery I could be kept off line for the remainder of the mission, both batteries could be used one at a time by switching batteries on and off periodically, additional loading could be applied to both batteries in parallel, both batteries could be kept on line until one of the batteries became unbalanced and then that battery could be deep cycled by commanding additional loads on with only that battery on line. The decision was made to minimize the potential hazards to the spacecraft by maintaining cell imbalance as low as possible, disabling the automatic cell monitor function and reaching a minimum voltage of 24.5 volts at least twice a day.

BATTERY ONE DISABLED

During the first 215 orbits of the mission (6 Oct 1981 - 21 Oct 1981) the loading on the batteries resulted in an average depth of discharge (DOD) of 1 AMP-HR out of 12 AMP-HR or 8% of the name plate capacity. This resulted in a minimum voltage on the spacecraft of 26.8 volts. During this time the positive cell imbalance (upper cell voltage greater than lower cell voltage) on both batteries rose until the cell monitor logic disabled charging to battery I. To condition the batteries the dummy load was turned on for 2 full orbits with charging disabled to battery I. The clamp voltage was also reduced by switching to VT level 4

for the remainder of the mission. This resulted in a DOD of 11%. On orbit 306 the dummy load was turned on for 7 consecutive orbits with charging disabled to battery II. This resulted in a DOD of 14%. The cell monitors on both batteries improved in both the negative and positive excursions During this conditioning period it was noted that when the dummy load was turned on for a full orbit the average temperature of the batteries rose .75 degrees C per orbit. This deviated from the optimum operating temperature of nickel-cadmium cells.

BATTERY HISTORY

DISCHARGE

During the course of the mission the maximum voltage (FIG 3 MIN-MAX EP28V) on the SME bus has varied from 30 volts to 29 volts. The current drop in maximum voltage is caused by using the lowest VT level as the temperature of the batteries (FIG 4 AVE TPBAT1) increases. The depth of discharge of the batteries (FIG 3 MIN-MAX EP28V) has steadily decreased from 25.5 volts to the current 24.5 volts. This has been achieved by increasing the amount and duration of loading (FIG 5 MAX EPL0I) during eclipse. Currently twice each day all available loads are turned on for the duration of two uniformly separated eclipses.

CHARGE

The charging of the batteries has been controlled by the number of solar array panels turned on (FIG 6 AVE EPSAST). Due to changes in the solar intensity (FIG 7 MAX EPSAI) it has been necessary to switch some of the arrays on and off to adjust for incorrect charge rates (FIG 8-11 EPB1C,EPB2C). The number of solar array panels turned on has been adjusted from the maximum of 13 panels to the minimum of 11. Currently all switchable arrays are off.

CELL IMBALANCE

The cell imbalance monitor (FIG 12,13 AVE EPB1CF,AVE EPB2CF) have responded to changes in charging and discharging. While battery one was the only battery to go offline before the automatic cell monitoring was disabled both batteries have experienced high cell imbalances at various times. The major contributors to high cell imbalance seem to be too high charge rates, too low charge rates, too high a discharge rate at DOD and too shallow DOD.

FUTURE PREDICTIONS

FACTORS AFFECTING BATTERY LIFE

The most important consideration for the power system is the expected battery life. SME was launched with a one year mission which has now been extended. Due to changes in the ascending node time the power system will experience several changes in the next few years. The duration of eclipse of each orbit is shortening from a maximum of 32 minutes during the second year of mission to an expected value of zero during the ninth year of mission The daylight portion of each orbit is lengthening during this same period. The change is a continuous one and has caused the following problems:

1) Temperature of the batteries is increasing. (FIG 14)

2) Duration of battery discharge is decreasing.

3) Rate of discharge at deepest discharge is too high

4) Duration of trickle charge to the batteries is too long.

5) Cell imbalances increasing.

6) Life of the batteries is decreasing.

BATTERY MODELS FOR PREDICTING BATTERY LIFE

Three battery models for life prediction have been considered: McDermott model, Lander model, JPL failure model[ref 7]. The temperature predictions for the remainder of the mission are a least squares fit of empirically determined factors that affect battery temperature. These factors in order of there significance are:

1) Ratio of daylight/eclipse

2) Distance of satellite from the sun.

3) Effective solar array surface area.

4) Amount of loading on the satellite

The McDermott and Lander models give similar results for the life of the SME batteries at the predicted battery temperatures (FIG 15).

EFFORTS TO EXTEND BATTERY LIFE

The first two factors are outside of our control. The effective solar array surface can be partially controlled and currently all switchable solar arrays are off and the satellite is torqued to provide the minimum possible effective solar array surface area. The amount and duration of loading is the only variable over which we have direct control at this time.

Currently twice per day at approximately 12 hour intervals all available loads are turned on and the load current is increased to a maximum value for the duration of eclipse (FIG 16,17). This discharges the batteries to within .8 volts of the undervoltage cutoff. During this period we see two ominous signs from the batteries. The first is an increase in the cell imbalance in either of the batteries sometimes to levels in excess of .5 volts. This imbalance has occurred at various times on both of the batteries and either just before or just after the transition from eclipse to daylight (FIG 18,19). This high imbalance does not occur when the voltage is above 25.Ø volts. The second problem is an uneven sharing between battery I and II near the end of discharge period below 25 volts the current from battery I increase with a corresponding decrease from battery two (FIG 2Ø,21). This uneven sharing has been a feature of the batteries since the second year of mission.

SUMMARY

The temperature of the SME batteries will be increasing over the next 5 years. This will degrade the performance of the batteries and shorten their life. The life of the batteries may be extended beyond the predicts if they can be conditioned sufficiently and if the shortened eclipse puts increasingly less demand on the them.

REFERENCES

1. Paul Bauer
"Batteries for Space Power Systems", NASA SP-172, 1968

2. Paul J. Rappaport and Arthur M. Frink Jr.
"Sealed Nickel-Cadmium, and Silver-Sink Batteries", Progress in Astronautics
and Aeronautics, vol 11, 1963, pp 211-219

3. R. C. Shair and W. Gray
"Hermetically Sealed Nickel-Cadmium Batteries for the Orbiting Astronomical Observatory Satellite", Progress in Astronautics and Aeronautics, vol 11, 1963, pp 221-239

4. Irwin M. Schulman
"Secondary Batteries for Energy Storage in Space", Progress in Astronautics
and Rocketry, vol 3, 1961, pp 479-476

5. Robert C. Hamilton
"Ranger Spacecraft Power system", Progress in Astronautics and Rocketry, vol 4, 1961, pp 19-27

6. Seymour H. Winkler, Irving Stein, and Paul Wiener
"Power Supply for the Tiros I Meteorological Satellite"
Progress in Astronautics and Rocketry, vol 4, 1961, pp 29-47

7. I. Schulman
"Life Prediction Model Comparisons",
The 1981 Goddard Space Flight Center Battery Workshop,
NASA Conference Publication 2217,Nov. 17-19,1981,P201-222

8. G. HALPERT
"A Comparision of Charge Control for
Fixed Array and Sun Oriented Array Missions",
The 1982 Goddard Space Battery Workshop,
NASA Conference Publication 2263, Nov 16-18,P 230-258

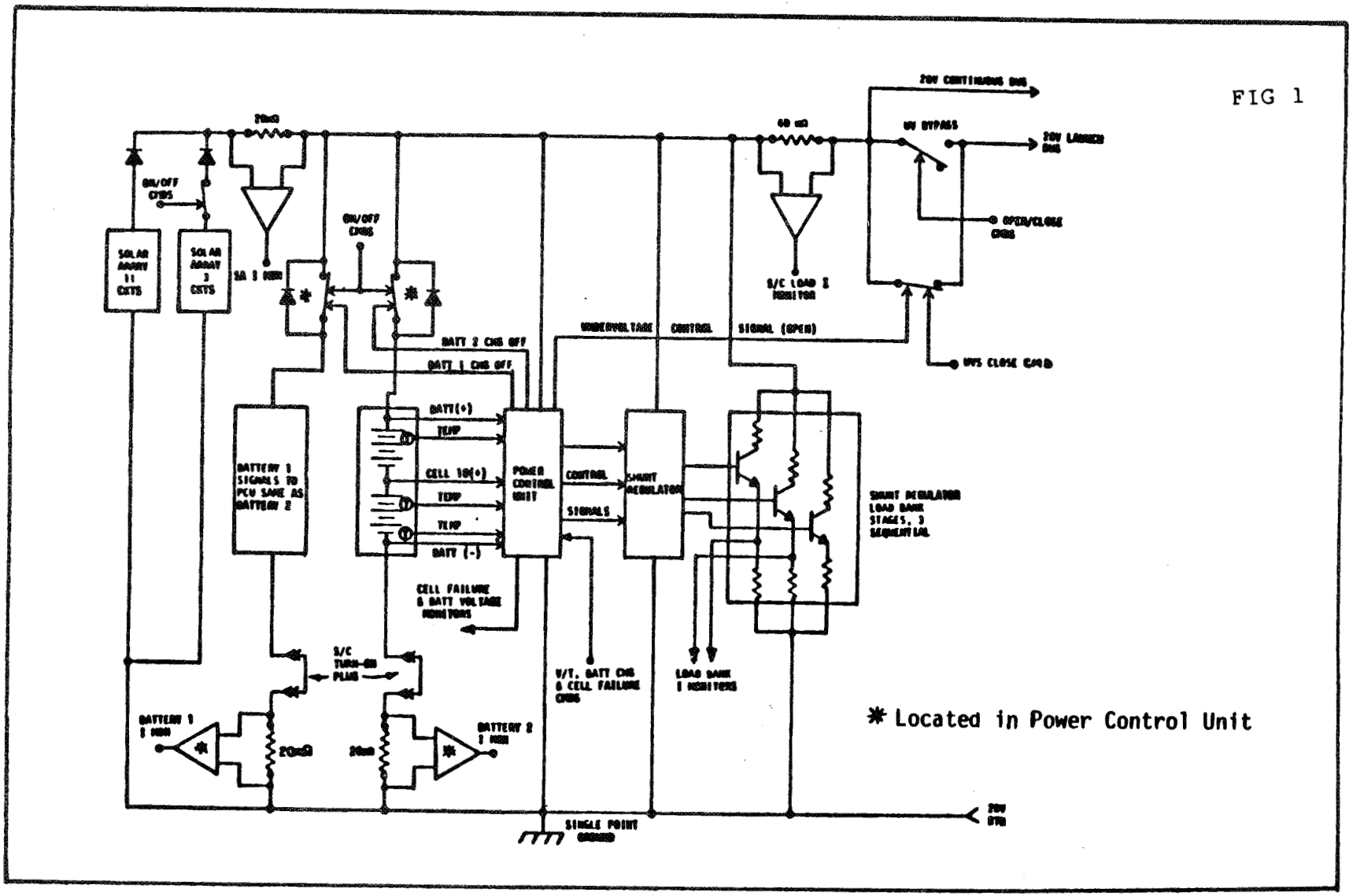

Figure 1. EPS Functional (Simplified)

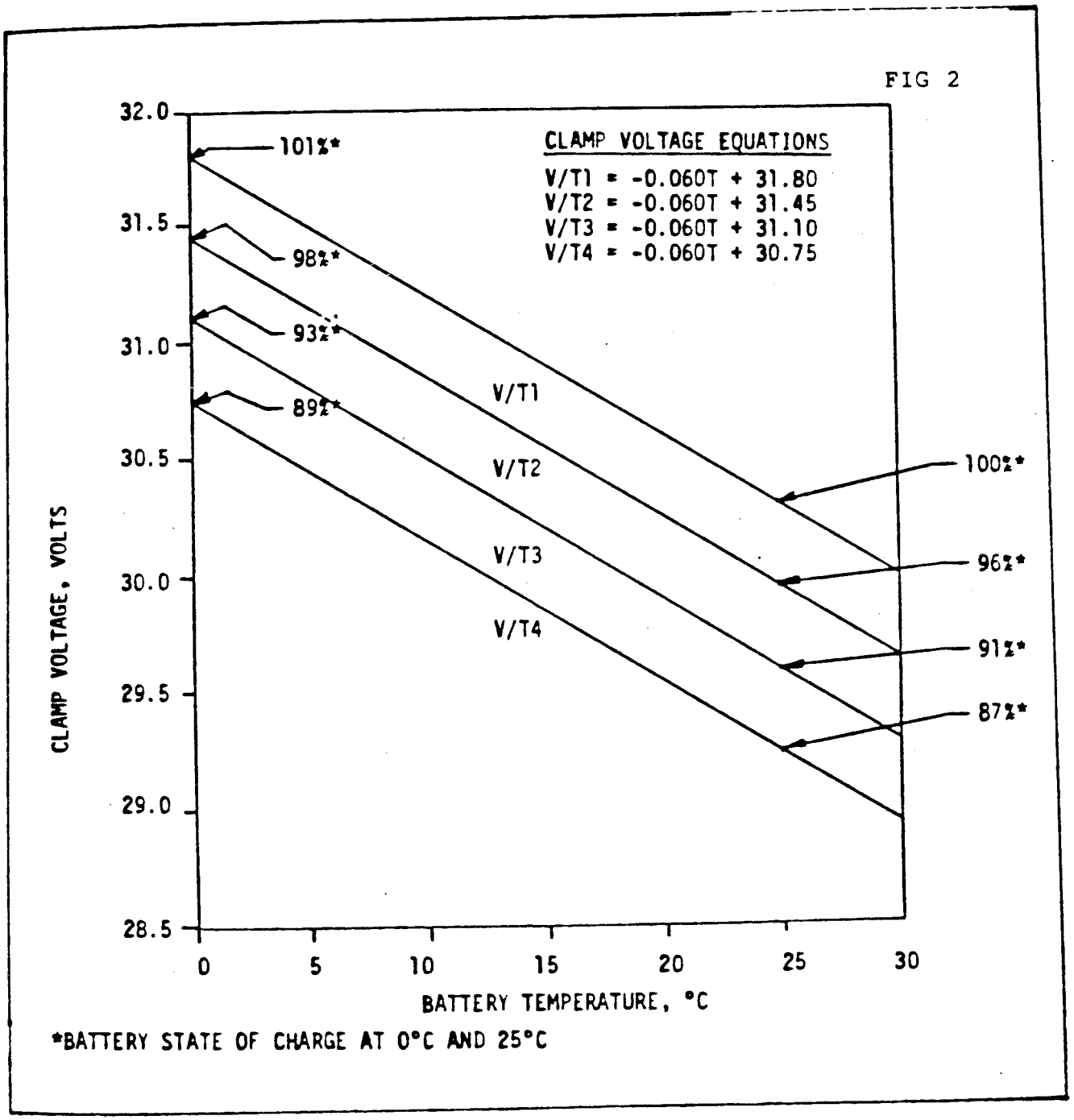

Figure 2. SME Voltage-Temperature Control Levels

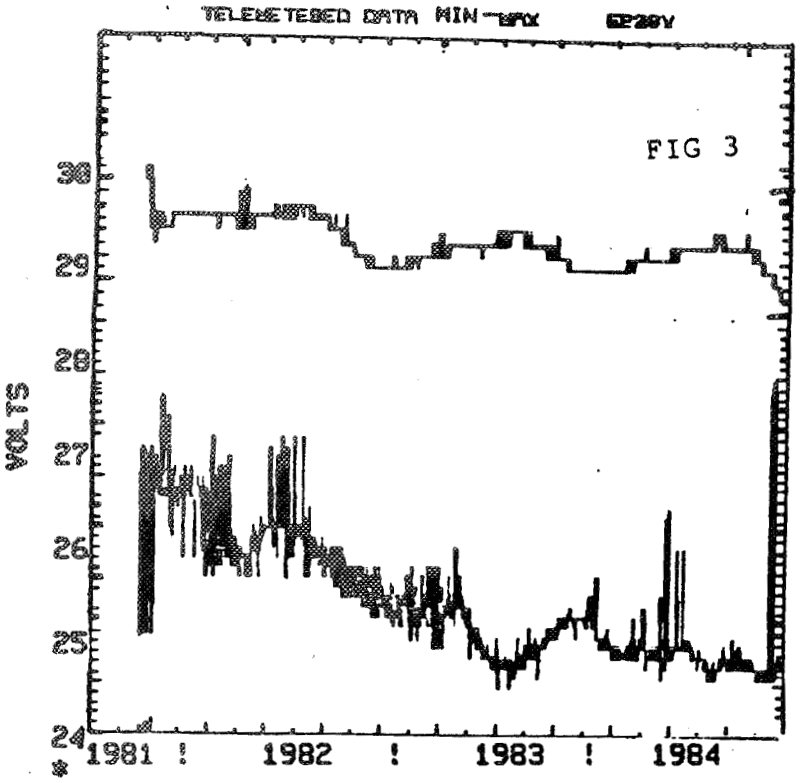

Figure 3.

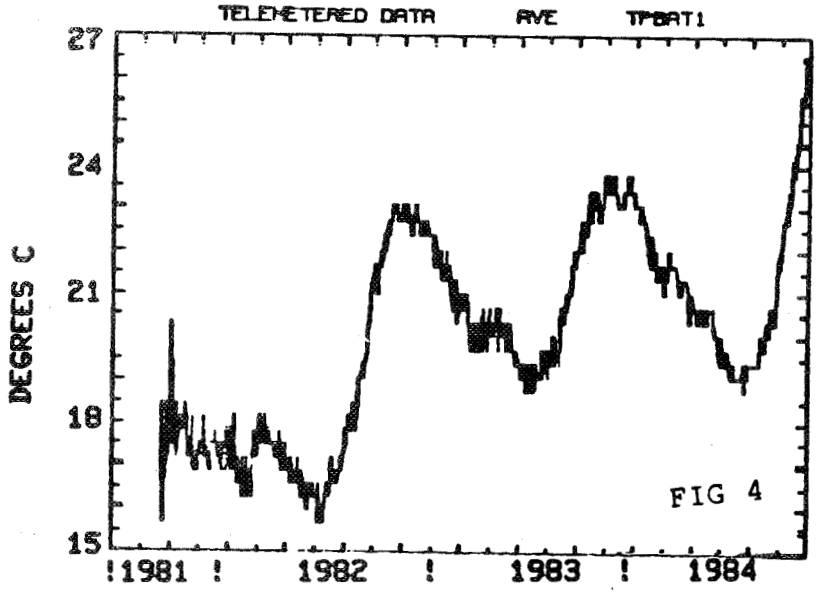

Figure 4.

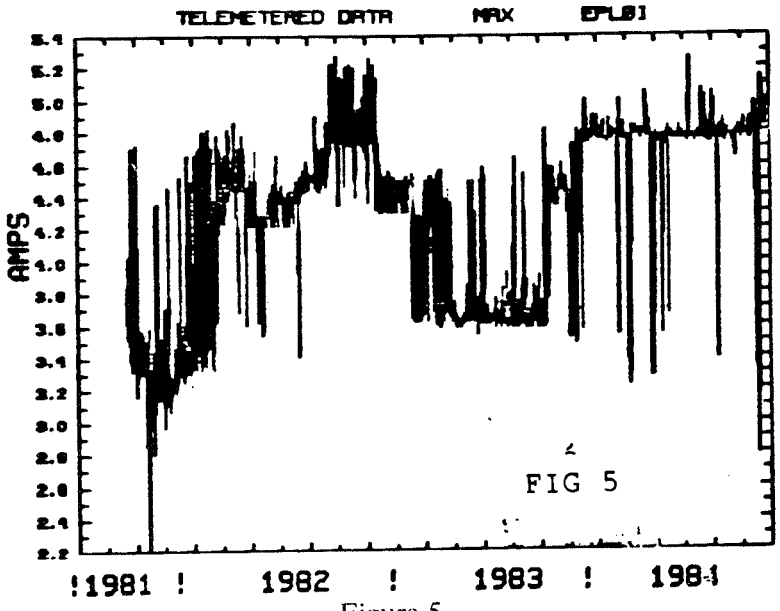

Figure 5.

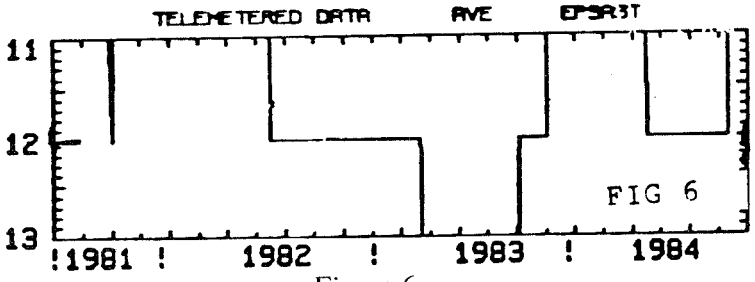

Figure 6.

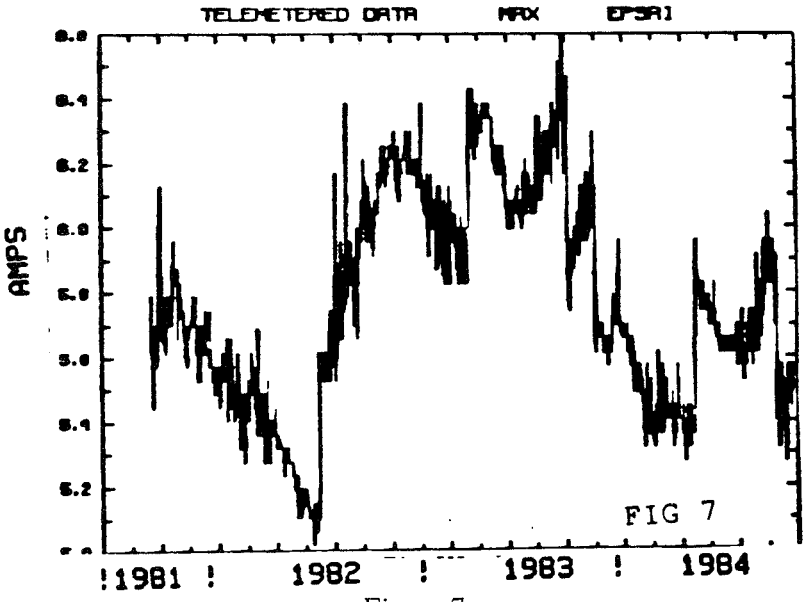

Figure 7.

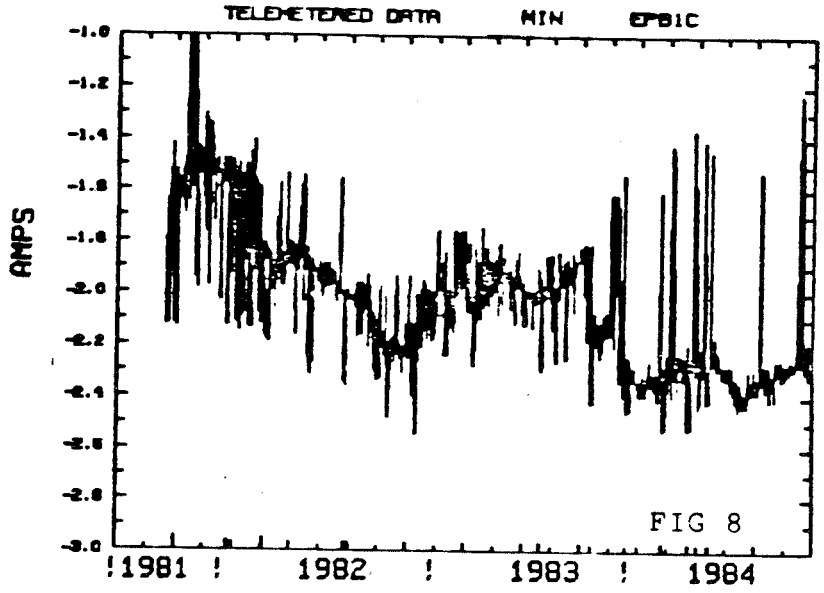

Figure 8.

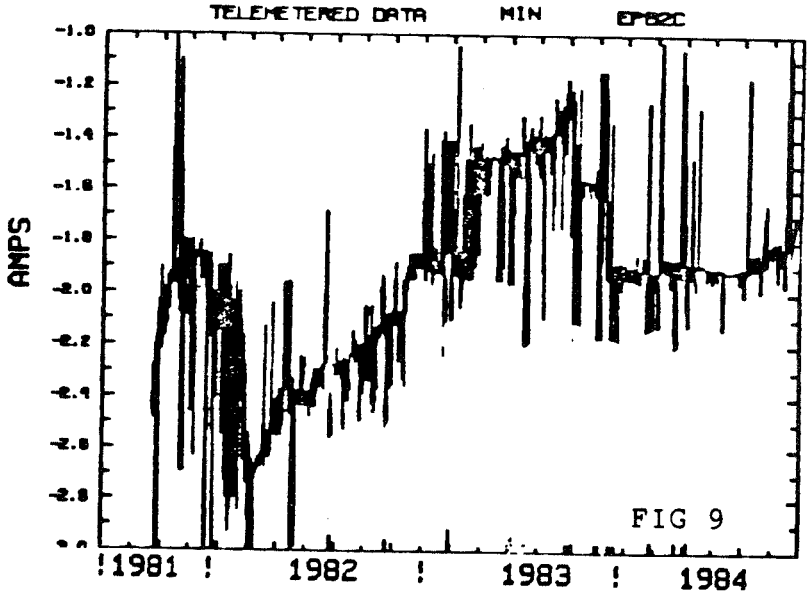

Figure 9.

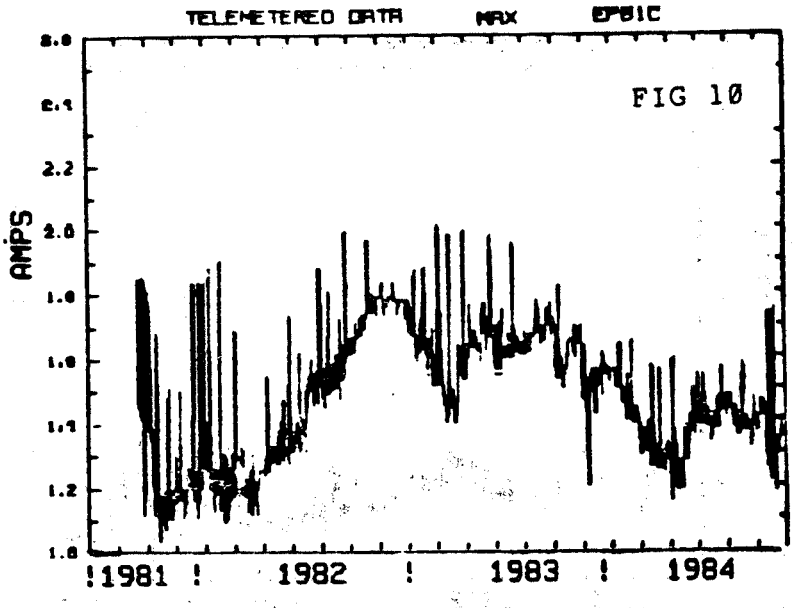

Figure 10.

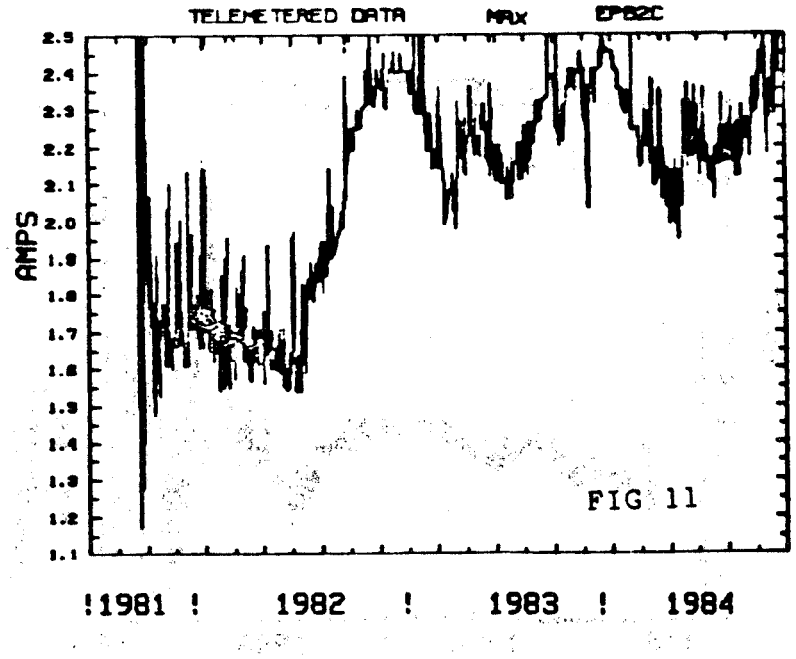

Figure 11.

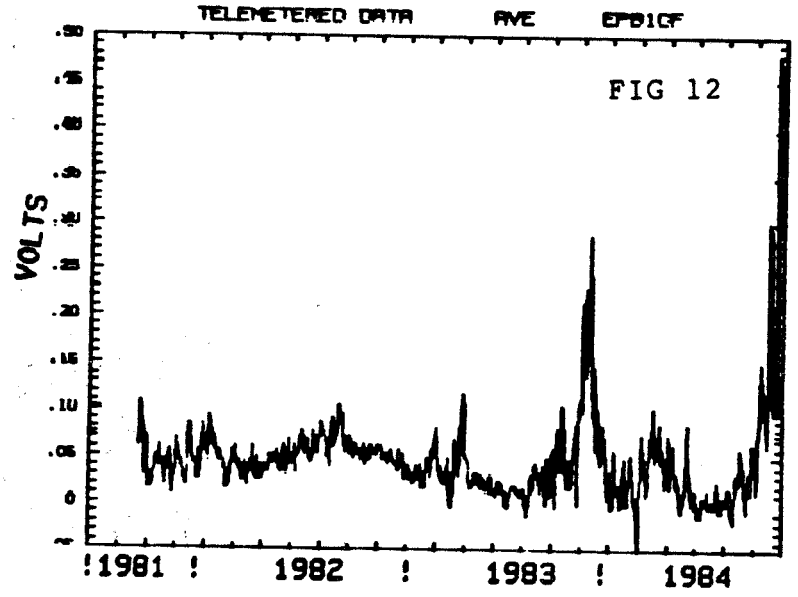

Figure 12.

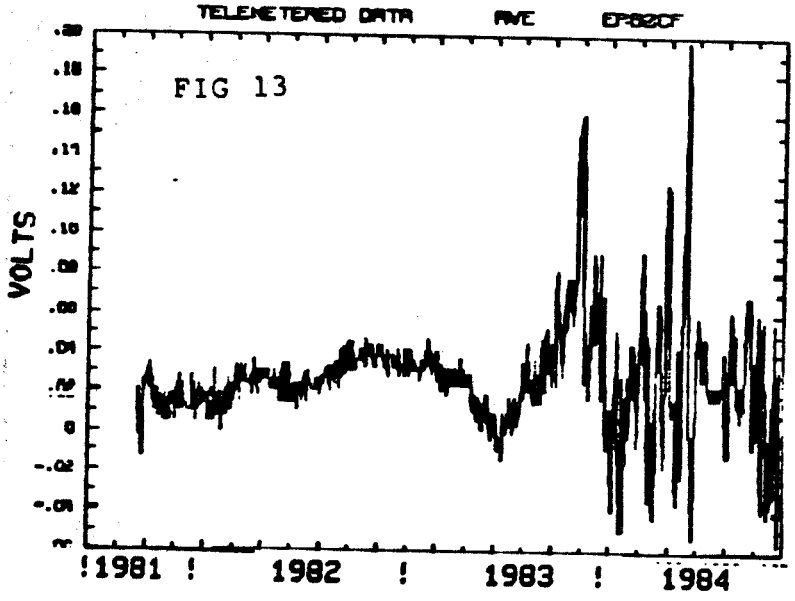

Figure 13.

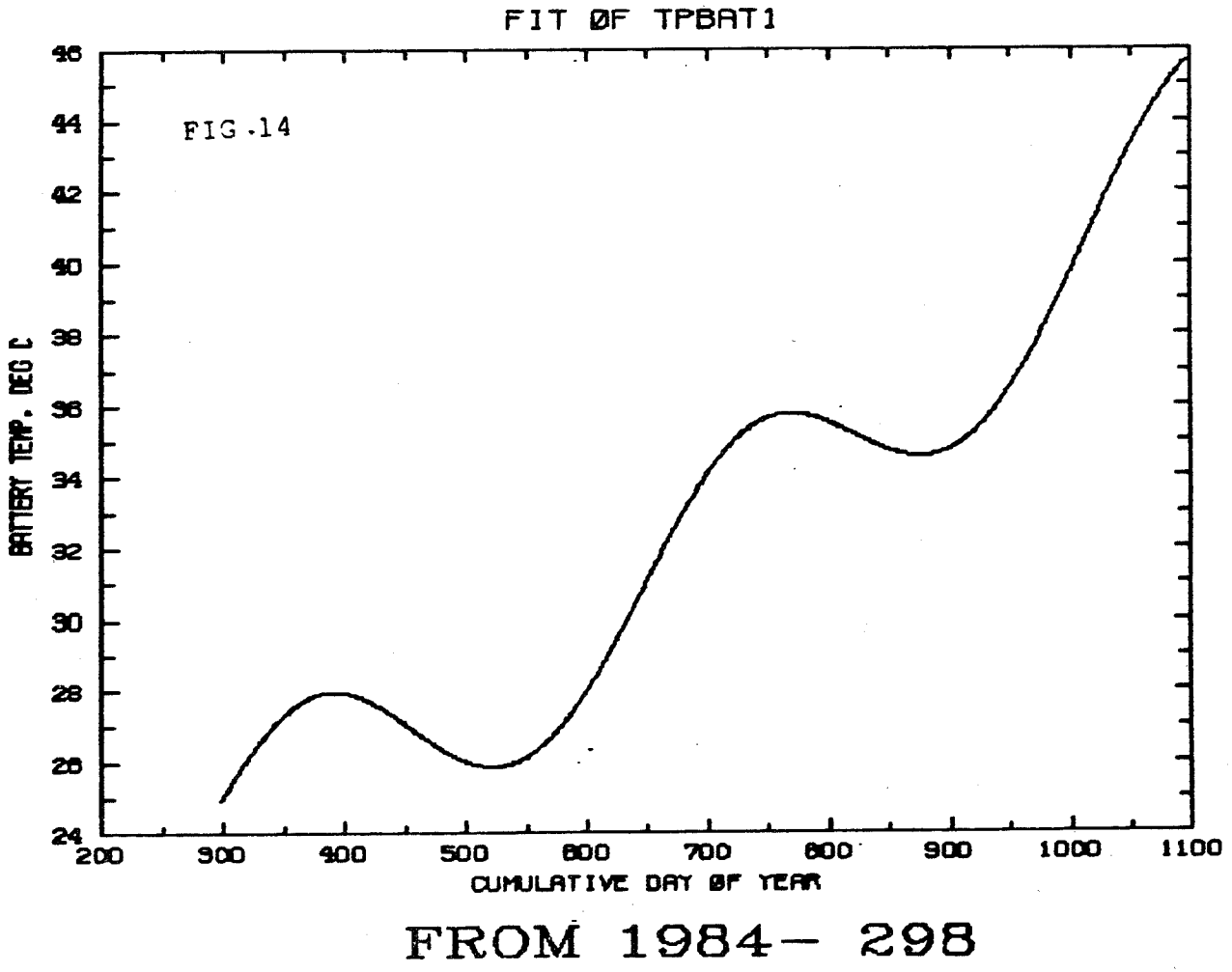
FIT ØF TPBAT1
FIG.14
BATTERY TEMP. DEG C
46
44
42
40
38
36
34
32
30
28
26
24
200
300
400
500
600
700
800
900
1000
1100
CUMULATIVE DAY ØF YEAR
FROM 1984- 298

Figure 14.

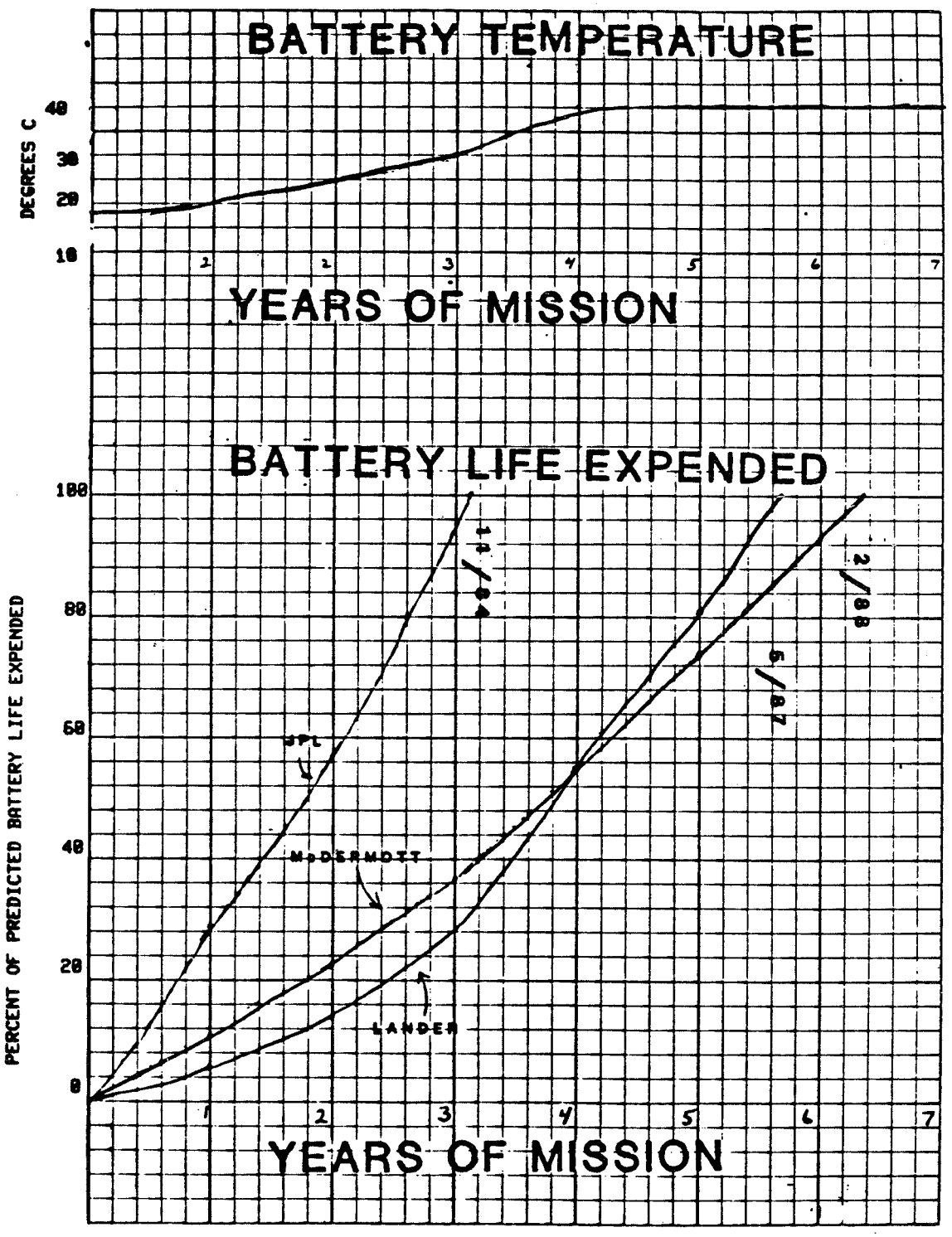
BATTERY TEMPERATURE
DEGREES C
40
30
20
10
1
2
3
4
5
6
7
YEARS OF MISSION
BATTERY LIFE EXPENDED
PERCENT OF PREDICTED BATTERY LIFE EXPENDED
100
80
60
40
20
0
JPL
McDERMOTT
LANDER
YEARS OF MISSION

Figure 15.

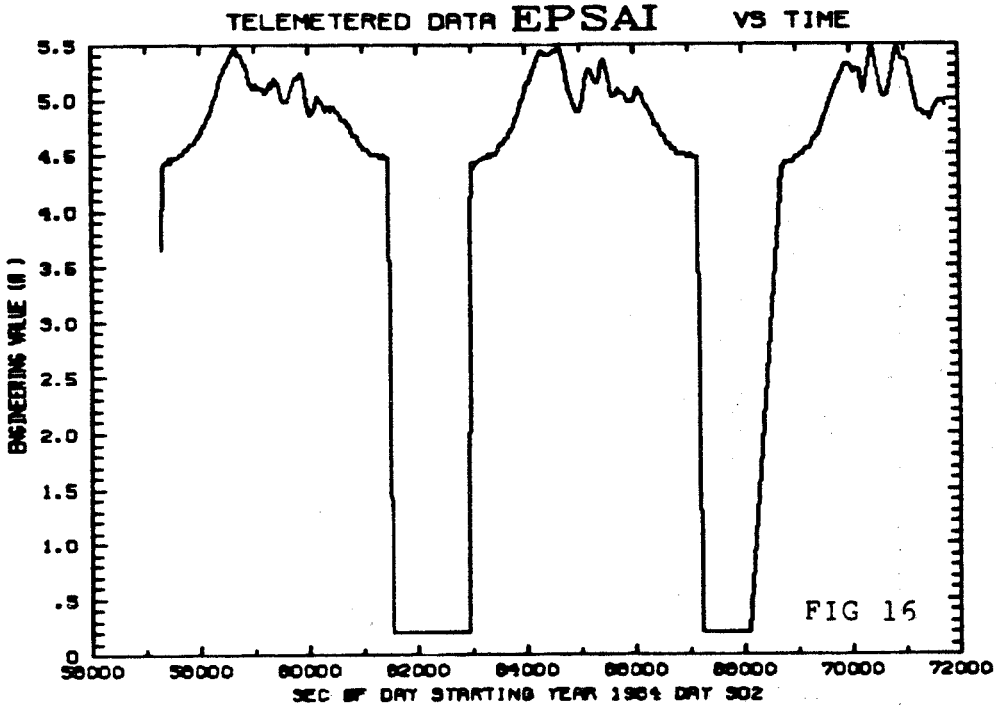

Figure 16.

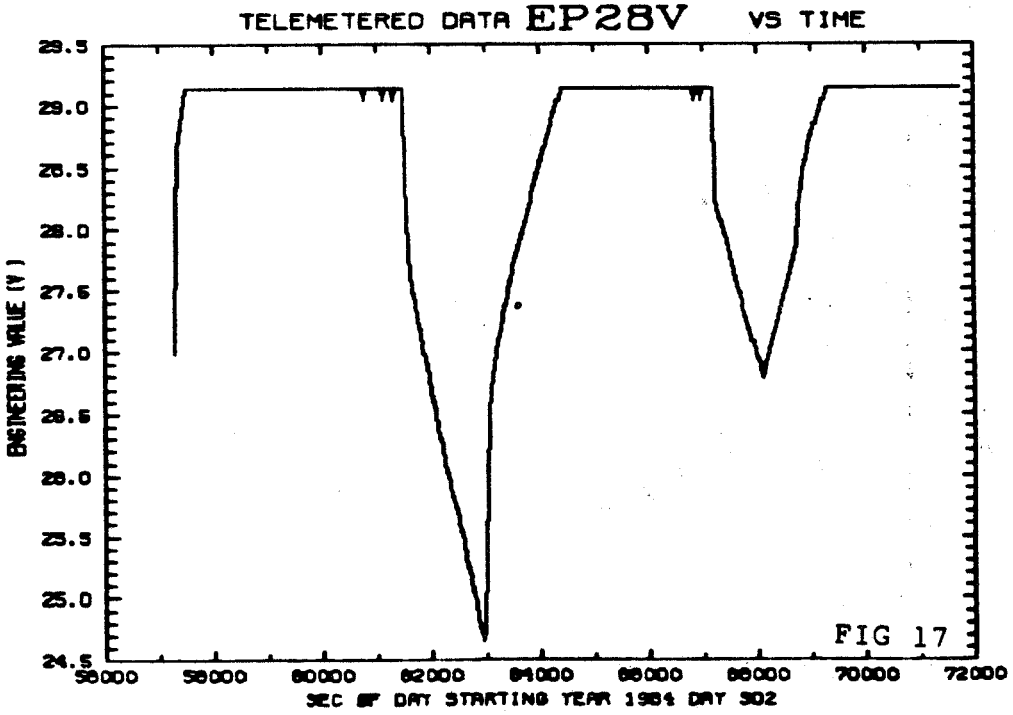

Figure 17.

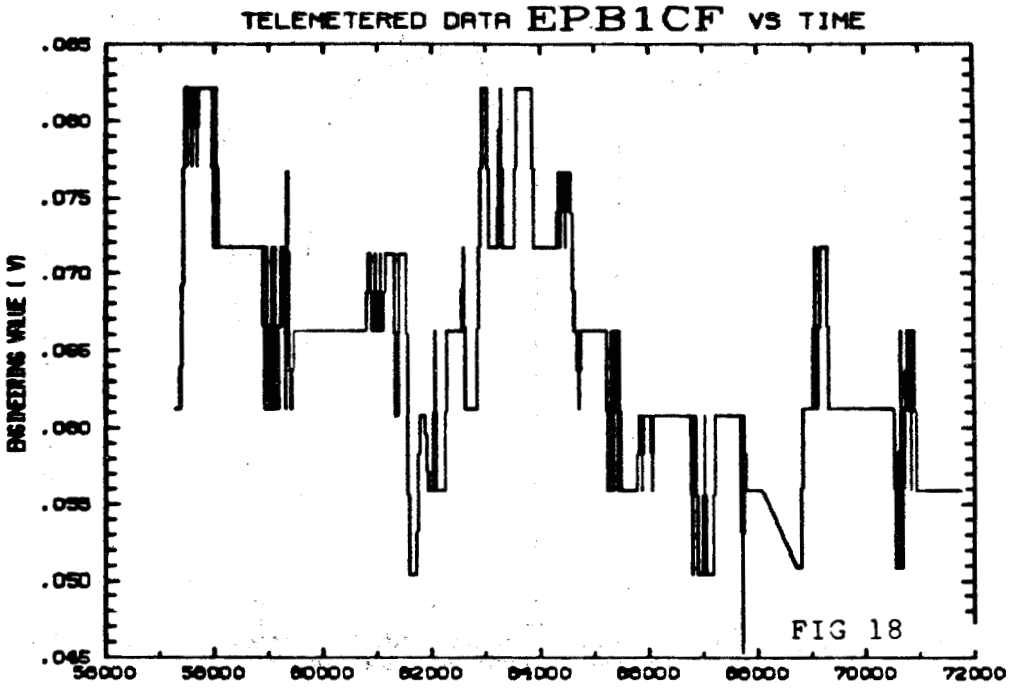

Figure 18.

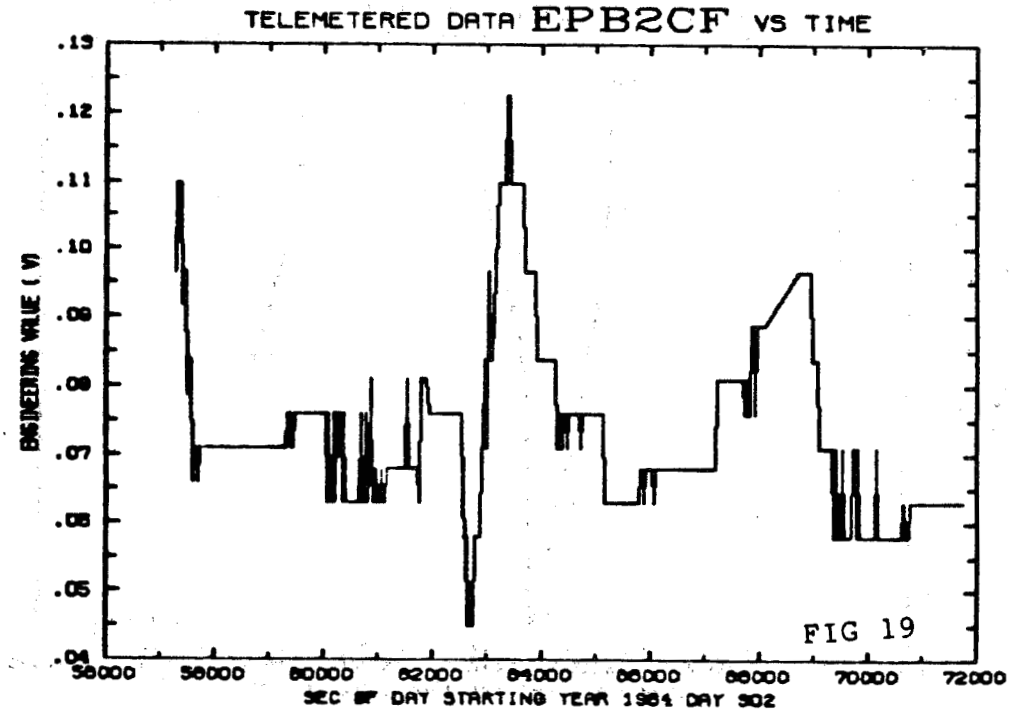

Figure 19.

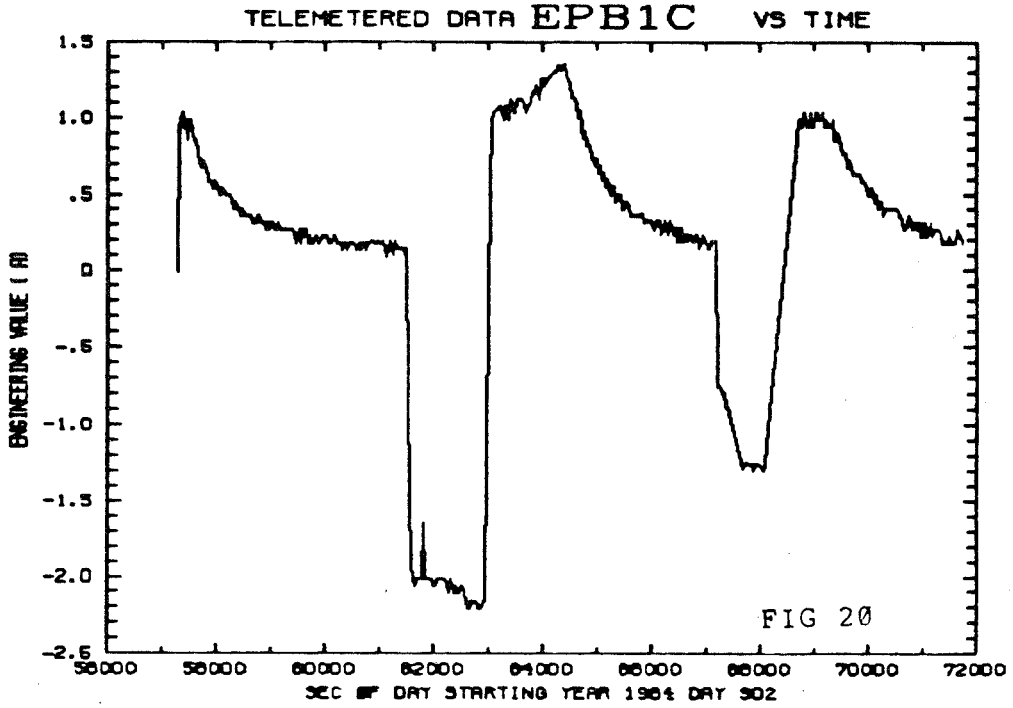

Figure 20.

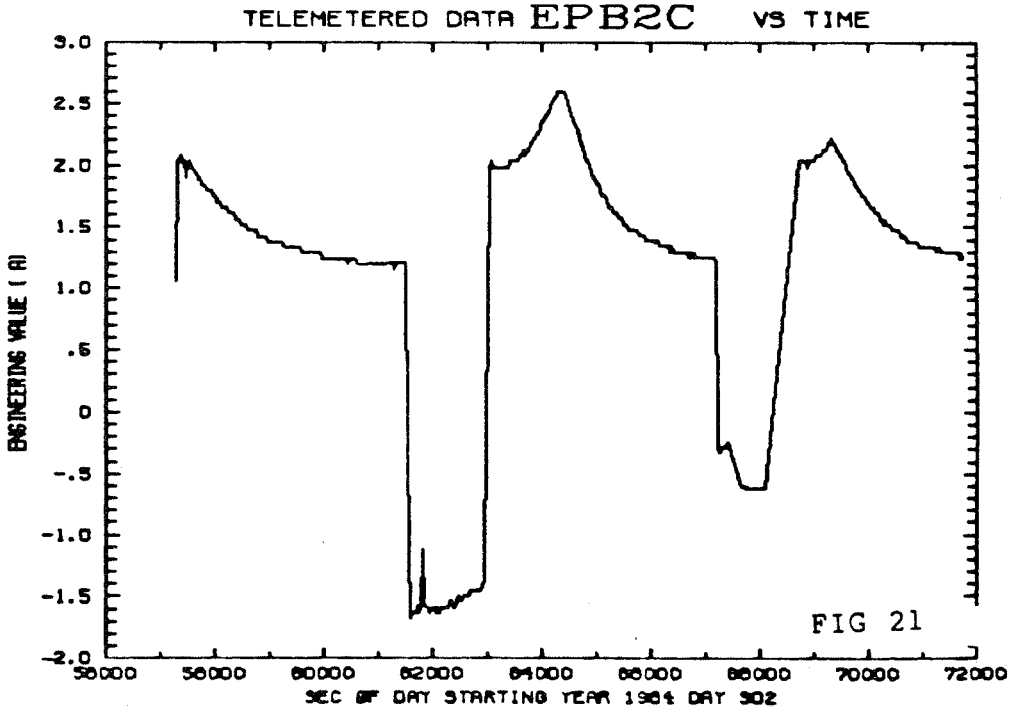

Figure 21.

DEEP RECONDITIONING OF BATTERIES

DURING DSCS III FLIGHT OPERATIONS*

H. E. Thierfelder, R. J. Stearns and P. W. Jones

General Electric Space Systems Division

ABSTRACT

Deep reconditioning of batteries was defined at the 1982 Workshop as "discharge below the 1.0 volt/cell level to a value of about 1.0 volt/battery". This type of reconditioning was investigated for use on the Defense Satellite Communications System (DSCS) Spacecraft, and has been used during the first year of orbital operation. Prior to launch of the spacecraft, the deep reconditioning was used during the battery life test, which has now completed fourteen eclipse periods. Reconditioning was performed prior to each eclipse period of the life test, and is scheduled to be used prior to each eclipse period in orbit. The battery data for discharge and recharge is presented for one of the life test reconditioning cycles, and for each of the three batteries during the reconditioning cycles between eclipse period #1 and eclipse period #2 in earth orbit.

INTRODUCTION

During the 1982 Goddard Space Flight Center Battery Workshop, battery reconditioning was the subject of Session IV. The panel presented four aspects of reconditioning:

- Deep Reconditioning - discharging lower than 1.0 volts per cell with a resistor across a battery.
- Deep Reconditioning - discharging lower than 1.0 volts per cell with resistor across each cell.
- Cost versus benefits.
- Effect of reconditioning on the nickel electrode .

In 1981, we presented a progress report of the DSCS III battery life test, which included the reconditioning procedure. The DSCS III power subsystem includes a reconditioning circuit for each of the three batteries. By command, each of the batteries can be disconnected from its charge regulator and connected across a single reconditioning resistor. The resistor is sized to limit the discharge current to the one hundred hour rate for a fully charged battery. When the battery voltage drops to 18 volts (1.125 volts per cell), a second resistor is automatically added to the discharge circuit, to limit the discharge current to about the two hundred and fifty hour rate. The discharge is terminated by command when the battery voltage is lower than four volts.

*Air Force Contract F04701-77-C-0004.

This procedure is in the category of "deep reconditioning" as discussed in the 1982 workshop.

LIFE TEST RECONDITIONING DATA

Before examining the flight data, we will review a typical reconditioning cycle from the life test. Figure 1 is data for the discharge and recharge performed between eclipse periods five and six. Battery voltage and current are plotted versus time. The time for discharge is 225 hours (between 9 and 10 days), and the time for recharge is about two days. We budget two weeks for a reconditioning cycle. At the start of battery discharge, the current is .35 amperes, the c/100 rate for the 35 ampere hour battery, and the battery voltage is 21 volts, 1.313 volts per cell for the 16 cell battery. After about 112 hours, the battery voltage has dropped to 18 volts and the discharge current is automatically reduced to .13 amperes, the c/270 rate. The discharge was allowed to continue until the battery voltage dropped to approximately 1.0 volts. At that time, the current had reduced to about 10 milliamps. We have annotated the time when the first cell went into reversal, at about 125 hours, at which time the discharge current was .12 amperes or about the c/300 rate.

In the life test, the battery is recharged by constant current at 2.8 amperes, with the voltage limit at 1.40 volts per cell for the 20°C temperature. After approximately five hours, the battery voltage reaches the limit, the current tapers and reaches steady state at approximately 36 hours.

FLIGHT RECONDITIONING DATA

The DSCS III electrical power subsystem includes three 16 cell, thirty five ampere hour nickel cadmium batteries. Each battery has a dedicated charge regulator and reconditioning circuit. Figure 2 is data for the reconditioning cycle for battery #1 between eclipse period #1 and #2. The time, voltage and current scales are identical to the scales used for the Figure 1 life test plot. The discharge current is not plotted because the discharge current telemetry is not calibrated below 0.5 amperes. However, the temperature is plotted. The automatic switch from high current to low current came at 109 hours, so we can conclude that the battery capacity was about 37 ampere hours, the same as the life test battery. The battery temperature can be seen to remain stable at about 3°C. The discharge was terminated when the battery voltage reached 4.0 volts.

In orbit, the battery is switched from reconditioning discharge to charge by command. When the charge regulator is turned on, it automatically is in the lower current limit mode, and after the battery voltage reaches 16 volts, a command is given to switch to the high current limit mode. The rise to 16 volts occurred within one minute, and so Figure 2 shows an instant rise to 4.65 amperes charge and 21.9 volts. The initial drop-off of charge current is due to rise in battery voltage. After about 13 hours, the battery reached the temperature compensated voltage limit and went into taper charge. Finally, the battery charge current returned to the stable 0.2 ampere charge.

The reconditioning data for battery #1 is very similar to the life test data, and when we look at Figures 3 and 4, the data for batteries 2 and 3 respectively, these data are also very similar. Battery #1 data for DSCS A-1 differs slightly from batteries #2 and #3 in general, because there is an eighteen month difference in the age of the cells.

SUMMARY

Based on the life test data and the flight data, we have confidence that deep discharge reconditioning is beneficial. A comparison of flight A-1 eclipse period #1 data, which was not proceeded with a reconditioning cycle, with eclipse period #2 data, which was proceeded with a reconditioning cycle, is shown in Table 1.

Table 1.

	BTRY #	ECLIPSE PERIOD #1	ECLIPSE PERIOD #2
Max Depth of Discharge	1	54%	58%
	2	51%	53%
	3	53%	57%
Min. Battery Voltage	1	18.6	18.7
	2	18.7	18.8
	3	18.7	18.7

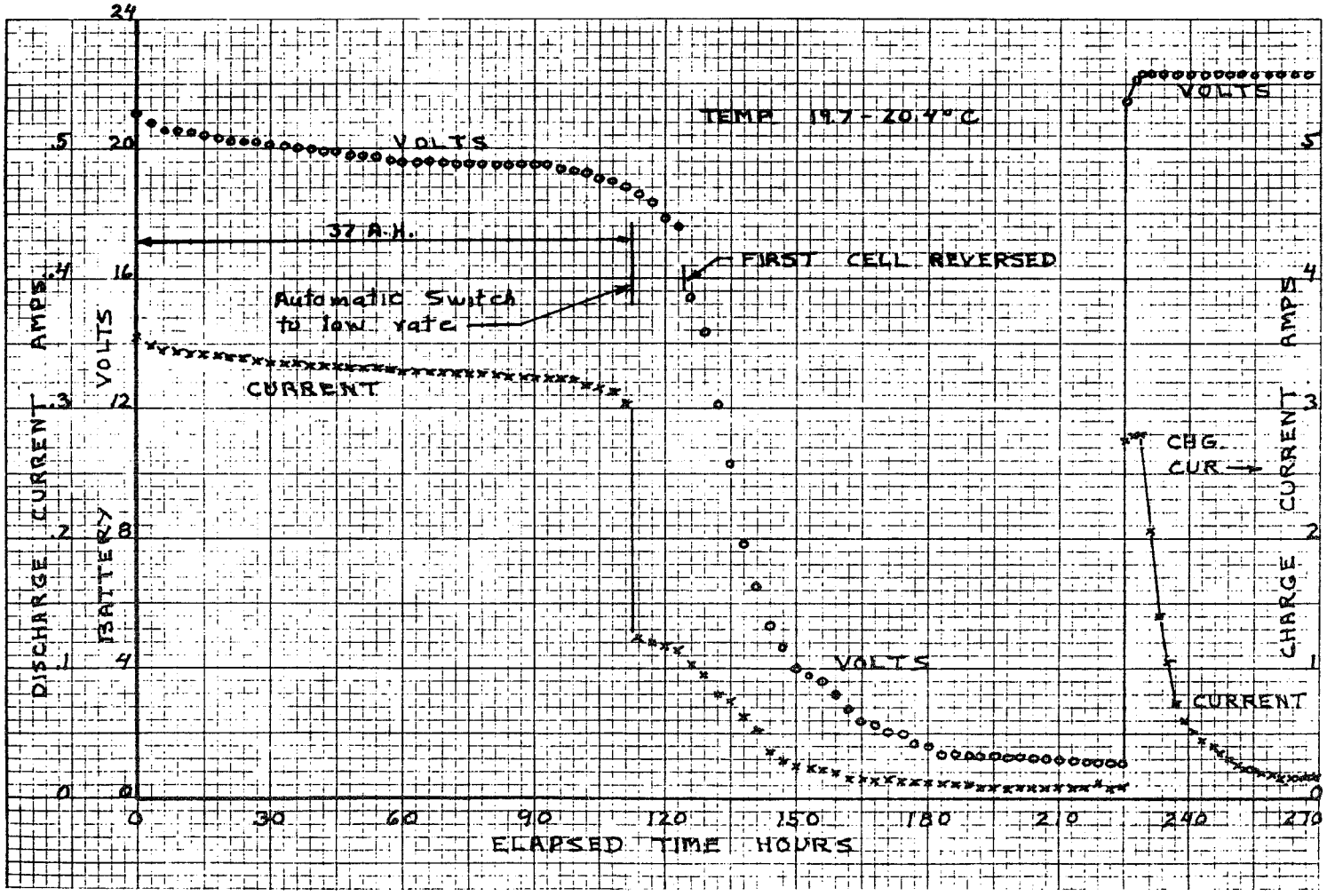

Figure 1. DSCS III Life Test Battery Reconditioning After Eclipse Period No. 5

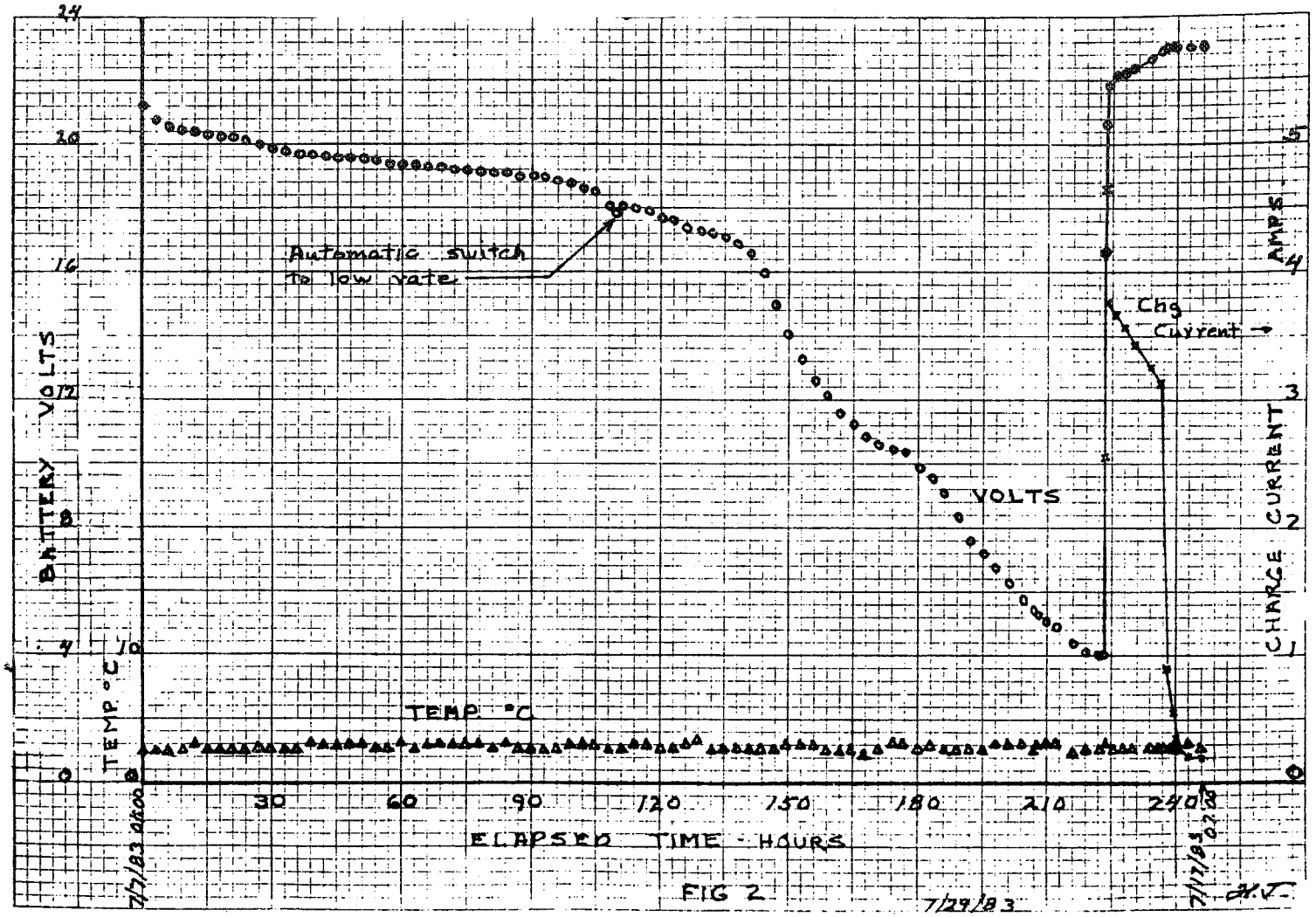

Figure 2. OSCS III A-1 Battery No. 1 (19) Reconditioning 7/7/83 0100 to 7/17/83 0700

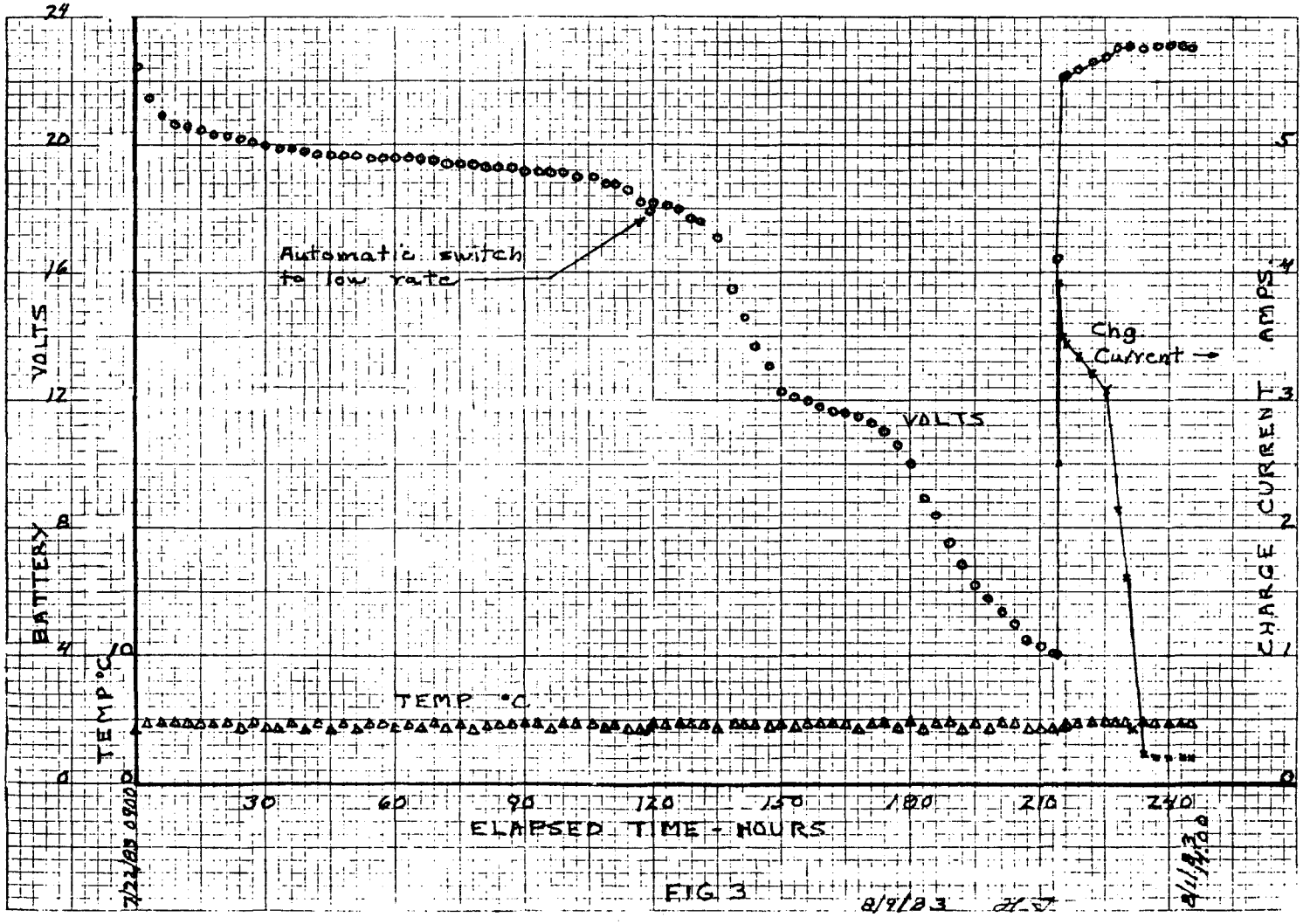

Figure 3. DSCS III A-1 Battery No. 2 (24) Reconditioning 7/22/83 0900 to 8/1/83 1400

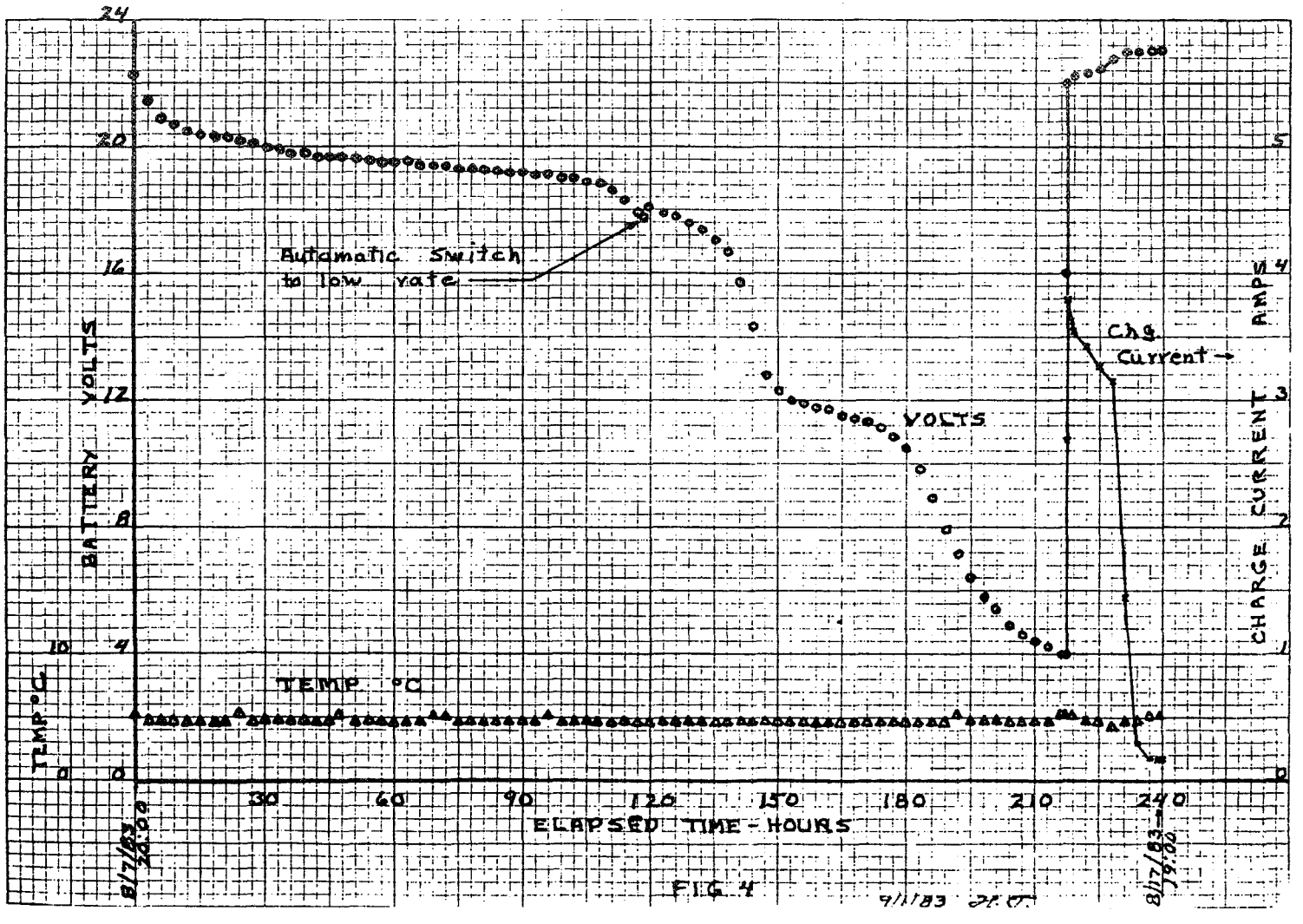

Figure 4. DSCS A-1 Battery 3 (25) Reconditioning 8/7/83 2000 to 8/17/83 1900

SESSION V

NICKEL-HYDROGEN TECHNOLOGY

Chairman: L. H. Thaller
Lewis Research Center

DESIGN PRINCIPLES FOR NICKEL HYDROGEN CELLS AND BATTERIES

Lawrence H. Thaller
National Aeronautics and Space Administration
Lewis Research Center
Cleveland, OH 44135

ABSTRACT

Nickel hydrogen cells and, more recently, bipolar batteries have been built by a variety of organizations. The design principles that have been used by the technology group at the Lewis Research Center (LeRC) of the NASA draw upon their extensive background in separator technology, alkaline fuel cell technology, and several alkaline cell technology areas. These design principles have been incorporated into both the more contemporary individual pressure vessel (IPV) designs that were pioneered by other groups, as well as the more recent bipolar battery designs using active cooling that are being developed at LeRC and their contractors. These principles are rather straightforward applications of capillary force formalisms, coupled with the slowly developing data base resulting from careful post test analyses. The objective of this overall effort is directed towards the low earth orbit (LEO) application where the cycle life requirements are much more severe than the geosynchronous orbit (GEO) application. Nickel hydrogen cells have already been successfully flown in an increasing number of GEO missions.

INTRODUCTION

Reviews of the history, status, progress, and projections related to nickel hydrogen have appeared in a variety of meetings and publications. The IECEC proceedings over the last few years probably contain the best selection of formal papers. The nickel hydrogen technology group at the Lewis Research Center of the NASA has contributed about a dozen or so papers over the last three years on various aspects of nickel hydrogen technology. The intent of this short paper is to briefly describe the underlying principles upon which all of the aforementioned papers are based. The relatively recent entry into this technology area by NASA was precipitated by a desire to modify existing cell designs to increase their cycle life for low earth orbit (LEO) applications. Contemporary IPV designs may roughly be divided into those based on back-to-back designs (Comsat) and those based on recirculating designs (Air Force/Hughes). Several different types of electrode impregnation procedures are currently in use, as well as several types of separator materials. It was not the intent of the LeRC effort to develop completely new IPV designs but rather to first try to understand the operating characteristics of these cells and then to formulate design guidelines or component requirements or constructional philosophies that would result in increased cycle life at deep depths of discharge. The cycle life history of nickel hydrogen devices in simulated LEO orbits at deep DOD's can best be

described as widely dispersed. The gradual accumulation of post test analysis has been very important in formulating our design principles and, in fact, cells made to our specifications by a commercial supplier which incorporate these principles are currently under test. These design (Ref. 1) modifications have already been fully described in the most current IECEC proceedings and will not be repeated here. Instead, a summary of our design principles is presented for comment, criticism, and review. Besides the growing amount of post test analysis that has been helpful in formulating corrective design strategies, the nearly twenty year background in the alkaline fuel cell area has also been a contributing factor. The background in the alkaline fuel cell area has been responsible for being able to lay out a number of principles that are based on the constructive use of capillary forces to perform some very delicate electrolyte and gas management tasks.

THE BASIC CELL

The basic nickel hydrogen cell consists of a gas electrode for the anode, a separator to form an ionic bridge to the catnode, and the cathode consisting of nickel hydroxide that is contained within the pores of an electrically conductive substrate. Beyond these basic components, there is a wide variety of options for other components, depending on the methods or techniques used to assist in electrolyte management and oxygen management. The fact that nickel hydrogen devices do not consistently display attractive cycle lives when tested to LEO regimes at deep depths of discharge indicates that not all of the variables are fully under control. Since at the single cell level nickel hydrogen and nickel cadmium device weigh about the same, (a 40 to 50 Ahr cell at 100% DOD has an energy density of about 40 Whr/Kg), then nickel hydrogen cells only display significant improvements in energy density when they can be cycled at depths of discharge that are well beyond 25% DOD. The types of shortcomings that are currently associated with nickel hydrogen devices can be divided into two categories: 1) those that are obvious based on the results of post test analysis:

a) unaccommodated for cathode expansion

b) uncontrolled recombination of hydrogen and oxygen

c) unreplenished loss of electrolyte within the cell components

and 2) those decay processes that have gone undetected due to the rapid loss of performance of the device due to the first type of decay processes. It is this second class of cell decay processes that are of particular interest since the ones in the first group will eventually recede as proper design principles are applied. The work of Lim (ref. 2), as well as others, is slowly culminating in a non phenomenological decay model for nickel electrodes. Fuel cell experience can shed some light on the long term sintering (with the resultant loss of catalyst activity) of highly dispersed catalyst surfaces, and the very gradual loss of the hydrophobic nature of the

gas electrode. The design principles to be outlined here are meant to address both classes of cell decay modes. By their very nature then, they are based on preconceived assumptions relative to how these devices work and how they might be designed so that they will display long cycle lives at deep DOD's.

CONCEPTS AND PHENOMENOM

For a clearer understanding of the terminology to be used to explain the basis for these principles, a series of concepts and phenomenon that are closely related to this subject will be presented. A minimum of mathematics will be used so as to make the conversion from battery terminology to fuel cell terminology as simply as possible.

OPTIMUM VOLUME

Nickel hydrogen cells are assumed to have an optimum volume. That is, there is a volume of electrolyte that when placed within the basic anode/separator/cathode grouping will result in the highest performance. This is due mainly to the properties of the gas electrode. If there is too much electrolyte (flooded), then the catalyst sites are covered over with a thick liquid film and poor performance results. On the other hand, if there is too little electrolyte (starved), then there are not enough catalyst sites connected to the electrolyte network. The matrix resistance will not go through a minimum, but as the amount of electrolyte is reduced the resistance of the cell will increase. In like manner the nickel electrode performance will be effected more by being starved than flooded. How the electrolyte distributes itself between the three or more components that make up a single cell is a very important topic and deserves the utmost consideration. The combination of pore size, pore size distribution and wettability will dictate how the electrolyte is partitioned between the components as a function of the amounts of electrolyte that is added to a cell. In general, the smallest, most wettable pores are filled first followed by successively larger pores. It should be obvious that each particular grouping of components which is intended to be identical may have slight variations in its optimum volume. In a typical IPV cell, there are many groups of components connected together in parallel. One cannot individually place the optimum amount of electrolyte volume into each one of these groupings. Some groupings will therefore be on the wet side of the optimum volume, while others will be on the dry side. What is desired then is a cell design that is said to have "volume tolerance." That is to say, the performance should not be too highly dependent upon the amount of electrolyte volume contained within the grouping of components.

VOLUME TOLERANCE

Figure 1 illustrates now volume tolerance is incorporated into the fuel cells of the type used on the Shuttle Orbiter. It consists of a thin cathode that incorporates a certain degree of wet proofing (hydrophobicity), a fully wettable, high bubble pressure, electrolyte matrix, a thin anode similar to

the cathode and an electrolyte reservoir. The pore size and pore size distribution is engineered such that the electrolyte reservoir will have the largest pores and as such will have the "last call" on electrolyte. The cell is initially filled with electrolyte in such a manner that the reservoir will be only partially filled. As conditions arise that result in an excess or a deficiency in electrolyte, the reservoir either empties or fills. In effect, volume tolerance has been incorporated into the cell. The virtues of volume tolerance go well beyond being able to accommodate "wet" or "dry" conditions. It also permits a number of groupings of components that possess a certain degree of stochastic variability to be assembled together and filled in some average manner and still have proper performance of the device as a whole.

RESERVOIRING

Reservoiring is the technique of providing for a certain amount of extra electrolyte at the beginning of life for use at some later time when either more electrolyte is required or some of the original electrolyte has been displaced for one reason or another. In current nickel hydrogen designs a variety of schemes have been used to provide a reservoir of extra electrolyte. Besides the electrolyte plate as used in hydrogen oxygen fuel cells, wall wicks used with excess free electrolyte, specially constructed pore sizing in the nickel electrode and separators containing bimodel pore size distributions have been proposed and or used to perform this reservoiring function. Reservoiring must work very closely with volume tolerance in terms of employing capillary forces to maintain proper electrolyte quantities in the individual cells and components.

OXYGEN MANAGEMENT

One of the most important aspects of cell design deals with oxygen management. The nickel electrode evolves oxygen during recharge and this gas must be directed out of the nickel electrode and chemically recombined with hydrogen. This requires a certain degree of care so as to not ruin the hydrogen electrode. Based on our knowledge of the sintering tendencies of noble metal based catalysts, we have made the decision to employ a separate catalyst surface for the recombination procedure. The LeRC technology group has devised and brought into practice several novel concepts to this end. The catalyzed wall wick is felt to be of special interest for modified IPV designs since it helps in the heat dissipation process.

ISOPIESTIC REDISTRIBUTION

One of the fundamental physical chemical principles taking place within nickel hydrogen devices is the tendency for the vapor pressure in all parts of the device to be equal. When temperature and or concentration differences are set up, then water vapor will move from place to place in an attempt to bring about the equilibrium of the vapor pressure. This is helpful for returning the water resulting from the recombination of oxygen and hydrogen back into the cell electrolyte. It can also be a source of difficulty when a hot spot

occurs and water vapor leaves for a cooler or a more concentrated portion of the electrolyte within the cell. The resulting localized "wet" or "dry" conditions may result in an undesired flooding of the anode in the former case or an undesired increase in the cell internal resistance in the latter case. The thermal management scheme used has as one objective the elimination of any large thermal gradients within a cell that might result in local dry out or flooding.

VAPOR/LIQUID DISENGAGEMENT

As hydrogen gas is generated within the anode during the charging process, it can dislodge and carry away small amounts of electrolyte. One technique used to correct this situation is to place a microporous, hydrophobic film on the back side of the electrode. This will permit the free passsage of hydrogen through the small pores, while at the same time prohibit the small droplets of electrolyte form passing through. For monopolar cell designs this scheme is a viable option, whereas teflon's electrical insulating characteristics precludes its use in bipolar configurations.

AGING EFFECTS

If it were not for changes that take place within the individual cell components, one would be ready to draw up the specifications for the design of an IPV cell or a bipolar battery. The results of post test analysis are very important in supplying the required information on this matter. There are three types of changes that must be followed if one is to begin with a proper cell design.

Wettability

Since the entire electrolyte management philosophy is built upon the capillarity characteristics of the individual cell components, then some knowledge is needed as to how the wettability of the components change during the course of cell testing. For instance, so called "wettable" material used as the separator can very quickly lose this wettable character. This will disrupt the entire "pecking order" as to where the electrolyte will be. The internal resistance in a cell containing a wettable matrix that goes non-wettable increases rather abruptly. The more gradual loss of hydrophobicity of the hydrogen electrode caused by constituents within the matrix, perhaps, that are deposited onto the anode by electrophoritic processes can be another problem. In the fuel cell area it is felt that asbestos contains some constituents that migrate or are electrophoretically deposited within the anode and ultimately lead to a loss in the hydrophobic nature of the electrode. Since in a fuel cell the operating temperatures are much higher 90° C vs 20° C and the ionic flow is only in one direction (due to the primary character of the fuel cell), it is not apparent that properly reformulated asbestos is an unsuitable separater material for nickel hydrogen devices.

Pore size/Poresize Distribution

Due to the morphological changes brought about by cycling the active material between two valence states, there is a gradual change in not only the average pore size, but the pore size distribution. With nickel electrodes there is a tendency to develop more small pores as the electrode is cycled. The reader is referred to the post test analysis work of Lim (Ref. 2) and others on this matter. The properties at the end of the required service life must be known and accounted for in the proper design of a nickel hydrogen cell or stack.

Electrode Growth

Probably the most bothersome change that takes place during the course of cycling is the increase in thickness of the nickel electrode. The reasons for this vary depending on the investigator and there have been a variety of claims for ways to reduce this expansion by using certain impregnation procedures. The growth management schemes are of utmost importance because the cycling of a nickel hydrogen cell can be prematurely terminated due to this phenomenon. This problem can be attacked using several different approaches.

In fuel cell terminology a "locked up" stack is the term used to describe an assembly of cells or components that is of fixed dimensions (see figure 2(a)). The only way the stack could expand in length would be via the stretching of the tie bolts. Thermal expansions in thickness of the metallic and plastic stack parts are accommodated by the slight amount of elastic stretching of the tie bolts in flight weight hardware or the use of compression springs along with the oversize tie bolts in laboratory hardware. From what is known about the expansion characteristics of cycled nickel electrodes, a "locked up" stack can lead to certain difficulties that have been documented over the years; most recently by Mackowski and Mueller, (Ref. 3). One solution to this problem as proposed by Smithrick, et al (Ref. 1) is to employ a "floating" stack that is designed to accommodate a certain degree of stack expansion. The spring constant is set once the compression characteristics of the separator material and the expansion characteristics of the nickel electrode structure are known. In the design of a floating stack the resevoiring and electrolyte volume management schemes become very important so as to be able to make up for the extra electrolyte required by the expanding cathode. A collapsible reservoir would represent another alternative for maintaining a proper quantity of electrolyte within each cell grouping. A set of compression strength/conductivity plots (Fig. 3) are required to fully assess the effects on cell performance that results from a certain amount of compression on the cell components. It can be seen that a highly compressible matrix material would make the design of a "floating" stack very difficult. Further, there is some evidence that the expansion characteristics of an electrode are somewhat related to the degree of compression it is under in the stack assembly.

CELL AND BATTERY DESIGN PRINCIPLES

The foregoing list of topics form the basis of developing the required design principles for a nickel hydrogen device. It should be noted that the actual electrochemistry that goes on inside the device was never mentioned. Only as the electrochemistry effects the electrolyte volume, the component pore size/pore size distribution, or the expansion characteristics, is it important. Measurement of the pore size and the distribution of that pore size for each one of the cell components as a function of cycle life and degree of compression is the essential starting point for this procedure. This permits one (with the help of some wettability information) to calculate the distribution among cell components of the electrolyte as a function of electrolyte content. The pore size characteristics of the matrix material used as the separator is subject to a certain amount of adjustment depending on the particle size and physical nature of the ingredients used in their formulation. This is followed by a series of measurements whereby the ionic/electrical conductivity is measured as a function of the compressive forces placed on the component. This is usually done in a fully saturated condition but can also be done as a function of electrolyte content.

There is probably not any one best way to design a cell or battery but there is a certain degree of formalism required to adequately account for all the changes that take place over the course of the useful life of a cell or battery. Once the oxygen management, electrolyte reservoiring, thermal management, and the component growth management techniques are all decided upon, then a series of rather straight forward calculations based on pore size engineering principles (Ref. 4) can be applied to insure proper cell and stack performance over the expected cycle life of the cell. The overall output of these principles have resulted in the cell and stack designs that have been produced by the nickel hydrogen technology group at the Lewis Research Center. These designs have been fully documented at earlier conferences and current cycle life results will be reported at this current workshop session. It is the current philosophy of the group to:

1) Use a separate recombination catalyst (rather than the hydrogen electrode) to recombine the oxygen coming from the nickel electrode. This then dictates the use of a separator matrix that will have a sufficiently small pore size to preclude the passage of oxygen through open pores within the separator.

2) Use a "floating" stack rather than a "locked up" stack to circumvent the problems associated with positive plate growth. The modified IPV designs use springs which permit actual stack expansion, whereas the bipolar designs employ collapsible components.

3) Provide electrolyte management schemes which will maintain proper electrolyte content within the cell components. These are all based on pore size engineering principles in conjunction with the knowledge of matrix fabrication techniques.

By applying these principles, cells and stacks have already been made and are being tested with results that have led us to believe that much of the mystique that currently enshrouds contemporary electrochemical device technology should be able to be replaced with a rather simple set of straight forward formalisms based on elementary principles of physical chemistry.

CONCLUDING REMARKS

Nickel hydrogen cells have been made by a number of groups over the past fifteen years or so. These devices are intended to replace nickel cadmium cells and batteries in aerospace applications. They have already been successfully introduced in GEO applications where the cycle life requirements are rather limited. In simulated LEO applications, the cycle life history of nickel hydrogen cells has been somewhat erratic but by in large disappointing in terms of being able to consistently display 10's of thousands of cycles at deep DOD's. The nickel hydrogen technology group at the Lewis Research Center of the NASA has been developing both IPV cells that are modifications of the basic back to back and recirculating designs, as well as large bipolar battery systems. These designs are intended primarily for LEO applications but will be extended to GEO applications as well. Over the past two years these designs have been translated to working hardware. This short paper is a discussion of the design principles that have been used in developing these new designs. They are based on a combination of the existing data base coming from post test analyses of several cell types, as well as the use of capillary forces to provide the required electrolyte volume management. A number of novel schemes have also been factored into these designs in an attempt to rectify some of the documented failure mechanisms. An active program to address other anticipated decay and failure mechanisms is also underway both on contract, as well as via inhouse projects. Cell hardware incorporating these design concepts are currently under test. As newer information becomes available on factors that will effect cell cycle life, it will be factored into upgraded cell designs.

REFERENCES

1. Smithrick, J. J., Manzo, M. A., and Gonzalez-Sanabria, O. D.: Advanced Designs for IPV Nickel-Hydrogen Cells. Proceedings of the 19th IECEC, Vol. 1, Aug. 1984, pp 631-634.

2. Lim, H. S. and Verzwyvelt, S. A.: Long Life Nickel Electrodes for a Nickel-Hydrogen Cell: III - Results of an Accelerated Test and Failure Analyses. Proceedings of the 19th IECEC, Vol. 1, Aug. 1984, pp 312-318.

3. Mackowski, M. J. and Mueller, V. C.: Cycling Characteristics and Failure Modes of Prototype Nickel-Hydrogen Cells. Proceedings of the 19th IECEC, Vol. 1, Aug. 1984, pp 146-151.

4. Abbey, K. M. and Thaller, L. H.: Pore Size Engineering Applied to Starved Electrochemical Cells and Batteries. Proceedings of the 17th IECEC, Vol. 2, Aug. 1982, pp 757-764.

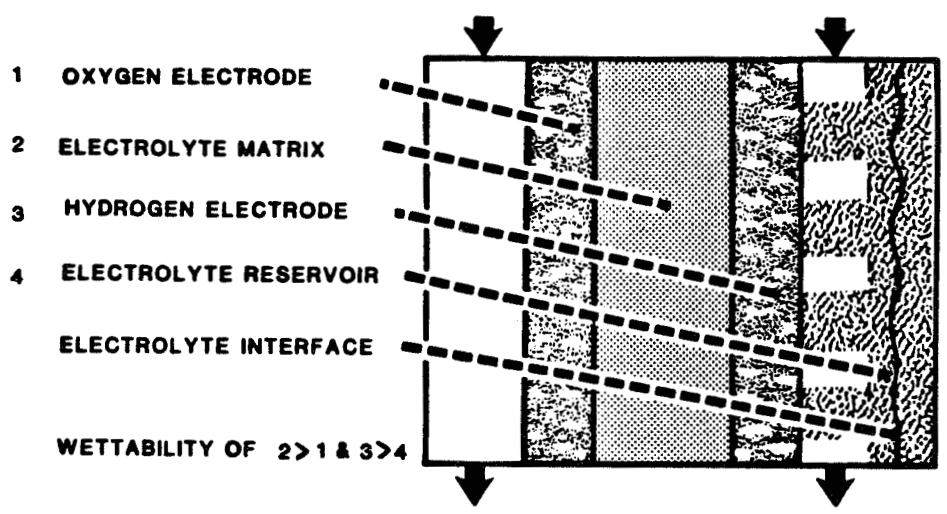

Figure 1. Fuel Cell Employing Reservoir to Bring About Volume Tolerance

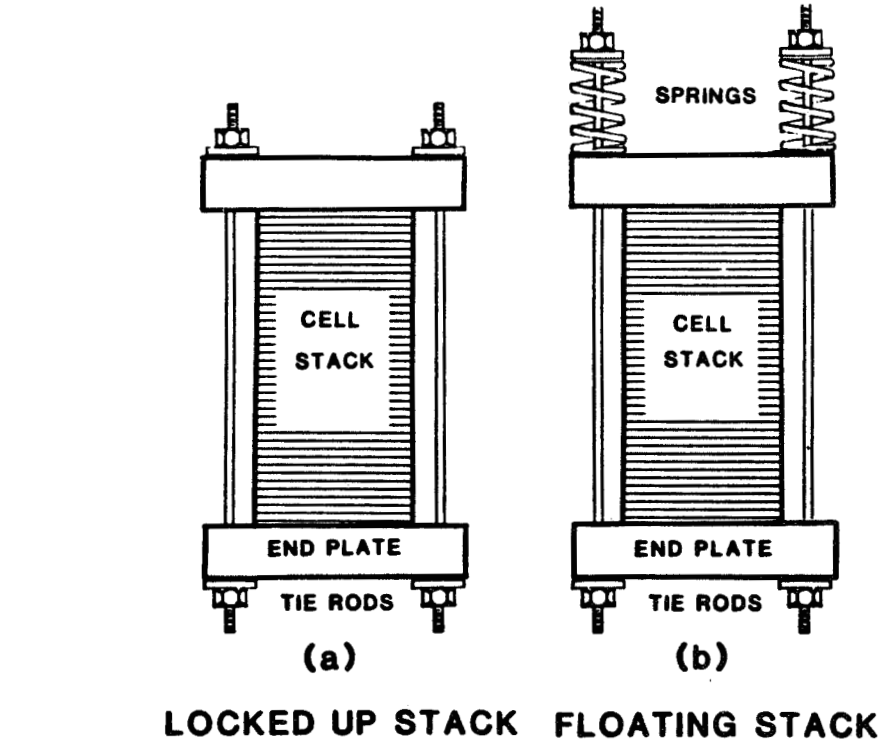

Figure 2. Two Different Stack Assembly Types

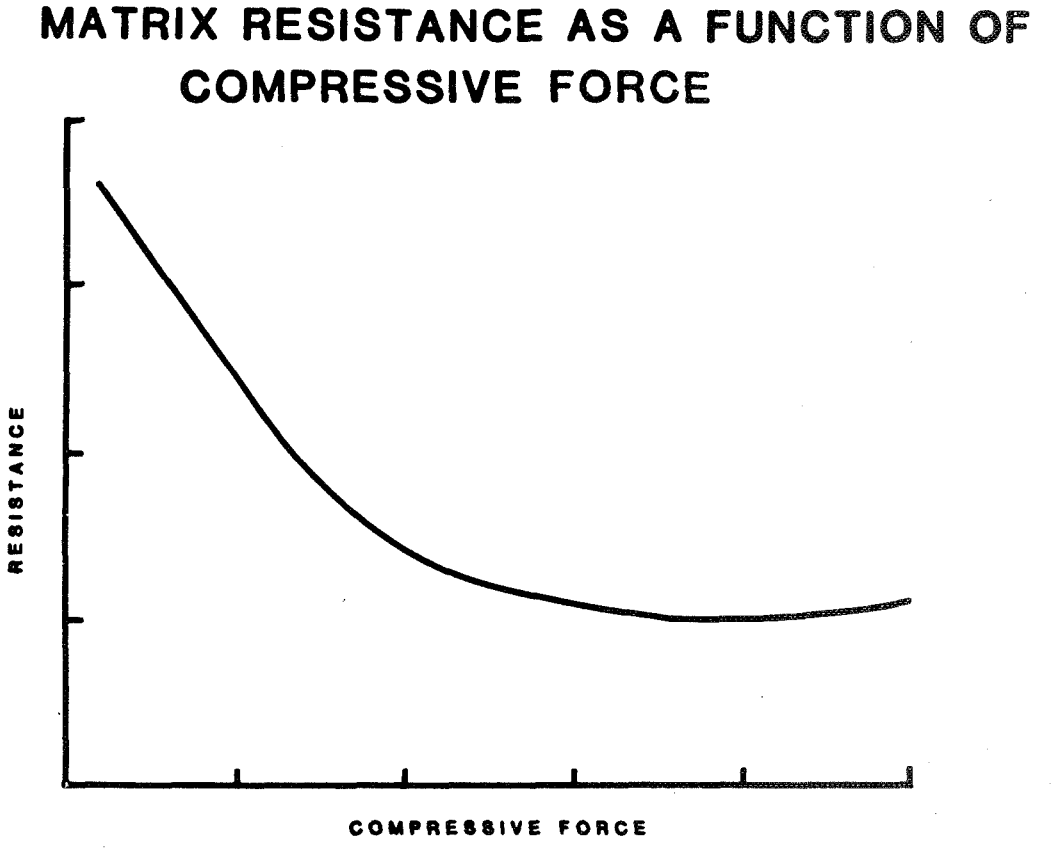

Figure 3. Matrix Resistance as a Function of Compressive Force

IMPROVED SPECIFIC ENERGY NI-H_2 CELL

Lee Miller

Eagle-Picher Industries, Inc.

ABSTRACT

Significant improvements in specific energy for Ni-H_2 battery cells have been and will be achieved. Current flight cell designs in operation on multiple satellites have achieved a specific energy of 52 Whr/Kg (this value may be compared to 45 Whr/Kg for advanced, light-weight Ni-Cd space cells). Battery cells operating at increased pressures (600 to 900 psi) have been manufactured and successfully tested demonstrating a specific energy of 63 Whr/Kg. Further optimization of electrode substrate and cell terminal/conductor assembly designs will permit achievement of specific energies between 75-80 Whr/Kg. Energy density (outline volume) will be improved from 49 Whr/L to 73 Whr/L.

INTRODUCTION

To achieve a Ni-H_2 battery cell offering a specific energy of 75-80 Whr/Kg, system design optimization was undertaken in the following specific areas which evolved from previous work (1): 1. The specific energy of the electrode stack was increased primarily through the enhancement of the specific capacity of the positive electrode. 2. Pressure vessel mass savings were achieved through size reduction associated with higher pressure operation and weld ring/center rod redesign. 3. The weight consumed by the electrical feedthru/current conductor assemblies was reduced by more efficient, shorter path designs.

This paper discusses the results of design validation testing and planned design validation steps to be undertaken.

The "Intelsat" type Ni-H_2 battery cell design has been chosen for expository purposes. However, it should be recognized portions of the improved technology could be applied to the "Air Force" type Ni-H_2 battery cell design with equal benefit.

DESIGN OPTIMIZATION

ELECTRODE STACK

Negative electrode design improvement has been achieved by the simple reduction of platinum catalyst loading. A reduction of 67% from the current flight production level produced the electrode thickness and mass improvements presented in Table I (17 and 28% reduction respectively).

With respect to design validation, work was initiated in this technoloty in 1974 with the goal of component cost reduction. Comparative testing reported in 1975 (2) demonstrated equivalent performance and these results were subsequently corroborated by multiple Ni-H_2 and Ag-H_2 cell production and testing. More recently, COMSAT Laboratories reported equivalent performance (3) with a platinum loading reduction of 94% of current flight production levels.

Planned validation for this component and the remaining design improvements discussed below will involve 75-80 Whr/Kg specific energy battery cell production for qualification and life testing. This activity is now in the tooling and part procurement phase.

A major advance was achieved with respect to the positive electrode. As indicated in Table I, a small increase (17%) in sinter substrate (nickel) thickness permitted a 5% increase in sinter porosity. Since the sinter substrate contributes more than 60% of the finished electrode weight but occupies only 20% of the volume, a small increase in porosity translates into a significant mass savings.

The resulting increase in void volume (vv) allows the further deposition of active material without violating the present, proven flight level limit. The measured capacity of the conventional "Intelsat" positive electrode is increased by 35%. In fact the weight of the additional active material is almost exactly off-set by the reduction of nickel sinter permitting the statement the specific capacity of the positive electrode has been increased by 35%.

Design validation has been successfully carried through sinter substrate mechanical strength characterization, and finished electrode dynamic stress and boilerplate performance cycling.

When these advanced electrode technologies are combined into a stack, a shorted stack (25%) offering higher capacity per unit mass is achieved (33% increase in specific energy) as presented in Table I. An initial analysis might indicate the specific energy at the stack level should be higher because of the component count reduction (37%). However, the electrolyte level associated with the positive electrode group remains unchanged and the total cell electrolyte is reduced by only 12%.

PRESSURE VESSEL

Figure 1. presents a photograph of the redesigned pressure vessel weld ring. This light-weight design offers enhanced dynamic load tolerance in the critical cell longitudinal axis. In addition, the design is intended to specifically accommodate the more universal "dual stack" cell assembly technique.

By shifting the fulcrum stress to a more centralized location, a lighter weight hollow center rod may be utilized. Total mass savings for these redesigned components is estimated to be 30%.

The redesigned weld ring has been validated by a centralized dynamic loading technique. If the photograph of Figure 1. is observed closely, the permanent deformation of the current weld ring design, after the same level of testing, can be noted.

The reduced length and corresponding pressure vessel mass savings associated with increased cell nominal operating pressure (900 psi) is straight forward and has been the subject of previous papers (1). The present vessel is quite conservatively designed with a nominal burst pressure in excess of 3,000 psi and an estimated yield pressure in excess of 2,700 psi.

Design validation has been accomplished via hydraulic pressure cycling at Eagle-Picher and through a fracture analysis performed for Eagle-Picher by Martin Marietta Aerospace, Denver, Colorado.

ELECTRICAL FEEDTHRU/CURRENT CONDUCTORS

To minimize the number of current conductors (electrode leads) required, the reduced stack component design described above is further enhanced as depicted in Figure 2. The "notched" lead access and reduced "wall gap" (0.20 cm to 0.10 cm) accommodates a 12% increase in electrode area. A 33% increase in electrode edge perimeter is also accommodated enhancing the heat rejection capability of the electrode stack.

Figure 2. further depicts elimination of the busbar arrangement in preference for the more mass efficient, continuous lead design.

Figure 3. offers an overview comparison between the current and advanced cell designs. Shown are the internally mounted, 45^{o} off-set electrical feedthru's considerably reducing the current conductor path length. The feedthru design features a redundant sealant (teflon), hydraulic seal mechanism.

Also shown is the relative reduction in pressure vessel length and the continuous lead, electrode stack conductor arrangement. A 50% mass savings with respect to the electrical conductors and a 17% mass savings with respect to the reduced pressure vessel size are projected. In addition, an overall outline volume reduction of 33% is achieved.

Design validation of the basic concepts associated with the 0.10 cm wall gap, continuous lead design and the hydraulic seal is assumed as the result of the successful work conducted by the Hughes Aircraft Company, Technology Division, El Segundo, California under the Air Force "Nickel-Hydrogen Battery Advanced Development Program" (4).

CONCLUSION

This paper has summarized design optimization activities which have evolved and validated the necessary technology to produce Ni-H_2 battery cells exhibiting a specific energy of 75-80 Whr/Kg (energy density approximately 73 Whr/L). Final design validation is currently underway with the production of battery cells for qualification and life testing.

The significance of the progress which has already been achieved is shown in Table II which begins with state-of-the-art, light-weight Ni-Cd. The photograph presented in Figure 4. shows two 70 Ah rated cells (nominal capacity 80 AH) mounted in aluminum thermal collars in preparation for life cycle testing. The pressure vessels for these cells are approximately 1 cm shorter than current flight production 50 AH rated cells and the measured specific energy is 63 Whr/Kg.

REFERENCES

1. Miller, L. (Eagle-Picher Industries): A High Energy-Density Nickel-Hydrogen Battery Design. Proc. 4th ESTEC Spacecraft Power-Conditioning Seminar, Noordwijk, (ESA SP-186, September 1982).

2. Final Report, Nickel-Hydrogen Prototype Cell, 29 August 1975. Contract No. CSC-IS-550B, International Telecommunication Satellite Organization (Intelsat), 950 L'Enfant Plaza, S.W. Washington, D.C.

3. Dunlop, J. et al (COMSAT Laboratories): Design and Development of a Sealed 100-Ah Nickel-Hydrogen Battery. Contractor Report SAND84-7155, August 1984, National Technical Information Service, U.S. Department of Commerce, 5285 Port Royal Road, Springfield, VA 22161.

4. Stadnick, S. J. et al (Hughes Aircraft Company): Nickel-Hydrogen Battery Advanced Development Program. AFWAL-TR-80-2-44, April 1980, Aero Propulsion Laboratory, Air Force Wright Aeronautical Laboratories, Air Force Systems Command, Wright-Patterson Air Force Base, OH 45433.

Table I. ADVANCED ELECTRODE DESIGNS

ADVANCED ELECTRODE DESIGNS

NEGATIVE ELECTRODE

PLATINUM LOADING	67% DECREASE
ELECTRODE THICKNESS	17% DECREASE
ELECTRODE MASS	28% DECREASE

POSITIVE ELECTRODE

SINTER THICKNESS	17% INCREASE
SINTER POROSITY	5% INCREASE
ELECTRODE LOADING	NO CHANGE
ELECTRODE CAPACITY	35% INCREASE

STACK SPECIFIC CAPACITY	33% INCREASE
STACK COMPONENT COUNT	37% DECREASE
STACK LENGTH	27% DECREASE

Table II. BATTERY CELL SPECIFIC ENERGY

BATTERY CELL SPECIFIC ENERGY	
LIGHT-WEIGHT NI-CD	45 WHR/KG
CURRENT (600 PSI) NI-H_2	52 WHR/KG
HIGHER PRESSURE (900 PSI) NI-H_2	63 WHR/KG
ADVANCED (900 PSI) NI-H_2	75-80 WHR/KG

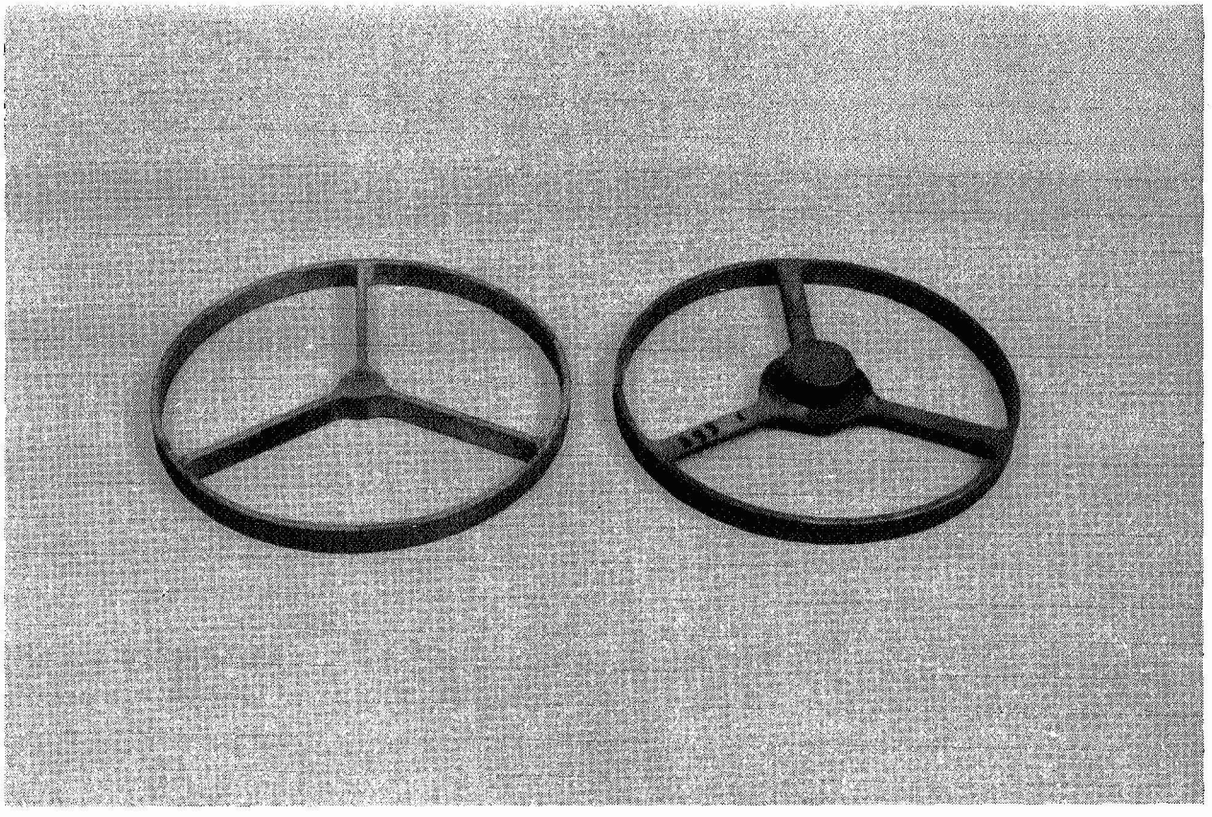

ADVANCED WELD RING CURRENT WELD RING

Figure 1

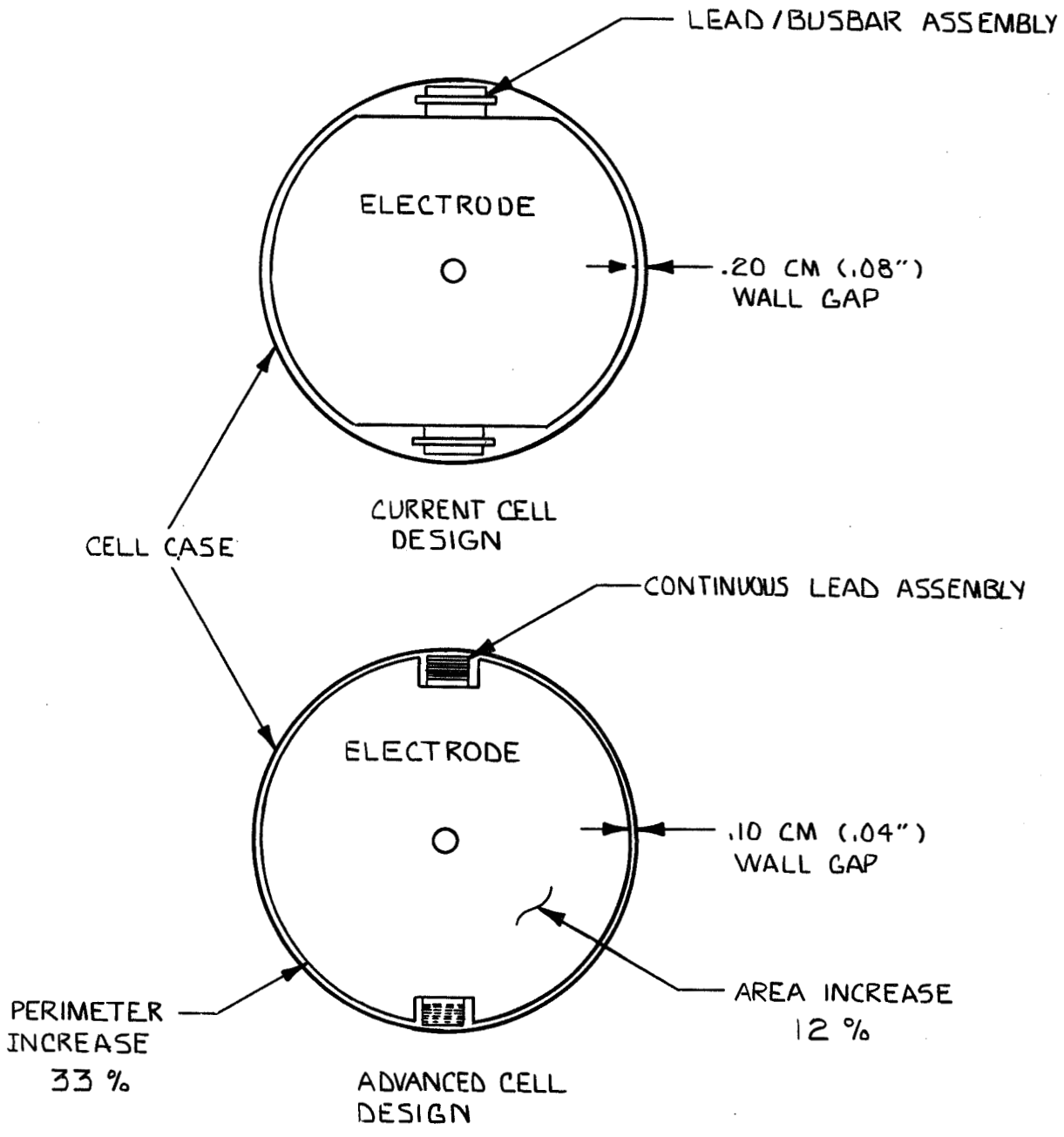
LEAD/BUSBAR ASSEMBLY
ELECTRODE
.20 CM (.08")
WALL GAP
CURRENT CELL
DESIGN
CELL CASE
CONTINUOUS LEAD ASSEMBLY
ELECTRODE
.10 CM (.04")
WALL GAP
AREA INCREASE
12 %
PERIMETER
INCREASE
33 %
ADVANCED CELL
DESIGN

Figure 2.

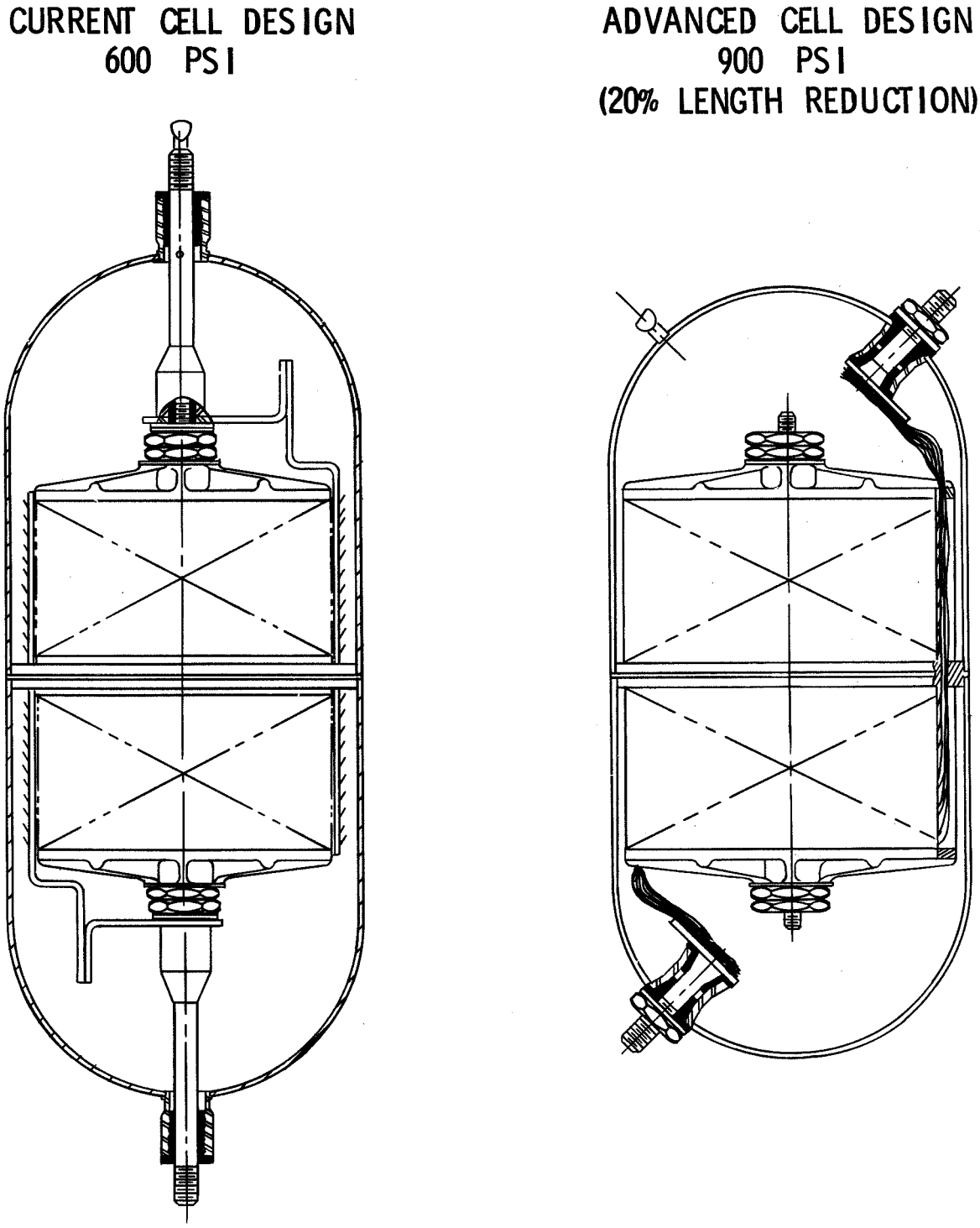

Figure 3. Projected 17% Mass Saving in Pressure Vessel and 50% Saving in Electrical Conductors. Outline Volume Reduction 33%.

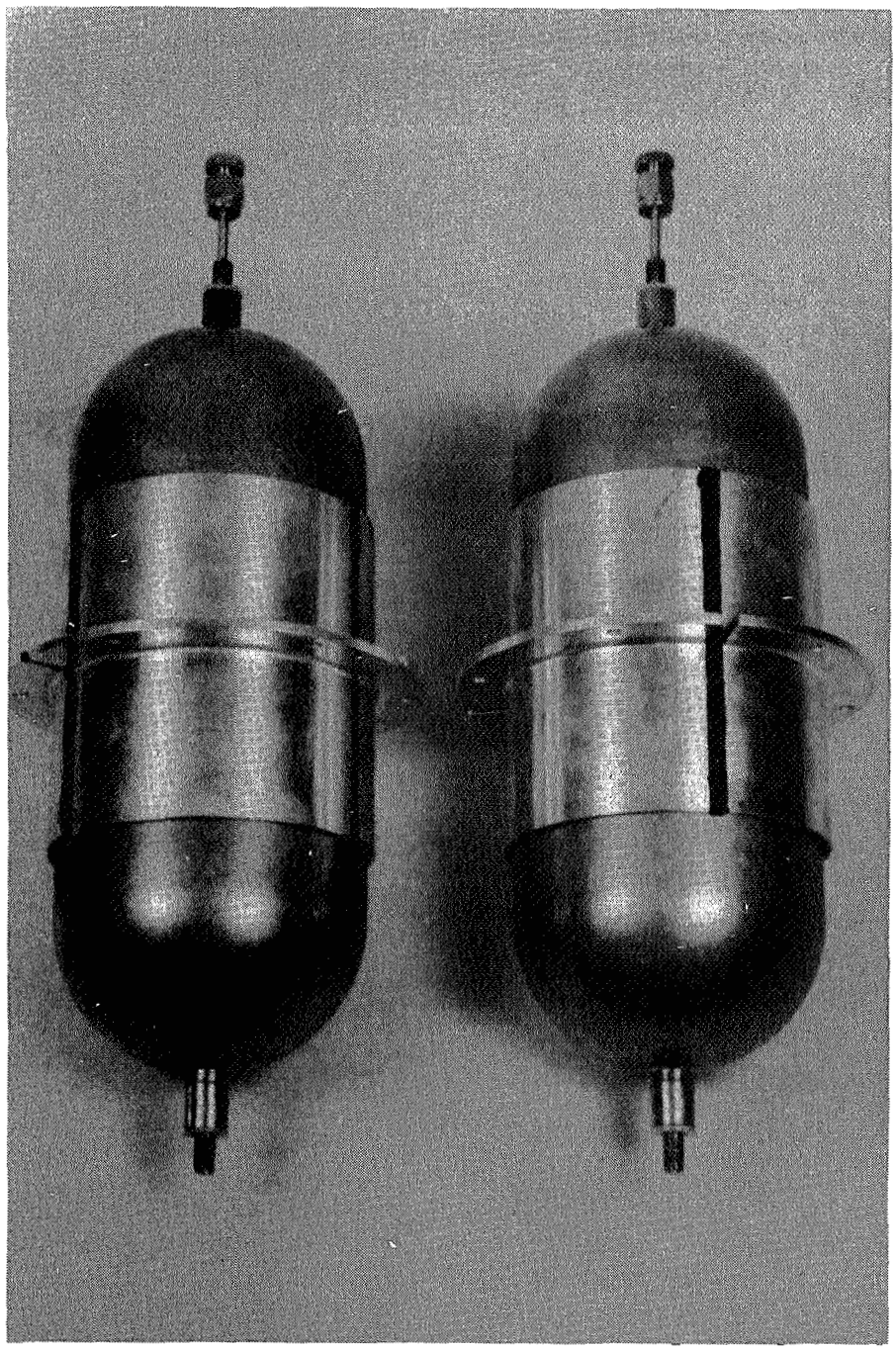

Figure 4. 70 AH Rated Cells (Nominal 80 AH), Specific Energy 63 Whr/Kg.

BIPOLAR NICKEL-HYDROGEN BATTERY DESIGN

C. W. KOEHLER, A. Z. APPLEWHITE, & Y. KUO

FORD AEROSPACE & COMMUNICATIONS CORPORATION

PALO ALTO, CA. 94303

INTRODUCTION

Ford Aerospace & Communications Corporation and Yardney Battery Division are now completing the design of a bipolar nickel-hydrogen battery stack. This initial design is the first of three design phases being conducted on the Advanced Nickel-Hydrogen Battery Development Program. The program is sponsored by the NASA-Lewis Research Center and the technology is being considered as one of the energy storage concepts for the Space Station.

The initial stacks which will soon begin fabrication were designed with several objectives in mind (Reference 1):

- o Maximization of reliability and life
- o High specific energy and energy density
- o Reasonable cost of manufacture, test, and integration
- o Ease in scaling for growth in power requirements

To meet these objectives the battery design must provide for careful material and thermal management (Reference 2).

This paper presents the results of the design effort which has resulted in the initial bipolar nickel-hydrogen battery design. Specifically, this paper will discuss the thermal and mechanical design of the battery. The electrochemical design considerations of the battery are described in Reference 3.

THERMAL DESIGN

The thermal design of a bipolar nickel-hydrogen battery is critical to the life and reliability of the battery. Materials balance and electrical performance are quite dependent on the thermal design. Thermal imbalances between individual cells can lead to premature failure of the battery since the transfer of materials from cell to cell via the gas or vapor phase is possible. A warmer cell can lose water to the cooler cells and thus dry out causing it to be less efficient. This inefficiency will result in higher heat dissipation during electrical cycling which will compound the temperature differences between this cell and the others of the bipolar stack. The runaway condition will ultimately result in battery failure.

Not only should cell-to-cell temperature gradients be eliminated but intracell gradients must be minimized. Large temperature gradients over the electrode surface would result in performance imbalances which could be detrimental to long term performance. The following thermal performance goals have been established for the bipolar nickel-hydrogen battery design:

- o Operational temperature range: 0 to 25°C
- o Cell-to-cell temperature gradient: 1°C (maximum)
- o Intracell temperature gradient: 5°C (maximum)

The cell-to-cell temperature gradient of 1°C is for equivalent locations on each cell.

To meet these thermal requirements the bipolar battery stack will be edge cooled. The electrodes will be rectangular in shape and a flat cooling panel containing a pumped cooling fluid will be assembled onto the two long sides of the stack. The bipolar conduction plate of each cell will have sufficient thickness to conduct the heat generated by the inefficiencies of the cell to the cooling plate. Cooling plates on opposite sides of the cell stack will contain fluid flowing in opposite directions. This counterflow cooling also helps minimize intracell temperature gradients.

The temperature gradient across a cell is dependent on the cell heat dissipation and the heat path thermal conductivity. The battery design is based on a 75Ah cell operating at 80% depth of discharge in a typical low earth orbit having a 90 minute period. Reference 4 discusses the considerations which affect the thermal design utilizing edge cooling. Specifically, the battery weight and volume can be optimized by selecting the nickel electrode width and sizing the bipolar conduction plate thickness so that the thermal requirements are met.

Ford Aerospace has analyzed the thermal design of the battery as a function of nickel electrode width and battery depth of discharge. Two depths of discharge were considered, 40% and 80%. Significant weight differences result in these two designs mainly due to the thicker bipolar conduction plates required for the higher depth of discharge (Reference 5).

Figure 1 shows the effect the nickel electrode width has on the bipolar conduction plate thickness for the two depths of discharge being considered. Both curves result in equivalent thermal performance with respect to operating temperature range and temperature gradients.

Since the bipolar conduction plate is in direct electrical contact with the cell the plate must be isolated from the cooling plate. Unfortunately, electrical insulators are poor thermal conductors. The poor thermal conductivity coupled with the small conduction area at the bipolar conduction plate/cooling panel interface makes it necessary for a special intermediate thermal conductor known as an 'L' fin. The concept, shown in Figure 2, provides the thermal contact area necessary for the thermal conduction of the waste heat from the cell edge to the cooling plate. The 'L' fin is electrically isolated from the bipolar conduction plate. Heat is trans-

ferred from the bipolar conduction plate to the 'L' fin through a larger insulated contact area then directly to the fluid cooling channel.

MECHANICAL DESIGN

The cell frame is the only component in the stack design which controls material management, particularly electrolyte isolation and water. In a bipolar battery stack relatively short distances in the stack direction perpendicular to the electrode area results in sizeable voltage differences making electrolyte isolation very important. An electrolyte bridge between two cells will electrically short the two cells and all cells in between.

The cell frame must be capable of sealing the electrolyte within the frame. Features in the frame, such as an o-ring and groove detail can seal the frame. Alternatively, compression of stack on the frame surfaces can be used to make a seal.

As shown in Figure 2, the 'L' fin must be insulated from the bipolar conduction plate with which it is directly in contact. If this insulation material is semi-rigid and has hydrophobic properties then an electrolyte seal can be established by compressing the cell stack and the insulation material. The 'L' fin is bonded to the cell frame and the cell frame is bonded to the bipolar conduction plate at the lower frame interface. Thus the cell frame seal is made by either compression of the insulation material or a bonded interface.

End plates at the top and bottom of the cell stack will provide the stack compression via tie rods. The stack components will be under approximately 23 psi of compression while the cell frame seal will be under approximately 230 psi of compression. The bipolar conduction plate in contact with the compression seal will be teflon coated, thus enhancing the hydrophobic characteristics of the compression seal.

The cell frame must also provide gas access to the hydrogen electrode. This is accomplished by allowing the hydrogen gas screen under the negative electrode to protrude to the outer edge of the cell frame's narrow side (Figure 2). The amount of gas screen under the cell frame will be teflon coated as will the bipolar conduction plate in this area. The hydrophobic surfaces in these areas are the only electrolyte barrier.

As the cell goes into overcharge oxygen will be generated at the nickel electrode. The cell stack components must recombine this oxygen with hydrogen producing water. It is important to recombine the oxygen in the cell where it was generated. If the oxygen were allowed to escape the cell it was generated in this cell would effectively be loosing water and other cells would gain water where it finally recombines. This would result in drying out of one cell and potential flooding of others.

To prevent this from occurring each cell will have a recombination site and electrolyte reservoir for oxygen recombination. The nickel electrode, located between the recombination site/reservoir and hydrogen electrode will produce oxygen on overcharge. The asbestos separator, having

high oxygen bubble pressure, will force the oxygen to the recombination site/reservoir area and to recombine there. The water will flow directly into the reservoir and nickel electrode creating a continuous water balance in the cell.

If the oxygen were allowed to recombine at the hydrogen electrode, the water produced could get trapped in the gas screen or flood the hydrogen electrode. In either event the performance of the cell would be impaired. Using asbestos as the separator and having the separator touch the cell frame at all four edges gaskets oxygen from getting to the hydrogen electrode.

INITIAL DESIGN AND PERFORMANCE GOALS

To meet the design capacity objective of 75Ah it is necessary for the nickel electrode area to be 192 in^2 (1239 cm^2), based on a 0.083 in (2.11mm) thick electrode chosen for the initial design. This area can be accommodated in almost any combination of electrode length and width but the configuration chosen for the initial design will be three (3) 4.0 inch wide by 16.0 inch long (10.2cm x 40.6cm) modules, each contained in a cell frame mounted on a single bipolar conduction plate. This configuration was established by the thermal design of the battery and manufacturing constraints on the cell frames.

The cell stack will consist of a bipolar conduction plate, electrolyte reservoir/recombination site plate, nickel electrode, separator, integrated-hydrogen electrode, and gas screen. The nickel electrode within each cell frame will be split in two equal parts. The split electrode will be adequately spaced and the gap will be filled with a wick made of separator material. The wick serve two purposes: (1) to provide a space for area expansion of the electrode, and (2) to provide a direct return path for water from the reservoir to the separator. A wick will also be placed at each end of the nickel electrode.

The bipolar conduction plate thickness for the initial design will be 0.040 inches (1.02mm). This thickness was based on an operating depth of discharge of 80% and a nickel electrode width of 4.0 inches (10.2cm). Selection of this nickel electrode width and bipolar plate thickness is discussed in Reference 5.

The hydrogen electrode is an integrated structure. The application of this new development by Yardney came about when the negative electrode originally considered for design experienced flooding during operation.

The separator and electrolyte wicks are beater treated asbestos (BTA) fabricated using similar techniques which NASA-LeRC has been successfully using. The reservoir material will be nickel foam metal. Two types of gas screen will be used. One is a fine mesh in direct contact with the negative electrode to provide good electrical conductivity; the second is a larger mesh for gas access.

A cross-section of the cell is shown in Figure 2. The thicknesses of the various components are summarized in Table 1.

Each cell module is contained within a plastic cell frame. The cell frame provides the necessary gas access, isolates the cell components from the cooling channels, seals the cell from electrolyte leakage which would result in cell bridging, and provides a internal oxygen seal which won't allow oxygen to recombine at the negative electrode. The cell frame is slightly thinner than the sum of the cell component thicknesses so that when the stack is compressed each cell is uniformly compressed providing a good electrical contact with the bipolar conduction plate between cells and uniform interelectrode spacing.

Stack compression is maintained by end plates and tie rods. The tie rods pass through the cell frames and bipolar conduction plates and are insulated with a teflon sleeve. The tie rods cannot pass outside the cell frames because they would interfere with the cooling panels.

The cooling panels are assembled onto the long sides of the stack. 'L' fins bonded onto the cell frame provide the necessary heat transfer surface for the heat path between the bipolar conduction plate and the cooling panels. Since the bipolar conduction plate is in direct contact with the cell it is insulated from the cooling plate as previously discussed.

The performance goals shown on Table 2 have been established for the initial design battery stack.

SUMMARY

Ford Aerospace and Yardney have established the initial design for the NASA-Lewis advanced nickel-hydrogen battery. Fabrication of two 10-cell boilerplate battery stacks will soon begin. The test batteries will undergo characterization testing and low earth orbit life cycling.

The design effectively deals with waste heat generated in the cell stack. Stack temperatures and temperature gradients are maintained to acceptable limits by utilizing the bipolar conduction plate as a heat path to the active cooling fluid panel external to the edge of the cell stack.

The thermal design and mechanical design of the battery stack together maintain a materials balance within the cell. An electrolyte seal on each cell frame prohibits electrolyte bridging. An oxygen recombination site and electrolyte reservoir/separator design does not allow oxygen to leave the cell in which it was generated.

REFERENCES

1. "Bipolar Nickel-Hydrogen Batteries for Aerospace Applications", C. W. Koehler, G. van Ommering, N.H. Puester, and V.J. Puglisi, 1983 Goddard Space Flight Center Battery Workshop, p.495.

2. "Bipolar Nickel-Hydrogen Battery System Design", G. van Ommering and C. W. Koehler, Proceedings of the 19th Intersociety Energy Conversion Engineering Conference, Volume I, p. 625.

3. "Nickel-Hydrogen Bipolar Battery Electrode Design", V.J. Puglisi, 1984 Goddard Space Flight Center Battery Workshop (to be published).

4. "Thermal and Geometrical Considerations in a Bipolar Nickel-Hydrogen Battery Design", C.W. Koehler and G. van Ommering, 31st Power Sources Symposium Proceedings, (to be published).

5. "System Considerations for a Bipolar Nickel Hydrogen Battery", G. van Ommering and C. W. Koehler, 1984 Goddard Space Flight Center Battery Workshop (to be published).

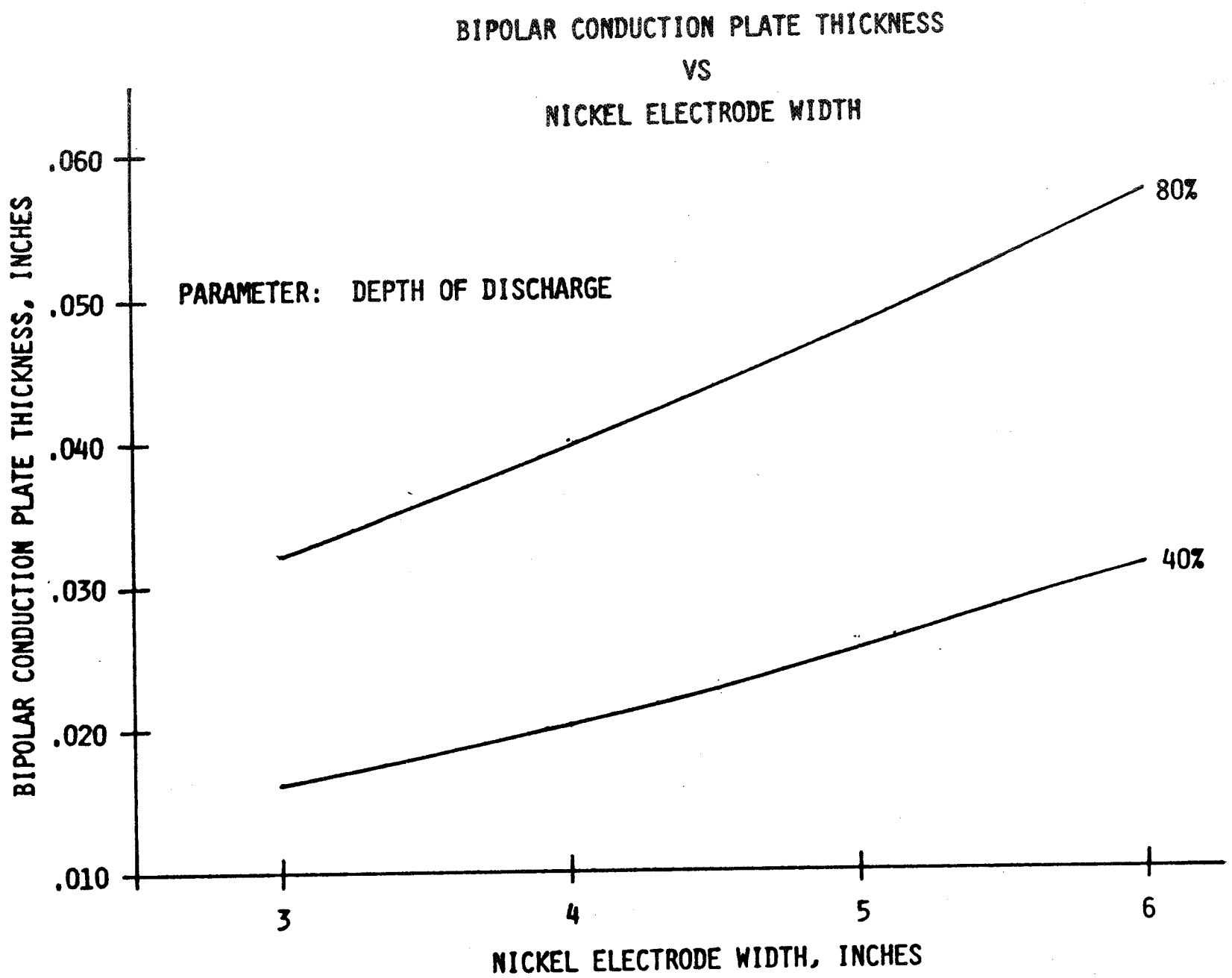

Figure 1. Bipolar Conduction Plate Thickness vs Nickel Electrode Width

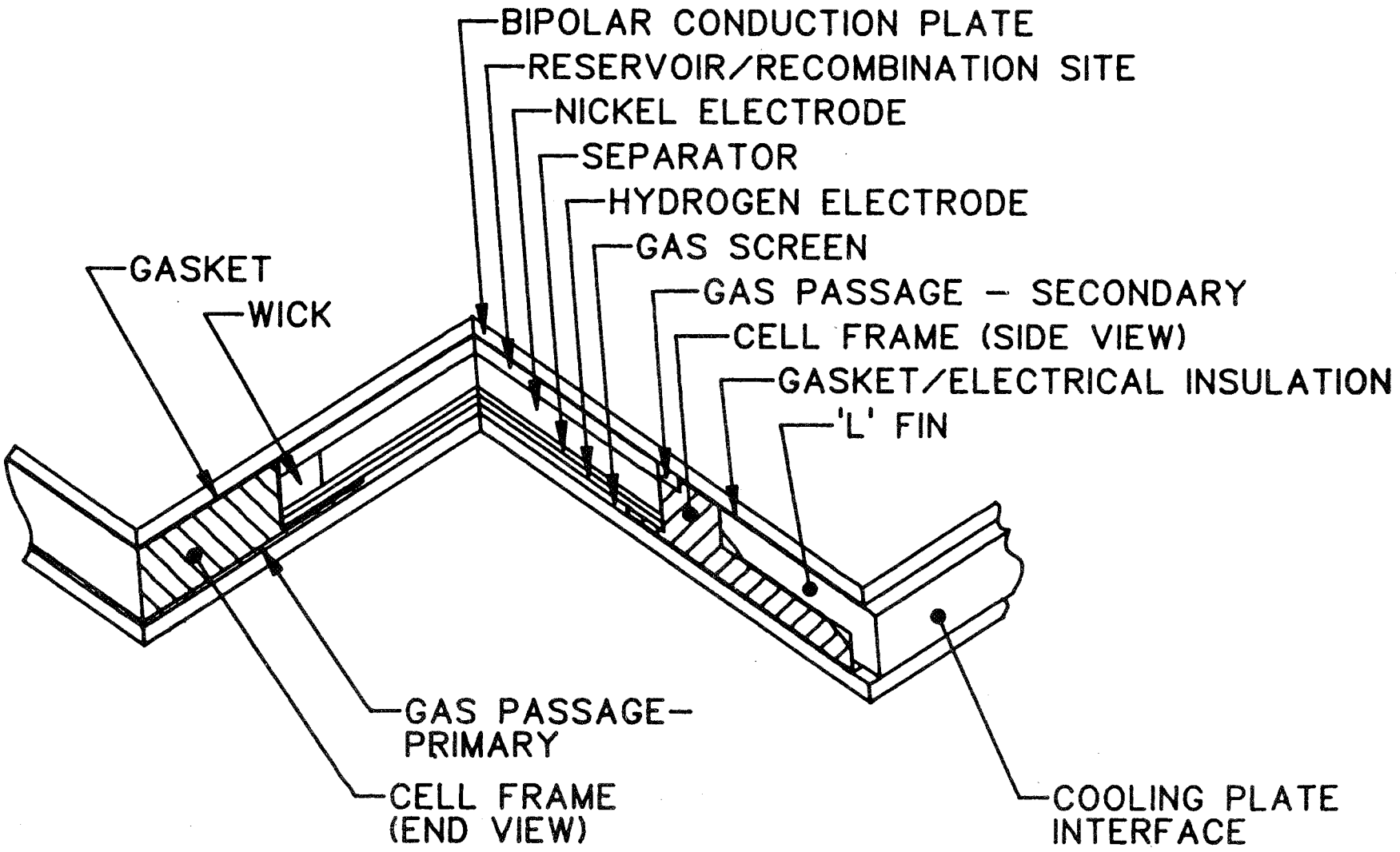

Figure 2. Bipolar Nickel-Hydrogen Cell

Table 1. CELL COMPONENT THICKNESSES

Component	Thickness	
1. Bipolar Conduction Plate	0.040 inch	1.02 mm
2. Electrolyte Reservoir	0.038	0.97
3. Nickel Electrode	0.083	2.11
4. Separator	0.015	0.38
5. Integrated Negative Electrode	0.015	0.38
6. Nickel Gas Screen (Total)	0.023	0.58

Table 2. BATTERY PERFORMANCE GOALS

Characteristic	Performance Goal
Electrical Performance:	
Charge Current	72 A (.96C)
Recharge Fraction	1.10
Charge Voltage (Maximum)	1.58V/cell (10^{o}C)
Discharge Current	103A (1.37C)
Discharge Capacity (Minimum)	75 Ah (to 1.0V/cell)
Discharge Voltage (Minimum)	1.20V/cell average to 80% DOD
Pulse Load	30C for 5 seconds
Minimum Voltage	1.00V/cell
Specific Energy	50 wh/kg (22.7 wh/lb)
Energy Density	0.06 wh/cm^3 (0.98 wh/in^3)
Cycle Life	30,000 cycle at 80% DOD
Thermal Performance:	
Cooling	Active, pumped fluid cooling
Operating Temperature	0^{o}-25^{o}C during 90 minute orbit
Qualification Temperature	-10^{o} to $+35^{o}$C
Temperature Gradients	5^{o}C within single cell; 1^{o}C from cell-to-cell

NICKEL-HYDROGEN SPACECRAFT MODULE CONFIGURATIONS STUDY

William B. Collins
Joseph K. McDermott
Owen B. Smith
Martin Marietta Denver Aerospace
Denver, Colorado

ABSTRACT

The incorporation of nickel-hydrogen technology into spacecraft power system designs for LEO vehicles offers significant power system weight reductions by increasing the power storage watt-hour efficiency. Several possible module configurations exist for the power system. The module configurations were compared utilizing reliability, weight, volume and load capability as evaluation parameters. This paper summarizes the results of this study.

INTRODUCTION

The NASA Standard Multi-Mission Spacecraft (MMS) module was the baseline volumetric constraint for the energy storage system for this study. The MMS module has the following dimensions:

LENGTH - 44"
WIDTH - 44"
HEIGHT - 16"

For the Low-Earth-Orbit (LEO) application pertaining to this study, the entire MMS module was allotted for batteries. The battery chargers, shunt banks, power control units and power control and distribution units will be located outside the MMS module. The Electrical Power Subsystem Design Criteria for the LEO application specifies a 24 volt minimum battery voltage. Twenty-two series connected nickel-hydrogen cells could support this minimum battery voltage requirement. The conventional battery would thus consist of 22 series connected nickel-hydrogen cells. The 22 cell battery could be divided into submodules which could be series connected to comprise the battery. The

one-cell module configuration would differ from the conventional 22 series connected cells in that each one-cell module would have the capability for bypass in the event of a failure. Important considerations relative to module size determination are reliability, weight and load growth capability. Volume was not considered a critical selection parameter due to the allocation of the entire MMS module for cells/batteries.

The basic ground rules and assumptions for this study were:

1) The nickel-hydrogen cell specified in this report is the 50 Ampere-Hour, Air Force design cell per Hughes Aircraft Company specification PS32014-031.

2) Battery discharge current was limited to a 1.3 C rate, or 65 amps.

3) Battery System Operational Life is 3 years.

4) The battery shall utilize redundancy so that a single module or component failure does not reduce the capability of the battery to support mission requirements.

5) The reliability allocation for the Electrical Power Subsystem is 0.946. It is assumed for this study the reliability of the battery system must be at least 0.99.

6) There will be only one module configuration for the battery system. This will simplify design and structural requirements.

7) The maximum number of 50 Ampere-Hour cells, depicted in Figure 1, that will fit in the NASA MMS module is 126.

DESCRIPTION OF SELECTION PARAMETERS

Selection parameters considered for the nickel-hydrogen battery system application included weight, reliability, safety, charge/discharge characteristics and requirements, maintainability, support requirements and load growth capability. Three parameters have been selected from this list in which a significant difference exists among the module configuration candidates. The other parameters, while important, are not significantly impacted by the module configuration selected. The three selection parameters utilized for this study are reliability, weight and load growth capability.

Battery reliability is quantitatively described as the probability that the system reliability will deliver rated power for the required mission duration. The main factors affecting battery reliability are cell reliability, pressure vessel reliability and the quantities of cells per module and per battery. The two main failure modes for a nickel-hydrogen cell are the short-circuit and open-circuit conditions. The short-circuit failure mode usually affects only one cell in a module, and the module or battery may still be capable of supporting loads at a lower voltage. The open-circuit failure mode will affect the entire module and generally arises from mechanical damage within a battery or from the loss of electrolyte within the cells. The capability of bypass protection circuitry can enhance the overall system reliability and alleviate the failure modes of short-circuit and open-circuit. For this study reliability is considered the most important of the selection parameters. If the total battery system does not provide a reliability of at least 0.99, then the battery system is considered unacceptable and does not even deserve further consideration. A cell reliability number for a 50 ampere-hour nickel-hydrogen cell does not exist due to the absence of a LEO data base. For this study, a cell reliability of 0.99 is assumed. It should be noted that a 0.99 cell reliability is somewhat optimistic based on the lack of an adequate data base.

Weight is considered an important selection parameter due to its impact on life cycle costs. The overall significance of weight has been reduced by the fact the entire MMS module may be utilized. For this study however, weight has also been evaluated for each module as a function of the available power. This allows a comprehensive weight evaluation of each module.

The average electrical load of successive iterations of a spacecraft design normally increases. The capability of a battery system for load growth would be advantageous for future missions. The load growth capability of each module configuration with associated weight and reliability factors were evaluated for the load capability parameter.

NICKEL-HYDROGEN MODULE CONFIGURATIONS

A twenty-two cell nickel-hydrogen battery may be constructed by use of submodules in numerous ways. The requirement that the nickel-hydrogen battery system will utilize only one module configuration reduces the possible module candidates to four:

1) Twenty-Two Cell Module - The most simplistic approach to a battery configuration is to have the module level equivalent to the battery. The maximum number of identical twenty-two cell modules that could fit in the NASA MMS module is five (5). The following paragraphs evaluate the twenty-two cell module configuration for reliability, weight and load capability.

The LEO application defines the operational life for Electrical Power Subsystems as three (3) years. If time t is assumed to be three years, and the cell reliability (P_C) is assumed to be 0.99, then the reliability of a twenty-two cell module (P_B) may be expressed as:

$$P_B = (P_C)^N = (0.99)^{22} = 0.802$$

If k batteries out of m total batteries in the system must survive for the system to survive, and P_B is the battery reliability, then the overall system reliability may be expressed as:

$$S_R = \sum_{x=k}^{m} \frac{m!}{x!(m-x)!} (P_B)^x (1-P_B)^{m-x}$$

Table 1 illustrates the battery system reliability when the module reliability is 0.802 and the total number of modules is five. Table 1 shows the twenty-two cell module configuration is unacceptable for meeting the reliability requirement of 0.99 when three or more operational batteries are required for load support. In order for the overall battery system reliability to be above the Electrical Power Subsystem reliability requirement, only two batteries out of the five total can be required for mission success. If only two of the five total batteries are required, the overall system reliability would be 0.9935.

The weight of a 50 Ampere-Hour nickel-hydrogen cell is assumed to be approximately 3.0 pounds. If a 1.35 weight packaging factor is assumed for wiring, structure and thermal control, then the weight of a 22-cell module would be:

$$(22 \text{ Cells})(3.0 \text{ Lbs/Cell})(1.35) = 89.1 \text{ Lbs}$$

Each battery would require two relays to permit switching the battery on and off the Bus. A 1.3 C rate limit for the nickel-hydrogen cell dictates a possible charge/discharge current of 65 amps. If the relays are sized based upon a maximum contact rating of 65 amps, then 100 amp relays (derated) weighing approximately 0.75 lbs each would be required for switching. Smaller and lighter relays would suffice if the contact rating of the relays was reduced to 25 amps or less. For this study, a 25 amp relay weighing 0.3 lbs is utilized. The total battery weight would then be approximately 89.7 pounds. The total battery system weight for the five, 22-cell module battery system would be 448.5 pounds.

Table 1 shows the twenty-two cell module configuration is capable of meeting the Electrical Reliability Subsystem reliability requirement only if two operational modules are required out of the five total. A redundancy requirement of operation with one unit failed results in a design usable energy from only a one battery system. Using 1.2 volts as the end-of-life, end-of-discharge voltage for a nickel-hydrogen cell, the energy available from one battery from full charge to 100% DOD is:

(1 battery)(26.4 V/battery)(50 A-Hr) = 1320 Watt-Hours

For a three year mission, the maximum allowable DOD for the nickel-hydrogen battery is 60%. The usable available energy for the MMS module based upon the 22-cell module configuration would be:

(1320 Watt-Hours)(.60 DOD) = 792 Watt-Hours

A 1.3 discharge rate limit dictates a peak load capability of 65 amps. The peak load capability for a twenty-two cell module configuration based upon a one battery system would be:

(1 battery)(65 amps)(26.4 V/battery) = 1716 Watts

The twenty-two cell module configuration has the design capability to support a maximum load of 1716 watts for a maximum time of 27.7 minutes or until 792 watt-hours have been removed.

2) Eleven Cell Module - An eleven cell module consisting of eleven series connected cells is another viable nickel-hydrogen battery module configuration candidate. Two of the eleven cell modules electrically series connected would comprise a battery. The maximum number of eleven cell modules that could fit in the NASA standard MMS module is eleven. The following paragraphs evaluate the eleven cell module configuration for reliability, weight and load capability.

The reliability of the eleven cell module may be expressed as:

$$P_B = (P_c)^N = (0.99)^{11} = 0.895$$

If k modules out of m total in the system must survive for the system to survive, and P_B is the module reliability, then the overall battery system reliability, S_R, with the eleven cell module configuration may be expressed as:

$$S_R = \sum_{x=k}^{11} \frac{11!}{x!(11-x)!} (.895)^x (1-.895)^{11-x}$$

Table 2 summarizes the battery system reliability for k operational modules out of eleven total modules when the eleven cell module reliability is 0.895. Table 2 shows that the eleven cell module configuration is capable of meeting the battery system reliability requirement of 0.99 if seven of the total eleven modules are required for operational support. Seven modules could be connected to comprise a three battery system with one spare. The spare would meet the redundancy requirement of operation with one unit failed. From a reliability standpoint, the eleven cell module configuration would be acceptable if the load requirements do not exceed a three battery system capability.

If the weight of a 50 Ampere-Hour cell is assumed to be 3.0 pounds and a weight packaging factor of 1.35 is utilized, the weight of an eleven cell module would then be:

(11 Cells)(3.0 Lbs/Cell)(1.35) = 44.55 lbs

The switching configuration of relays required to connect eleven cell modules into various pairs to comprise a battery is rather complex. A minimum number of 144 relays are estimated to allow the independent switching to comprise 3 batteries out of 11 total modules. The total weight of the 11, eleven cell modules plus switching relays would be:

(11 modules)(44.55 lbs/module) + (144 relays)(0.3 lbs/relays)
= 533.3 lbs

The minimum acceptable battery system reliability requirement of 0.99 and the redundancy requirement of operation with one unit failed results in a maximum design load capability based upon a three battery system. The energy available from three batteries from full charge to 100% DOD would be:

(3 Batteries)(26.4 V/Battery)(50 AHr) = 3960 Watt-Hours

For a three-year mission, the maximum allowable DOD is 60%. The usable available energy from a three battery system comprised of eleven cell modules is:

(3960 Watt-Hours)(.60 DOD) = 2376 Watt-Hours

The battery system peak load capability would be:

(3 Batteries)(65 amps)(26.4 V/Battery) = 5148 Watts

The eleven cell module configuration battery system has the capability to support a maximum load of 5148 watts for a maximum time of 27.7 minutes or until 2376 watt-hours have been removed.

3) Two Cell Module - A two cell module consisting of two series connected cells is another possible module configuration. Eleven, two cell modules connected in series could comprise a battery. The following paragraphs evaluate the two cell module configuration for reliability, weight and load capability.

The reliability of a two cell module may be expressed as:

$$P_B = (P_c)^N = (0.99)^2 = 0.9801$$

The maximum number of modules that could fit in the NASA MMS module is 63. Eleven modules would be required per battery, thus a maximum number of five batteries are available. The reliability of a 22 cell battery consisting of eleven series connected two cell modules may be expressed as:

$$P_B = (P_c)^N = (0.9801)^{11} = 0.8016$$

This is unacceptable for a battery reliability. If, however, in each battery there is a spare two cell module, then the battery system reliability would be enhanced. Table 3 summarizes the battery reliability for k operational modules out of m total modules when the two cell module reliability is 0.9801 and the total number of modules is 12, 13 and 14. The 13 and 14 module concepts provide a battery reliability greater than 0.99. However, the overall battery system reliability has not yet been calculated. Table 4 summarizes the overall battery system reliability for the battery configurations reviewed in Table 3. The 14, two cell module configuration per battery provides a high overall battery system reliability of 0.9992. The redundancy requirement of operation with one unit failed has been met through the additional modules per battery. From a reliability standpoint, the two cell module configuration is an excellent candidate if the load requirements do not exceed a four battery system capability.

The weight packaging factor for a two cell module configured battery will be significantly greater than the twenty two or eleven cell module configurations due to the extra connections and cabling. For the two cell module configuration, a 1.50 weight packaging factor has been assigned. The weight of a two cell module would then be:

$$(2 \text{ Cells})(3.0 \text{ Lbs/Cell})(1.50) = 9.0 \text{ Lbs}$$

The switching configuration of relays required to comprise a twelve, thirteen or fourteen module battery would involve the capability to series connect various two cell modules or place the two cell modules in an open circuit condition. The advantage to this configuration is, off-line charging is probably not necessary if the capability to periodically switch modules in and out of the string exists. Twenty-six total relays (including redundancy) would be required for a 13, two cell module battery. The relays would be rated at 25 amps and

weigh 0.3 lbs each. The total weight of a a twelve, thirteen or fourteen module battery would be:

(12 modules)(9 lbs/module) + (24 relays)(0.3 lbs/relay) = 115.2 lbs

(13 modules)(9 lbs/module) + (26 relays)(0.3 lbs/relay) = 124.8 lbs

(14 modules)(9 lbs/module) + (28 relays)(0.3 lbs/relay) = 134.4 lbs

The NASA MMS module can accommodate five, 12 module batteries or four, 13 or 14 module batteries. The total battery system weight for the two cell module configuration is summarized in Table 5.

Five batteries consisting of twelve modules each would have a maximum available capacity of 250 ampere-hours. The energy available from full charge to 100% DOD would be 6600 Watt-hours. The redundancy requirement of operation with one unit failed has been met at the module level. The usable energy available from five batteries based upon a maximum allowable DOD of 60% would be:

(6600 Watt-Hours)(.60 DOD) = 3690 Watt-Hours

Four batteries consisting of thirteen or fourteen modules each would have a maximum available capacity of 200 Ampere-hours. The energy available from full charge to 100% DOD would be 5280 Watt-hours. The usable energy based upon a maximum allowable DOD of 60% would be:

(5280 Watt-Hours)(.60 DOD) = 3168 Watt-Hours

The 1.3 C discharge rate limit would dictate a peak load capability of 65 amps per battery. The battery system peak load capability of a four or five battery system would be:

(4 batteries)(65 amps)(26.4 V/battery) = 6864 Watts

(5 batteries)(65 amps)(26.4 V/battery) = 8580 Watts

Table 6 summarizes the load capabilities of the two cell module configurations.

4. One Cell Module - A one cell module is the smallest possible configuration candidate. Twenty-two, one cell modules connected in series would comprise a battery. The following paragraphs evaluate the one cell configuration for reliability, weight and load capability.

The reliability of a one cell module would simply be the cell reliability, or 0.99. If 22 one cell modules were series connected, the battery reliability would be:

$$P_B = (P_c)^N = (0.99)^{22} = 0.802$$

This is an unacceptable battery reliability. The battery reliability may be enhanced by having additional one cell modules per battery. The addition of spare modules would require the capability to switch cells in or out of the series. Table 7 summarizes the battery reliability for k operational modules out of m total modules for a cell reliability of 0.99. Table 8 summarizes the overall battery system reliability for the one cell module candidates. Five batteries consisting of 23 cells will fit in the MMS module, while four batteries consisting of 24 or 25 cells will fit in the MMS module. The redundancy requirement of operation with one unit failed has been met at the cell level within a battery. From a reliability standpoint, the one cell module configuration is an excellent candidate if the load requirements do not exceed a four battery system.

The weight packaging factor for the one cell module is assigned the same value as the two cell module, 1.50. The weight of a one cell module would then be:

(1 Cell)(3.0 Lbs/Cell)(1.50) = 4.5 Lbs

The switching configuration of relays required to comprise a 23, 24 or 25 cell battery would involve the capability to series connect 22 total modules and place the spare cells in an open circuit condition. A total of 50 relays are required for such a configuration for a 25 cell battery. The total weight of 23, 24 and 25 cell battery would be:

(23 cells)(4.5 lbs/cell) + (46 relays)(0.3 lbs/relay) = 117.3 lbs

(24 cells)(4.5 lbs/cell) + (48 relays)(0.3 lbs/relay) = 122.4 lbs

(25 cells)(4.5 lbs/cell) + (50 relays)(0.3 lbs/relay) = 127.5 lbs

The NASA Standard MMS module can accommodate five 23 cell batteries or four 24 or 25 cell batteries. The total battery system weight for the one cell module configurations is summarized in Table 9.

The load capabilities of a five or four battery system were calculated in the two cell module configuration paragraph. Table 10 summarizes the load capabilities of the one cell module configurations.

CONCLUSION

Table 11 summarizes the results of this study for a battery system with a minimum reliability of 0.99. The twenty-two and eleven cell module configurations require a large number of spare modules in order to meet the reliability requirements, resulting in poor specific energy densities for the configurations. The redundancy requirement of operation with one unit failed also significantly reduces the available design capacity for the twenty-two and eleven cell module configurations. The two and one cell module configurations provide the highest reliable battery system and appear to be the optimum configuration candidates for the NASA Standard MMS module.

It should be noted that this study was the initial investigation of nickel-hydrogen module configurations. Many system components of the Electrical Power System were not evaluated as to the impact of nickel-hydrogen modular implementation. The reliability of the relays for switching cells in or out of the series was assumed to be very high (1.00 for the study) and was not evaluated any further. The study does indicate, however, that the one cell module configuration is the optimum candidate for a nickel-hydrogen energy storage system.

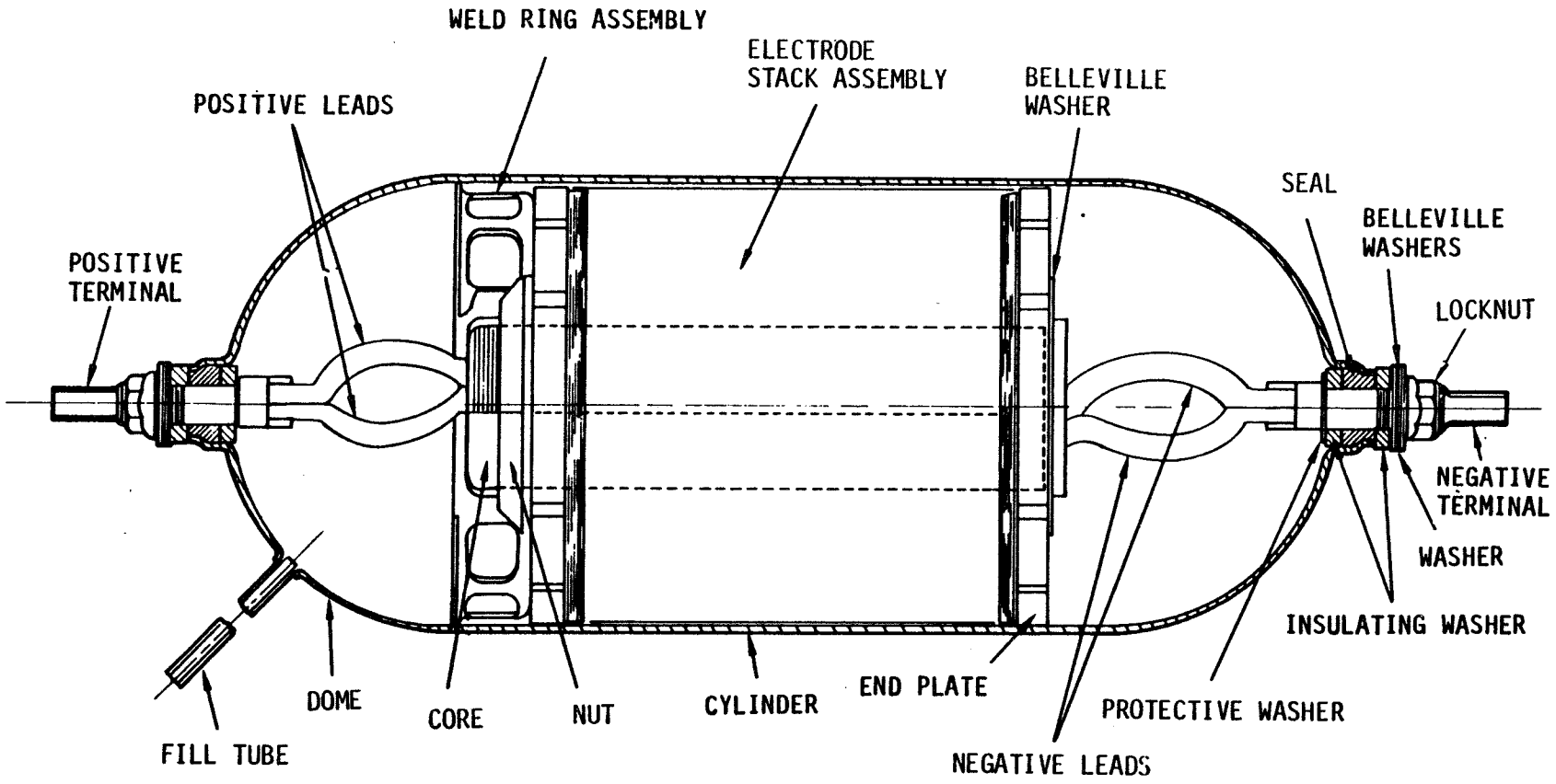

Figure 1. Individual Pressure Vessel Nickel-Hydrogen Cell

Table 1. TWENTY-TWO CELL MODULE OVERALL SYSTEM RELIABILITY

Number of Operational Batteries (k) Required Out of m Total (5) for Mission Success (0.95 Cell Reliability)	Overall Battery System Reliability
5	0.3310
4	0.7414
3	0.9436
2	0.9935
1	0.9997

Table 2. ELEVEN-CELL MODULE OVERALL SYSTEM RELIABILITY

Number of Operational Batteries (k) Required Out of m Total (11) for Mission Success	Overall Battery System Reliability
11	0.2952
10	0.6761
9	0.8995
8	0.9781
7	0.9966
6	0.9996
5	0.9999

Table 3. TWO-CELL MODULE BATTERY RELIABILITY

Number of Operational Modules (M) Required Out of N Total for a Battery		Battery Reliability
k	m	
11	12	0.9771
11	13	0.9980
11	14	0.9998

Table 4. TWO-CELL MODULE OVERALL BATTERY SYSTEM RELIABILITY

Number of Two-Cell Modules per Battery	Battery Reliability	Number of Batteries per MMS Module	Battery System Reliability
12	0.9771	5	0.8906
13	0.9980	4	0.9920
14	0.9998	4	0.9992

Table 5. TWO-CELL CONFIGURATION BATTERY SYSTEM WEIGHT PROFILE

Number of Two-Cell Modules per Battery	Number of Batteries per MMS Module	Total Battery System Weight (Lbs)
12	5	576.0
13	4	499.2
14	4	537.6

Table 6. TWO-CELL MODULE LOAD CAPABILITY

Modules per Battery	Number of Batteries per MMS Module	Load Capability (Watt-Hours)	Peak Load Capability (Watts)
12	5	3960	8580
13	4	3168	6864
14	4	3168	6864

Table 7. ONE-CELL MODULE BATTERY RELIABILITY

Number of Operational Modules (M) Required Out of N Total for a Battery		Battery Reliability
k	m	
22	22	0.8016
22	23	0.9780
22	24	0.9983
22	25	0.9999

Table 8. ONE-CELL OVERALL BATTERY SYSTEM RELIABILITY

Number of One-Cell Modules per Battery	Battery Reliability	Number of Batteries per MMS Module	Battery System Reliability
23	0.9780	5	0.8947
		4	0.9149
24	0.9983	5	0.9915
		4	0.9932
25	0.9999	5	0.9995
		4	0.9996

Table 9. ONE-CELL CONFIGURATION BATTERY SYSTEM WEIGHT PROFILE

Number of Cells per Battery	Number of Batteries per MMS Module	Total Battery System Weight (Lbs)
23	5	586.5 Lbs
23	4	469.0 Lbs
24	4	489.6 Lbs
25	4	510.0 Lbs

Table 10. ONE-CELL MODULE LOAD CAPABILITY

Cells per Battery	Number of Batteries per MMS Module	Load Capability (Watt-hours)	Peak Load Capability (Watts)
23	5	3960	8580
24	4	3168	6864
25	4	3168	6864

Table 11. BATTERY CONFIGURATION EVALUATION SUMMARY

Module Configuration	Battery System* Reliability	Battery System Weight (Lbs)	Capacity (Watt-Hours)	Peak Load Capability (Watts)
22 (Five, 22-cell batteries)	0.9935	448.5	792	1716
11 (Eleven, 11-cell modules; five batteries total)	0.9966	533.3	2376	5148
2 (13, 2-cell modules/battery; 4 batteries total)	0.9920	499.2	3168	6864
1 (24, 1-cell modules/battery; 4 batteries total)	0.9932	489.6	3168	6864

* Minimum acceptable reliability for battery system is 0.990. All module configurations listed in this table were based on this minimum acceptable battery system reliability. Redundancy requirement of operation with one unit failed also included in this table.

NICKEL HYDROGEN BIPOLAR BATTERY ELECTRODE DESIGN

PRESENTED BY
V. J. PUGLISI
YARDNEY BATTERY DIVISION
YARDNEY CORPORATION

NICKEL HYDROGEN BIPOLAR BATTERY

ELECTRODE DESIGN

V. J. Puglisi, P. Russell, D. Verrier and A. Hall

Yardney Battery Division

ABSTRACT

Nickel Hydrogen technology is broadening to meet the expanding power requirements of the aerospace industry. This is occurring not only with the individual pressure vessel (IPV), as exemplified by the MILSTAR 70AH cell development and the Air Force Advance Development 4.5 inch diameter cell initiative, but also with multi-cell common pressure vessel development sponsored by NASA (Lewis Research Center). This latter effort is being performed by Ford Aerospace with Yardney Battery Division supporting (1).

The preferred approach of the NASA development effort utilizes a bipolar plate stacking arrangement to obtain the required voltage-capacity configuration. In a bipolar stack, component designs must take into account not only the typical design considerations such as voltage, capacity and gas management, but also conductivity to the bipolar (i.e., intercell) plate. The nickel and hydrogen electrode development specifically addressing bipolar cell operation is the subject of this paper.

Nickel oxide electrodes, having variable type grids and in thicknesses up to .085 inch are being fabricated and characterized to provide a data base. A selection will be made based upon a system level trade-off. Negative (hydrogen) electrodes are being screened to select a high performance electrode which can function as a bipolar electrode. Present nickel hydrogen negative electrodes are not capable of conducting current through their cross-section. An electrode has been tested which exhibits low charge and discharge polarization voltages and at the same time is conductive. Test data is presented.

INTRODUCTION

Nickel hydrogen cell technology is currently being utilized as the basis upon which many of the new satellite power systems are predicated. Current IPV cells have plates connected in parallel to provide an ampere

hour (AH) capacity which is the sum of the plate capacities, and exhibit the characteristic couple voltage (about 1.2V). Cells are grouped in a series string to yield a higher voltage battery. The total available power is typically under 2KW. The MILSTAR satellite program is requiring the development of a 70AH cell capability with a growth potential to 100AH, thereby advancing the state-of-the-art from the current 50AH plateau. In addition, the USAF has initiated an advanced development effort which seeks to obtain a higher capacity cell by increasing the cell's diameter from 3.5 inches to 4.5 inches. This should allow higher capacities, possibly up to 200AH, to be attainable within a passively cooled individual pressure vessel.

NASA (Lewis Research Center) has identified nickel hydrogen technology as a potential candidate to meet the multi-kilowatt power requirements of planned future missions (2). To meet these higher power demands in an efficient manner, NASA is not relying on the existing individual pressure vessel approach, but has embarked on exploration of large common pressure vessel designs (3). These design approaches have been the subject of several publications to date (4-7). Because of the size of the eventual battery (150V, 75AH) and derivatives thereof, the design will require active cooling to maintain the stack components within a 5°C range during the course of the low earth orbit duty cycle. This is a marked departure from passive cooling utilized in the present nickel hydrogen cell technology.

The preferred stack approach, based on projected superior voltage, capacity and relative simplistic design, is the bipolar arrangement shown in Figure 1. This has however necessitated a tailoring of the component design and in many instances, new developments.

This paper reports the status of nickel oxide and hydrogen electrode development being performed under the first task, entitled Initial Design, of the NASA funded effort.

NICKEL OXIDE ELECTRODE INVESTIGATION

The key desirable attributes of the nickel oxide electrode are as follows:

- high energy density and specific power
- cycle life to achieve mission goals
- thick electrodes exhibiting high performance
- conductivity with the bipolar plate

The first two attributes are required in all aerospace designs. The third, a high performance thick electrode, is particularly important with

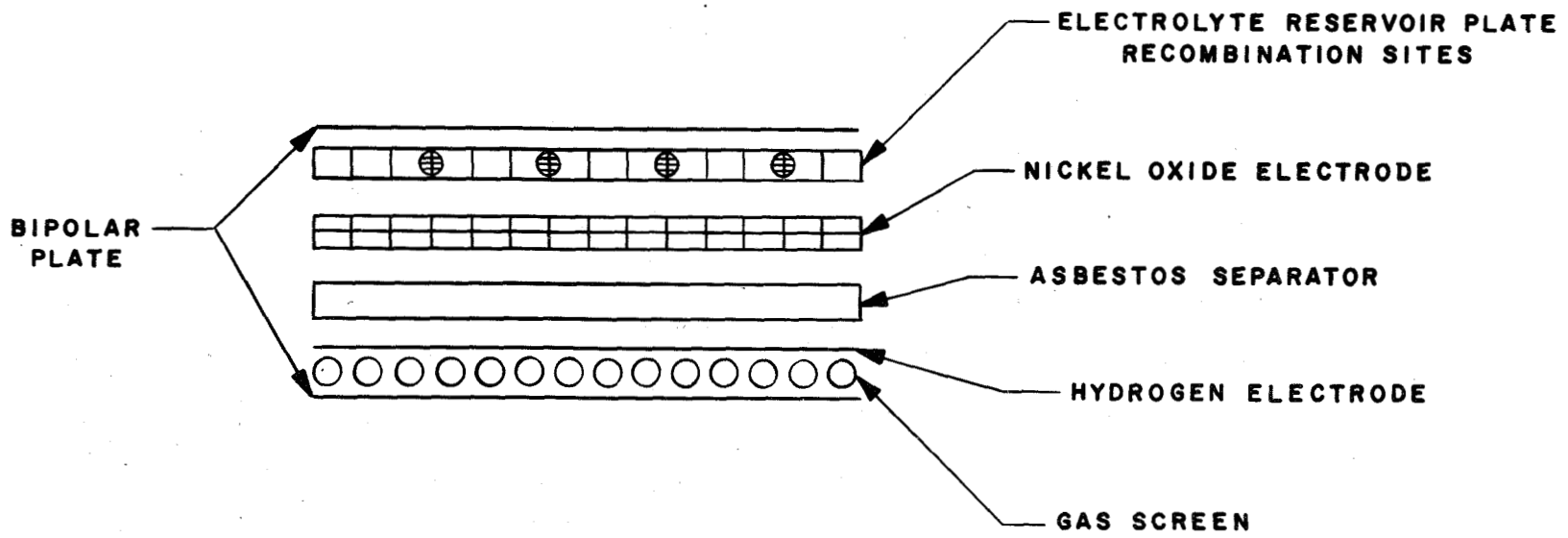

Figure 1. Bipolar Cell Stack Schematic

a bipolar configuration because a reduction in plate area results in a complimentary reduction in ancillary component weight (e.g., cooling system, bipolar plate, electrolyte reservoir plate, etc.) assuming an electrode efficiency independent of thickness. The fourth desirable attribute, conductivity of the nickel electrode with the bipolar plate was, at the program's inception, a key development question. The concern was that oxide formation on the bipolar plate during overcharge would render the interface less conductive and thereby inefficient.

Assessment of the available nickel oxide electrode types relative to a proper selection can only be made with the total system in mind. In particular, the selection must be based on the optimum 75AH battery weight and volume attainable as a function of nickel electrode thickness. For example, a minimal capacity gain, when translated in ancillary component weight savings, may be advantageous in spite of the small corresponding capacity increase with thickness.

To arrive at an electrode data base such that the type of trade-off described above can be made, characterization tests are being performed on a number of electrode types. These types include grid variations (either screen or exmet), variable number of grids per electrode (either 1 or 2), and finally variable electrode thickness (up to .085 inch). All electrodes have been fabricated employing a slurry method to manufacture sintered plaque and an aqueous electrochemical impregnation to deposit the active material within the plaque.

Characterization cycling of these electrodes is being carried out in a nickel hydrogen bipolar test cell. To ensure consistent voltage measurements, a gold-plated, nickel bipolar plate is being utilized and nickel electrode voltages are recorded versus a hydrogen (platinum) reference electrode. Characterization of each electrode type is being performed at two charge rates (15 and 100 mA/cm^2) and four discharge rates (15, 50, 100 and 150 mA/cm^2). A ten percent overcharge is used in all instances and discharges are terminated at 1.0 volts for purposes of capacity calculation.

Data obtained for screen grid type electrodes is shown in Figures 2 and 3. Figure 2 illustrates the capacity obtained as a function of discharge current density for various electrode thickness. All charges were at 15 mA/cm^2 and the ambient temperature was maintained at 20 ± 3°C. It is apparent that the dependence of capacity is relatively independent of discharge rate for all thicknesses investigated. It should be noted that the capacities obtained at the lowest discharge rate are virtually identical to the theoretical values calculated from actual active material weight gain.

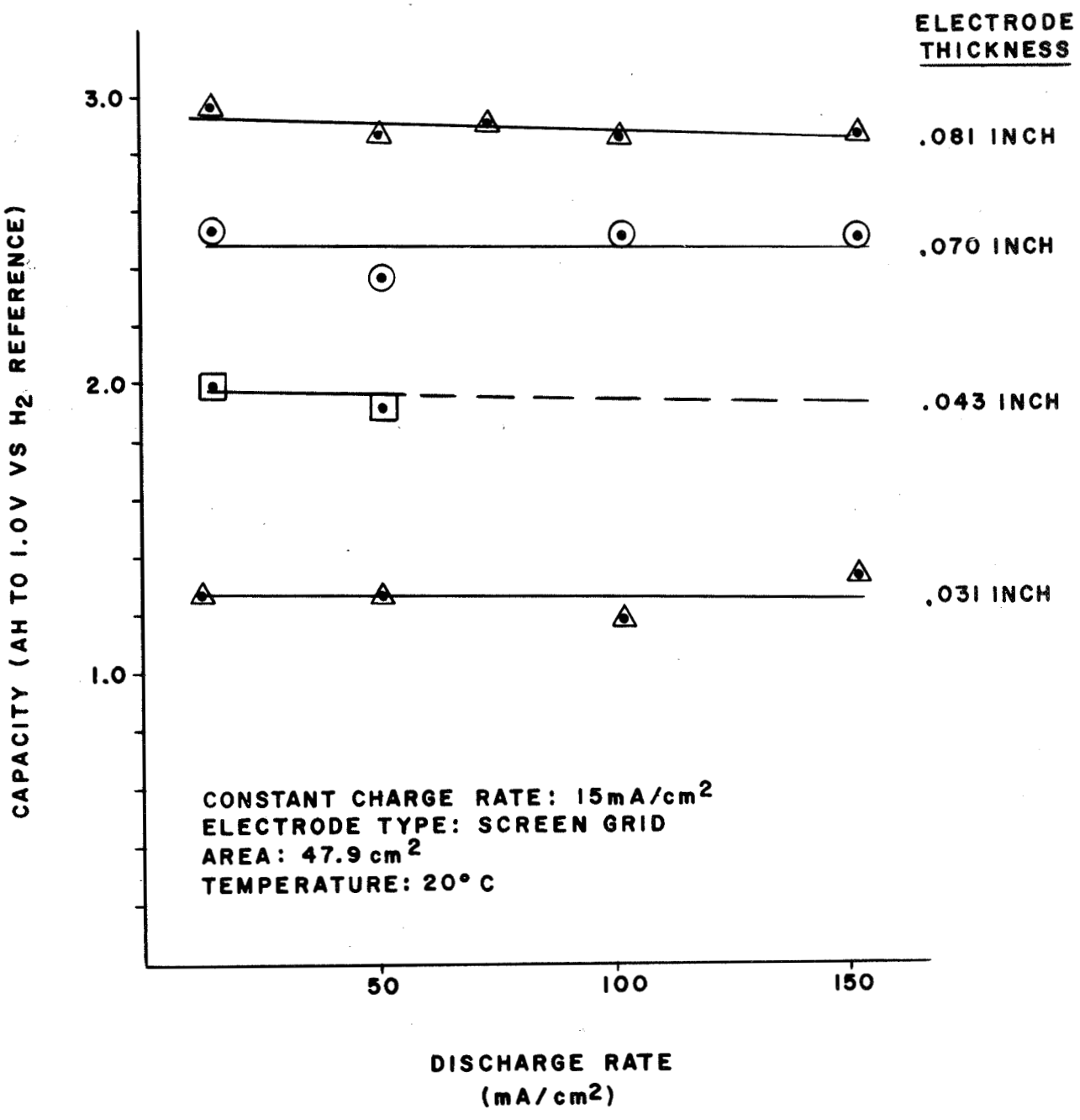

Figure 2. Nickel Electrode Capacity vs Discharge Rate

Figure 3 illustrates the dependence of plate capacity as a function of charge current density for various electrode thicknesses. All discharges were at 50 mA/cm^2. Although only two charge current densities (i.e., 15 and 100 mA/cm^2) were used to generate the curves, the negative influence of higher charge current densities with increasing thickness is apparent.

Table I illustrates the required charge and discharge regime of a 75AH battery operating in a Low Earth Orbit as a function of depth of discharge (DOD). The discharge rate is predicated on having a total plate area of 1238 square centimeters and a discharge time of 35 minutes. The charge rate assumes a 1.10 charge input to discharge output (i.e., C to D) ratio and an allowed charge time of 55 minutes. It can be seen that for operation at 80% DOD, a discharge current density of 83 mA/cm^2 is required to remove the 60AH in the allowed time. Further, to return that taken out plus 10% (i.e., 66AH) in 55 minutes requires a charge current density of 58.1 mA/cm^2. By definition, the battery would be rated employing these 80% DOD rates by discharging to 1.0V.

To examine the performance of a bipolar cell under various conditions identified in Table I, a .079 inch thick nickel electrode (denoted type A12) was assembled as shown in Figure 1. The bipolar plates were nickel and an 0.04 inch thick electrolyte reservoir plate was interposed between the nickel electrode and the bipolar plate. The actual end-of-charge and end-of-discharge voltages of the nickel electrode versus a hydrogen (platinum) reference electrode are given in Table I. Data obtained at 20°C is presented for 40 and 80% DOD and at 10°C for an 80% DOD. Continued discharge at the 80% DOD rate and 10°C yielded an equivalent battery capacity of 87AH. The voltage data was recorded following 20 such cycles and has shown that the conductivity of the nickel electrode to the bipolar plate is not affected by cycling.

HYDROGEN (PLATINUM) ELECTRODE

The key desirable attributes for a hydrogen electrode operating in a bipolar cell configuration are as follows:

- low polarization on charge and discharge (<25 mV at 15 mA/cm^2)
- cycle life to achieve mission goals
- conductivity through the electrode's cross-section

The first two attributes are common to all aerospace applications. The third is unique to bipolar cell operation.

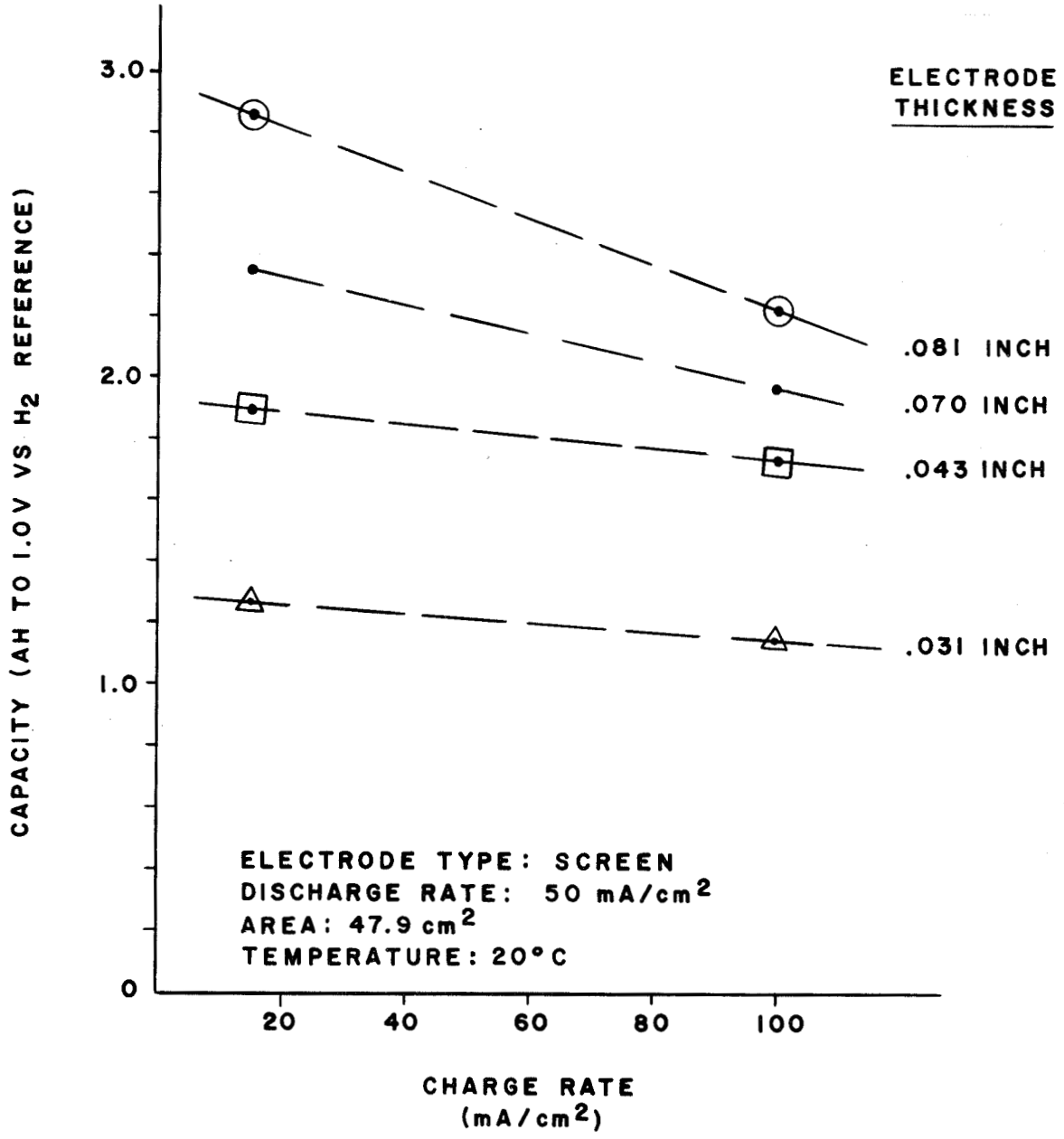

Figure 3. Nickel Electrode Capacity vs Discharge Rate

Table I. LEO[1] CHARGE/DISCHARGE PERFORMANCE VERSUS PERCENT DOD FOR A 75 AHR BATTERY[2]

	DISCHARGE		CHARGE		ACTUALS[3]	
% DOD	AHR DEL'D.	RATE(MA/CM^2)	AHR RET'D.	RATE(MA/CM^2)	EOCV	EODV
10	7.5	10.4	8.25	7.3		
20	15.0	20.8	16.50	14.5		
30	22.5	31.1	24.75	21.8		
40	30.0	41.5	33.0	29.1	1.44	1.28
50	37.5	51.9	41.25	36.3		
60	45.0	62.3	49.50	43.6		
70	52.5	72.7	57.75	50.9		
80	60.0	83.0	66.00	58.1	1.47/1.49[4]	1.21/1.20[4]

(1) CHARGE TIME OF 55 MINUTES FOLLOWED BY A 35 MINUTE DISCHARGE
(2) POSITIVE PLATE AREA IS 1238 CM^2
(3) ELECTRODE A12 IN A BIPOLAR CONFIGURATION @ 20°C, VOLTAGE MEASURED VS H_2 REFERENCE
(4) SAME AS (3) BUT AT 10°C

The commonly employed aerospace hydrogen electrode has demonstrated both low polarization and good cycle life. However, since it has a non-conductive hydrophobic backing, it is not suitable for use in a bipolar configuration. The polarization performance of this type of electrode can serve as a benchmark upon which to grade other electrode types.

Several types of available Fuel Cell electrodes were tested. These electrodes were attractive since they are conductive through their cross-section and since they have demonstrated long-term operational life. Electrodes ranging in platinum loading from 0.5 to 12 mg/cm^2 have been tested. It was found that although voltage performance on charge was adequate, voltage performance on discharge was variable at best. This latter behavior appears to result from flooding of these electrodes with the production of H_2O during discharge. This tended to make the voltage unstable, increasing as the discharge proceeded. A third type of electrode, developed at Yardney specifically for bipolar use, was tested. Its charge and discharge voltage performance is shown in Figure 4.

The performance of hydrogen electrodes tested showed a dependence on hydrogen pressure, with improved performance corresponding to higher hydrogen pressures. For that reason, charge and discharge curves are presented at two pressures (i.e., 100 and 600 PSIG). These pressures are projected to be close to the eventual battery end-of-discharge and end-of-charge pressures, respectively. Charge and discharge polarization curves for the standard aerospace electrode are also given as a basis for comparison.

As can be seen from Table I, the full 75AH battery is projected to operate at maximum charge and discharge current densities of 58 and 83 mA/cm^2, respectively. Anticipated hydrogen electrode polarization at these current densities, taken from Figure 4, are about 35 and 60 mV.

SUMMARY

Nickel electrode characterization is proceeding. Electrodes having thicknesses of up to .085 inch have been fabricated employing slurry plaque and electrochemical impregnation techniques. The dependence of capacity on discharge current density has shown thusfar to be minimal, whereas the dependence on charge current density is significant for the thicker electrodes. Data, typified by that presented above, will be generated for additional electrode types. This data base will be employed in trade-off studies to make an electrode selection yielding the optimum battery.

Candidate hydrogen electrodes have been investigated. Table II summarizes the findings to date. The aerospace type electrode was dismissed for lack of conductivity through its cross-section. The fuel cell type electrodes were found deficient in discharge performance, exhibiting evidence of flooding. A third electrode type, developed by Yardney, appears to be suitable, but must be tested to determine its life cycle capability.

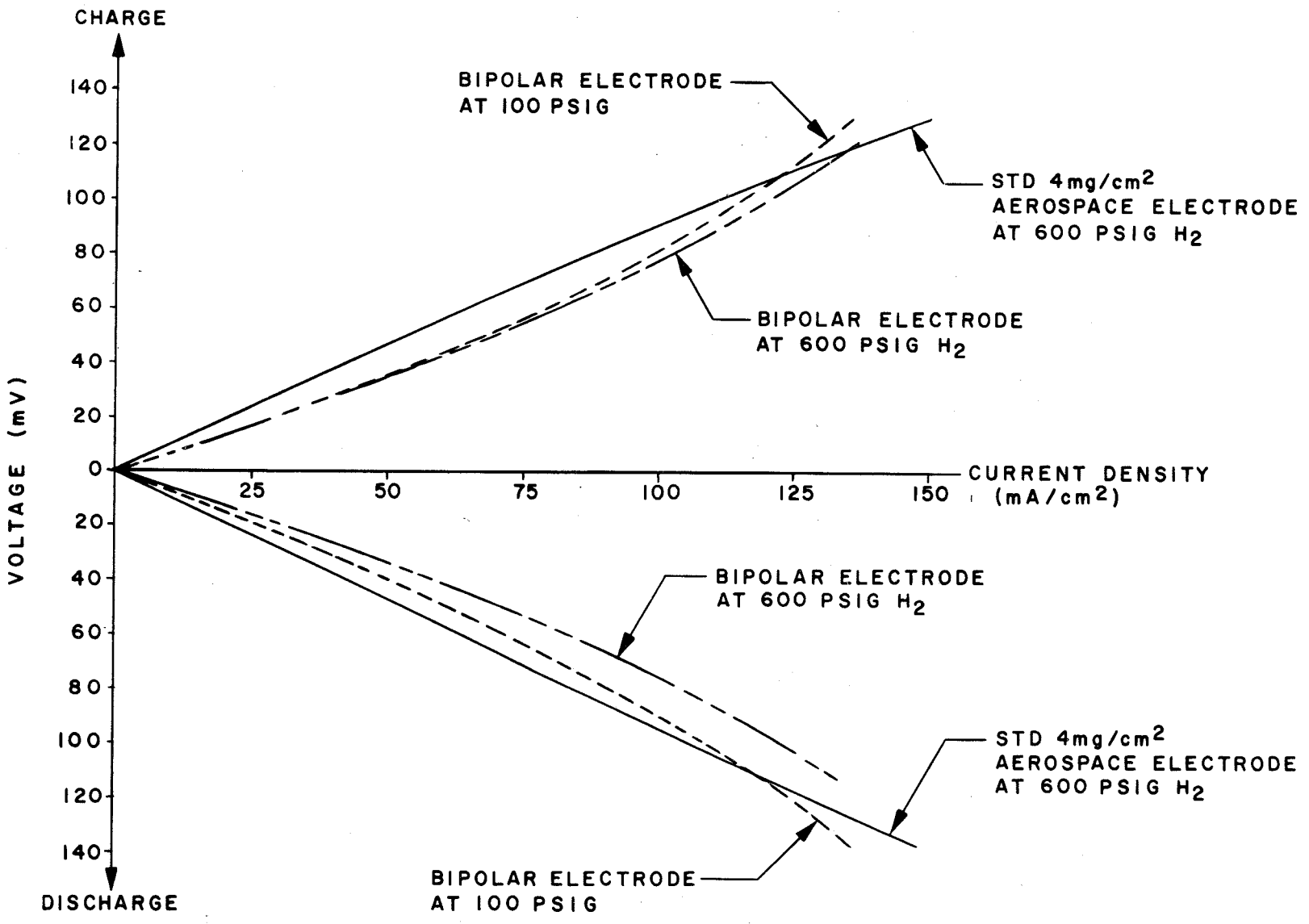

Figure 4. Hydrogen Electrode Polarization

Table II. HYDROGEN ELECTRODE ASSESSMENT

ELECTRODE TYPE	ASSESSMENT OF CHARACTERISTIC			
	CONDUCTIVITY	POLARIZATION		CYCLE LIFE
		CHARGE	DISCHARGE	
1. STATE-OF-ART AEROSPACE (4MG/CM^2)	NO	GOOD	GOOD	GOOD
2. FUEL CELL ELECTRODES	YES	ADEQUATE	POOR	GOOD
3. YARDNEY BIPOLAR ELECTRODE	YES	GOOD	GOOD	TBD

REFERENCES

1. NASA (Lewis Research Center) Contract NAS 3-23879 awarded to Ford Aerospace & Communications Corporation, March 1984, entitled Advanced Nickel Hydrogen Battery Development.

2. Joint Nickel-Hydrogen Technology and Advanced Battery Development Plan presented to the SSTAC sub-committees on Energy Storage Technology by Electrochemistry Branch, S&ED, LeRC, June 1981.

3. NASA RFP 3-377289, Advanced Nickel Hydrogen Battery Development, 1982.

4. "Bipolar Nickel-Hydrogen Batteries for Aerospace Applications", C.W. Koehler, G. van Ommering, N. H. Puester, and V. J. Puglisi, 1983 Goddard Space Flight Center Battery Workshop, p. 495.

5. "Bipolar Nickel-Hydrogen Battery System Design", G. van Ommering and C. W. Koehler, Proceedings of the 19th Intersociety Energy Conversion Engineering Conference, Volume I, p. 625.

6. "Thermal and Geometrical Considerations in a Bipolar Nickel-Hydrogen Battery Design", C. W. Koehler and G. van Ommering, 31st Power Sources Symposium Proceedings, (to be published).

7. "System Considerations for a Bipolar Nickel Hydrogen Battery", G. van Ommering, 1984 Goddard Space Flight Center Battery Workshop (to be published).

NICKEL-HYDROGEN CELL LIFE TEST

James R. Wheeler and Dwaine K. Coates
Eagle-Picher Industries, Inc.

ABSTRACT

Over 6,900 LEO cycles have been accumulated at 30% DOD on twelve Intelsat-design nickel-hydrogen cells. Physical equipment and cells are described. Performance characteristics are seen to be uniform. Further testing is planned to seek a failure mode, and also to investigate the effects of a new additive for nickel-hydrogen cells. Initial results indicate improved performance at higher temperatures and diminished swelling of positive nickel plates.

INTRODUCTION

Nickel-hydrogen battery cells are now in general use for geo-synchronous (GEO) satellites. Five satellites with nickel-hydrogen batteries have been successfully launched in the last two years and over a dozen are scheduled for the near future. All of these use the Intelsat design. However, the use of this design for low earth orbit (LEO) has not been widely explored.

To investigate the efficacy of the Intelsat design for LEO applications twelve standard production cells (RNH-30-1) with nominal 30 ampere-hour capacities each are being cycled in a LEO regime. The results to-date are described herein. Future plans are also discussed.

CELL DESCRIPTION

The twelve cells were constructed as part of standard production cell lots. A typical RNH-30-1 cell is shown in Figure 1. Eight cells were of completely normal construction. Two (numbers 2 and 4 in accompanying figures) contain negative plate substrates of a unique patented design and two (numbers 1 and 3) contain special positive plates. However, the latter four cells are normally constructed in every other respect and were processed and given acceptance testing with a production cell lot.

The new negative plate substrates, Figure 2, are designed to enhance electrical efficiency by minimizing the electrical current path length to the tab. At the same time, the tab area is considerably

strengthed structurally in comparison with previously-used designs by a concentration of radial ribs near the tab-rib and by tapering of the tab-rib itself. The overall geometric design provides roughly-rectangular structural sectors which are essentially identical in surface area, thus providing a relatively homogenous surface for adhesion of platinum catalyst.

The two cells with special positive plates were designed to investigate performance characteristics of a particular nickel-oxide sinter lot.

TEST FIXTURING

The test fixture is shown in Figure 3. Each cell is mounted in an aluminum thermal flange which is bonded to it with RTV-560 and which is electrically isolated by a layer of photo-etched mylar. The cells are mounted in a common vertical aluminum fixture which is 0.8 inches thick. Its large mass enables it to serve effectively as a stabilizing heat reservoir.

The entire fixture is contained in a refrigerated chamber which is able to regulate temperature to $4 \pm 3^{\circ}C$. Each cell is mounted horizontally. Some additional cells may be seen in Figure 3 alongside the vertically-standing fixture. These are part of another life test being run concurrently with this one.

As safety features the test chamber contains a catalytic hydrogen gas sensor and a temperature-sensitive switching element. These are wired to a fault-relay which will terminate cycling and trigger an audible alarm in the event of a hydrogen leak or excessive heat build-up. Over/under voltage protection is also provided.

Ancillary equipment includes a small computer which controls cycling automatically, a power supply, and a monitor for recording voltage.

CYCLE REGIME AND PERFORMANCE

The cells have, as of November 1984, completed over 6,900 LEO cycles at a 30% depth-of-discharge (DOD), i.e., 55 minutes of charge at C/3 and 35 minutes of discharge at C/2 for 16 cycles per day.

The initial charge/discharge (C/D) ratio of 1.08 was reduced to 1.04 after 3,300 cycles to maintain an EOC V near 1.57 volts per cell. C/D was further reduced to 1.02 at 6,000 cycles and then re-adjusted to 1.03 at 6,400 cycles.

EOC and EOD voltages have remained quite uniform throughout cycling. Data representative of the lowest and highest cell at each measurement are displayed in Figures 4 and 5.

Discharge capacities are measured at intervals to monitor cell performance. This typically consists of a C/2 discharge to 1.0 volt which is preceded by a C/10 charge for 16 hours. Capacities are shown in Figure 6. Note that capacities increased significantly at cycle 4200. A mechanical failure occurred at that time which caused the unintended reversal of all twelve cells to an average of -0.25 volts per cell.

Charge retention is also measured at intervals. The cells are charged at C/10 to knee-over (typically eighteen hours) and EOC voltages obtained. After a four to twelve day open-circuit stand another OCV is obtained. Capacity after one such stand is shown in the last column of Figure 6. Charge-retention voltage data are tabulated in Figure 7.

FUTURE PLANS FOR LIFE TESTING

It is planned to continue life-testing of the twelve cells indefinitely with the intention of eventually determining a failure mode. In addition, life testing of two additional RNH-30-1 cells is planned. These are identical to those of a recent production cell lot except that they contain a special additive.

The additive used increased cell capacity at higher temperatures and also improved charge retention at 10°C. Figure 8 shows capacity comparisons between the two additive cells (cells A and B) and the production cell lot in which they were built and tested. The change is most striking at 30°C where an eight ampere-hour improvement is seen. The improvement in 10°C capacity after a 72-hour charge-retention stand is nearly four ampere-hours.

Figures 9 through 19 show time/voltage comparisons between one of the additive cells (labeled "A") and one cell representative of the production lot average. The abrupt, brief rise in voltage near the end of some discharge curves is an artifact of the curve-smoothing algorithm and should be disregarded.

Beyond the improvements in capacity and charge retention an interesting feature is a rise in voltage near EOC for the additive cell which invariably crosses-over the non-additive cell's voltage.

As a check on possible effects of the additive used, a 10C stress test was performed on similar positive plates, using a 12-minute charge/6-minute discharge cycle. Six plates were immersed in normal KOH (1.300 SpG) and six in the same KOH with the additive. Thickness measurements were made before testing and after cycles 55, 160, 240 and

320. The measurements are tabulated in Figure 20. Notably, the plates in the additive grew only 1 to 4 mils compared to those in the regular KOH which thickened 4 to 8 mils. This stress test was extremely severe and went far beyond the number of cycles normally employed.

SUMMARY

Over 6,900 LEO cycles have been accumulated at 30% DOD on twelve Intelsat-design nickel-hydrogen cells. Although the cells are from two different production lots, voltage and capacity performances have been very uniform and charge retention characteristics remain nominal. Voltage reversal on one discharge was seen to have a posi-tive effect on capacity and did not otherwise affect performance. New design negative-plate substrates have not affected performance at the low charge/discharge rates used.

Future plans include continued testing of the twelve cells with the intent of determining a failure mode. Two cells with a special additive will also be tested in a regime yet to be determined. Initial results indicate improved capacity at higher temperatures and improved charge-retention characteristics. Plate growth may also be reduced because of the additive.

Not least of all, the efficacy of nickel-hydrogen cells without wall-wicks in LEO cycles is being shown as superior to previous esti-mates. A useful life-test data base in this regard continues to be generated.

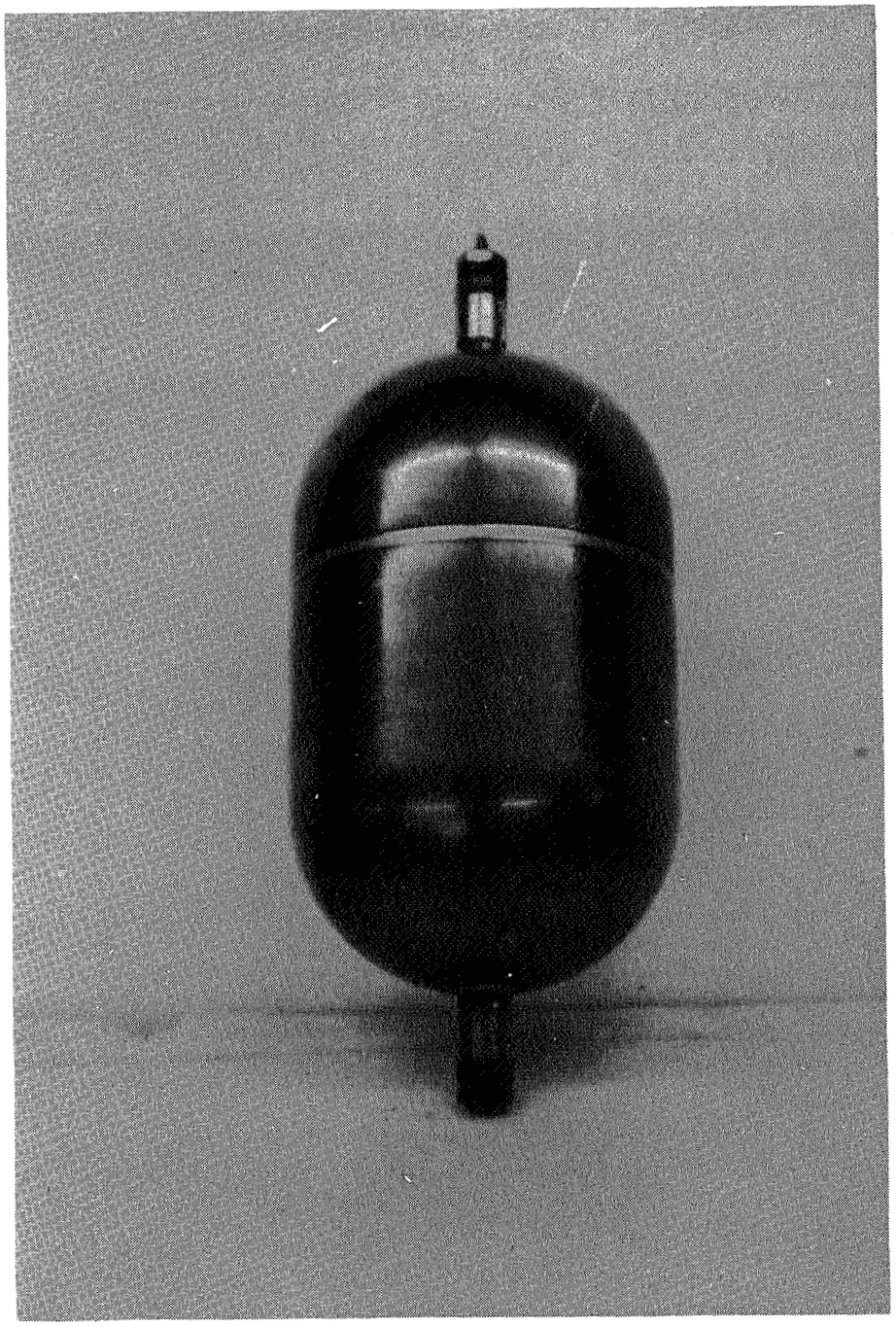

Figure 1. Typical RNH-30-1 Nickel-Hydrogen Cell

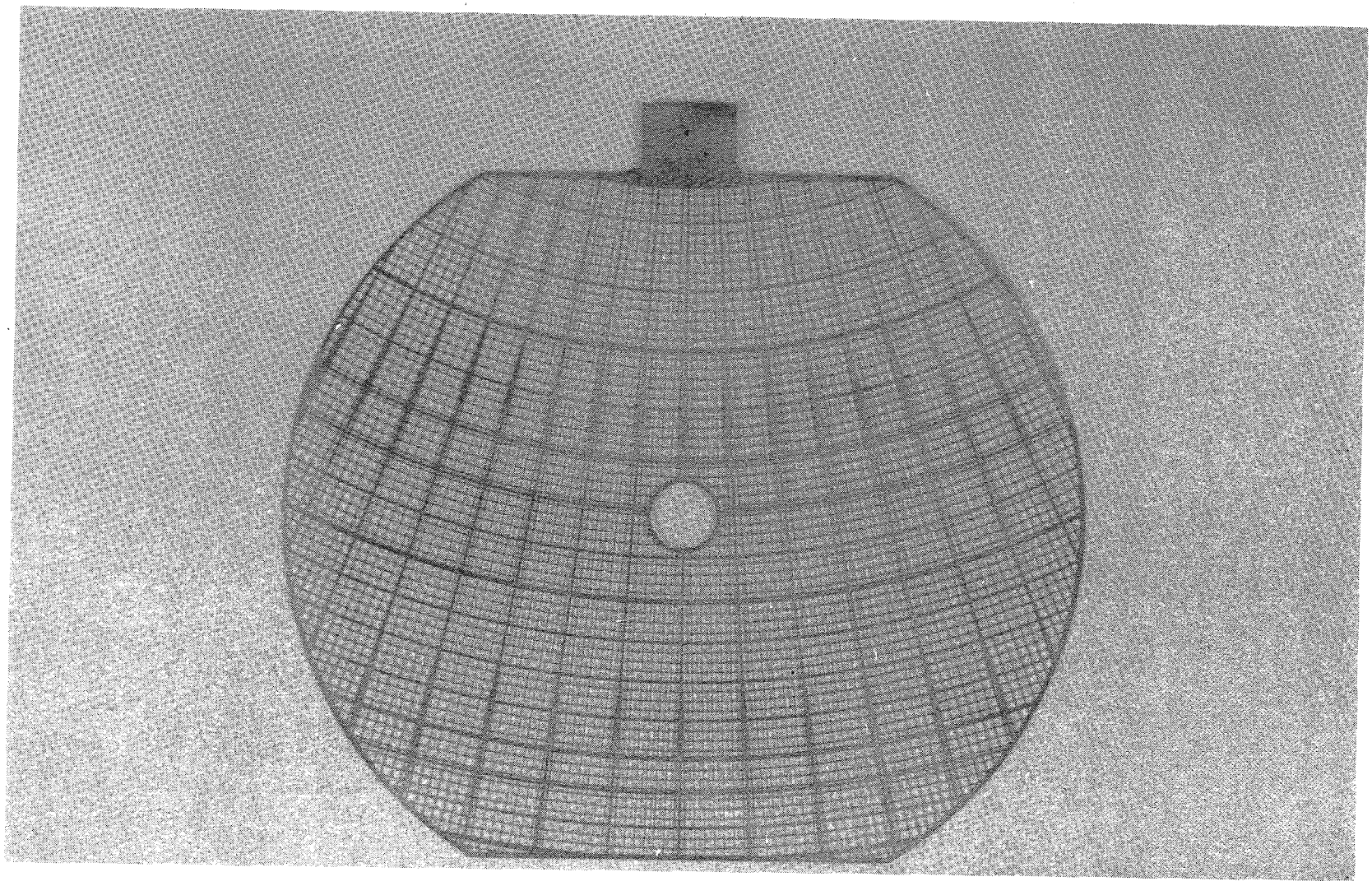

Figure 2. Negative Plate Substrate (U.S. Pat. No. 4,477,546)

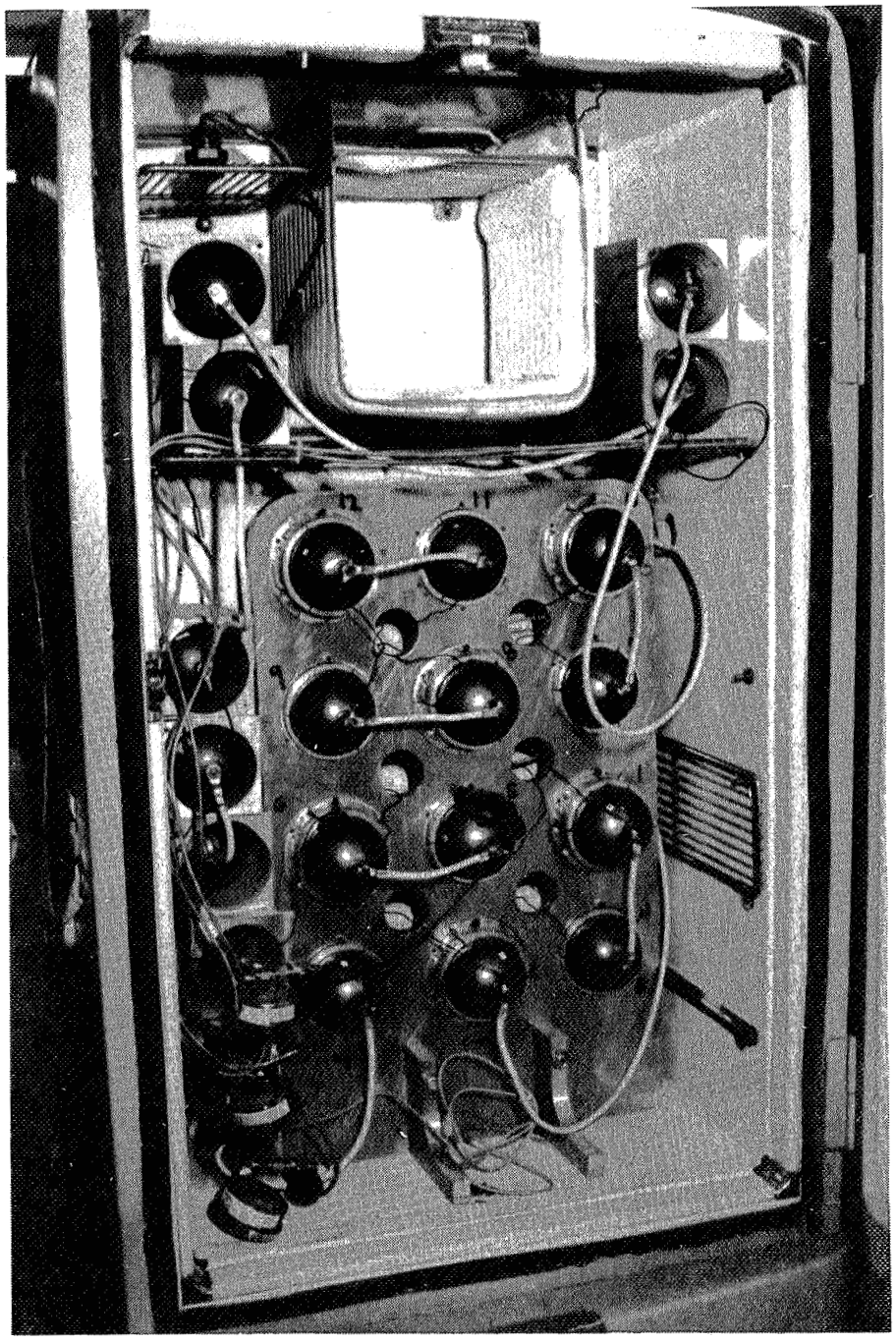

Figure 3. Test Fixture and Refrigeration Chamber

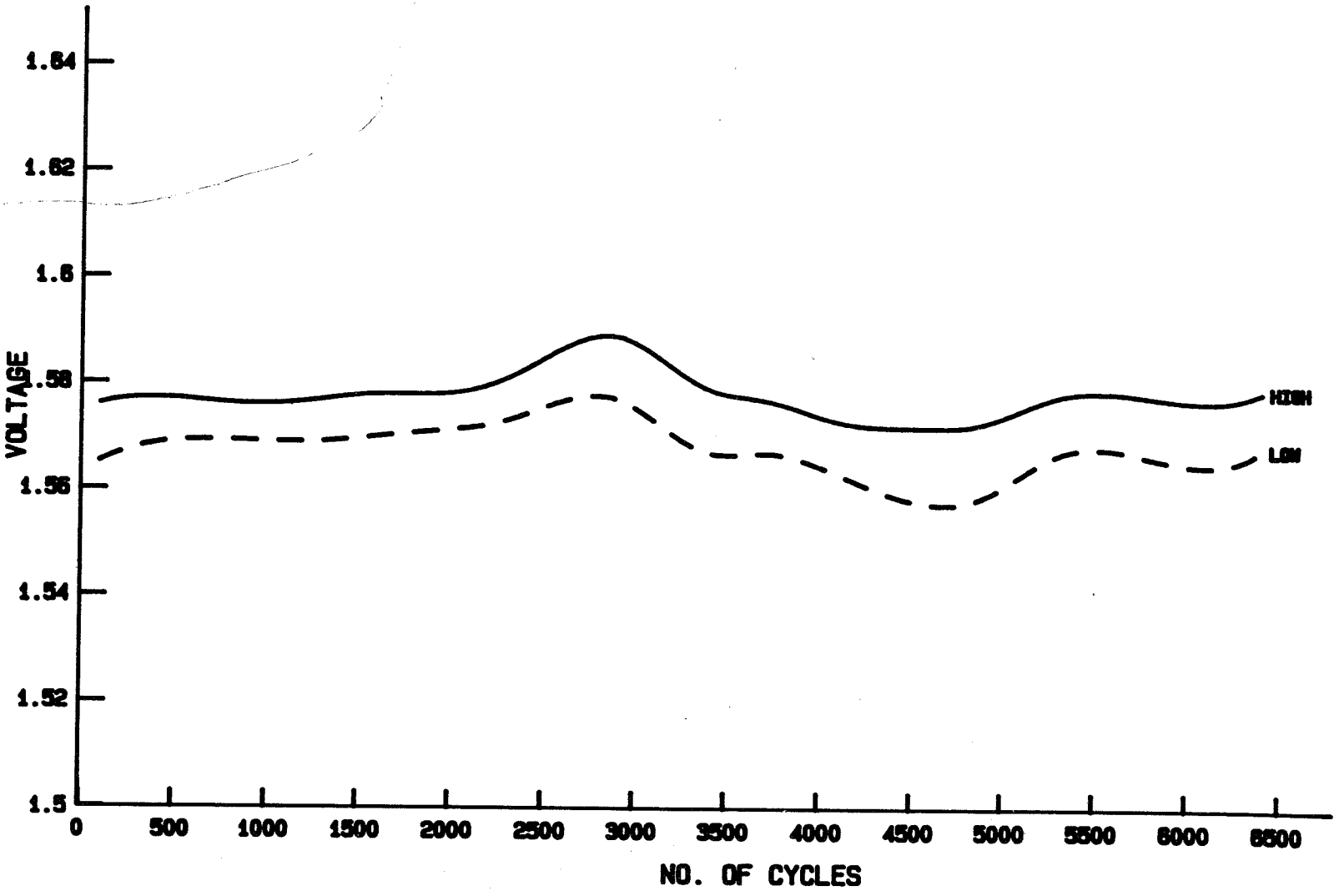

Figure 4. End-of-Charge Voltages

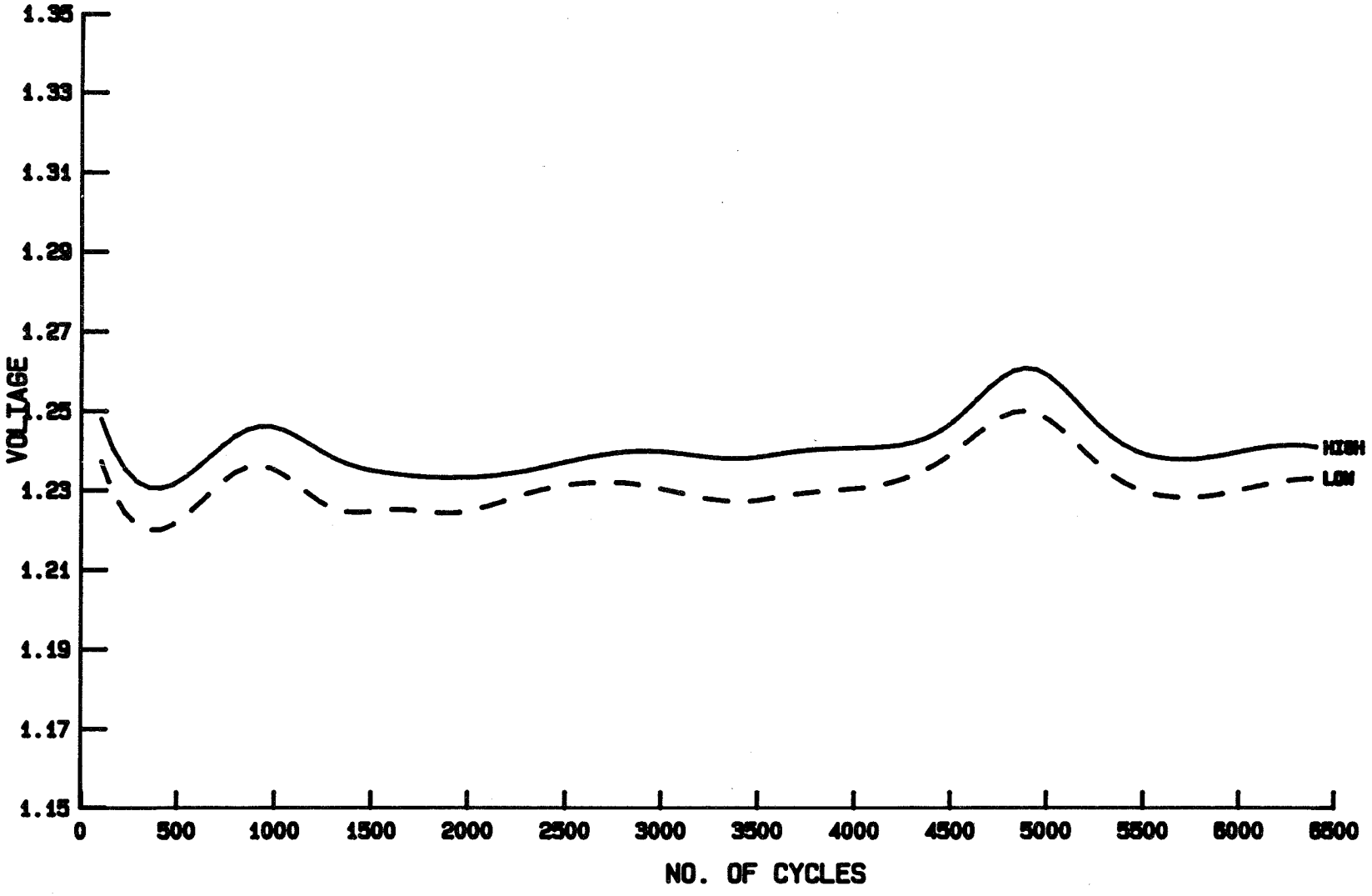

Figure 5. End-of-Discharge Voltages

S/N	INITIAL	CYCLE #2300	CYCLE #4200 (1)	CYCLE #4200 (2)	CYCLE #4400 (3)
01	36.0	36.0	37.0	40.0	34.6
02	35.4	30.8	32.3	35.1	30.8
03	36.0	36.0	37.5	40.0	35.7
04	35.6	35.4	36.7	39.8	34.4
05	35.0	32.3	33.6	38.0	33.1
06	35.8	32.1	34.1	38.0	33.1
07	35.3	32.6	34.1	38.2	33.1
08	36.0	32.3	34.4	38.2	33.1
09	35.8	32.6	34.4	38.2	32.3
10	35.8	32.9	35.4	38.5	33.6
11	35.3	32.3	33.9	38.2	32.9
12	35.3	32.3	33.9	38.2	33.1
AVG:	35.6	33.1	34.8	38.4	33.3
S.D:	0.87	1.69	1.56	1.30	1.22

(1) IMMEDIATELY PRIOR TO REVERSAL

(2) AFTER REVERSAL TO -0.25V

(3) AFTER 96 HR. OPEN CIRCUIT STAND

Figure 6. Discharge Capacities (Ampere Hours) RNH-30-1 Life Test

S/N	CYCLE #70 96 HOUR STAND BEGIN OCV	CYCLE #70 96 HOUR STAND END OCV	CYCLE #1000 120 HOUR STAND BEGIN OCV	CYCLE #1000 120 HOUR STAND END OCV	CYCLE #2200 288 HOUR STAND BEGIN OCV	CYCLE #2200 288 HOUR STAND END OCV
01	1.532	1.369	1.528	1.352	1.392	1.339
02	1.534	1.369	1.529	1.354	1.394	1.340
03	1.530	1.371	1.526	1.353	1.397	1.339
04	1.529	1.368	1.526	1.352	1.395	1.338
05	1.526	1.371	1.521	1.353	1.400	1.338
06	1.530	1.371	1.524	1.355	1.400	1.337
07	1.524	1.371	1.520	1.354	1.401	1.338
08	1.528	1.370	1.522	1.354	1.400	1.337
09	1.527	1.371	1.522	1.355	1.400	1.338
10	1.531	1.372	1.526	1.356	1.403	1.339
11	1.522	1.369	1.518	1.353	1.401	1.338
12	1.520	1.369	1.516	1.353	1.400	1.339

S/N	CYCLE #2500 288 HOUR STAND BEGIN OCV	CYCLE #2500 288 HOUR STAND END OCV	CYCLE #4200 96 HOUR STAND BEGIN OCV	CYCLE #4200 96 HOUR STAND END OCV	CYCLE #4500 96 HOUR STAND BEGIN OCV	CYCLE #4500 96 HOUR STAND END OCV
01	1.523	1.339	1.515	1.358	1.472	1.353
02	1.527	1.339	1.518	1.364	1.472	1.357
03	1.523	1.339	1.515	1.362	1.474	1.356
04	1.523	1.339	1.514	1.360	1.472	1.354
05	1.518	1.341	1.514	1.358	1.467	1.352
06	1.521	1.340	1.513	1.361	1.471	1.355
07	1.515	1.342	1.510	1.360	1.465	1.351
08	1.519	1.341	1.511	1.361	1.469	1.354
09	1.518	1.341	1.511	1.361	1.469	1.354
10	1.518	1.340	1.511	1.362	1.470	1.356
11	1.514	1.341	1.509	1.359	1.467	1.351
12	1.514	1.341	1.509	1.358	1.468	1.350

Figure 7. Charge Retention, RNH-30-1 Life Test

CYCLE	CELL A	CELL B	LOT AVG. (80 CELLS)	SIGMA
30°C Capacity	35.5	35.3	27.0	1.4
20°C Capacity	35.4	35.4	31.7	.8
10°C Capacity	36.8	36.9	34.2	.5
0°C Capacity	37.0	38.4	37.3	.2
10°C Chg. Ret.	33.6	33.6	29.8	.7

Figure 8. Performance of Additive Cells, Capacities in Ampere-hours

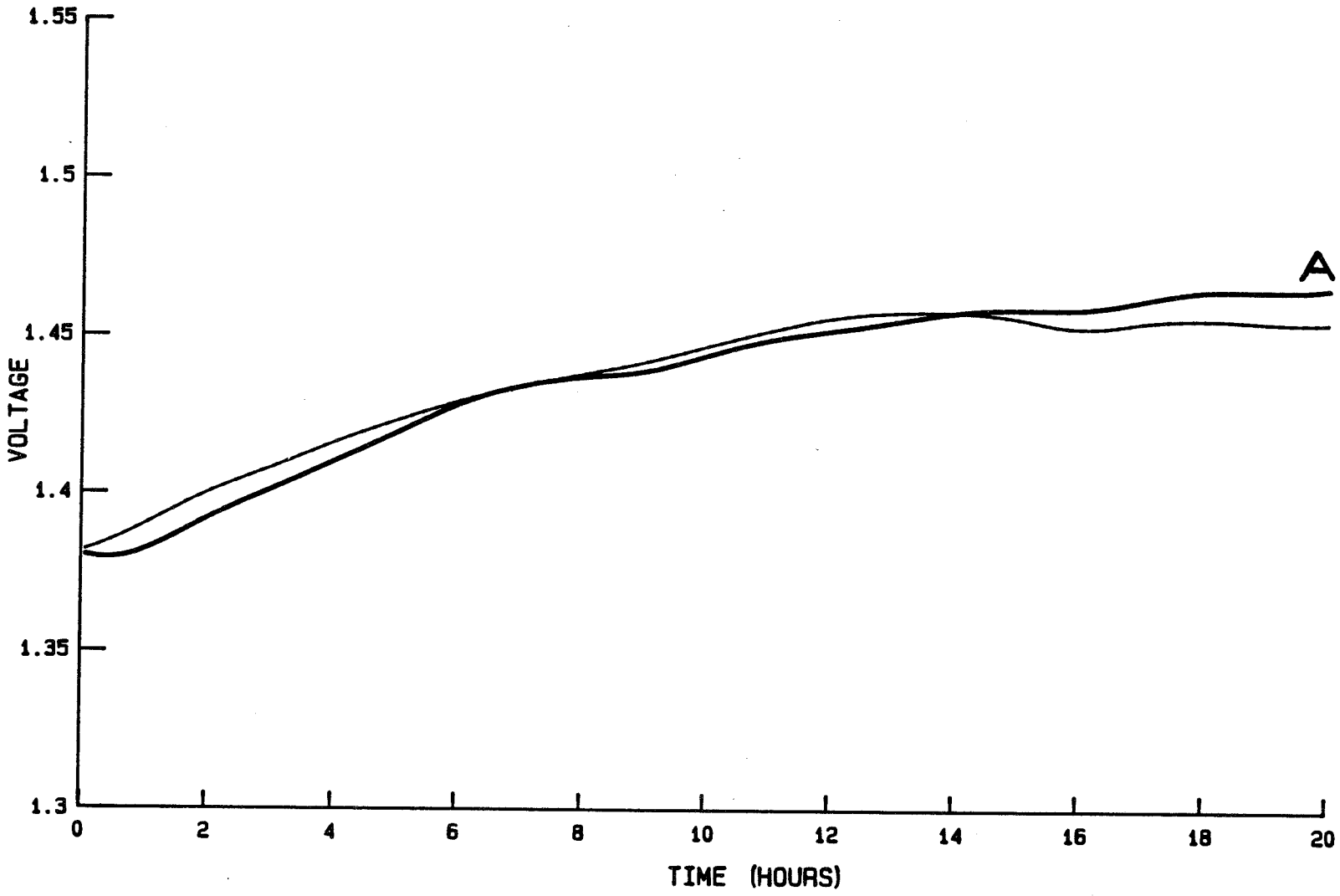

Figure 9. 30 Degree Charge

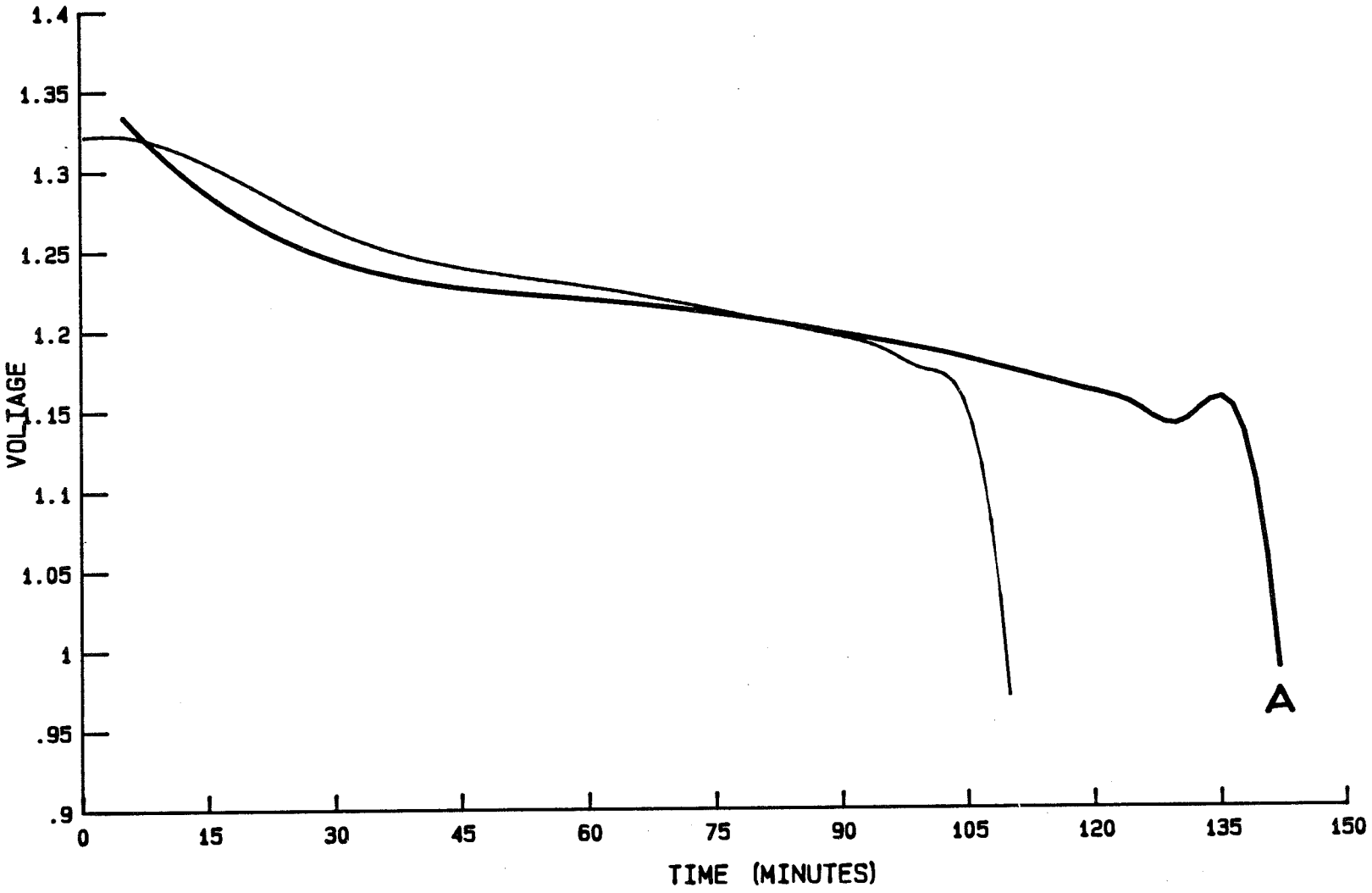

Figure 10. 30 Degree Discharge

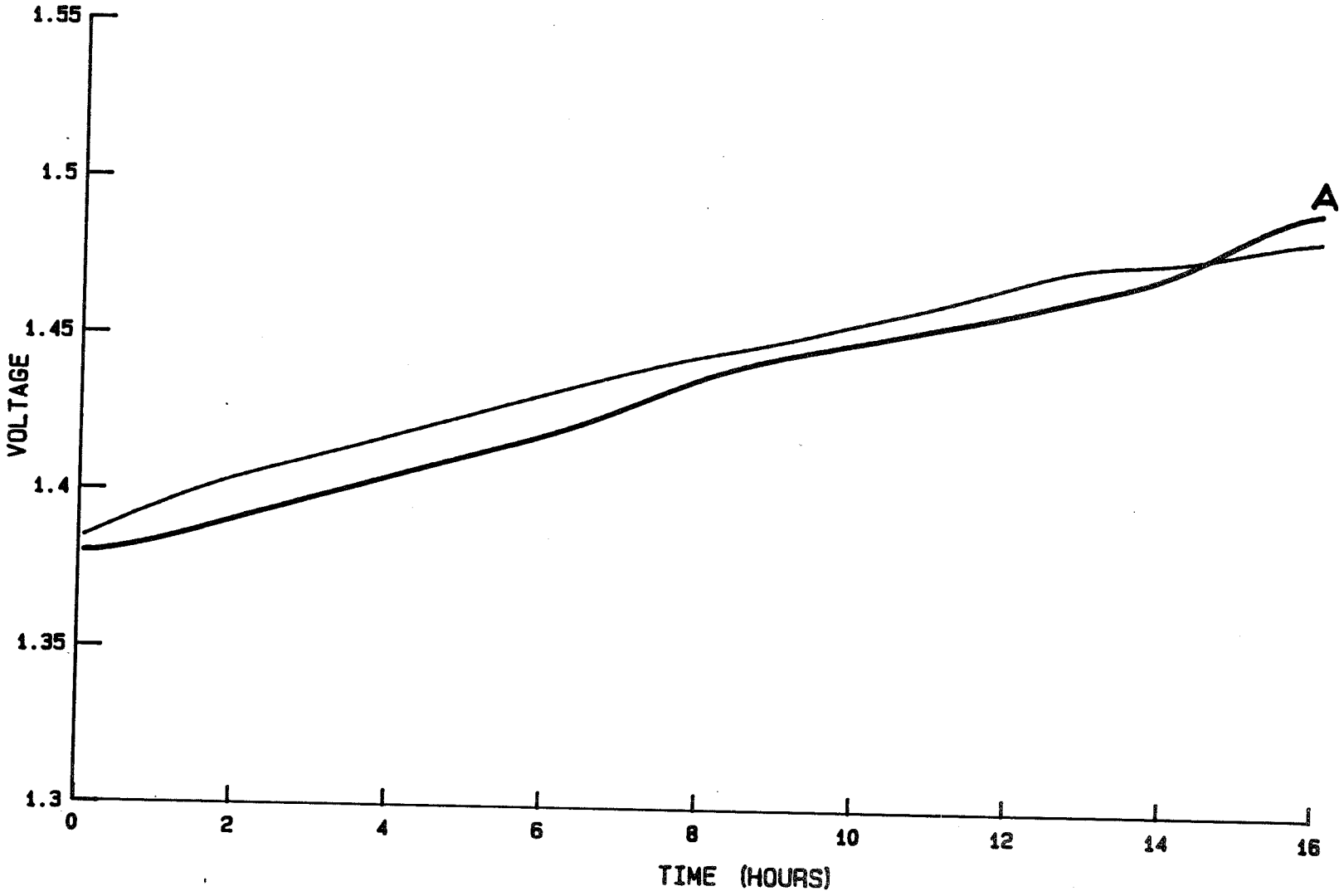

Figure 11. 20 Degree Charge

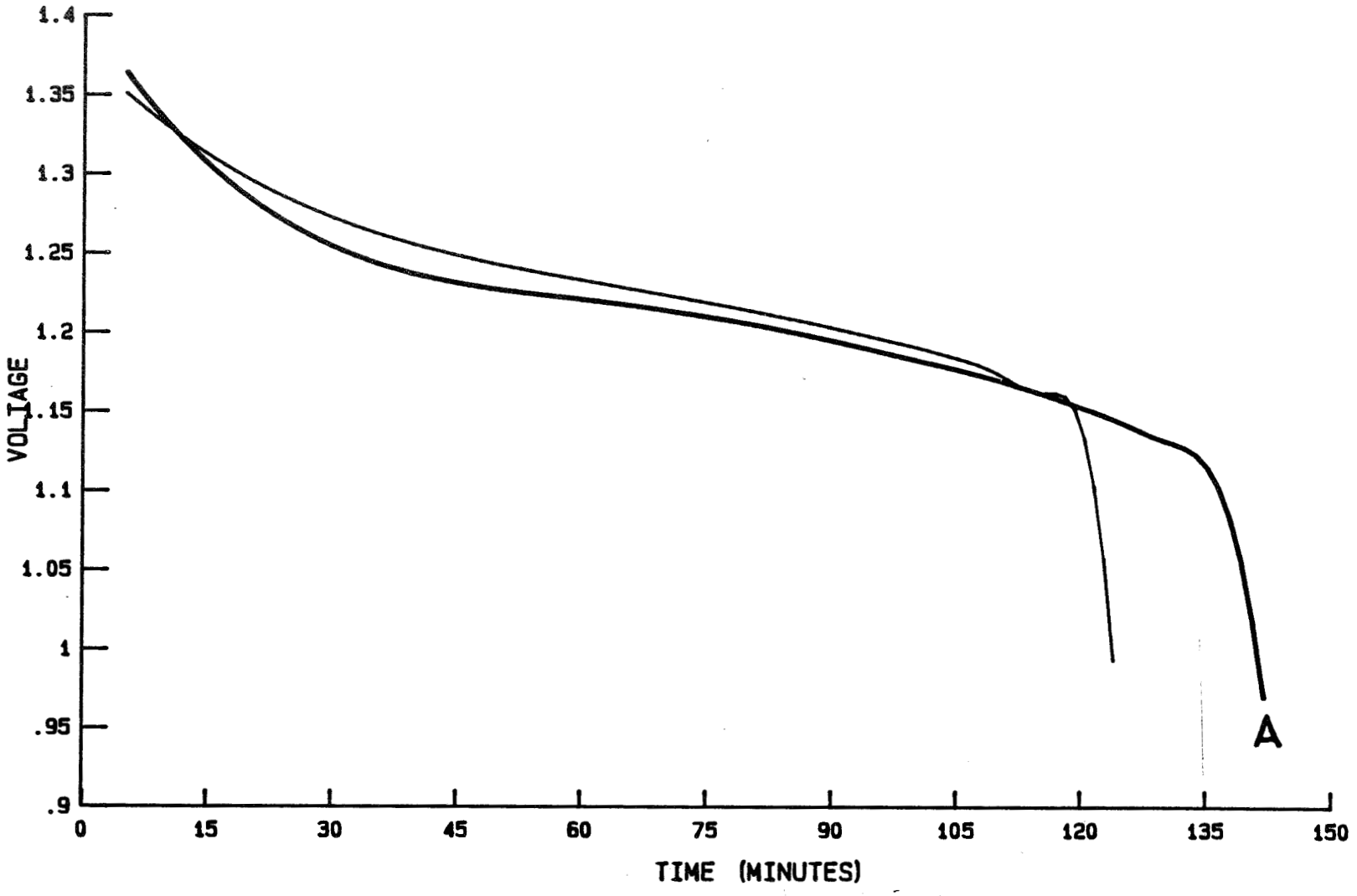

Figure 12. 20 Degree Discharge

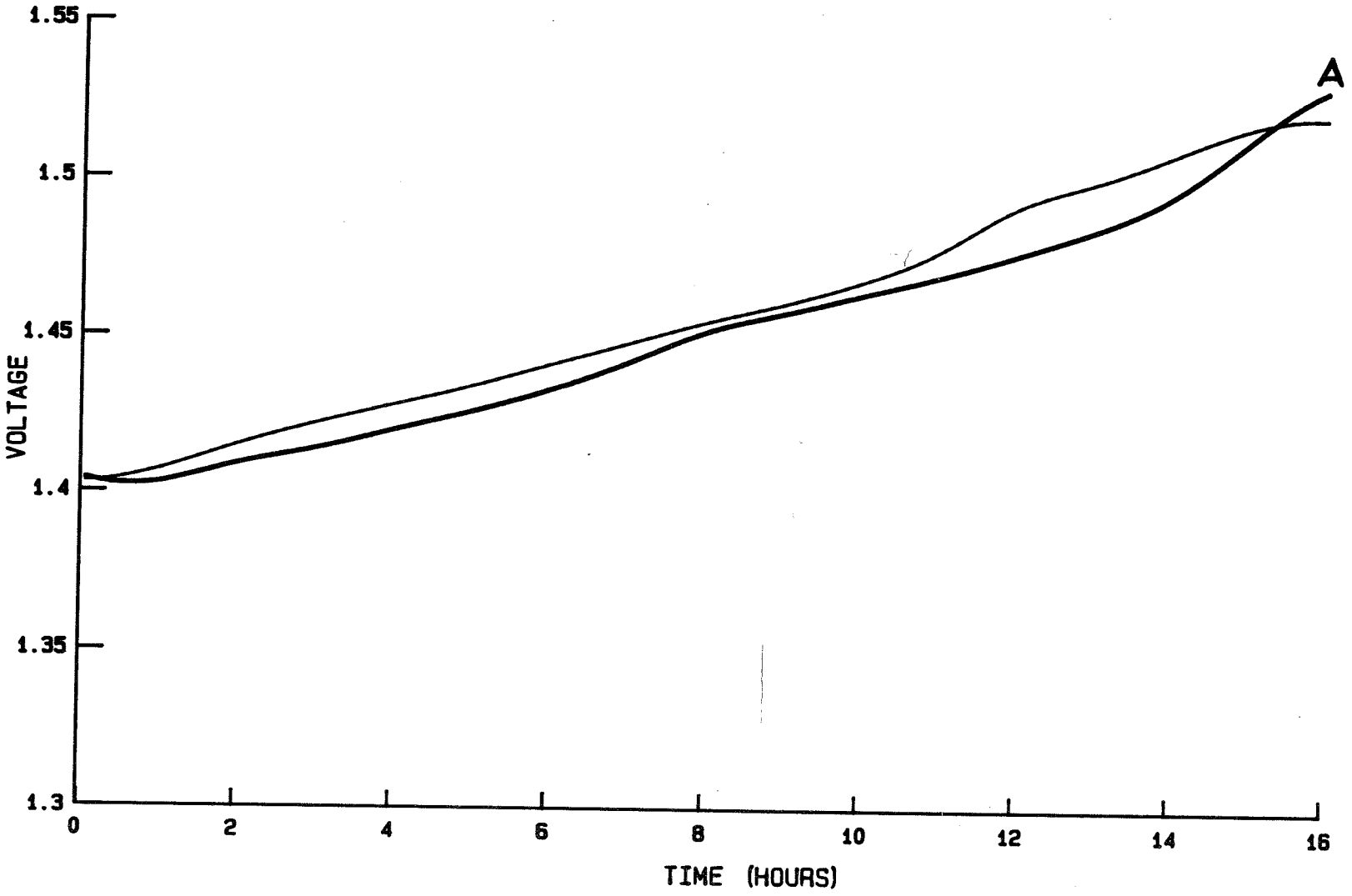

Figure 13. 10 Degree Charge

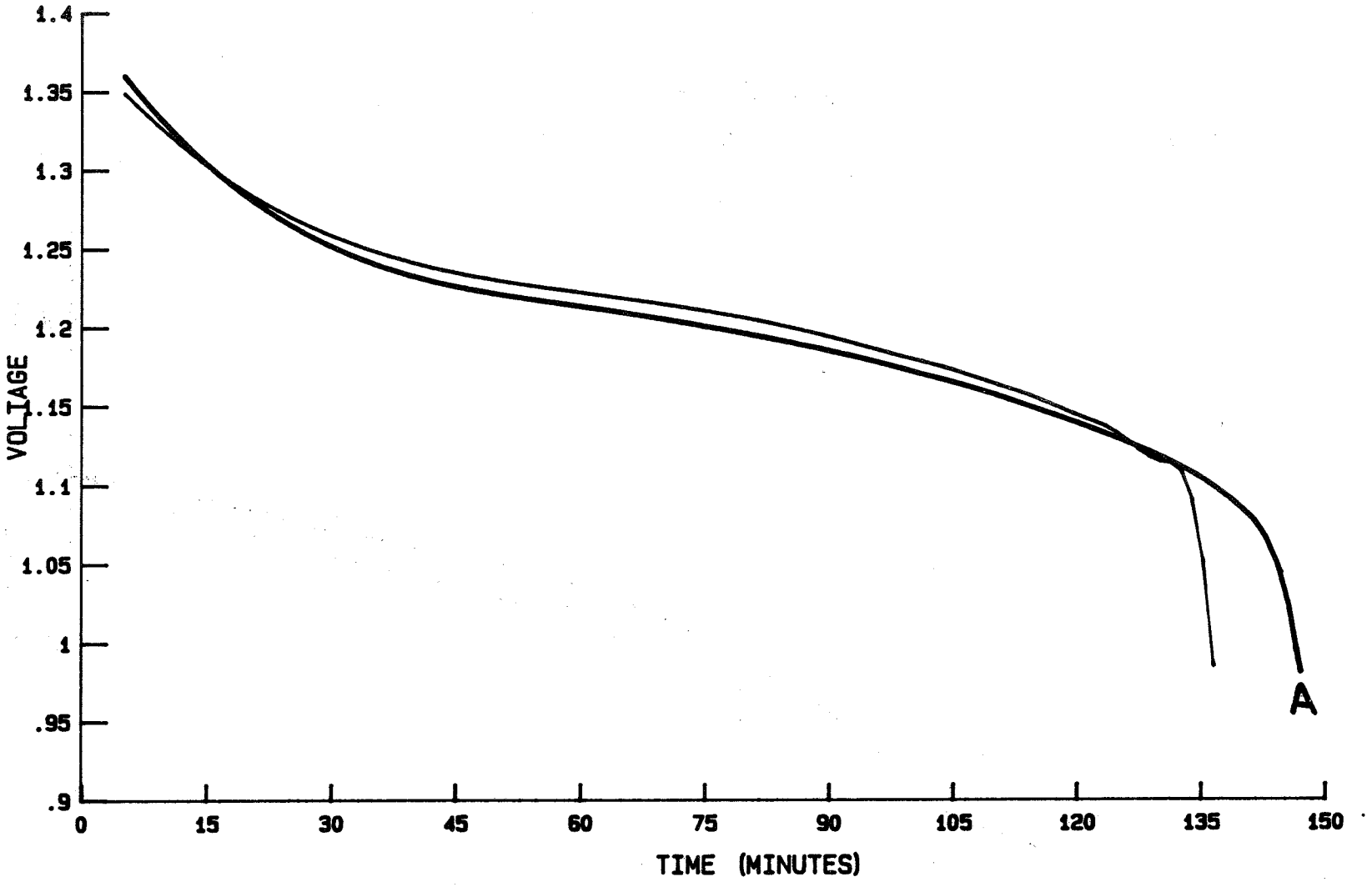

Figure 14. 10 Degree Discharge

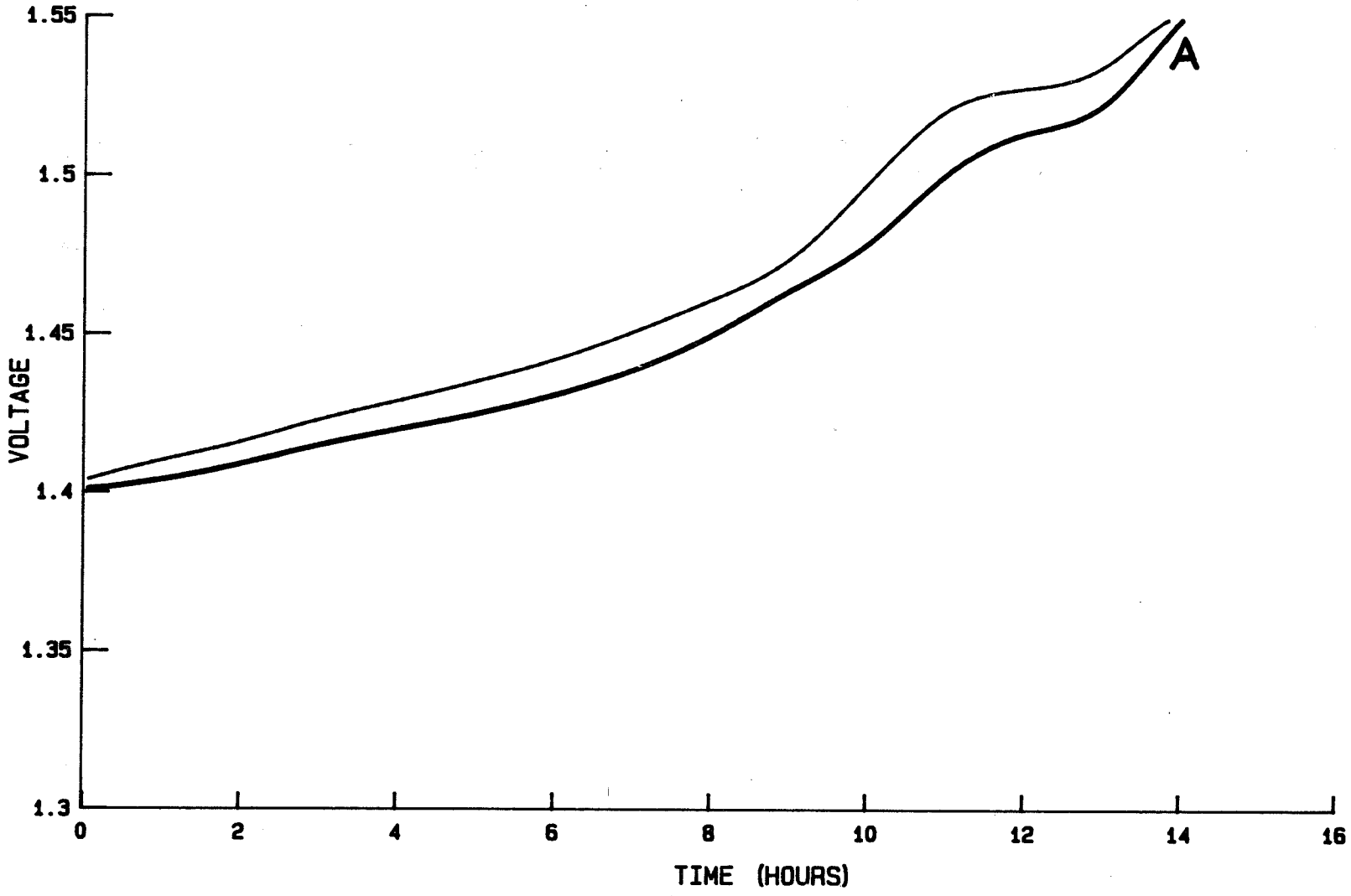

Figure 15. 0 Degree Charge

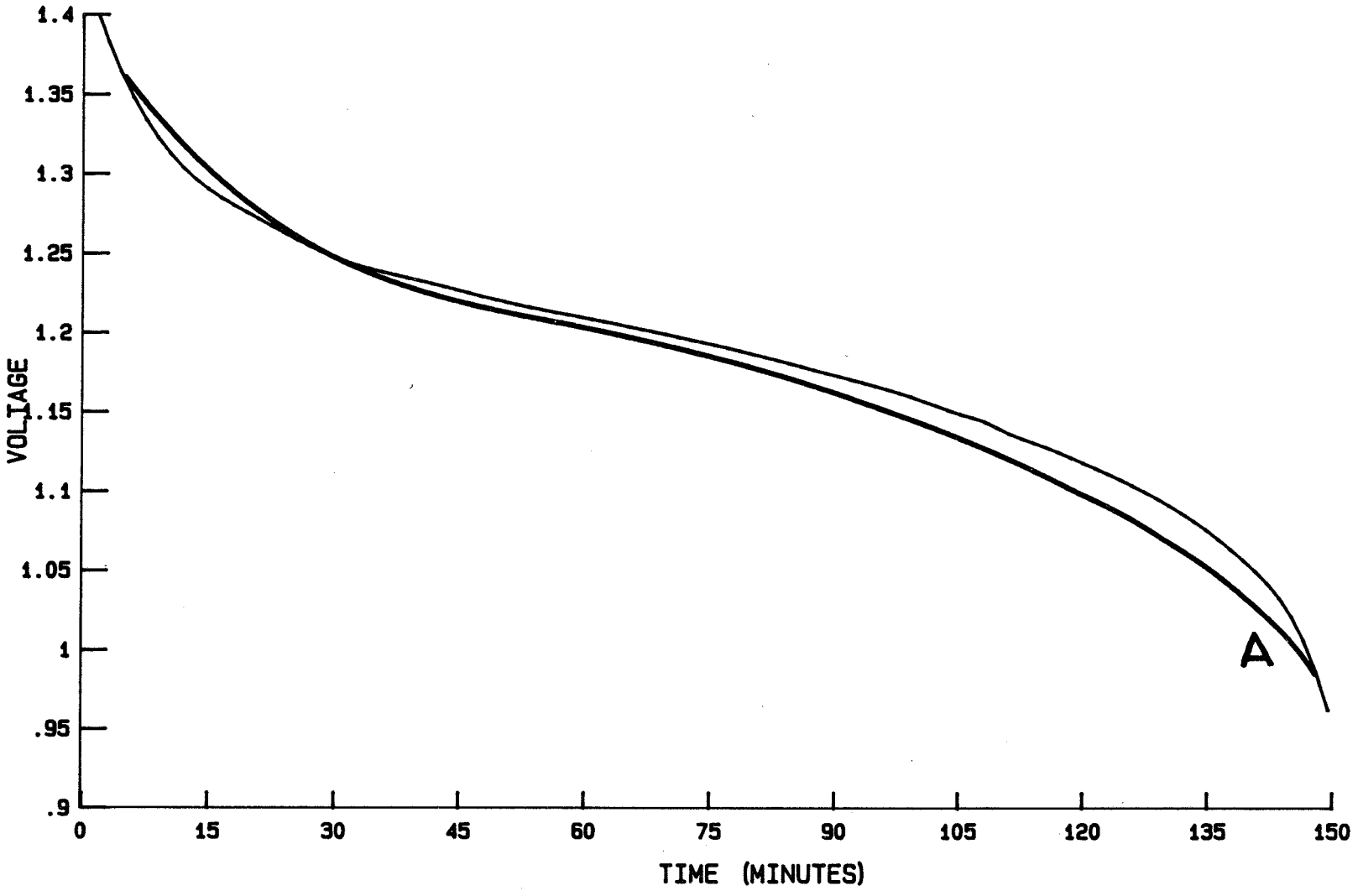

Figure 16. 0 Degree Discharge

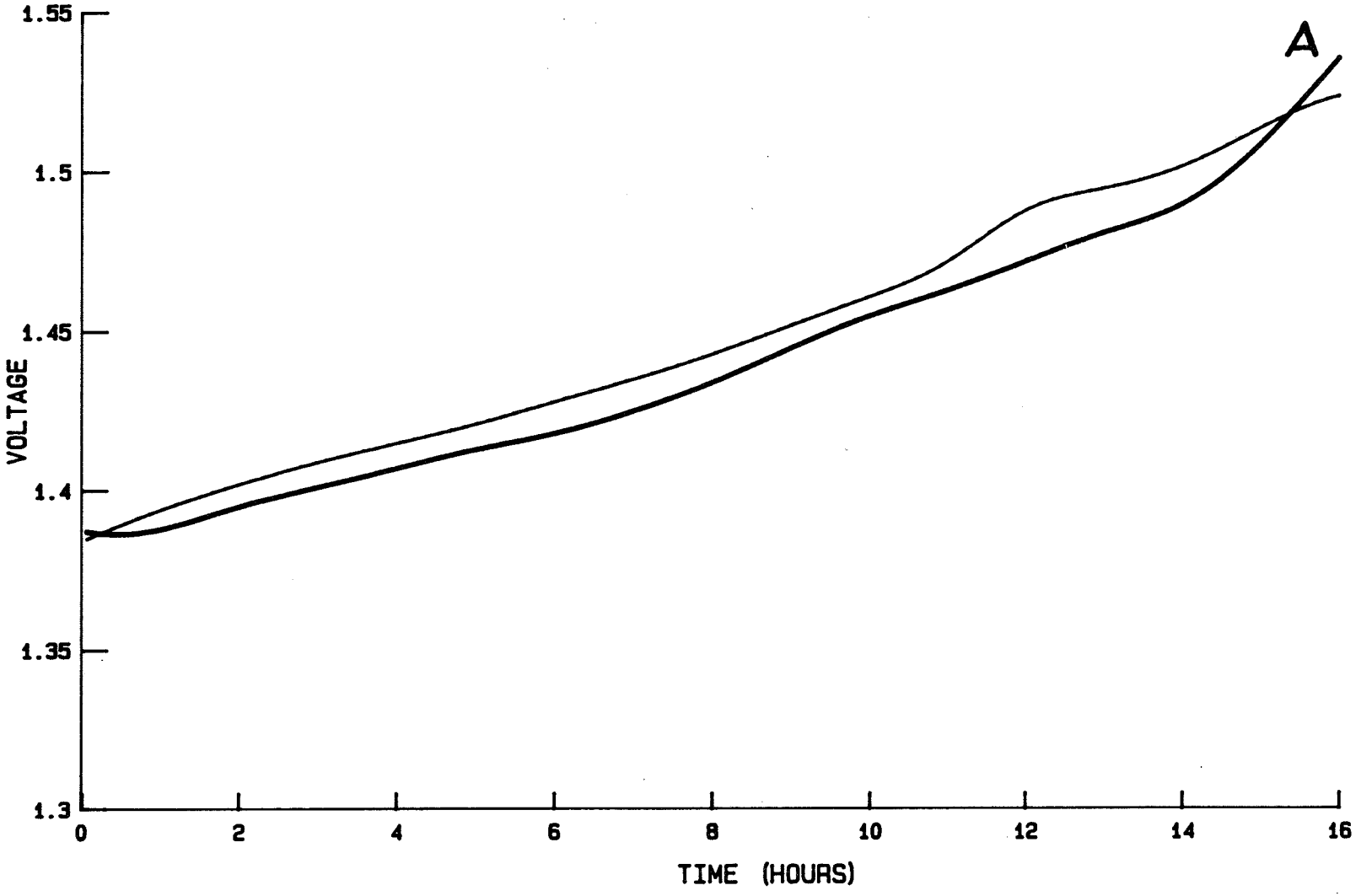

Figure 17. 10 Deg Charge Ret Charge

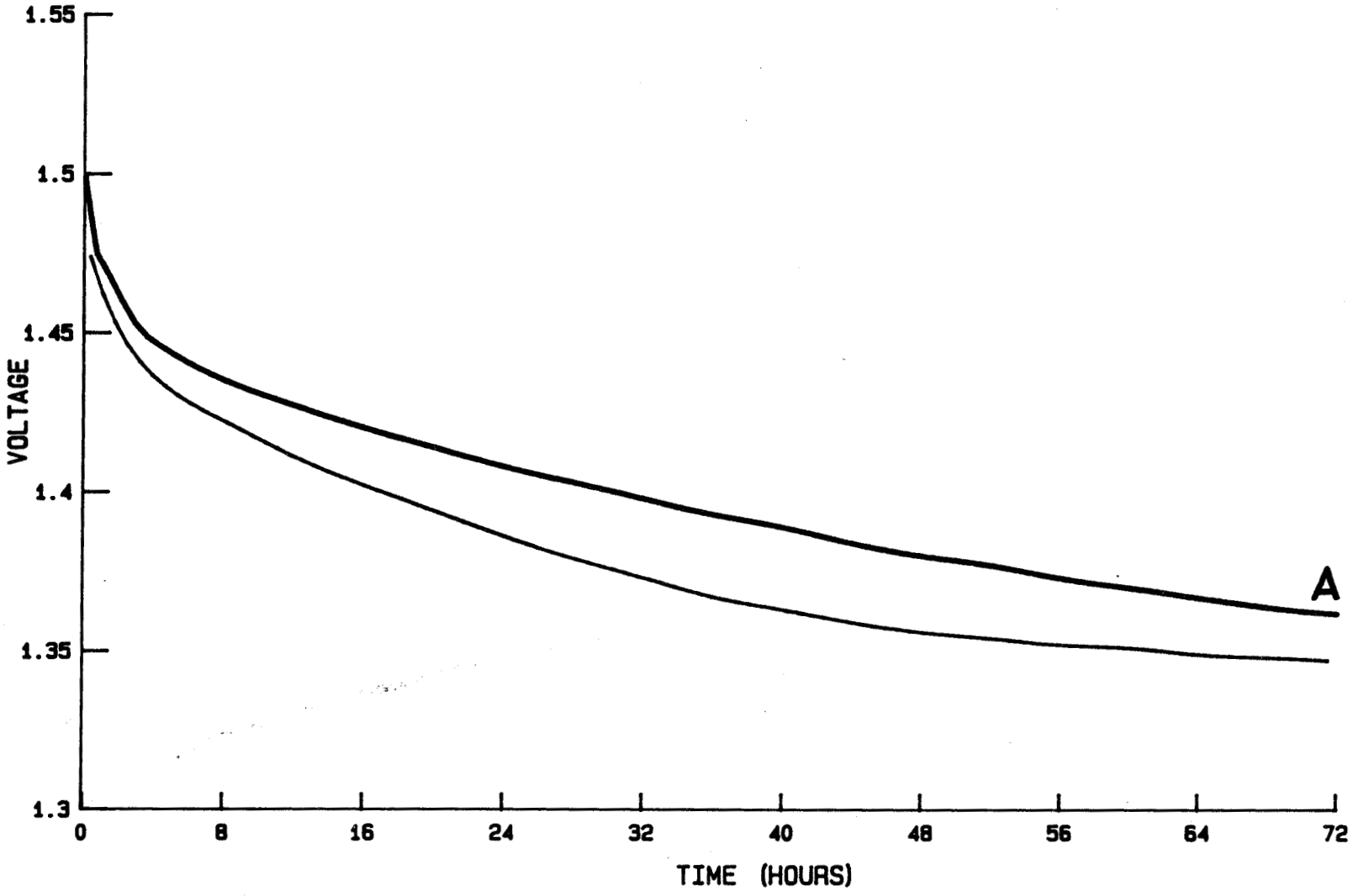

Figure 18. 10 Deg Charge Ret 72 hr. OCV

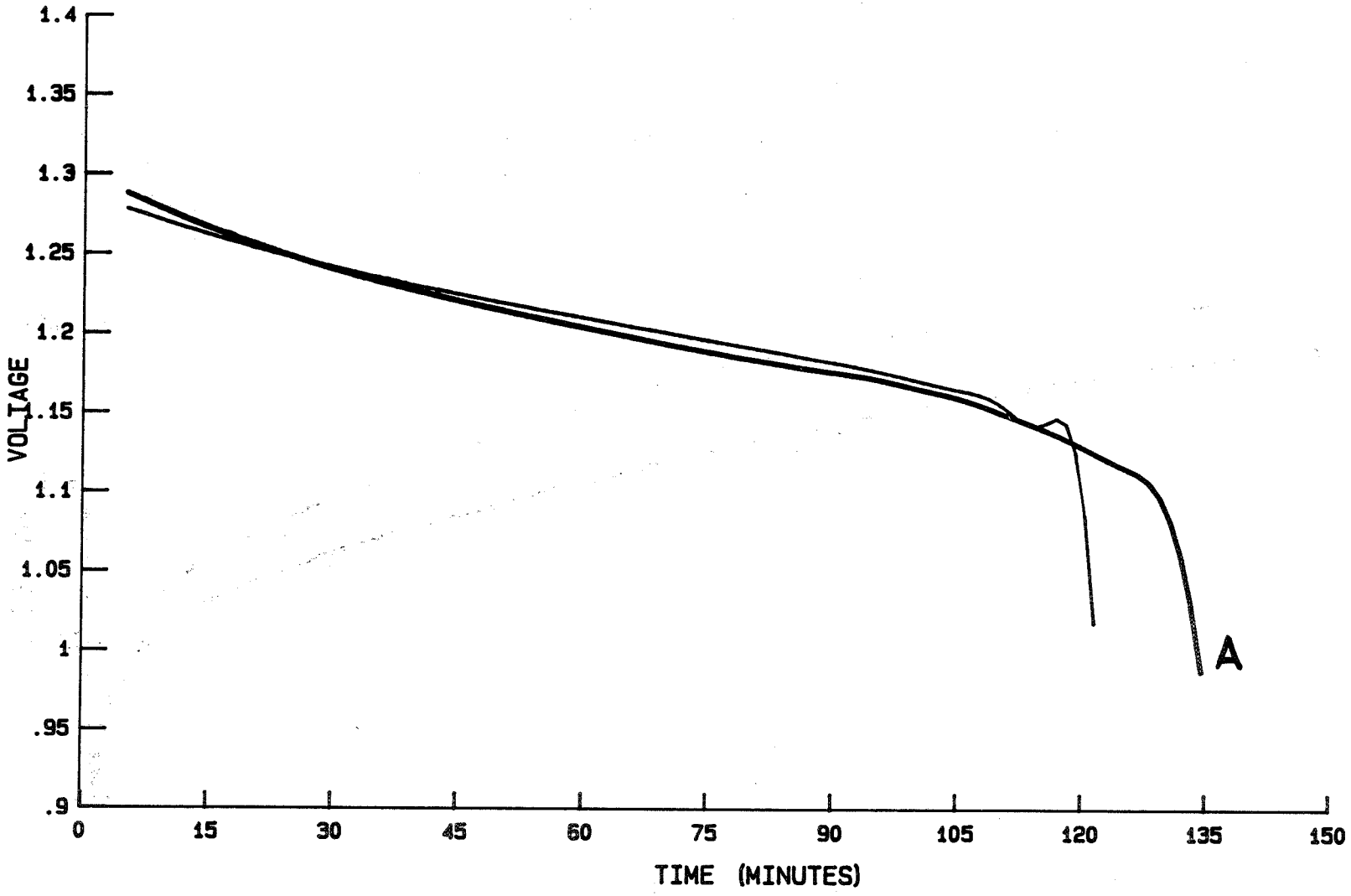

Figure 19. 10 Deg Charge Ret Discharge

NORMAL KOH	CYCLE - 0	THICKNESS (IN.) AT: 55	160	240	320
1	.031	.031	.031	.035	.035
2	.031	.031	.031	.036	.036
3	.030	.030	.030	.037	.037
4	.031	.031	.031	.039	.039
5	.031	.031	.031	.036	.036
6	.031	.031	.031	.035	.036
ADDITIVE KOH					
1	.031	.031	.031	.034	.035
2	.030	.030	.030	.031	.032
3	.030	.030	.030	.031	.032
4	.030	.030	.030	.031	.031
5	.029	.029	.029	.029	.030
6	.030	.030	.030	.031	.031

Figure 20. Thickness of Positive Plates During Stress

INITIAL PERFORMANCE OF ADVANCED DESIGNS FOR IPV NICKEL-HYDROGEN CELLS

John J. Smithrick, Michelle A. Manzo, and Olga Gonzalez-Sanabria
National Aeronautics and Space Administration
Lewis Research Center
Cleveland, OH 44135

ABSTRACT

Advanced designs for individual pressure vessel nickel-hydrogen cells have been conceived which should improve the cycle life at deep depths-of-discharge. Features of the designs which are new and not incorporated in either of the contemporary cells (Air Force/Hughes, Comsat) are: (1) use of alternate methods of oxygen recombination, (2) use of serrated edge separators to facilitate movement of gas within the cell while still maintaining required physical contact with the wall wick, and (3) use of an expandable stack to accommodate some of the nickel electrode expansion. The designs also consider electrolyte volume requirements over the life of the cells, and are fully compatible with the Air Force/Hughes design.

Boiler plate cells based on each of the designs have been fabricated. They are in the process of being evaluated in a continuing cycle life test.

INTRODUCTION

As part of an overall effort to advance the technology of nickel-hydrogen batteries for possible use in an energy storage system, in low earth orbit (LEO), improved advanced designs for individual pressure vessel (IPV) cells have been conceived. The purpose of this effort is to improve the cycle life at deep depths-of-discharge (DOD). The approach has been to effect cell improvements through a continuing combined in-house and contractual effort. Comtemporary IPV nickel-hydrogen cell designs and results of cycle life tests conducted in-house and by others were reviewed to identify areas where improvement could result in a longer cycle life. A component improvement effort directed towards the physical properties of each of the individual components was initiated and improvements will be factored into the cell as evolved. Design philosophies have been developed related to oxygen and electrolyte management requirements. Existing technology was utilized where possible to minimize development cost and time.

The contemporary design cells (Air Force/Hughes, Comsat) are adequate for the geosynchronous orbit (GEO) applications, where not many cycles are required over the life of the storage system. However, for the demanding LEO applications, the current cycle life at deep depths-of-discharge (2000 to 8000 cycles) is not acceptable (1,2). Some investigators report that this limited cycle life is mainly due to degradation of the nickel electrode. However,

there are also indications that modifications to the contemporary designs should result in an improved cycle life(3). Some possible causes of degradation are: density changes of the active material during cycling which could cause fatigue of the nickel plaque (4) and structural damage to itself resulting in capacity loss; active material could flake or extrude from the electrode causing a loss of capacity and possible shorting of the cell (1,5). Extrusion of active material may also cause channeling of oxygen generated during charge. This could lead to "popping" caused by large concentrations of oxygen reacting with hydrogen at the hydrogen electrode (5) which could damage the electrode (4). Blistering of the nickel electrode during cycling could cause capacity loss (6). Change in pore distribution and electrode surface area can also result from active material expansion and contraction, which could effect electrolyte distribution and performance. It has been reported that the nickel electrode expands significantly during cycling (3). This could cause compression of the separators, drying of the stack, rupture of the polysulfone core and cell failure. This failure mode can be eliminated by modifying the cell design to accommodate expansion.

In this report advanced designs for IPV nickel-hydrogen cells are described. Initial cycle life performance of boiler plate cells, based on each of these designs, is presented and compared to the Air Force recirculating design.

EXPERIMENTAL

TEST FACILITY

The test facility used to cycle life test the nickel hydrogen cells is illustrated in Fig. 1. The facility design incorporates two main features: safety and versatility. Since the nickel-hydrogen cells are precharged with hydrogen and also generate hydrogen during charge, special attention was given to personnel safety. The cells were located on top of the instrumentation cabinets. There were two cells for each cabinet. Each cell was located within a cylindrical shrapnel shield in case of the improbable event of an explosion or rupture of the cell pressure vessel. During a test, the cylindrical shield was purged with nitrogen to create an inert atmosphere. The nitrogen gas, and hydrogen gas if any, would be exhausted from the test laboratory through a hood located above the cells. If the exhaust fan would fail or the nitrogen purge would become interrupted, the test would be automatically terminated. A test can also be terminated on a preset upper and/or lower limit of cell voltage, current, pressure, and temperature.

The facility's versatility allows for testing over a wide range of cycle regimes. A geosynchronous earth orbit (GEO) cycle regime can be run in real time using a programmable timer. Various accelerated GEO and low earth orbit cycle regimes can be run using a Texas Instrument timer. The cell discharge current is controlled by an electronic load, which can be varied from 0 to 100 amps. The charge current can also be varied in the same range. Test data are printed out locally using a Fluke data collector. Strip chart recorders are

used to record cell voltage, current, and pressure as a continuous function of charge and discharge time for selected cycles. A maximum of twelve cells can be tested at the same time.

TEST CELL DESCRIPTION

Air Force Design Cell

The Air Force cell is illustrated in Fig. 2. It consists of a stack of nickel electrodes, separators, hydrogen electrodes, and gas screens assembled in a non back-to-back electrode configuration. The stack is packaged in a cylindrical pressure vessel, with hemispherical end caps. This is made of Inconel 718 and lined with zirconium oxide which serves as a wall wick. The components are shaped in a "pineapple" slice pattern. The electrodes are connected electrically in parallel. In this configuration electrodes of different types directly face each other. Hence, since a high bubble pressure separator is used, the oxygen generated at the nickel electrode on charge is directed to the hydrogen electrode of the next unit cell, where it recombines chemically to form water. The fuel cell grade asbestos separators are extended beyond the electrodes to contact the wall wick. Hence, electrolyte which leaves the stack during cycling will be wicked back into the stack. The nickel electrode consists of a sintered nickel powder plaque containing a nickel screen substrate which is electrochemically impregnated with nickel hydroxide active material by the Pickett process. The gas screens are polypropylene. The electrolyte is a 31 percent aqueous solution of potassium hydroxide. The stack configuration is referred to as a recirculating design.

NASA Advanced Cells

Overall Designs - Two different but similar advanced design IPV nickel-hydrogen cells have been conceived. They are illustrated in Figures 3 and 4. One is referred to as the catalyzed wall wick and the other as the recombination capsule design. They differ only in the method of oxygen recombination. Initially the nickel electrodes, hydrogen electrodes, gas screens, pressure vessel, and potassium hydroxide electrolyte concentration will be identical to the ones used in the state-of-the-art Air Force/Hughes cells. However, a component improvement effort directed towards the physical properties of each of the individual components has been initiated and improvements will be factored into the cells as they evolve. For both designs the electrode configuration is back-to-back as is the case for the Comsat cell. Both designs also use a wall wick, however portions of the wall wick are catalyzed for the catalyzed wall wick design.

Features of the advanced designs which are new and not incorporated in either of the contemporary cells are: (1) use of alternate methods of oxygen recombination; (2) use of serrated edge separators; (3) and use of an expandable stack. The designs also consider electrolyte volume requirements over the life of the cells, and are fully compatible with the Air Force/Hughes design.

Boiler plate cells of both designs are in the process of being cycle tested to verify design feasibility.

Oxygen Management - During the later part of charge and on overcharge oxygen is evolved at the nickel electrodes. For both contemporary designs oxygen management consists of chemically recombining the oxygen generated during charge on the catalyzed hydrogen electrode surface to form water. This chemical reaction is very exothermic; hence care must be taken to limit the rate at which these two reactants come together. If a separator is used which has a pore size distribution that permits a certain degree of gas permeability, oxygen bubble buildup occurs and "popping" results as these accumulations of oxygen abruptly recombine. This can result in sintering of the catalyzed surface and/or local melting of the Teflon/catalyzed agglomeration that makes up the hydrogen electrode. If high bubble pressure separators are used in the back-to-back electrode configuration (Comsat design) the oxygen must travel along the face of the nickel, leave the stack and then reenter to recombine on the hydrogen electrode. In this case, the recombination would be expected to take place around the outer perimeter of the electrodes. The concentration of chemical reactants could result in damage to the electrocatalyst surface of the electrode.

An improved method of oxygen recombination is to use a catalyzed wall wick. The oxygen evolved on charge between the back-to-back nickel electrodes to the catalyzed wall wick where it recombines. The water formed is wicked into the stack because the asbestos separators are in contact with the wall wick. An oxygen seal is used at the inner edge of the nickel electrodes to preclude oxygen from bypassing the catalyzed wall wick by escaping into the stack core, and reentering to recombine at the hydrogen electrodes. The asbestos separator pore size distribution is such that it has a high bubble pressure, thus denying the oxygen a direct path to the hydrogen electrode.

The catalyzed wall wick is fabricated by first depositing a thin zirconium oxide layer of wicking material on the inner surface of the pressure vessel, as is the case in the Air Force design. A platinum Teflon mixture is coated in stripes onto the zirconium oxide surface. The mixture is similar to that used to fabricate SOA hydrogen electrodes, and is cured in the same manner.

The advantages of using a catalyzed wall wick are (1) aids thermal management, as the heat of oxygen recombination is deposited at the pressure vessel wall rather than at the hydrogen electrodes in the stack, and (2) prevents damage to the hydrogen electrode due to concentrated bubbles of oxygen reacting (popping problem).

Another method of oxygen management would be to use oxygen recombination capsules between the back-to-back nickel electrodes. The high bubble pressure asbestos separator directs the oxygen into the capsule, which consists of recombination sites catalyzed with platinum. They are encapsulated with a vapor permeable coating to allow passage of the gases in and water vapor out, but remain hydrophobic to liquid. The coating must also isolate the catalyst

electrically, otherwise it will react with the nickel electrode as a parasitic reaction. The water formed within the capsule is returned to the nickel electrodes in the vapor form. This method of oxygen management benefits the overall electrolyte management scheme, and helps prevent damage to the hydrogen electrode.

Expandable Stack - The SOA electrochemically impregnated nickel electrodes expand significantly due to cycling at deep depths-of-discharge compressing the separators. The electrolyte forced out is absorbed by the increased pore volume of the nickel electrodes. Hence, expansion of the nickel electrodes effects electrolyte volume (as a percentage of stack saturation) and electrolyte distribution. This failure mode applies to the Comsat cell, which does not use a recirculation stack. In the Air Force cell, the proper electrolyte volume should be maintained by the recirculation stack design. However, it has been reported by others that the Air Force cell has also failed due to nickel electrode expansion (7). In this case, the expansion was so great (about 1/2 in., 40 electrode stack) that the polysulfone core of the stack ruptured. This failure mode can be eliminated by modifying the cell design to accommodate expansion.

To accommodate the nickel electrode expansion and improve cycle life, an expandable stack has been proposed. One way of implementing this is to use Inconel 718 Belleville disc springs at each end of the stack between the end plates and tie rod nuts. The springs will maintain stack compression throughout the life of the cell. Another way is to share the accommodation with the separator. The spring constant can be selected so that some of the electrode expansion is absorbed by the asbestos separator. A 10 mil separator, which is the standard thickness used in contemporary nickel-hydrogen cells, can be compressed to about 5 mils without any performance degradation provided it has adequate electrolyte. In SOA cells, the asbestos separators are initially compressed 1 mil to insure good component contact. As a matter of fact, the performance of the separator may improve due to the decrease in thickness. However, this could be offset by a change in tortuosity due to compression. The separator can be thought of as a spring in series with the Belleville spring. The relative deflection will depend on the respective spring constants.

An effort has been initiated in-house to investigate the effect of separator compression on resistance and electrolyte content.

Serrated Separator - The separators are made of beater treated asbestos (BTA) rather than conventional fuel cell grade asbestos. BTA is reconstituted fuel cell grade asbestos that has 5 percent by weight butyl latex binder added (8). The sheet is formed in one ply and is approximately 7 mils thick. The properties of BTA are comparable to those of the fuel cell grade asbestos (resistivity, electrolyte retention, porosity, pore size, bubble pressure). In addition, the BTA is more uniform and stronger. The edges of the separator are serrated to facilitate gas movement inside the cell. The (duty cycle) of the serration is about 25 percent. Hence, 75 percent of the separator edge will still be in contact with the pressure vessel wall for electrolyte management.

Electrolyte Management - Cell performance is very sensitive to stack electrolyte volume and distribution (9). There are many factors which effect this quantity, and some are difficult to control. However, by good design, proper electrolyte volume can be maintained over the life of the cell for good performance.

One way of maintaining the proper electrolyte volume is to provide extra electrolyte in the bottom of the cell (about 20 ml) and a means of transporting it to the stack as required. This can be done by extending the separators beyond the electrodes to contact the wall wick, which is in contact with the electrolyte reservoir, as is the case in the Air Force design.

MEASUREMENTS AND PROCEDURE

For this experiment the quantities measured for each cell at the end of charge and discharge, and their accuracies were: Current (±0.3 percent), voltage (±0.5 percent), pressure (±1 percent), temperature (±1° C limit of error), and charge and discharge ampere-hours capacity (±0.5 percent). Charge-to-discharge ampere-hour ratio was calculated. Cell current, voltage, and pressure were recorded continuously as a function of time, for selected cycles, on a strip chart recorder.

Cell charge and discharge currents were measured across a shunt, using an integrating digital voltmeter. Cell voltage was also measured using an integrating digital voltmeter. Cell pressure was measured using a conventional pressure transducer. Temperature was measured using an iron-constantan thermocouple located on the center of the outside pressure vessel wall. Charge and discharge ampere-hours were measured using a conventional ampere-hour meter. Charge-to-discharge ratio (ampere-hours into cell on charge to ampere-hours out on discharge) was calculated from the ampere-hour measurements.

Prior to cycling the cell, the ampere-hour capacity loss due to self discharge after a 72-hour open circuit voltage stand was measured for all cells.

Three, 6 ampere-hour boiler plate cells of each design will be cycled to failure. In addition, one 4 ampere-hour boiler plate cell of the catalyzed wall wick design will also be cycled to failure. The cycle regime will be a LEO regime. The depth-of-discharge will be 80% of name plate capacity. For this test cell failure was defined to occur, when the discharge voltage degraded to 0.9 volts during the course of a constant current 35-minute discharge at the 1.37C rate. For the first test cycle, the cells were charged for eighteen hours at a C/10 rate (0.6 amps) followed by discharge at the 1.37C rate for 35 minutes. Then the normal LEO charge/discharge regime was initiated which consisted of charging the cells at about a constant 0.96C rate (5.76 amps) for 55 minutes immediately followed by discharge at a constant 1.37C rate (8.2 amps) for 35 minutes. The charge-to-discharge ratio was set at 1.10.

RESULTS AND DISCUSSION

SELF DISCHARGE

The average percentage ampere-hour capacity loss and confidence interval (standard deviation about the mean) for three cells of each design is summarized in figure 5. The capacity loss was measured after a 72-hour open circuit voltage stand. The cell temperature was not controlled during the measurements. Room temperature was 25° C. The spread in the data indicates no significant difference in the average percentage capacity loss. This suggests that the new designs do not introduce any new self discharge mechanisms.

CYCLE PERFORMANCE

The effect of cycling on the end of discharge voltage for the best cell (least voltage degradation) for each design is shown in figure 6. There was no apparent difference between the performance of the oxygen recombination capsule design and the Air Force design cell (control). The voltage for both designs was stable and relatively constant throughout the test. At cycle 1500 the end of discharge voltage was about 1.14 volts for each design. The catalyzed wall wick design cell exhibited a beginning of life variability in end of discharge voltage (not shown in figure 6), and then stabilized. Once stabilized, it showed relatively little degradation in voltage and was about 1.08 volts at cycle 2800. This lower voltage compared to the Air Force control cell (cycle 1500) is probably not inherent to the catalyzed wall wick design. It could be due to several factors such as; high contact resistance between cell components due to inadequate stack compression; maldistribution of electrolyte; or partial passivation of the hydrogen electrodes. The oxygen seal used in this design was tested in 31% potassium hydroxide, which was used as the electrolyte, and was partially soluble. This could have been a source of passivation. A cell with a different oxygen seal material, that is not soluble in KOH, has been fabricated and will be evaluated.

The cycle test of tnese cells will be continued until failure. A post-cycle cell teardown and failure analysis will be conducted to evaluate the cause(s) for failure. This information be factored into further improving the cell design.

CONCLUDING REMARKS

Advanced designs for IPV nickel-hydrogen cells have been conceived, which could have a longer cycle life at deep depths-of-discharge. The features of the designs which are new are: use of alternate methods of oxygen recombinations, use of an expandable stack to accommodate nickel electrode expansion, and use of serrated edge separators to facilitate gas movement within the cell while still maintaining required physical contact with the wall wick. The designs also consider electrolyte volume requirements over the life of the cells, and are fully compatible with the Air Force/Hughes design.

Boiler plate cells of both designs have been fabricated and are in the process of being cycle tested to verify the design feasibility.

REFERENCES

1. Adler, E., Duranti, T., Frisch, P, Jacewicz, T., Rogers, H. Samoss, L., Stadnick, S., and Tinker, L.: Nickel-Hydrogen Battery Advanced Development Program. AFWAL-TR-80-2044, Hughes Aircraft Company, (1980).

2. Warnock, D.: Life Test of 50 AH NiH_2 Battery. The 1981 Goddard Space Flight Center Worksnop, Halpert, G., ed., NASA CP-2217, pp. 487-500, (1982).

3. Smithrick, J. J.: Cycle Life Test and Failure Model of Nickel-Hydrogen Cells. Proc. 18th. IECEC, Orlando, FL, pp. 1535-1542, (1983).

4. Fritts, D. H.: J. Power Sources, 6, pp. 171-184, (1981).

5. Pickett, D. F., Rogers, H. H., Tinker, L. A., Bleser, C. A., Hill, J. M., Meador, J. S.: Establishment of Parameters for Production of Long Life Nickel Oxide Electrodes for Nickel-Hydrogen Cells. Proc. 15th IECEC, Seattle, WA, Vol. 3, pp. 1918-1924, AIAA, NY (1980).

6. Fritts, D. H.: J. Power Sources, Vol. 6, pp. 327-336 (1981).

7. Muller, V. C.: Failure Analysis of Ni-H_2 Cell Subject to LEO Cycling. The 1983 Goddard Space Flight Center Workshop Proceedings, to be Published.

8. Schmidt, G. F. and Weber, R. E.: Development of Battery Separator Composites. NASA CR-165508, Kimberly-Clark Corporation (1981).

9. Abbey, K. M. and Britton, D. L.: Electrolyte Management in Porous Battery Components-Static Measurements. NASA TM-83073, (1982).

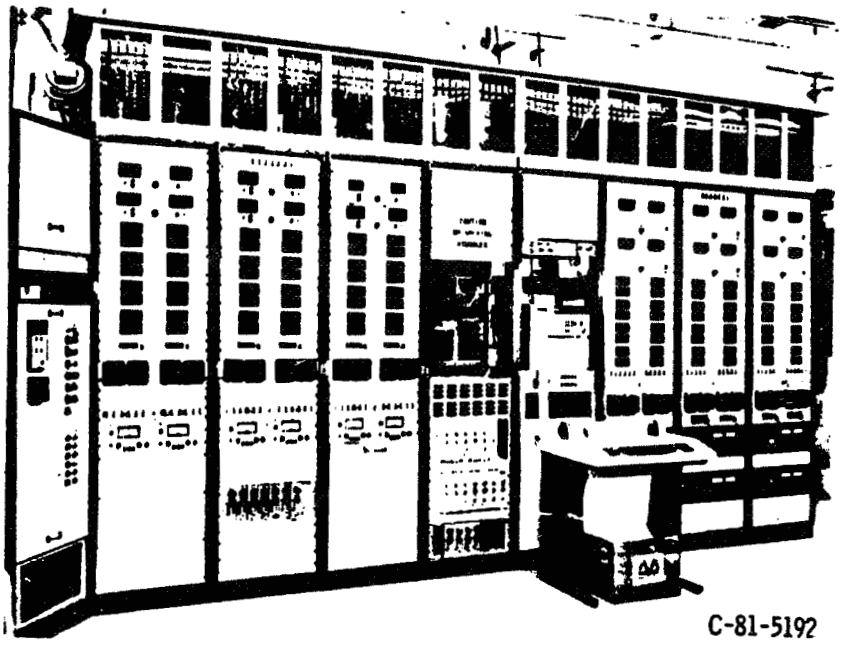

Figure 1. Nickel-hydrogen Cell Test Facility

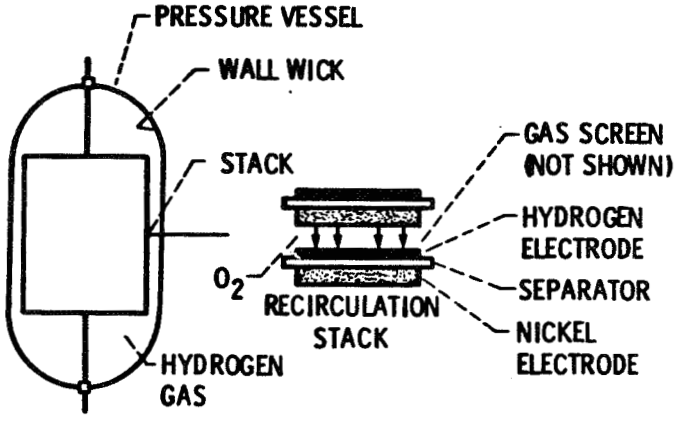

Figure 2 - Illustration of Air Force/Hughes design individual pressure vessel nickel-hydrogen cell.

Figure 2. Illustration of Air Force/Hughes Design Individual Pressure Vessel Nickel-Hydrogen Cell

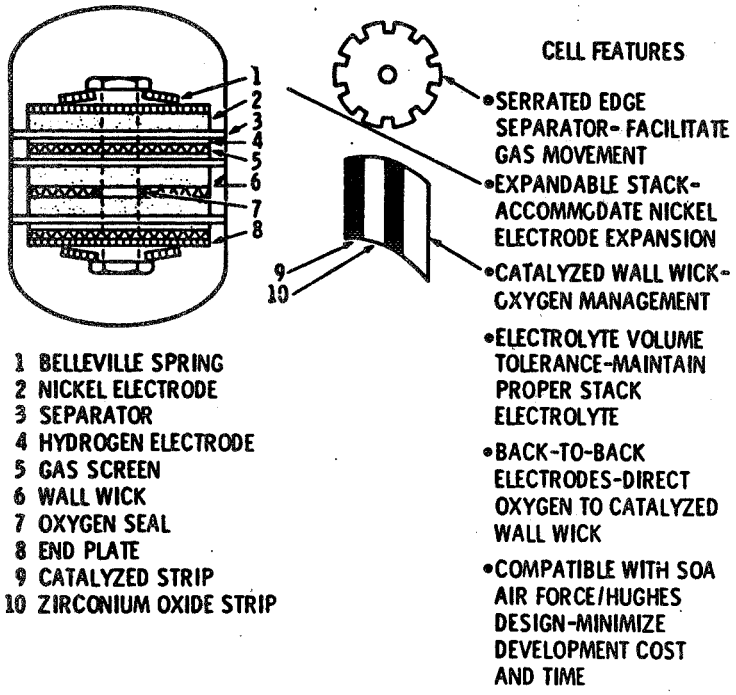

Figure 3. NASA Advanced Design IPV Nickel-Hydrogen Cell-catalized Wall Wick

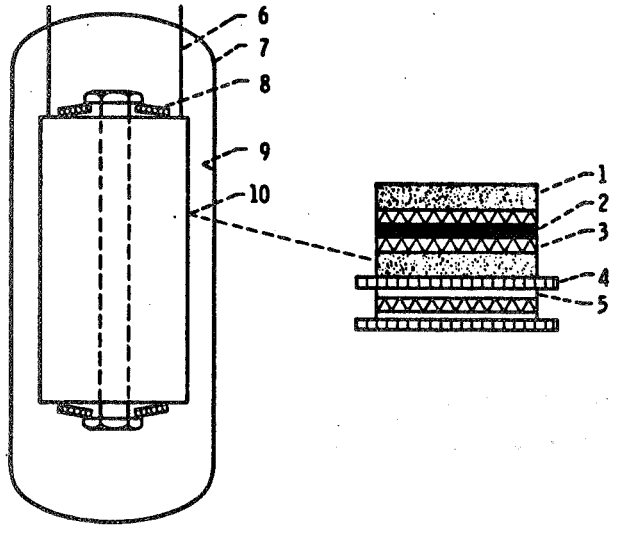

Figure 4. NASA Advanced Design Nickel-Hydrogen Cell–Oxygen Recombination Capsule

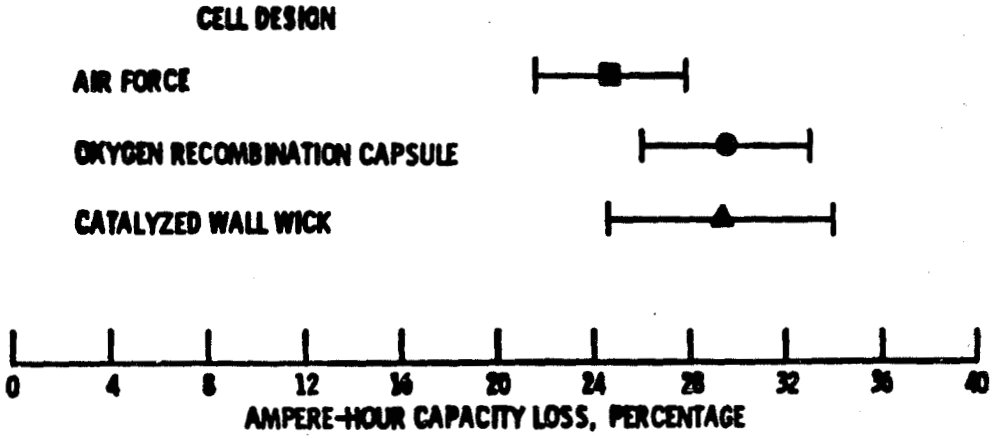

Figure 5. Self Discharge—Average Capacity Loss and Confidence Interval After 72-hour Open Circuit Voltage Stand

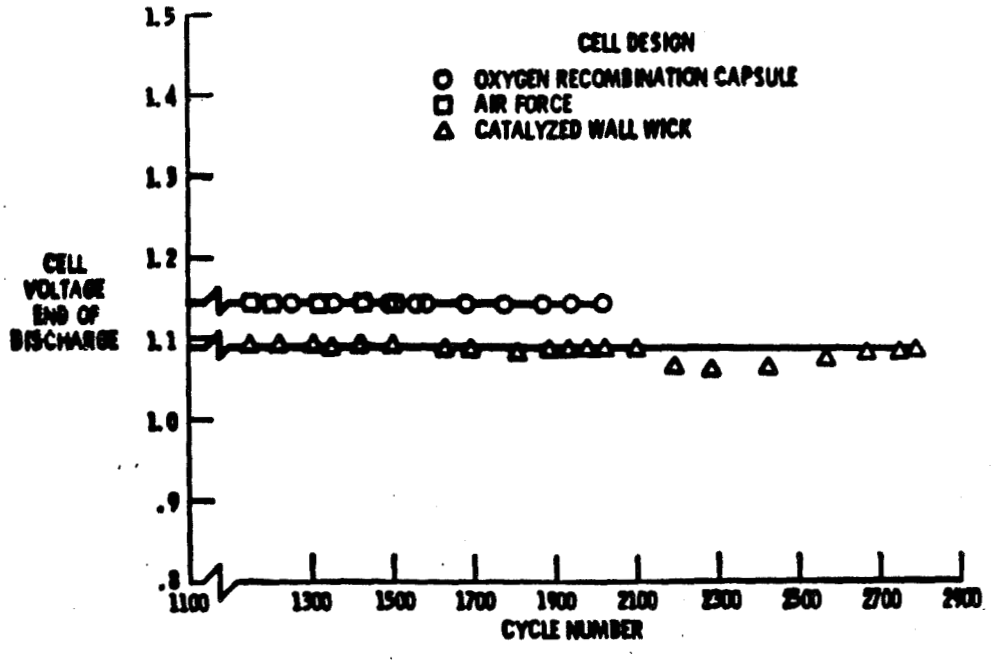

Figure 6. Effect of Cycling on End of Discharge Voltage of Best Cell of Each Design

ACCELERATED AND REAL-TIME GEOSYNCHRONOUS LIFE CYCLING TEST PERFORMANCE OF NICKEL-HYDROGEN BATTERIES

Robert S. Green
RCA Astro-Electronics
Princeton, New Jersey

ABSTRACT

RCA Astro-Electronics currently has four nickel-hydrogen storage battery modules (11 cells each) on test in simulated geosynchronous life cycle regimes. These battery modules are of identical design to those used on the GSTAR (GTE Satellite Corp.) and Spacenet (GTE Spacenet Corp.) communications satellites as previously reported.[1]

The batteries are being tested using an automated test station equipped with computer-controlled environmental chambers and recording equipment. The two battery types, 30 ampere-hours and 40 ampere-hours (GSTAR and Spacenet, respectively), are being electrically cycled using identical 44-day eclipse sequences at 5°C and vary with respect to depth of discharge, recharge ratio, duration of accumulated suntime, and the use of a reconditioning sequence. This paper outlines the test parameters and presents the preliminary test data and results.

INTRODUCTION

As part of RCA Astro-Electronics development and qualification of the nickel-hydrogen energy storage system for the GSTAR and Spacenet communications satellite programs, three 30 AH nameplate battery modules (GSTAR type) and one 40 AH nameplate battery module (Spacenet type) are currently being tested in a simulated geosynchronous life cycle, both real-time and accelerated (reduced suntime) regimes. This test sequence is being performed to demonstrate satisfactory performance of the batteries over the mission life of their respective spacecrafts. All depth-of-discharge (DOD) values are given as a function of actual measured capacity at 10°C unless otherwise noted. The C/2, C/20, and C/60 rates are based on nameplate capacity values.

EXPERIMENTAL

TEST EQUIPMENT

All electrical performance testing of nickel-hydrogen batteries at RCA is performed using an automated battery test system. This test system consists of three major units:

1. Test Station - Combining environmental control chamber, charge power supply, and discharge load

2. Computer System - Providing parameter control, monitoring, and data acquisition

3. Operator CRT and printer for command-control and programming

ELECTRICAL

44-day Eclipse Season

All four battery modules are operating using the same 44-day geosynchronous eclipse simulation, as shown in Table 1. The 30 AH GSTAR modules 005, 006, and 007 are represented as test modules A, B, C, and the 40 AH Spacenet module is represented in test as module D. Note here that the charge time at C/20 is directly proportional to the recharge ratio selected, and that the C/60 charge rate is used to "top-off" and maintain the battery at full state-of-charge.

Suntime: Real-Time vs. Accelerated

The suntime is defined as that period of time when the spacecraft is not in eclipse. One battery in test (Module C) is operating in real-time, that is, there are approximately 3200 hours between eclipse seasons. Because station-keeping maneuvers use the batteries and are performed every 3 to 4 weeks during this period, this module is operating as detailed in Table 2A.

The three remaining modules (A, B, D) are operating in a reduced suntime test. Here the suntime has been reduced to approximately 5% of real-time (Tables 2B and 2C). The simulated stationkeeping discharges have been reduced to 1 per season, and are placed at the beginning of the suntime.

Reconditioning vs. Non-Reconditioning

Reconditioning is that sequence of events when the battery cells are all discharged and drained of all their capacity, immediately followed by a full charge. This usually occurs 1 to 3 weeks prior to beginning a new eclipse season.

The NiH_2 batteries on board the GSTAR and Spacenet spacecraft have the capabilities of being reconditioned[1] should the need arise. Of the four battery units in test, only module A is being reconditioned. This started at the commencement of eclipse season 5.

Depth-of-Discharge and Recharge Ratio

When the full load on the GSTAR and Spacenet spacecraft is applied to the batteries, a depth of discharge of approximately 52% of actual capacity is expected. This being the case, three of the modules (A, C, and D) are operating in constant current discharge mode to 52% DOD (60% of nameplate capacity). In addition, these three modules have a 1.2 recharge ratio at the C/20 rate followed by C/60 for the duration of the daily charge time.

Table 1. 44-DAY ECLIPSE SEASON DAY-BY-DAY ECLIPSE DURATION, RECHARGE TIMES

Day No.	Day No.	Discharge Time (hours)*	Total Charge Time (hours)
1	44	0.200	23.800
2	43	0.367	23.633
3	42	0.483	23.517
4	41	0.583	23.417
5	40	0.667	23.333
6	39	0.773	23.227
7	38	0.800	23.200
8	37	0.867	23.133
9	36	0.933	23.067
10	35	0.983	23.017
11	34	1.033	22.967
12	33	1.067	22.933
13	32	1.110	22.890
14	31	1.133	22.867
15	30	1.150	22.850
16	29	1.167	22.833
17	28	1.167	22.833
18	27	1.167	22.833
19	26	1.183	22.817
20	25	1.183	22.817
21	24	1.183	22.817
22	23	1.183	22.817

NOTE: The total charge time is divided into charge time at nominal C/20 rate and charge time at the nominal C/60 rate. The duration of the C/20 charge is dependent upon the recharge ratio selected, and the remaining time is used to trickle charge the battery at C/60 rate.

*Discharge current determined from average spacecraft load, nominal C/2 rate.

Table 2A. REAL-TIME SUNTIME, MODULE C

Mode	Current	Time
1. Discharge	11 Amperes	1.5 Hours (Stationkeeping)
2. Charge	C/20 (1.5A)	13.2 Hours
3. Charge	C/60 (0.5A)	307 Hours

Repeat Step 1-3 10 times, totaling 3217 hours of suntime.

Table 2B. ACCELERATED SUNTIME*, MODULES A AND B

Mode	Current	Time
1. Discharge	11 Amperes	1.5 Hours (Stationkeeping)
2. Charge	C/20 (1.5A)	13.2 Hours
3. Charge	C/60 (0.5A)	166 Hours

*Approximately 5% of real-time

Table 2C. ACCELERATED SUNTIME*, MODULE D

Mode	Current	Time
1. Discharge	16.5 Amperes	1.5 Hours (Stationkeeping)
2. Charge	C/20 (2.0A)	14.9 Hours
3. Charge	C/60 (0.67A)	166 Hours

*Approximately 5% of real-time

Battery module B was originally operating at 70% DOD (80% of nameplate capacity) with a 1.2 recharge ratio. Although no test difficulty was encountered (e.g., cell reversal), the DOD was reduced to 65% (approximately 75% nameplate), because the minimum voltage requirement of 25.0 volts was being exceeded at the higher DOD. The recharge ratio was increased to 1.4 to overcome charge inefficiency and maintain uniform end-of-charge pressures at the relatively high DOD.

ENVIRONMENTAL

All four test units are each in an environmentally controlled chamber. The chamber is temperature controlled to 5° ±2°C using dry nitrogen. The real-time test, Module C, operates at 10°C (increasing 1°C every year) during the long suntime operation. There is, in addition, a hydrogen sensor in the chamber monitoring for the lower explosion limits of hydrogen, and can abort the test and alert the operator of a potential hazard.

DATA

Module A (GSTAR 005) is operating in an accelerated test regime with a reconditioning sequence prior to each eclipse season (beginning with season 5) at 5°C. The end-of-discharge voltage versus eclipse day for seasons 1, 3, and 5 are shown in Figure 1. At 52% DOD for the 72-minute maximum eclipse period, no degradation has been observed to date. The addition of a reconditioning sequence at the beginning of season 5 appears to have no appreciable effect at this time. The relative uniformity of the end of charge voltages for seasons 1, 3, and 5 can be observed from Figure 2.

Module B (GSTAR 006) is currently being tested in an accelerated test regime at a high depth of discharge at 5°C. During the first two simulated eclipse seasons, this battery was discharged at 70% maximum DOD during the longest days. The charge return for the first half of season 1 was 120% and was increased on day 20 to 130%. Season 2 operated with 140% charge return. The end-of-discharge voltages for seasons 1 and 2 are shown in Figure 3. An increase in end-of-discharge voltage was observed with a 140% charge return in season 2.

Beginning with day 20 of season 3, the depth of discharge was lowered to 65% (for programmatic reasons), and a 1.4 recharge ratio maintained. Figure 4 shows significant voltage increase of approximately 0.7 volt for season 3 when the DOD was reduced from 70% to 65%. Note here the relatively uniform EOD voltages for seasons 4, 5, and the latter half of season 3. Uniform end-of-charge voltages were observed regardless of DOD and recharge ratios, as seen in Figure 5.

Module C (GSTAR 007) is proceeding through test in a real-time test regime, 52% DOD. The approximately 3200 hours of suntime are broken up into ten test portions, each beginning with a simulated stationkeeping maneuver that discharges the battery at approximately a C/3 rate to a DOD of approximately 47%. The 1.2 recharge ratio is maintained for all discharges in this battery.

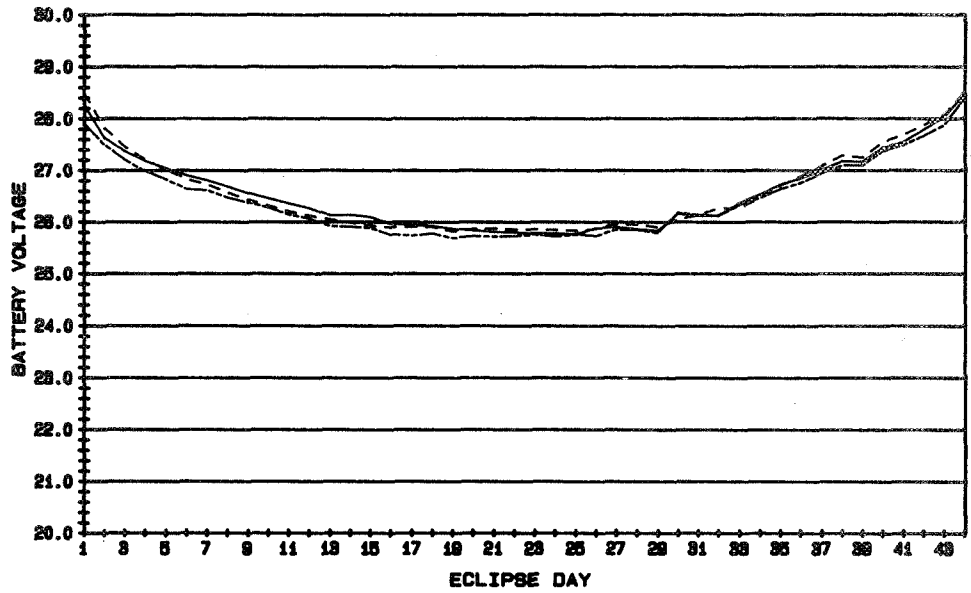

Figure 1. GSTAR Module 005, Accelerated Life Test, End-of-Discharge Voltage vs. Eclipse Day

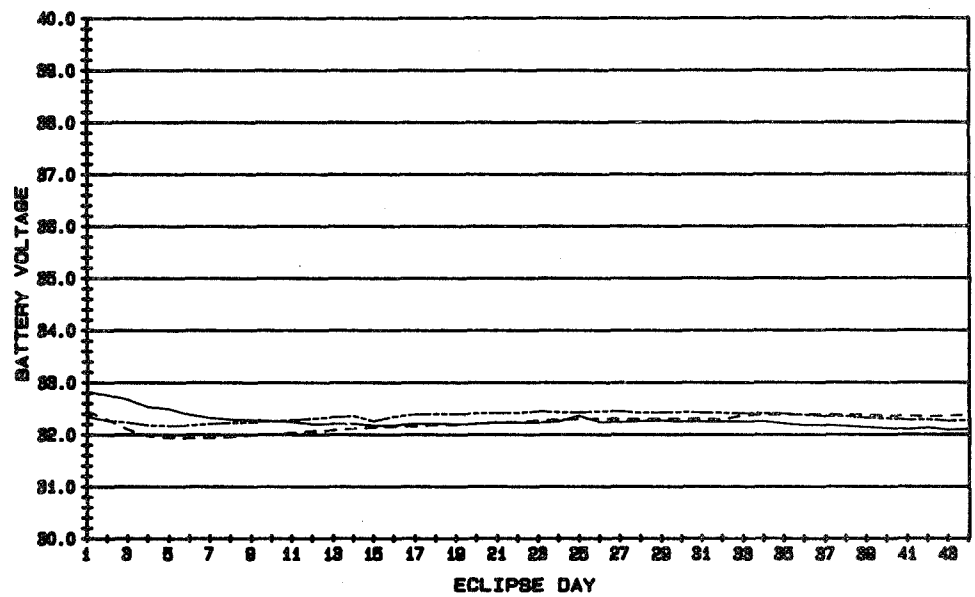

Figure 2. GSTAR Module 005, Accelerated Life Test, End-of-Charge Voltage vs. Eclipse Day

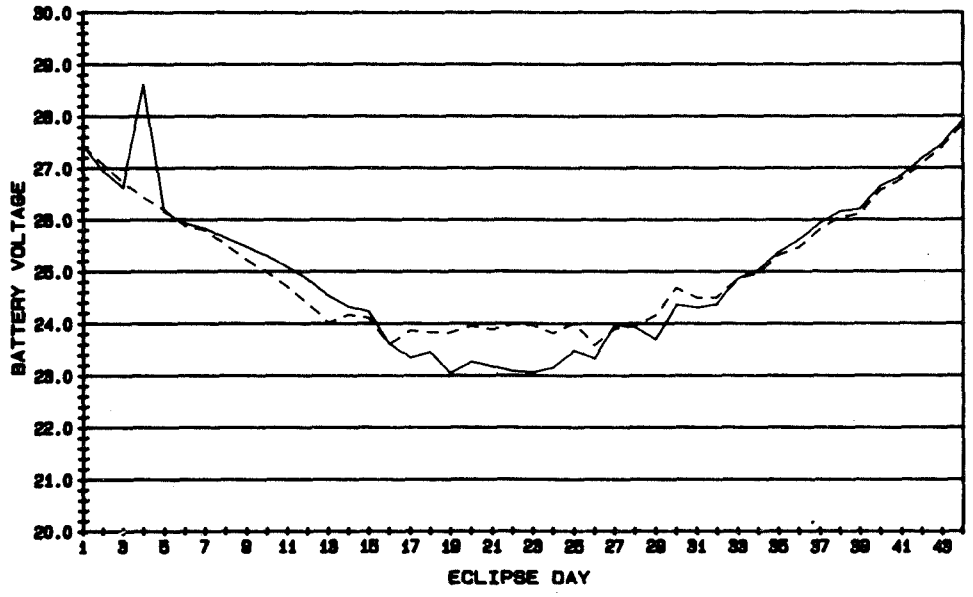

——— VTOTAL. SEASON 1. 12/22/83–2/8/84 (BATT. VOLTAGE = 2 x MODULE V.)
- - - - - - VTOTAL. SEASON 2. 2/18/84–4/1/84

Figure 3. GSTAR Module 006, Accelerated Life Test, 70% DOD, End-of-Discharge Voltage vs. Eclipse Day

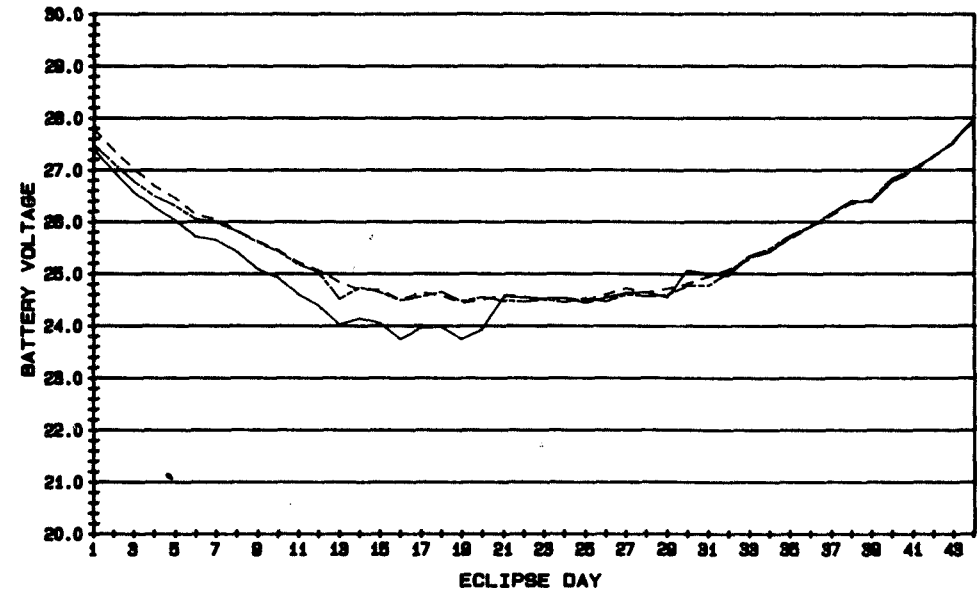

——— VTOTAL. SEASON 3. 3/31/84–5/24/84 (BATT. VOLTAGE = 2 x MODULE V.)
———— VTOTAL. SEASON 4. 8/4/84–7/20/84
- - - - - - VTOTAL. SEASON 5. 7/28/84–9/10/84

Figure 4. GSTAR Module 006, Accelerated Life Test, High DOD, End-of-Discharge Voltage vs. Eclipse Day

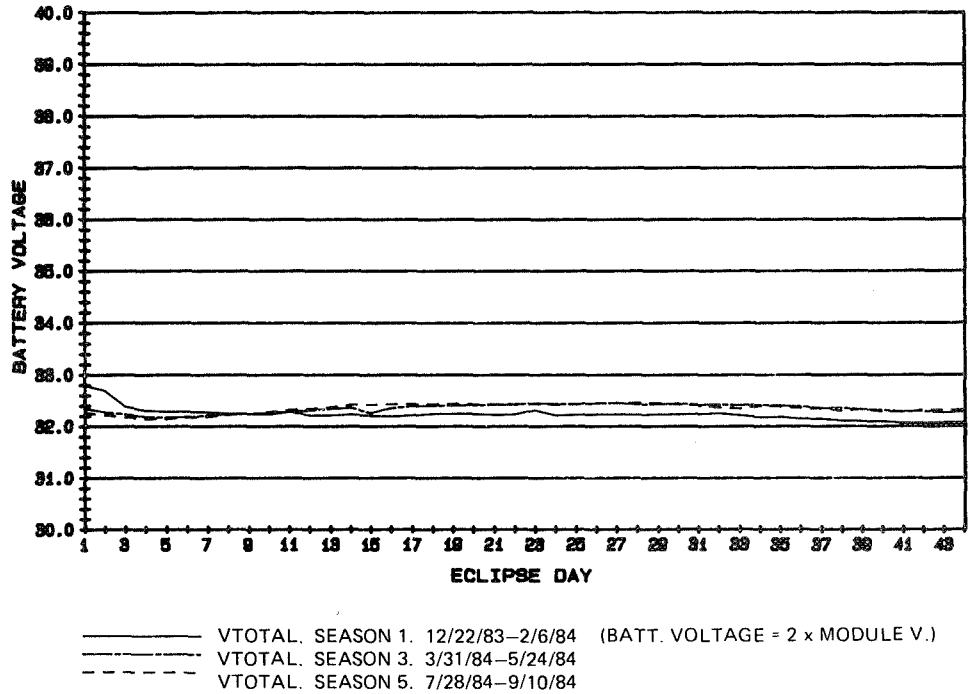

Figure 5. GSTAR Module 006, Accelerated Life Test, High DOD, End-of-Charge Voltage vs. Eclipse Day

The test temperature is 10°C for suntime (increase 1°C/year) and 5°C during eclipse simulation. Figures 6 and 7 are the EOD and EOC voltages versus eclipse day for seasons 1 and 2, respectively.

The fourth nickel-hydrogen battery in this test is Module D (Spacenet 005), a 40-AH qualification unit identical to that launched in the Spacenet F1 spacecraft.[1] Operating in a 52% maximum eclipse day DOD accelerated test mode employing a 1.2 recharge ratio, two simulated eclipse seasons have been witnessed to date. The uniformity of both the EOD voltages and the EOC voltages during the simulated eclipse seasons can be seen in Figures 8 and 9, respectively.

DISCUSSION

All three modules being evaluated at 52% DOD are operating normally. End-of-charge voltages are as expected, above 32 volts/battery (1.46 volt/cell) at the trickle rate of C/60, and the end of discharge voltages are above 25 volts/battery (1.18V/cell) at the C/2 rate for 72-minute discharge.

The nickel-hydrogen energy storage system is clearly capable of being discharged to a 70% DOD on the maximum eclipse day at the C/2 rate. The end-of-discharge voltage is above 23.1 volts/battery (1.05V/cell) without any test difficulty.

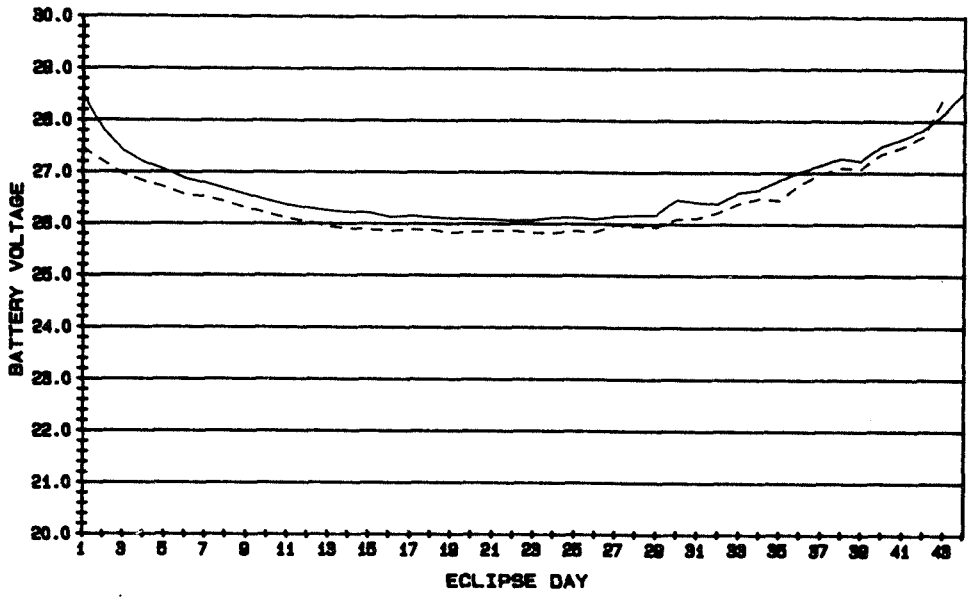

Figure 6. GSTAR Module 007, Real-Time Life Test, End-of-Discharge Voltage vs. Eclipse Day

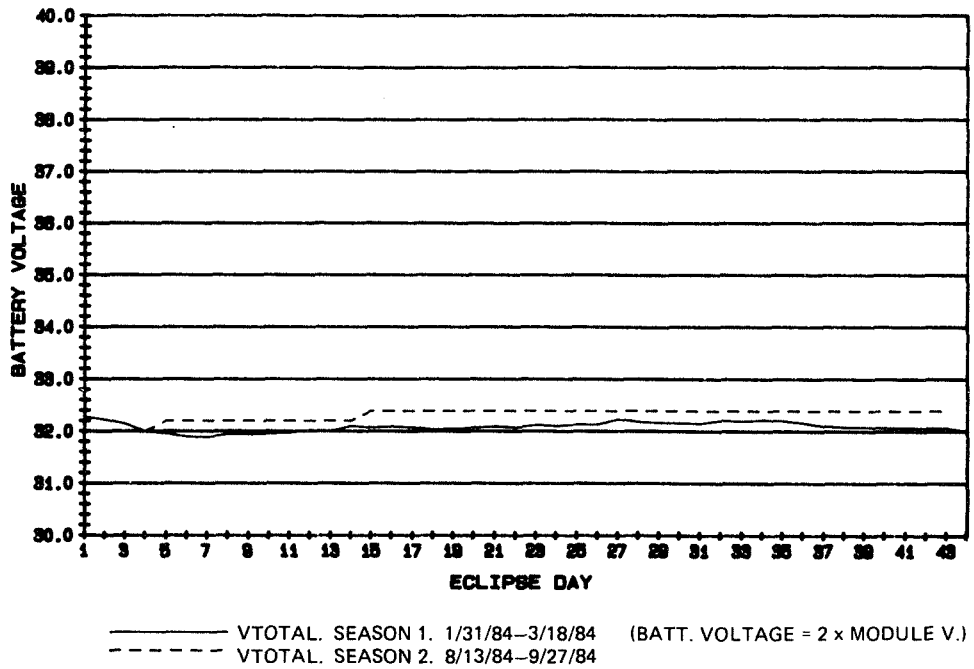

Figure 7. GSTAR Module 007, Real-Time Life Test, End-of-Charge Voltage vs. Eclipse Day

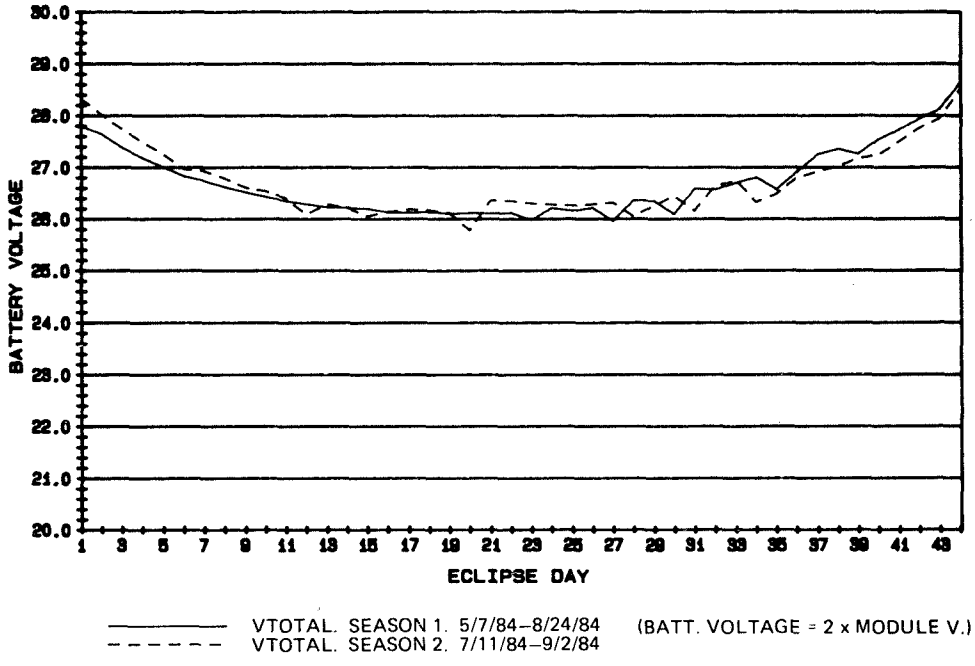

Figure 8. Spacenet Module 005, Accelerated Life Test, End-of-Discharge Voltage vs. Eclipse Day

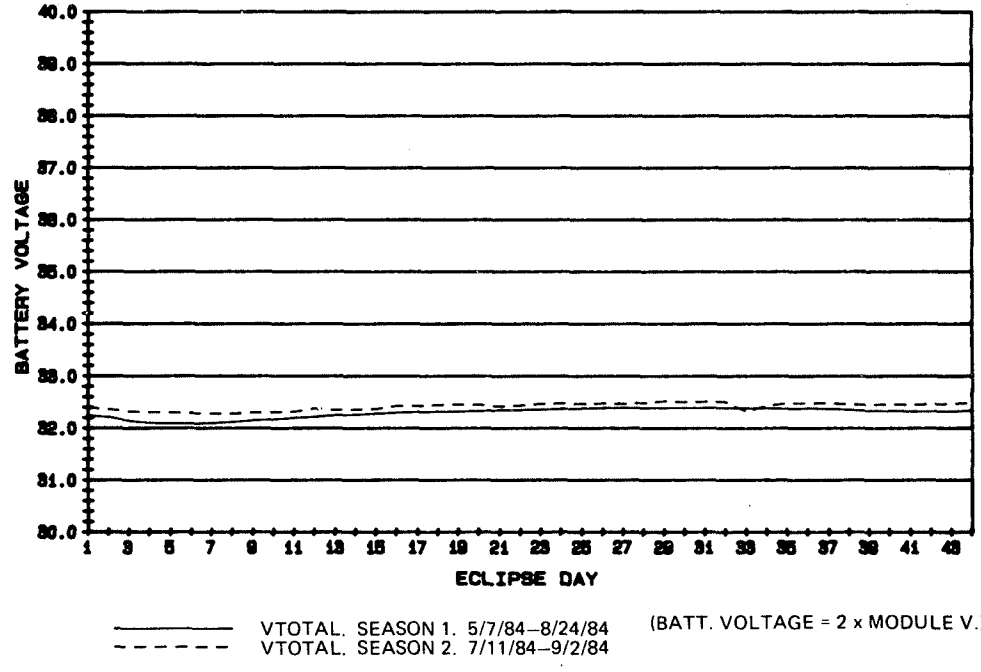

Figure 9. Spacenet Module 005, Accelerated Life Test, End-of-Charge Voltage vs. Eclipse Day

CONCLUSION

The database for the terrestrial testing of nickel-hydrogen batteries in terms of expected life in geosynchronous orbit is still quite small (compared to nickel-cadmium battery technology), and the in-orbit data even smaller. With the successful launch and deployment of the Spacenet F1 spacecraft and the launch of other NiH_2-equipped GSTAR and Spacenet spacecraft in the near future, in-orbit data will be obtained to increase this database. Demonstration of these nickel-hydrogen batteries to perform satisfactorily over their respective mission lives is well under way, and further data and results will be presented periodically.

REFERENCE

1. S. J. Gaston, "The GSTAR and Spacenet Nickel-Hydrogen Batteries for Geosynchronous Orbit Applications," Proc. 19th Intersociety Energy Conversion Engineering Conference, 1984, pp. 257-263.

ACKNOWLEDGEMENTS

The author would like to thank all the members of the Power Systems Group, GSTAR Program Office and Spacenet Program Office of RCA Astro-Electronics, R. Dalebout of GTE Spacenet Corp. and R. Broderick of GTE Satellite Corp. for their support in this project.

LIFE CYCLE TEST RESULTS OF A BIPOLAR NICKEL HYDROGEN BATTERY

Robert L Cataldo
National Aeronautics and Space Administration
Lewis Research Center
Cleveland, Ohio 44135

ABSTRACT

This paper presents a history of low earth orbit laboratory test data on a 6.5 ampere-hour bipolar nickel hydrogen battery designed and built at the NASA Lewis Research Center. During the past several years the Storage and Thermal Branch has been deeply involved in the design, development, and optimization of nickel hydrogen devices. The bipolar concept is a means of achieving the goal of producing an acceptable battery, of higher energy density, able to withstand the demands of low-earth-orbit regimes.

INTRODUCTION

Over the past several years the NASA's Lewis Research Center has been actively engaged in the development of a bipolar configured nickel hydrogen battery. Several studies have pointed out that battery simplicity and weight savings can be realized by employing bipolar construction techniques. The actual weight savings compared to conventional nickel hydrogen designs is in the neighborhood of 20 to 30 percent, and is largely dependent on the particular mission and its specific requirements. The aspect of modularity, where the complete system of storage and heat rejection is integrated into one package, provides the ability to accommodate the growing needs of large systems with little or no impact on the whole system.

In August of 1982, a concept verification program was initiated. A 6.5 ampere-hour 10 cell battery was placed on test. The battery was successfully cycled on a low-earth-orbit regime at 80 percent depth-of-discharge for 2000 cycles. At this point the battery was disassembled and components evaluated for early failure mechanisms.

A second battery was assembled in November, 1983 and has now accrued over 4000 low-earth-orbit cycles.

The remainder of this paper will summarize the performance characteristics of this second stack design that is currently under test.

DESIGN FEATURES

Several special features are found in this battery that are not common to the more conventional nickel hydrogen cells made to date. These features are as follows: electrolyte reservoir plate, that aids in the function of both oxygen and water/electrolyte management; oxygen recombination sites other than the hydrogen electrode (Ref. 1). Figure 1 shows the layout of the cell components.

Some components and the method of electrolyte activation were changed from the first battery built and the one currently on test. Table I displays these modifications. These changes were made as a result of the teardown analysis performed on Build I (Ref. 2) and the battery performance during those 2000 cycles. For example, the chemically impregnated nickel electrode expanded about 50% in thickness. The bipolar plate was edge coated with teflon to eliminate shunt currents that developed within the manifolds after 1000 cycles in the first stack. The activation process was changed because the vacuum backfill method was difficult to carry out and posed problems in electrolyte clean up.

TEST DATA

The stack was assembled in November of 1983. A series of formation tests were performed to establish an actual battery capacity. The charge ampere-hour input was increased from 8.6 Ah to 9.6 Ah over 13 cycles, charging at 3.75 A for appropriate times . The discharge current, 1.875 A remained the same for each discharge. The ampere-hours discharged to 0.5 V (lowest cell) increased from 7.82 Ah to 8.1 Ah. The nominal capacity asymptotically reached 8.1 Ah as the charge ampere-hours was increased. The capacity discharged to 1.0 V of the weakest cell was 7.8 Ah as shown in Table II, and this value was used as "C" for the characterization tests.

The characterization test matrix contained charge rates of C/4, C/2, and C and discharge rates of C/4, C/2. C and 2C, as well as one 10C discharge. The results are shown on Figure 2 and compared to similar results of Build I.

LEO cycling to 80 percent depth (based on the 1.6C rate capacity of figure 2) at the 9.6A rate was started following the characterization tests. Twenty cycles were performed with decreasing end-of-discharge (EOD) voltages. A decision was made to pull a vacuum on the vessel. A hard vacuum was pulled on the vessel because we had not done this prior to pressuring the vessel with hydrogen. During Build I we found electrolyte in the vessel and thought that evacuating the air from the vessel prior to the hydrogen fill expelled

electrolyte from the stack. The battery EOD voltage increased by 1.0 volts as shown in Figure 2. The vacuum was thought to have relocated some electrolyte into the smaller pores and into the hydrogen electrode. The battery degraded about 0.5 volts in fifty cycles and then stabilized. The stack was removed from the vessel and vacuum back filled with electrolyte. This procedure had a longer lasting effect on EOD performance; however, voltages were still degrading.

The performance of Build II was not a good as Build I. Some design changes had been made as indicated in Table I. At this point it was decided to rebuild cells 1, 2 and 3 to try to determine the effects of the changes that had been made.

Cell 1 received all new components. The hydrogen and nickel electrode were vacuum filled prior to assembly and 21 mils of separator was used. Cell 2 only received a vacuum filled hydrogen electrode and 14 mils of separator. Cell 3 got a change of separator from 14 mils to 21 mils. These modifications were made in an attempt to isolate the design changes that were not improvements. However, the following cycle data did not provide a basis for any judgements, other than a vacuum filling of the hydrogen electrodes is necessary. A performance increase was noted in the other 7 cells that were undisturbed.

A performance increase was observed by doing several LEO rate discharges to 0.5 volts of the lowest cell. The deep discharge reconditioning made a significant increase in battery voltage for 20-30 cycles and also decreased the rate of degradation of EOD voltages.

Several times during cycling the stack was deep discharged and electrically shorted out over night. This procedure also provided marked improvements in EOD voltages. Several self-discharge open circuit stands were performed. No shunt currents were observed and a 30 percent loss in the C/4 capacity was recorded in a 3-day period with the hydrogen pressure a constant 400 psi. This proved the teflon edge coating of the bipolar plate provides a means of prohibiting shunt currents from forming.

After 2800 cycles were run, a 4 mil nickel shim was added to each cell. The shim was added to increase the stack component compression. Compression tests on various materials and separator thicknesses indicated that our stac pre-load was not sufficient to compress the separator and provide good conta with the bipolar plate. Table II shows the individual cell voltages for ove 300 cycles prior to and after the installation of the shims. It is of interest to note that all the cells had declined in EOD voltage prior to the shim installation; however, six cells increased and four cells decreased in voltage afterward. Again, the results are not clear about the merit of increased compression.

The nickel electrode was removed from cell 10 during the shim installation and replaced with a new electrode. The cycled electrode expand 3-4 mils or 10 percent of the original thickness, which furthur increases th compression. It is possible the cells with reduced voltage have been over compressed, which may have forced electrolyte from the active areas.

Table II displays the C/4 capacities measured to 1.0 volts throughout battery cycling. A loss in capacity is noted in all cells. Cell 6 has experienced the greatest decline, 35 percent, while the other cells have degraded about 30 percent. The nickel electrode removed from cell 10 at 28C cycles measured a loss of about 15 percent in capacity at C/4 rates and 25 percent at the 2 C rate in flooded capacity tests while the electrodes under cell conditions at 3350 cycles showed a 20 percent decrease. In the span of cycles 3100 to 3860 the depth of discharge was adjusted to 70% corresponding to their original capacity as noted in Figure 3. Following the last C/4 capacity discharges at cycle 3906, the depth of discharge was resumed to the 80 percent level. The ampere-hours discharged is almost 90 percent of the actual electrode capacity.

CONCLUDING REMARKS

Over 4100 LEO cycles have been established on a ten cell battery. It seems that any perturbation on normal cycling effects the cells performance. Explanations and theories of the battery's behavior are varied and widespre among those closely associated with it. Deep discharging does provide a reconditioning effect and further experimentation is planned in this area.

The battery watt-hour efficiency is about 75 percent and the time averaged, discharge voltage is about 1.26 volts for all cells at both the C/4 and LEO rate.

Since a significant portion of the electrode capacity has degraded, the LEO cycle discharges are approaching depths of 90-100 percent of the high rate capacity. Therefore, the low end-of-discharge voltages occur precipitously after the knee of the discharge curve and is more an indication of electrode capacity and is a lesser indicator of overall cell performance.

REFERENCES

1. Cataldo, R. L.: Test Results for a Ten Cell Bipolar Nickel-Hydrogen Battery, 18th IECEC Proceedings, NASA TM 83384.

2. Manzo, M. A., Gonzalez-Sanabria, O. D., Herzau, J. S. and Scaglione, L. J.: Teardown Analysis of a Ten Cell Bipolar Nickel-Hydrogen Battery, 19th IECEC Proceedings, NASA TM 83618.

	Build I	Build II	Remarks
Nickel Electrode	Chemically Loaded 2.1g/cc	Electrochemically Loaded 1.6g/cc	Electrode expanded 50%
Hydrogen Electrode	Fuel Cell Type Non-backed	Fuel Cell Type Non-backed	Need to vacuum fill
Separator	Asbestos 21 mils 5% Binder	Asbestos 14 mils 5% Binder	
Electrolyte Reservoir	Nickel Foam	Nickel Foam	
Recombination Sites	H_2 Electrode Open Gortex	H_2 Electrode Sealed Gortex	
Bipolar Plate	Gold Plated Nickel	Gold Removed, Teflon Coated Edges	Shunt currents developed
Activation Process	Vacuum Backfill with KOH Drain	Vacuum Fill Nickel Electrodes; Metered Amount Added to Each Cell	Simplify process

Table I.

	CELL NUMBER									
CYCLE #	1	2	3	4	5	6	7	8	9	10
16[e]	7.8[a]	8.0[b]	8.0[b]	8.0[b]	8.0[b]	8.0[b]	8.0[b]	8.0[b]	8.0[b]	8.0[b]
2363[c]	5.76	5.76	5.73	5.82	5.9	5.7	5.7	5.9	5.6[a]	5.7
2364[c]	6.7	6.7	6.3[a]	6.45	6.74	6.74	7.0	6.9	7.0	7.0
3350[d]	6.5[b]	6.34	6.34	6.5[a]	6.5[b]	5.93	5.85	6.47	6.5[b]	6.5[b]
3862[d]	5.9[b]	5.8	5.7[a]	5.8	5.9[b]	5.2	5.6	5.7	5.9[b]	5.9[b]
390b[d]	5.6[b]	5.55	5.4[a]	5.5	5.6[b]	5.0	5.23	5.3	5.6[b]	5.6[b]

Table II. DISCHARGE CAPACITIES TO 1.0 V AT THE C/4 RATE OF 1.9 A

a = first cell to reach 0.5 Volts
b = cells not reaching 1.0 Volts before event a
c = charge; 8 A-H; 4 A for 2 Hrs.
d = charge; normal LEO cycle interuption
e = charge; 9.1 Ah

CELL NO	CYCLE NO.					
	2410	2800	ADDED SHIM	2807	3167	
1	1.173	1.129	-.044	1.123	1.162	+.039
2	1.164	1.125	-.039	1.122	1.117	-.005
3	1.156	1.095	-.061	1.096	1.031	-.065
4	1.192	1.145	-.047	1.138	1.158	-.020
5	1.209	1.173	-.036	1.166	1.187	-.021
6	1.175	1.112	-.063	1.102	1.109	-.007
7	1.192	1.139	-.053	1.133	1.026	-.107
8	1.139	1.097	-.042	1.092	1.074	-.018
9	1.186	1.127	-.059	1.125	1.154	-.029
10	1.168	1.121	-.047	1.112	1.178	+.066
NET			-.491			-.013

Table III. CELL VOLTAGES BEFORE AND AFTER ADDING SHIM TO EACH CELL

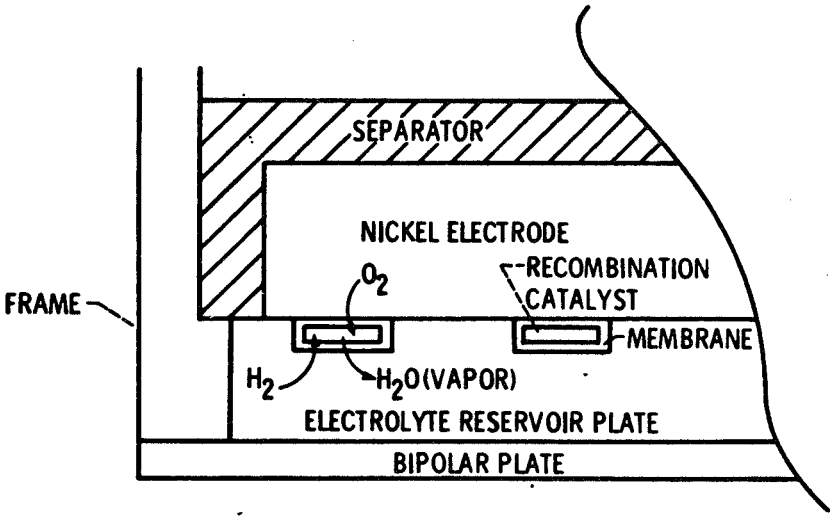

Graphic representation of oxygen - hydrogen recombination.

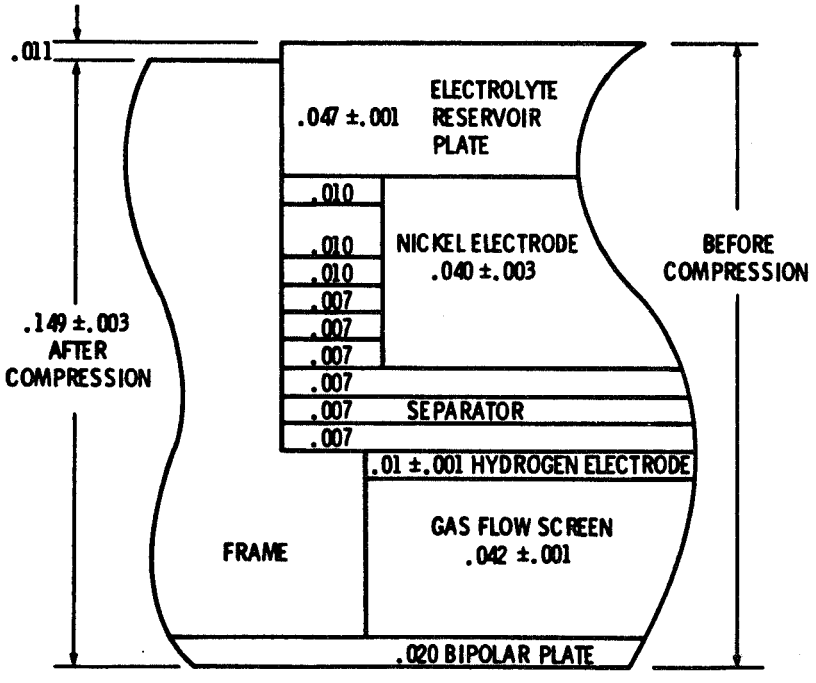

Cell cross section with dimensions of components, in.

Figure 1. Cell Component Layout

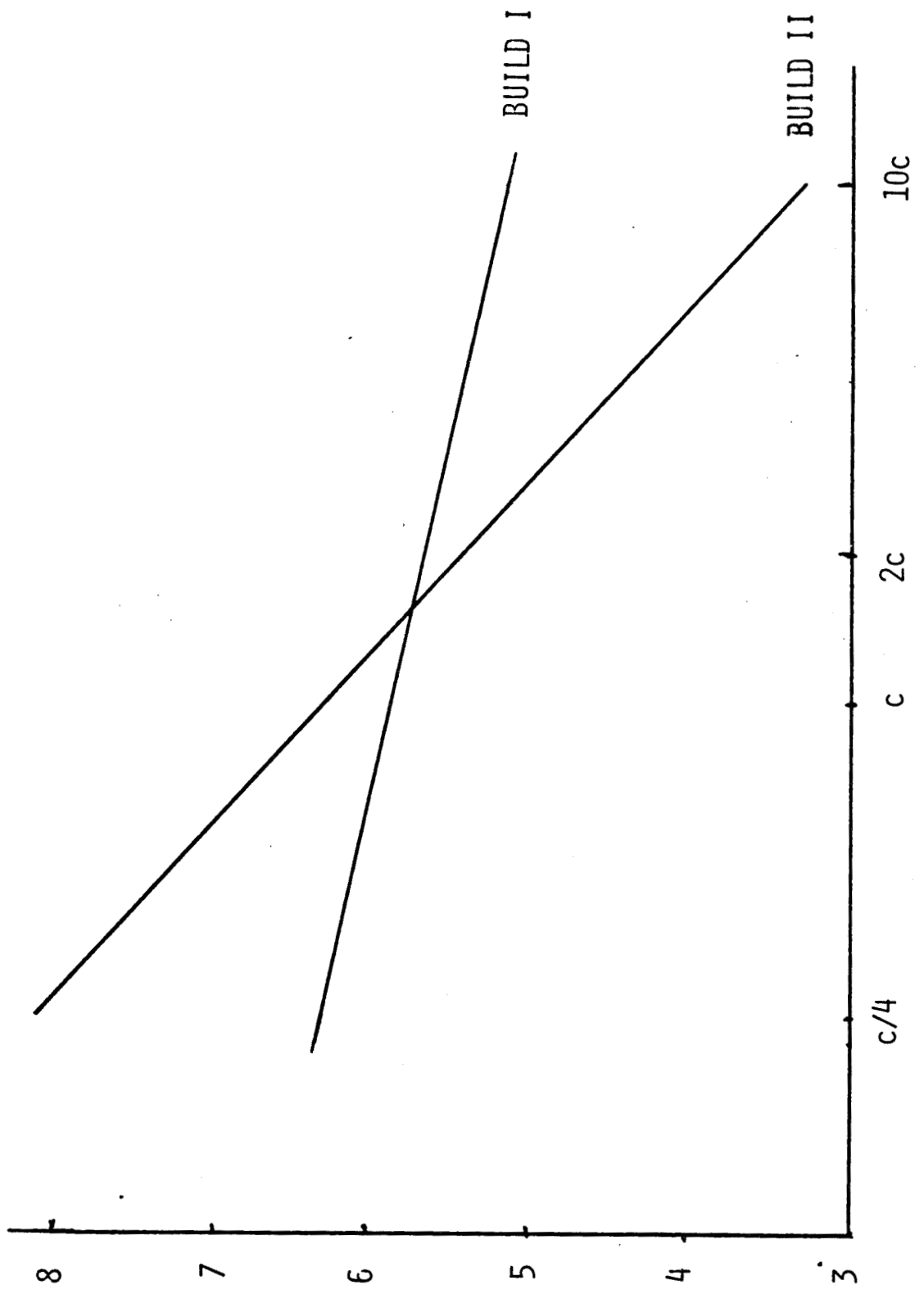

Figure 2. Discharge Capacity vs. Current Rate

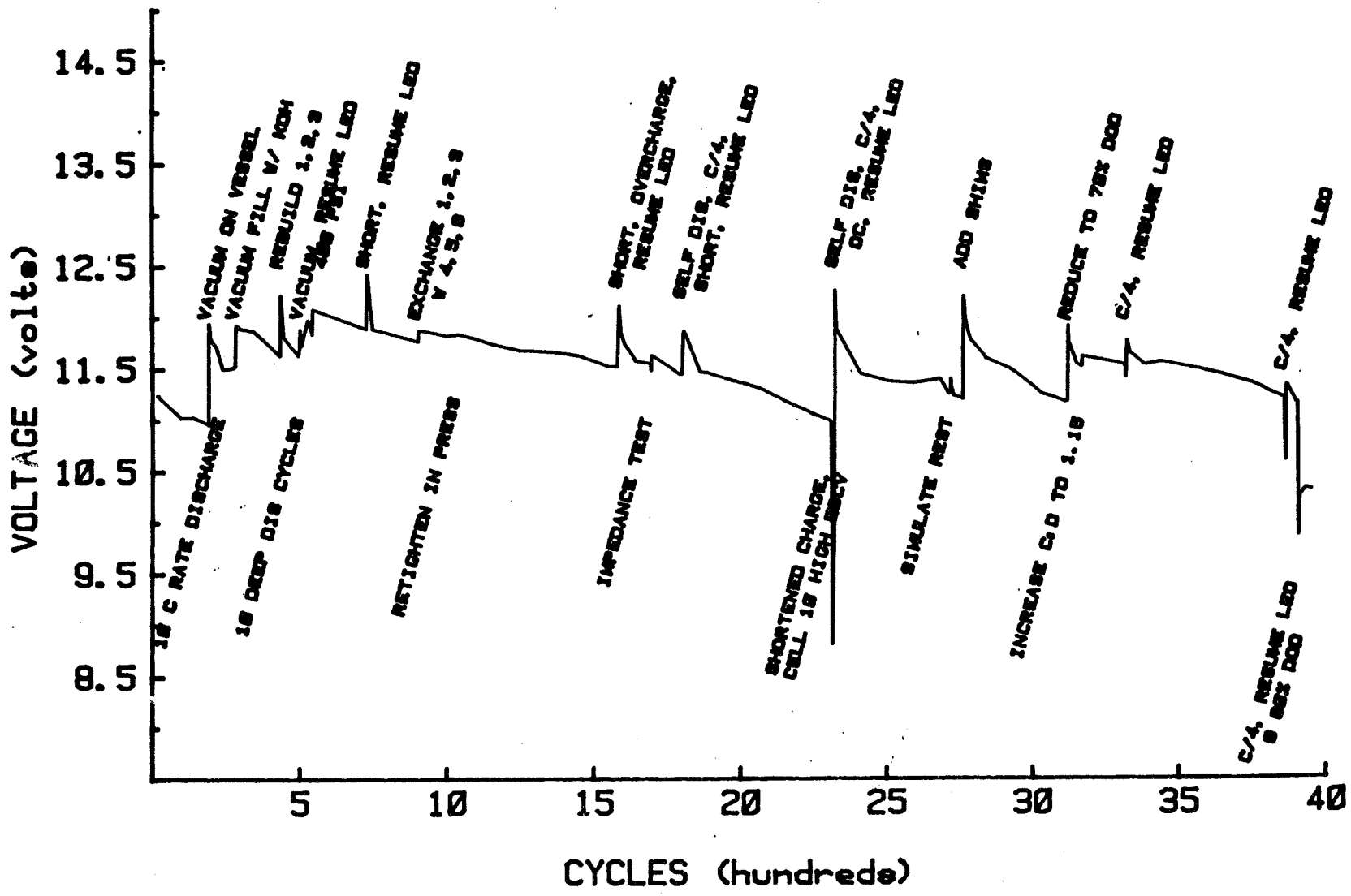

Figure 3. End of Discharge Voltage vs. Cycles for Build II

NICKEL-HYDROGEN CELL TEST PROGRAM SUMMARY

Vernon C. Mueller

McDonnell Douglas Astronautics Company - St. Louis Division

ABSTRACT

Three prototype 50 ampere-hour (AH) nickel-hydrogen cells of the Air Force Wright Aeronautical Laboratories (AFWAL) design have been cycled to failure by the McDonnell Douglas Astronautics Company-St. Louis Division (MDAC-STL). A summary of the life cycling tests and failure analyses of the cells are presented in this paper. The cells were cycled in a simulated low earth orbit regime at depths of discharge ranging from 25 to 80 percent. Trend data, such as end of discharge voltage and cell capacity, was recorded during test. Cells 1, 2, and 3 completed 17167, 2473, and 10080 charge/discharge cycles, respectively, prior to failure. All failed due to internal shorts, and were disassembled to determine cause of failure.

INTRODUCTION

Three NiH_2 cells rated at 50 AH were provided to MDAC-STL by AFWAL for a test program consisting of parametric tests followed by life cycling in a simulated low-earth orbit regime. Two of the cells had a zirconium-oxide, single-layer square weave separator (Cell 1/SN 104 and Cell 2/SN133), and the third had asbestos separators (Cell 3/SN148). All cells were manufactured in 1978 by Hughes Aircraft Company and contained Yardney positive electrodes made with a slurry process sinter and electrochemically impregnated. Figure 1 shows the cell general arrangement. MDAC-STL began the test program in November, 1979, concluding with failure of the last surviving cell in August, 1983. Test progress and interim results have been presented in earlier Goddard Space Flight Center Battery Workshops beginning in 1980. A summary of the life cycling tests and cell failure analyses are discussed in this paper.

During test, the cells were mounted horizontally in a fixture which gripped the cell about the cylindrical section and permitted heat to flow from the cell to the aluminum clamp and then to a supporting aluminum plate. Figure 2 shows the three cells in the test fixture. The one-inch aluminum baseplate was cooled by a circulating liquid coolant bath to provide temperature control of the cells. To assure that all heat was removed from the cells by conduction through the mounting clamp to the temperature controlled baseplate, insulation was applied completely around the cells. Temperature measured at a point on the side of the middle cell near the support fixture was used as the control point for temperature control.

LIFE CYCLING TESTS

Objectives of the cyclic tests were to obtain life data in a low-earth orbit regime and to identify and evaluate cell performance degradation. The cells were cycled by discharging into a fixed resistor such that the desired depth-of-discharge (DOD) was achieved in a 35-minute discharge period, followed by charging at approximately 50 amperes to a voltage limit, which was then held constant while the current tapered for the balance of the 55-minute charge interval. Cycling was controlled automatically to permit unattended operation. In order to prevent cell damage due to equipment malfunction, alarms were provided to shut down the test (open-circuit the cell) for over/under voltage, excessive discharge current, overtemperature, overpressure, and loss of facility power. At approximately 500 cycle intervals, cell capacity was determined by discharging at 25 amperes to a 1.0 volt cutoff. Capacity checks were accomplished immediately after a normal cyclic charge interval. Data was recorded at one-minute intervals during the capacity discharge and for one cycle at roughly 200 cycle intervals. For intervening cycles, data was recorded at 10-to 20-minute intervals as an aid to reconstruct anomalies, should they occur.

Cell 1 was cycled independently and Cells 2 and 3 were cycled in series. The control point temperature was set to 8°C for the first 2000 cycles, and to 23°C subsequently. Figure 3 shows energy removed on discharge as a function of cycles completed for these cells. The desired depth of discharge (DOD) for Cells 2 and 3 was 80 percent of rated capacity. However, this resulted in low end of discharge (EOD) voltage and DOD was reduced to 70 percent after 585 cycles. Further reduction occurred subsequently, again in response to low EOD voltage. Cell 1 DOD was reduced to 25 percent early in the test for 500 cycles to obtain data to support another study then in progress. It was then returned to 50 percent DOD to cycle 15706 at which time it was reduced due to low EOD voltage.

Cycling test trend data is shown in Figures 4 and 5. Cell 2 had recurring problems with low EOD voltage. At cycle 2473, cycling was stopped to perform a capacity check. Following the capacity check, Cell 2 failed to recharge. Three days later, a 5-ampere charge was again attempted, but Cell 2 failed to respond. Apparently an internal short had developed and the cell was removed from test. Cells 1 and 3 continued to cycle with relatively few problems. Degradation of EOD voltage and reduction of measured capacity was observed, as noted in Figures 4 and 5. Cell 3 failed abruptly after completing 10,080 charge/discharge cycles. Evidently, a massive short had developed, as evidenced by a high cell temperature. At this point, the cell was disconnected electrically, but physically left in the test fixture.

Cell 1 lost a significant portion of its hydrogen gas when a leak developed in a pressure fitting, which attached a pressure transducer to the cell at Cycle 6229. The loss of hydrogen caused shutdown of Cell 1 cycling due to an undervoltage alarm during discharge. During investigation of the failure, the cell was shorted for several weeks. The leak in the external plumbing was corrected and the cell was backfilled with 50 psi of hydrogen several times to replenish the cell. When the cell was recharged, it showed good voltage recovery and was returned to cycling. As shown in Figure 4, the reconditioning effect on EOD voltage was soon diminished and remained relatively stable for several thousand cycles after the anomaly occurred.

At Cycle 11891, Cell 1 was inadvertently overcharged for 20 hours, with a total input energy of 118.4 ampere-hours due to an equipment malfunction. There was no apparent cell damage; therefore, the cell was returned to cycling after equipment repair. The effect of this long overcharge can be seen in the increase in measured capacity after Cycle 12015. Measured capacity was 59 ampere-hours at this point.

Cell EOD voltage was degrading on Cell 1 at approximately 15,000 cycles. The charge limit voltage was increased slightly, but the voltage continued to degrade and an undervoltage alarm caused shut down at Cycle 15690. At this time, the cell was recharged and a capacity check was performed. Measured capacity was only 23.9 ampere-hours, so the discharge energy was reduced from 25 to 15 ampere-hours. The effect on EOD voltage is reflected in Figure 4. As shown in Figure 5, measured capacity improved considerably after the low reading of 23.9 ampere-hours. Reasons for the behavior are not known. Cycling continued smoothly until failure occurred at Cycle 17168. Failure occurred about 20 minutes into the discharge of Cycle 17168 and was accompanied by a high-cell temperature pulse.

FAILURE ANALYSES

Each of the cells was dissected to determine the cause of failure. A dry nitrogen purge was used prior to disassembly to eliminate any residual hydrogen. Then the cell was cut open with a lathe just below the weld toward the negative terminal (see Figure 1). The negative end of the pressure vessel was then removed, exposing the electrode stack assembly. Figure 6 is a sketch of the electrode stack assembly. For purposes of identification, the electrodes are numbered consecutively from the positive end of the cell (weld ring end). Elements of the electrode stack assembly were removed individually, and photos, observations, etc. were accomplished as the disassembly progressed.

CELL 2

Cell 2 (SN 133) failed after 2473 charge/discharge cycles. This cell had a Zircar separator. Cells 2 and 3 were connected in series during cycling, and were discharged in series during a capacity check after 2473 cycles. Cells 2 and 3 delivered 27.3 and 46.9 ampere-hours to a one-volt cutoff, respectively. The discharge characteristic for Cell 2 showed a second voltage plateau at approximately 0.85 volts, and the continuing discharge of Cell 3 drove Cell 2 into reversal at -0.06 volts. It remained reversed for 14 minutes until Cell 3 reached one volt. After the discharge, Cell 2 remained at an open-circuit voltage of 0.004 volts for three days before a five-ampere recharge was attempted and the voltage failed to recover.

After Cell 2 was cut open and the polysulfone nut was removed to free the stack, a voltage measurement of 0.908 volts was observed indicating that the short was removed as electrode stack compression was relieved. Disassembly of the electrode stack revealed no obvious evidence of a mechanical short. Three anamolous areas were found where active material had bridged through burnholes from a positive electrode to an adjacent negative. If this material

was conductive, it could have provided a shorting path when the stack was tightly compressed. Tests by Hughes Aircraft Company have shown that such a bridge will remain nonconductive for at least 1500 cycles. If these anomalies were formed early enough for sufficient positive material to be reduced to conductive nickel, it would account for the condition. This seems the most likely failure mechanism. Numerous gas screens and negative electrodes had tiny burn holes randomly spaced due to rapid oxygen recombination (popping). The damage was most noticeable on the gas screens and the teflon surface of the negative. However, this phenomenon was not a contributing factor to the observed failure.

CELL 3

Cell 3 (SN 148) completed 10,080 charge/discharge cycles prior to failure. Cell failure analysis was discussed in detail at the 1983 Battery Workshop. Therefore, this discussion will be somewhat abbreviated. At approximately five minutes into the charge period of cycle 10,080, a cell overtemperature was sensed and, on the next data scan a few seconds later, the voltage was less than 0.5 volts. The automatic circuitry open-circuited the cell. When the next data set was recorded 18 minutes later, the highest temperature was 89.6°C, measured at the top of the cylindrical section furthest removed from the coolant bath. Intermediate data points were not recorded, and the peak temperature excursion is not known. The cell was disconnected electrically after failure, but physically left in the test fixture for approximately 11 months before the failure analysis was done.

Something loose could be heard rattling within the pressure vessel prior to dissection. After the negative end of the pressure vessel was removed, the ceramic insulating washer at the negative terminal was found broken into four pieces, which accounted for the rattling noise. The shoulder at the end of the polysulfone core had fractured completely around the intersection with the central part of the core. This allowed the electrode stack to relieve, leaving the first negative roughly flush with the broken end of the polysulfone core. The shoulder, belleville washer, and honeycomb end plate were loose on the negative leads. The reservoir had melted completed acróss the annular section in the area of the negative tab and the electrode stack was indented. Forces applied to the plates by the negative tabs when the stack relieved may have caused this indentation.

The electrode stack assembly was disassembled, element by element. Shorting of adjacent positive and negative plates was found at the inner perimeter of the plates in the area of the negative tab. In many cases, active material from the positive plate was imbedded in the adjacent negative. Gas screens and reservoirs between negative and positive plates had melted and shrunk and were fused to the teflon-coated side of the negative electrodes. Damage was observed to extend from the negative end of the electrode stack to plate set 27, with the most extensive damage seen in plate sets 34 to 37. The heat pulse generated when the shorting occurred appeared to discolor and swell the polysulfone core, such that a ribbed appearance was created and a black deposit was left where the positive plates restricted this swelling. The dimension from the end of the core to the first indentation caused by a positive plate

was less than the combined thickness of the end plate and belleville washer, which implies that the end of the core fractured prior to the occurrence of the short. Positive plate thicknesses were measured during disassembly and, assuming each was fabricated at the maximum dimension, electrode stack height increased 0.395 inches during cycling.

We have concluded that positive plate growth during cycling was the primary reason for cell failure. A chronological history of the failure can be postulated as follows:

- Positive plate growth during cycling causes fracture of the shoulder from the polysulfone core.
- Forces applied to the electrodes when the stack expands creates pressure points between adjacent pairs of electrodes, most pronounced at the tab attachments.
- A short occurs at a pressure point after some period of time.
- The heat pulse and mechanical forces generated by the short cause the failure to propagate to adjacent plate sets.

CELL 1

Cell 1 (SN 104) completed 17,167 charge/discharge cycles prior to failure. Failure occurred on 23 August 1983, at about 20 minutes into discharge of cycle 17,168. Cycling was terminated by an undervoltage alarm which open-circuited the cell, but it continued to self-discharge and heat up. The bottom of the cell reached 183°C seven minutes after shutdown, indicating a short circuit. At thirty minutes after failure, cell temperature was 115°C. During an automatic shutdown, active cooling is terminated. An hour after shutdown, the voltage had dropped to zero and the pressure fell to approximately 100 psi. A five-ampere, five-minute recharge was attempted without success. The cell was left in the test fixture until the failure analysis was begun on 17 October 1983.

On the basis of our failure analysis of Cell 3, we decided to X-ray Cell 1 prior to disassembly to determine whether a similar condition existed. Inspection of the radiographs showed the belleville washer and end plate were free and that the electrode stack assembly had relieved. Also, loose parts could be heard rattling inside the pressure vessel.

The ceramic washer from the negative terminal was found fractured into five segments inside the cell when the negative end of the pressure vessel was removed, which caused the rattling noise. Again, the shoulder of the polysulfone core had fractured completely around the intersection with the core. The shoulder, end plate, and belleville washer were retained by the negative leads. The electrode stack had relieved with the first negative electrode extending slightly past the fractured end of the core. Also the

electrodes were indented along an axis corresponding to the axis in which the plate tab to positive and negative leads is made. This depression is believed to have been caused by forces exerted through the leads when the stack relieved. Figure 7 is a view of the electrode stack prior to disassembly showing the indentation. Also, the negative reservoir had shrunk and necked in at one point, probably due to heating. Visual examination of the fractured end of the core showed striations similar to that seen in fatigue failure of metals.

An electrode-by-electrode disassembly revealed shorting of adjacent positive and negative plates at the inner perimeter of the plates in the area where the negative leads attach. Active material from the positive plate was imbedded in the adjacent negative in many cases. Also, the gas screen between negative and positive plates had melted and shrunk and was fused to the teflon coated side of the negative plate. Most severe damage to the gas screen was at a point where shorting had occurred at the negative lead to plate attachment. As the gas screen shrunk, it apparently fused to the outer periphery of the negative plate and peeled the teflon backing away from the underlying screen structure. Figure 8 is a photograph of negative plate 35 showing active material from positive plate 34 imbedded at the inner periphery where the negative lead attaches to the tab. Note also how the gas screen peeled back the teflon coating as it shrank due to heating. Gas screen shrinkage, melting, and fusing to the negative plate, and shorting of positive and negative electrodes extended throughout the stack assembly. Pin holes were found in many of the negative plates, indicating that "popping" occurred. As disassembly progressed toward the positive end of the electrode stack assembly, the plates became more planar.

Examination of the polysulfone core after disassembly showed the discoloration and swelling which is apparently caused by the heat pulse generated when shorting occurs. Figure 9 shows the polysulfone core attached to the positive hemisphere after the electrode stack elements have been removed. The degree of discoloration is believed to be proportional to the heat generated at that point. Applying that premise, the short is believed to have occurred first at a point approximately one-third of the stack thickness from the positive end and progressed outward in both directions. The swelling of the core causes a ribbed appearance and a black deposit is left where the positive plates restrict the swelling. The dimension from the fractured end of the core to the first indentation caused by a positive plate is less than the combined thickness of the end plate and belleville washer, which implies that the shoulder fractured from the end of the core prior to the occurrence of the short.

Positive plate thicknesses were measured during disassembly and ranged from 0.038 to 0.048 inches. Assuming that each positive plate was fabricated at the maximum dimension of 0.032 inches, the thickness of the electrode stack assembly increased by 0.451 inches during cycling. the cell failed in a nearly identical manner to Cell 3, and we believe the failure history was also the same. Positive plate growth of this magnitude cannot be accommodated; and, after the stack relieves, a short occurs at a pressure point between adjacent pairs of electrodes which ultimately results in the massive internal damage observed.

CONCLUSIONS

The prototype cells tested do not exhibit the cyclic life necessary for spacecraft power systems operating in low-earth orbit. However, when one considers the high depth of discharge used for the cyclic tests, the performance of Cell 3/SN148 and Cell 1/SN 104 are certainly respectable as compared to nickel-cadmium cell life. Cells used for these tests are prototypes, and do not represent a mature technology. Also, considerably more data needs to be acquired to obtain a statistically significant data base for low-earth orbit applications. The most significant cause of failure is the positive plate growth experienced with these early design positive electrodes. More recent positive electrodes show significantly less growth with cycling, and should retard or eliminate the type of failure seen in Cells 1 and 3. Testing of current generation cells incorporating the improved positive electrodes, as well as other design improvements, are required to obtain necessary cyclic life data. MDAC-STL plans to test a 21-cell, nickel-hydrogen battery in a simulated low-earth orbit regime in the near future.

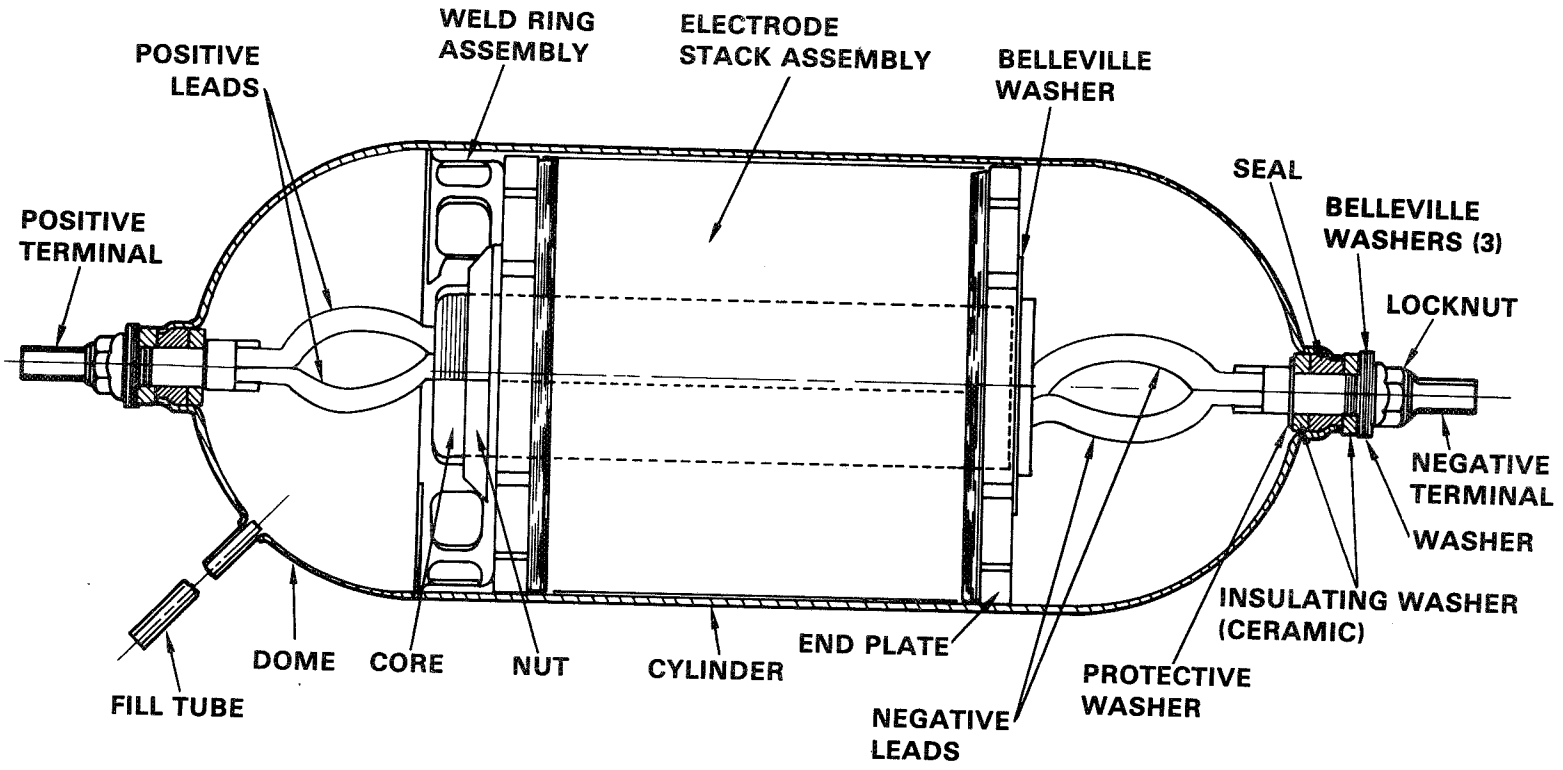

Figure 1. 50 Ampere-Hour Nickel-Hydrogen Cell

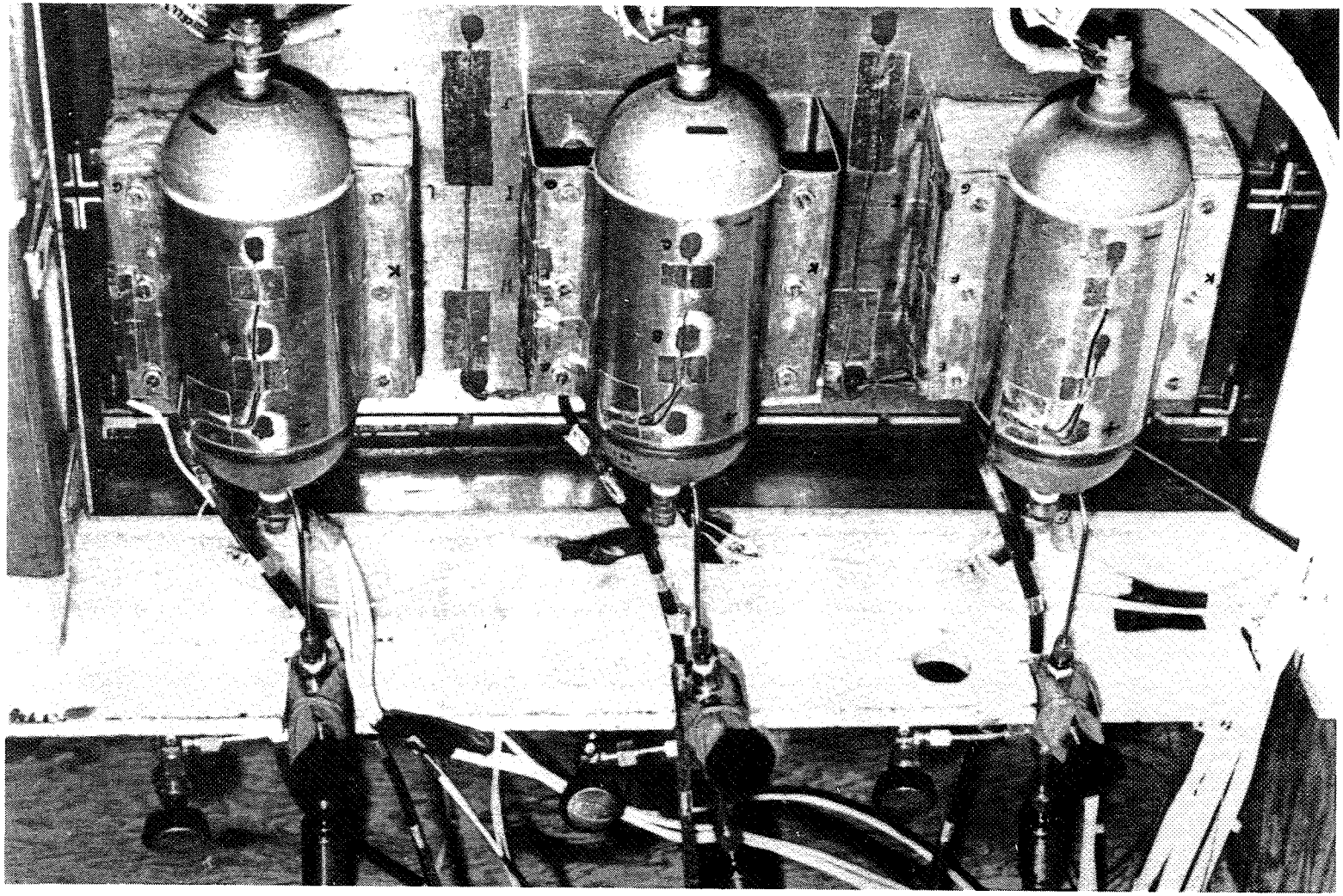

Figure 2. Nickel-Hydrogen Cells Mounted in Test Fixture

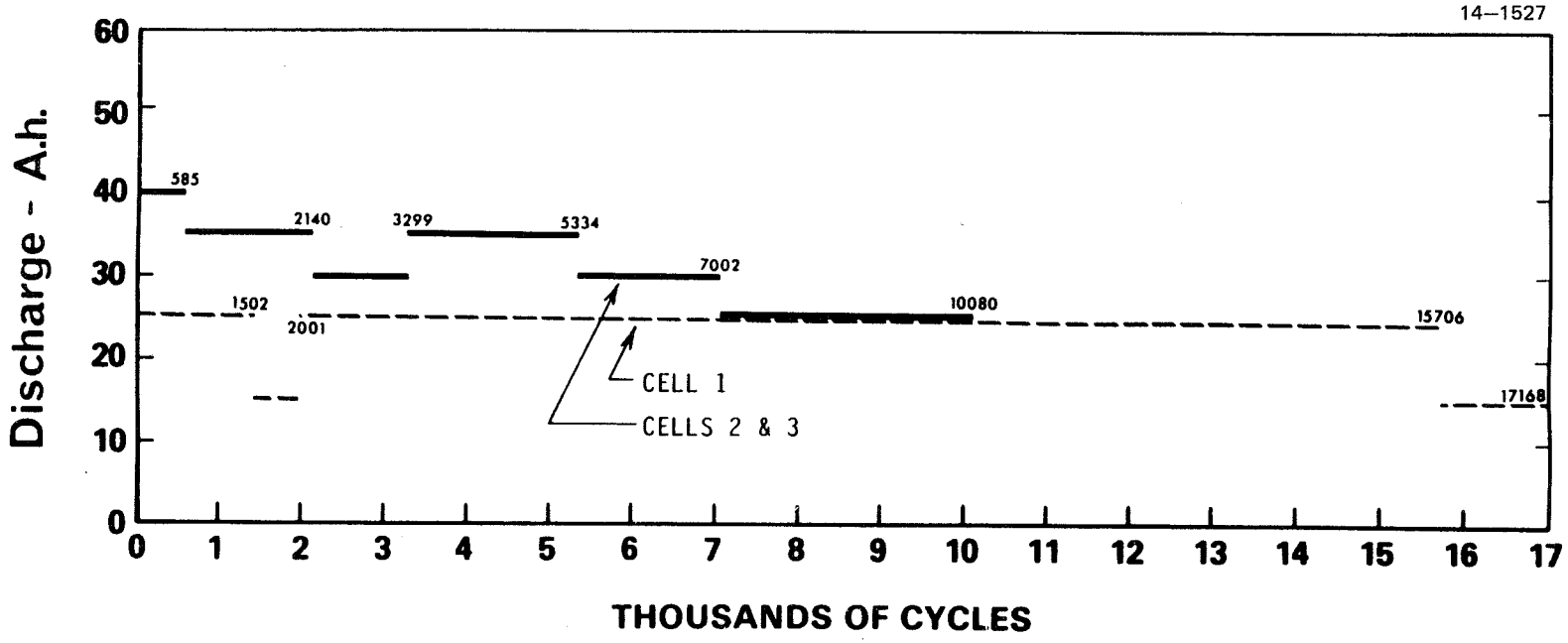

Figure 3. Discharge versus Cycles

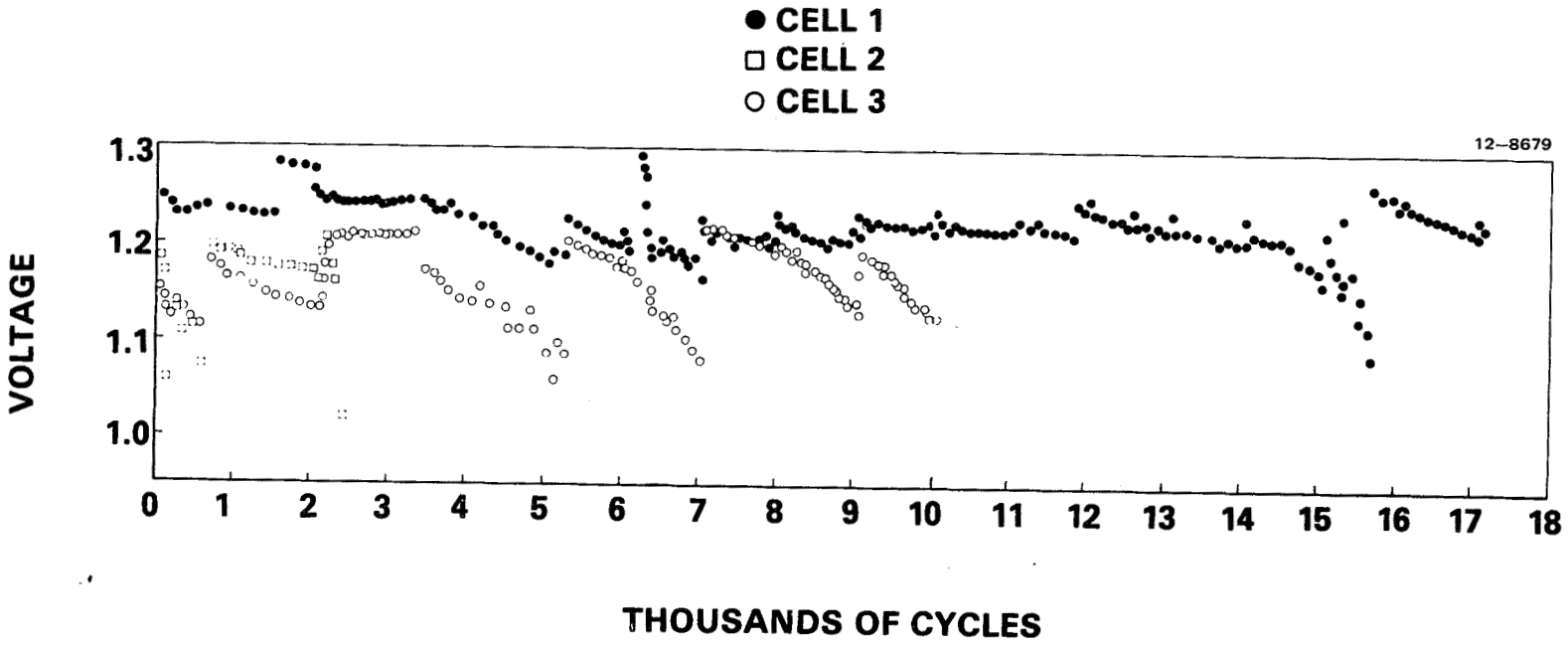

Figure 4. Cell End-of-Discharge Voltage versus Cycles

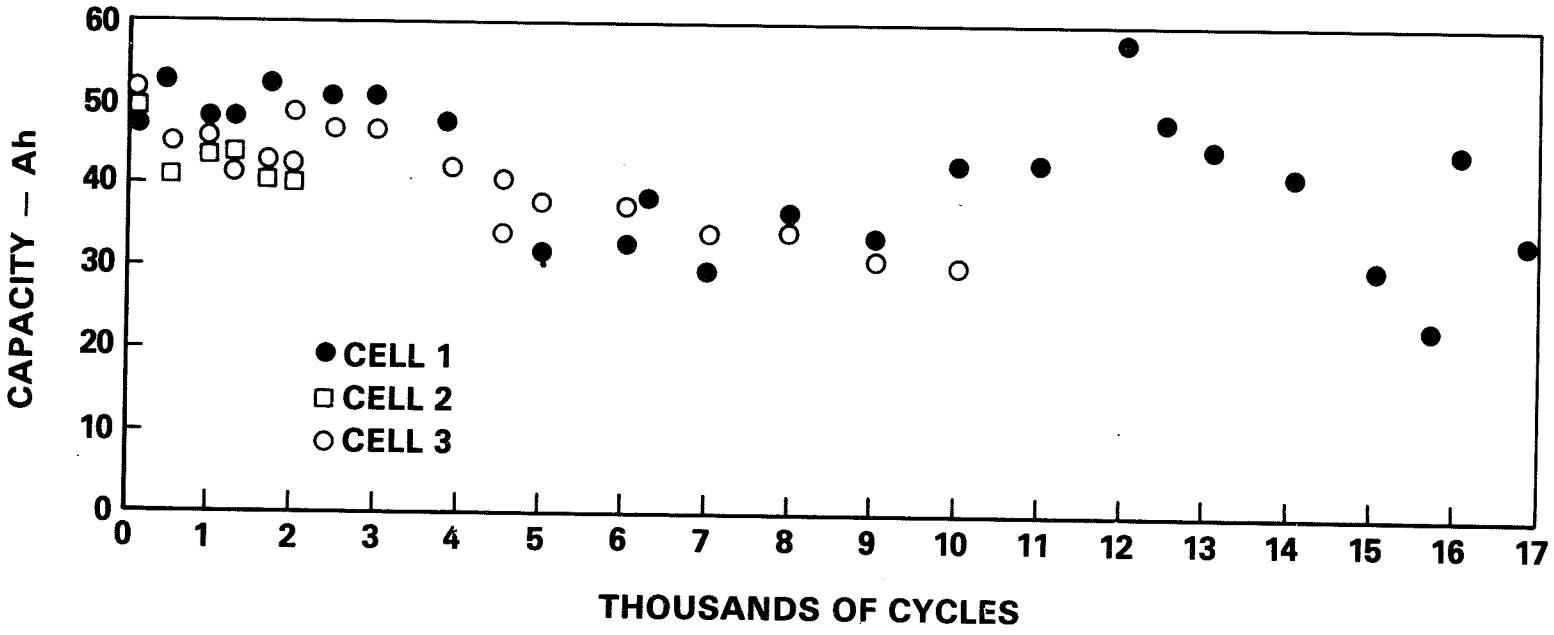

Figure 5. Cell Measured Capacity versus Cycles

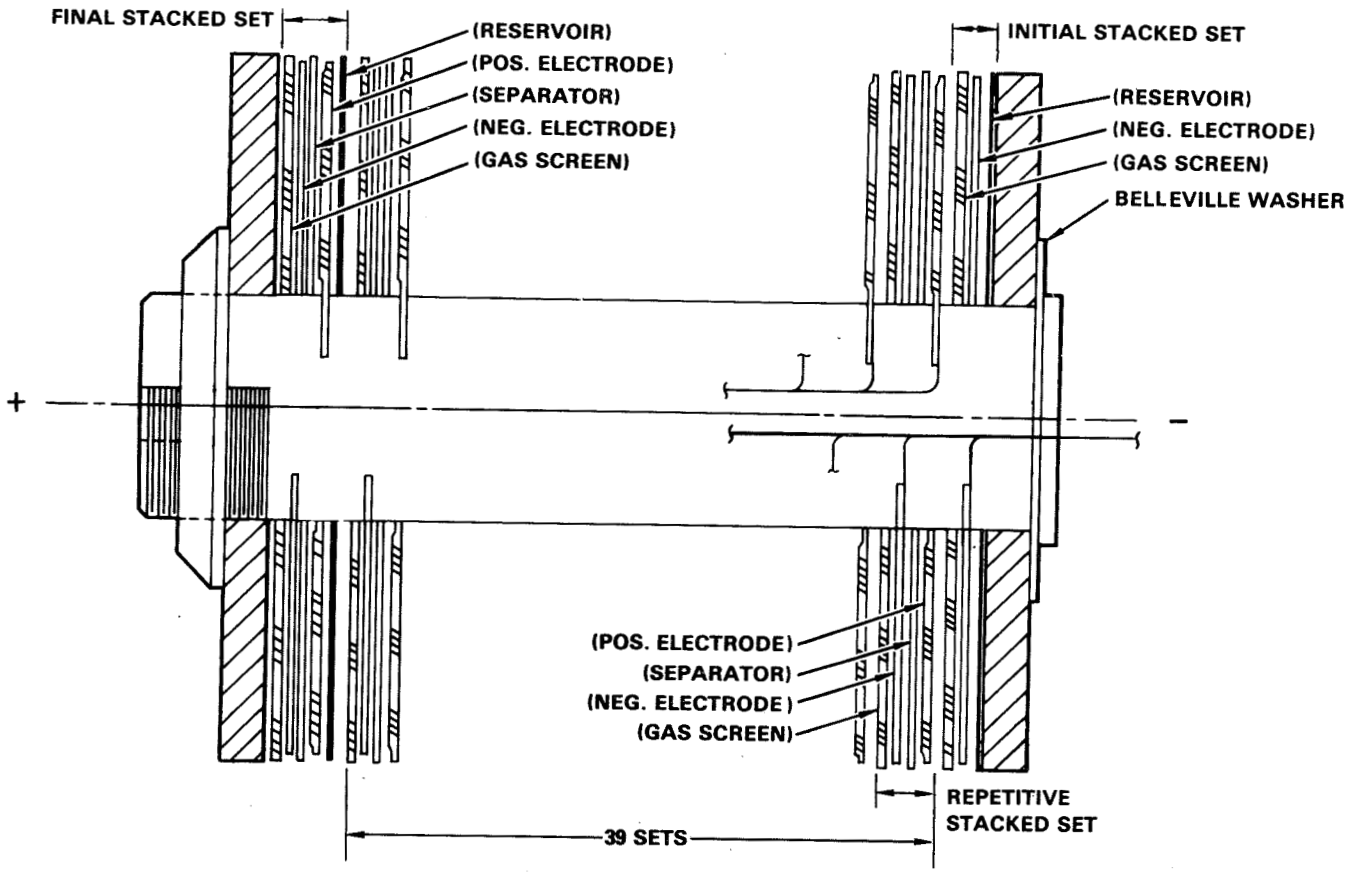

FIGURE 6

Figure 6. Electrode Stack Sketch

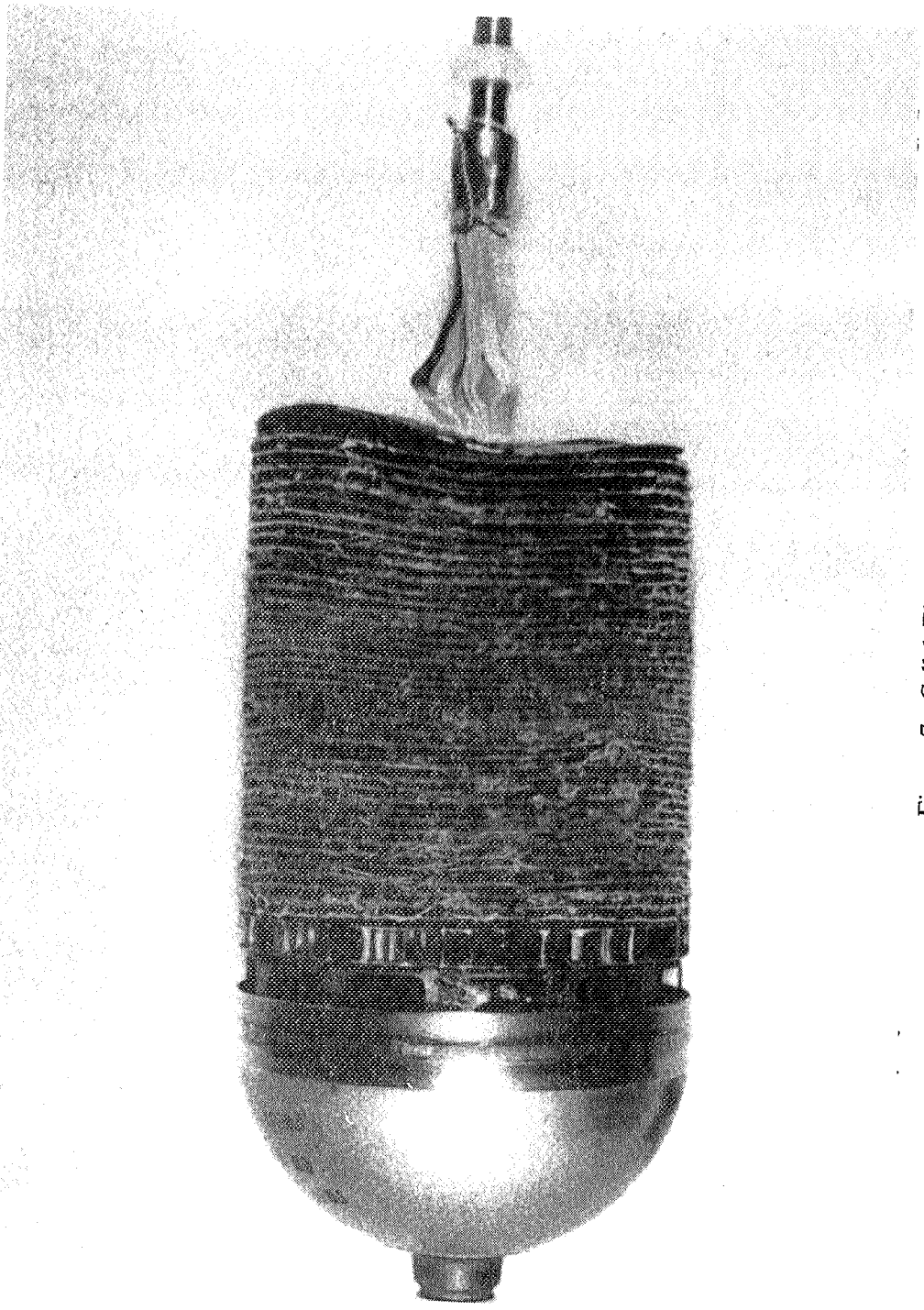

Figure 7. Cell 1 Electrode Stack Assembly

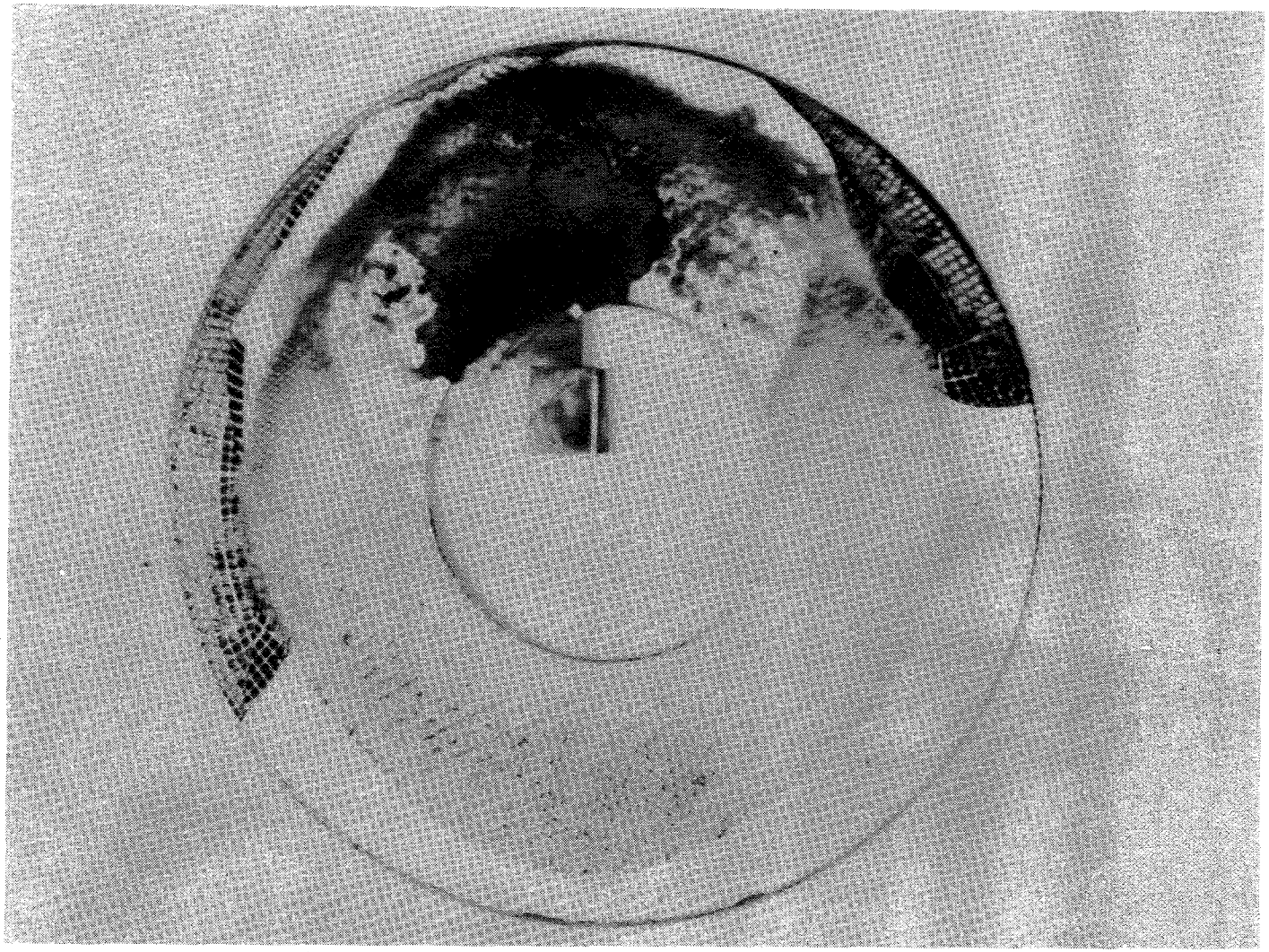

Figure 8. Cell 1 Negative Plate 35 and Gas Screen

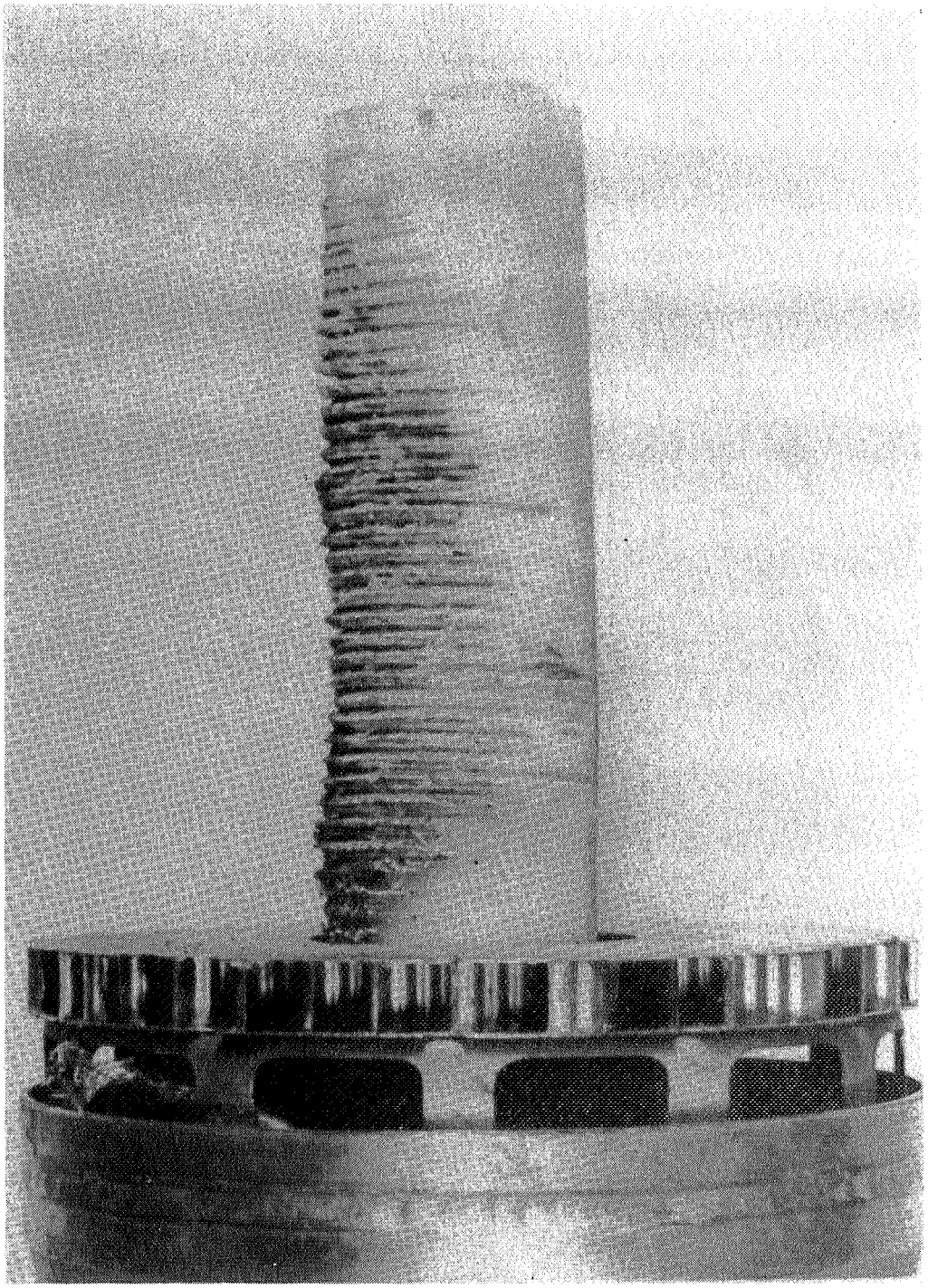

Figure 9. Cell 1 Polysulfone Core

THE FAILURE MECHANISM OF A NICKEL ELECTRODE IN A NICKEL-HYDROGEN CELL*

H.S. Lim and S.A. Verzwyvelt

Hughes Research Laboratories

ABSTRACT

Studies on a number of types of nickel electrodes after cycle failure in a Ni/H_2 cell showed that the failure is due to the loss of high rate discharge capability rather than an absolute capacity loss. The failure mechanism is speculated to be a combination of migration of the active material away from the current collecting nickel sinter, increased porosity of the active material caused by cycling, and an electrical isolation process of the active material during discharge.

INTRODUCTION

Nickel-hydrogen cells are used for spacecraft energy storage systems which require a long cycle life and low weight batteries. The useful weight and cycle life of the cell are closely related to each other. When the depth-of-discharge (DOD) of the cell operation is increased, the effective cell weight is decreased in an inversely proportional manner; however, the cycle life will also decrease. The cycle life and the weight of a Ni/H_2 cell can be exchanged for a lighter weight if necessary.

Nickel electrodes have been recognized as key life-limiting components of the Ni/H_2 cell. Therefore, understanding the failure mechanism of the nickel electrode is of paramount importance for understanding the limitations of the Ni/H_2 cell and for further improvements of the cell.

NICKEL ELECTRODE TYPES AND TEST CELLS

All electrodes used in this study were sinter type of various designs. The details of electrode types and test cells have been described elsewhere (Ref. 1-3), except for those electrodes used for BET surface area and the sinter damage studies. The electrode samples for these studies were typical flight quality nickel electrodes for Ni/H_2 cells of the standard Hughes/USAF design. These electrodes were evaluated before and after a 6400 cycle life test at 80% DOD in a Ni/H_2 cell.

CHANGES OF ELECTRODE CAPACITY AND RATE DEPENDENCE DURING CYCLE LIFE TEST

The change in nickel electrode capacity by cycling is shown in Figure 1 in terms of the active material utilization. The utilization is defined as

*This work was partially supported by NASA-Lewis Research Center under Contract No. NAS 3-22238 (Contract Manager, John Smithrick).

the ratio of the measured capacity to the theoretical capacity which represents the total amount of the active material in the electrode. The capacity or utilization decreased gradually as the electrode was cycled. Capacities of a Ni/H_2 cell before and after a 12960 cycle test are shown in Figure 2 as a function of discharge rates. The capacity of the cell was limited by the nickel electrodes.

The capacity depended on the discharge rate showing decreased capacity at an increased rate. The average difference in the initial capacities of 19 cells between the discharge rates of 2.74C and 0.5C was 3.3%. After the cycle life test this dependence increased markedly, in addition to the overall capacity decrease, as shown in Figure 2. The cell capacity decreased sharply as the discharge rate increased. The average capacity at the discharge rate of 2.74C was 19% less than at the 0.5C rate. At a very low discharge rate (C/10 rate) the cell capacity after the cycle test approached its initial value, indicating that the absolute cell capacity did not decrease significantly. These results also indicate that the cycling failure of a Ni/H_2 cell is due to this loss of high rate discharge capability in nickel electrodes rather than an absolute loss of the electrode capacity. In summary, these results indicate that the electrode degradation involves a gradual loss of the high rate discharge capability as the electrode is aged by cycling.

CHANGES OF NICKEL ELECTRODES AFTER CYCLE LIFE TESTS

Many changes of nickel electrodes have been observed after a cycle life test of various Ni/H_2 cells. These changes include dimensional (thickness) expansion, rupture of sinter structure, loose black powder formation, increase of BET surface area, change of pore distribution, increase of pore volume, and active material migration as described below.

The thickness of the electrode expands as the electrode is cycled. The degree and the rate of the expansion depend strongly on the level of the active material loading in the electrode, as shown in Figure 3. This electrode expansion often accompanies the rupture of the substrate sinter structure, as shown in Figure 4. Loose black powder of the active material was observed on the surface of nickel electrodes and other cell components adjacent to the electrode in cycled cells. The powder on the gas screen and back side of a hydrogen electrode from a cycled cell is shown in Figure 5.

The BET surface area of a nickel electrode increased after cycling. The increase of the surface area appears to be mainly in the pore range of 50 to 100 Å, as shown in Figure 6. Direct measurements of the pore distribution using a mercury intrusion porosimetry also showed a large increase of pores in the same pore radius range, as shown in Figure 7. These increases in pore volume and surface area indicate that the active material expands with the formation of additional pores in the range of 50 to 100 Å as the electrode is cycled.

The expansion of active material inside the porous sinter structure inevitably leads to active material migration, as shown in Figures 8 and 9. The light dots and the large circular area in the picture are nickel sinter

and nickel wire mesh substrate, respectively. The grey area represents the active material. New electrodes have a relatively uniform pore structure of sinter in which the active material is impregnated. Because of this uniformity, the active material in the new electrode is distributed more closely (roughly within 10 μm) to the current collecting nickel sinter particles. In cycled electrodes, however, the distritution of the active material is no longer uniform due to the migration of the active material. The change is readily noticeable, regardless of the active material loading level, sinter structure, or degree of the electrode expansion (Figures 8 and 9). All of the changes discussed above were apparently the result of irreversible active material expansion which occurred during cycling (Ref. 4). As the active material expanded inside the pores of the nickel sinter, a portion of the active material was extruded out of the pores to the outside of the sinter or into void pockets of the sinter. This extrusion appeared to occur without sinter damage in a large pore (16 μm) sinter such as 2540 type plaque (Ref. 1). However, when there was an insufficient amount of void volume (e.g., in heavily loaded electrodes) and the extrusion was restricted by small pores of the plaque, the active material expansion fractured the sinter structure, often into layers along the plane of the electrode, as shown in Figures 4 and 8. Regardless of whether the sinter was ruptured or not, the extrusion of the active material resulted in a migration in which a significant portion of the active material moved away from the vicinity of the current collecting sinter.

FAILURE MECHANISM OF NICKEL ELECTRODES

Although several physical changes have been observed, as discussed above, only two of these are apparently related to the failure of the nickel electrode at the high rate cycling of a low earth orbit regime. These two are the active material migration away from the current collecting nickel sinter particles and the density reduction of active material by the increase of the pore volume in the pore radius range of 50 to 100 Å.

Other changes such as the dimensional expansion and the rupture of the sinter structure were not observed with every failed electrode, indicating that these changes are not a necessary condition of the failure. In addition, some failed electrodes with severe expansion and sinter rupture cycled much longer than those without such changes. The formation of black powder in varying degrees, was observed in all failed electrodes. However, the amount of the black powder material was estimated to be fairly minor portion of the active material. In addition, the capacities of some failed electrodes were close to the initial capacity when measured at a very low discharge rate (Figure 2), indicating that the capacity loss due to the black powdering is relatively small. An increase of the BET surface area was also observed with all the failed electrodes. However, the magnitude of the increase varied depending on the number of cycles to the failure, lacking a consistent value for the failure.

The active material migration away from the current collector and the pore volume increase (density reduction) of the active material were observed with every failed electrode. It appears that the failure mechanism has to be

closely related to these two changes. An explanation of the capacity decrease at the high rate discharge has been speculated to be a combination of an electrical isolation mechanism of charged active material during discharge (Ref. 5-7) and the presently observed migration and density reduction of the active material. The mechanism of the charge propagation through the active material may be complex (Ref. 6-7), especially in view of the porous nature of the active material. For example, no information is available on the polarization of electrolyte in the micropores of the active material and the tortuosity of the pore structure. However, a rough model is offered below to explain the capacity reduction, assuming that the polarization of the electrolyte in the micropores is not the major factor in the propagation of the discharge reaction.

In a new electrode the active material is relatively uniformly distributed in the vicinity (roughly within 10 μm) of the current collecting nickel sinter, as illustrated schematically in Figure 10(a) and 10(b). In an electrode cycled to failure, however, a significant portion of the active material has moved away from the sinter, as shown schematically in Figure 10(c) and 10(d). When a new electrode is charged and discharged the active material is more or less fully and uniformly utilized. In a cycled electrode, as shown in Figure 10(c) and 10(d), however, the active material is expected to be fully charged, but a portion of the active material may not be fully discharged (Figure 10(d)). This is because the active material in the charge state is a good conductor (Ref. 8) while the one in the discharged state is a poor conductor (Ref. 6). The active material in the vicinity of the current collector may be discharged before the portion away from the current collector has a chance to be fully discharged because of the potential drop accross the porous active material. When this occurs the undischarged active material will be electrically isolated from the current collector.

The electrical isolation process of the charged active material is expected to depend on the discharge rate. The anticipated discharge rate effect of a microscopic area of the electrode (Figure 11) is illustrated in Figure 12. As the active material becomes more porous by cycling, the electrical isolation process will occur more readily becuase the overall conductivity of the material will be reduced progressively. Although we do not fully understand the pressure behavior of Ni/H_2 cells during cycle tests (Ref. 2), this overall scheme of the speculated failure mechanism of the nickel electrode appears to be consistent with the physical changes of the electrode after cycling.

REFERENCES

1. H.S. Lim and S.A. Verzwvelt, "Long Life Nickel Electrodes For a Nickel-Hydrogen Cell: III. Results of an Accelerated Test and Failure Analyses," Proc. 19th Intersociety Energy Conversion Engineering Conference, August 1984, p. 312.

2. H.S. Lim and S.A. Verzwyvelt, "Long Life Nickel Electrodes For a Nickel-Hydorgen Cell: Cycle Life Tests," Proc. 31st Power Sources Symposium, Cherry Hill, N.J. June, 1984.

3. H.S. Lim, S.A. Verzwyvelt, C. Bleser, and K.M. Keener, "Long Life Nickel Electrodes For a Nickel-Hydorgen Cell: I. Initial Performance," Proc. 18th Intersociety Energy Conversion Engineering Conference, August 1983, p. 1543.

4. H.S. Lim and S.A. Verzwvelt, "Expansion Mechanisms of the Nickel Electrode in an Alkaline Storage Cell: I. Electrode Bending Experiments," Proc. 15th Intersociety Energy Conversion Engineering Conference, Aug. 1980, p. 1619.

5. C.K. Dyer, "Chargeability of Ni Electrodes Studied by Optical Microscopy," The Nickel Electrode, ed. by R.G. Gunther and S. Gross (The Electrochemical Society, Pennington, N.J. 1982), Proceeding Vol. 82-4, p. 118.

6. R. Barnard, G.T. Crickmore, J.A. Lee and F.L. Tye, J. Appl. Electrochem., 10, 61 (1980).

7. R. Barnard, C.F. Randell and F.L. Tye, J. Appl. Electrochem., 10, 109 (1980).

8. D. Tuomi and G.J.B. Crawford, J. Electrochem. Soc., 115, 450 (1968).

FIGURE CAPTIONS

1. Active material utilization of various nickel electrodes as a function of number of cycles. Electrode types: A; 8740M, B; 8770M, C; 8755M, D; 5540M, E; 5555M, and F; 5570M. The utilization was measured by discharging Ni/H_2 cells to 1.0 V at 1.37C rate after charging for 80 min. at C rate.

2. Capacities of a Ni/H_2 cell (BP13 of Ref 1) at various discharge rates before and after a cycle life test.

3. Nickel electrode expansion as a function of the number of 80% depth-of-discharge cycles. Active material loading level of the electrode is indicated by various symbols.

4. Cross sectional view of nickel sinter substrate of a new nickel electrode (A) and a similar electrode after 6400 cycles. The samples were prepared after the active material was dissolved out.

5. Photograph of the gas screen and back side of the hydrogen electrode from a cycled Ni/H_2 cell.

6. Change of BET surface area of a nickel electrode by cycling.

7. Cumulative pore volume distribution of various new and cycled nickel electrodes by a mercury intrusion porosimetry.

8. SEM cross sectional view of new (A) and cycled (B) (12,960 cycles) nickel electrodes (8740M) with 1.52 g/cc void of active material loading.

9. SEM cross sectional view of new (A and C) and cycled (B: 2330 cycles and D: 2340 cycles) nickel electrodes of various types. (A) and (B): 2540L type; 1.37 g/cc void loading. (C) and (D): 2540H type; 1.64 g/cc void loading.

10. A schematic illustration of nickel electrode capacity decrease.

11. A schematic representation of a microscopic portion of a nickel electrode.

12. A schematic illustration of discharge rate dependence of electrode capacity.

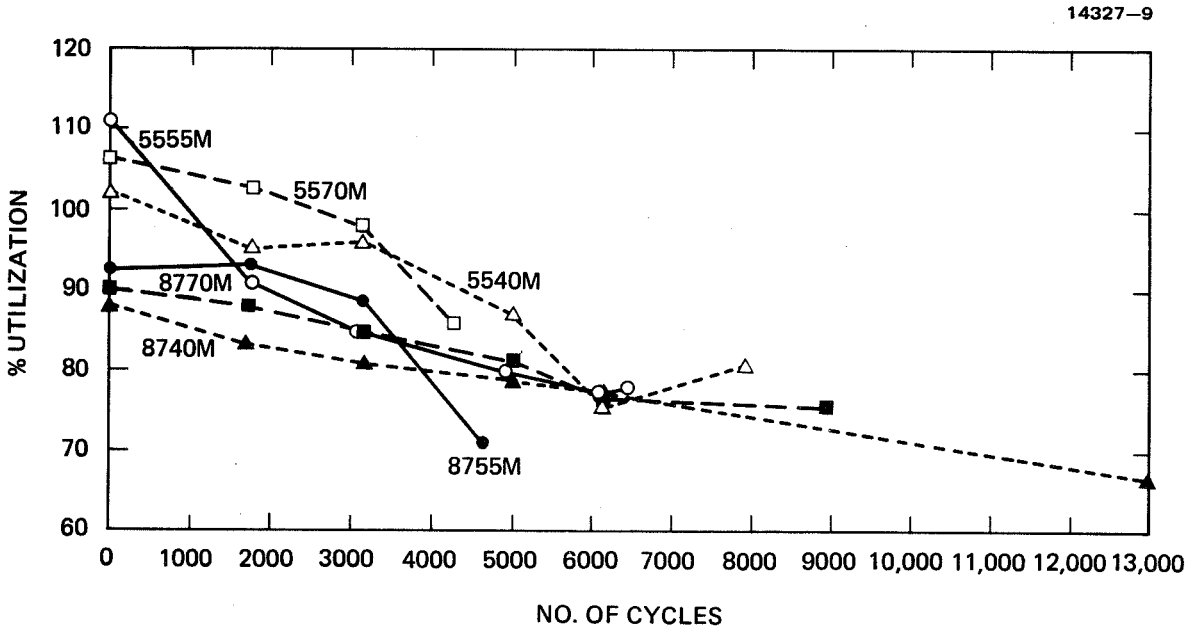

Figure 1. Active material utilization of various nickel electrodes as a function of number of cycles. Electrode types: A, 8740M; B, 8770M; C, 8755M; D, 5540M; E, 5555M; and F, 5570M. The utilization was measured by discharging Ni/H_2 cells to 1.0V at 1.37C rate after charging for 80 min. at C rate.

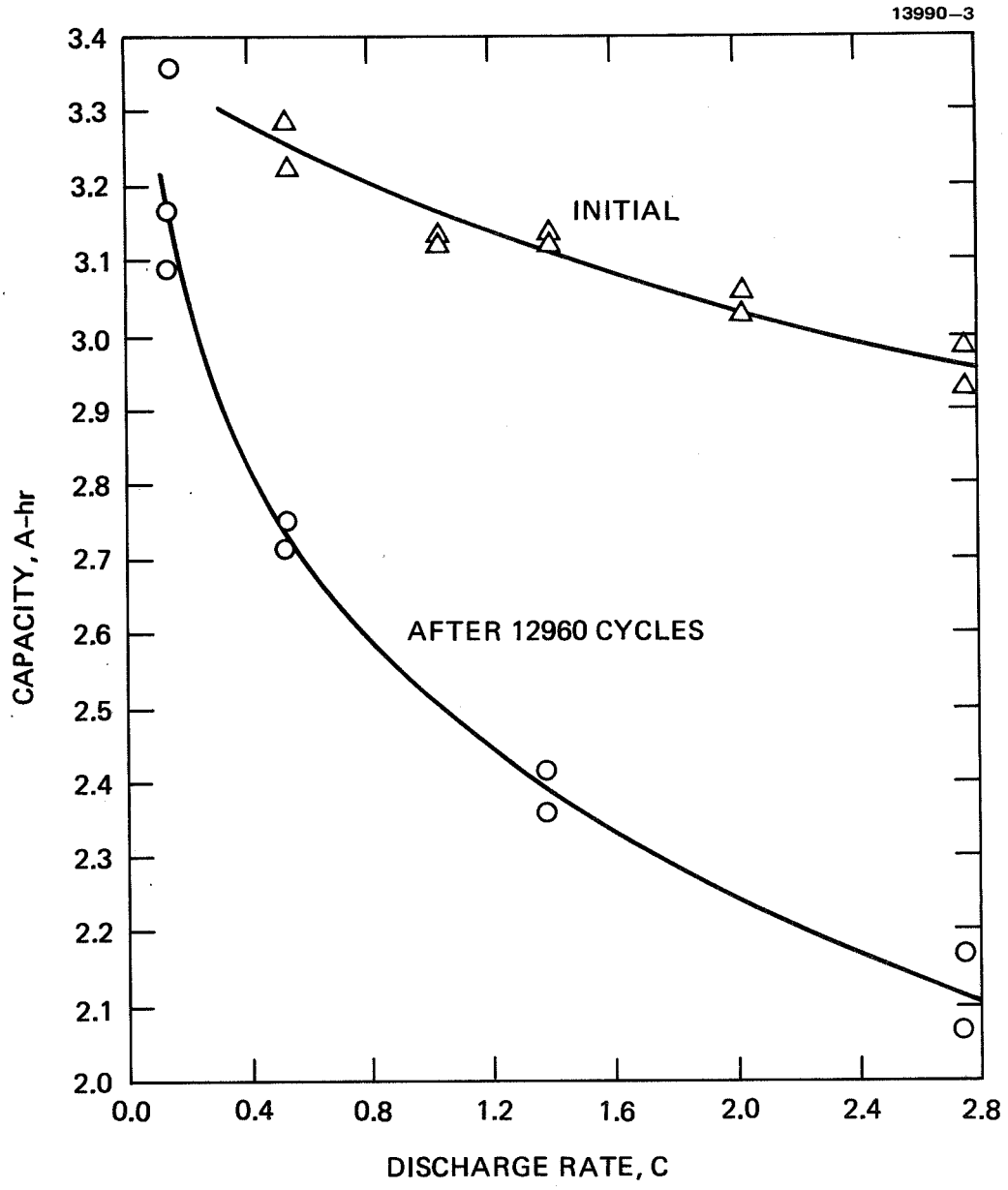

Figure 2. Capacities of a Ni/H_2 cell (BP13 of Ref. 1) at various discharge rates before and after a cycle life test.

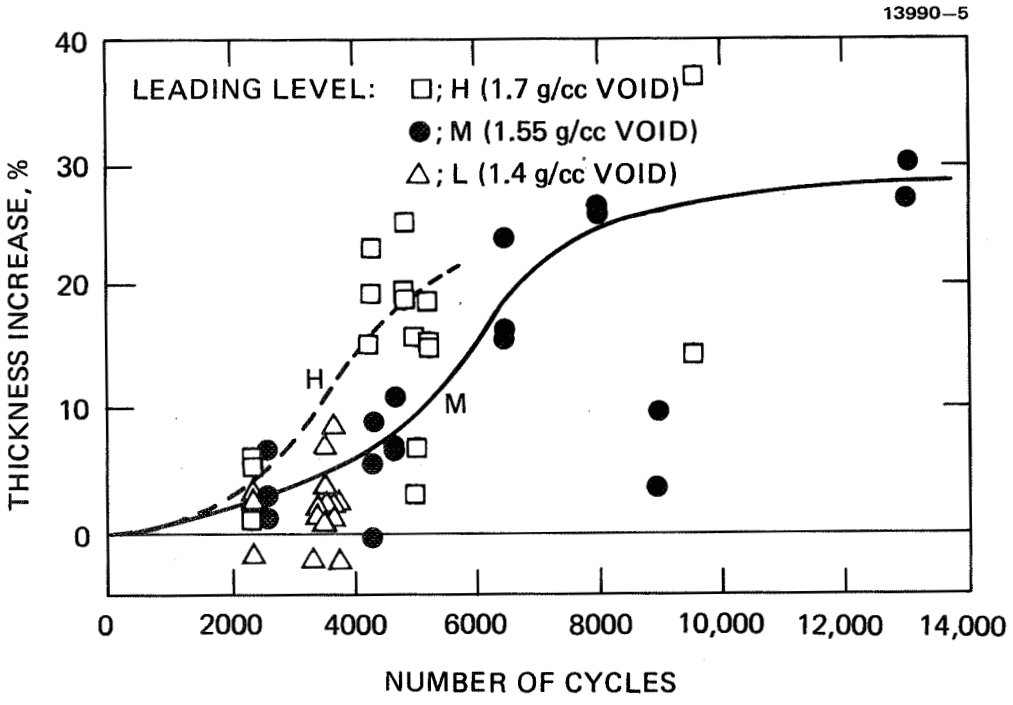

Figure 3. Nickel electrode expansion as a function of the number of 80% depth-of-discharge cycles. Active material loading level of the electrode is indicated by various symbols.

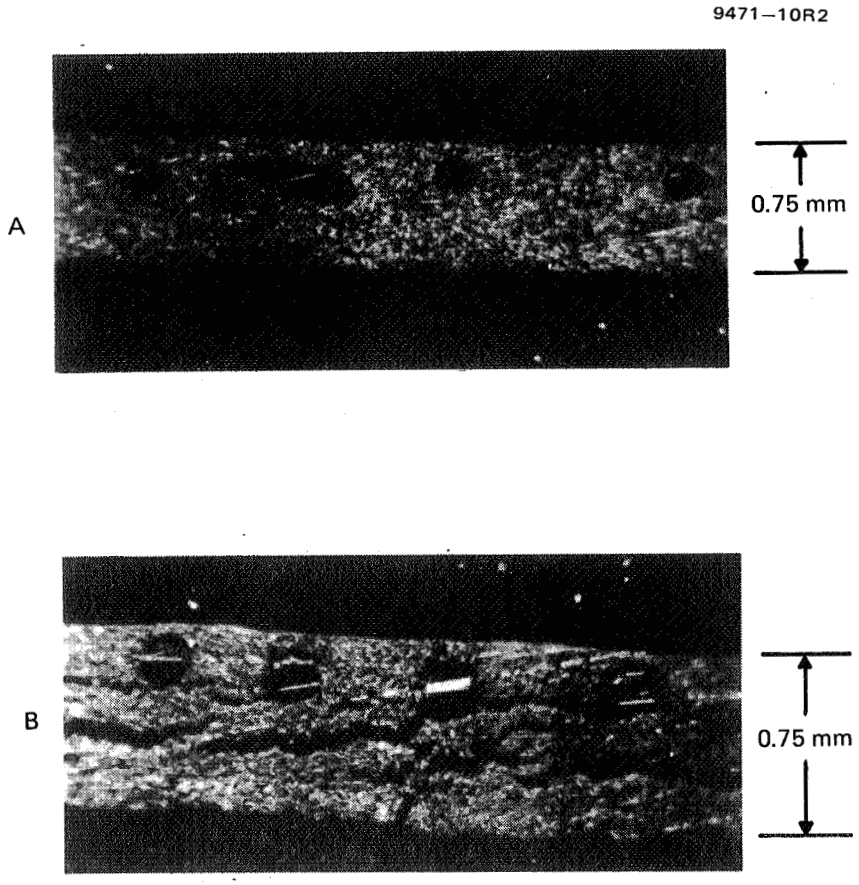

Figure 4. Cross sectional view of nickel sinter substrate of a new nickel electrode (A) and a similar electrode after 6400 cycles. The samples were prepared after the active material was dissolved out.

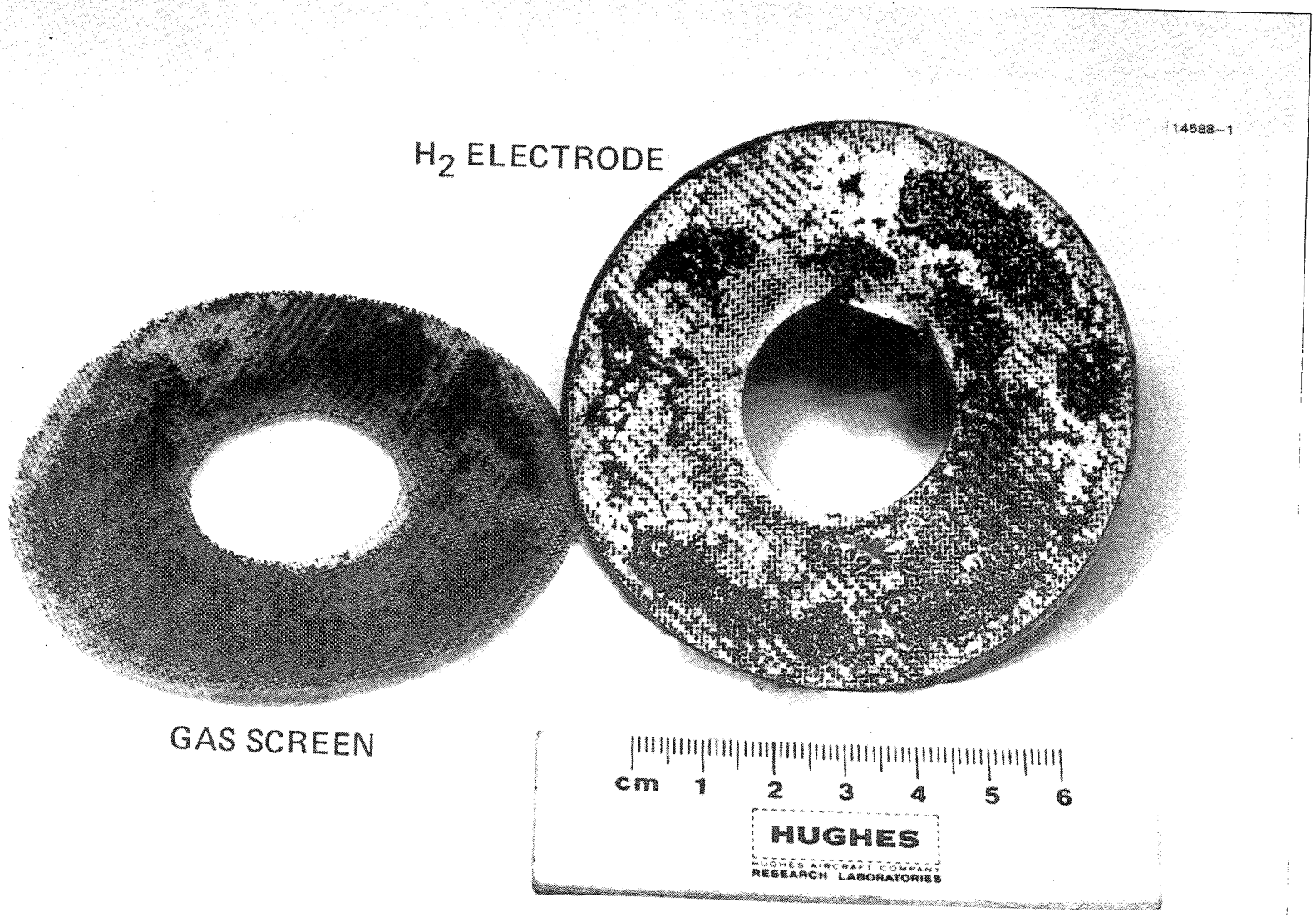

Figure 5. Photograph of the gas screen and back side of the hydrogen electrode from a cycled Ni/H_2 cell.

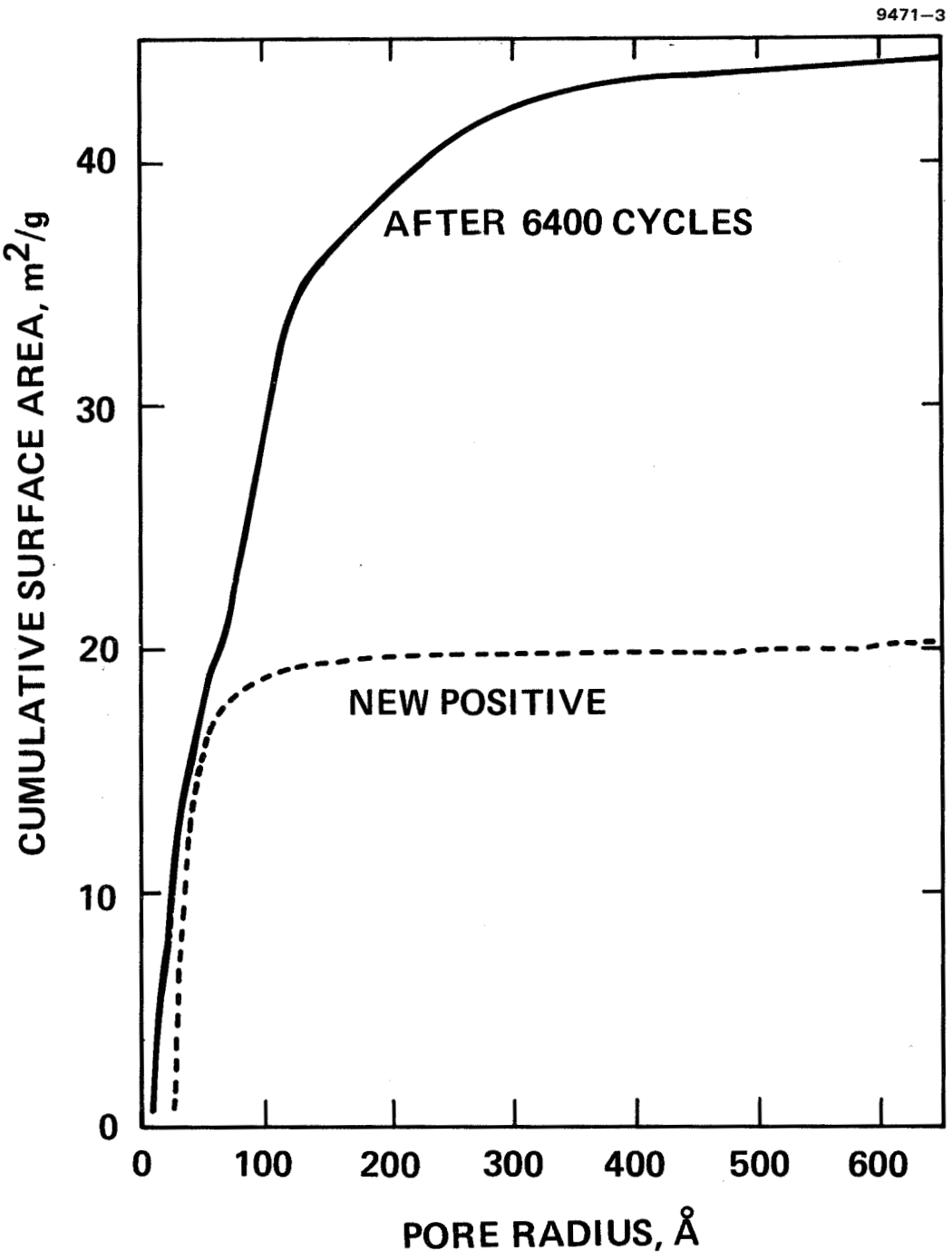

Figure 6. Change of BET surface area of a nickel electrode by cycling.

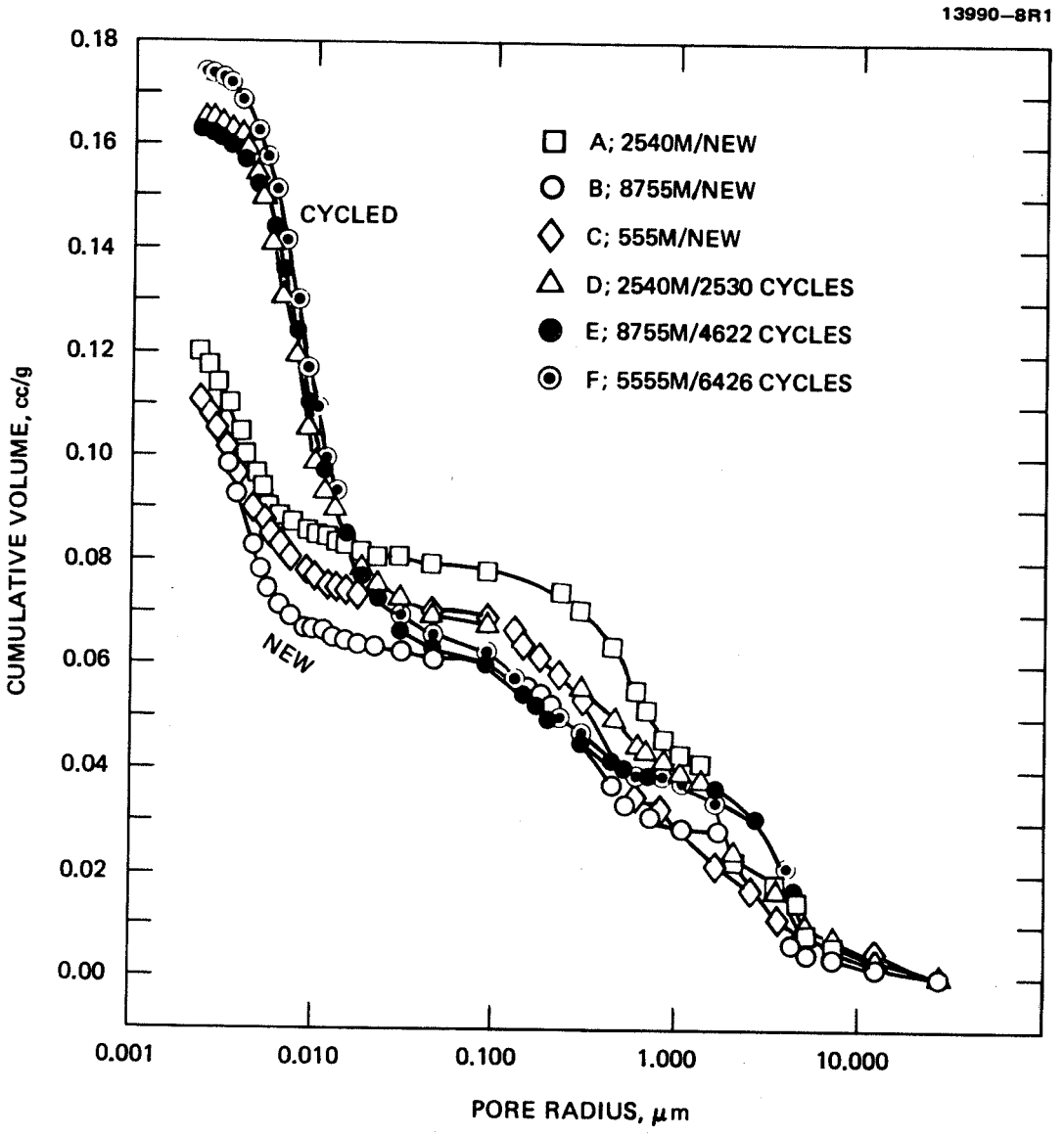

Figure 7. Cumulative pore volume distribution of various new and cycled nickel electrodes by a mercury intrusion porosimetry.

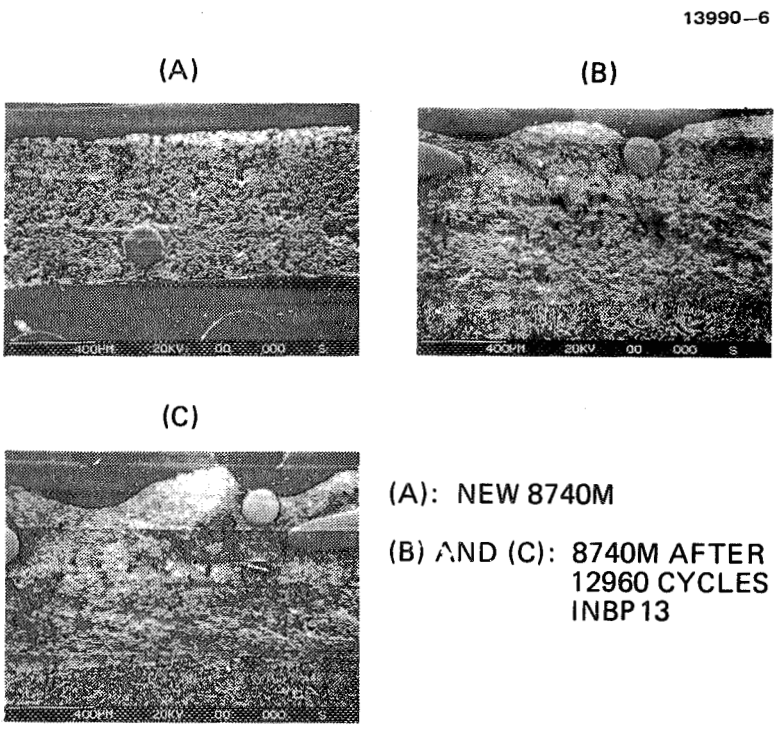

Figure 8. SEM cross sectional view of new (A) and cycled (B) (12,960 cycles) nickel electrodes (8740M) with 1.52 g/cc void of active material loading.

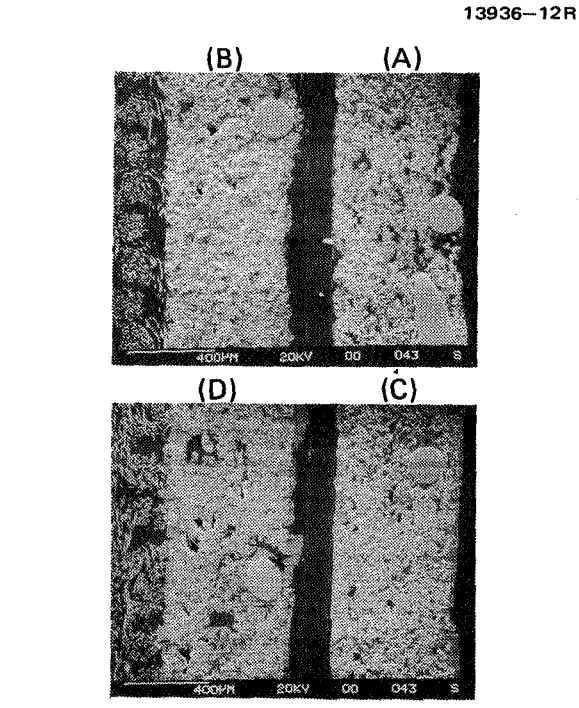

Figure 9. SEM cross sectional view of new (A and C) and cycled (B: 2330 cycles and D: 2340 cycles) nickel electrodes of various types. (A) and (B): 2540L type; 1.37 g/cc void loading. (C) and (D): 2540H type; 1.64 g/cc void loading.

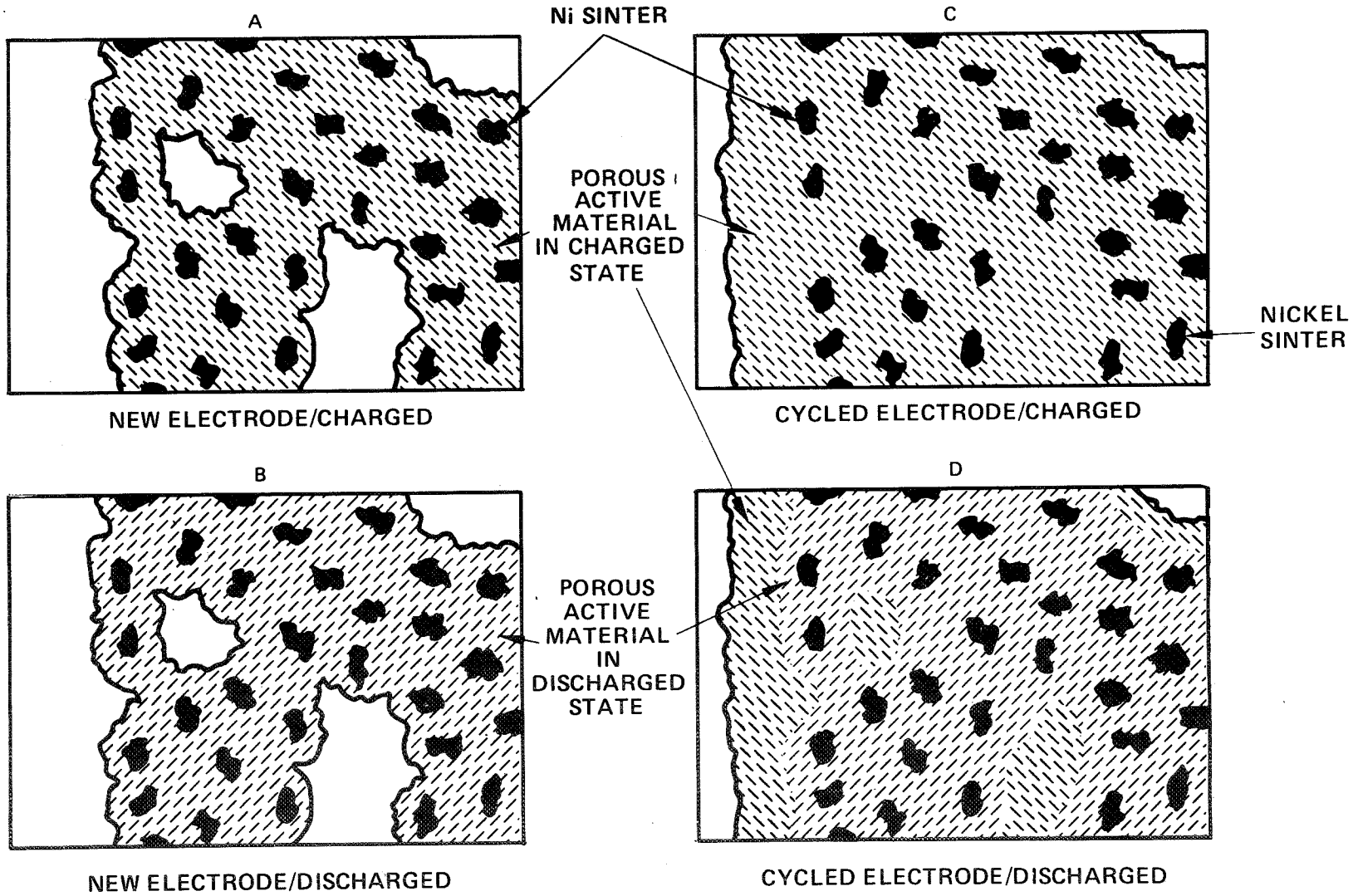

Figure 10. A schematic illustration of nickel electrode capacity decrease.

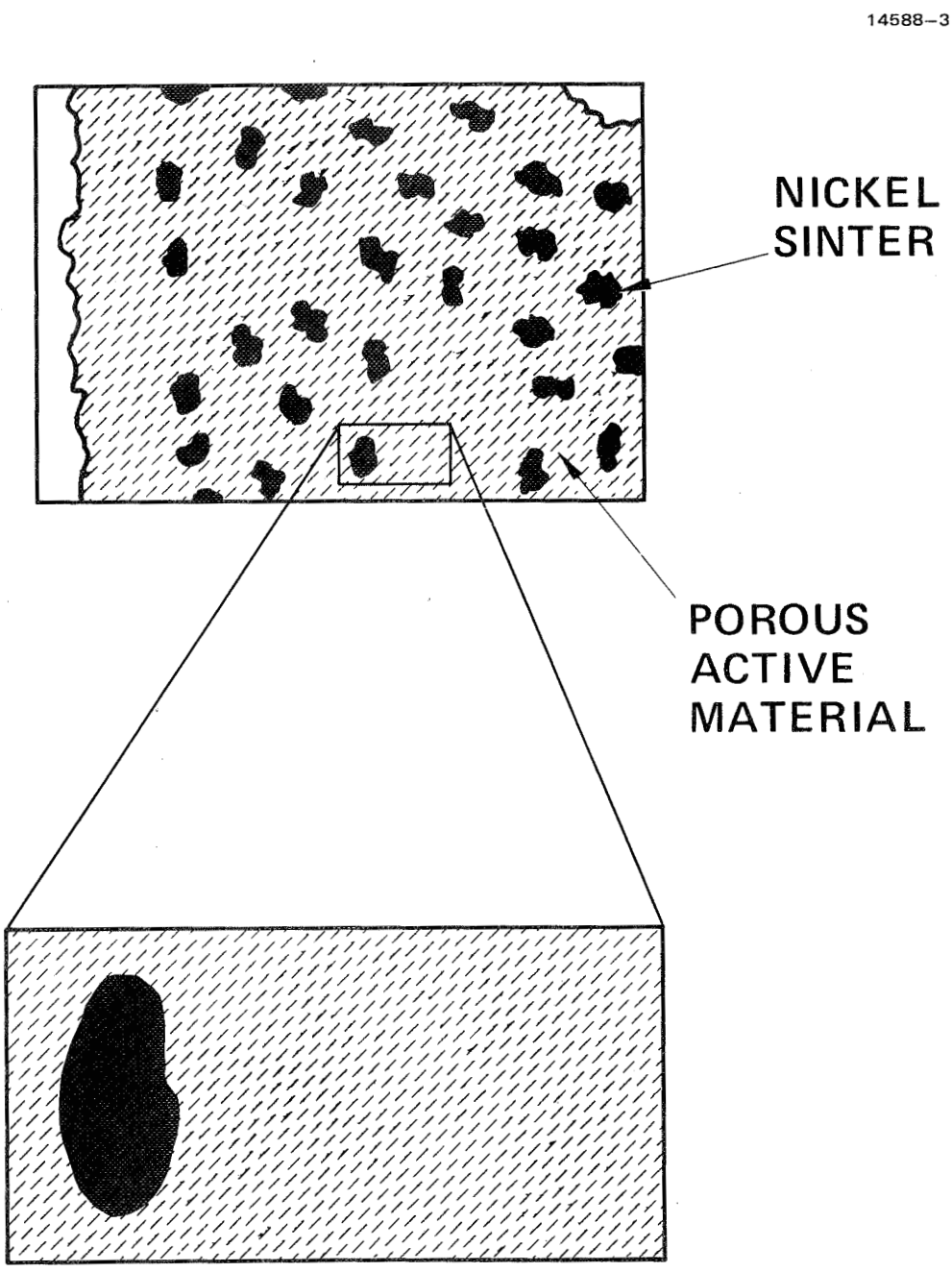

Figure 11. A schematic representation of a microscopic portion of a nickel electrode.

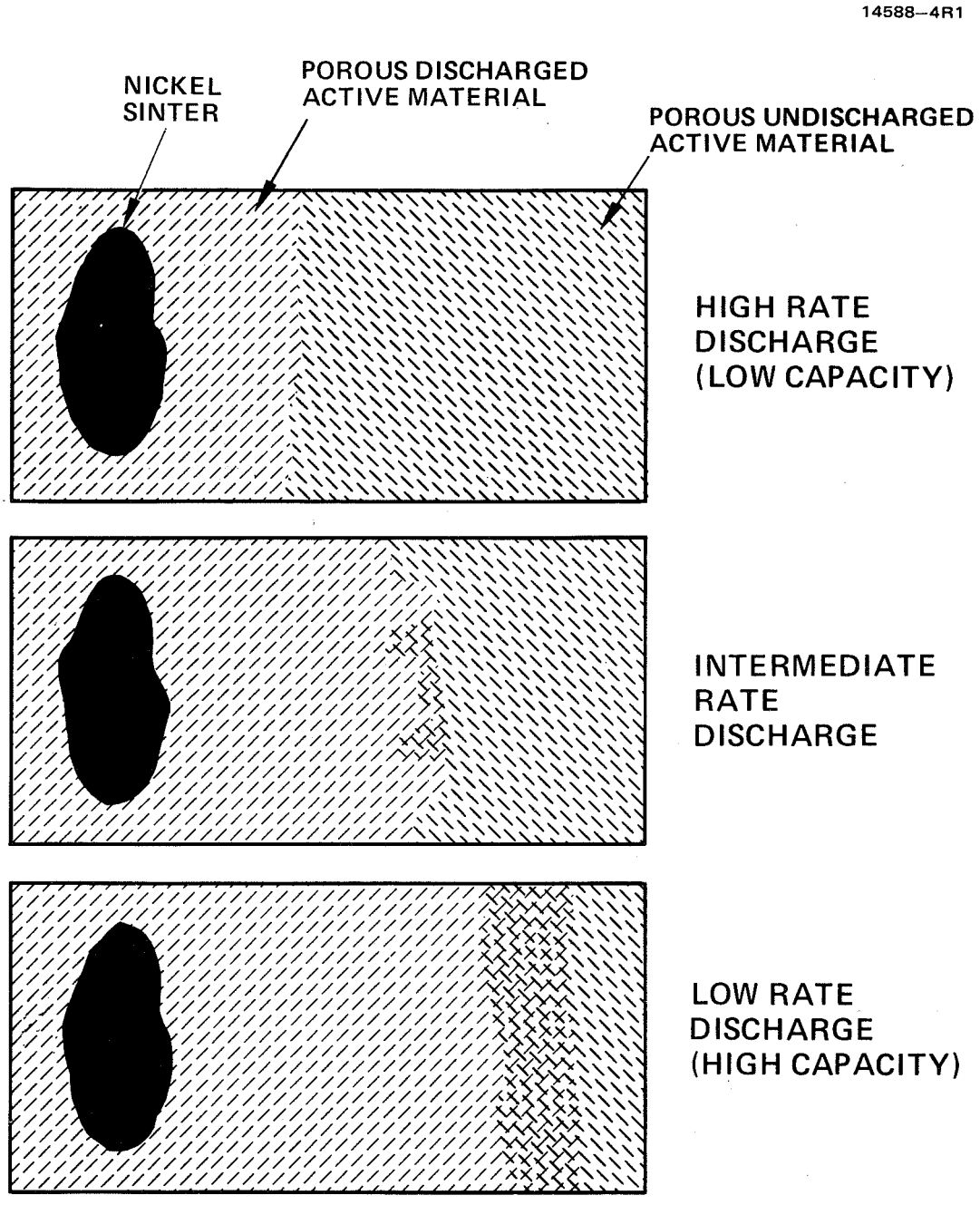

Figure 12. A schematic illustration of discharge rate dependence of electrode capacity.

AN INDUSTRY AND GOVERNMENT SURVEY: A NICKEL-HYDROGEN TESTING DATA BASE

Charles Badcock and Martin Milden
The Aerospace Corporation

ABSTRACT

The government and industry were surveyed to determine the level of testing of nickel hydrogen (NiH_2) battery cells and to evaluate the demonstrable capabilities of tne couple. Only flight-type cells undergoing ground test were incorporated in the data base, no boilerplate cells or flight batteries were included. Both USAF design and COMSAT design cells as well as a few cells produced by SAFT were listed. The USAF design is in test in both high and low earth orbit simulations, whereas the COMSAT design, intended specifically for high orbit applications, is being tested predominantly in high orbits. The data from over 400 cells show that the reliability and capability of both designs for high orbit applications are reasonably established out to ten years in geosynchronous orbit and to approximately 3000 cycles in other high orbit applications. However, the data base is weak and incomplete for applications of the USAF cell in low earth orbit. This probably arises because of the harsh testing environment to which these cells have been subjected as well as various minor design questions that were not resolved when these cells began testing. It must also be pointed out that most of the testing data base is constructed from cells that were developmental in design or manufacture (all cells purchased for a test are used, even if performance is questionable) as contrasted to a flight program where it can be assumed that many of the failures listed would have been rejected prior to either life test or to use in a flight battery.

INTRODUCTION

A survey of the testing data base for nickel-hydrogen (NiH_2) battery cells has been performed. The objective of this survey was to evaluate the status of testing of cells in general and of the Air Force design nickel-hydrogen cell in particular. Sufficient detail was sought so that a critical evaluation of the test results and of cell performance could be made. Realizing that subtle differences in test conditions can result in large differences in cell performance, an effort was made to define the actual test environment as closely as possible. These data were obtained in the time period February to May 1984, and reflect the status of tests at that time. Periodic updates of the information are planned.

THE DATA BASE

Potential sources of test data in the United States and Canada were asked to provide results of testing of any and all NiH_2 cells. These sources were provided with a questionnaire that was either completed by the respondent or by the interviewer from data received by telephone. These inputs were supplemented by reviewing IR&D reports and reports in Proceedings of the IECEC and the GSFC Battery Workshop. COMSAT Laboratories testing is not included in this report. This omission results in the loss of a significant portion of the COMSAT design NiH_2 cell data base.

In this survey the term USAF design applies to cells with annular electrodes, leads placed on the inner perimeter of the electrodes, and generally, a recirculating stack. Electrolyte has a net flow within the recirculating stack, wherein the negative and positive plates alternate in the plate pack so that the gas screen separates the rear of the positive and negative plates. The front faces of the plates are separated by asbestos or zirconia fabric (Zircar) separators. The gas screen provides for delivery of hydrogen gas and for transport of oxygen gas during overcharge, directly across the screen from the adjoining positive to the catalytic negative. The COMSAT design indicates cells with circular electrodes with chords removed for leads on the outer perimeter and a back-to-back plate pack design. In this design two positives are placed back-to back, separated by asbestos from negatives that are also back-to-back wih a gas screen separating them; during overcharge oxygen escapes from the positives along the plate pack edge to the backs and sides of the negative. This design does not produce a net electrolyte flow. Th COMSAT cell was designed for high orbit use and is not a high rate, high cycle frequency cell. The USAF cell was originally designed for high rate, high cycle frequency, low earth orbit (LEO) use however, it can be used in any less stressful orbit.

The data obtained relate to some 412 cells from several generations of both COMSAT and AF designs. Thus, some of the longest tests and most impressive data are from cells of earlier designs. Differences in designs are, for the most part, evolutionary in nature: changes in seals, improvements in positive electrodes, and minor changes in construction are typical. From a performance standpoint the most significant change in cell design in this data base was the introduction of the wall wick for electrolyte management in the USAF design. The earliest test data are for cells without this feature. All cells manufactured in the U.S. included in this survey utilize electrochemically impregnated positive plates. Ten Saft cells manufactured in France and included in the COMSAT grouping may utilize chemically impregnated positives and a different separator system than the asbestos used universally in the COMSAT design.

The distribution of cells in test by design shows that at least 192 cells of the COMSAT design are either in test, in preparation for testing, or have been tested. All but four of these have been tested in some type of high orbit simulation. Of the 271 USAF cells tested, in-test, or in preparation for testing, well over half have been subjected to, or are planned to be tested in simulated low earth orbit regimes. No "boiler plate" test data were included in the data base because of the questionable relevance of such data to flight type cell performance. Generally "boiler plate" data are applicable but instances of rework during test and variation in electrolyte quantity, pressure and plate-to-volume ratios compared to flight-type cells are sufficiently common that these data cannot readily be evaluated.

DISTRIBUTION OF FAILURES AND TESTING

Figures 1 through 4 present summaries of the data on the distribution of test durations and failures in bar graph form. The definition of failure is taken from the data reviewed. Most failures are defined as the inability of the cell to maintain a minimum of 1.0 V during discharge. Less than one-half of the failed cells shorted. The rest were low voltage failures without confirmed shorts. No cells were reported to have failed open circuit. If a test was terminated without cell failure, it is reported as a discontinued test.

Figure 1 summarizes all low earth orbit test experience for the USAF design cell. These data are skewed somewhat by 20 of 21 cells that have experienced over 8000 cycles and the 20 of 21 cells that exceed 10,000 cycles from the two ground test batteries of the Air Force Flight Experiment. These cells are of an older design (ca. 1975) and do not represent current state-of-the-art; they used back-to-back electrodes and had no wall wick. Only one cell in each group of 21 failed early. The remaining 20 cells are either continuing in test or were discontinued without additional failures. Removal of these Flight Experiment test batteries from the distribution results in the distribution shown in figure 2. The data for the USAF design in low earth orbit suggest that a significant difference in performance exists between cells tested predominantly at 80% depth of discharge (DOD) and those tested at less than that depth. There are insufficient data to make a finer distinction. The cross-hatched bars indicate cells tested at 80% depth of discharge in figures 1 and 2.

Figure 3 summarizes the experience for both USAF cell design in high orbit simulations. Figure 4 shows similar data for the COMSAT cell design except that the testing is all for simulated geostationary orbit conditions. Both accelerated and real time testing are combined in both of these figures. There is no apparent difference between 80% and lower depths of discharge in the performance under these conditions. Most failures, ten for the COMSAT design and one for the USAF design, can probably be attributed to workmanship or design defects that have since been corrected or would not have been included in a flight cell selection process.

DISCUSSION

The data available at this time suggest that both the USAF and COMSAT cell designs can be used in high orbit with high reliability. This assumes that the observed failures were for the most part manufacturing defects and activation problems that have been solved or would be screened out in a flight program. Certainly the number of cells that have survived at least 1000 cycles (ten year geostationary orbit) at up to 80% DOD is impressive at so early a point in the technology development cycle. Taking total numbers and including both high and low orbit testing for the USAF design, some 148 cells have been tested to 1000 or more cycles at DOD's greater than 50%; there have been seven failures prior to reaching 1000 cycles. A similar comparison for the COMSAT design shows that at least 65 cells have provided 1000 cycles or more with seven failures. The failures that have occurred must be considered to be from development lots of cells; the failures would be reduced or eliminated in an actual flight program. It must be pointed out that these data do not support use at 80% DOD because no contingency for acceptable degradation or system failures has been included. The ultimate capability of the cells from which power system designs can be derived is, however, demonstrated.

Low earth testing has not demonstrated the long life at the great depths of discharge that the USAF-design cell promises. Examining the data and coupling it with other information suggests that several elements may well serve to cause premature failure of cells. The streses in low earth orbit can be much greater, particularly at greater depths of discharge. First, recognizing that the nickel electrode is inherently the weakest component of the cell, steps must be taken to minimize the possible stresses. Second, designs and procedures that might prove satisfactory for high orbit use, but that may not permit cell performance to be maintained over the more than 25,000 cycles required for LEO must be scrutinized. Finally, the charge procedures (the discharge is largely dictated by mission considerations) and thermal environment must be adjusted to assure that these do not limit cell life. It is important to note that the capability of NiCd batteries to perform for more than 3 years at 20 to 25% DOD has been developed over the years by a better understanding of how the cells work, by improvements in cell components, and by fine tuning of cell designs. Similar attention to NiH_2 batteries could result in very significant improvements.

The positive electrode is subject to stresses due to charge-discharge cycling and especially to overcharge. These are caused by molecular volume changes between the various phases of charged and discharged material, by relaxation of these phases, by oxygen gas evolution, and by a host of design variables involved in the plate manufacturing process. Research and

development can certainly lead to more stress-resistant and efficient nickel electrodes. Similarly the stresses can be mitigated by minimizing overcharge, by limiting charging and discharging that cause high strain rates, and by keeping temperatures low so that electrode efficiency is maximized.

The design and production of NiH_2 cells is still evolving. Improvements in design such as those shown by MANTECH will continue to make the cells that are under test less than the state-of-the-art. Recent problems with asbestos separators in both cell designs and the historic problems with pinholing of the negative electrode in Zircar separated cells suggests that a better separator material is needed. The test data show that neither separator is superior in terms of life or performance. However, it may be that both separators are satisfactory and that activation or other handling procedures are deficient. The performance of some recently manufactured cells may be related to testing or specific manufacturing problems because other cells produced near the same time with similar materials have not shown similar anomalies. Careful review of past procedures and of any proposed changes must be made and acceptability demontrated by test.

The electrical environment must also be adjusted to minimize stress. Overcharge, particularly at high rate, must be avoided. Constant voltage charging does not appear to be an acceptable charge control procedure because the slope of the voltage vs capacity-returned curve is shallow in NiH_2 cells and the abrupt voltage rise near the end of charge characteristic of NiCd cells may not be reliable in NiH_2 cells. Tests have given good results using constant voltage charge; however, the variations in the charge return indicate that the better control of overcharge may be useful. The easiest way to minimize the quantity of overcharge required is to maintain the cells in a cool environment. By minimizing the thermal gradients in the cell and keeping the temperature low, the charge efficiency is maximized and the necessity for large charge return ratios is eliminated. Although it is enticing to treat NiH_2 batteries as "super" NiCd batteries, the cell is a different couple with unique charge control and environmental requirements.

CONCLUSIONS

The testing data collected from most North American sources indicates that the basis for use of NiH_2 cells in high orbits is firm. Results from over 227 cells have produced only 14 failures up to 1000 cycles. The failures are of the type that have either been corrected or would be screened out in a flight program. Recent flight experience appears to support this position.

The data base is very weak and insufficient for low orbit applications. Few cells have more than 8000 cycles (1.4 years in low orbit) before failure or test discontinuance. However, tests have generally been run under unrealistically harsh conditions of high depth of discharge, large charge return ratios, and temperatures near ambient. A particular problem is that the charge return ratios that have been used appear small until it is realized that even 105% charge return results in a large quantity of extra charge at high DOD's. In comparison, a typical NiCd run with 107% charge return at shallow DOD receives much smaller quantity of extra charge. It is such problems as these, coupled with minor design and procedural changes that may not have been beneficial, that lead to the lack of sufficient, demonstrable capability for NiH_2 cells in low earth orbit. A carefully controlled low earth orbit test using reasonable conditions with properly specified and quality-controlled cells would appear to be mandatory in order to demonstrate life.

FIGURE CAPTIONS

Figure 1. Distribution of testing and failures for all USAF design cells (128 cells) in low earth orbit (LEO) simulations is shown. Cross-hatched bars are numbers of cells tested at 80% depth of discharge. Asterisks indicate the major contribution from cells in the two USAF Flight experiment batteries.

Figure 2. Distribution of testing and failures for USAF design cells in LEO simulations excluding those 42 cells in the two Air Force Flight Experiment test batteries. Cross-hatched bars are numbers of cells tested at 80% depth of discharge.

Figure 3. Distribution of testing and failures for USAF design cells in high earth orbit simulations are shown for 66 cells. The cross-hatched bars are numbers of cells in elliptical orbit simulations.

Figure 4. Distribution of testing and failures for COMSAT design cells in geostationary orbit simulations are shown for 132 cells.

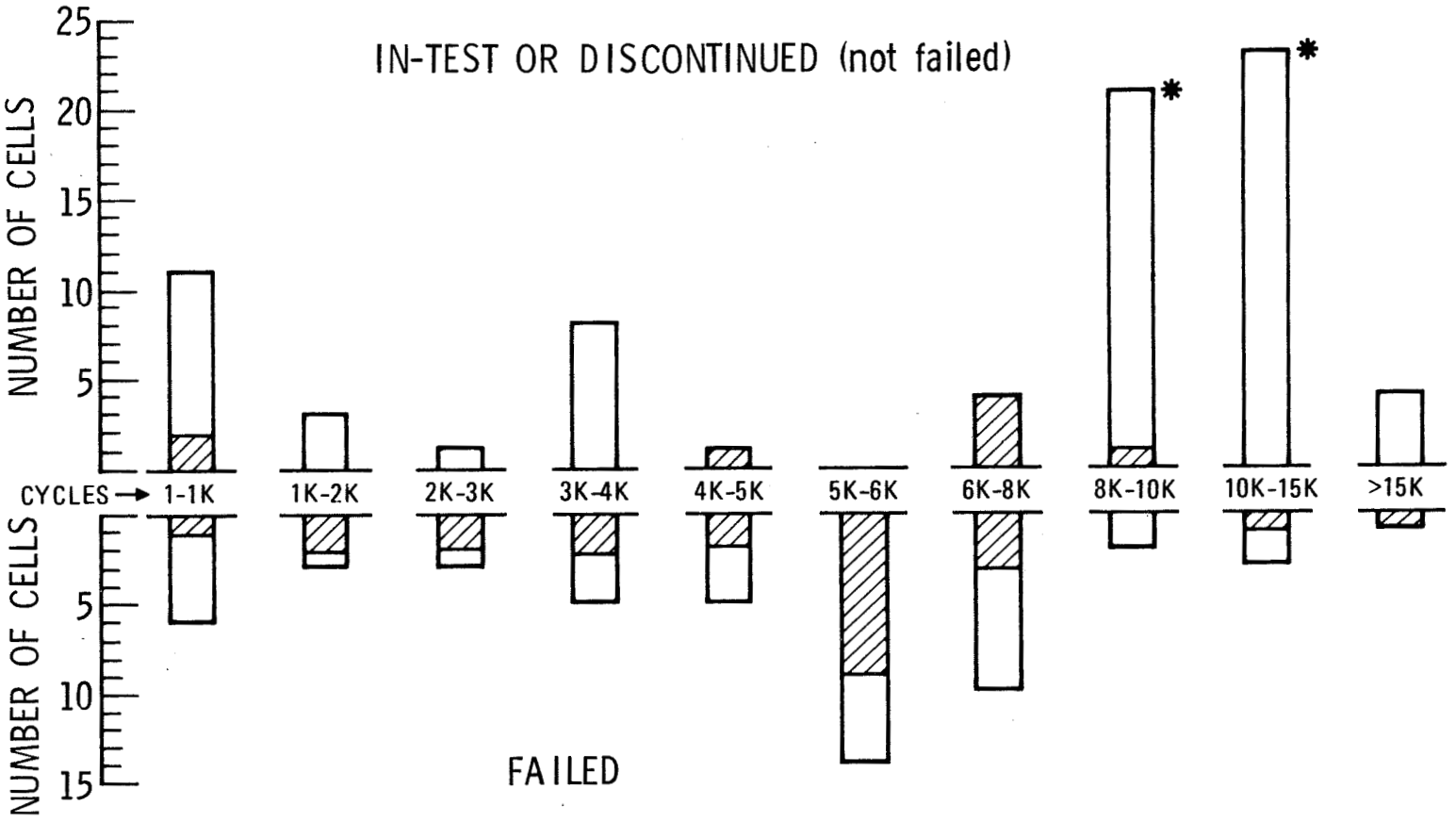

Figure 1. Distribution of testing and failures for all USAF design cells (128 cells) in low earth orbit (LEO) simulations is shown. Cross-hatched bars are numbers of cells tested at 80% depth of discharge. Asterisks indicate the major contribution from cells in the two USAF Flight experiment batteries.

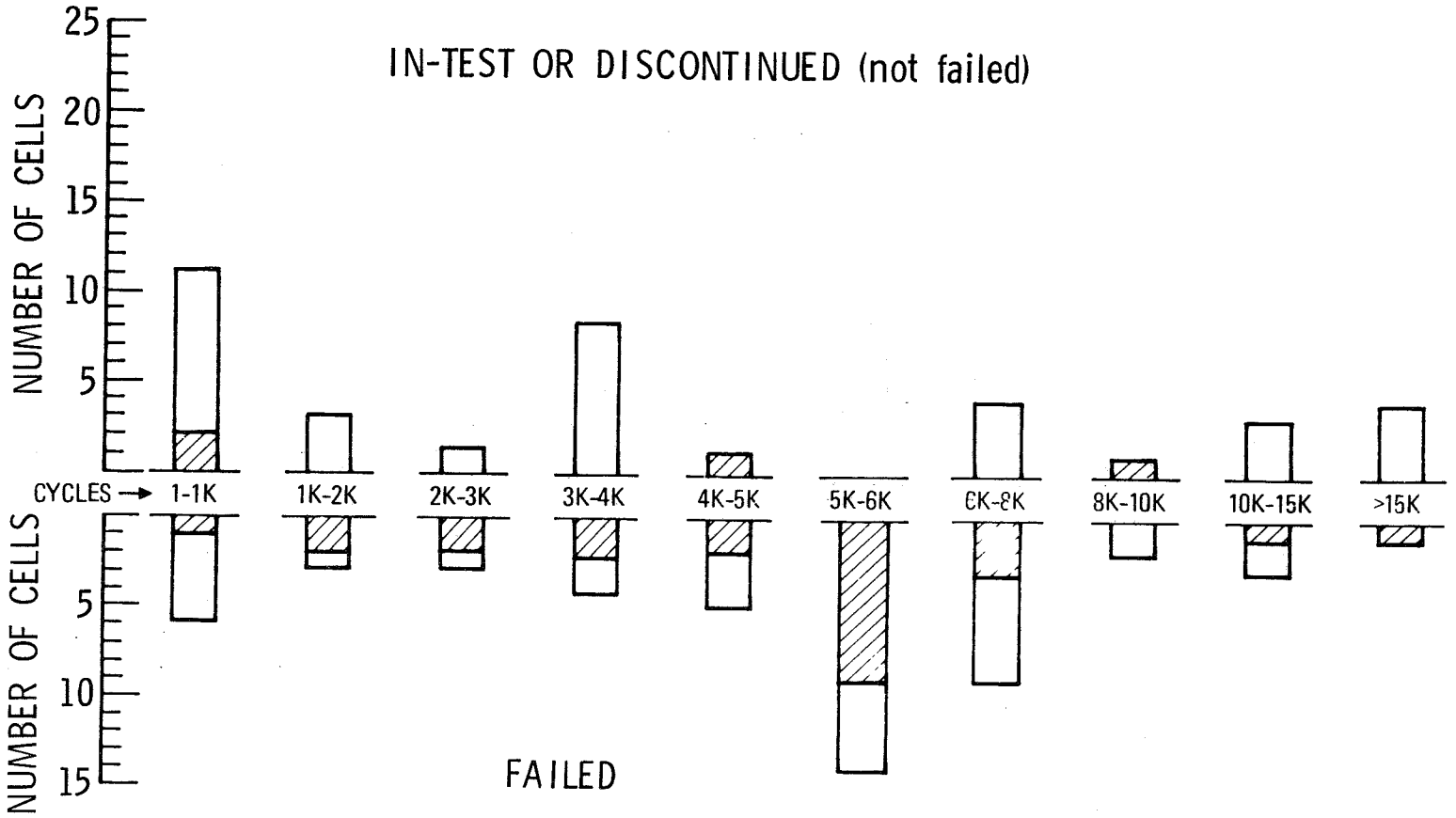

Figure 2. Distribution of testing and failures for USAF design cells in LEO simulations excluding those 42 cells in the two Air Force Flight Experiment test batteries. Cross-hatched bars are numbers of cells tested at 80% depth of discharge.

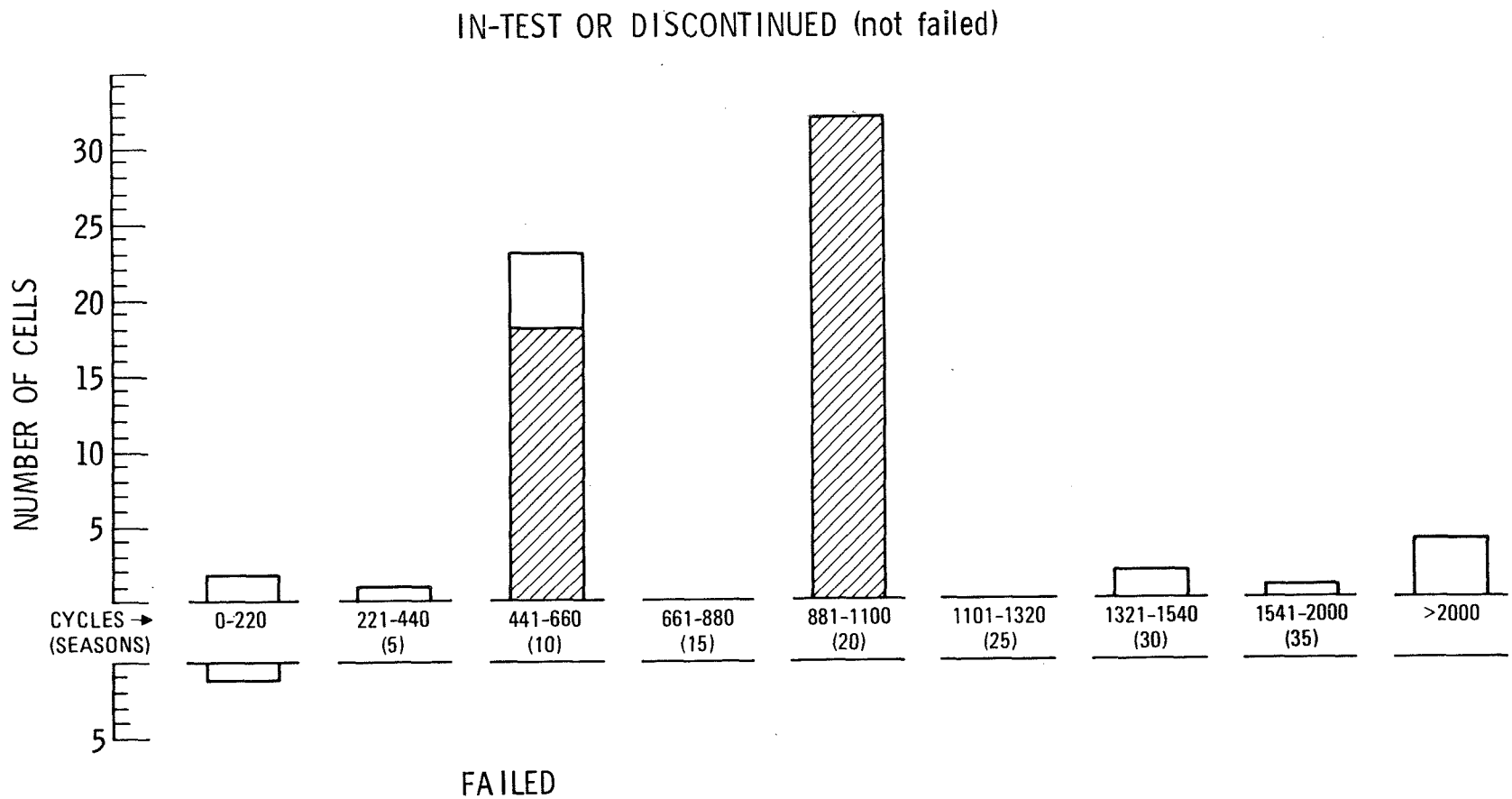

Figure 3. Distribution of testing and failures for USAF design cells in high earth orbit simulations are shown for 66 cells. The cross-hatched bars are numbers of cells in elliptical orbit simulations.

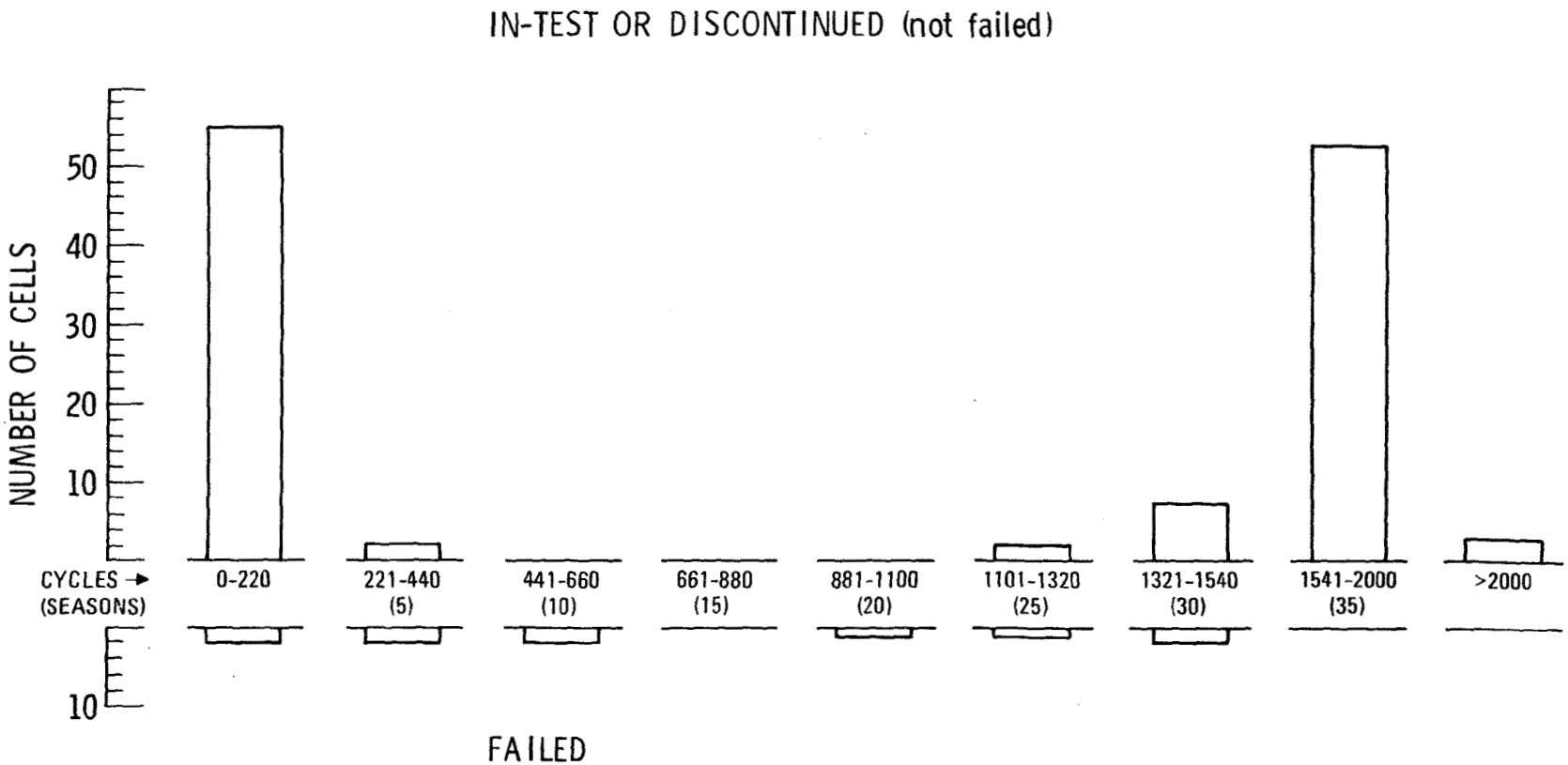

Figure 4. Distribution of testing and failures for COMSAT design cells in geostationary orbit simulations are shown for 132 cells.

GODDARD SPACE FLIGHT CENTER
November 13-15 1984 BATTERY REGISTRATION

Arthur E. Anderson
AT&T Bell Laboratories
600 Mountain Avenue
Murray Hill, NJ 07974

J. J. Auborn
AT&T Bell Labs
500 Mountain Avenue
Murray Hill, NJ 07974

Charles Badcock
Aerospace Corporation
P.O. Box 92957
MS M2-275
Los Angeles, CA 90009

David Baer
Hughes Aircraft Company
MS S12/V330, P.O. Box 92919
Los Angeles, CA 90009

James A. Barnes
Code R33
Naval Surface Weapons Center
Silver Spring, MD 20910

Wilbert L. Barnes
Naval Research Lab
4555 Overlook Avenue, S.W.
Washington, DC 20375

Fr. Baron
European Space Agency
ESTEC Post Bus. 299, 2200 AG
Noordwijk, Netherlands
FRANCE

Jospeh Barrella
Power Conversion, Inc.
495 Boulevard
Elmwood Park, NJ 07407

Richard Beauchamp
Johnson Controls
900 E. Keefe Avenue
Milwaukee, WI 53212

Jim Bell
Hughes Aircraft Company
Building S12
P.O. Box 92919
Los Angeles, CA 90009

Charles Bennett
General Electric Co. - RSO
3198 Chestnut Street
Philadelphia, PA 19101

Christian Beres
Quantex Corporation
1 Riverwood Court
Potomac, MD 20854

George Bernard
Fairchild Industries
c/o NRL
4555 Overlook Avenue, S.W.
Code 7712
Washington, D.C. 20375

E. R. Berry
Aerospace Corporation
P.O. Box 92957, M.S. M4/988
Los Angeles, CA 90009

Jacob Bineth
TADIRON
1 Linden Place
Great Neck, Long Island, NY 11021

Samuel Birken
Aerospace Corporation
P.O. Box 92957
M4-988
Los Angeles, CA 90009

Frank Bis
Code R33
Naval Surface Weapons Center
Silver Spring, MD 20910

Wayne S. Bishop
USAF
AFWAL/POOC-1
WPAFB, OH 45433

GODDARD SPACE FLIGHT CENTER
November 13-15 1984 BATTERY REGISTRATION

Harlan Bittner
Aerospace Corporation
Mail Station M2-988
P.O. Box 92957
Los Angeles, CA 90009

Ms. Carole Blesser
Eagle-Picher Industries, Inc.
3820 S. Hancock Exp.
Colorado Springs, CO 80931

John Boldt
The Applied Physics Laboratories
John Hopkins Road
Laurel, MD 20707

Christine K. Bonniksen
United States Air Force
SD/YASB P.O. Box 92960
Worldway Postal Center
Los Angeles, CA 90009

William A. Boyd
Utah Research & Development
Company, Inc.
7915 South 1530 West
West Jordan, UT 84084

Dr. Klaus Brandt
Moli Energy, LTD.
3958 Myrtle Street
Burnaby, BC
Canada VYC4DZ

Philip Branot
RCAS
GSFC Code 513
Greenbelt, MD 20771

Douglas Brasco
SAFT-America, Inc.
107 Beaver Court
Cockeysville, MD 21034

Veronica S. Brence
11235 Oakleaf Drive
Apt. #609
Silver Spring, MD 20901

Mr. Eric Brill
Eagle-Picher Industries, Inc.
3820 S. Hancock Exp.
Colorado Springs, CO 80931

Jack Brill
Eagle-Picher Industries, Inc.
P.O. Box 47
Joplin, MO 64802

Al Britting
The Aerospace Corporation
M4/988
P.O. Box 92957
Los Angeles, CA 90009

Ralph Brodd
Standard Oil of Indiana
Amoco Research Center
P.O. Box 400
Napeville, IL 60566

Richard J. Broderick
GTE Satellite
1700 Old Meadow Road
McLean, VA 22102

Mr. Michael Brookman
SAFT-America, Inc. Inc.
107 Beaver Court
Cockeysville, MD 21030

John Bruder
Quadri
1725 West 17th Street
Tempi, AZ 85282

Richard C. Buchman
Energy Technology, Division of Medtronic
6700 Shingle Creek Parkway
Brooklyn Center, MN 55430

Gernot Buerger
Pellon Corporation
20 Industrial Avenue
Chelmsford, MA 01824

GODDARD SPACE FLIGHT CENTER
November 13-15 1984 BATTERY REGISTRATION

Robert B. Byrnes
Department of Army
RT 2 Box 595
Stafford, VA 22554

Josip Caja
Oak Ridge Precision Industries
111 Flint Street
Oak Ridge, TN 37830

J. Carami
D. Kendall Company
95 West Street
Walpole, MA 02081

Matt Carns
OAO Corporation
7500 Greenway Center
Greenbelt, MD 20770

Robert L. Cataldo
NASA/Lewis Research Center
MS 309-1
21000 Brookpark Road
Cleveland, OH 44135

R. Donald Chartier
AMAX Nickel, Inc.
599 West Putnam Avenue
Greenwich, CT 06836

Captain Allen L. Chesley
United States Air Force
HQ AFSC/IGF
Andrews AFB, MD 20334-5000

P. R. K. Chetty
D-8
Fairchild Space Company
Germantown, MD 20874

Stewart Chodosh
Power Conversion, Inc.
495 Boulevard
Elmwood Park, NJ 07407

Lee C. Christensen
Pellon Corporation
20 Industrial Avenue
Chelmsford, MA 01824

James Ciesla
Electrochem Industries
10,000 Wehrle Drive
Clarence, NY 14031

Maj. Michael B. Cimino
USAF AFWAL-POOC-1
Wright Patterson AFB, OH 45433

Karla Clark
Hughes Aircraft
Building S12
P.O. Box 92919
Airport Station
Los Angeles, CA 90009

Steven Cohen
RCA American Communications (Americom)
400 College Road East
Princeton, NJ 08540

J. F. Connolly
AT&T Technology Systems
50 Lawrence Road
Springfield, NJ 07081

Dennis B. Cooper
INTELSAT
490 L'Enfant Plaza, S.W.
Washington, DC 20024

Glenn F. Cruze
Duracell U.S.A.
Berkshire Industrial Park
Bethel, CT 06801

F. S. Cushing
Consultant
209 Krewson Terrace
Willow Grove, PA 19090

George Dakermanji
M/S E 13
Century Boulevard
Fairchild Space Company
Germantown, MD 20879

GODDARD SPACE FLIGHT CENTER
November 13-15 1984 BATTERY REGISTRATION

Steven Dallek
Naval Surface Weapons Center
Code R33
Silver Spring, MD 20910

Ivan F. Danzig
United States Army
6812 Wild Rose Court
Springfield, VA 22152

E. Thomas Dawson
Space Division USAF YF
2616 Vargas Way
Redondo Beach, CA 90278

C. T. Dils
Honeywell Power Sources Center
104 Rock Road
Horsham, PA 19044

Michael Domeniconi
Lockheed Missiles and Space Company
Building 582, P.O. Box 504
Sunnyvale, CA 94086

G. R. Drengler
Union Carbide Corp. - Tech.
P.O. Box 45035
Westlake, OH 44135

Orville O. Dunham Jr.
National Standard Company
P.O. Box 1620
Corbin, KY 40701

J. Dunlop
COMSAT Laboratories
22300 Comsat Drive
Clarksburg, MD 20871

Andrew Dunnet
INTELSAT
490 L'Enfant Plaza, S.W.
Washington, DC 20024

Davids Dwyer
Sanders Associates
HUD-2A
95 Canal Street
Nashua, NH 03061

Martin Earl
COMSAT Laboratories
22300 Comsat Drive
Clarksburg, MD 20871

Jack Faber
University of Colorado
Laboratory for Atmospheric
and Space Physics
5525 Central Avenue
Boulder, CO 80301

David O. Feder, Consultant
Electrochemical Energy Storage Systems
35 Ridgedale Avenue
Madison, NJ 07940

Mr. Vladimir Feiman
Motorolla, Inc.
8000 W. Sunrise Boulevard
Room 2609
Ft. Lauderdale, FL 33322

Dennis P. Ferry
MIT Lincoln Laboratory
Lexington, MA 01824

Floyd E. Ford
NASA/GSFC
711.2
Greenbelt, MD 20771

Robert W. Francis
Aerospace Corporation
P.O. Box 92957
Los Angeles, CA 90009

James D. Frawley
F.B.I., Room 1B035
10th & Pennsylvania Avenue
Washington, D.C. 20535

Gary B. Freebern
(Dept. 354, Bldg. 34/3, MS416)
McDonnell Aircraft Company
P.O. Box 516
St. Louis, MO 63166

GODDARD SPACE FLIGHT CENTER
November 13-15 1984 BATTERY REGISTRATION

Mr. Anthony Galassi
Hughes Aircraft Company
7221 Calamo Street
Springfield, VA 22150

David Garner
Naval Research Lab
Code 7714
Washington, DC 20375

K. F. Garoutte
Honeywell Power Sources Center
104 Rock Road
Horsham, PA 19044

Stephen J. Gaston
RCA Astro-Electronics
P.O. Box 800
Princeton, NJ 07726

Capt. Gregory M. Gearing
USAF AFWAL - POOC-1
Wright Patterson AFB, OH 45433

Lawrence J. George
NASA/Marshall Space Flight Center
EB12
MSFC, AL 35812

Joe Gessler
SAFT-America, Inc., Inc.
Advanced Battery Systems Division
107 Beaver Court
Cockeysville, MD 21030

James Gleeson
Standard Oil of Indiana
Amoco Research Center
P.O. Box 400
Napeville, IL 60566

Donald R. Glenn
Energy Research Corporation
Washington, DC 20585

Dirk Gleysteen
SAFT-America, Inc.
107 Beaver Court
Cockeysville, MD 21030

Dr. Ned Godshall
Sandia National Labs
ORG. 25-23
Albuquerque, NM 87185

Mr. Paul Goldsmith
TRW
One Space Park
R4-2182
Redondo Beach, CA 90278

L. T. Goliaszewski
RCA Astroelectronics, MS 111
P.O. Box 800
Princeton, NJ 08540

Lester Gordy
U.S. Army
420 N. Van Dorn Street
Tower Hotel, Room 216
Alexandria, VA 22304

Peter W. Gorian
AUSSAT PTY LTD.
Suite 616
999 N. Sepulveda Blvd.
El Segundo, CA 90245

Mr. J. Goualard
Saft - France
A56 Avenue De 7ETZ
Romainville, France 93230

H. R. Grady
Foote Mineral Company
Route 100
Exton, PA 19341

Robert S. Green
RCA/ASTRO Electronics
MS 111, P.O. Box 800
Princeton, NJ 08540

Frank Gross
Martin-Marietta-Denver Aerospace
S0550
Denver, CO 80202

GODDARD SPACE FLIGHT CENTER
November 13-15 1984 BATTERY REGISTRATION

Sidney Gross
Boeing Aerospace Company
Mail Stop 3A-03, P.O. Box 3999
Seattle, WA 98124

Randy Haag
Naval Weapons Support Center
Code 30524
Crane, IN 47522

Ronald Haas
LSMC
1111 Lockheed Way
Sunnyvale, CA 94064

Douglas Hafen
Lockheed Missiles and Space Company
D/62-16, B/151A
P.O. Box 504
Sunnyvale, CA 94086

Steve Hafner
SAFT-America, Inc.
107 Beaver Court
Cockeysville, MD 21030

Steve Hall
Naval Weapons Support Center
Code 30524
Crane, IN 47522

Dr. Gerald Halpert
Jet Propulsion Laboratory
MS 277-102
4800 Oak Grove Drive
Pasadena, CA 91109

Dr. Alan Harkness
Ballard Research Inc.
1164 15th Street, West VIP 1M9
North Vancouver, BC Canada

Albert F. Heller
The Aerospace Corporation
M4-988, P.O. Box 92957
Los Angeles, CA 90009

Thomas J. Hennigan
T. J. Hennigan Associates
900 Fairoak Avenue
West Hyattsville, MD 20783

Gregg Herbert
The Applied Physics Lab
Johns Hopkins Road
Laurel, MD 20707

Jerry Herridy
Hughes A/C
El Segundo CA
Los Angeles, CA 90009

Donald C. Hess
NESSEA
St. Inigoes, MD 20684

George Higgins
Dow Chemical
Building 566
Midland, MI 48640

R. Higgins
Eagle - Picher Industries
C & Porter Streets
Joplin, MO 64802

Mr. Jim Hill
Eagle-Picher Industries, Inc.
3820 S. Hancock Exp.
Colorado Springs, CO 80931

Charles B. Hodgson
Canadian Astronautics Limited
1050 Morrison Drive
Ottawa, Ontario K2H 8K7
Canada

Mr. Gerhard L. Holleck
EIC Laboratories, Inc.
111 Downey Street
Norwood, MA 02062

Lt. Javier E. Hopun
USAF Space Division
SD/YDEA, P.O. Box 92960
Los Angeles, CA 90009

GODDARD SPACE FLIGHT CENTER
November 13-15 1984 BATTERY REGISTRATION

Mark A. Hoberecht
NASA/LERC
21000 Brook Park Road, MS 301-3
Cleveland, OH 44135

Donald M. Horan
Naval Research Laboratory
Code 7714
Washington, DC 20375

F. L. Hornbuckle
Fairchild Communications and Electronics
20301 Century Blvd.
Germantown, MD 20874

Paul L. Howard
P.L. Howard Associates, Inc.
P.O. Box K
Millington, MD 21651

R. E. Hudak
Ford Aerospace & Communications Corporation
3939 Fabian Way, M/5 G45
Palo Alto, CA 94303

Daniel L. Hutchins
The Aerospace Corporation
P.O. Box 92957, MS M4-988
Los Angeles, CA 90009

Warren Hwang
Aerospace Corporation
Mail Station M2-275
P.O. Box 92957
Los Angeles, CA 90009

Rikio Ishikawa
Central Research Institute of Electric Power Industry (CRIEPI)
Ohtemachi Bldg., 1-6-1
Ohetemachi Chiyoda-ku
Tokyo 100 Japan

Bruce Jagid
Power Conversion, Inc.
495 Boulevard
Elmwood Park, NJ 07407

James Martin Jagielski
NASA/GSFC
Code 711.1
Greenbelt, MD 20771

Stan D. James
Naval Surface Weapon Center
Silver Spring, MD 20910

D. H. Johnson
Union Carbide Corporation Technology
P.O. Box 45035
Westlake, OH 44145

Joseph D. Jolson
Catalyst Research
1421 Clarkview Road
Baltimore, MD 21209

Charles Kelly
Honeywell Power Sources Center
104 Rock Road
Horsham, PA 19044

J. J. Kelley
Exide Corporation
19 W. College Avenue
Yardley, PA 19067

Koichi Kibe
National Space Development Agency of Japan
2-1-1, Sengen, Sakura-mura
Niihari-gun, JAPAN 305

R. C. Kientz
General Electric Company
P.O. Box 114
Gainesville, Florida 32605

Michael Paul Kimmey
Catalyst Research
1421 Clarkview Road
Baltimore, Maryland 21209

GODDARD SPACE FLIGHT CENTER
November 13-15 1984 BATTERY REGISTRATION

Alice King
Hughes Aircraft Company
P.O. Box 92919
Building S12
Los Angeles, CA 90009

Eddison W. Kipp
TRW
One Space Park, M4/1028
Redondo Beach, CA 90278

Peter Kitchener
MIT Lincoln Laboratory
244 Wood Street
Lexington, MA 02173

Mr. Martin Klein
Energy Research Corporation
3 Great Pasture Road
Danbury, CT 06804

C. W. Koehler
Ford Aerospace & Communications Corporation
3939 Fabian Way, M/S G45
Palo Alto, CA 94303

W. H. Koh
Lockheed Missiles and Space Company
P.O. Box 504
Sunnyvale, CA 94086

Dr. Robert Kosak, Jr.
Lithium Corporation of America
449 N. Cox Road
Gastonia, NC 28053

David N. Kramer
Ridgetech Associates, Inc.
P.O. Box 464
Owings Mill, MD 21117

Paul W. Krehl
Wilson Greatbatch LTD
10,000 Wehrle Drive
Clarence, NY 14031

Marvin L. Kronenberg
Duracell
37A Street
Needham, MA 02194

Mr. Joseph L. Lackner
Department of National Defense
DRGO/ECD
Shirley Bay
Ottawa, Providence Ontario, Canada
K1AOZ4

Gabriel Lastro
SAFT-America, Inc.
107 Beaver Court
Cockeysville, MD 21034

John W. Lear
Martin Marietta Denver Aerospace
6819 N. Ridgeway Circle
Parker, CO 80134

Thomas T. Lee
Electrochem Industry
10,000 Wehrle Drive
Clarence, NY 14031

Dr. Charles Levine
Dow Chemical Company
2800 Mitchell Drive
Walnut Creek, CA 94598

Samuel C. Levy
Sandia National Laboratories
ORG. 2523
P.O. Box 5800
Albuquerque, NM 87185

C. C. Liang
Omnion Enterprises, Inc.
9460 Greiner Road
Clarence, NY 14031

Hong S. Lim
Hughes Research Laboratories
MS RL70
3011 Malibu Canyon Road
Malibu, CA 90265

GODDARD SPACE FLIGHT CENTER
November 13-15 1984 BATTERY REGISTRATION

David Linden, Consultant
78 Lovett Avenue
Little River, NJ 07739

Joseph Lindmayer
Quantex Corporation
1 Riverwood Court
Potomac, MD 20854

Jim Low
Hughes Aircraft Company
P.O. Box 92919
El Segundo CA, Building S12
Los Angeles, CA 90009

Charles Lurie
TRW
1 Space Park, R4-1028
Redondo Beach, CA 90278

Phil Lyman
Ball Aerospace
P.O. Box 1062
Boulder, CO 80306

Mr. Gary Lyons
Howard Textile Mills
20 Roosevelt Avenue
Rosslyn, NY 11576

Tyler X. Mahy
U.S. Government, CIA
c/o OTS
Washington, DC 20505

B. Mani
Energy Conversion Devices, Inc.
197 Meister Avenue
P.O. Box 5357
North Branch, NJ 08876

Dominic Manzer
NASA/GSFC
Code 711.2
Greenbelt, MD 20771

Suzanne L. Maras
Ford Aerospace & Communications Corporation
Code 435.7
GSFC
Greenbelt, MD 20771

Lynn Marcoux
Hughes Aircraft Company
Building S12, MS V330
P.O. Box 92919
Los Angeles, CA 90009

Charles H. Marcus
GSFC, Health and Safety Branch
Code 205.2
Greenbelt, MD 20771

Nikola Marincic
Hellesens Bei
1636 Hyde Park Avenue
Hyde Park, MA 02136

Jean M. Marinkovich
Hughes Aircraft Company
Building, S12
Los Angeles, CA 90009

Anthony Matthews
6614 Tenth Street
Alexandria, VA 22307

Dr. Dean Maurer
Bell Laboratories, Room 1E207
Murray Hill, NJ 07974

Keith Mauter
Duracell, United States of America
Berkshire Industrial Park
Bethel, CT 06801

Joseph H. McCann
RCA
9012 Stevens Lane
Lanham/Seabrook, MD 20706

GODDARD SPACE FLIGHT CENTER
November 13-15 1984 BATTERY REGISTRATION

D. A. McCoy
Communications Research Center
3701 Carling Avenue
P.O. Box 11490, Shirley Bay
Ottawa, Ontario, Canada KZH 8S2

Joseph K. McDermott
Martin-Marietta-Denver Aerospace
8583 South Everett Street
Littleton, CO 80123

Dr. Patrick McDermott
B&K Dynamics
3204 Monroe Street
Rockville, MD 20805

Greg McDonald
Satellite Business Systems
P.O. Box 291
Clarksburg, MD 20871

George McKhann
McDonnell Douglas
4301 Bolsa Avenue, MS 14-3
Huntington Beach, CA 92647

W. C. Merz
Consultant
Tracor Battery Technology Center
3805 Mt. Vernon Avenue
Alexandria, VA 22305

John R. Metcalfe
Canadian Astronautics Limited
1050 Morrison Drive
Ottawa, ON K2H8K7
CANADA

George J. Methlie
2705 N. Jefferson Street
Arlington, VA 22207

Mr. John R. Meyer
Johns Hopkins University
Applied Physics Laboratory
Johns Hopkins Road
Laurel, MD 20707

Ronald P. Mikkelson
General Dynamics/Convair
MZ 24-6390, P.O. Box 85357
San Diego, CA 92138

Martin Milden
Aerospace Corporation
P.O. Box 92957, MS M2-275
Los Angeles, CA 90009

Marvin Milewits
Flopetrol Johnston
P.O. Box 36369
Houston, TX 77036

Mr. Gene J. Miller
Johns Hopkins University
Applied Physics Laboratory
Johns Hopkins Road
Laurel, MD 20707

Lee Miller
Eagle-Picher Industries, Inc.
P.O. Box 47
Joplin, MO 64802

Thomas Miller
NASA/Lewis Research Center
c/o Goddard Space Flight Center
Code 711.2
Greenbelt, MD 20771

Anthony J. Miserendino
GTE Power Systems
520 Winter Street
Waltham, MA 02254

Dr. Jim Moore
Rensselear Polytechnic Institute
110 8th Street
Troy, NY 12181

Ms. Georgina More
Motorola, Inc.
8000 W. Sunrise Boulevard
Room 2609
Ft. Lauderdale, FL 33322

GODDARD SPACE FLIGHT CENTER
November 13-15 1984 BATTERY REGISTRATION

George W. Morrow
NASA/GSFC
Code 711.2
Greenbelt, MD 20771

H. C. Moses
Naval Research Laboratories
828 Glen Allen Drive
Baltimore, MD 21229

Dr. Carl E. Mueller
NSWC/WO
Code R33
Silver Spring, MD 20910

Vernon C. Mueller
McDonnell Douglas Astronautics Co
St. Louis Division
P.O. Box 516
Dept.: E454, Mail Stop 409
St. Louis, MO 63166

Buddy D. Murray
Martin-Marrietta Corporation
P.O. Box 179
Mail Stop S0550
Denver, CO 80201

Stephen Nicholas
Naval Electronic Systems Command
PDE 106-6
Washington, D.C. 20363

Mr. Phillip D. Olbert
Ball Aerospace Division
P.O. Box 1062
Boulder, CO 80306

G. Van Ommering
Ford Aerospace & Communications
Corporation
3939 Fabian Way, M/S G45
Palo Alto, CA 94303

Kathleen O'Neill
Naval Surface Weapons Center
Silver Spring, MD 20910

L. T. Ostwald
Ball Aerospace Systems Division
P.O. Box 1062, Mail Station BE-9
Boulder, CO 80306

T. D. O'Sullivan
AT&T Bell Labs
Room 1E209
Murray Hill, NJ 07060

Burton Otzinger
Rockwell Institute, SSD
2600 Westminister Blvd.
P.O. Box 3644, M/C SL-10
Seal Beach, CA 90740

Dr. Boone B. Owens
Energy Technology/Medtronic
6700 Shingle Creek Parkway
Mail Stop G207
Brooklyn Center, MN 55430

Charles F. Palandati
NASA/GSFC
Code 711.2
Greenbelt, MD 20771

Wendy A. Parkhurst
Code R33
Naval Surface Weapons Center
Silver Spring, MD 20910

Ken Parkany
Power Systems
UTC P.O. Box 109
S. Windsor, CT 06074

Peter Paschakarnis
Hoppecke
c/o Utah Research & Development
Company, Inc.
7915 South 1530 West
West Jordan, UT 84084

Robert E. Patterson
TRW
One Space Park, R4/1120
Redondo Beach, CA 90278

GODDARD SPACE FLIGHT CENTER
November 13-15 1984 BATTERY REGISTRATION

Eugene Pearlman
RCA Astro-Electronics
P.O. Box 800
Princeton, NJ 07726

Frank Perez
Hughes Aircraft Company
P.O. Box 92919
El Segundo CA S12/V330
Los Angeles, CA 90009

Mr. Leo Pessin
Fairchild Space Company
20301 Century Boulevard
Germantown, MD 20874

Dave Pickett
Hughes Aircraft Company
P.O. Box 92919
Airport Station
Los Angeles, CA 90009

Philip Pierce
RCA Astro-Electronics
P.O. Box 800
Princeton, NJ 07726

Michael J. Pollack
Three E Laboratories, Inc.
840 W. Main Street
Lansdale, PA 19446

F. John Porter
The Applied Physics Laboratories
Johns Hopkins Road
Laurel, MD 20707

William Price
FBI
1B475 9th & Pennsylvania Avenue
Washington, D.C. 20535

Vincent J. Puglisi
Yardney Battery Division
82 Mechanic Street
Pawcatuck, CT 02891

Dr. Hamid Rahnamai
Intelsat
Intelsat, 490 L'Enfant Plaza
Washington, D.C. 20024

Nachiappan S. Raman
SAFT-America, Inc.
107 Beaver Court
Cockeysville, MD 21030

Mr. Guy Rampel
General Electric
Gainesville, FL 32602

David A. Reed
COMSAT
22300 Clarksburg Drive
Clarksburg, MD 20871

Gail K. Regan
GSFC, Health & Safety Branch
Code 205.2
Greenbelt, MD 20771

Dr. Margaret A. Reid, M.S. 309-1
NASA Lewis Research Center
21000 Brookpark Road
Cleveland, OH 44135

Frank Rhoback
Honeywell Power Sources Center
104 Rock Road
Horsham, PA 19044

R. N. Richards
Martin-Marietta-Denver Aerospace
P.O. Box 179
Denver, CO 80201

Paul Ritterman
COMSAT
2250 W. Imperial
El Segundo, CA 90245

Robert L. Robinson
NASA/JSC
Code EP4
Houston, TX 77058

G. Ernest Rodriguez
NASA/GSFC
Code 711.1
Greenbelt, MD 20771

GODDARD SPACE FLIGHT CENTER
November 13-15 1984 BATTERY REGISTRATION

Gilbert L. Roth
NASA HQ's
LB
Washington, D.C. 20546

John J. Rowlette
Jet Propulsion Laboratory
Pasadena, CA 91109

Ted Russell
Space Communications Company
1300 Quince Orchard Blvd.
Gaithersburg, MD 20878

Al Sadilek
Johns Hopkins Applied Physics Lab
Johns Hopkins Road
Laurel, MD 20707

William R. Sadler
2705 N. Jefferson
Arlington, VA 22207

Ms. Lisa S. Sapp
Johns Hopkins University
Applied Physics Laboratory
Johns Hopkins Road
Laurel, MD 20707

G. Sarre
SAFT-America, Inc.
156 Avenue de Metz
Romainville, FRANCE 93230

Stephen F. Schiffer
RCA Astro Electronics
P.O. Box 800, MS 111
Princeton, NJ 08540

David F. Schmidt
General Electric Company
P.O. Box 861
Gainesville, FL 32602

J. A. Schmidt
RCA Americom
#2 Edsal Road
Sussex, NJ 07461

Dean Schneebeck
Martin-Marietta Corporation
P.O. Box 179
Denver, CO 80236

A. Dan Schnyer
NASA HQ-RP
Washington, DC 20546

Nile Schwabauer
Gates Corporation
Denver, CO 80236

Eddie Tatsu Seo
The Gates Corporation
P.O. Box 5887
Denver, CO 80217

H. Shields
Eagle & Picher Industries
C & Porter Streets
Joplin, MO 64802

Robert Siegler
Electrochem Industries
10,000 Wehrle Drive
Clarence, NY 14031

Bob Siegling
Quadri
1725 West 17th Street
Tempi, AR 85282

Dennis Sieminski
Electrochem Industries
10,000 Wehrle Drive
Clarence, NY 14031

David E. Simm
OAO Corporation
1304 North Road
Severna Park, MD 21146

Jack Sindorf
Johnson Controls
900 E. Keefe Avenue
Milwaukee, WI 53212

GODDARD SPACE FLIGHT CENTER
November 13-15 1984 BATTERY REGISTRATION

Luther Slifer
7023 Dolphin Road
Lanham, MD 20706

Houston Smith
Lithium Corporation of America
449 N. Cox Road
Gastonia, NC 28053

Jerry J. Smith
Office of Naval Research
Code 413
Arlington, VA 22217

Dr. Patricia Smith
Naval Surface Weapons Center
R-33
Silver Spring, MD 20910

John J. Smithrick
NASA/Lewis Research Center
MS 309-1
21000 Brookpark Road
Cleveland, OH 44135

D. G. Soltis
NASA LERC
21000 Brook Park Road
Cleveland, OH 44135

Steven J. Specht
Gould Defense Systems, Inc.
18901 Euclid Avenue
Cleveland, OH 44117

Nath Srinivas
COMSAT
950 L'Enfant Plaza
Washington, DC 20024

Dr. Robert Staniewicz
SAFT-America, Inc.
107 Beaver Court
Cockeysville, MD 21030

Robert Stearns
General Electric Company
P.O. Box 8555
Building 100 M2412
Philadelphia, PA 19101

Jay Stedman
United Technologies Corporation
P.O. Box 109
S. Windsor, CT 06074

Irv Stein
JPL 198-220
4800 Oak Grove Drive
Pasadena, CA 91109

David Stewart
RCA American Communications (Americor
400 College Road East
Princeton, NJ 08540

Dr. J. A. Stiles
Moli Energy, LTD.
3958 Myrtle Street
Burnaby, BC
Canada VYC4DZ

Russell C. Stinebring
Wilson Greatbatch LTD
10,000 Wehrle Drive
Clarence, NY 14031

J. Stockel
COMSAT Laboratories
22300 Comsat Drive
Clarksburg, MD 20871

Phil Studer
NASA/Goddard Space Flight Center
Code 716.2
Greenbelt, MD 20771

Martin Sulkes
USAERADCOM
DELET-PL
Fort Monmouth, NJ 07703-5302

Ralph M. Sullivan
The Applied Physics Laboratories
Johns Hopkins Road
Laurel, MD 20707

GODDARD SPACE FLIGHT CENTER
November 13-15 1984 BATTERY REGISTRATION

David Surd
Catalyst Research
1421 Clarkview Road
Baltimore, MD 21209

Larry L. Swette
Giner, Incorporated
14 Spring Street
Waltham, MA 02154

James Symanski
Johnson Controls G3
Milwaukee, WI 53201

Bob Taenaka
Hughes Aircraft Company
P.O. Box 92919
Building 512/V330
Airport Station
Los Angeles, CA 90009

Mike Takao
Senior Sales Engineer
Sanyo Electric, Inc.
200 Riser Road
Little Ferry, NJ 07643

Yoshihiro Takizawa
Furukawa Battery Company, LTD
No. 16-1, Hoshikawa Z Chome, Hodogaua-ku
Yokohama 240, Japan

C. Michael Tasevoli
NASA/GSFC
Code 711.2
Greenbelt, MD 20771

Dr. Lawrence H. Thaller
NASA/Lewis Research Center
21000 Brook Park Road
Cleveland, OH 44135

Helmut E. Thierfelder
G. E. Space Systems Division
Box 8555
Philadelphia, PA 19101

Bill Thompson
NASA/GSFC
Code 711.2
Greenbelt, MD 20771

Stephen Thornell
Dept. of the Army
U.S. Army ET & D LABS
Fort Monmouth, NJ 07703-5302

Smith Tiller
NASA/Goddard Space Flight Center
Code 711.2
Greenbelt, MD 20771

Paul J. Timmerman
Martin-Marietta-Denver Aerospace
8376A S. Upham Way 1-305
Littleton, CO 80123

James E. Triner
Gould Defense Systems, Inc.
18901 Euclid Avenue
Cleveland, OH 44117

Dr. Hari Vaidyanathan
COMSAT Laboratories
22300 Comsat Drive
Clarksburg, MD 20871

Dr. K. L. Vasanth
Bowie State College
c/o GSFC, Code 711.2
Greenbelt, MD 20771

Donald C. Verrier
Yardney Battery Division
82 Mechanic Street
Pancatuck, CT 02891

Capt. Carl Wabs, Jr.
United States Air Force
HQ/AFSC/IGF
Andrews AFB, MD 20334-5000

James R. Waggener
Catalyst Research Corporation
1421 Clarkview Road
Baltimore, MD 21209

GODDARD SPACE FLIGHT CENTER
November 13-15 1984 BATTERY REGISTRATION

C. Richard Walk
Tracor Battery Technology Center
3805 Mt. Vernon Avenue
Alexandria, VA 22305

Don R. Warnock
U.S. Air Force
AFWAL/POOC
Wright-Patterson AFB, OH 45433

Tom Watson
Catalyst Research
1421 Clarkview Road
Baltimore, MD 21209

Hubert C. Watton
General Dynamics Convair
P.O. Box 85357
MZ 34-6200
San Diego, CA 92138

Bruce Webber
SAFT-America, Inc.
107 Beaver Court
Cockeysville, MD 21034

Howard Weiner
The Aerospace Corporation: M4-988
P.O. Box 92957
Los Angeles, CA 90009

Max M. Wertheim
Grumman Aerospace Corporation
M/S T02-05
Bethpage, NY 11714

John L. Westrom
G.E. Space Division
P.O. Box 8555
Philadelphia, PA 19101

Jim Wheeler
Eagle-Picher Industries, Inc.
P.O. Box 47
Joplin, MO 64802

Eileen G. Whitlock
U.S. Army - SLAG
5925 Quantrell Avenue #202
Alexandria, VA 22312

Mark Williams
Catalyst Research
1421 Clarkview Road
Baltimore, MD 21209

Alvin H. Willis
Boeing Aerospace Company
P.O. Box 3999
Seattle, WA 98124

P. Williman
CNES-DRT/QPE/CP
18 Avenue Edouard Belin
Toulouse, France 31055

T. H. Willis
AT&T Technologies
600 Mountain Avenue
Murray Hill, NJ 07974

Richard Wilson
Standard Oil of Ohio
Midland Building (808HB)
Cleveland, OH 44115

Dave Wormstone
SPAR Aerospace
Trans Canada Highway
Montreal, Canada ___

I. David Yalom
Consultant
10813 East Nolcrest Drive
Silver Spring, MD 20903

David Yedwab
ARDC
Building 61 South
Dover, NJ 07801-5001

Albert Zimmerman
Aerospace Corporation
Mail Station M2-275
P.O. Box 92957
Los Angeles, CA 90009

LIST OF CONFERENCE PARTICIPANTS
WITHOUT ADDRESSES

1. Elmer G. Brungardt
2. Gabriel Castro
3. Guy Chagnon
4. Miles O. Dustin
5. John P. Everritt
6. Detlef H. Kurpanek
7. Warid Martin
8. Don Mattson
9. Joseph McCartney
10. Jim Parry
11. Krushow Press
12. Christopher T. Shapen
13. W. Zajae

BIBLIOGRAPHIC DATA SHEET

1. Report No.	2. Government Accession No.	3. Recipient's Catalog No.
NASA CP-2382		

4. Title and Subtitle	5. Report Date
The 1984 Goddard Space Flight Center Battery Workshop	July 1985
	6. Performing Organization Code: 711
7. Author(s): G. Morrow, Editor	8. Performing Organization Report No.: 85B0328
9. Performing Organization Name and Address: Goddard Space Flight Center, Greenbelt, Maryland 20771	10. Work Unit No.
	11. Contract or Grant No.: S-14764-D
12. Sponsoring Agency Name and Address: National Aeronautics and Space Administration, Washington, D.C. 20546	13. Type of Report and Period Covered: Conference Publication
	14. Sponsoring Agency Code

15. Supplementary Notes

16. Abstract

This document contains the proceedings of the 17th annual Battery Workshop held at Goddard Space Flight Center, Greenbelt, Maryland on November 13 to 15, 1984. The workshop was attended by manufacturers, users and government representatives interested in the latest results in battery technology as they relate to high reliability operations and aerospace use. The subjects covered included advanced energy storage programs, lithium cell technology, nickel-cadmium technology, testing and flight experience, and metal hydrogen technology.

This document contains the formal papers presented in each session.

17. Key Words (Selected by Author(s))	18. Distribution Statement
Batteries, Electrochemical, Lithium Cells	Unclassified–Unlimited Subject Category 33

19. Security Classif. (of this report)	20. Security Classif. (of this page)	21. No. of Pages	22. Price
Unclassified	Unclassified	611	A99

For sale by the National Technical Information Service, Springfield, Virginia 22161

GSFC 25-44 (10/77)

☆U.S. GOVERNMENT PRINTING OFFICE: 1985 -537 -086/ 20004 REGION NO. 4

National Aeronautics and
Space Administration

Washington, D.C.
20546

Official Business
Penalty for Private Use, $300

NASA

National Aeronautics and
Space Administration

Washington, D.C.
20546

SPECIAL FOURTH CLASS MAIL
BOOK

Postage and Fees Paid
National Aeronautics and
Space Administration
NASA-451

Official Business
Penalty for Private Use $300

1 1 1U,D, 850730 S905o9ASR
NASA
SCIEN & TECH INFO FACILITY
ATTN: ACCESSIONING DEPT
P O BOX 8757 BWI ARPRT
BALTIMORE MD 21240

NASA

POSTMASTER: If Undeliverable (Section 158
Postal Manual) Do Not Return